Fate and influence of inorganics and heteroatoms during the hydrothermal carbonisation of biomass

Aidan Mark Smith

Submitted in accordance with the degree requirements of Doctor of Philosophy as part of the integrated PhD with MSc in Low Carbon Technologies

Doctoral Training Centre in Low Carbon Technologies, School of Chemical and Process Engineering,

The University of Leeds

November 2018

The candidate confirms that the work submitted is his own, except where work which has formed part of jointly-authored publications has been included. The contribution of the candidate and the authors to this work has been explicitly indicated below. The candidate confirms that appropriate credit has been given within the thesis where reference has been made to the work of others.

The details in chapters 4 and 5 of the thesis are based on the following published papers respectively.

Smith A.M., Singh S. and Ross A.B. (2016), Fate of inorganic material during hydrothermal carbonisation of biomass: influence of feedstock on combustion behaviour of hydrochar *Fuel Volume 169, 135-145*

The candidate performed all the experiments, analysis and write up. Dr Singh supported in the experimental and analytical techniques. Dr. Ross contributed with comments, guidance and proof reading.

Smith A.M. and Ross A.B. (2016) Production of bio-coal, bio-methane and fertilizer from seaweed vial hydrothermal carbonisation *Algal Research Volume 16, 1-11*

The candidate performed all the experiments, analysis and write up. Dr. Ross contributed with comments, guidance and proof reading.

Smith A.M., Whittaker C., Shield I and Ross A.B. (2018) Potential for production of high quality bio-coal from early harvested miscanthus by hydrothermal carbonisation *Fuel volume 220, 546-557*

The candidate performed all the experiments, analysis and write up. Dr Ross, Dr Shield and Dr Whittaker contributed with comments, guidance and proof reading.

Planned Publication:

Smith A.M., Ekpo U. and Ross A.B. (under review) Influence of pH on the combustion properties of hydrochar following hydrothermal treatment of Swine manure. *Fuel*

The candidate performed the analysis of samples made by a previous PhD student, Dr Ugo Ekpo, re-interpreted the data and wrote the bulk of the manuscript. Dr. Ross contributed with comments, guidance and proof reading.

Acknowledgements

Firstly, I would like to thank my supervisor Dr Andrew Ross for his support and guidance over the last four years and his openness to discuss ideas and develop concepts, be those good or bad. I would also like to thank his two former post-doctoral researchers Dr Patrick Biller and Dr Surjit Singh as their guidance in the initial year was invaluable. I would also like to thank the technical staff at the University of Leeds, in particular, Dr Adrian Cunliffe, Simon Lloyd, Karen Alves Thorne, Sara Donna and Ed Woodhouse, who were a tremendous source of advice and their continual support enabled this PhD. I must also thank the administration staff at the University of Leeds particularly Emily Bryan-Kinns, David Hayes, James McKay and Rachael Brown who were always on hand to help and enabled me to focus on the research and not the administration.

Acknowledgement of my fellow student researchers is also required, in particular, Dr Douglas Phillips, Dr Niamh Ryall, Dr Victoria Hoolohan, Dr Robert Bloom, Dr James Hammerton, Dr Katrina Adam, Dr Kate Palmer, Dr Kelly Marsh and Dr Patrick Mason who have been a continual source of distraction and support. In addition, I am very grateful for the support outside of Leeds by Dr Nicolas Pooley and Dr Emma Pooley.

I would also like to thank the Engineering and Physical Science Research Council (EPSRC) for the financial support via EP/G036608/1.

Finally, I would like to express my greatest thanks to Katharine and my two children Eleanor and Phoebe for being so tolerant. Without Kate's help and support, none of this would be possible and I will be forever grateful for her allowing me to have a wonderful family while fulfilling a dream.

I would like to dedicate this work to Eleanor, Phoebe and Laurence

Abstract

Hydrothermal carbonisation (HTC) is an emerging biomass pre-treatment that works by converting biomass into a coal like material, in the process overcoming some of the inherent limitations of biomass. To date, there have been limited publications looking into the fate and influence inorganics and heteroatoms have on the HTC chemistry. This is surprising given these elements are of critical importance when it comes to the fuel's utilisation. This work sets out to understand the role and fate of key inorganics and heteroatoms during HTC, but goes on to develop a mechanistic understanding of the HTC process chemistry.

This work primarily focuses on the feedstocks *Miscanthus*, willow, brown kelp (macroalgae) and swine manure. Additionally, this work has also looked into the processing of food waste, secondary sewage sludge, AD press cake, microalgae, municipal solid wastes and oak wood, providing a large database of samples.

Reaction parameters investigated as part of this work include how temperature, retention time, particle size, pH and recycling of process waters influence product yields, energy density, combustion properties, the bio-chemical composition of the bio-coal, the process water chemistry and the retention and removal of inorganics and heteroatoms. The results show that under the correct conditions HTC can produce a fuel with a HHV ranging from 25 to 30 MJ/kg (db) and the resulting bio-coal can burn like a coal, grind like coal and can overcome many of the limitations of burning biomass in pulverised coal plant. By recycling the process waters *Miscanthus* can be made into a fuel with an energy density of 29 MJ/kg (db), with an energy yield of 91 % and fuel properties comparable to a high volatile sub-bituminous coal.

The behaviour of the inorganics and heteroatoms during HTC appear dependent on feedstock, the feedstocks inorganic chemistry and the HTC processing conditions. Generally speaking, alkali metals, which are primarily responsible for the slagging and fouling behaviour of solid fuels, are largely removed (>80%) during HTC. Moreover, when processing at 250 °C retention of calcium and reincorporation of phosphorus occurs. The combination of reduced alkali metals and relative increase in calcium and phosphorous in the ash brings about significant improvement in the fuels slagging and fouling propensity as demonstrated by the ash fusion test. It hypothesised that any residual potassium within the fuel should form calcium potassium phosphate complexes in the ash. These complexes are thermally stable and prevents the formation of low melting temperature potassium silicates or the volatilisation of potassium chloride, further

reducing slagging, fouling and corrosion beyond that expected for alkali metal leaching. This can be applied to a range of low value fuels such as green harvested *Miscanthus* and seaweeds. This demonstrates the technologies potential to valorise low quality feedstock and produce a direct substitute bio-coal from an expanded range of terrestrial and aquatic biomass.

Recycling process water brings about an increase in bio-coal energy density, energy yield and produces a fuel with more coal-like properties. It is hypothesised that the recycled process waters contain organic acids that hydrolyse the hemicellulose and cellulose to furfural like compounds at a lower temperature and increase saccharide concentrations within the process water at lower temperatures. The increased saccharide concentrations favour aromatization and repolymerisation, which better enables the decomposition products to undergo polymerisation and form the bio-coal before the increasing process temperature brings about their further degradation to organic acids. Once degraded to organic acids these acids appear to only undergo limited reincorporation into the bio-coal, but do appear to play a role in the demineralisation of the fuel. Based on this it is proposed that the slow heating rates followed by an hour retention time is favourable to overcome kinetic limitations otherwise imposed by faster heating rates and shorter retention times.

The heteroatom oxygen plays a critical role in the reactions involved in HTC. The energy densification of the bio-coal is largely due to the deoxygenation of the fuel. Removal of this oxygen forms unsaturated compounds that polymerise quickly, and intermolecular dehydration results in polymerisation, condensation and aromatisation of these fragments. Oxygen is also critical in repolymerisation, with aromatic structures initially chemisorbed though reactive oxygen functionalities that dehydrate to form stable oxygen bonds linking a polymeric matrix of cyclic aromatic carbon rings. The retention of calcium also suggests it may play catalytic role in the repolymerisation process with the literature supporting this. There is however evidence that at high calcium concentrations, calcium in the process water can have an adverse effect on carbonisation, binding to surface oxygen functional groups on the biomass feedstock and preventing hydrolysis and decomposition of the feedstock.

Table of contents

Table of figures

Table of tables

Table of equations

Nomenclature

AAS	Atomic Absorption Spectroscopy
AD	Anaerobic Digestion
ad	as determined
AFT	Ash Fusion Test
AI	Alkali Index
ar	as received
ASTM	American Society for Testing and Materials
BAI	Bed Agglomeration Index
BBOT	2,5-(Bis(5-tert-butyl-2-benzo-oxazol-2-yl) thiophene
BECCS	Bioenergy Carbon Capture and Storage
BET	Brunauer–Emmett–Teller theory analysis
BMP	Biological Methane Potential
BS	British Standard
BSE	Back Scattered Electrons
BSPP	British Standard Pipe parallel thread
BSPT	British Standard Pipe Taper thread
CCS	Carbon Capture and Storage
CEC	Cation Exchange Capacity
CEN	European Committee for Standardisation
COD	Chemical Oxygen Demand
-COOH	Carboxyl
CPMAS	Cross polarisation magic angle spinning
CV	Calorific Value
daf	dry ash free
db	dry basis
DDGS	Dried Distillers Grains with Solubles
DPMAS	Direct Polarisation Magic Angle Spinning
DSC	Differential Scanning Calorimetry
DT	Deformation Temperature
DTG	Differential Thermal Gravimetric
EDTA	Ethylenediaminetetraacetic acid
EDX	Energy-Dispersive X-ray Spectroscopy
EDXRF	Energy Dispersive X-ray Fluorescence
EMC	Equilibrium Moisture Content
EN	European Norms
EPSRC	Engineering and Physical Sciences Research Council
ESP	Electrostatic Precipitator

FDG	Flue Gas Desulphurisation
FI	Fouling Index
FT	Flow Temperature
GC	Gas Chromatography
GCMS	Gas chromatography Mass Spectroscopy
GJ	Gigajoule
HGI	Hardgrove Grindability Index
HHV	Higher Heating Value
HMF	Hydroxymethylfurfural
HPLC	High-Performance Liquid Chromatography
HPLC-MS	High-performance Liquid Chromatography Mass Spectroscopy
HT	Hemisphere Temperature
HTC	Hydrothermal Carbonisation
HTG	Hydrothermal Gasification
HTL	Hydrothermal Liquefaction
IC	Ion Chromatography
ICP AES	Inductively Coupled Plasma Atomic Emission Spectroscopy
ICP-MS	Inductively Coupled Plasma Mass Spectrometry
IPPC	Intergovernmental Panel on Climate Change
ISO	International Organization for Standardization
LCFA	Long Chain Fatty Acids
LHV	Lower Heating Value
MAS	Magic Angle Spinning
MIC	Multi Ion Counting
MSW	Municipal Solid Waste
NMR	Nuclear magnetic resonance spectroscopy
NOx	Nitrogen oxides
NPS	National Pipe Straight
NPT	National Pipe Taper
OH	Alcohol functional group
PF	Pulverised Fuel
PID	Proportional Integral Derivative
PTE	Potential to Emit
PTFE	Polytetrafluoroethylene
Py-GCMS	Pyrolysis Gas chromatography Mass Spectroscopy
Rb/a	Base to acid ratio
RF	Radio Frequency

RH	Relative Humidity
RPW	Recycled Process Water
RT	Retention Time
SCWG	Supercritical Water Gasification
SEM	Scanning Electron Microscope
SI	Slagging Index
SIPS	Sample Induction Pump System
SST	Shrinkage Temperature
STP	Standard Temperature Pressure
SVI	Slag Viscosity Index
TAG	Triacylglycerides
TCD	Thermal Conductivity Detector
TGA	Thermo-Gravimetric Analysis
TIC	Total Ion Count
TOC	Total Organic Carbon
TPO	Temperature Programmed Oxidation
TS	Technical Standard
VFA	Volatile Fatty Acid
WDXRF	Wavelength Dispersive X-ray Fluorescence
XPS	X-ray Photon Spectroscopy
XRF	X-ray Fluorescence

1. Introduction

Today most of our industrial materials including fuels, polymers, chemicals, pharmaceuticals, packaging and construction products are made from fossil based resources. This was not always the case; up until the early part of the 20th century many industrialised chemicals such as solvents, fuel, synthetic fibres and chemical products were made from plant resources [1, 2]. Issues however arise in this fossil fuelled world when you consider that not only are these resources finite and the global resources diminishing; most of fossil-fuel derived products eventually end up as carbon dioxide in the Earth's atmosphere. During the last 150 years there has been a rapid increase in the carbon dioxide concentrations in the atmosphere, from 228 ppm, to 383 ppm in 2007 [3] and exceeding 400 ppm for the first time in 2015 [4]. This increase is our own fault and is due primarily to the combustion of fossil fuels.

It is now widely accepted throughout the scientific community that the climate is changing as the result of these anthropogenic emissions [5]. This acceptance has spread to political leaders with 195 parties adopting the first universal, legally binding global climate deal in Paris at the COP21 climate conference. The Paris agreement aims to keep the global averaged temperature increase below 2 °C by the end of the century compared to pre-industrial levels, and if possible to no more than a 1.5 °C rise through the reduction in global emissions [6]. In order to meet the <2 °C temperature rise target agreed on in the Paris Agreement, concentrations of carbon dioxide equivalents (CO_2eq) must not exceed 450 ppm in the atmosphere and if the 1.5 °C target is to be met then concentrations must not exceed 430 ppm by 2100 [7]. In order to meet these targets, peak emissions must be reached as soon as possible in order to reduce long term climate change, preferably by the mid-2020s [8].

Adoption of renewable energy is one of the more important issues in reducing emissions and in the UK and Europe the need to replace coal combustion with a reliable, renewable, sustainable technology has driven many coal fired power stations to switch from coal to biomass as a combustion fuel. In the future it is also envisioned that the use of carbon capture and storage (CCS) technologies in conjunction with biomass could even potentially provide negative emissions (removal of carbon dioxide from the atmosphere). The basic concept of a Bioenergy CCS is that the carbon dioxide is removed from the atmosphere by the growth of biomass and is released, captured and stored when the biomass is converted using CCS technology, thus removing emissions from atmosphere. Given most emission scenarios modelled in the Intergovernmental Panel on Climate

Change (IPCC) Fifth Assessment assume negative emissions in order to meet the 430 ppm target, development of bioenergy CCS appears an important technology if emissions targets are to be met [8, 9].

While biomass maybe an attractive energy resource in terms of its potential sustainability and carbon neutrality, when compared to solid fossil fuels such as coal the physiochemical properties of biomass are different and this brings about challenges. Even high quality lignocellulosic biomass suffers due its low bulk density, high moisture content, low calorific value and high hydrophilic nature. This combined with milling difficulties brought about through the fibrous nature of biomass means that the handling properties of raw biomass negatively influence the economies of biomass. This has prompted considerable interest in pre-treatment techniques that may overcome some of these limitations. One such process is torrefaction, which has received increasing interest in recent years. Torrefaction is a thermal process that involves the heating of biomass to between 180°C and 300°C in an inert atmosphere, driving out moisture and various low calorific components to increase the fuel's calorific value [10].

This work looks at an alternative pre-processing technology, Hydrothermal Carbonisation (HTC). HTC is an emerging pre-processing technology for upgrading the physical and chemical properties of biomass before further conversion or combustion. HTC involves submerging biomass in water and heating to between 180 and 260 °C while maintaining pressures high enough to keep the water in a liquid phase. Under these conditions, the physical properties of water change at the molecular level, with the water providing a medium for a complex series of reactions which promote a natural coal formation process [11]. The resulting coal like product, known as a hydrochar is: (i) more energy dense, (ii) easily friable and (iii) more hydrophobic than the starting material and because of these properties there is now interest in its potential as a biomass pre-treatment prior to combustion or gasification.

While HTC is only now an emerging pre-processing technology for upgrading the physical and chemical properties of biomass before further conversion or combustion, research in this area began as early as 1911; albeit in an attempt to make hydrogen from coal as opposed to finding alternative fuels to the fossil based ones. In 1911, German scientist Friedrich Bergius was convinced that it should be possible to carry out the "water gas reaction" and produce hydrogen gas while inhibiting the troublesome formation of carbon monoxide by reacting coal / carbon and water at the right temperature according to Equation 1.1, assuming the right temperature and pressure conditions are satisfied [12].

Using temperatures below 600°C (a temperature at which even steam does not act on coal), Bergius managed to oxidise coal using liquid water at 200 bar producing carbon dioxide and hydrogen, however reaction rates which would have made such a reaction of commercial interest failed to be achieved.

$$C + 2H_2O = CO_2 + 2H_2 \qquad (1.1)$$

While a reaction of commercial interest had failed, in experiments where Bergius and co-workers had substituted peat for coal it was observed that exceptionally large amounts of carbon dioxide was formed and that the carbonaceous residue remaining in the vessel had the same elemental composition of natural coal. This observation prompted Bergius to study the decomposition process of plant substances more closely as he thought the process would be similar to the process of coalification, a metamorphic process that plant-based compounds undergo in their gradual transition into coal in the course of millions of years.

By 1913 many researchers had already attempted to convert biomass into coal but most had attempted to do so by heating the biomass (pyrolysis), decomposing the cellulose in the process. The secret that Bergius discovered was that the biomass precursor had to be in intimate contact with the liquid water, which, at mild temperatures (200-330 °C) and high pressures, prevented super-heating of the cellulose and thus prevented its decomposition. The resulting carbonisation products had a very similar composition to natural coal [13]. This important discovery was followed by numerous studies by Bergius and his assistant Hugo Specht on the production of this artificial coal [14]. Their experiments also become the basis for the production of liquid and soluble compounds from coal, a process which they named “coal liquefaction” [15]. Bergius was awarded the Nobel Prize in 1931 for all his studies on the production of synthetic coal as well as his work on hydrogenation and his contributions to high-pressure reactions [16].

Following the discovery by Bergius, a number of authors and studies between 1920 and 1960 developed coalification. For example, Berl and Schmidt [17] varied the biomass source and treated the different samples, in the presence of water, at temperatures between 150 °C and 350°C in order to better understand the behaviour of cellulose when heated in water and later the authors published a review on the origins of coal in Berl et al. [18]. Later, Van Krevelen and co-workers further developed this area further, analysing amongst other parameters the influence of pH on the outcome of the carbonisation reaction, and found substantial differences in the decomposition behaviour and final products, as identified by the C/H/O composition of the product [19, 20].

A renaissance of HTC started around 2000, with interest focused on carbon materials not fuel. Initially research focused on the hydrothermal synthesis of carbon spheres (~200°C) using sugar or glucose as precursors in 2001 [21, 22], and the synthesis developed towards various metal/carbon nanoarchitectures [23], carbon nanofibers [24] and spheres [25]. It was through the publication of 'Back in the Black' in 2007 by Titirici et al. [26] that HTC started to receive attention outside of geochemistry and carbon materials. Titirici et al. [26] highlighted the potential of HTC for producing biochar for carbon sequestration as opposed to slow pyrolysis and soon after several papers were published on the potential HTC had on carbon sequestration and soil improvement [27, 28]. This was at a time when there was growing interest in using biomass as a future energy source and the application of HTC in energy was soon explored. Early studies suggested the potential coal-like properties of the hydrochar would exhibit favourable behaviour with respect to combustion, gasification, and other thermal conversion processes and the technology quickly developed both academic and commercial interests in the utilisation of HTC in energy [29]. With the recent interest in using HTC to make fuel, the term bio-coal is now being commonly used as an alternative to hydrochar in order to differentiate the hydrochars for energetic applications from hydrochars intended for other applications [30-35]. Given this research looks into the energetic application of hydrochar, the author favours the term 'bio-coal' in the context of this research and will be used going forward.

Since the renaissance in HTC, the handling improvements brought about though HTC are now well documented and 100 years of research into coal formation has meant that the basic underlying chemistry behind the HTC of lignocellulosic material is at least in part understood. There has, however, been little research on the fate and influence of inorganics and heteroatoms during HTC [11, 36]. Inorganics in biomass generally refer to the metal oxides in the fuel that make up the ash. Typical heteroatoms are nitrogen (N), oxygen (O), sulphur (S), phosphorus (P), chlorine (Cl), bromine (Br), and iodine (I). As biomass is organic material from living or recently living organisms, biomass contains a number of essential minerals which are required for growth; these include silicon (Si), calcium (Ca), potassium (K), aluminium (Al), iron (Fe), magnesium (Mg), titanium (Ti), sodium (Na), nitrogen, phosphorus and sulphur [37, 38]. Inorganics are a particular issue for biomass during combustion and gasification as large amounts of alkali and alkaline metals, particularly potassium and sodium, along with sulphur and chlorine influence ash chemistry. The ash chemistry influences the behaviour of the fuel in terms of its tendency to corrode equipment and cause slagging, fouling and bed agglomeration; nitrogen,

sulphur, chlorine and phosphorus can also be associated with airborne emissions [39-41]. To reduce the adverse effects of inorganic metals, there is now interest in the leaching of biomass with water and acids in order to extract nutrients as a way to reduce the ash deposition and airborne emissions before combustion, gasification or further pre-treatment such as torrefaction [41-43].

As HTC processes biomass in water, it is possible to remove inorganic salts and ionic bonded inorganics along with heteroatoms from the bio-coal, in a way which is not possible with dry thermal pre-treatments [44-46]. Moreover it may be possible to modify the inorganic and heteroatom chemistry of the compounds remaining in the bio-coal in such a way to reduce the ash deposition and airborne emissions [47]. It is also known that certain salts have catalytic effects on the hydrothermal process [44, 48, 49]. By understanding the behaviour of inorganics and heteroatoms during the HTC process it may also be possible to modify the inorganic chemistry in such a way to utilise the catalytic effects certain salts have on hydrothermal processes, simultaneously enhancing the yields and products while reducing their adverse impacts.

This research aims to understand the role and fate inorganics and heteroatoms have during hydrothermal carbonisation of a range of biomass. The objectives are: (i) to identify the behaviour of inorganics and heteroatoms in a range of biomass resources and their implications in combustion; (ii) to understand how reaction parameters influence a fuels inorganic and heteroatom chemistry; (iii) to develop an understanding of the mechanisms behind the extraction of key metals and heteroatoms during the HTC of lignocellulosic biomass; and (iv) to understand the potential catalytic mechanisms and roles inorganics and heteroatoms have during HTC.

These aims and objectives are addressed throughout this study with an outline of each chapter given in the following paragraphs:

Chapter 2 is a literature review that gives both an introduction to HTC as well as a review of the current ‘state of the art’ in HTC. This review will cover the fundamental chemistry behind HTC, the influence of reaction parameters on the bio-coal product and review of the current research and literature. In addition, this section will set out the principles behind solid fuel combustion, set out best practice when combusting biofuels in pulverised fuel power plant, explain the challenges associated with fuel inorganic and heteroatom chemistry and give a brief introduction to coal and coalification.

Chapter 3 provides a description of the methodologies used in the experiments and the analysis of the results seen in this work. This chapter includes brief overviews of

the principles behind the analytical techniques along with a brief methodology for their use. Throughout this work, methods were adapted between chapters in order to improve the reliability and repeatability of the data. Alongside the description of the experimental methodologies, this chapter provides the logic behind their adaption and refinement.

Chapter 4 is the first data chapter within this thesis. In this chapter a range of ten feedstocks with different biochemical compositions are treated at 200 °C and 250 °C. Changes in the fuel properties are then assessed against the starting feedstock, including quantification of the changes in inorganic chemistry. The fuels suitability as a combustion fuel is then assessed using slagging and fouling indices and ash fusion tests. The findings show that HTC has a strong influence on the slagging propensity of the fuel, with ash fusion temperatures for the processed fuels melting at higher temperatures to that of the raw feedstock. The behaviour and mass balance is however very feedstock dependent and the higher lignin biomass produce higher yields of bio-coal.

Chapter 5 develops the work presented in Chapter 4, focusing on two low quality biomasses, *Miscanthus* and brown kelp and the specific application of HTC. Based on the findings in Chapter 4, HTC could be a promising pre-treatment in the valorisation of these low quality, problematic biofuels, offering the potential to exploit an extensive and largely unutilised biomass resource in the form of kelp and increase conventional yields of *Miscanthus* by up to 40 % per hectare. This is demonstrated in this chapter.

Chapter 6 looks into the influence of retention time on bio-coal combustion chemistry of *Miscanthus*. The study looks at how temperature and retention time influences product yields, energy density, combustion properties, the bio-chemical composition of the bio-coal, the process water chemistry and the retention and removal of inorganics and heteroatoms. The chapter then goes on to develop a mechanistic understanding of the HTC process chemistry and the process chemistry underlying the retention and removal of inorganics and heteroatoms.

Chapter 7 looks at the influence and implications of recycling process waters on the bio-coal fuel properties, yields and process chemistry when processing *Miscanthus*. Recycling process waters is often cited as a route to dispose of the aqueous product, of which disposal is potentially challenging, however few studies have looked into its impact. The study looks at; product yields, energy density, combustion properties, the bio-chemical composition of the bio-coal, the process water chemistry and the retention and removal of inorganics and heteroatoms. The findings show an increase in yield and a

bio-coal with properties similar to a high volatile subbituminous coal. The results also give further insight into the HTC process chemistry.

Chapter 8 looks into the influence particle size has on the HTC of willow (lignocellulosic biomass). This aspect is often overlooked in the literature with many studies stating HTC increases the grindability of HTC bio-coals but almost every study carbonising already ground biomass. The study looks at how size influences energy density, combustion properties, bio-chemical composition of the bio-coal, grindability, hydrophobicity and the retention and removal of inorganics and heteroatoms. The chapter then applies the mechanistic theory developed in the previous chapters and demonstrates how particle size is influenced by the diffusion limitations in terms of heat and the diffusion of products into the process water. These limitations can however be advantageous as by avoiding diffusion of preliminary products into the process water, these products enhance hydrolysis and polymerisation within the particle/ cylinder for cylinders up to 2.5 cm in diameter. The results go on to suggest when operating at 250 °C with one-hour retention time, cylinders up to 4 cm diameter can be treated without adverse impact on fuel properties.

Chapter 9 looks at the influence pH and temperature has on the combustion properties of swine manure. The results demonstrate how pH and temperature influences the dehydration and repolymerisation of the bio-coals and offers insights into how pH and temperature influence metal and heteroatom retention and removal. The results look at the fuel properties of the manure derived bio-coals and demonstrate that a fuel suitable for pulverised fuel combustion may be possible, albeit appropriate blending maybe required to account for ash loading, fuel nitrogen and fuel sulphur.

Chapter 10 draws together the findings within this thesis outlining the specific fate and influence of oxygen, nitrogen, sulphur, chlorine, phosphorous potassium, calcium, magnesium, silicon, iron and aluminium during HTC. Chapter 10 also brings together the findings of this thesis in relation to fuel's handling, combustion chemistry and process chemistry.

2. Current Literature

2.1. Introduction to biomass

The term biomass can include a wide range of material that is directly or indirectly derived from photosynthesis reactions such as wood fuel, wood derived fuel, fuel crops, agricultural by-products or waste and animal by-products [39].

2.1.1. The structure of lignocellulosic biomass

Woody biomass has a complicated structure and comprises of three major organic compounds; cellulose (40-50%), hemicellulose (15-30%), lignin (16-33%), along with minor substances such as pectin, protein, extractives, starch and inorganics (ash) making up the remaining constituents [50]. Herbaceous crops such as *Miscanthus* typically comprise of the same structural components albeit with lower lignin contents and higher cellulose and hemicellulose content [51]. An example of the structure of lignocellulosic biomass can be seen in Figure 2.1.

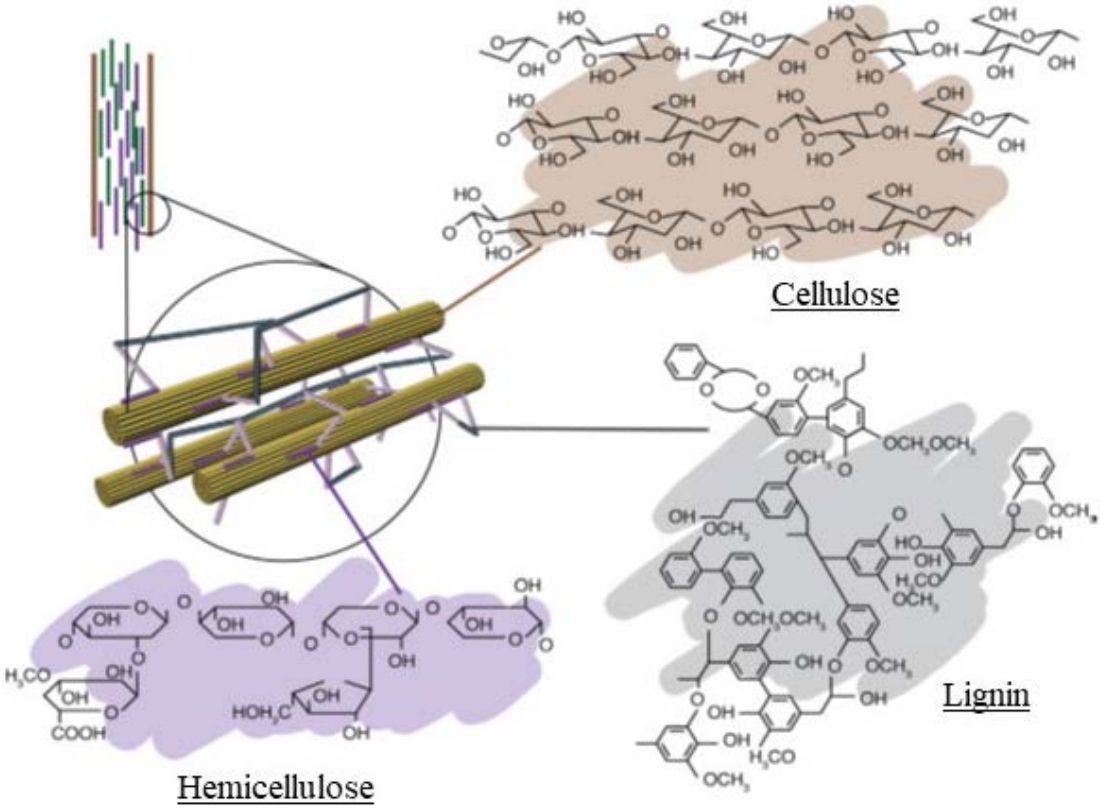

Figure 2.1: Plant cell wall and lignocellulosic biomass composition, with hemicellulose (purple), cellulose (brown) and lignin (grey) [52]

2.1.1.1.Cellulose

Cellulose is a fibrous material that provides strength to the biomass cell walls. Cellulose is a long chain, linear polymer that contain 5,000-10,000 glucose monomers, and has high molecular weight (10^6 or more). The cellulose polymers organise to form cellobiose units consisting of two glucose anhydride units [53].

2.1.1.2.Hemicellulose

Hemicellulose molecules are a mixture of polysaccharides derived from glucose, galactose, mannose, xylose, arabinose and glucuronic acids. Hemicellulose molecules are less structured than cellulose and consist of only 100-200 sugar monomers resulting in a lower molecular weight and the exact composition varies widely among different plant species and cell types [54].

2.1.1.3.Lignin

Lignin is a complex polymer that penetrates the spaces between cellulose and hemicellulose adding strength to the cell wall [52]. Lignin has no exact structure and is mainly derived from three aromatic alcohols, p-coumaryl, coniferyl and sinapyl, which are connected in weakly linked branched structures. Lignin is rich in carbon and due to this carbon contributes a larger proportion of the energy within the biomass compared to the other fractions [55, 56].

2.1.1.4.Inorganics

Inorganics in biomass generally refer to the metal oxides in the fuel which make up the ash. As biomass is organic material from living or recently living organisms, biomass contains a number of essential minerals which are required for growth; this primary group includes silicon, calcium, potassium, aluminium, iron, magnesium, titanium, and sodium, along with the non-metallic elements sulphur and phosphorus. These elements make up the bulk of the ash formed after combustion [37, 38]. In addition to the main ash forming elements there are also a secondary group of metals known as the heavy metals, which include copper, zinc, cobalt, molybdenum, arsenic, nickel, chromium, lead, cadmium vanadium and mercury which are up taken by the plant act as nutrients during the plants growth but at lower concentrations to the main ash forming elements [57].

2.1.2. The structure of brown kelp

Aquatic plants offer an alternative solution to terrestrial biomass, offering an extensive and largely unutilised biomass resource which does not compete with agriculture or forestry for land and freshwater; thus offering a potentially large biomass resource which should not be to the detriment of food production or carbon sinks. Brown kelp (Class: Phaeophyceae) is a variety of multicellular eukaryotic aquatic plant collectively known as seaweed or macroalgae. Brown kelp is significantly different from terrestrial plants in terms of their chemical composition, as well as physiological and morphological features [58]. Their different physiological and morphological features mean they exhibit exceedingly high growth rates fuelled by their high photosynthetic activity (6-8 % compared with 2 % for terrestrial biomass) [59] and with modern cultivation technologies can yield 15-20 dry tonnes of macroalgae per hectare per year [60].

Since brown kelp needs to be able to withstand stormy marine conditions, brown kelp typically does not contain lignin due to a higher requirement for flexibility. Consequently kelp is predominantly comprised of carbohydrate in the form of mannitol, laminarin, fucoidan, alginic acid and other polysaccharides [61]. To give the algae support in the absence of lignin, brown algae use parallel chains of polymeric alginic acid bound by alkali and alkaline metals to provide the seaweed with support [62]. Consequently brown algae in particular are prone to accumulating alkali and alkaline earth metal ions, notably K^+, Na^+ and Ca^{2+}, giving high inorganic/ ash contents [63]. The remaining organic fraction is predominantly protein, which results in comparatively high levels of nitrogen along with fucoidan, a structural sulphated polysaccharide comprising of fucose (a hexose deoxy sugar) with glucuronic acid, xylose or glucose substitutions [61].

2.2. Introduction to coal

Coal is a solid fossil fuel utilised by humankind for thousands of years as a source of energy [64]. The pressures of climate change are resulting in the overall decline of coal use within Europe, though coal remains the world's most used fuel for generating electricity, producing steel and making cement due to its relatively low cost and favourable handling properties. In 2015, coal provided almost 30% of the world's primary energy, with forecasts predicting decline to 27% by 2021. It is however responsible for 45% of all energy-related carbon emissions, in addition to other types of pollution [65]. Despite pressures of climate change, emerging economies, particularly in Asia, with growing populations are seeking affordable and secure energy sources to power their

economies and fuel their economic growth, resulting in the continued construction of new coal power generation [65]. This can lead to the lock-in of large amounts of carbon emissions for decades to come unless suitable biomass based fuels or carbon capture and storage is adopted.

Coal is found in seams in the Earth's crust and originated form deposited vegetation that underwent chemical and physical changes due to a process called coalification. The deposited coal differs throughout the world due to the localised conditions at the seams at the time of coalification and is typically characterised by three parameters: (i) coal rank, (ii) coal type and (iii) coal grade. *Coal rank* is determined by the degree of metamorphism (or coalification) the plant debris has been subjected to (i.e. the extent of the chemical and physical processing). *Coal type* is determined by the material from which the coal has been derived (wood leaves, algae etc.) and the remaining plant derivatives (macerals). *Coal grade* is determined by the amount to which the accumulated plant material has been kept free of contamination of inorganic material. For a coal to be classed as 'high-grade' it must have low overall inorganic content, regardless of rank or type [66].

The organic fraction within coal are known as macerals, which are microscopic components of coal that can be linked to the type of plant material originally deposited. The macerals are classified into three main categories, vitrinites, liptinites and intertinites. Vitrinite is formed from the woody tissue derived from lignin and cellulose of the original biomass and tend to contain more oxygen than other macerals. Liptinites derive from plant resins, spores and algal remains and contain higher levels of hydrogen than other macerals. Intertinites derive from the same source as vitrinites but have undergone thermal or biological oxidation (such as forest fires) resulting in a high inherent carbon content [66-68].

2.2.1. The coalification process and coal classification system

Coalification, the geochemical process that transforms deposited plant material into coal, can be described by the following steps:

Peat → Lignite → Subbituminous coal → Bituminous coal → Anthracite

The overall coalification process can be split into three stages: (i) a microbial degradation stage whereby plant material has accumulated in nearly stagnant water, typically not solely associated with thick peat bogs, whereby plant material undergoes degradation of the cellulose present in the plant material. (ii) The conversion of lignin

into humic substances, and (iii) the condensation of these substances to form larger coal molecules [67, 69]. The type of vegetation decaying and the decomposition environment are important factors in determining the nature and quality of the coal seams. The chemical and biological composition of the plant material deposited over geological periods and the depth, temperature, acidity and movement of water differed between deposit sites all affecting the coal composition. The geochemical phase is the result of increased temperatures and high pressure experienced over millions of years, due to the burying of the vegetation, and is the most important factor in the coalification process. The greater the extent of the coalification process the less moisture, volatiles, hydrogen and oxygen are present in the coal while the carbon content is increased relative to the original vegetation deposited [67]. The chemical processes that occur during each stage of coalification are outlined in Table 2.1.

Table 2.1: The coalification process [69]

Materials	Partial Process	Main Chemical Reaction
Vegetation	Peatification	Bacterial and fungal life cycles
↓		
Peat	Lignification	Air oxidation, followed by decarboxylation and dehydration
↓		
Lignite	Bituminization	Decarboxylation and hydrogen disproportioning
↓		
Bituminous Coal	Preanthracitization	Condensation to small aromatic ring systems
↓		
Semianthracite	Anthracitization	Condensation of small aromatic ring systems to larger ones; dehydrogenation
↓		
Anthracite	Graphitization	Complete carbonification

The extent of the coalification process and the conditions at the deposition sites result in coals with different measurable properties, these are used to rank and classify coal types. The classifications of coals are shown in Table 2.2 with anthracite coals undergoing coalification to the greatest extent. Figure 2.2 shows the influence on atomic H/C and O/C ratio using a Van Krevelen plot [20]. Formal classification systems have not been developed for coal grading but coal grade details information such as the amount of mineral matter present, the sulphur content, the ash fusion temperatures and the quantity of trace metals are highly important to the coal user [67].

Table 2.2: Classification of coals (adapted from Smith et al. [64])

Coal Rank	Volatile Matter (%)	H (wt%)	C (wt%)	O (wt%)	HHV (MJ/kg)	H/C	O/C
Anthracite							
Meta	1.8	2.0	94.4	2.0	34.4	0.25	0.02
Anthracite	5.2	2.9	91.0	2.3	35.0	0.38	0.02
Semi	9.9	3.9	91.0	2.8	35.7	0.51	0.02
Bituminous							
Low–Vol	19.1	4.7	89.9	2.6	36.3	0.63	0.02
Med-Vol	26.9	5.2	88.4	4.2	35.9	0.71	0.04
High-Vol A	38.8	5.5	83.0	7.3	34.7	0.80	0.07
High-Vol B	43.6	5.6	80.7	10.8	33.3	0.83	0.10
High-Vol C	44.6	5.4*	77.7	13.5	31.9	0.83	0.13
Subbituminous							
Sub A	44.7	5.3	76.0	16.4	30.7	0.84	0.16
Sub B	42.7	5.2	76.1	16.6	30.4	0.82	0.16
Sub C	44.2	5.1	73.9	19.2	29.1	0.83	0.19
Lignite							
Lignite A	46.7	4.9	71.2	21.9	28.3	0.83	0.23

Values determined on a dry ash free basis

*4.4 % stated in literature but does not fit with trend

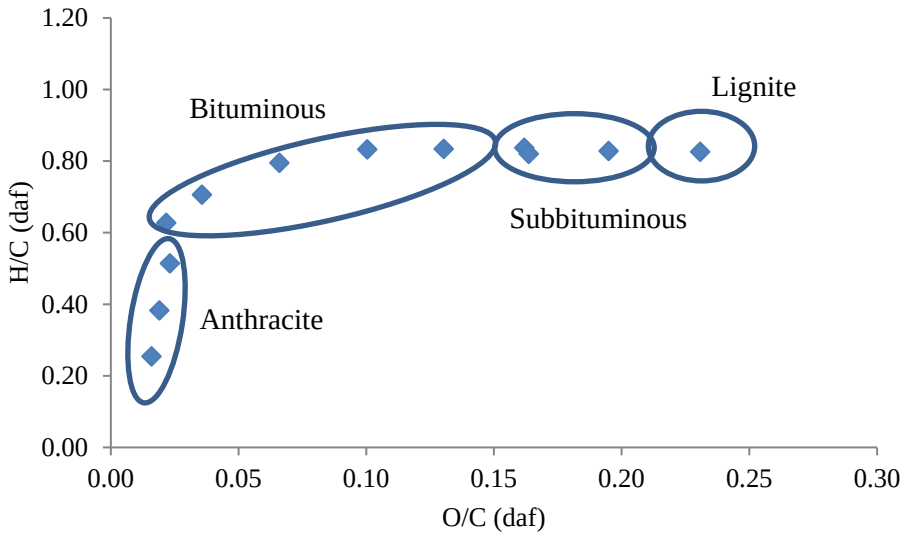

Figure 2.2: Atomic H/C-O/C ratios of coals with increasing classification

2.2.2. Chemical composition of coal

The structure of coal is complex and a general structure of a high-volatile bituminous coal as described by Shinn [70] can be seen in Figure 2.3. The coal is

presented as a polymeric matrix of cyclic aromatic carbon rings (benzene and polycyclic aromatic hydrocarbons) linked with other aromatic structures by bridges consisting of aliphatic groups, oxygen functional groups and oxygen or sulphur atoms [64]. Nitrogen may also be present in forms such as amines but as the coal matures the nitrogen forms into more condensed structures (pyridines and pyrroles). Sulphur is present as sulphide, disulphide or mercaptan in both aliphatic and aromatic structures [64].

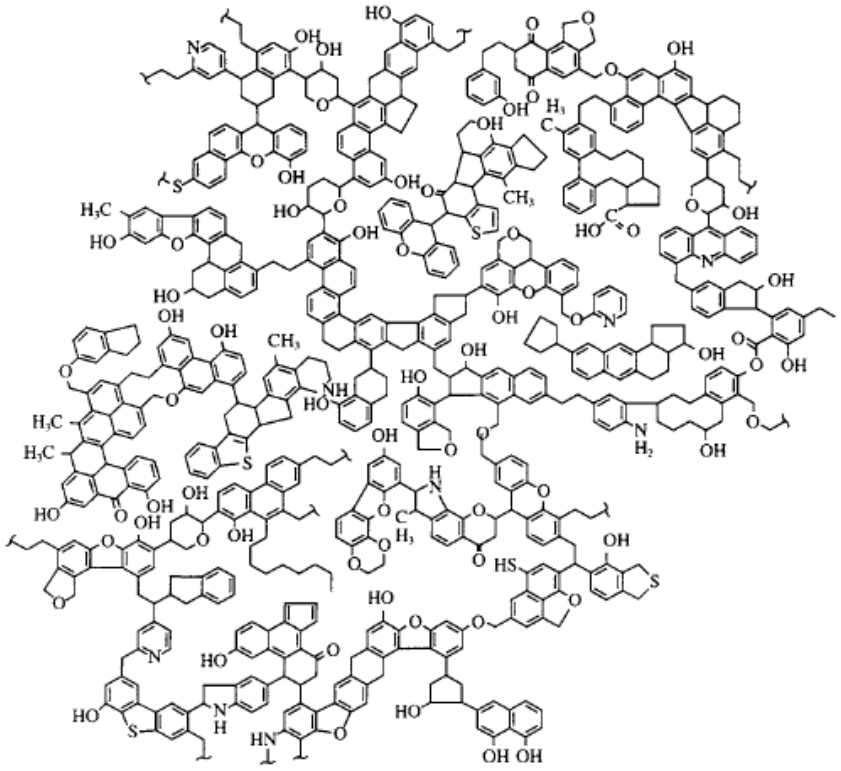

Figure 2.3: Representation of the chemical composition of high-volatile bituminous coal [70]

2.3. Fundamentals of hydrothermal processing

2.3.1. Hydrothermal Processing

HTC is a form of hydrothermal processing. Hydrothermal processing is a collective term used for three main processes: hydrothermal carbonisation (HTC), hydrothermal liquefaction (HTL) and hydrothermal gasification (HTG). In hydrothermal processing biomass is submerged in water and is subjected to high temperatures at pressures, which prevent the water from evaporating. Under these conditions, water undergoes changes at the molecular level which in turn influence its solvation power, viscosity and polarity [71]. As the water is heated and compressed, its density and polarity change reversing its properties from a highly polar hydrogen-bonded solvent to properties more like a non-polar solvent such as hexane at just below the critical point [71]. The

conditions promoting the three hydrothermal processes are largely governed by temperature and pressure, which determines the solvent properties of the water. Figure 2.4 illustrates how the ionic product, density and dielectric constant change with temperature.

At temperatures below 250 °C the main yield is a solid char like residue fraction, known as a hydrochar or bio-coal with similar properties to that of a low rank coal, in the process known as HTC. As the temperature increases to between 250-374°C, an additional liquid oil fraction known as biocrude is formed and this becomes the target product in a process referred to as HTL. The transition between HTC and HTL appears to be feedstock dependent, with some HTC studies using temperatures above 250° C. Temperature appears to be the most dominant parameter in HTC although the efficiency of the hydrothermal process is also influenced by the percentage solids in the feed [11, 28]. Above the critical point at 374 °C and 214 bar, the density of water becomes interchangeable without any phase transitions over a wide range of conditions, allowing radical reactions to dominate. This results in gasification of the biomass, with the biomass predominantly converted into carbon dioxide (CO_2), hydrogen (H_2) and methane (CH_4) [72, 73]. This supercritical process is referred to as HTG or supercritical water gasification (SCWG).

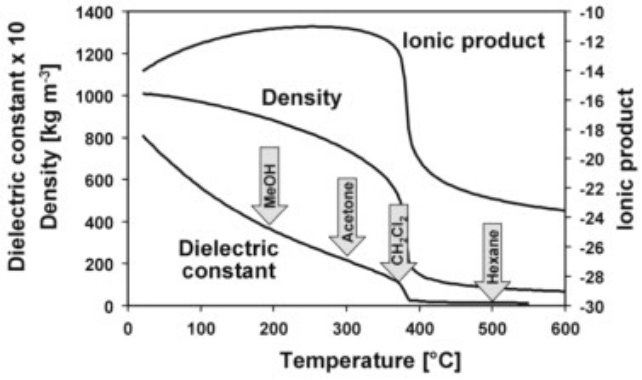

Figure 2.4. Physical properties of water at a pressure of 24 MPa versus temperature. Dielectric constants of typical organic solvents at room temperature are indicated [74]

2.3.2. The chemistry of HTC

The chemistry behind HTC is best understood for the HTC of lignocellulosic biomass; largely because HTC has historically been used to investigate and understand coalification and coal largely originates from lignocellulosics. Funke and Ziegler [11] extensively reviewed the literature on coalification from which their review gives good insight into the possible chemical mechanisms involved in the process by bringing together an extensive array of coalification studies. A later publication by Libra et al. [28]

complemented this study and gave a more in-depth insight into how the process works and compares technologies such as slow pyrolysis, with the report predominantly geared toward production of biochar (carbon sequestration) and soil amendment. Between the two publications the HTC process can however be summarised as follows. The aim of HTC is to produce a coal like bio-coal, which is: (i) more energy dense, (ii) easily friable and (iii) more hydrophobic than the starting material. This is achieved though the modified aqueous conditions providing a medium for a complex series of reactions which involve removal of hydroxyl groups through dehydration, removal of carboxyl and carbonyl groups though decarboxylation, and cleavage of many ester and ether bonds through hydrolysis under the modified aqueous conditions. This process reduces the oxygen and hydrogen content (described by the molecular O/C and H/C ratio), destroys the colloidal structures and reduces the hydrophilic functional groups, giving the bio-coal its enhanced properties [11, 28].

HTC is a complex series of reactions but it is generally understood that the following reactions take place for lignocellulosic biomass. Initially the hemicellulose and cellulose are readily degraded at temperatures of 180 °C and 200 °C respectfully. This degradation largely takes the form of hydrolysis of the hemicellulose and cellulose into oligomers and monomers such as (oligo-) saccharides [71]. The lignin does not start to degrade until slightly higher temperature, between 230 °C and 260 °C [28, 75, 76] and as it degrades it is hydrolysed into phenolic fragments, which are highly reactive and recombine quickly [28]. This maintains a coke like macromolecular structure which becomes increasingly aromatised with phenolic structures derived from the dehydration of lignin [11]. Dehydration and decarboxylation reactions remove carboxyl and hydroxyl groups leaving unsaturated compounds which can polymerise easily, resulting in condensation and polymerisation of oligomers and monomers derived from the hydrolysis hemicellulose and cellulose which also simultaneously undergo aromatisation and condense onto the aromatic macromolecule [11].

For material with lower lignin content, cellulose appears to play an important role in the formation of the char. For biomass with a structural crystalline cellulose scaffold, such as is present in grasses, this structural scaffold appears to play an important role as a nucleus for the recondensation reactions, from which the char is largely derived [28, 77]. For biomass without a structural crystalline cellulose structure the bio-coals appear different, with carbonaceous nanoparticles obtained and the particle size depending mainly on the carbonisation time and concentration, which is determined by the water to

solids ratio [77, 78]. It should however be stressed that the detailed nature and the relative significance of the above mechanisms appear strongly dependent on the type and composition of the feed [11].

For lignocellulosic biomass the reaction chemistry is believed to follow the following process. As the water heats and becomes subcritical the increasing high dissociation of H^+ and OH^- brought about under hydrothermal conditions promotes the hydrolysis of the hemicellulose and cellulose giving rise to their corresponding oligosaccharides, monosaccharides (glucose, fructose and maltose through isomerization, along with pentose) and aldehydes derived from the hydrolysis of cellulose and starch [79-81]. The high dissociation of H^+ (in the form of hydronium – H_3O^+) and OH^- then leads to the decomposition of these early monosaccharides to organic acids (e.g. acetic, lactic, propionic, levulinic and formic acids) bringing about a rapid drop in process water pH to approximately 3 [82, 83]. These acids go on to generate hydronium ions which go on to catalyse the further degradation of the oligosaccharides generated from the hydrolysis of the hemicellulose and cellulose to monosaccharides [84]. These monosaccharides then undergo dehydration and fragmentation (i.e. ring opening and C-C bond breaking) processes giving rise to different soluble products, such as furfural-like compounds and hydroxymethylfurfural (HMF) related compounds, 1,2,4-benzenetriol, acids and aldehydes (acetaldehyde, acetonitrilacetone) [84, 85]. These decomposition products undergo polymerization and condensation leading to the formation of soluble polymers. The polymerization or condensation reactions can be induced by intermolecular dehydration (two –OH groups react to leave a –O- bond removing water) or by aldol condensation. The formation of C=C can result from keto-enol tautomerism of dehydrated species (see Figure 2.5) or by intramolecular dehydration (see Figure 2.6) [85]. Increased saccharide concentration along with increased organic loadings within the process water favour the aromatization and repolymerisation of the soluble polymers [85].

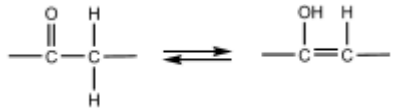

Figure 2.5: Formation of C=C can result from keto-enol tautomerism of dehydrated species

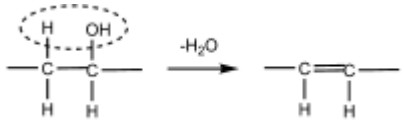

Figure 2.6: Formation of C=C can result from intramolecular dehydration

The formation of the bio-coal is believed to be produced by condensation through the intermolecular dehydration of the aromatized molecules described above [85]. The structure this takes is dependent on the biomass from which it is formed, with biomass with 'hard' plant tissues, such as crystalline cellulose, maintaining hierarchical shape (as is the case for *Miscanthus*), while soft plant tissues, without a scaffold do not keep their structure and form globular carboniferous particles [77]. Both structures are believed to follow the LaMer model of particle formation whereby when the concentration of aromatic structures reaches a certain point a burst nucleation takes place [22].

Initially the aromatic structures would be chemisorbed though reactive oxygen functionalities (hydroxyl, carboxyl, carboxylic etc.) which are present on the surface, and dehydrate to form stable oxygen groups, ether or pyrone, within the char formation, as shown in Figure 2.7. Reactive oxygen functionalities will remain on the surface and provide binding sites for more aromatic structures [85]. Figure 2.8 is a schematic of the process chemistry for the hydrothermal carbonisation of cellulose, obtained from Sevilla and Fuertes [86] and shows the formation of a hydrothermal sphere. The reactive oxygen functionalities on the hydrophilic surface providing binding sites for more aromatic structures and the dehydrated stable oxygen groups within the hydrophobic core. This results in a chemical composition very similar to that of high-volatile bituminous coal, shown in Figure 2.3.

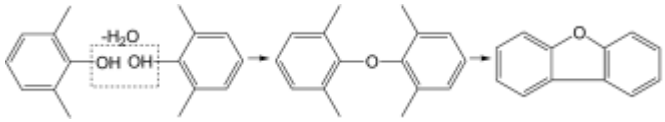

Figure 2.7: Formation of aromatic clusters via intermolecular dehydration / condensation of aromatized molecules

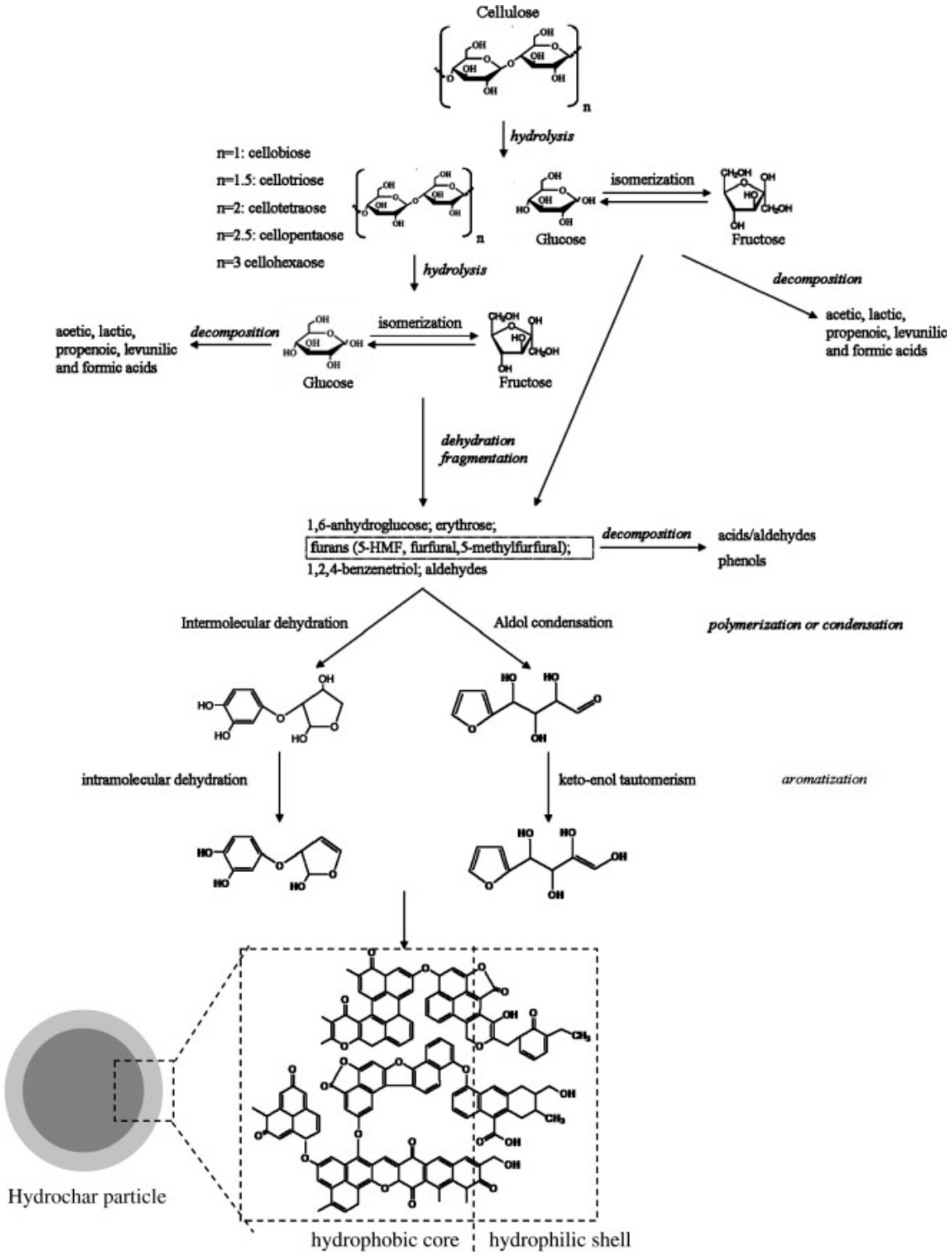

Figure 2.8: Schematic of the process chemistry for the hydrothermal carbonisation of cellulose, obtained from Sevilla and Fuertes [86]

HTC of components such as proteins and lipids are less well known, with a limited number of studies looking into the behaviour of these components in the HTC of microalgae and DDGS [87-90]. Heilmann et al. [89] undertook a mechanistic study of the HTC of DDGS by constructing 'synthetic DDGS' out of model compounds and found that during the HTC process triacylglycerides (TAG) along with monounsaturated oils and polyunsaturated oils were largely unaffected the HTC process and were simply found

deposited on the surface of the char. This has also been shown to happen during the HTC of microalgae [88, 90]. Heilmann et al. [89] also found that during the HTC process the protein fraction does not appear to carbonise unless accompanied with carbohydrate. The carbohydrate fraction appears to play an important role in the HTC of protein containing feedstock, with the hydrolysis derived oligomer and monomer intermediates denaturing and insolubilizing the protein which then becomes part of the char as opposed to it carbonising and becoming a nuclei around which the char forms.

Malliard chemistry plays an important role in the behaviour of proteins within HTC and is likely the main route for nitrogen incorporation within the bio-coal [91-93]. The Malliard reaction is not just one specific reaction but rather refers to a group of reactions occurring between reducing sugars and amino acids. The reaction is most commonly associated with the reaction which gives browned foods (bread, biscuits, seared meats etc.) their distinctive flavour but also play a key role in HTC. In the process, hundreds of different compounds can be created that can themselves react further in various ways. It is therefore impossible to provide a definitive mechanistic pathway for the incorporation of nitrogen within the bio-coal from saccharides and nitrogen containing compounds (amino acids etc.) [16, 94].

Figure 2.9 is adapted from Titirici [16] and shows some relevant steps in the Malliard reaction. This demonstrates how heteroatoms, such as nitrogen, can be incorporated into hydrothermal carbon derived from glucose (but applicable to other reducing sugars). The process starts with the nucleophilic attach of an amine (e.g. an amino acid) on the aldehyde of the sugar to produce glycosylamines (Figure 2.9, **I**), which loses water to give a Schiff base (Figure 2.9, **II**). The α-hydroxy aldehyde motif allows for the rearrangement of the Schiff bases to aminoketoses or so-called Amoadori compounds (Figure 2.9, **III** and **IV**) [95]. Compound III can form α dicarbonyl species (Figure 2.9, **V**) which could go through successive dehydrations to form HMF, which as discussed before is one of the main reactive intermediates in HTC [16].

Sulphur, another heteroatom, can also be incorporated into hydrothermal carbon via Malliard reactions however due to the valence of sulphur, sulphur nuclides cannot form Schiff bases and thus cannot go through the classical Malliard reaction cascade shown in Figure 2.9 and alternative reactions must take place. Wohlgemuth et al., [96] demonstrated that when incorporating the sulphur containing compounds cysteine and thienyl-cysteine both molecules cultivate an additional nucleophile (either a thiol or thienyl moiety) to the free amine enabling the Malliard reaction cascade to take place.

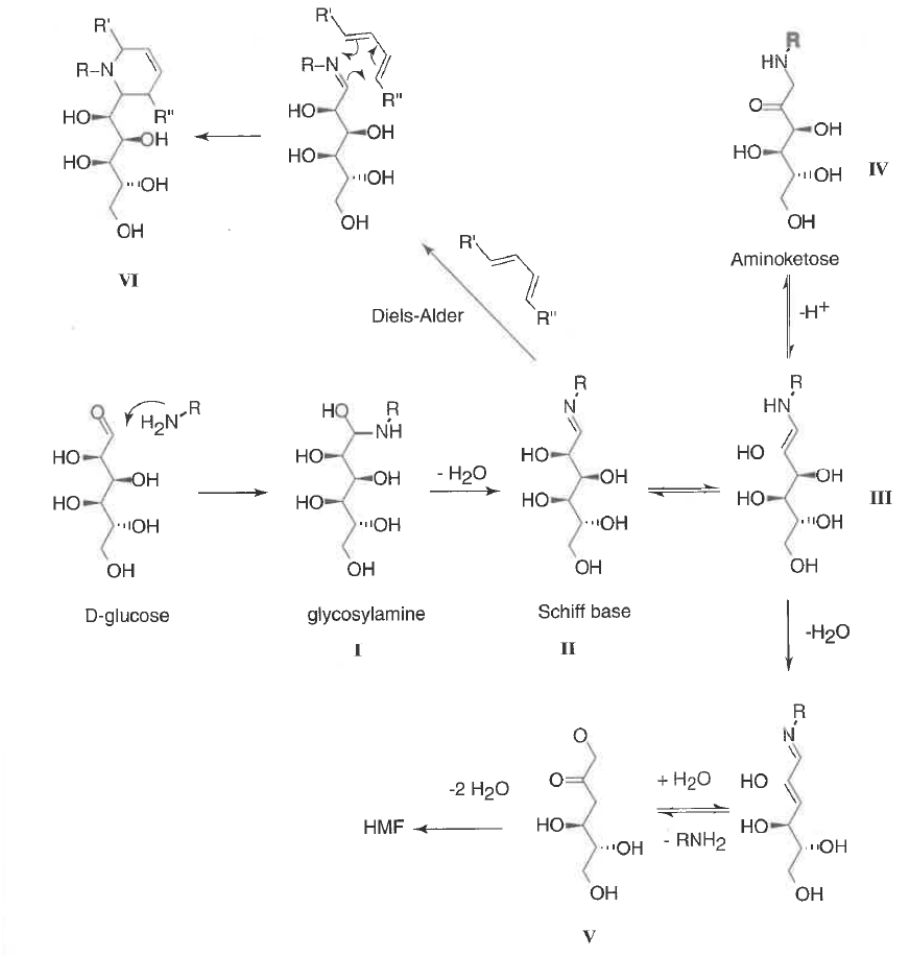

Figure 2.9: Examples of the Maillard reactions applicable to HTC [16]

2.3.3. Influence of reaction parameters on HTC

2.3.4. Temperature

The reaction rate and products of HTC are governed to a large extent by reaction temperature. The rate of hydrolysis, dehydration and polymerisation within a reaction are governed by temperature [11, 97], and the onset of degradation of key components such as cellulose, hemicellulose and lignin are also controlled by temperature [28, 75, 76, 97]. This is also combined with the changes in solvent properties of water as the temperature changes [71, 74].

Increasing the reaction temperature has been shown to reduce overall mass yield, and decarboxylation and dehydration reactions are more favourable at higher temperatures, demonstrated by decreasing oxygen to carbon (O/C) and hydrogen to carbon (H/C) ratios [29]. Decarboxylation degrades the carboxyl (-COOH) and carbonyl groups (C=O), forming CO_2 and CO respectively. Dehydration removes hydroxyl groups (-OH) from the feedstock leading to less hydrophilic functional groups. Both reactions can therefore reduce the oxygen content significantly, in turn upgrading the energy

density, for oxygen adversely influences higher heating value (HHV) as shown by Dulongs equation (see Equation 2.1). It has also been shown that as you increase the reaction temperature re-condensation reactions become increasingly prevalent, with this shown to become increasingly prevalent by 230 ^{0}C for willow [97]. Consequently by increasing heating you significantly increase the energy content of the char, with the net energy yield a trade-off between the fuel's energy content and the mass yield [29].

$$HHV = (0.3383 * \% \text{ Carbon}) + (1.422 * \% \text{ Hydrogen}) - (\% \text{ Oxygen} / 8) \quad (2.1)$$

2.3.5. Residence time

Residence times vary throughout the literature with some reports using residence times from less than five minutes to up to several days. It is generally assumed that longer residence times generally increase reaction severity [11]. It has been suggested by several authors that HTC is a two stage process with the initial hydrolysis reactions along with dehydration and decarboxylation reactions believed to have gone to completion by the time the hold temperature is reached [29, 98]. The advantage of retaining the reactor at temperature is it allows the ongoing repolymerisation of dissolved fragments in the liquid phase which finally lead to the precipitation of insoluble salts [11]. Hoekman et al. [29] experimented with varying retention times with a spruce / fir mix and analysed the acids and sugars present in the process water by IC and the mass yields and energy density of the chars. The results showed that sugars within the process water decreased as retention times increased, with organic acid increasing slightly. Overall, total organic carbon decreased, which is indicative of repolymerisation, and despite a small but noticeable decrease in mass recovery, energy content was shown to increase with residence time. Kruse et al. [99] demonstrated that increasing retention time at between 180 °C and 250 °C reduced nitrogen content of the bio-coal.

With residence time there appears to be a trade-off between the costs associated with retaining a process at temperature (influence on throughput, increased energy costs etc.) and an enhanced product. This is now dividing the HTC community, with a low retention time process now being marketed as hydrothermal torrefaction or wet torrefaction [100]. Within the literature "hydrothermal torrefaction", "wet torrefaction" and "hydrothermal carbonization" are often used interchangeably which can be confusing. As discussed, HTC is a wet process, involving reaction of biomass with hot, pressurized liquid water and during this process, numerous chemical reactions take place, including hydrolysis, condensation, decarboxylation, and polymerization and aromatization occur. Hydrothermal torrefaction, should have the same aims as dry

torrefaction whereby it aims achieve an improved product though the removal of hydroxyl and carboxyl groups, but the energy densification is merely being achieved though the removal of components with a low heating value. Consequently, HTC should now be regarded as a longer process whereby the process has a long enough retention to incorporate aromatization and repolymerisation. Short retention times impose kinetic limitations which prevent aromatization and repolymerisation [101] and in this instance should be regarded as hydrothermal torrefaction.

Influence of particle size, and solids loading are additional factors that will influence the required residence time, as both diffusion-controlled transport mechanisms during biomass decomposition and condensation polymerisation are likely to govern the overall rate of reaction.

2.3.6. Severity factor

A number of authors in HTC have combined both the temperature and pressure parameters into a single factor known as the severity factor and is given in Equation 2.2 [84, 101-103]. The severity factor being the logarithm of the reaction ordinate; this reactivity factor was developed by Overend and Chornet [104] to characterize hydrolytic depolymerisation processes during wood pulping and similar operations. The principle dictates that similar products are obtained through increased retention times at either a lower temperature or increased temperature with lower retention times. The equation is advantageous when predicting hydrolytic depolymerisation processes and will be suited to 'hydrothermal torrefaction' applications but becomes limited when you consider kinetic limitations imposed by aromatization and repolymerisation. Consequently shorter reaction times influence chemical composition of the products and simply operating hotter may not overcome this [101].

$$\text{Severity Factor} = \text{Log (time (min))} * e^{[(\text{temp (°C)} - 100)/14.75]} \qquad (2.2)$$

2.3.7. Pressure

The influence of pressure is often overlooked during HTC, with most research pressuring the reactor autogenically [28, 36], with the saturation vapour pressure of water corresponding to the reaction temperature as shown in Figure 2.10. The reaction pressure influences the reaction network according to the principles of LeChatelier and elevation in pressure is known to reduce dehydration and carboxylation, however in practice this has been shown to have little impact on HTC [11]. There could however be advantages in terms of extraction of inorganics and heteroatoms from increasing reaction pressure as

it will result in encapsulated gases within the biomass being compacted or dissolved, which will allow broader access of the water phase [97]. There could also be advantages to pre-pressurising the reactor over autogenic pressurisation, as autogenic pressurisation generates steam to pressurise the reactor and this will come with a latent heat penalty and could be significant on bigger reactors.

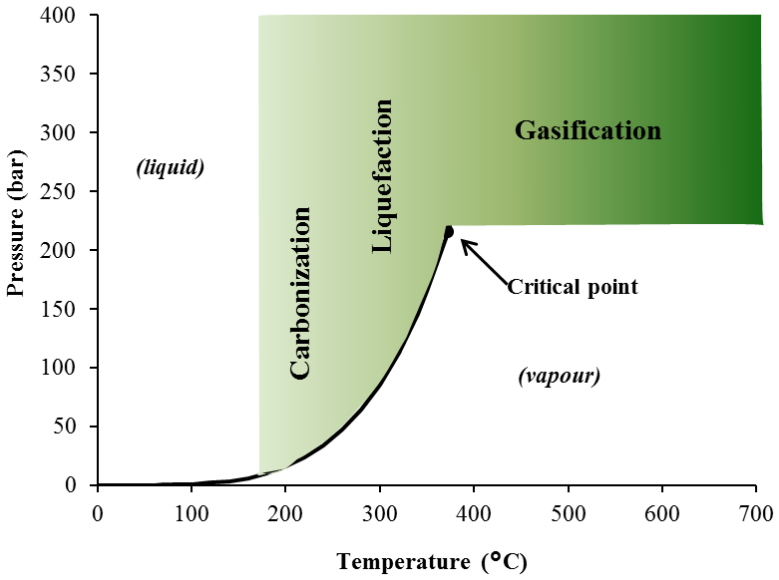

Figure 2.10: Temperature – pressure phase diagram for water

2.3.8. Solid loading

Solid loading is the amount of organic or solid material to water on a weight basis and appears to be a significant parameter. Low water to solid ratios (e.g. 5:1) are shown to favour char formation and high water to solids ratio (e.g >10:1) favouring dissolution of the organic material into the aqueous phase and at high enough temperatures production of an oil phase (liquefaction) [28, 105]. The reason for this increase in solid formation is due to the simple principle that greater amount of solids will result in higher concentrations of monomers within the liquid phase, which will then enhance the chance of polymerisation [106].

To date, the effect of solid loading on yield is not well established in the HTC literature, and caution is needed when trying to generalise from the data available. Previous research into HTC of olive waste [107], *Opuntia* Spp. (an agricultural cactacee crop) [108] and woody biomass [109] have demonstrated a slight increase in bio-coal yield with an increase in solid loading. Likewise it has also been noted by Álvarez-Murillo

et al. [110] and Sabio et al. [111] who investigated the HTC of olive stone and tomato-peel waste that in general an increase in solid loading results in a slight increase in bio-coal yield. The same authors however noted that such correlations between bio-coal yield and solid loadings do not necessarily hold across other operational conditions, such as retention time and temperature. Likewise, Mäkelä et al. [112] found no statistically significant effect of solid loading on multiple process outputs (including bio-coal yield) for HTC of lignocellulosic paper sludge.

An increase in solid loading is highly advantageous for HTC as low water to solid ratios is likely to lead to more favourable process economies. HTC is an exothermic process, with the process governed by the sum of dehydration and decarboxylation [71], however in order to process the biomass, the water in which it is resides requires heating. Based on enthalpy change, heating requirements to heat water to 250 °C is 0.9 MJ/kg so to process 1 kg of dry biomass at 10:1 it will involve 9 MJ of heat, increasing the water to biomass ratio to 5:1 would reduce the heat input to 4.5 MJ. It is worth noting that it is likely that a large portion of the initial heat input can be recovered but reductions in the initial heat input are beneficial. Care is however required when reducing the biomass to water ratio when trying to extract inorganics from biomass since there is a risk of saturation and reduced extraction.

Recycling the process waters back into the HTC process has been suggested by a number of authors [113-115] and may be one of the most efficient means of heat recovery [116]. By recycling the process waters back into the reaction the dissolution of the organic material into the aqueous phase, which reduces char formation, should be reduced as the recycled process reintroduces the organic acids generated in the previous reaction, including: acetic, formic, lactic and luvulinic acids [11, 29], moving reaction equilibriums toward greater char yield [26, 28]. Consequently when recycling process waters, water to solid ratios maybe less important.

It has also been shown that evaporating water can shift solution equilibria to form solid precipitation [117]. The reaction equilibrium of condensation polymerization which proceeds under formation of water is generally shifted toward polymers by removing reaction water from the system [117]. Consequently lowering the reactor pressure below the saturation vapour pressure of water in the latter phases of HTC, once hydrolysis, dehydration and decarboxylation reactions are believed to have gone to completion, could further increase bio-coal yield though shifting equilibriums to favour repolymerisation of monomers in the aqueous phase.

2.3.9. Particle size

There appears to be limited reports on the influence of particle size on HTC and even HTL, with most work published using ground biomass, typically < 1 mm in diameter [98]. This appears surprising given that a batch HTC process would, like torrefaction, be conducted on chipped fuels to avoid energy-intensive size reduction prior to processing, taking advantage of the improved grind-ability [43]. Consequently, there is uncertainty as to how the HTC mechanism works in larger particles. On smaller particles it was assumed that the solid product of bio-coal is largely formed by re-condensation reactions, some of which were aliphatic in nature [28]. With larger particles it is more uncertain how a particle behaves, with recent research by Mosteiro-Romero et al. [98] indicating that under HTC there are two distinct zones; a hydrolysis zone on the outside of the particle which is in contact with the process water and a pyrolysis zone within the particle which forms due to limited contact with water [98]. The extent of the pyrolysis zone is determined by the thickness of the hydrolysis zone [98]. This could be highly significant when trying to extract inorganics and heteroatoms from biomass as development of the hydrolysis zone may reduce or prevent the extraction of these elements. This will be due to the hydrolysis layer preventing diffusion though the particle and consequently understanding this process is of high importance if large biomass particles are to be used in HTC.

It should also be noted that particle size will have an influence on the water to solid ratio discussed previously. Given any reactor will have a finite volume and for the process to work biomass needs to be submerged in water, increasing particle size will increase void size between particles, voids which will be filled with water. Consequently increasing particle size will invariably increase the water to solid ratio. Consequently, energy penalties brought about though energy-intensive size reduction needs to be balanced against the potential greater heat requirement and lower char yields as discussed in the previous section.

2.3.10. Use of pH and catalysts during HTC

The use of catalysts in HTC have largely revolved around the use of acid catalysts as it was reported early on that weekly acidic conditions improve the overall rate of reaction in HTC [26]. Consequently many HTC processes report the addition of such acids as citric acid [26, 44, 118], acrylic acid [119], and sulfuric acid [120, 121]. The use of organic acids appear to complement the HTC process as it is generally accepted that during HTC a variety of organic acids are generated, with acetic, formic, lactic and

luvulinic acids identified as common reaction intermediates [11, 29]. Caution is however required when referring to the use or organic acids as ‘catalysts’ as many organic catalysts are consumed in the reaction and become part of the reaction products. In this instance, these organic catalysts are strictly reagents and not catalysts. Addition of acetic acid has been shown to change reaction mechanisms, with Lynam et al. [44] demonstrating that additional acetic acid is not generated during HTC if acetic acid is added at the start. This could indicate that reactions to produce acetic acid could be reversible reactions, with added acetic acid pushing the equilibrium in the direction of reduced acetic acid production possibly resulting in hemicellulose, from which acetic acid is largely derived [120, 121], remaining within the char and improving yields [44].

Experiments with alkaline catalysts have shown an initial pH of greater than 7 leads to a liquid rather than solid product [118, 122] consequently alkaline catalysts are not commonly used in HTC but are commonly applied in HTL as base catalysts such as sodium hydroxide have been shown to favour oil yields by inhibiting repolymerisation, thus reducing char yield [123]. This said alkalis are added during HTC along with acids to accelerate the hydrolysis/degradation process by changing ion products [124, 125].

2.3.10.1. Influence of pH

2.3.10.1.1. pH on cellulose and lignocellulosics

In a study presented by Reza et al. [126] the influence of feed water pH on the HTC of wheat straw was investigated. An initial process water pH of between 2–12was studied using acetic acid and potassium hydroxide as the acidic and basic medium. The results demonstrated that the starting feed water pH influences carbon density and HHV in wheat straw, with higher carbon densities associated with lower pH. Mass yields indicated that pH between 4 and 8 gave the highest mass yields although a reported standard deviation was as great as the variation between pH. Given the lower pH was brought about though use of acetic acid it is also difficult to tell whether the increase in carbon density is simply due to an increase in acetic acid and thus more organic carbon within the reaction media or the influence of pH. The same authors had previously demonstrated in Lynam et al. [44] that acetic acid enhances the fuel value of bio-coal, principally though the additional addition of carbon.

The results did show that the resulting bio-coal and process waters become acidic regardless of any feed water pH. This would fit with work by Antal et al., [82] and Jin et al., [83] that decomposition of monosaccharides to organic acids (e.g. acetic, lactic, propionic, levulinic and formic acids) bring about a rapid drop in process water pH to

approximately 3 when starting at around pH 7. The results presented in Reza et al., [126] showed that removal and reactivity of hemicellulose and cellulose was less in alkaline feed water but lignin follows the opposite path. Some caution is required here as the fibre method used is a modified van-Soest method [127] using ANKOM A200 Filter Bag Technique. The technique works by separating the components using two detergents: a neutral detergent consisting of sodium lauryl sulfate and EDTA, with a pH of 7.0 and an acid detergent, cetyl trimethyl ammonium bromide in 1 molar sulphuric acid. Extractives, hemicellulose, cellulose and lignin can then be determined accordingly. The method is however developed to determine hemicellulose, cellulose and lignin in grains, feeds and forages in unprocessed biomass. Figure 2.8 gives the process chemistry and char structure for the hydrothermally carbonised cellulose it is likely that carbonised, repolymerised and aromatised material will be more lignin like in structure (see Figure 2.1), despite not necessarily being from lignin origin. Consequently, to draw the conclusion that the lignin content is recalcitrant using this technique is not strictly correct.

The results of Reza et al., [126] did show that relative yields of more sugars, less furfural derivatives, and less organic acids were produced, when wheat straw was treated with alkaline feed water. This result is not necessarily surprising as introducing potassium hydroxide should neutralize the generated organic acids [124], which would otherwise go on to catalyse the further degradation of the sugars generated from the hydrolysis of the hemicellulose and cellulose [84, 128].

Work by Yang et al. [124] also demonstrated that the hydrothermal process can be influenced by the exchange of sodium ions in sodium hydroxide at high pH, reducing polymerisation and, while work in Reza et al., [126] used potassium, both elements are group one elements and should behave similarly. Yang et al. [124] in a similar study also demonstrated that sodium hydroxide in the HTC process results in the decomposition of lignin and found changes in pH from 4 to 9 had no significant influence on the bio-coal H/C, O/C, and proximate characteristics. Like Reza et al., [126] bio-coals produced at pH 2 had more suitable fuel properties, including high higher heating values and fixed carbon contents, but this was accompanied with lower yields.

Lu et al. [128] evaluated how changes in initial process water pH influenced the carbonization mechanisms and product composition, yields, and energy value of bio-coal derived from cellulose. The study used normalised concentrations of mineral acids and bases hydrochloric acid, sulphuric acid, sodium hydroxide and calcium, along with the organic acid, acetic acid. Cellulose dissolution appears to be accelerated in the presence of initially acidic process water (0.0001–0.01 N HCl and H_2SO_4), as evidenced by lower

solid recoveries at early reaction times (<1.5 h) when compared against a control experiment in deionised water. Yields beyond 1.5 hours were similar for all experiments, this would indicate that acidic conditions appears to catalyse cellulose dissolution and the mineral acids are not acting as reagents. The results also showed a difference between the mineral acids at the same pH, with the addition of 0.01 N sulphuric acid appearing to promote more decarboxylation than the 0.01 N hydrochloric acid, based on the observed carbon yields in the gas phase.

Carbonising in initially basic conditions (0.001–0.01 N NaOH and 0.001–0.01 N $Ca(OH)_2$) also influences initial cellulose dissolution. Calcium hydroxide has an effect similar to that observed when carbonizing in the presence of acids; initial cellulose dissolution increases as base concentration increases. The inverse was however observed for sodium hydroxide, with cellulose dissolution decreasing as the sodium hydroxide concentration increases; with solid recovery obtained when carbonising in the presence of sodium hydroxide appeared similar to that of the control. Analysis of the process waters of the sodium hydroxide addition at 0.01 N indicated the presence of glucose at 1.5 hours, along with high concentrations of 5-HMF (a major decomposition product of glucose). The decrease of these products with time suggest that rather than catalyse the carbonisation reaction the sodium hydroxide may inhibit the reaction. This would fit with the trends seen in Reza et al., [126] and Yang et al. [124]. Lu et al. [128] put this down to the degree of cellulose swelling in the HTC reaction; cellulose swelling has been shown to decrease with increasing alkali concentration [129]. Normalisation of the solutions mean that the hydroxide should not vary between the sodium and calcium runs, so the results indicate that sodium ions (Na^+) and calcium ions (Ca^{2+}) influence cellulose dissolution / decomposition differently.

2.3.10.1.2. pH on lignin

Wikberg et al. [130] looked into the influence of 0.15 molar sodium hydroxide on the HTC of kraft lignin at 240 °C for 22 hours. In this research, it was found that under HTC conditions a thermally more stable, rigid and cross-linked structure was formed with a slightly higher energy density than the starting lignin. This was brought about through changes in the lignin structure caused by the cleavage of carbon side chain structures as well as demethylation causing increasing amount of catechol structures to be present within the char. The use of sulphuric acid as a catalyst promoted the faster degradation of lignin under HTC conditions resulting in higher solid yields and carbon recoveries, creating at the same time a more stable carbonaceous structure.

2.3.10.1.3. pH on manures

Acid catalysed HTC appears most commonly applied to manures, with Ekpo et al. [131] and Dai et al. [132] investigating the influence of acids on the recovery of phosphorus and nitrogen in swine and cattle manures respectively. Ekpo et al. [131] investigated sodium hydroxide, sulphuric acid, acetic acid and formic acid at 0.1 molar concentration and the results indicated that operating hydrothermal treatment in the presence of acidic additives has benefits in terms of improving the extraction of phosphorus and nitrogen. It was generally observed that phosphorus extraction is pH and temperature dependent and is enhanced under acidic conditions. The highest level of phosphorus is extracted using sulphuric acid, reaching 94% at 170 °C. The phosphorus is largely retained in the residue for all other conditions. Extraction of nitrogen is not as significantly influenced by pH, although the maximum extraction is achieved using sulphuric acid.

Dai et al. [132] undertook HTC at 190 °C for 12 h using hydrochloric acid at varying concentrations. The results showed that HTC in 2% hydrochloric acid extracted almost 100% phosphorus and 63 % nitrogen. Decreasing pH saw a small increase in carbon content and a large decrease in oxygen content, which should increase energy content (not stated). Decreasing pH did however have an impact on yield with yields reducing from 70 % (db) to 53 % (db), albeit this reduction appeared predominantly associated with removal of oxygen. Fuel volatile matter was seen to decrease with increasing fixed carbon with decreasing pH. These results suggested that HTC in dilute acid could simultaneously facilitate nutrient recovery from manure and bio-coal upgrading.

Ghanim et al. [133] looked into the HTC of poultry litter at 250 °C for 2 h using various initial pH and acetic and sulphuric acid. The results indicated that undertaking HTC in the presence of acids at decreasing pH increased the carbon content and HHV of the bio-coal. Increasing sulphuric acid content appeared to both increase yield and decrease ash content. The reduction in yield does however go against other trends with low pH, moreover higher volatile matter contents in these chars also contradicts the findings in Chen et al. [134] who used sulphuric acid and bagasse.

2.3.10.1.4. pH on electrokinetic potential

pH should also play a key role in the flocculation repolymerisation during hydrothermal carbonisation due to its influence on the zeta potential. Zeta potential, or as it is more correctly known: electrokinetic potential, is a key indicator of the stability of

colloidal dispersions and the magnitude of the zeta potential indicates the degree of repulsion of likewise charged particles in a dispersion. A high zeta potential will give a high dispersion stability, which will mean the solution or dispersion will resist agglomeration; a low zeta potential will result in the dispersion flocculating. The most important factor affecting zeta potential is pH.

Bio-coals have a negative zeta potential as the HTC materials have a negative acidic oxygenated groups on the surface, making them behave like week acids [91]. Moreover the bio-coals will remain acidic during repolymerisation and the removal of the oxygenated surface functionality due to the incorporation stable oxygen groups, ether or pyrone, within the char formation [91]. If alkali is added to a hydrothermal suspension then the particles will tend to acquire a more negative charge [135]; and this will reduce the chance of them flocculating and forming the char. If acid is added to the suspension, a point is reached where the negative charge is neutralised. The point, at which zeta reaches zero is the isoelectric point and this would be the point the suspension is most likely to flocculate.

Yu et al. [135] demonstrated that for glucose, sucrose and starch, a zeta potential of -15 is present at pH 3; xylose had a zeta potential of -25. When the isoelectric point is reached further addition of acid will result in the build-up of positive charge on the bio-coal [136]. Consequently, at very low pH it would be possible that a positive zeta potential will be created which could make the suspension stable and prevent flocculation. In zeta potential experiments presented in Zhao et al. [137] the isoelectric point is reached at approximately pH 2 got glucose chars following hydrothermal treatment at 180 °C overnight. For chitosan and glucosamine, it was between pH 5 and 6.

2.3.10.2. Influence of salts

The use of salts as catalysts have also been researched, although are less common than acid catalysts. Lynam et al. [48] investigated the influence of lithium, calcium and magnesium chloride, formate and acetate salts on their catalytic role in HTC. Salts were used in high concentrations (1:1 biomass to salt and 5:1 water to biomass ratio) and the results showed chloride salts generally lead to an increase in energy density of the fuel, with a net increase in the energy recovered by HTC. The formate and acetate salts were shown to result in a lower HHV than the control although it was reported that yields were higher. Authors have hypothesised that the presence of acetate and formate in the process water is changing reaction equilibriums and reducing the production of acetic and formic acid, resulting in a greater proportion of hemicellulose and cellulose within the char. The energy yields through the addition of these salts were largely not changed but a lower

energy density product would be less favourable. The higher HHV and greater energy yields for chloride salts was attributed to chloride ions being known to disrupt the hydrogen bonding between adjacent cellulose polymer strands [138, 139], facilitating their solubilisation and removal from biomass. It has also been suggested that lactate might perform a similar action in disrupting cellulose hydrogen bonding. If more cellulose is removed from the biomass, a higher proportion of lignin remains, increasing the biochar's HHV [48].

In addition to the effects on yield, salts were also shown to reduce reactor pressure, with chloride salts resulting in the greatest pressure reductions, with pressures 30% lower for lithium chloride [44, 48] and 19% lower for calcium chloride [48]. Other salts, excluding calcium formate, reduce pressure by about 7%, with about 10% of salts remaining in the bio-coal product [48]. This pressure drop could have additional catalytic benefits for the HTC process as pressure has been demonstrated to supress dehydration and decarboxylation and the lower reaction pressures may favour enhanced dehydration and decarboxylation.

It was suggested by Lynam et al. [44] and Yu et al. [140] that the added salts also may catalyse condensation reactions which cause the formation of products with greater HHV, which may precipitate into the biochar pores. This would seem less likely if the role of salts is to reduce reaction pressure. It is suggested in coal studies that compaction enhances polymerisation as polymerisation is a slow process due to low diffusivity [11] and lowering pressure would not enhance this.

In addition to pH, Lu et al. [128] evaluated how salt addition influenced the carbonization mechanisms, product composition, yields, and energy value of bio-coal derived from cellulose. It was shown that salt addition to the initial process water accelerated cellulose dissolution, but sodium chloride and calcium chloride (at equivalent Cl^- concentrations) influence solid recoveries differently. By increasing sodium chloride concentration cellulose dissolution was increased but with the final solid yield being similar to that of the control experiment in deionised water. Calcium chloride initially increased the rate of cellulose dissolution but then after one hour yields stop decreasing and a higher solid yield is achieved. Analysis of the carbon content indicates that the carbon content of this char is lower, with lower carbon contents observed for all the calcium chloride runs (0.01, 0.025 and 0.5 N $CaCl_2$) when compared with the deionised water control. The inverse was observed for the sodium chloride runs. The largest difference between the solids generated in the presence of calcium chloride and sodium chloride was the change in oxygen content, which generally has a significant impact on

solids energy content. As the sodium chloride concentration in the initial process water increases, the oxygen content of the recovered solids at a reaction time of 3 h decreases. The opposite trend was observed when carbonizing in the presence of calcium chloride.

The reduction in energy content with the addition of calcium chloride differs from that reported by Lynam et al. [48] albeit both studies used different temperatures, reaction times, and feedstock and it is possible this has resulted in the difference. In previous work presented in Lu et al. [141] it was reported that the majority of oxygen initially present in the feedstock is transferred to the liquid-phase during HTC. The results seen in Lu et al. [128] would then suggest that the Na^+ and Ca^{2+} cations influence the transfer of oxygen from the solids to the liquid-phase, influencing solids energy content [128]. Analysis of the process waters of the calcium chloride runs did however indicate that liquid phase reactions had advanced with complete removal of glucose and 5-HMF at longer retention times, with higher yields of levulinic acid, with reducing formic acid yields, which was suspected to be being converted to hydrogen gas. This result is consistent with work by Patwardhan et al. [142] which showed that mineral salt addition may accelerate the formation of low molecular weight compounds, including formic acid. The results presented in Lu et al. [128] showed significantly more hydrogen was measured in the gas-phase when carbonizing in the presence of $CaCl_2$ indicating conversion to hydrogen gas. The authors hypothesised that despite an increase in liquid phase reactions that full cellulose conversion from the solid phase had not occurred because of solid surface passivation (formation of a protective micro coating), preventing chemical corrosion of the cellulose. The greater amount of oxygen remaining integrated within the recovered solids after suggesting this surface passivation is preventing dehydration, which is increased with larger $CaCl_2$ concentrations.

2.3.10.2.1. Salts as Lewis acids

In addition to salt addition influencing reaction mechanisms due to their ionic products; many metal salts are Lewis acids. There has subsequently been some interest in using metal salts as Lewis acids as an alternative to mineral acids due to the greater ease in recovery of the metal salts making the catalysed carbonisation process more friendly [143]. Zinc chloride [144], copper (II) acetate [23], ammonium iron (II) sulphate [145], iron (II) chloride [143] and iron (III) chloride [143, 146] have been investigated as Lewis acid catalysts and the lithium, calcium and magnesium catalysts in Lynam et al. [48], sodium chloride and calcium chloride catalysts in Lu et al. [128] will also influence acidity being Lewis acids.

Cui et al., [145] demonstrated that iron ions and iron oxide nanoparticles can effectively catalyse the hydrothermal carbonization of starch and rice grains under mild conditions (≤200 °C). The iron oxide acts as an alkali catalyst. The difference between the acid and alkali is the significant influence on the formation of carbon nanomaterials with different shapes. In the presence of Fe^{2+} ions, both hollow and massive carbon microspheres can be obtained. In contrast, the presence of Fe_2O_3 nanoparticles leads to very fine, rope-like carbon nanostructures. In Hamid et al. [143] the iron Lewis acid catalysts promoted the complete carbonisation of cellulose at 200 °C where incomplete carbonisation was observed in the absence of the salt. Differences between iron (II) chloride and iron (III) chloride was observed, with the greater C=O functionality when compared to iron (III) chloride. The authors put this down to differences between the Fe^{2+} and Fe^{3+} ions as opposed to the iron (III) chloride being a stronger Lewis acid, albeit the latter does not appear to be considered.

Wikberg et al. [130] looked into the influence of 2 wt % iron (II) chloride (percentage catalyst to biomass) on the HTC of kraft lignin at 240 °C for 22 hours. This work found that Fe^{2+} ions had only minor effects on the final structure of the lignin derived bio-coal compared with the uncatalysed lignin derived bio-coal. There is also evidence that under liquefaction conditions alkali salts are known to improve C-C scission rates [49] although this research has yet to be done under HTC conditions.

2.3.10.3. Role of metals in polymerisation

There is some evidence that cations do play a role in polymerisation, with experiments looking into the formation of carbon microspheres from alginate finding that divalent cations, such as calcium and magnesium, bind acid units, in this case poly-guluronic acid units, forming stable cross linking chains which then carbonise as spheres [147]. Cui et al. [145] demonstrated that iron ions and iron oxide nanoparticles alter the shape of the carbon formation. In the presence of Fe^{2+} ions, both hollow and massive carbon microspheres can be obtained. In contrast, the presence of Fe_2O_3 nanoparticles leads to very fine, rope-like carbon nanostructures.

The influence the metals have on polymerisation is not yet clear. In fossil coal, metals are known to exist within the coal matrix as salts of carboxylic acids, alcohols and phenols [148]. Removal of metals from within the coal matrix of low rank coals is known to lead to the solubilisation of low rank coals. Likewise the addition of divalent cations (Ca^{2+}, Mg^{2+} Fe^{2+}) and trivalent cations (Fe^{3+} and Al^{3+}) has been shown to re-precipitate the coal (taking into account potential for acid precipitation), while monovalent cations

(Na^+) had no effect on precipitation [148]. This would suggest that metals present, specifically the multivalent cations, may play a role in the formation of the bio-coal.

Work modelling brown coal formation has shown that di-valiant cations aid the formation of energetically favoured, undistorted structures. The metal ions appear to become surrounded by oxygen functional groups, with carboxyl groups potentially acting as bi-dentrate ligands to calcium ions (e.g. R-$COO^-(Ca^{2+})^-OOC$-R). The trivalent cation iron was modelled and found to form less energetically favoured, distorted structures, associating with carboxyl and phenoxy groups [149]. This binding would suggest that multivalent cations play a role in the bio-coal formation through the chelating of aromatic structures though carboxyl groups and interactions with the surrounding functional groups which then dehydrate to form stable oxygen groups.

It is unclear what role mono-valiant cations have in the bio-coal formation. It has been modelled in Domazetis and James [149] that sodium ions form week ionic bonds with carboxyl functional groups (e.g. R-$COO^-(Na^+)$) and it appears likely there will be similar interaction with potassium. The solubilisation and metal precipitation experiments of low rank coals presented in Quigley et al. [148] would suggest sodium and potassium play no role in the chelating of aromatic structures. It appears likely addition of divalent cations (Ca^{2+}, Mg^{2+} Fe^{2+}) and trivalent cations (Fe^{3+} and Al^{3+}) would likely remove these sodium and potassium ions through ion exchange. Without surplus multivalent cations it appears likely that sodium and potassium will remain within the bio-coal. Moreover ammonium within the process water would likely exchange with potassium, sodium, calcium and magnesium ions due to its higher affinity in cation exchange. There is also evidence that under liquefaction conditions alkali salts are known to improve C-C scission rates [49] although this research has yet to be done under HTC conditions.

Silicon has also been demonstrated to aid formation of carbon structures during HTC, with silicon forming ‘hard templates’ to which carbon structures may be deposited [150-153]. While this may in part be due to the low solubility of silicon dioxide, partial dissolution of silicon, as reported in Fellinger et al. [150] would suggest some role for silicon in char formation being a tetra-valiant metalloid. Use of metals and inorganics for templating has been less used for fuel but long been associated with formation of mesoporous carbon synthesis via HTC for catalytic purposes [118] and has long aided the formation of metal/carbon nanoarchitectures [23], carbon nanofibers [24] and spheres [25]. There has been a move toward naturally synthesised inorganic structures, with the use of calcium carbonate from crustacean shells used as a template in White et al. [154] and Soorholtz et al. [155]. The use of calcium over silicon is favourable over the more

conventional silicon templates as there is usually a requirement to remove the inorganic structure. Calcium carbonate can be easily removed using week Brønsted acids such as acetic acid, whereas silicon relies on hydrofluoric acid, ammonium fluoride and caustic sodium hydroxide, which bring with it safety concerns [156]. More recently template assisted carbon structures using HTC have moved away from inorganic templates favouring carbon based materials such as polystyrene, phloroglucinol, phenol-formaldehyde and latex [157-164].

2.3.10.4. Influence of catalysts on inorganic chemistry

The role catalysts have on inorganics within the final bio-coal is currently unknown, although the results of Lynam et al. [48] have shown that addition of salts increases the salt content and thus inorganic content with the char, with about 10 % of the salt added found in the ash. Zhai et al. [165] looked at the influence of pH on the fixation of heavy metals within bio-coal derived from sewage sludge and found that alkaline reaction condition was beneficial to form stable chelates between heavy metal ions and carbon. Acids have been shown to aid leaching of salts in biomass washing [42, 43] and organic acids should react and leach salts during the HTC reaction. Whether this leaching will be enhanced by the addition of organic acids is unknown as the results presented in Lynam et al. [44] suggests addition of acetic acid inhibits further acetic acid production and the same mechanism may happen with formic acid and its influence on cellulose degradation [166].

As the formate and acetate salts of calcium and magnesium appear to show the same inhibition to formic and acetic acid production as shown with acid addition [48], it is likely the same amount of inorganics (cations) will be leached irrespective of the amount of organic acid added as a catalyst for cellulose and hemicellulose containing feedstock. Loading organic acids at concentrations in excess of the equilibrium concentration, whereby more organic acid is in the process water than would otherwise be produced may simply result in the acid being reformed into another compound and leading to no enhanced acid leaching. Because of the potential equilibrium issues with formic and acetic acid, increasing the water to biomass ratio maybe the solution to enhancing the leaching of inorganics though organic acids as this will allow a greater organic acid to biomass ratio while not exceeding the reaction equilibrium. Addition of mineral acids may however not have the same influence on reaction equilibriums and lead to far greater inorganic leaching.

2.3.10.5. Influence of atmosphere

The addition of carbon dioxide (CO_2) to hydrothermal processes has also been developed as an alternative catalyst in hydrothermal processing [167, 168] and applied to HTC in [169]. In an aqueous medium, carbon dioxide reacts with water to form carbonic acid, which promotes an acid catalysed hydrothermal reaction. Moreover, due to the volatile nature of carbon dioxide, the catalyst recovery is almost complete at no cost. Similar to other catalysts, the addition of carbon dioxide was found to enhance the hydrothermal reaction [168, 170, 171]. Most studies on carbon dioxide enriched hydrothermal treatment focused on a hydrolysis process, which aims at maximization of the water-soluble products (e.g., sugars) yield for chemicals production. In Bach et al. [169] carbon dioxide was found to improve the reactivity of forest residues during mild HTC treatment at between 175 to 225 °C with 30 minute retention time compared with the control. The bio-coals produced in carbon dioxide had lower heating value, lower mass yield and energy yield, but better grindability and hydrophobicity, compared with the controls. The addition of carbon dioxide was however shown to enhance ash removal with HTC with carbon dioxide addition reducing ash content by 60–69% compared to only 14–26% for the control. Analysis of the changes in ash chemistry was not undertaken. Increasing temperature and retention time may allow for increased polymerization, which could enhance energy content.

2.3.10.6. Influence of catalysts on fuel nitrogen

During the HTL of microalgae the heteroatom, nitrogen, is known to have catalytic influence on the liquefaction reaction. In HTL of microalgae the reaction does not require the alkali catalysts (KOH, NaOH, Na_2CO_3) used in HTL of lignocellulosics to promote alkaline conditions which favour oil production. Instead the high protein content of microalgae gives a high nitrogen content which in turn gives alkaline conditions which favour liquefaction [172, 173]. It is likely that nitrogen will have a similar catalytic effect on the products of HTC if protein or nitrogen is at high enough concentrations.

The use of catalysts to remove nitrogen from fuel has also been researched. While denitrogenation is known to occur under hydrothermal conditions, reductions are feedstock specific with leaching from antibiotic residue wastes reaching 45 % of nitrogen at 200 °C [174] but denitrogenation of organic nitrogen compounds in municipal wastes not occurring until 275 °C in pure water [175]. Broch et al. [173] showed denitrogenation occurs in microalgae, pine and sugarcane bagasse but the percentage of nitrogen in the char did not change significantly at 175 and 215 °C. Addition of alkaline, alkaline earth

metal salts and the alkaline metal hydroxides by Akimoto et al. [175] have however shown the pH of the aqueous solution plays a significant role in the hydrothermal removal of the organic nitrogen, indicating hydrothermal denitrogenation occurred readily under acidic or basic conditions. Alkaline metal hydroxides were found to be the most effective for the hydrothermal denitrogenation, with more nitrogen removed with increasing the basicity of the alkaline metals, with the results indicating that hydrothermal denitrogenation occurred primarily via an ionic reaction path catalysed by OH^- ions in aqueous alkaline solutions [175].

2.4. Combustion of solid fuels

Solid fuels have been utilised for energy production through combustion in pulverised fuel power plants for decades. The fundamental combustion process of solid fuels whether coal, biomass or treated biomass is the same [39, 68] and can be described by the process outlined in Figure 2.11 and discussed in the following sections.

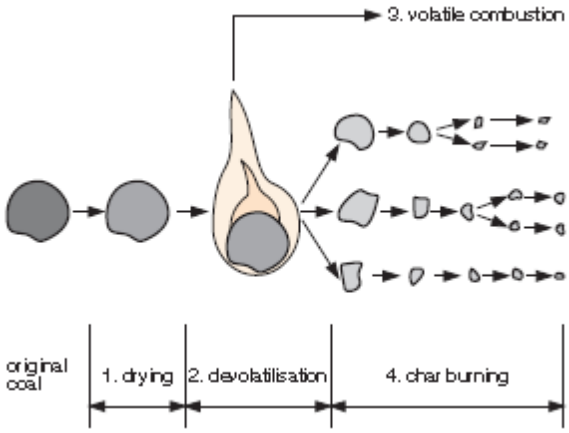

Figure 2.11: Overall combustion process of coal [176]

2.4.1. Heating and drying

In a combustion system the pulverised fuel (PF) particle enters a boiler at relatively low temperatures and is rapidly heated whereby the surface temperature increases and inherent moisture within the particles porous structure evaporates [68]. Since vaporisation uses energy released from the combustion process, it lowers the temperature within the combustion temperature, which slows down the combustion process. High moisture content can delay particle heating, which in turn can increase the overall combustion time and is a problem in biomass fuels where moisture contents can be up to 60 wt% [39] compared to bituminous coals that contains 1-12 wt% [176]. Wet biomass can require so much energy to heat water vapour that temperatures can be

reduced to below the minimum temperature requires to sustain combustion [39]. Consequently, moisture content is a very important fuel variable and appropriate control is required to achieve flame stability, a critical variable when safely operating combustion plant [68]. In most bio-fuel based literature, energy values are stated as Higher Heating Value (HHV) or gross calorific value and HHV assumes water vapour formed during combustion is condensed and this energy is recovered. Lower Heating Values (LHV) (net calorific value) takes into account the latent heat requirements for the water within the fuel. Moreover, LHV also takes into account the water generated and evaporated from the fuel bound hydrogen. Biomass and lower rank coals typically have higher hydrogen contents than higher rank coals and this hydrogen generates water on combustion, which requires heat to vaporise it. Given that in many combustion applications (e.g. coal power station) the latent heat is not recovered, LHV is often the more significant value as it represents the overall energy available.

HTC has been demonstrated to have enhanced hydrophobicity and dewaterability (mechanical water recovery) compared to biomass due to the dehydration of the fuel and removal of biomass structures [47, 177-180]. Water immersion tests of bio-coal pellets, presented in Kambo and Dutta [179], along with equilibrium moisture content (EMC), indicates the moisture content of the bio-coal appears dependent on the hydrothermal reaction severity but do not appear to rehydrate like biomass and have more coal like moisture contents of 1-12 wt% even after submersion [177, 179]. Moreover bio-coals are more hydrophobic than the equivalent torrefaction fuels [177, 180]. The results of EMC and submersion tests could also suggest that open air storage could be possible with bio-coal due to the enhanced hydrophobicity. Storage outside would be significant advantage as it may overcome issues with silo storage. For biomass, spontaneous combustion is associated with storage as the hydrophilic nature of biomass means biomass must usually be stored in silos to avoid wetting which could result in high moisture contents on combustion and biological decomposition of the fuel. Issues with stored biomass and silos arise when the biomass undergoes biological and chemical processes which consume oxygen, generate heat and release combustible gases, which when hot can ignite [181]. Coal, being far less hydrophilic than biomass can undergo open-air storage avoiding this issue. The hydrophobicity of coal does however deteriorate with time as a product weathering processes during handling and transport or when the coal is stockpiled under different environmental conditions leads to coal oxidation and increasing coal functionality [66]. It would appear likely that the hydrophobicity of bio-coal would do the same.

Determining the moisture content is undertaken using an oven dry method, whereby a biomass sample is heated at 105 °C until a steady mass is achieved. The moisture content taken as the change in mass.

2.4.2. Devolatilisation

The second step in the combustion process, outlined in Figure 2.11, is the devolatilisation step. As the particle is heated (typically to temperatures above 200 ºC) the fuel starts to decompose and light volatile gases are released in a process known as pyrolysis. This pyrolysis step is highly important for lignocellulosic materials as cellulose and lignin are not directly combustible but decompose to form combustible compounds when subjected to a sufficient source of energy [68]. These volatiles are driven out of the fuel particle and prevent oxygen, present in the combustion environment, from penetrating the particle and oxidising the carbon, hydrogen, and sulphur present in the particle. As the thermal energy is able to penetrate the particle but the oxygen is not, a solid fuel particle undergoes pyrolysis until devolatilised [182]. The escaping volatiles burn much more quickly than the char, the fraction remaining after devolatilisation, and therefore understanding the devolatilisation behaviour of a fuel is important in terms of flame ignition, flame stability, flammability limits and the formation of pollutants such as nitrogen oxides [68].

From a practical standpoint, volatility is influenced by two factors: fuel particle size and combustion temperature. Particles that are smaller release more volatiles and at a faster rate. In addition, higher temperatures cause more volatiles to be released, whereas lower-temperature environments promote char formation [68]. Increasing particle size generally results in larger char yields but to what extent the particle size influences volatile yield is fuel dependent. As discussed in Section 2.1.1. lignocellulosic biomass comprises of three major organic compounds; cellulose, hemicellulose and lignin with the respective ratios not only varying between woody and herbaceous biomass but also within each category. For lignocellulosics the hemicellulose and cellulosic component is mostly converted to the combustible and non-combustible volatiles. Lignin components, on the other hand, contribute to the char fraction [68]. Due to the high proportion of hemicellulose and cellulose within lignocellulosic biomass, biomass contains higher volatile fraction and a much smaller char fraction than those seen in coals [183]. This changes the temperatures and nature of the fuel's heat release, with 70% of the heat output associated with volatile combustion for biomass and 36% of the total heat output associated with volatile combustion for coal [183]. Moreover the devolatilisation process

determines the properties of the remaining char such as char yield, porosity and composition, all important factors in the overall char combustion properties [184].

In addition to the amount of volatiles released, heating rates and final temperatures influence the nature of the pyrolysis products released. The devolatilisation and pyrolysis mechanisms of a biomass can be seen in Figure 2.12. Wide ranges of gaseous products and vapours are released during the devolatilisation stage and these are dependent on which part of the biomass is undergoing pyrolysis. For lignocellulosics, the hemicellulose initially decomposes followed by the cellulose and then the lignin, with the long polymeric chains cracking to produce vapours which leave the particle via the pores formed during the drying stage [185]. On leaving the particle these vapours react with oxygen, ignite and result in flaming combustion. During this stage a wide range of gases and vapours are produced dependent on the temperature and part of the plant undergoing devolatilisation.

Hemicellulose is the first to decompose (200-260 ºC) forming acetic acid, formaldehyde, carbon monoxide, hydrogen, furfural and furan. Decomposition of cellulose starts between 240 ºC and 350 ºC, with the first stage in the decomposition of cellulose is the production of active cellulose which will then produce charcoal by dehydration or levoglucosan depending on the temperature. The levoglucosan will then decompose further to form hydroxyl-acetaldehyde, acetol, furfural, CO and a range of other compounds. The final fraction of the plant that starts to decompose is the lignin, which decomposes between 280 ºC and 500 ºC producing aromatic compounds and the largest fraction of the char. The aromatics are produced as the straight chain links of the lignin decompose releasing phenols, carbon dioxide, hydrocarbons, formic acid, acetic acids, methanol and higher fatty acids also being produced [186]. Typically, the conditions seen in pulverised fuel combustion favour light volatiles rather than tar formation [183]. The temperature at which pyrolysis starts in biomass is about 200 ºC to 250 ºC compared to 350 ºC for bituminous coal.

Determining the volatile content is achieved using an international method (BS EN ISO 18123:2015) whereby a fuel sample is devolatilised in specially designed crucibles for 7 minutes in a furnace at 900 ºC.

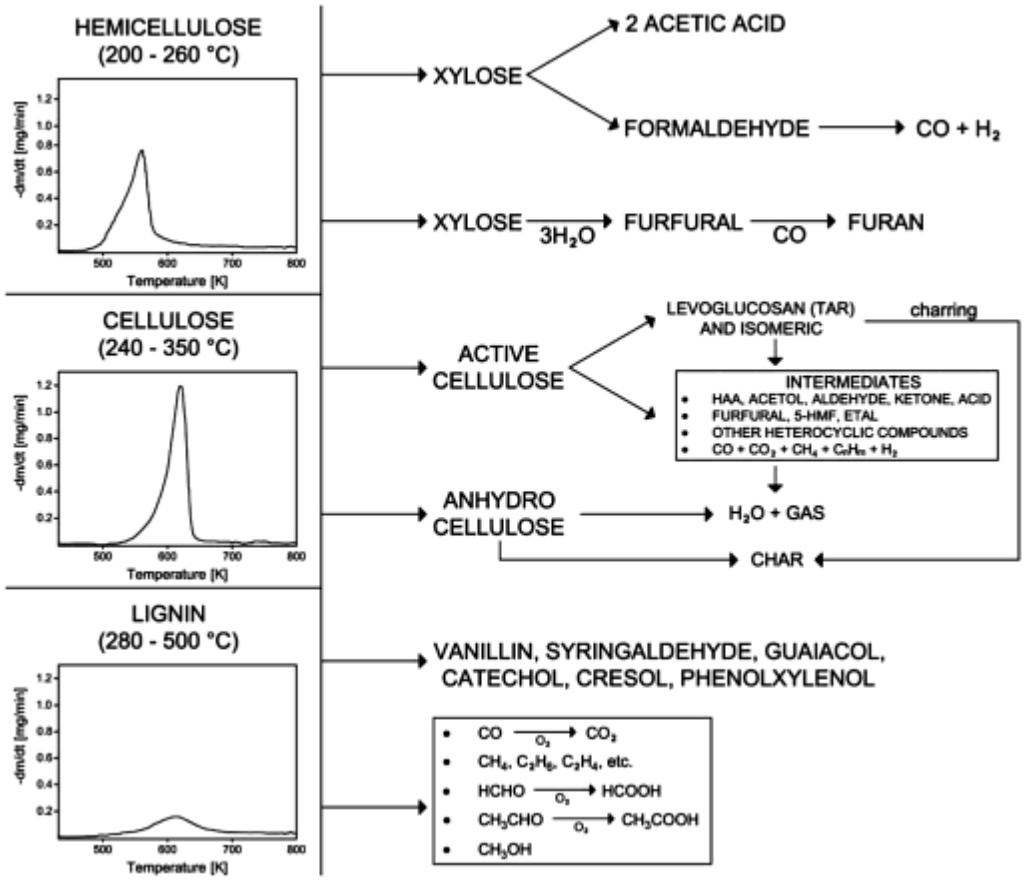

Figure 2.12: Devolatilisation pathway of ligno-cellulosic biomass [186]

2.4.3. Char combustion

The char burnout is the final step of solid fuel combustion (Figure 2.11) whereby ignition of the char occurs though the direct oxidation of the char matrix by the furnace atmosphere. The char oxidation step can be several orders of magnitude slower than the devolatilisation step and is often the rate determining step in the overall combustion process [64]. During the combustion of char, the reactant, usually oxygen, diffuses from the combustion atmosphere through the boundary layer to the surface of the char and penetrates the porous particle. The oxygen reacts with the carbon on the surface and at the pore walls producing CO, which can react in the gas phase in the area surrounding the particle to form CO_2, with changes to the pore structure within the char either enabling or inhibiting the combustion process [64].

2.4.4. Combustion of solid fuels in relation to co-firing and pulverised fuel applications

Application of biomass in pulverised coal-fired power plants is often favourable as it involves utilising existing infrastructure. Most of these pulverised coal-fired power

plants have usually been built to burn a ‘design’ fuel, whereby the design fuel is usually a typical coal from the locality. These design fuels use parameters including ash content, Hardgrove Grindability Index (HGI), volatile matter content, combustion behaviour, and slagging and fouling characteristics (collectively referred to as the coal grade) in an attempt to account for boiler performance [187]. Consequently, for pulverised coal applications, fuel specifications are often site-specific and for pulverised fuel applications, where the design fuel becomes unavailable, different coals are typically blended to best match the performance parameters.

2.4.4.1. Influence of combustion profile on co-firing

When burning fuel, it is important to achieve flame stability to sustain the flame and ensure safe boiler operation. To achieve a stable flame you first need to achieve ignition, whereby you attain substantial burning of a combustible material. To achieve ignition there is an initial heat loss due to the evaporation of any residual water and heating of the particle to the point of ignition, which results in a heat loss. This heat loss needs to be balanced by the heat release at the ignition temperature. Flame stability requires the rate of burning (flame velocity) to match the rate of material feed. If these are not matched, the flame will either blow off or flash back [187]. Thermo-gravimetric analysis (TGA) is one method originally developed by Babcock and Wilcox for comparing and evaluating fuels and by calculating the first derivative thermogravimetric (DTG) curve, with the characteristic temperatures being typically interpreted [68]. This method is discussed in detail in Section 3.8 but in essence, the method looks to identify differences in fuel burning characteristics (as shown by the burning profile). If the burning profiles are mismatched it could either result in a fuel burning in a way a furnace is not designed for or lead to poor burn interaction if co-fired (i.e. two fuels burning independently of each); either way resulting in an unstable flame.

As discussed in section 2.4.2. lignocellulosic biomass contains higher volatile fraction and a much smaller char fraction than those seen in coals, moreover 70% of the heat output is associated with volatile combustion for biomass and 36% of the total heat output associated with volatile combustion for coal [183]. The nature in which the particle ignites can also bring about issues with flame stability. Higher rank low volatile coals can undergo a process called heterogeneous ignition, whereby devolatilisation, ignition and combustion of the volatiles and char oxidation / combustion occur almost simultaneously [188]. Biomass along with high volatile coals undergoes a process called homogeneous ignition, which begins with the ignition of the volatiles and oxygen close to the particle

surface. Once ignited a gas flame surrounds the particle and prevents oxygen from reaching and igniting the char [188]. This brings about two phase combustion and firing or co-firing lignocellulosic biomass in a pulverised fuel coal plant. When co-firing these differences in burning characteristics can bring about challenges in maintaining flame velocity and flame stability as the homogeneous ignition of the biomass may prevent the heterogeneous ignition of the coal. This may allow the particles to became entrained in the gas stream and move higher in the furnace while burning [68].

There have only been limited investigations within the literature into the co-firing of coal with HTC chars, with Liu et al., [189] investigating the co-firing behaviours of lignite and two bio-coals produced from hydrothermal treatment at 250 ºC for 20 minutes of coconut fibre and eucalyptus leaves, using 25 % and 50 % bio-coal blends. Similar ignition temperatures were observed for both 250 ºC fuels and lignite, which would suggest that existing combustion furnaces suitable for lignite could accommodate these blends directly, or with only minor modifications. DTG plots indicated that there were synergistic interactions between bio-coal and lignite, resulting in improved energy conversion during co-firing, especially for the coconut fibre-derived bio-coal lignite blends. In contrast, co-combustion of unprocessed biomass-coal blends indicated little or no overlap in the combustion regions due to different ignition temperatures between coal and raw biomass. This difference in the combustion profiles resulted in a lack of interaction between the coal and biomass burn, which, in a combustion furnace could bring challenges in maintaining flame velocity and flame stability.

Parshetti et al. [190] investigated the co-firing of hydrothermally carbonised oil palm biomass at 150 ºC, 250 ºC and 350 ºC with 20 minute retention times with a low rank Indonesian coal using 50 % blends. The combustion behaviour of fuels and their blends show that the burning process was improved using 250 ºC derived bio-coal, when co-fired with 50 % coal, the 250 ºC derived bio-coal, when co-fired with 50 % coal having the lowest amounts of gaseous pollutants (CO_2, CO, CH_4, NO and SO_2). The improved combustion performance seen in both Liu et al. [189] and Parshetti et al. [190] could be due to the higher volatile matter content of the bio-coals, along with the lower initiation temperature, which promote early ignition of the total fuel mass when co-fired; leading to better and more complete combustion. This early ignition in turn can also be beneficial for nitrogen oxide emissions as it will consume additional oxygen, increasing the fuel staging effects of low-NOx burners [68].

When comparing bio-coals to coal, bio-coals compare most closely with vitrinite group macerals. Vitrinite macerals are typically derived from the humification of woody tissues and can possess remnant cell structures or may be structure-less and tend to have more oxygen than other macerals for any given coal rank [191]. Bio-coals can also compare with liptinites, which have high hydrogen and higher volatile fractions, depending on the reaction conditions and feedstock. Vitrinite identification and quantification is useful in evaluating coals for combustion and gasification, as the greater content of liptinite and vitrinite brings about greater ignition, flame stability and fuel coal burnout, greatly increasing the combustion efficiency [192-195]. This would suggest favourable combustion for bio-coal if fired or co-fired with coal in PF applications or even used as gasification feedstock. Vitrinite identification and quantification in coal is also essential to the steel-making industry as vitrinite macerals are the principal reactive components of a coking coal. During the heating process in a reducing atmosphere, vitrinite becomes plastic, devolatilizes, and then solidifies to form the porous, carbonaceous matrix of a metallurgical coke. The reactivity of the liptinite macerals are also useful as they are highly reactive but contribute more to the by-products of the coking process because of their higher volatile content [191]. This would strongly suggest that bio-coals could be well suited to biomass coke production in addition to PF application. Alkali loading in blast furnaces has a negative influence on coke reactivity [191] so removal by the hydrothermal process would be of benefit.

2.4.4.2. Influence of particle size on co-firing

Flame instability can be further exacerbated by differences in particle size, as large particle sizes can act as heat sinks, increasing the residence time of the particle before ignition and influencing the balance of heat loss and heat release. For a stable flame in a pulverised coal operation, pulverisation of fuel to 70% below 75µm is typically required. The ease in which fuels can be pulverised to 70% below 75µm is described using the Hardgrove Grindability Index (HGI). Coals typically lie between 30 (increased resistance to pulverization) and 100 (more easily pulverized) on the scale. The HGI of unprocessed *Miscanthus*, a common herbaceous bio-energy crop given in Bridgeman et al. [196] has an HGI of zero. This essentially implies under the test conditions, that no fuel would reach the desired 75µm and thus, assuming co-milling, there would be either a greater energy requirement for milling to achieve 75µm or the pulverised fuel particles would be greater than 75µm in diameter. It is argued by authors that the lower pyrolysis temperature and thus devolatilisation temperature of biomass, typically 200 ºC to 250 ºC compared to 350

ºC for bituminous coal would to a certain extent offset a larger particle diameter as heat loss due to the greater heat sink would be balanced by the earlier heat release. This is in part true but will be dependent on biomass moisture content as biomass can have considerably higher moisture content compared with coal. Higher moisture content can delay particle heating, which in turn can increase the overall combustion time and larger particles, on drying and de-volatilization, will became entrained in the gas stream and move higher in the furnace while still burning promoting flame instability [39, 68]. The lower decomposition temperatures associated with many biomass fuels also bring about further challenges as operation of the pulveriser mills when using pulverising biomass require lower temperatures compared to coal to avoid fuel decomposition so additional milling may not be possible.

It is widely accepted in the literature that HTC increases grindability of biomass [33] because HTC degrades the hemicellulose and cellulose (fibrous material that provides strength to the biomass cell walls) at temperatures of 180 °C and 200 °C respectively [71]. At present, there appears no literature on the quantifiable gridability of the bio-coal using HGI. There is however literature on the torrefaction of biomass with Bridgeman et al. [196] investigating the influence of torrefaction at between 230 °C and 290 °C with holds between 10 and 60 minutes for willow and *Miscanthus*. Results showed that the HGI went from zero for both fuels to between 5 and 38 for willow and 6 and 53 for *Miscanthus*, with higher HGI associated with greater reaction severity. Ndibe et al. [197] investigated torrefied straw and poplar at between 250 °C and 300 °C, along with steam exploded wood and A1 wood pellets. His findings showed that A1 wood pellets had an HGI of 15, with torrefied materials between 30 and 43. For reference, a change in HGI from 15 to 43 represents a 50% reduction in the energy requirement for milling [197].

Torrefaction works by heating biomass is the absence of oxygen between 200 °C and 300 °C to drive off oxygen rich volatiles that have a low calorific value. The loss of volatiles is associated with the decomposition of the hemicellulose component which binds the cellulose structures in the cell wall enabling an increase in the friability [198]. HTC, dependent on reaction temperature, is associated with the decomposition of the hemicellulose, cellulose and to some extent the lignin, with the char derived from the recalcitrant biomass fractions and condensation and repolymerisation of oligomers and monomers derived from the biomass. The derived spherical shaped structures and the

remaining plant scaffolds around which the char is formed should facilitate a significant increase in HGI when compared with torrefaction.

2.5. Issues associated with inorganics and heteroatoms during combustion

2.5.1. Inorganic related issues

Inorganics and heteroatoms are a particular issue for biomass during combustion, pyrolysis and gasification as the alkali and alkaline metals, particularly potassium and sodium, along with sulphur and chlorine influence ash chemistry and influence the behaviours of the fuel in terms of its tendency to corrode equipment and cause slagging, fouling and in certain furnaces bed agglomeration [39].

2.5.1.1. Slagging

Slagging is a phenomenon brought about though the melting of ash when ash deposits are exposed to radiant heat, such as flames in a furnace. As most furnaces are designed to remove ash as a powdery residue, having a high ash melting temperature is often desirable as if it softens or melts it then fuses into a hard glassy slag, known as a clinker; extraction is difficult and the furnace requires cleaning [39]. Chlorine within the ash is very corrosive to stainless steel and can also react with silicates and the alkali metals to form an undesirably stable and corrosive slag [199]. Bed agglomeration is similar to slagging but is an issue specific to fluidised bed furnaces and comes about though the formation of potassium silicates within the ash which melt and lead to adhesion of the bed material [200]. For slagging and bed agglomeration, the temperature at which the ash melts and fuses is strongly influenced by the alkali and alkaline metals, with alkali metals acting as a flux for alumina-silicate ash, while the alkaline earth metals tend to increase melting temperatures [39].

2.5.1.2. Fouling

Fouling is brought about when potassium and sodium, often in combination with chlorine, partially evaporate when exposed to radiant heat and form alkali chlorides, which condense on cooler surfaces such as heat exchangers. These deposits do not just reduce heat exchanger efficiency, they also play a major role in corrosion as these deposits react with sulphur in the flue gas to form alkali sulphates releasing chlorine in the process. This chlorine has a catalytic effect which results in the active oxidation and corrosion of the furnace material [39, 201]. Consequently, to reduce the propensity for an ash to slag or foul it is important to minimise the alkali metals, particularly potassium and sodium within the ash along with chlorine and other halogens.

2.5.1.3.Role of phosphorus in slagging and fouling

The role of phosphorus within the ash is currently under debate as it has generally been observed that phosphorus is a controlling element in the ash transformation reactions during biomass combustion due to the high thermal stability of phosphate compounds [200]. Phosphate ashes do however contribute to slagging and bed agglomeration once the ash becomes molten [200]. This phosphorus is also beneficial from a fouling perspective, as potassium chloride present within the ash or char during combustion, can bind with calcium rich phosphates, or become potassium phosphates, which then further react with calcium oxides. These calcium potassium phosphate complexes are stable and removes the potassium available to form low temperature melting potassium silicates [200, 202]. Calcium oxide, calcium carbonate and calcium hydroxide would otherwise dissolve into potassium silicate melts, bringing about the release of the potassium into the gas phase [203, 204].

2.5.1.4.Prediction of slagging and fouling

Controlling slagging, fouling and bed agglomeration is currently done through careful fuel selection and blending of fuels and additives with known ash chemistry so to tailor a fuel with favourable ash chemistry to best minimise their effects. To predict the likelihood of fouling during combustion, various slagging and fouling indices have been derived based on the chemical composition of the fuels. The equations for alkali index (AI), bed agglomeration index (BAI), acid base ratio ($R\frac{b}{a}$), slagging (Babcock) index (SI), fouling index (FI), and slag viscosity index (SVI) are given as equations 1-6 in Table 3.3 in Chapter 3, along with the methodology got their use (see Section 3.7.2). While these indices have been developed over a number of years to predict the likelihood of slagging and fouling, some caution is needed when interpreting these results as they have been developed specifically for coal ashes, and biomass ashes are very different and consequently will behave differently.

Differences between coal and biomass indices are particularly prevalent for fouling indices, as fouling indices for coal ashes are predominantly based around the sodium content of the fuel. This is due to potassium being principally present as a consistent of clay minerals within the coal and as such is not considered to be in a form readily volatilised in a flame. Consequently the deposition of sodium compounds by a volatilisation / condensation mechanism is considered the principle driving force behind convective pass fouling in coal boilers [39]. In biomass, potassium tends to be the most predominant alkali metal, and as is the case for sodium, generally in a form which is

available for release by devolatilisation [205]. Table 3.3 gives slagging and fouling indices, which are based on the total alkali content of the fuel and as such are more suited to biomass materials [205]. Other approaches for the prediction of fouling and slagging propensity are based around the use of phase diagrams for the appropriate alumino-silicate ash [39].

In coal science the ash fusion test is often a good indicator of the fuel's propensity to slag and foul with generally high ash melting usually indicative of a low slagging and fouling propensity [39]. The ash fusion test results are also one of the most commonly quoted parameters in coal grade, during the sale and procurement of steam coal. The ash fusion test has been developed to describe the melting behaviour of biomass ash. A test piece is prepared from biomass ash and is heated at a constant rate with constant observation. The key stage temperatures are subsequently recorded when the test piece changes shape, with the key stages as described in the standard method for the determination of ash melting behaviour (DD CEN/TS 15370-1:2006) as follows: beginning of shrinkage (SST), sample deformation temperature (DT), hemisphere temperature (HT) and flow temperature (FT). Figure 3.13 gives images of the various transition states.

As most furnaces are designed to remove ash as a powdery residue and slagging is a phenomenon brought about though the melting of ash when ash deposits are exposed to radiant heat, having a high ash melting temperature is often desirable. For most power station applications, the 'deformation' temperature is taken as the safe combustion temperature limit, as this is the onset point where ash becomes sticky and issues start arising, although sometimes 'hemisphere' temperature is reported. Given the temperature at which the ash melts and fuses is strongly influenced by the alkali metal content (potassium and sodium acting as a flux for aluminium and silicon based ash), a high ash melting temperature is usually indicative of a low alkali metal content and thus low fouling propensity [39]. This is however a rule of thumb and not necessarily correct in all applications.

2.5.1.5.Role of metals in catalysing combustion

In addition to the impact on slagging and fouling certain inorganic elements are known to have a significant impact on the devolatilisation and char reactivity during combustion [206, 207]. There is strong consensus in the literature that the alkali metals, potassium and sodium, catalyse char reactivity [160, 207-209]. The alkaline earth metals, calcium and magnesium, are understood to catalyse char reactivity but to a lesser extent

than the alkali metals [209-211], with iron known to behave using similar mechanisms [212]. These metals are known to increase reactivity though metal catalysed oxidation of the carbon surface through the intimate bonding of metals with oxygen functionalities [160, 207, 209]. Through this mechanism, carbon-carbon bonds are broken at temperatures where they would not otherwise be broken. This is due to the oxidisation of the bonded metal, followed by donation of the acquired oxygen to the carbon structure breaking the stable carbon-carbon bonds at lower temperatures. Silicon has been reported to reduce char reactivity by forming inactive alkali silicates and the overall catalytic effect of the inorganic matter likely depends on the relative proportions of inorganic elements in the char [210].

As discussed in further detail in Section 2.5.3.2, inorganic elements are extracted to different extents during HTC [76, 213] the overall catalytic effect of the inorganic matter will almost certainly be different for bio-coals than for untreated biomass [214]. A few studies have investigated the impact of HTC on the reactivity of biomass chars. Bach and co-workers recently published a series of papers on the effect of HTC pre-treatment on the conversion of microalgae [215], wood [216, 217] and wood-derived biomass [218] during combustion in air. Lane et al. [214] looked into the reactivity of hydrothermally carbonised grape marc, sugar cane bagasse and a freshwater macroalgae. In all cases, the conversion of char was shifted toward higher combustion temperatures following HTC, potentially indicating lower char reactivity for the bio-coals when compared with the untreated biomass feedstocks [214]. Caution is however required as the authors place a strong emphasis on the influence of metals catalysing the devolatilisation behaviour; citing studies where the physical structure of the biomass has not been changed. This is not the case for HTC. HTC is a series of hydrolysis, condensation and polymerisation reactions and as such, the compounds, which make up the char, are different to that of the starting material. Changes in devolatilisation temperatures can as much be because different compounds and structures will be present and different compounds volatilise at different temperatures. While metals will play a role, it cannot be said that changes in metal concentration is catalysing the devolatilisation behaviour without discounting changes in volatile chemistry.

2.5.2. Heteroatom related issues

Heteroatoms during combustion are predominantly responsible for a range of airborne emissions during combustion, although as shown in the earlier section chlorine, phosphorus and sulphur also play key roles in fouling, slagging and bed agglomeration.

2.5.2.1.Nitrogen

Nitrogen within the fuel largely ends up being released as N_2, nitrogen oxides and to a lesser extent nitrous oxide during complete combustion [39]. Nitrogen oxides are formed two ways during combustion, with nitrogen originating from fuel nitrogen and nitrogen in the air, with the latter referred to as thermal nitrogen oxides [39]. Thermal nitrogen is a plant operating consideration and is usually controlled though fuel staging effects using low-nitrogen oxide(s) burners. In this process, initial combustion occurs in a zone where the air to fuel ratio is above stoichiometry, consuming additional oxygen and reducing nitrogen oxides back to gaseous nitrogen [68]. As thermal nitrogen is not necessarily a fuel consideration, this section will focus purely on fuel-derived nitrogen.

Nitrogen oxides are formed in both the gas phase and char combustion phases and the main emission is nitric oxide (NO) (>90 %) which is later converted to nitrogen dioxide (NO_2) in the atmosphere. Initial nitrogen evolution from the fuel occurs in the pyrolysis phase of combustion where nitrogen is volatilised as ammonia (NH_3) and hydrogen cyanide (HCN) which is then converted to NO though different reaction routes. By operating the fuel mixture rich in the near-burner zone is it however possible to subsequently react the NO with NH_3 and HCN to produce N_2, to reduce NO and NO_2 emissions from volatile-N [219-221]. Rapid release of the nitrogen during the volatile burn can promote nitrogen evolution within a fuel-rich environment. In contrast to an oxygen-rich environment, this promotes the formation of diatomic nitrogen (N_2) instead of NO_x molecules such as NO, NO_2, etc. To achieve this however, understanding of the kinetics of fuel pyrolysis and combustion is essential [68]. Nitrous oxide (N_2O) emission during complete combustion is thought to be less important in pulverised fuel combustion [39].

2.5.2.2.Sulphur

Sulphur oxides are a result of complete oxidation of fuel sulphur. Emissions are largely in the form of sulphur dioxide (SO_2) (>95 %), with sulphur trioxide (SO_3) occasionally formed at low temperatures [39]. During combustion, fuel sulphur is not completely converted to gaseous sulphur oxides with between 57-65 % released into the gas phase and the remaining fraction remaining in the ashes, interacting with inorganics as described in the earlier sections [222]. Sulphur dioxide within the flue gas plays an important role in corrosion and active oxidation of fouling deposits on heat exchangers, reacting with potassium and sodium chloride deposits within ash deposit layers, forming potassium and sodium sulphates, which liberate chlorine in the process. This chlorine

goes on to react with iron forming iron chloride which is then oxidises and forms a layer of iron oxide between the ash deposit and the heat exchanger, as shown in Figure 2.13 [201].

Fuel sulphur content however plays an important role in reducing suspended particle matter from thermal power stations, so its presence within the flue gas is not necessarily adverse. Combustion of solid fuel results in the formation of ash, of which a portion becomes entrained within the gas flow, known as fly ash, and contributes to an increase in suspended particulate matter within the surrounding environment. Particulate matter is known to exert an impact on human health [223] and in larger furnaces abatement of particulate matter is requires to avoid emission to the environment, the use of electrostatic pacificators (ESP) being a typical abatement technology [224]. Electrostatic precipitation is a technique that employs the application of an electric field to separate out the suspended particles from the flue gas [224]. With the adoption of low sulphur fuels, be it biomass or low sulphur coal, it has been noted that the electrical resistivity of the fly ash generally increases as the ratio of sulphur-to-ash content in the coal decreases, which potentially results in a low collection efficiency of ESP [225].

The role sulphur plays in ESP is due to sulphur trioxide within the flue gas combining with moisture vapour as the flue gas cools below 315 °C to form sulphuric acid in the flue gas vapour. The sulphuric acid within the flue gas vapour is absorbed onto the fly ash particles [226] which effects the surface electrical conductivity of the fly ash/dust and increases the fly ash/dust cohesion to reduce losses during dislodgement and fly ash collection (rapping) [224]. When combusting fuel sulphur emissions are largely in the form of sulphur dioxide however when a fuel with high sulphur content is combusted, there is generally enough sulphur trioxide formed to bring the electrical resistivity of the fly ash into a range which results in good precipitator operation [225]. When burning a fuel with a low sulphur content, flue gas conditioning is requires which involves injection of chemical additives (for example sulphur trioxide, sulphuric acid, ammonium sulphate, ammonium bisulphate, sulphamic acid and ammonia) into the flue gas to alter the physico-electrical properties of the fly ash, to increase ESP efficiency [224]. Consequently, sulphur is typically required when operating a furnace with ESP, albeit either within the fuel or added in flue gas conditioning. Many modern power plants use flue gas desulphurisation (FDG), a set of technologies used to remove sulphur oxides from exhaust flue gases, post ESP with a view to reducing sulphur emissions to the environment and abate the impact on both health and global warming [227].

2.5.2.3.Chlorine

Chlorine is an essential micronutrient for higher plants and is used as a major solute in maintaining the plants turgor, controlling osmoregulation, regulation of pH gradients, electrical excitability and membrane potential [228]. Chlorine exists within biomass in the form of water soluble ionic salts (NaCl, KCl, $CaCl_2$, $MgCl_2$ and ionic chloride (Cl^-)) [37, 38] with the ionic salts often making up a large proportion of the total inorganics within the starting biomass. Chlorine becomes an issue during combustion as it is very corrosive to stainless steel, a common material in power plants [201]. During combustion, chlorine within the fuel is partially released as hydrogen chloride (HCl), volatilised potassium or sodium chloride, or remains within in the ash. Chlorine within the ash will go onto react with silicates and the alkali metals within the ash and if slagging is encountered will to form an actively corrosive and undesirably stable slag [199].

When volatilised as sodium or potassium chloride, these alkali chlorides go on to condense on the heat exchanger surfaces (fouling). While these deposits bring about reductions in heat exchanger efficiency, they also play a major role in corrosion as these deposits react with sulphur in the flue gas to form alkali sulphates releasing chlorine in the process. This chlorine has a catalytic effect, which results in the active oxidation and corrosion of the furnace material as shown in Figure 2.13 [39, 201]. Chlorine volatilised as hydrogen chloride is often not problematic in terms of corrosion as it is transported out of the furnace in the flue gas. It can however undergo further reactions and can be emitted as dioxins and other organic chlorine compounds, polychlorinated dioxins and furans which are a group of highly toxic components which can be created by this process [39]. Corrosion can be a particular problem when combusting *Miscanthus*, grass and straw which contain higher amounts of chlorine than wood [39].

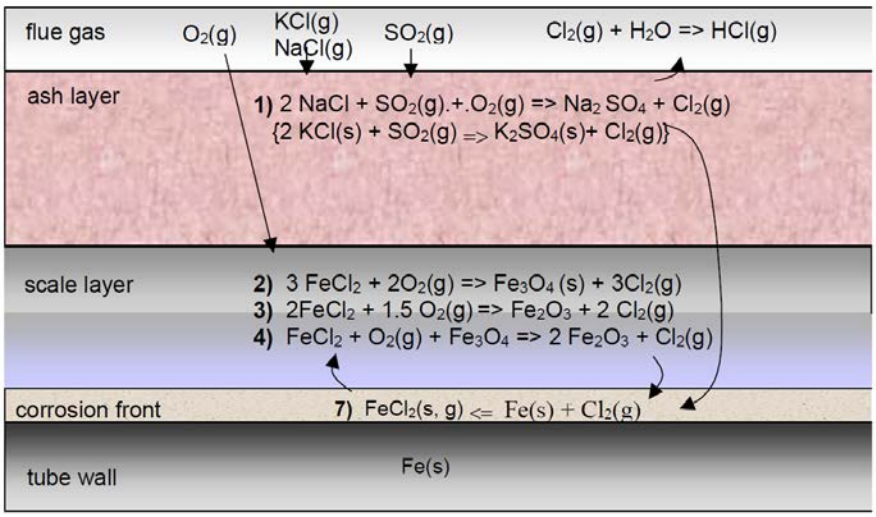

Figure 2.13: Active oxidation corrosion mechanisms as a consequence of ash fouling deposits on iron surfaces [201]

2.5.2.4.Oxygen

Oxygen is arguably the most important heteroatom in fuel science, yet it does appear largely overlooked in the literature, with few specifically measuring for it. It's most notable impact is its adverse impact on energy content, reducing HHV, as demonstrated by Dulongs Equation (see Equation 2.1), yet is it also associated with many of the handling issues associated with biomass. Oxygen is present in both biomass and coal but in coal oxygen often forms the stable bridges between cyclic aromatic carbon rings, which makes up the coal's polymeric matrix, as shown in Figure 2.3 [64, 70]. The structure of lignocellulosic biomass on the other hand largely consists of sugar monomers linked by oxygen ether bonds, with a series of alcohol functional groups (OH), along with carboxyl and carbonyl functional groups, as shown in Figure 2.1 [52-54]. It is this structure that gives lignocellulosic biomass a higher oxygen content, and in part its lower energy density. In addition to reduced energy density, the alcohol functional groups influence the polarity of the biomass giving it its hydrophilic properties [229]. The hydrophilic nature of biomass means, for energetic applications, biomass must usually be stored in silos to avoid wetting and decomposition [181]. Wetting can also adversely affect calorific value due to the latent heat requirements for evaporating water within the fuel and associated issues with flame stability [39].

The highly oxygenated structure of biomass can also bring about fire and explosion hazards when storing and handling. When finally milled or as a dust, oxygen within the biomass is readily released during devolatilisation and gives biofuels both a low lean flammability limit along with a high reactivity increasing its explosion risk [230, 231]. Moreover, the oxygenated nature of biomass means the upper flammability limit

can often be well above stoichiometric, this combined with the low mean flammability gives biomass a large flammability range, not seen for flammable gases such as methane [230]. The oxygen within the biomass structure can also influence metal catalysed reactivity as it is known surface oxygen functional groups can bind to cations such as sodium, potassium, magnesium, calcium [232]. These bonded metals go on to oxidise and then donate their oxygen to neighbouring carbon-carbon bonds, breaking carbon-carbon bonds at temperatures where they would not otherwise be broken [160, 207, 209]. The binding of cations to these surface oxygen functional groups can also effect a fuel's propensity to foul, as it has been shown by Baxter and co-workers that during the devolatilisation stage, functional groups containing oxygen, can transport associated cations, assisting the volatilisation of both volatile and non-volatile metals [232].

While oxygen in biomass appears to largely be detrimental to the fuel, it should however be noted that organically bound oxygen appears to play a key role in gasification and coking, HTC and coal formation. During HTC, it is through the reactive oxygen functionalities on the derived aromatic structures that the structures superficially link though chemisorption before dehydrating to form stable oxygen groups, ether or pyrone, within the char formation [85, 86]. These same ether and pyrone bonds are present in the coal formation, presented in Figure 2.3. The stable oxygen groups in coal also play an important role in the efficiency of gasification, with the more oxygenated vitrinite fraction increasing the reactivity and fuel conversion [191-195]. Oxygen content may also be linked to grindability, with a very close correlation between vitrinite content and coal HGI [233].

2.5.3. Mitigation of issues associated with inorganics and heteroatoms during combustion

While control of the aforementioned issues has up-until recently been controlled though the careful selection and blending of fuels, increasing demand for biomass resources mean that selection of low ash, low chlorine fuels will become less of an option and higher ash, higher chlorine biomass will have to be exploited in bioenergy. One promising solution has been washing biomass, where by biomass is leached with water and acids in order to extract nutrients as a way to reduce the ash deposition and airborne emissions before combustion, gasification or further pre-treatment such as torrefaction [41-43]. This technology is particularly well suited to high chlorine fuels such as *Miscanthus*, grasses and straw [39, 41] and a review of biomass washing is available in

Gudka et al. [42]. Other mitigative measures includes the use of fuel additives, and, as hypothesised in this work HTC.

2.5.3.1. Utilisation of additives

Utilisation of additives to abate problems associated with alkali metals and chlorine have also been developed and now being utilised in biomass combustion [234, 235]. Various additives can mitigate ash related issues by the following possible mechanisms: i) capturing problematic ash species via chemical adsorption/ reactions with additives so that low melting temperature elements in biomass fuels can be converted into high temperature melting substances [236-240]; and ii) increasing the biomass ash melting temperature and reducing sintering by enhancing inert elements/compounds in ash residues via addition of additives [234]. Additives are typically grouped into four groups: (i) aluminium-silicate based additives, (ii) sulphur based additives, (iii) calcium based additives, and (iv) phosphorus based additives. These additives are typically introduced into the biomass combustion systems by blending it directly with the fuel; either through pelletizing the fuel together with additives or mixing the additives with the fuel while on transport conveyors. Alternatively they are fed into the combustor as a powder or solutions via a separate installed spraying system [234].

Aluminium silicate based additives work predominantly by reacting the aluminium silicate additive with potassium chloride within the fuel forming potassium aluminium silicates, as shown in Equation 2.3. A common commercial aluminium silicates additive is kaolin, which when reacted with gaseous potassium chloride forms Kalsilite ($KAlSiO4$) and leucite ($KAlSi2O6$) and have melting temperatures of about 1600 °C and 1500 °C, respectively [241, 242]. Other aluminium silicates include zeolites, emathlite and bentonite and work using a similar mechanism, albeit forming more complex potassium aluminium silicates [243]. In addition, silicon dioxide and aluminium oxide also react with potassium chloride at high enough temperature (see Equation 2.4 and Equation 2.5 respectively), but with lower efficiency and capacity compared to commercial additives such as kaolin [243-245].

Coal fly ash is also being used as an aluminosilicate-based additive ($Al_xSi_yO_z$) in biomass power plants such as Drax (Selby, United Kingdom), which operates three biomass and three coal boilers giving it abundant availability for the power plant. Results presented in Clery et al. [235] support the case for potassium being retained within the ash due to the use of the fly ash additive, albeit the experiences of Drax Power would suggest fly ash addition is predominantly restraining biomass ash sintering by diluting the

potassium within the ash (personal communication). There is also increasing interest in the potential for sewage sludge as it contains different aluminium silicates, silica and alumina, which showed ability to increase biomass ashes sintering temperatures and reduce fouling deposition in different studies. Therefore, sewage sludge is classified as an aluminum silicate based additive [237, 240, 246-249].

$$Al_2O_3.xSiO_2 + 2\ KCl + H_2O \rightarrow K_2O.Al_2O_3.xSiO_2 + 2\ HCl_{(g)} \quad (2.3)$$

$$Al_2O_3 + 2\ KCl + H_2O \rightarrow 2\ KAlO_2 + HCl_{(g)} \quad (2.4)$$

$$SiO_2 + 2\ KCl + H_2O \rightarrow K_2O.SiO_2 + 2\ HCl_{(g)} \quad (2.5)$$

Sulphur based additives convert potassium chloride into potassium sulphate, with the reactions given in Equation 2.6 to 2.10 [250-253]. The primary purpose is sulphation of the potassium chloride so that the chlorine will be released as hydrogen chloride and flows away with flue gas, as opposed to forming potassium chloride deposits on heat exchangers [250, 253]. Hydrogen chloride is seen as less problematic than potassium chloride as reductions in the amount of potassium chloride will considerably reduce the amounts of chlorine in the fouling deposits. The implications are discussed in section 2.5.2 and Figure 2.13 [236]. The potassium sulphate generated through sulphur addition also has a slightly higher melting temperature, about 840 °C, compared to the potassium chloride which makes potassium sulphate less problematic in terms of deposition [250, 253]. Typically sulphur based additives are added in the form of a solution, since water soluble sulphates may decompose in a wide temperature range [253].

$$2\ SO_{2(g)} + O_{2(g)} \rightarrow 2\ SO_{3\,(g)} \quad (2.6)$$

$$(NH_4)_2SO_{4(l)} \rightarrow 2\ NH_{3(g)} + SO_{3\,(g)} + H_2O_{(g)} \quad (2.7)$$

$$Fe_2(SO_4)_{3(l)} \rightarrow 3\ SO_{3\,(g)} + Fe_2O_3 \quad (2.8)$$

$$Al_2(SO_4)_{3(l)} \rightarrow 3\ SO_{3\,(g)} + Al_2O_3 \quad (2.9)$$

$$SO_{3\,(g)} + 2\ KCl_{(g)} + H_2O_{(g)} \rightarrow 2\ HCl_{\,(g)} + K_2O_4 \quad (2.10)$$

Calcium based additives often take the form of lime, limestone and marble sludge. As discussed in section 2.5.1 increasing calcium content within the ash will increase ash melting temperature and will restrain ash melting, ash sintering and slagging in bottom ash. This mechanism works as calcium, an alkali earth metal can dissolve into potassium silicate melts (as ionic calcium (Ca^{2+})) (see Equation 2.11) [203, 204]. The resulting potassium calcium silicates have higher melting temperatures than potassium silicates. This reaction could however result in the release of potassium into the gas phase (see Equation 2.12) which can bring about the issues of fouling and corrosion as previously discussed [203, 204]. Calcium additives are however more active in combustion of

biomass fuels that are rich in phosphorus and potassium [202, 242, 254]. This is due to potassium chloride present within the ash or char, can either binding with calcium rich phosphates (see Equation 2.13), or become potassium phosphates (see Equation 2.14) which then further react with calcium oxides (see Equation 2.15). These calcium potassium phosphate complexes are stable and removes the potassium available to form low temperature melting potassium silicates [200, 202]. Consequently calcium based additives appear best suited to fuels rich in phosphorus and potassium.

$$K_2O.SiO_2 + 2\ CaCO_3 \rightarrow 2\ CaO.K_2O.SiO_2 + 2\ CO_{2(g)} \quad (2.11)$$

$$K_2O.SiO_2 + 2\ CaCO_3 + ½\ O_2 \rightarrow Ca_2SiO_4 + K_2CO_3 \quad (2.12)$$

$$KCl_{(g)} + 2\ CaHPO_4.2H_2O \rightarrow 2\ CaKPO_4 + 2\ H_2O + HCl_{(g)} \quad (2.13)$$

$$4\ KCl_{(g)} + 2\ CaHPO_4.2H_2O + O_2 \rightarrow 2\ K_2PO_4 + 5\ H_2O + 2\ CaCl_2 \quad (2.14)$$

$$K_2PO_4 + 2CaO \rightarrow 2\ CaKPO_4 + O_2 \quad (2.15)$$

For biomass fuels containing high contents of potassium, silicon and a certain amount of calcium, phosphorus rich additives have been suggested. Grimm et al. [200] tested phosphoric acid as an additive to reduce ash sintering and bed agglomeration in a fluidized bed reactors. The investigation concluded that with more phosphorus in the ash residues potassium may react with the phosphorus forming potassium rich phosphates that may further react with calcium oxide. Addition of calcium phosphate would allow the conversion of potassium chloride into more stable calcium rich phosphates as shown in Equation 2.13. In both these mechanisms the potassium available to form low melting temperature silicates is reduced, which is observed as a reduction of low temperature melting potassium silicates [200, 202].

2.5.3.2.Utilisation of HTC

Demineralization of the fuel through dissolution of these alkali salts into the process water during HTC could potentially remove a large fraction of the fuel mineral content thereby reducing the above mentioned ash problems. Likewise, it is possible that through HTC less soluble but unwanted compounds and elements maybe modified in such a way to reduce or remove their role in the for-mentioned processes. This would result in a fuel that is not only (i) more energy dense, (ii) easily friable and (iii) more hydrophobic than the starting material but also one with lower inclination to slag and foul through the removal of alkali metals and chlorine.

Previous work by Saddawi et al. [43] has demonstrated that simple washing of biomass in distilled water (at room temperature and pressure) can remove simple ionic salts such as alkali earth chlorides which dissolve easily. Washing in solutions such as

ammonium acetate can further increase recovery, recovering inorganic elements that are bound to the organic structures of the biomass with ionic bonds, though ion exchange. Finally washing in a hydrochloric acid solution dissolves alkali earth carbonates, sulphates and sulphides. Consecutive leaching using these three methods can subsequently remove the ionic bonded inorganics from the biomass structure, leaving only silicates and elements bound to the organic matrix with covalent bonds [43]. During HTC the subcritical water used has a lower density and viscosity than that of water under normal conditions [255] and as such removal of simple ionic salts within the biomass matrix can be enhanced. The increased dielectric content [256], increased ionic dissociation constant [257] and lower pH [11] of the subcritical water could also aid the removal of ionic bonded inorganics though ion exchange and dissolve the inorganic salts, thus removing ionic bonded inorganics from the biomass structure. The modification of the biomass structure during HTC will also further aid the removal of the inorganic elements.

Reza et al. [76] investigated the fate of inorganics during HTC for *Miscanthus*, corn stover, switch grass and rice hull. The results have shown reductions in the amount of calcium, sulphur, phosphorus, magnesium and potassium in the original biomass when the biomass is processed under hydrothermal conditions at 200° C, 230° C and 260° C. Removal of silicon appears limited at 200° C and 230° C although there was some indication that silicon content starts to decrease when the lignin starts to degrade at 260° C. It should be noted that despite a decrease in the inorganic content relative to the starting biomass, the overall concentration of inorganics within the char can increase. More recent studies in Benavente et al. [45] looked into the HTC of olive mill waste, artichoke waste and orange juice wastes and observed reductions in ash content between the feedstock and chars, with x-ray florescence (XRF) analysis showing slight reductions in K_2O content of the char, and significant reductions in silicon dioxide (SiO_2), MgO, CaO and Cl. Both studies compared the results with slagging and fouling indices but no further investigation of the ash properties was carried out. Analysis of process waters by Broch et al. [173] also confirmed the extraction of alkaline metals from herbaceous and woody biomass. Consequently based on the results given in Reza et al. [76], Broch et al. [173] and Benavente et al. [45] it looks like modification of the ash chemistry is possible via HTC, with optimisation possible though varying the HTC parameters.

When starting this study there was limited information beyond these three studies and the impacts in terms of slagging and fouling propensity was limited to slagging and

fouling indices presented in Reza et al. [76]. Data presented in Chapter 4 was presented in Smith et al. [213] was the first to demonstrate a tangible benefit in terms of slagging and fouling and since undertaking this study these results have been validated in additional studies [258-260]. The work presented in Smith et al. [213] demonstrated that at higher temperatures calcium and phosphorus are retained within the bio-coal, giving an additive effect similar to that described for calcium and phosphorus additive described earlier in this section. This has also been investigated and supported in Mäkelä and Yoshikawa [261]. Other authors looking into HTC have demonstrated either alkali metal or ash reductions [108, 169, 214, 262, 263] however they have largely drawn the conclusion that slagging, fouling and corrosion will be reduced based on the reduction of alkali metals as opposed to use of empirical methods (slagging index etc) and retention/ reduction of other influencing metals.

HTC should also reduce the chlorine within the fuel. Chlorine exists within biomass in the form of water soluble ionic salts (NaCl, KCl, $CaCl_2$, $MgCl_2$ and ionic chloride (Cl^-)) [37, 38] with the ionic salts making up a large proportion of the total inorganics extracted under HTC. The extraction of these chloride based salts will result in the extracted chlorine appearing as chloride in the process waters. Biomass washing experiments have shown that between 85 % and 100 % of total chlorine within the biomass is extracted though washing [43, 205, 264]. Simultaneous denitrogenation of the fuel may also be possible under the right conditions [131]. Within the hydrothermal literature chlorine measurement appears limited to date with published data largely limited to the published work presented in Chapter 5 [259] and [260]. Most authors make the assumption that given chlorine exists within biomass in the form of water soluble ionic salts most chlorine within the biomass is extracted, as demonstrated in washing experiments, during HTC.

Liu et al. [265] has also proposed that HTC reduces the fouling risk due to a combination of decreased oxygen and volatile matter content of the bio-coal. This is because in addition to evaporation mechanisms discussed above, organic transport mechanisms also appear important in understanding a fuels propensity to foul. Baxter and co-workers demonstrated that volatile matter is importance in transport and volatilisation of both volatile and non-volatile metals during combustion and thus effects a fuel's propensity to foul. During the devolatilisation stage, functional groups containing oxygen, can transport associated cations, assisting the volatilisation of both volatile and non-volatile metals [232]. While the reduction in oxygen and volatile carbon is true, the

assumption that this then reduced the fouling propensity of the bio-coal may not be correct This is because this mechanism does not take into account the re-uptake of metals from the process water onto the surface of the bio-coal.

It is known that surface oxygen functional groups can bind to cations such as sodium, potassium, magnesium, calcium, which can then be released upon thermal treatment [232] and as discussed in Section 2.3.2 reactive oxygen functionalities are present on the char surface, which will provide binding sites for more aromatic structures [85]. Binding of alkali metals to the surface of the chars during HTC treatment may result in rapid volatilisation of these bound metals, which may still lead to fouling issues. The contribution of this effect requires further investigation but a reduction in O/C would limit reabsorption of metals and reduce this potential mechanism. Moreover release of volatile metals, such as potassium, is complicated and the release also depends upon the content of chlorine and silica in the fuels rather than on the potassium content alone [266]. Consequently, caution is required when predicting fouling propensity as the hydrothermal process could lead to a greater fouling propensity than would otherwise be expected, due to an increase in the proportion of cations associated with surface functional groups.

To fully understand the fouling risk posed, it is important to understand the availability of potassium and when working with bio-coals this appears largely unknown. As previously stated fouling in coal combustion is predominantly associated with the sodium within the fuel as the potassium is principally present within clay minerals in the coal and typically not volatilised in the flame [39]. In biomass, potassium is mostly present as free K^+ ions in solution within the xylem cells generally in a form which is available for release by devolatilisation and evaporation [205]. While the removal of potassium has been documented, there is at present no information on the partitioning of potassium during HTC. It is thus unclear whether potassium is still in ionic form, formed carbonates or has reacted with other inorganic elements present in the fuel to form minerals such as K_2CaSiO_4 and $KAlSi_3O_8$ during HTC. Chemical fractionating techniques are one method of predicting the release on inorganics into the vapour phase. The method was initially developed for use in coal and involves a standardised leaching process using progressive and more severe chemical reagents, for example water, then ammonium acetate and then hydrochloric acid. It is generally considered that water and acetate leachable elements are those that are more readily released into the vapour phase, while the remaining acid soluble and residual elements considered to remain within the

ash [39, 205, 267]. To the best of the author's knowledge, such analysis has not been undertaken for bio-coals.

2.6. Production of higher value chemicals and enhanced energy recovery by HTC

In addition to the bio-coal, HTC produces an aqueous co-product, which contains about 10 to 15 % of the original organic matter in the form of sugars and organic acids for the HTC of herbaceous and woody biomass [268]. These process waters also contain alkaline metals extracted by the HTC process [173]. The process water composition appears to vary with feedstock and reaction temperature, with lower temperature HTC being high in sugars but organic acids dominating above 235 °C. Of the sugars present 5-hydroxy-methyl furfural (5-HMF) appears in significant quantities (up to 5 % original mass) in the HTC of pine, juniper, spruce, fir and sugarcane bagasse. Furfural appears in significant quantities (up to 4 % original mass) in woody materials, sugarcane bagasse, corn stover and rice hulls; and galactose, xylose and mannose are also present in pine and fir at 200 °C or below [268]. For the organic acids, at higher temperatures concentrations of acetic acid are around 8 % for many of the herbaceous and woody feedstock, with lactic acid the next most common acid, followed by formic acid succinic acid and glutaric acid [268].

Recently there has been growing interest in the potential utilisation for the process waters as their utilisation may offer yet more technical or economic advantages over conventional biomass processes. Recycling of these acids back into the HTC process has been suggested as organic acids have been shown to catalyse the reaction and can improve the yields at little or no cost [44]. Recycling the whole process water back into the reaction has been demonstrated in Stemann et al. [113], Weiner et al. [269], Uddin et al. [114] and Kambo et al. [115] and may even be one of the most efficient means of heat recovery [116]. Results presented in these studies have predominantly looked at the impact on yield and energy density of the resulting fuel. The studies overlooked the impact the alkaline metals, chlorides, sulphates and nitrogen based compounds initially extracted by the HTC process will have on the fuel's inorganic chemistry and the potential implications discussed in sections 2.5.1 and 2.5.2. Moreover as discussed in section 2.3.10 acids and salts can act as both catalysts and reagents in the process which will alter the process chemistry and the resulting product and detailed analysis of this is currently absent. Recycling would have the advantage of removing the need to treat waste process water although the issues associated with accumulation of extracted inorganics and heteroatoms would need to be addressed.

Alternative suggestions have been to recover and purify the organic acids, sugars and 5-HMF [115], although the feasibility of doing this has yet to be demonstrated. Some caution is however needed, as recovery of sugars, 5-HMF and other furfural compounds is likely to have a significant impact on fuel quality. As discussed in section 2.3.2 it is the generation of oligosaccharides, monosaccharides and aldehydes derived from the hydrolysis of hemicellulose, cellulose and starch which then undergo dehydration and fragmentation processes giving rise to different soluble products, such as furfural-like compounds and HMF related compounds, 1,2,4-benzenetrol, acids and aldehydes. It is these decomposition products which then undergo polymerization and condensation leading to the formation of the soluble polymers which then repolymerise and condense to form the hemicellulose, cellulose and starch derived component of the bio-coal [85, 86]. By removing these products it is likely to have an adverse influence on the char formation which will lower fuel yield and fuel quality. Consequently while HTC does produce many 'high value' products, these same 'high value' products are the same products which go on to repolymerise and form the char. The idea of producing both appears less likely as the processes appear diametrically opposed and to obtain the sugars, 5-HMF and other furfural compounds it appears likely one would have to inhibit repolymerisation.

Removal of organic acids may be more feasible as unreacted 5-HMF and furfural-like compounds appear to decompose to products such as levulinic acid [128, 270]. While these acids go on to generate hydronium ions which go on to catalyse the further degradation of the oligosaccharides generated from the hydrolysis of the hemicellulose and cellulose to monosaccharides [84], they appear to play little further role in char formation and their extraction may not have too adverse impacts on char formation.

In Lynam et al. [44] it was suggested that extraction of specific compounds followed by recirculation of the remaining product could be possible and this point made again in Kambo et al. [115]. These papers however make the assumption that the products will remain the same when recycling which would not be the case, for example organic acids which have been shown to catalyse the reaction, so the products will be different to the products of the first cycle. Moreover accumulation of acids and salts within the process water have been shown to favour formation of low molecular weight compounds [128, 142] and even the production of hydrogen gas [128]. With the production of hydrogen gas and smaller acids such as formic acids it may be possible that the organic acid chemistry may change with the formation of products such as valeric acid; valeric

acid being a product of the hydrogenation of the levulinic acid, by either hydrogen or formic acid [271]. While this is not an argument against the extraction specific compounds followed by recirculation of the remaining product, caution is required as the impacts of doing this appears unknown.

The other main area receiving a lot of interest of late is the anaerobic digestion or fermentation of the aqueous co-product as a potential route to optimise energy recovery, with the bulk of the literature focusing on the production of methane. Anaerobic digestion (AD) of the organic compounds within the aqueous phase resulting from HTC has been suggested in various reports as a potential route to optimise energy recovery. The degradation of complex organic matter during the HTC process to organic acids, particularly formic acid and acetic acid, should enable relatively fast degradation, providing the absence of inhibition [272]. When first undertaking this research literature with relation to integration of HTC and AD was predominantly but not exclusively limited to Wood et al. [273], Wirth and Mumme [272] and Danso-Boateng et al. [274]; based on this information the biological methane production (BMP) tests were developed and utilised in Smith and Ross [259].

Wood et al. [273] undertook BMP tests on process waters derived from the HTC of corn silage derived at 220 °C and 240 °C and compared it to the digestibility of thin stillage (the aqueous product derived from the fermentation of corn silage). The investigation looked at using chemical oxygen demand (COD) and compared actual methane yields to the yields predicted by COD. COD essentially expresses the amount of oxygen required to oxidise organic carbon to carbon dioxide and due to stoichiometry is directly proportional to the potential for methane production. Results generally showed that 83% of the initial COD was converted into methane; compared with 91 % for thin stillage, indicating good digestibility. Wirth and Mumme, [272] has demonstrated AD of process waters from the HTC of corn silage, comparing their results to the process waters Total Organic Carbon (TOC) demonstrating BMP in the region of 0.5-1 L methane per gram of TOC. Danso-Boateng et al. [274] looked into the HTC of sewage sludge with integration of AD to optimise energy recovery. In this paper, BMP can also be calculated by using the Buswell equation, given in Equation 2.16, with methane yields based off the elemental content of the process waters.

$$C_aH_bO_cN_d + ((4a-b-2c+3d)/4)\ H_2O \rightarrow ((4a+b-2c-3d)/8)\ CO_2 + ((4ab+2c+3d)/8)\ CH_4 + d\ NH_3 \quad (2.16)$$

Subsequent to the data published in Smith and Ross [259]; Wirth et al. [275] investigated the use of process liquor from HTC of sewage sludge (200 °C with a holding time of six hours) as sole substrate for AD in both mesophilic (37 °C) and thermophilic (55 °C) digesters operated for 20 weeks. During operation, the organic loading rate was stepwise increased from 1 to 5 grams COD L^{-1} d^{-1} and the hydraulic retention time decreased from 34 to 5 days. Significant differences in methane production were not observed as both reactors yielded up to 0.18 litres CH_4 grams COD^{-1}. Increased temperature had no effect on yield with both reactors yielding 68–75% of predicted yield based on COD. Methanogenesis was identified as the speed-limiting step in anaerobic digestion of HTC liquor. Nyktari et al. [276] went on to experimentally validate the integration of HTC and AD of sewage sludge presented in Danso-Boateng et al. [274], demonstrating a 92 % reduction in COD in the AD fermentation of process waters generated at 240 °C. The hydraulic retention times of the liquid was however either 21 hours or 42 hours, which does however rise the question of whether methane is being produced. Given the work presented in Wirth et al. [275] found that methanogenesis was the speed-limiting step in anaerobic digestion of HTC liquor, this result is surprising.

In AD one of the first stages is hydrolysis or acidogenesis as it is sometimes described, whereby the organic matter is broken down to acids such as butyric acid or acetic acid and in the process hydrogen is evolved. Methane production (methanogenesis) is a delayed second stage of a two stage process [277-280], with inhibition of the second stage possible though volatile fatty acid production by acidogenesis or organic acids derived from heat treatment [280]. Given that hydrolysis / acidogenesis was of an order of magnitude faster than methanogenesis in Wirth et al. [275], it appears plausible that the gas production was hydrogen in the case of Nyktari et al. [276].

Aragón-Briceño et al. [281] investigated the BMP of the aqueous product from the HTC of sewage sludge AD digestate, which has high organic matter content despite initial conversion into biogas. Three different temperatures were evaluated: 160 °C, 220 °C and 250 °C all using 30 min reaction time. The hydrothermal treatments improved the characteristics of the sewage digestate producing bio-coals and process waters rich in organic matter and nutrients. AD was demonstrated to be a suitable option to treat process waters from hydrothermal treatments for further biomethane production. Processing of digestate at 250 °C resulted in a bio-coal that enhanced the net production of volatile fatty acids but on the BMP tests limited methane production was observed until 14 days and methane was still be produced when the experiment ended at 21 days, consequently

higher methane production would be expected. Theoretical methane yields were also compared with experimental data from BMP tests and it was found that the Boyle's equation had closer agreement to BMP values.

Nuchdang et al. [282] also looked into the HTC of AD digestate, in this case digestate from microalgae treated at 200 °C with no retention time. In this instance, the aim of the treatment was not to produce a fuel but to treat the digestate and then re-digest it to enhance methane yield and while reducing the remaining solid mass (char). Their logic was if you assume 50 % of the algal biomass without pre-treatment digests to produce methane you would get 250 Nm^3 CH_4/ dry ton, with 0.5 dry ton of digestate. Applying hydrothermal treatment to that digestate and recycling the hydrothermal product to the primary AD would produce another 100 Nm^3, i.e. an overall methane yield improved by 40%, based on the results presented and hand halving the digestate mass (now bio-coal) requiring disposal.

Villamil et al. [283] investigated the mesophilic anaerobic digestion of the liquid fraction from hydrothermal carbonisation (208°C for 1 h) of dehydrated sewage sludge. In the investigation the process water was found to have a high COD of 96 g L^{-1} and along with high total nitrogen of 8.7 g N L^{-1} (Total Kjeldahl Nitrogen). Yields of 180 mL CH_4 STP g^{-1} COD was obtained, however high levels of inoculum compared to process water were required (>1:1) as low (≤ 0.5:1) were found to negatively affect the methane yields due to inhibition of methanogensis due to the high ammonia nitrogen and high volatile fatty acid release. It was also found that high levels of COD (>25 g COD L^{-1}) also brought about inhibition. Until Villamil et al. [283] few authors have touched upon the potential issues with inhibition.

Inhibition has been known to be an issue with the mildly alkaline conditions, presence of alkali cations, heavy meals and the presence of ammonia potentially inhibiting methanogenic bacteria [284, 285]. There are also a number of organic compounds which have been reported to be toxic to the anaerobic processes include long chain fatty acids (LCFAs), phenol and alkyl phenols, and alcohols [286]. Given alkali cations are known to be present within the process waters and the formation of recalcitrant or inhibitory compounds such as furfural, phenols and furan may occur during the hydrothermal process [287], inhibition appears a likely issue with the AD process. Consequently the AD route may favour alternative carboxylate routes such as hydrogen or ethanol production [288].

3. Methodological Development

This following chapter contains detailed information on the equipment and analytical techniques used and developed while undertaking this thesis. Based on the results and experience methodology was continually reviewed and developed throughout this work, albeit individual data sets are constant. Due to the methodology evolving as the thesis developed, each chapter contains a concise methodology for the data presented within that specific chapter.

3.1. Sample preparation

Specifics with regard to sample processing and materials processed are given in each individual chapter. These specifics include the origin of the feedstock and the size at which the material is processed. The following descriptions however detail specific methodologies common to all processes.

3.1.1. Retsch SM300 cutting mill

Most feedstocks were typically homogenised in a Retsch (Germany) SM 300 cutting mill before processing, albeit in some cases further size reduction was required in advance, in order to fit into the gravity feed. In most applications, a 4mm mesh sieve is used at the base of the cutting rotor. The 4 mm will give a size range typically give a particle size range suitable for hydrothermal processing; with particles typically 0.5 mm to 2 mm in diameter. Further size reduction to <100μm, a size where a fuel is generally considered homogenous, has shown to produce very reactive hydrothermal conditions with high levels of gas generation and thermal overrun. When undertaking further analytical work (e.g. thermo-gravimetric analysis of feedstock) further processing using a cryomill is typically required to achieve a particle size of <100μm, at which point the sample is homogenous and representative. In order to do this sub-sampling is required.

3.1.2. Sub-Sampling

Once the sample has been processed in the Retsch cutting mill, the sample is typically sub-sampled using an 18 chute riffle box (Pfeuffer, Germany). The riffle box works by adding a heterogeneous sample into the top part of the box. The sample is then divided across the 18 opposing inclined chutes. These chutes divide the sample into two half lots. One-half is discarded and the over half can be subsequently divided until the desired sample mass is achieved. A schematic of the process is given in Figure 3.1.

When processing bio-coals riffle box splitting is often not appropriate as the sample mass is typically small (approx. 50 grams for 250°C bio-coals). In this instance

coming and quartering is typically used, which is a method used to reduce sample size without creating a sampling bias. The technique involves pouring the sample so that it takes on a conical shape, and then flattening it out into a cake. The cake is then divided into quarters; the two quarters which sit opposite one another are discarded, while the other two are combined and constitute the reduced sample. The same process is continued until an appropriate sample size remains. A schematic of the process is given in Figure 3.2.

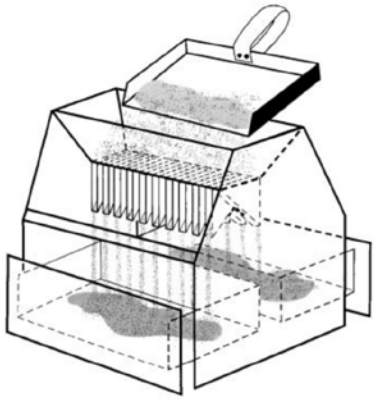

Figure 3.1. Chute riffle box schematic taken from Gerlash et al. [289]

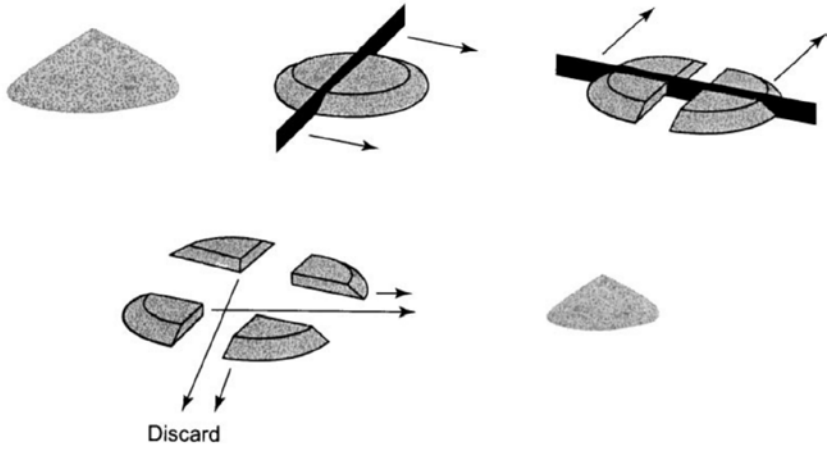

Figure 3.2. Coning and quartering, schematic taken from Gerlash et al. [289]

3.1.3. Retsch cryomill

The Retsch cryomill is a reciprocal impact /ball mill that is capable of cryogenically cooling biomass in the mill to -196 °C by cooling the ball mill enclosure. This is achieved by a continual feed of liquid nitrogen into a jacked surrounding the mill, avoiding any direct contact between the nitrogen and the biomass. By freezing biomass it becomes brittle and on impact with the ball baring and the mill casing the biomass undergoes attrition, without heating which can release volatile material. For biomass such as *Miscanthus*, the fibrous nature of the material means it has high resistance to milling

and it becomes challenging to grind a whole sample to <100µm, at which point the sample can be regarded as homogenous and representative in quantitative analysis. The Retsch cryomill has a capacity of 50 ml and can process up to 20 ml of biomass per cycle (approximately 10 grams). Once milled the samples were passed through a 100µm sieve and any parts too large were re-milled in the cryomill. The Cryomill is also capable of operating as an impact mill without liquid nitrogen at room temperature and consequently in this work it is utilised as a 50 ml ball mill in addition to a cryomill.

3.1.4. Retsch AS 200 vibratory sieve shaker

Retsch AS 200 sieve shakers were utilised to aid separation of the samples to the required size fractions. The shakers work by stacking a series of sieves in increasing mesh size and then oscillating at a set frequency for approximately 10 minutes. During this time, the size fractions are separated by gravity. Typical size fractions include <100 µm for thermogravimetric analysis, acid digestion, proximate and ultimate analysis. <1180 µm, <600 µm and <75 µm was used when undertaking the Hardgrove Grindability Index.

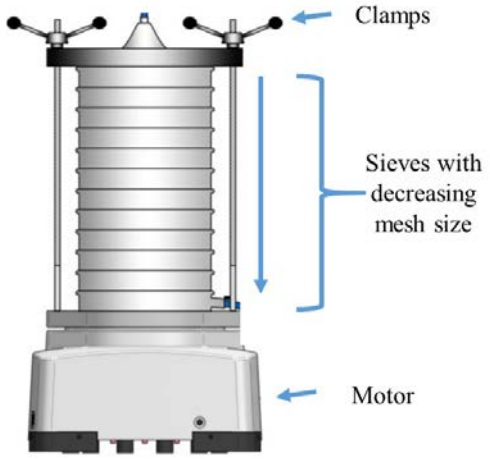

Figure 3.3. Vibratory sieve shaker schematic

3.2. Hydrothermal carbonisation

3.2.1. 600 ml Parr reactor

HTC was performed in a bench top reactors Parr (USA) reactors at 200 °C and 250 °C using a 10 % solids loading. Initial work was undertaken in a non-stirred, 600 ml, 4560 series reactor constructed in 316 stainless steel, using PTFE gaskets a schematic of the reactor is given in Figure 3.4. This reactor has a maximum temperature of 350 °C and a rated pressure of 200 bar. The reactor had been constructed in 2005 and had undergone modification by previous users, which included removal of the stirrer assembly and inbuilt cooling loop.

Temperature was controlled via a Parr 4836 temperature controller and an 1100 watt Parr ceramic fibre heating mantle. The temperature controller used a Proportional Integral Derivative (PID) heat controller, which was periodically recalibrated at 200 °C and 250 °C using the built in 'autotune' function. The PID temperature controller was attached to the central J-type thermocouple. Under typical conditions, the reactor is heated to the desired temperature at approximately 8 °C minute^{-1} and the reaction temperature held for one hour. After one hour the reactor was removed from the heating mantel and allowed to air cool to room temperature (approximately 2 ½ hours from 200 °C; three hours from 250 °C).

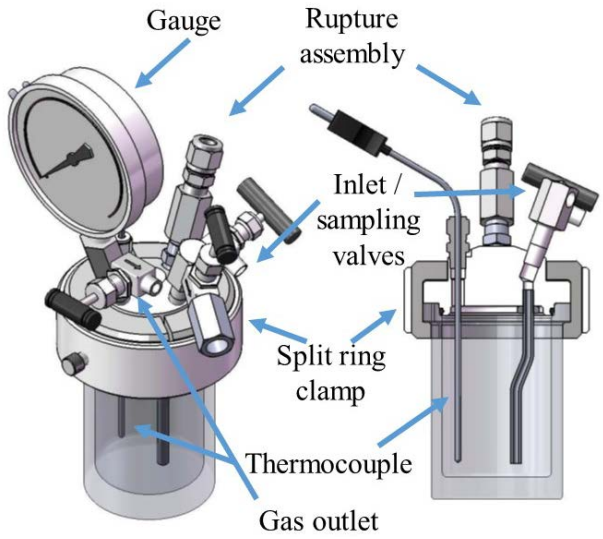

Figure 3.4, Schematic of 600 ml Parr reactor with pressure gauge and gas outlet removed in cross section.

During runs in the 600 ml Parr reactor a solid loading of 24 grams of biomass and 220 ml of water was used, which gives a 10% solid loading. This sample volume was decided based on previous experiments for HTL operating at 350 °C. At 350 °C water volume has expanded 73%, when compared to room temperature [290] and consequently this volume was calculated as the safe operation volume using Equation 3.1 and using data presented in Table 3.1. Due to pervious work at 300 °C and 350 °C the reactor loading was maintained at 24 grams of biomass and 220 ml water for consistency at 200 °C and 250 °C runs. The 600 ml Parr reactor was operated at isobaric pressures of 16 bar and 40 bar respectfully and the reactor pressure achieved through steam evolved as the reactor heats.

$$\text{Maximum Allowable Volume Loading} = \frac{(0.9*[\text{vessel volume}])}{(\text{Expansion Factor})} \quad (3.1)$$

Table 3.1: Thermal properties of water at elevated temperature

Temperature (°C)	Partial Pressure of Water (bar)	Specific Weight of Water (l) g/ml	Expansion Factor*
25	1.0	1.000	1.00
200	15.6	0.864	1.16
210	19.1	0.853	1.17
220	23.2	0.840	1.19
230	28.0	0.827	1.21
240	33.5	0.814	1.23
250	39.8	0.799	1.25
260	46.7	0.784	1.28
270	55.1	0.768	1.30
280	64.2	0.751	1.33
290	74.5	0.732	1.37
300	85.9	0.712	1.40
350	165.4	0.574	1.74

Expansion Factor = (1/ Specific Weight of Water)

In the initial work presented in Chapter 4, the gas product was released to the atmosphere (once cooled) and the solid and liquid products separated by filtration under gravity using 150 mm grade 1 qualitative circles (Whatman, UK) and a stemmed funnel. The sample was not washed in water or organic solvent and the bio-coal was air dried in a ventilated fume cupboard for a minimum of 48 hours.

For the work presented in Smith and Ross [259], the 600 ml Parr reactor method was adapted slightly with the incorporation of a 4.2 kg, 0.01g balance (ME4002, Mettler Toledo, Switzerland), enabling the reactor to be weighed before heating. When cooled, the reactor was depressurised into a gas sampling bag for gas analysis and the reactor reweighed to calculate gas and moisture loss along with the remaining combined mass of process water and bio-coal. The solid and liquid products were separated by filtration under vacuum using a 110 mm Buchner funnel and 110 mm qualitative circles (Grade 15, Munktell, UK). The process water was then stored and the reactor and char rinsed with a known volume of distilled water to recover any remaining sample. The bio-coal was allowed to air dry in a ventilated fume cupboard for a minimum of 48 hours. Mass of the recovered process water was calculated by subtracting the dry mass of bio-coal from the combined mass of process water and bio-coal.

3.2.2. 2000 ml Parr reactor

Following the seaweed work, a 2000 ml, 4622 series reactor constructed in 316 stainless steel, using PTFE gaskets was commissioned. This was done in order to increase the processing volume capability due primarily to high volumes of ash required for analysis and the low ash content of lignocellulosics. Temperature was controlled by a Parr 4838 temperature controller and heat supplied by a 1500 watt Parr calrod heating mantle. Temperature was controlled by a PID temperature controller, which was periodically recalibrated at 200 °C and 250 °C using the built in 'autotune' function.

Due to the mass of the reactor, Pyrex liners (399HC) were used, which can be removed with process water and solids contained within. These liners were weighed before and after the runs to give mass before and mass after minus gas loss. The Pyrex liners reduced the internal volume to 1700 ml, which gives a maximum safe operating volume of 1225 ml based on Equation 3.1. For consistency 96 grams of biomass and 880 g of water was used, giving a 10% solid loading. Due to the potential for thermal overshoot, an upper temperature limit of 260 °C, was programmed into the PID controller which isolated power to the heater is this temperature exceeded 260 °C or in the event of a 'loss of signal' from the thermocouple. Based on 260 °C a combined reactor loading of 1150 ml was imposed when operating at 250 degrees and using Pyrex liner. A schematic of the original reactor is given in Figure 3.5.

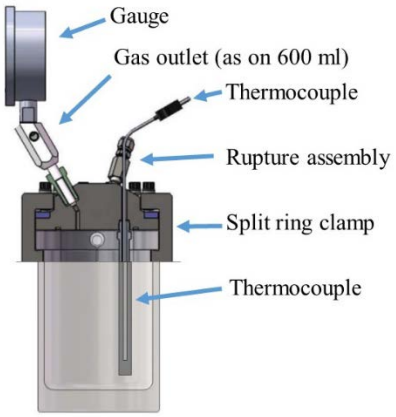

Figure 3.5 Unmodified 2000 ml Parr reactor

3.2.2.1. 2000 ml Parr reactor modification

Reactor commissioning revealed issues with thermal inertia when heating, with significant lag between heating the reactor and the response on the thermocouple, leading to significant thermal overshoot even when the reactor is calibrated using the 'autotune' function. To overcome this the thermowell (265HC7), which is standard on this reactor,

was removed and replaced with a 3 mm mineral insulated thermocouple enabling intimate contact between the thermocouple and the reaction media. To seal the reactor a parallel 9/16-18 male to ¼" tube stub fitting (Swagelok, USA) was used to seal the tread of the pervious thermowell and a ¼" to 1/8" tube union connector (Swagelok, USA) to connect the ¼" tube fitting to the thermocouple. To ensure a pressure tight seal the 1/8" union ferrules were replaced for 3 mm ferrules, supplied by Swagelok for this purpose.

A second thermocouple was added to sit between the Pyrex liner and the inner side of the 316 steel reactor. This thermocouple was fed though a second previously 'blanked' port in the reactor head. This was sealed using 1/8" male NPT thread to ¼" tube stump fitting (Swagelok, USA) into the reactor head. The ¼" tube stump goes into a ¼" union tee (Swagelok, USA) with a piezoelectric pressure sensor (PXM309-200G10V, Omega, UK) fitted to the 90° branch. The piezoelectric pressure sensor was connected via a ¼" female BSPP thread fitting to ¼" tube stub (Swagelok, USA) and sealed using Klinger SIL C-4400 gasket. The 180° branch was connected to a second ¼" union tee (Swagelok, USA), connected by a ¼" port to ¼" tub stub port connector (Swagelok, USA). The 90° branch of the second tee was connected by a ¼" port to ¼" stub port connector to a ¼" port to ¼" port needle valve (Swagelok, USA) to enable the reactor to be pressurised with different head gasses and to enable purging. The 180° branch on the second was connected to a ¼" port to 1/8" BSPT thread female connector, joined by a ¼" port to ¼" stub port connector, with a 50 cm, 0.5 mm J-type thermocouple sealed in via a Spectite (UK) PF-1/8"BSPT-0.5-L assembly. All fixings and fittings were in 316 stainless steel with tapered threads sealed with PTFE tape. Parallel threads were set with N-5000 nickel anti seize compound (Loctite, Germany).

The 0.5 mm J-type thermocouple fitted snugly between the Pyrex liner and the inner side of the 316 steel reactor, with this thermocouple used as the feedback thermocouple for the Parr 4838 temperature controller. The 3mm J-type thermocouple was positioned central within the reactor and taken as reaction temperature. Data from this thermocouple was logged via a Pico-Logger TC-08 (Pico Technology, UK) and PicoLog data logging software. Readings displayed in real time on a PC monitor. This setup overcame issues with thermal lag and thermal inertia, however a high failure rate of the mineral insulation on the 0.5 mm J-type thermocouple meant this design was revised and replaced for a 3mm J-type thermocouple, with the measurement tip in contact with the inside of the Pyrex liner. This setup gave good and stable temperature control once at temperature and was highly reliable.

While stable temperatures were achieved once heated, this setup did not overcome the issue with temperature overshoot. Observations however showed that by monitoring changes in pressure within the reactor it was possible to accurately gauge equilibrium points at which the heat within the reactor and the heat going into the reactor are matched as this gives a continuous and stable pressure. A stable pressure would indicate a stable temperature would soon be reached. The piezoelectric pressure sensor (PXM309-200G10V, Omega, UK) added as part of the reactor modifications was connected to a voltage logger (OM-CO-VOLT101A-15V, Omega, UK), with a 24 v DC bias. The pressure sensor works through resistance being directly proportional to pressure exerted, consequently change in voltage is directly proportional to chance in pressure. The voltage logger is then interphases though an OM-CP-IFC200 data logger interphase (Omega, UK) and changes in pressure and time are logged in real time on a PC monitor, along with temperature as previously discussed. Periodic calibration of the piezoelectric pressure sensor was undertaken by pressuring the reactor in argon using a 145 series piston regulator (Paxair, USA) capable of delivering pressure from 0 – 230 bar. The reactor was pressurised and the logged voltage taken every 10 bar, using the reactor primary gauge pressure (Wika, USA). Using this data, a regression equation was calculated using least squares and used to display pressure on PC screen.

To achieve a stable temperature and pressure it was found that for a 250 °C run, setting the PID controller would be typically set at 230 °C and on heating would typically bring about a 20 °C overshoot (thus 250 °C). By monitoring pressure during this overshoot, it was possible to gauge when the temperature within the reactor was stabilising due to stabilisation of pressure. At the point the pressure stops increasing, temperature could then be set at 250 °C on the PID controller and the PID controller should then be able to indefinitely maintain that temperature. For 200 °C the PID controller would typically be set at 170 °C.

Reactor heating behaviour did however appear to be feedstock specific, with overshoot typically associated with samples that result in increased gas production (e.g. high cellulose feedstock). This would be due to the generation of gas reducing the latent heat requirement, required to generate steam, which self-pressurises the reactor. It was also found by pre-pressuring the reactor using an inert gas substantially increased heating rate and enabled more stable temperature during operation. This will be due to the reduced steam requirements during self-pressurisation lowering latent heat requirements during heating. A heating rate of approximately 5 °C minute^{-1} is achieved when pre-pressurising

with 5 bar argon. Heating rates of 20 °C minute^{-1} can be achieved using the 600 ml reactors, using 5 bar argon. Argon was chosen as the principle head gas due to; (i) its use as the carrier gas in a GC-TCD commonly used for permanent gas analysis; (ii) nitrogen, a common inert gas used in hydrothermal research is a heteroatom of interest; (iii) its critical pressure of 49 bar is higher than nitrogen and helium; and (iv) it has good insulating properties.

Five bar argon will reduce the amount of steam generated but not replace it outright. In order to avoid steam generation it was calculated that an initial pressures of 7.6 bar and 14.1 bar of argon would be required to achieve the isobaric pressures of 16 bar and 40 bar for 200 °C and 250 °C respectively. This takes into account the thermal expansion of the gas and water. A schematic of the modified 2000 ml Parr reactor is given in Figure 3.6.

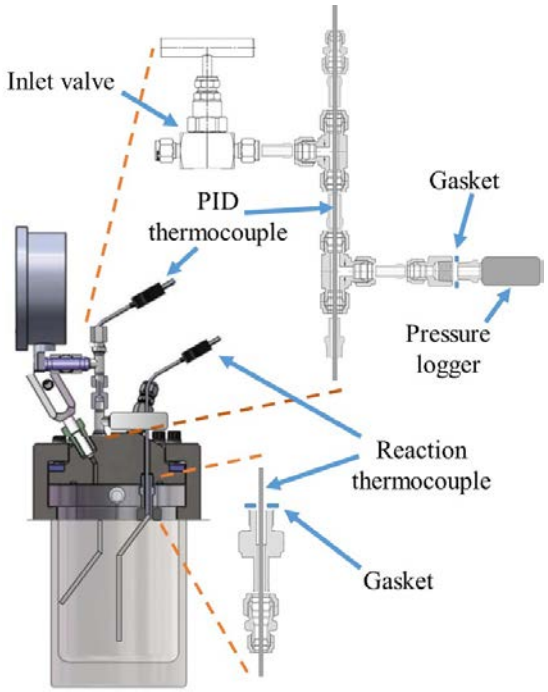

Figure 3.6. Modifications to 2000 ml Parr reactor

3.2.2.2.2000 ml Parr reactor operating procedure

When operating the reactor, the Pyrex liner, mass of biomass and mass of water was weighed before loading the reactor. Once loaded the reactor was sealed and cleared of air via a vacuum pump (RV8, Edwards, UK) via the gas outlet valve on the pressure gauge assembly. The reactor was subsequently flushed with argon via the inlet value, shown in Figure 3.6 via a 145 series piston regulator (Paxair, USA): the reactor was subsequently cleared and refilled twice before each run to remove residual air. When

clearing the reactor of air, a vacuum was applied until a constant pressure was displayed on the pressure logger.

Once cleared of air the reactor was pressurised to five bar and the reactor typically left for 30 minutes logging pressure prior the run. In this time the internal pressure will stabilise and become constant. The pressure logger is very sensitive and if pressure continues to decrease there is likely a leak that needs to be resolved prior operation. Following a satisfactory pressure check, the reactor pressure is taken and the reactor heated to the desired temperature. The thermocouple located in the centre of the reactor (reaction thermocouple in Figure 3.6) is connected to the Pico Logger, with temperature continually displayed and plotted on a PC monitor. This temperature is taken as reaction temperature. Hold times started when the desired temperature was achieved on this 'reaction' thermocouple. After the desired hold time (typically one hour) the reactor was removed from the heating mantel, and allowed to air cool to room temperature (approximately three hours from 200 °C; 3 ½ hours from 250 °C).

When cooled, the reactor pressure was noted along with the corresponding reactor temperature so that reactor pressures could be calculated as room temperature equivalent and directly compared. Reactor gas was subsequently depressurised into a gas sampling bag (Saint Gobain, France) fitted with a 3 way ball vale (Swagelok, USA) for gas analysis. Once opened the Pyrex reactor liner and contents was reweighed and any additional moisture on the reactor quantified using pre-weighed tissue paper. The solid and liquid products were separated by filtration under vacuum using 110 mm qualitative circles (Grade 3, Whatman, UK). Remaining solid sample in the Pyrex liner was recovered though repeated rinsing of the liner with the process water until the liner was clear of char.

The process water yield was subsequently calculated by subtracting the starting mass of the liner and the wet char from the post-run mass of Pyrex reactor liner and contents. The gas yield was taken as the starting mass of the liner and contents minus the mass of the liner and contents plus the mass of moisture recovered from the reactor.

In interest of safety the reactors were operated with rupture disk assemblies (Fike, USA), which was connected by flexible ¾" stainless steel tubing into the ventilation ducting. In the event of the reactor over-pressurising and the assembly rupturing, the steam and reactor content would be safely diverted by this stainless steel into the ducting as opposed to the laboratory. The reactor was operated in fume cupboard with the sash closed to prevent steam entering the laboratory in the event of a gasket or component

failure. Heating controls were located outside of the fume cupboard. Due to the high pressures encounters during some experiments the rupture assembly on the 2000 ml Parr reactor was upgraded from 1000psi to a 2000 psi Inconel rupture assembly (Fike, USA). This pressure is still within the rated pressure of the reactor; following upgrade of the pressure gauge (Wika, USA).

The Inconel steel appears to become brittle after prolonged exposure to chlorine, which can result in failure below rated pressure. Consequently, periodic replacement of the rupture disk was adopted as part of routine maintenance. Routine maintenance included, calibration of heaters using the 'autotune' function and calibration of pressure sensor. In addition to the routine maintenance and pre-run pressure testing, the reactor was subjected to annual hydrostatic pressure test (Craftsman Tools, UK) to ensure integrity of the reactor and additional components added.

3.3. Proximate analysis

The proximate analysis gives an understanding of the fuel composition in terms of the moisture, volatile, fixed carbon and ash content and can be used to help determine the bio-coals equivalent coal rank [64, 291].

3.3.1. Moisture Content

For moisture content an adapted method of BS EN ISO 13134-1: 2015 was used, where by moisture was determined using an oven dry method at 105(±2)°C under a stream of nitrogen in a specially designed moisture oven (Carbolite, UK) for one hour. Samples were dried in glass dishes with a maximum loading of 1g /cm^2. In a divergence to BS EN ISO 13134-1: 2015 a sample mass of 300 grams was not used, instead a mass closer to 3 grams for the bio-coals was used in addition to a laboratory balance accurate to 0.005 mg (Mettler Toledo, Switzerland), where the analytical standard requires a balance accurate to 0.1 g. In another divergence from BS EN ISO 13134-1: 2015, samples were removed from the sampling oven and allowed to cool in a desiccator prior to weighing.

Moisture determination via thermogravimetric analysis appeared less repeatable and consequently moisture values stated in this work are determined via this oven dried method. Likewise, ultimate analysis results presented on a dry basis were calculated based on this oven dried method. For all samples, a minimum of two determinations was undertaken.

3.3.2. Ash Content

Determination of fuel ash content was determined in accordance with BS EN ISO 18122:2015. The methods state that ashing should take place at 550 °C but also gives specific heating conditions. These conditions state that the sample should be heated from room temperature at an even heating rate to 250 °C at a heating rate of 5 °C min^{-1}. Once 250 °C is achieved, this temperature should be maintained for a minimum of 60 minutes to allow the volatiles to leave the test portion before ignition. Following the 250 °C hold samples are heated to 550 °C at a heating rate of 10 °C min^{-1} and held for a minimum of 120 minutes.

The ash analysis was undertaken in a Nabertherm B80 furnace with a temperature programmable PID controller. Typically, samples were cooled to approximately 200 °C in the furnace before removal. Samples were cooled to room temperature in a desiccator prior to weighing. Ashing was undertaken in either alumina or porcelain crucibles. Care was taken not to exceed a sample loading of 0.1g cm^2 to avoid incomplete incineration or absorption of carbon dioxide by calcium in the top layer of the ash (forming calcium carbonate). Crucibles were pre-conditioned and samples were weighed on a laboratory balance accurate to 0.005 mg (Mettler Toledo, Switzerland). For all samples, a minimum of two determinations was undertaken.

3.3.3. Volatile and fixed carbon content

Determination of volatile and fixed carbon content is described in BS EN ISO 18123:2015 and uses a pre-heated ashing furnace hated to 900 (±10) °C, whereby the sample is devolatilised for 7 minutes. Because of the low fixed carbon yields and high volatile carbon contents of many of the starting feedstocks used in this work, proximate analysis of the chars by the conventional British Standard methods is challenging. Consequently determination of volatile and fixed carbon content was undertaken by thermogravimetric analysis (TGA) using a Mettler Toledo TGA/DSC1 and later work a Mettler Toledo TGA/DSC3. It is recognised that volatile matter measured via TGA may differ to that measured by the British Standard method, and so the results are only applied in a comparative way. The TGA method has additional advantages in it offers additional information, for example offering information on the temperature and rate of volatile release, reactivity and heat flow information, which overcome the “approximate” nature of the analysis.

The proximate analysis was carried out using a programmed method consistent on both the TGA/DSC1 and TGA/DSC3, with both instruments fitted with automated gas

switching boxes. The main difference between the two instruments being the furnace limit, with 1100 °C and 1500 °C limits for TGA/DSC1 and TGA/DSC3 respectively. Both instruments were fitted nitrogen with an inline super clean gas filter and oxygen trap (Restek, USA) on the nitrogen lines. The proximate analysis involved heating the sample in nitrogen atmosphere from 30 °C at a rate of 25 °C min^{-1} to 105 °C, with a 10 minute hold at 105 °C to remove residual moisture. The sample was then heated at 25 °C min^{-1} to 900 °C in a nitrogen atmosphere, where they were held at 900 °C for an additional 10 minutes to ensure full devolatilisation. After 10 minutes the atmosphere was switched to pure bottled air at 900 °C, which was held for an additional 15 minutes to enable complete combustion.

Samples were typically treated in 70 µl alumina crucibles annealed at 1100 °C (Mettler Toledo, Switzerland). It was however observed that when processing samples with high alkali metal contents the alumina became permeable to molten sodium and potassium. This could result in fusing of the crucible to the ceramic balance arm. 70 µl platinum crucibles, annealed at 1100 °C (Mettler Toledo, Switzerland), were subsequently used for high salt containing samples, using the same heating rate but a platinum cubicle method. A sample mass of 10 mg was used per run. Multiple proximate runs with differing masses are given in Figure 3.7. Differences between the first derivative thermogravimetric curves (DTG) indicate there is minimal thermal transfer issues during devolatilisation. The results do however suggest sample size does limit the rate of oxidation during combustion. Consequently a sample mass of 10 mg is needed for all samples when analysing reaction rates and comparing DTG profile.

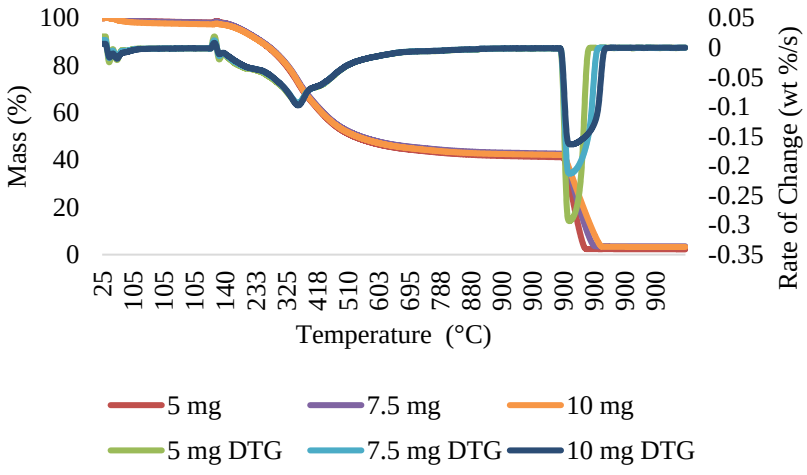

Figure 3.7, The first derivative thermogravimetric analysis of proximate runs at differing sample mass (5, 7.5 and 10 mg).

When analysing the proximate analysis, moisture was taken as the mass difference between the starting mass and the mass at the end of the 10 minute hold at 105 °C. Volatile matter was taken as the change in mass between the end of the 10 minute hold at 105 °C and the mass just before the point the atmosphere was switched to air at 900 °C. Residual material after 15 minutes at 900 °C should be the ash content of the fuel, when ashed at 900 °C. This is assuming complete combustion has occurred, as is the case in the example given in Figure 3.8. The difference between the mass just before the atmosphere was switched to air and the ash weight can be determined as the fixed carbon.

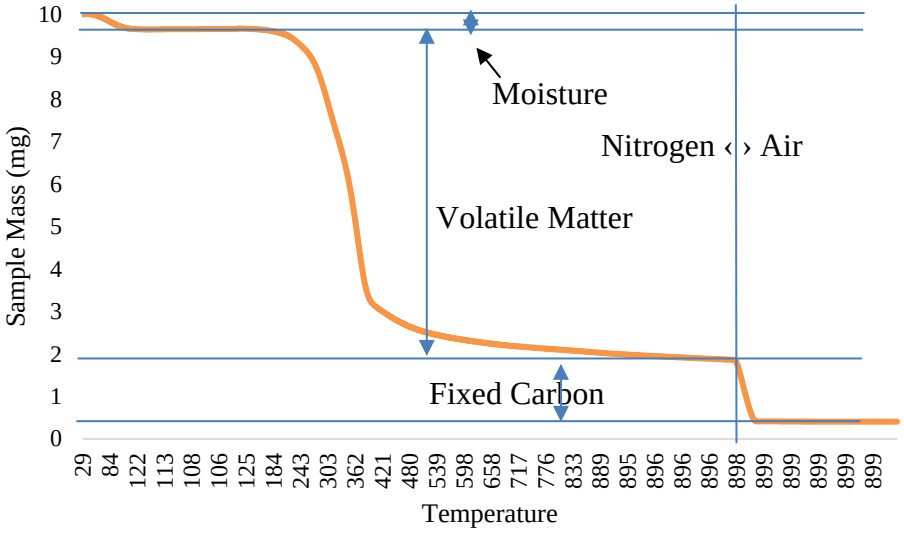

Figure 3.8, Proximate analysis of a unprocessed *Miscanthus* via TGA

Within this thesis, figures are given on a dry basis, unless otherwise stated. These values are determined following the method started in ASTM D3180-15 and following the definitions given in ASTM D3180-15 and respective formulae. These are as follows:

As-determined basis (ad) - analytical data obtained from the analysis sample after conditioning and preparation. As-determined data represents the numerical values obtained at the particular moisture level in the sample at the time of analysis. These values are normally converted, according to formulae 3.2-3.4 to conventional reporting bases.

As-received basis (ar) - analytical data calculated to the moisture condition of the sample as it arrived at the laboratory and before any processing or conditioning. If the sample has been maintained in a sealed state so that there has been no gain or loss, the *as-received* basis is equivalent to the *as sampled* basis.

Dry basis (db) - data calculated to a theoretical base of no moisture associated with the sample. The value obtained in accordance with BS EN ISO 18122:2015 is used for converting the as-determined data to a dry basis.

Dry, ash-free basis (daf) - data calculated to a theoretical base of no moisture or ash associated with the sample. Numerical values as established by Test Method D 3173 and Test Method D 3174 are used for converting the as-determined data to a moisture- and ash-free basis.

$$\text{As-received basis (ar)} = (100 - \text{Moisture}_{ar})/ (100 - \text{Moisture}_{ad}) \quad (3.2)$$

$$\text{Dry basis (db)} = 100 / (100 - \text{Moisture}_{ad}) \quad (3.3)$$

$$\text{Dry ash- free basis (daf)} = 100 / (100 - \text{Moisture}_{ad} - \text{Ash}_{ad}) \quad (3.4)$$

3.4. Ultimate analysis

Ultimate analysis is used to determine the carbon, hydrogen, sulphur, nitrogen, oxygen, ash and moisture contents of a fuel. The method to determine the ash and moisture were described above, while the carbon, hydrogen, sulphur, nitrogen and oxygen was determined using a CE Instruments Flash 1112 or a Thermo Scientific Flash 2000 Series elemental analyser. The specific instrument is stated in each chapter. Both analyses followed the methodology laid out in the British Standard BS EN ISO 16948:2015.

3.4.1. CHNS using CE Instruments Flash 1112

The calibration standards used to calibrate the CE Instruments Flash 1112 are: atropine, methionine, cystine, sulphanilamide and BBOT (2,5 Bis–(5–Tert-Butyl-Benzoxazol-2-yl)-thiopene) (Elemental Microanalysis, UK). Two standard reference materials were typically used; usually a reference coal, oatmeal reference or barley reference (Elemental Microanalysis, UK) depending on the expected carbon content of the fuel. These standard reference materials were run every 10^{th} sample as a control to check instruments performance. 2-3mg of calibration standard or fuel sample (in duplicate) were accurately weighed into small tin capsules (Elemental Microanalysis, UK) using laboratory balance accurate to 0.005 mg (Mettler Toledo, Switzerland) and crimped to remove any air.

Samples are loaded into the instrument via an auto sampler and the crimped sample capsule is loaded into a piston chamber and purged with helium to remove residual air. The samples then fall into a combustion reactor at 900 °C, along with an oxygen injection (10 seconds required for bio-coal combustion) to combust the sample. The combustion gases are transferred to a reduction tube / reactor primarily comprising of electrolytic copper and copper oxide at 650 °C via a helium carrier gas which ensures the combustion gases are converted to carbon dioxide, water, nitrogen and sulphur dioxide (e.g. nitrogen oxides are reduced to elemental nitrogen and carbon monoxide is converted

to carbon dioxide). These gases then enter a gas chromatography column where they are separated before being detected by a thermal conductivity detector (TCD). The TCD is among the most commonly used measuring devices for monitoring substances separated in a column. The detector measures a change in the thermal conductivity of the helium carrier gas caused by the presence of the eluted carbon dioxide, water, nitrogen and sulphur dioxide. Oxygen was calculated by difference. When dealing with samples suspected to contain sulphur vanadium pentoxide was used as an oxidising agent to aid combustion.

Results are given on a dry basis, as stated in BS EN ISO 16948:2015 and on occasion in terms of dry ash free. These values were determined following the method started in ASTM D3180-15 and the respective formulae are as follows:

$$C,N,S_{(db)} = C,N,S_{(ad)} *(100 / (100 – Moisture_{ad})) \quad (3.5)$$

$$H_{(db)} = (H_{(ad)} - (2 *(Moisture_{ad} /18))) *(100 / (100 – Moisture_{ad})) \quad (3.6)$$

$$O_{db}=100−C_{db}−H_{db}−N_{db}−S_{db}−A_{db} \quad (3.7)$$

3.4.2. CHNSO using Thermo Scientific Flash 2000

The Thermo Scientific Flash 2000 is essentially an updated CE Instruments Flash 1112 analyser. The instrument was however fitted with an additional reactor and column enabling the instrument to detect both CHNS (as above) and oxygen. CHNS was undertaken using the same reactor type as above although calibration was adapted slightly, with BBOT, oatmeal and barley flower typically used in duplicate as calibration standards as opposed to atropine, methionine, cystine, and sulphanilamide. This was done because it was observed using calibration reference materials, which match the samples being analysed, tended to give more repeatable results and tended to highlight issues with the instrument on calibration. Oxygen analysis was undertaken as a separate analysis consisted of 2-3mg of calibration standard or fuel sample into small silver capsules (Elemental Microanalysis, UK) and crimped to remove any air. Acetanilide and aspartic acid were used as the calibration standards with each standard used in duplicate. When analysing, every 10^{th} sample as a control standard consisting of atropine to check reactor performance.

It was found that when analysing low sulphur samples, analysis by BS EN ISO 16994-2 using an oxygen bomb (Parr, USA) and ion exchange chromatography (Dionex, USA) proved more appropriate, as the samples were often at or below the lower detection limit of the Flash 2000 instrument.

Oxygen analysis is similar to CHNS where by samples are loaded into the instrument via an auto sampler and the crimped sample is loaded into a piston chamber and purged with helium to remove residual air. The samples then fall into a pyrolysis reactor at 900 °C where any oxygen is emitted as carbon dioxide, carbon monoxide and water. The pyrolysis gases are transferred to a reactor primarily comprising of silica and nickel plated carbon at 650 °C via a helium carrier gas which then passes the gas though a soda lime and magnesium perchlorate adsorption filter. This ensures that all oxygen is converted to carbon monoxide. The gas then enter a gas chromatography column where they are separated before being detected by a TCD.

Results are given on a dry basis, as stated in BS EN ISO 16948:2015. These values were determined following the method started in ASTM D3180-15 and the respective formulae are as follows:

$$C,N,S_{(db)} = C,N,S_{(ad)} *(100 / (100 – Moisture_{ad})) \quad (3.8)$$

$$H_{(db)} = (H_{(ad)} - (2 *(Moisture_{ad} /18))) *(100 / (100 – Moisture_{ad})) \quad (3.9)$$

$$O_{(db)} = (o_{(ad)} - (16 *(Moisture_{ad} /18))) *(100 / (100 – Moisture_{ad})) \quad (3.10)$$

3.5. Determination of calorific value

The higher heating values of the feedstock and the fuels was determined by either Dulong's Formula for estimating higher heating value (HHV) or higher calorific value (HCV) as it is sometimes referred. Dulong's Formula is given as Equation 3.11 [292]. The values are based on the CHNSO data obtained using the methodology described in Section 3.4, above. HHV was also calculated using Parr (USA) 6200 bomb calorimeter and the results were found to correlate closely, validating Dulong's Formula for bio-coals. In this work the bomb calorimeter was primarily used as an oxygen bomb in order to undertake chlorine and sulphur analysis by BS EN ISO 16994-2016, as discussed in Section 3.6.7. Issues with the associated chiller did however bring about some erroneous data in Chapters 6 and 7. Consequently, in some sections HHV by bomb calorimeter has been omitted.

$$HHV (MJ/kg) = (0.3383*\% Carbon) + (1.422*\% Hydrogen) – (\% Oxygen / 8) \quad (3.11)$$

Lower Heating Values (LHV) (net calorific value) have also been calculated. The latter value taking into account the latent heat requirements for the water generated from the fuel bound hydrogen on a dry basis, and, the water within the fuel and fuel bound hydrogen on an as received basis. HHV assumes water vapour formed is condensed and this energy is recovered. Given in many combustion applications (e.g. coal power station)

the latent heat is not recovered and LHV is often the more significant value as it represents the overall energy available. LHV was calculated using Equation 3.12.

$$\text{LHV (MJ/kg)} = \text{HHV} - (2.442 * [\text{kg } H_2O \text{ in fuel} + \text{kg } H_2O \text{ from } H_2]) \quad (3.12)$$

Whereby:

$$\text{kg } H_2O \text{ in fuel} = \% \text{ Moisture(ar)}/1000$$

$$\text{kg } H_2O \text{ from } H_2 = (((\%H_{2(ar)}/1000)/2)*18)$$

$$H_{2(ar)} = H_{2(db)} *((100- \text{Moisture}_{(ar)})/100)$$

3.6. Inorganic and heteroatom analysis

With the exception of oxygen and nitrogen, quantitative determination of inorganic and heteroatom elements within the fuel involve the extraction of the elements on interest from the fuels matrix into a media in which they can be determined. For many of the methods discussed in the following section this involves completely transferring the analyses into a solution via acid digestion. This is however not exclusive as for substances which do not normally dissolve in acids can also be detected though ashing and then determined using quantitative techniques using x-ray fluorescence. This section discusses the methods and method development undertaken during this work.

3.6.1. Acid digestion

Acid digestions are employed to determine elements in a solid sample by completely transferring the elements of interest into solution so they can be determined in liquid form (for example by AAS or ICP-MS), while avoiding loss or contamination of the analyte. For biomass and biofuels acid digestion involves the decomposition of organic material and to achieve this an oxidising acid is required. Nitric acid (HNO_3) is typically used as, unlike other common acids such as hydrochloric acid (HCl), hydrofluoric acid (HF) and sulphuric acid (H_2SO_4), it's an oxidising acid and can decompose organic material as shown in Equation 3.13. In order to oxidise using the non-oxidising acids, oxidising agents are required, typically hydrogen peroxide (H_2O_2), which offers oxidation potential though decomposition, as shown in equation Equation 3.14 or though combination with nitric acid, as used with aqua regia, which is 3:1 hydrochloric acid and nitric acid.

$$(CH_2)n + 2HNO_3 \rightarrow CO_2 + 2NO + 2H_2O \quad (3.13)$$

$$2\ H_2O_2 \rightarrow 2H_2O + O_2 \quad (3.14)$$

Hot concentrated nitric acid (68 % w/w) is an oxidising acid and dissolves most metals [293] and was used to digest the samples in Chapter 4, with digestion undertaken

in an Anton Paar (USA) Multiwave 3000 microwave digester using quartz reactors. Microwave digesters use high frequency microwaves, high temperatures and increased pressure, as offered by the microwave digestion vessel to aid sample dissolution [293]. When undertaking acid digestion using the Multiwave 3000 microwave digester approximately 0.2 grams of sample was accurately weighed to four decimal places and added to the quartz reactor vessels, with mass taken by difference (mass of sample minus mass of sample left on weighing boat). 10 ml of nitric acid was then added to the digestion vessel and loaded into the microwave. The samples were then heated using 700 watts to 280 °C and 80 bar pressure over a period of 15 minutes. The temperature and pressure was then held for 45 minutes. After 45 minutes the samples were cooled and depressurised. Once cooled the samples were transferred into clean 50 ml volumetric flask and the digestion vessel thoroughly rinsed using a wash bottle containing ultra-high purity deionised water (Elga, UK) and a rubber policeman, to ensure full recovery of the analyte. Once clean the volumetric was made up to the meniscus line and the sample stored for analysis in 50 ml centrifuge tubes (LabCon SuperClear, USA). Acid blanks were also prepared alongside the digestion standards to assess contamination of the analyte.

While hot concentrated nitric acid dissolves most metals it does not form soluble nitrates with: gold, platinum, aluminium, boron, chromium, titanium and zirconium, nor does it break down silicon. It was also observed that the nitric acid digestions sometime left a white precipitate, which is believed to be a calcium aluminium silicate complex. Consequently, an alternative acid digestion method was developed using hydrofluoric acid, with the aim to volatilise the silicon. This enables full quantification of calcium and aluminium.

Hydrofluoric acid dissolves glassware so digestion could not be done in the quartz digestion vessels so open vessel digestion was adopted instead. Approximately 0.2 grams of sample was accurately weighed (by difference) to four decimal places and placed in a polypropylene beakers with 10 ml hydrofluoric acid added and sample heated on a steam bath. The hydrofluoric acid then proceeds to decompose silicates, forming silicon tetrafluoride gas, as shown in Equation 3.15. Residual hydrofluoric acid is then evaporated on the steam bath to ensure slow evaporation and to prevent vigorous boiling [293]. The residue is taken to dryness to remove residual hydrofluoric acid. Complexes of metal fluoride ions are very stable and consequently complete removal of the fluoride is required. This is typically done by adding sulphuric acid to form metallic sulphates [293], but in order to do this platinum crucibles are required, which were not available. Sulphuric acid will react with the polypropylene so the residue within the beaker was re-

digested in 10 ml hydrochloric acid (32 % w/w) and transferred to a 400 ml pyrex beaker. The contents of the beaker is then heated to dryness on a hotplate to form metal chlorides as opposed to metal fluorides. Residual organic material was then removed using a combination of 5 ml 1:1 sulphuric acid dehydrate to organic material and 10 ml nitric acid (68 % w/w) to oxidise and remove it. This was undertaken on a hotplate at the acid boiling temperature, with the 400 ml pyrex beaker covered by a Pyrex clockglass of slightly larger diameter than the beaker. This clockglass does not prevent the escape of gas but is enough to retain the acid vapours, refluxing the acid, whereas otherwise the vapour will escape freely [293]. This setup is shown in Figure 3.9.

Following digestion the acid was taken to insipid dryness before being made up to volume in a volumetric flask, with the aid a wash bottle containing ultra-high purity deionised water (Elga, UK) and a rubber policeman. Insipid dryness is required if the analyst intends to use ICP-MS as the residual sulphate could otherwise cause issues with ionic loading. Two certified biomass reference materials (Elemental Microanalysis, UK) were used to check the extraction efficiency. Samples are stored for analysis in 50 ml centrifuge tubes (LabCon SuperClear, USA). Acid blanks were also prepared alongside the digestion standards to assess contamination of the analyte.

$$4HF + SiO_2 \rightarrow 2H_2O + SiF_4 \quad (3.15)$$

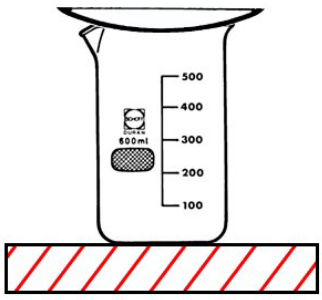

Figure 3.9. Beaker under reflux

3.6.2. Inorganic analysis via Inductively Coupled Plasma Mass Spectrometry

Inductively Coupled Plasma Mass Spectrometry (ICP-MS) is a multi-element determination system capable of determining ions at very low concentrations within a liquid sample. The system works by continually inputting sample into a stream of argon gas at slightly above atmospheric pressure. Electromagnetic induction then ionises the argon creating a thermal plasma up to 8000 °C, creating a high concentration of gas phase ions. These primary ions generated by the ICP are then analysed by a quadrupole mass spectrometer. The quadrupole filter then separates the ions, which are then channelled at an electron array detector [293]. A schematic of the system used is given in Figure 3.10.

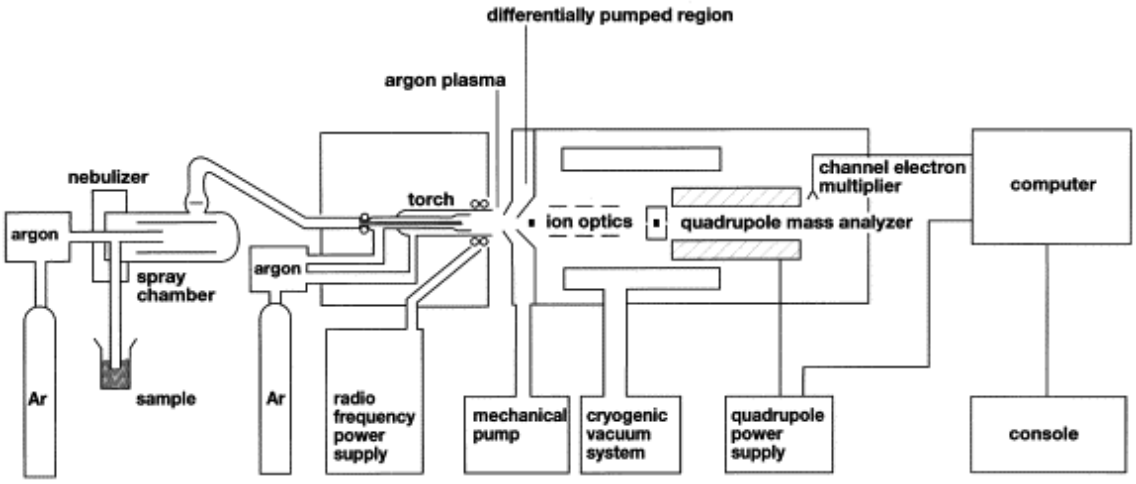

Figure 3.10 Schematic of an Perkin Elmer ELAN ICP-MS, obtained from Klinkenberg et al. [294]

Initially ICP-MS was the main method for multi-element determination in this thesis, using a Perkin Elmer ELAN DRC-e ICP-MS (USA). Issues however arose with the instruments upper limit of detection, which was around 1 ppm (1 mg/l). Given elements of interest within this project can be present in weight percentage concentrations, dilutions of 0.2 grams in 5000 ml were typically required. At this dilution, good resolution of the minor elements was not possible due to very low concentrations; moreover, error was added when diluting samples. Consequently, Atomic Absorption Spectroscopy (AAS) was adopted as the method of choice for potassium, sodium, calcium, magnesium and iron, while trace elements were analysed by ICP-MS, using dilutions of 0.2 grams in 50 ml or 500 ml. This exceeded the detection limits for the elements detected by AAS but gave good resolution to the minor elements present. Metal concentration within the sample was then determined using Equation 3.16.

$$\text{Element } (mg/kg_{sanple})_{ad} = (\text{Conc } (mg/l) \times \text{Dilution } (l))/ \text{ Sample Mass } (kg) \quad (3.16)$$

3.6.3. Inorganic analysis via Atomic Absorption Spectrometry

Atomic Absorption Spectrometry (AAS) is a single-element determination system, capable of determining metallic salts. The process works by aspirating a solution containing a metal salt into a flame. When in the flame the solvent is evaporated quickly, leaving a solid residue in the flame, this quickly dissociates into constituent atoms. When atoms are excited they can be undergo a change in energy level, which releases a photon of energy. This photon wavelength is element specific and can be detected by a detector, with the emission directly proportional to the element in the solution. This process is called Atomic Emission Spectroscopy (AES) and is typically used as an alternative detector to a mass spectrometer when combined with an inductively coupled plasma

(ICP). While atomic emission is possible using a flame, the temperature of the flame determines the excitation of the elements and the lower temperatures of a flame when compared to thermal plasma means most gaseous metals will remain in an unexcited state (will not emit photons), in what is known as a ground state. These elements are however capable of absorbing a photon of their own resonance frequency. AAS works by passing a beam of light (photons) at an element specific wavelength through the flame while the metals are dissociates into constituent atoms. The extent to which this beam is then absorbed is directly proportional to the number of ground state atoms in the flame [293]. The light source is typically a hollow cathode lamp, with the cathode usually comprised of the analyte. Single source xenon bulbs are however now available. A schematic of the process is given in Figure 3.11.

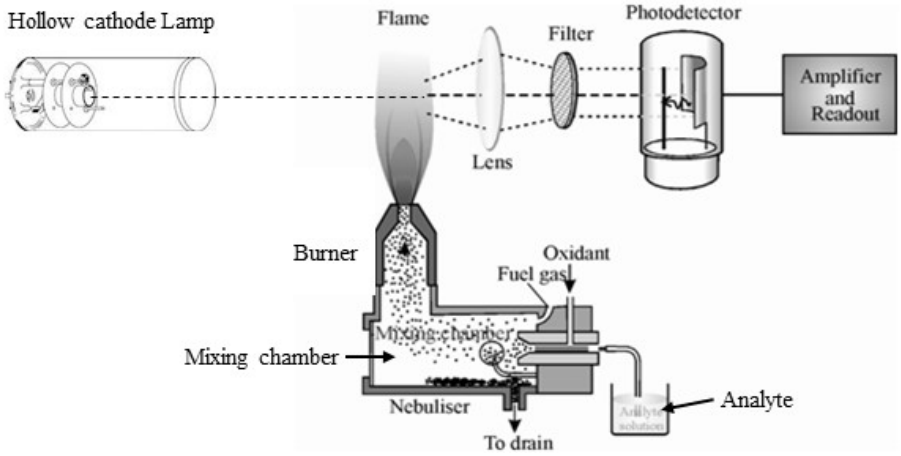

Figure 3.11, Schematic of an atomic absorption spectrophotometer

In this work sodium, magnesium, aluminium, potassium, calcium and iron were analysed by AAS following acid digestion, as they were found to main ash forming elements within the bio-coals and feedstock. Silicon cannot be determined by AAS. AAS was undertaken using a Varian (Australia) 240 FS Flame analyser, using single element hollow cathode bulbs and with air acetylene and nitrous oxide acetylene flame options. To determine elements via AAS, each element has specific optimum wavelength for a concentration range, along with specific flame stoichiometry, slit width and lamp current. The instrument s setup depending on the specific parameters required for that specific element, with the parameters given in Table 3.2. The instrument was fitted with a Sample Introduction Pump System (SIPS), which can automatically dilute samples to within the appropriate dynamic range (within reason).

Table 3.2 Optimum parameters for flame atomic absorption spectroscopy

Element	Working Range (PPM)	Wavelength (nm)	Slit Width (nm)	Fuel	Flame Stoichiometry	Lamp Current
Sodium	0.01-2.0	589.6	1	air-acetylene	oxidising	5 mA
	2-400	330.3	0.5	air-acetylene	oxidising	5 mA
Magnesium	0.15-20	202.6	1	air-acetylene	oxidising	4 mA
Aluminium	0.3-250	309.3	0.5	nitrous oxide-acetylene	reducing	10 mA
Potassium	0.1-6.0	769.9	1	air-acetylene	oxidising	5 mA
	15-800	404.4	0.5	air-acetylene	oxidising	5 mA
Calcium	0.01-3	422.7	0.5	nitrous oxide-acetylene	reducing	10 mA
	2-800	239.9	0.2	nitrous oxide-acetylene	reducing	10 mA
Iron	0.06-15	248.3	0.2	air-acetylene	oxidising	5 mA
	1-100	372	0.2	air-acetylene	oxidising	5 mA

3.6.4. Determination of phosphorus by colorimetry

Phosphorus determination via ICP-MS and AAS is not recommended and consequently phosphorus was determined by sample digestion in nitric acid followed by colorimetric determination using the phosphovanadomolybdate method. To achieve this, two 25 ml aliquots of sample were added to two separate 50 ml volumetric flasks, with one marked reagent and one marked blank. 10 ml of ammonium molybdavanadate solution (0.625 g ammonium matavanadate in 200 ml in 1:1 nitric acid added to 25 grams of ammonium molybdate in 200 ml of deionised water and made up to 500 ml) was added to the flask marked reagent and both volumetric flasks made up to volume. The colour change was allowed to develop over 30 minutes and measured at 430 nm in a Thermo Scientific Multiskan GO UV-visible light spectrophotometer (USA).

The process works by converting the phosphorus into a phosphovanadomolybdate complex, which absorbs light at 430 nm. A sample blank is required because iron present within the sample also absorbs within this wavelength and use of a sample blank ensured this is corrected for [293]. Samples were done in duplicate with triplicate readings taken to determine absorbance. Calculation of absorbance is given in Equation 3.17. Calibration was achieved by making a series of calibration standards using 1000 mg/kg phosphate stock solution (Spectrosol, UK), with care taken to convert from phosphate to total phosphorus. A regression equation calculated using least squares and used to determine the total phosphorus within the solution. Concentration of phosphorus in the feedstock or fuel was then calculated using Equation 3.16.

$$Abs_{total} = Abs_{sample} - Abs_{blank} \qquad (3.17)$$

3.6.5. Determination of silicon by colorimetry

Determination of silicon via ICP-MS and AAS is generally not possible due to the challenge of getting complete dissolution of silicon. Silicon can be determined through digestion into a liquid form however such digestions are more complex than most acid digestions as the silicon needs to be converted into a siliceous acid. Once silicon is in solution it can be determined by colorimetric determination.

To determine the silicon content the sample was initially ashed at 550 °C in accordance with BS EN ISO 18122:2015, as discussed in Section 3.3.2. 1.5 g of sodium hydroxide was weighed into a nickel crucible and then heated over a gas burner to form a dehydrated nickel hydroxide melt. This was allowed to cool before approximately 50 mg of ash, accurately weighed using a four-figure laboratory balance, was added to the

cold sodium hydroxide melt. The nickel crucible was then heated on a burner at a dull red heat until complete dissolution of the ash. Sample was heated for a further five minutes before being allowed to cool. Once cooled, 25 ml of distilled water was added and the sample heated on a steam bath for 30 minutes to dissolve the melt. The sample was then decanted and thoroughly rinsed into a 600 ml glass beaker, with the aid of a rubber policeman. The solution made up to approximately 400 ml with distilled water. 20 ml of 1:1 hydrochloric acid (HCl) was then added before the solution was decanted and rinsed into a 1000 ml volumetric flask, topping up with distilled water. Samples were stored in plastic bottles until analysis.

To undertake the colorimetric analysis 10 ml of siliceous acid solution was then transferred into a 100 ml volumetric flask, diluted to 50-60 ml with distilled water before 1.5 ml of ammonium molybdate solution was added (7.5 g ammonium molybdate, in 75 ml distilled water, followed by 10 ml 1:1 sulphuric acid and finally made up to 100 ml). The solution was allowed to stand for 10 minutes before 4 ml of tartaric acid solution added (10 g tartaric acid in 100 ml distilled water), followed immediately by 1 ml reducing solution (20 ml 45% sodium hydrogen sulphite solution in 90 ml water, mixed with 0.7 g sodium sulphate and 0.15 g 4-amino 3-hydroxynaphthalene 1-sulphonic acid dissolved in 10 ml distilled water). Solutions were allowed to develop for one hour and the concentration of silicon determined by absorbance at 650 nm in a Multiskan GO UV-visible light spectrophotometer (Thermo Scientific, USA).

This colorimetric analysis works by converting the silicon into silica acid which is then reacted with molybdate to form $H_8[Si(Mo_2O_7)_6]$ which gives an intense yellow colour. The intensity of the resulting yellow is measured at 650 nm with the intensity proportional to the silicon in the starting ash [293]. Samples were done in duplicate with triplicate readings taken to determine absorbance. Calibration was achieved by making a series of calibration standards using 1000 mg/kg silicon stock solution (Spectrosol, UK) and a regression equation calculated using least squares and used to determine the total silicon within the siliceous acid solution. Concentration of silicon in the feedstock or fuel was then calculated using Equation 3.18.

$$\text{Si (mg/kg)} = (\text{Conc (mg/l)} * \text{Dilution (l)} * 1000) / (\text{Mass of ash (g)} / (\%\text{Ash}_{ar}/100)) \quad (3.18)$$

3.6.6. Determination of chlorine by titration

A feedstock and fuel's chlorine content can be calculated when a fuel is dissolved in nitric acid using the Volhards method [295]. The method works by adding nitric acid-dissolved sample into a 0.1 mol silver nitrate solution in the presence of a ferric alum

indicator (ferric ammonium sulphate at cold saturation in water with a little nitric acid). The chloride in the sample reacts with the silver nitrate to form insoluble silver chloride and the remaining silver nitrate is then titrated with 0.1 mol potassium tyocyanate solution [295]. This method however proved more a method to determine total halogen as opposed to total chlorine and with the later adoption of hydrofluoric acid digestion, which requires hydrochloric acid, this method was replaced with total chlorine by oxygen bomb, as discussed in Section 3.6.7.

3.6.7. Determination of sulphur and chlorine by oxygen bomb

Determination of halogens, phosphorus, chlorine and sulphur can be achieved through the combustion of the feedstock or fuel in an oxygen atmosphere [293]. Chlorine and sulphur was analysed by BS EN ISO 16994-2016, whereby approximately 0.2-0.3 grams of sample is pressed using a 13 mm pellet press (Spex, UK) to 0.1 NM before being accurately weighed to 0.1mg. The sample is then combusted in an oxygen bomb (Parr 6200 (USA)). When analysing for chlorine, fuse wire should be used for ignition as opposed to cotton thread as this can add to the chlorine content measures. Prior to firing, 10 ml of deionised water added to the bomb, which acts as an aqueous absorption media. The combustion vessel is then flushed with oxygen to reduce the nitrous oxide formation, as nitrous oxide at high concentrations can be potentially problematic when analysing the chlorine and sulphur content using ion chromatography.

On firing, the bomb was left for approximately 15 minutes to let the vapours dissipate. Phosphoric acid mist generated within the bomb from phosphorus present does not dissipate into solution so a 24 volt dc current was passed through the electrodes in order to dissipate the mist to enable phosphorus determination [296]. Once vapours have had a chance to dissipate, gas was discharged and the bomb thoroughly rinsed into a 100 ml volumetric flask, with the aid a wash bottle containing deionised water (Elga, UK) and a rubber policeman. The halogens within the water are then determined using a Dionex DX 100 ion chromatograph fitted with a Dionex IonPac AS14A 250 x 4 mm column and an eluent solution composing of sodium carbonate (Na_2CO_3) (8 mM) and sodium bicarbonate $NaHCO_3$ (1mM). Halogen concentration within the fuel or feedstock was hen determined using Equation 3.16.

3.6.8. Determination of inorganics and phosphorus by x-ray fluorescence

While the inorganic and heteroatom methods discussed to this point involve completely transferring the elements of interest from a solid sample into solution, X-ray

fluorescence spectrometry (XRF) can be used as a quantitative method for solid samples. The technique works by bombarding a sample with high speed electrons. In this process the electron beam may displace electrons within inner electron shells of the elements present and this lost electron is subsequently replaced with an outer electron releasing an x-ray in the process. Like the photons in AAS/AES the resulting emission peaks are characteristic of the elements and the emission peaks can be related to the atomic number of the elements producing them [293]. A schematic of the process is given in Figure 3.12. When calibration is based on biomass reference materials, XRF can be used for a quantitative analysis of the total content of the specified elements within different solid biofuels.

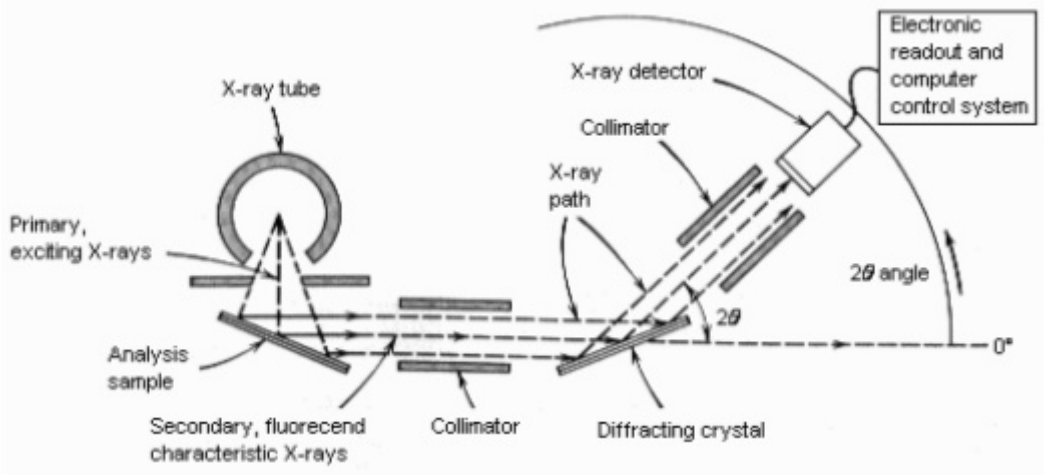

Figure 3.12. Schematic of the principle of wavelength dispersive x-ray fluorescence

In this work wavelength dispersive X-ray fluorescence (WDXRF) spectrometry was developed to analyse the main inorganics and phosphorus with the fuels and feedstock using a Rigaku Primus II (Japan). WDXRF is different to energy dispersive X-ray fluorescence (EDXRF) spectrometry, typically associated with scanning electron microscopes (SEM), in that WDXRF reads or counts only the X-rays of a single wavelength at a time, rather than producing a broad spectrum of wavelengths or energies simultaneously greatly increasing accuracy. PD ISO/TS 16996:2015 is applicable for the following elements: Na, Mg, Al, Si, P, S, Cl, K, Ca, Ti, V, Cr, Mn, Fe, Co, Ni, Cu, Zn, As, Br, Mo, Cd, Sb, and Pb. Concentrations from approximately 0.0001 %.

3.6.8.1. XRF fusion disk method

For XRF analysis, ash fusion disks were initially undertaken as it is generally accepted that this results in the homogeneous analysis. To undertake this, samples are ashed at 550°C in accordance with BS EN ISO 18122:2015. Once ashed the samples are further heated to 900°C at 10 °C minute^{-1} to convert any sulphates in the ash to oxides to

avoid interaction with platinum. The mass of ash is accurately weighed to 0.1 mg and taken as the ash content at 900 °C. Approximately 0.7 g of ash is ten accurately weighed into a platinum crucible and made up to 7 grams using lithium borates flux (SPEX, USA). The mixture is then heated to 1100°C and cast in a platinum fusion disk mould using a Katanax K1 (Canada) automated fusion system. The fused samples are then analysed using the Rigaku Primus II using a metal oxide programme. The instrument was calibrated using biomass reference materials prepared in Xing et al., [297].

To calculate the mass of the detected elements within the biomass, the Rigaku Primus II algorithms enable calculation of the elements within the starting ash (900 °C) to weight percent within the ash. These values were then converted to weight present within the biomass, based on the ash content at 900 °C. The values can then be corrected from mass as oxides to elemental mass. Due to the high temperatures required for glass fusion; potassium, sodium, calcium, magnesium are determined by AAS as the alkali metals are known to volatilise below 900°C thus XRF may underestimate their concentration, as specified in PD ISO/TS 16996:2015.

3.6.8.2.Logic behind development of pressed pellet method

In general, the sensitivity of XRF when using fusion disks is not sufficient for a determination of the content of minor elements (trace metals) in solid biofuels and consequently ICP-MS remains the optimum tool for trace metals. Moreover the proposed methodology whereby the weight percentage of elements found within the ash is taken as weight present within the biomass based on the ash content at 900 °C, is not strictly correct due to losses though decomposition of residual carbonates when the mixture was then heated to 1100°C. Consequently the method was subsequently further developed for the work presented in Chapters 6 to 9.

3.6.8.2.1. Ash and binder pressed pellets

In the revised methodology, samples were ashed to a final temperature of 550°C in accordance with BS EN ISO 18122-2005. Approximately 0.4 grams of ash was then accurately weighed and combined with a lithowax binder using 10:1 ratio. The ash and binder was thoroughly mixed using an Agate pestle and mortar and then palletised at 0.5 NM using a 13 mm pellet press (Spex, UK). Once pressed the pellet was reground in the Agate pestle and mortar before being repressed. The second pressing appeared to improve the properties of the pellet as well as leaving the pellet completely homogenous to the eye. The elemental composition of the ash was then determined by XRF (Rigaku, USA)

using a metal oxide method. Due to carbon within the ash, in the likely form of carbonate, carbon content of the ash (without binder) was determined by the Flash 2000 CHNS analyser (Thermo Scientific, USA) and carbon manually inputted to the XRF component list. Using this inputted data the Rigaku Primus II algorithm is able to take into account carbon within the existing sample.

3.6.8.2.2. Binderless pressed pellets

In work presented in Chapters 10 and 11, the sample process was continued without the lithowax binder, reducing carbon error obtained though using the carbon based binder. This revised method should overcome issues with metal losses encountered as the ash is heated between 900 °C and 1100°C. Moreover given the sample with the lithowax binder is 90 % ash and the sample without lithowax is 100 % ash, the increased error brought about though heterogeneity of the samples is offset by the increased count rates brought about though the higher ash content. This makes this technique more suitable for determination of minor elements within the ash as the concentration of minor elements is increased within the test piece.

As the sample target area is reduced from 30 mm, used for the 32 mm fusion disk to 10 mm, required for the 13mm pellet, scan time was increased for the pellets to further increase count rate. Due to the lower ashing temperature, losses of volatile metals should be less than in the fusion disk samples; however, determination of potassium, sodium, calcium and magnesium has continued to be determined by AAS, as specified in PD ISO/TS 16996:2015.

3.7. Determination of slagging and fouling propensity.

3.7.1. Ash fusion testing

Ash fusion testing (AFT) was performed using a Carbolite digital ash fusion furnace. The apparatus is essentially a temperature calibrated tube furnace with a digital camera fixed to the front to capture images of the ash every 5 °C while it is heated from 550 °C to 1570 °C at 7 °C minute^{-1}. The tests were conducted in an oxidising atmosphere with an air flow of 50 ml minute^{-1}. Cylindrical test pieces were formed using dextrin binder (Sigma-Aldrich, USA) and were run in duplicate. Photographs were taken at 5 °C intervals but as the test was performed in accordance with the standard method for the determination of ash melting behaviour (DD CEN/TS 15370-1:2006) stages were given to the nearest 10 °C as specified in the standard. The key stage temperatures are as follows: beginning of shrinkage, sample deformation, hemisphere and flow temperature

and based on the observation temperature of specific changes to the text pieces. Figure 3.13 shows the phases in the melting process. Deformation temperature, the temperature at which the first signs of rounding of the edges of the test piece occurs due to melting, is often an indicator of the onset of ash stickiness and ash issues. Lower onset temperatures suggest increased slagging propensity along with potentially increased fouling propensity.

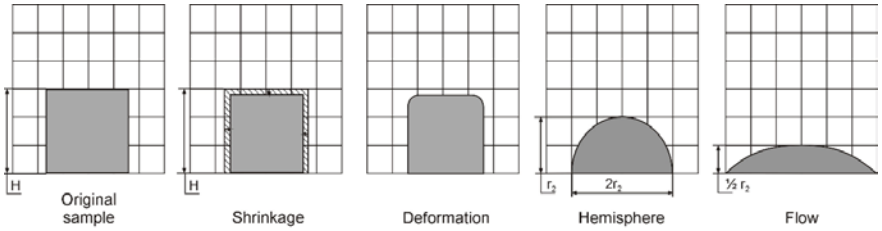

Figure 3.13: Phases in the melting process (Original shape= shape and size at 550°C)

3.7.2. Predictive slagging and fouling indices

There does not appear a standard test for fouling at present although in coal science the ash fusion test is often a good indicator of the fuels propensity to slag and foul with generally high ash melting usually indicative of a low fouling propensity [39]. As discussed in Section 2.5.1.4 slagging and fouling indices are empirical formula, which predict the likelihood of slagging and fouling based on the elemental chemistry determined in Section 3.6. Various slagging and fouling indices have been derived based on the chemical composition of the fuels, however to predict the likelihood of fouling during combustion of biomass, it is important that they also contain potassium, something which can be omitted from coal indices. The equations for alkali index (AI), bed agglomeration index (BAI), acid base ratio (R_a^b), slagging (Babcock) index (SI), fouling index (FI), and slag viscosity index (SVI) are given in Table 3.3 and are appropriate for biomass combustion.

For the AI an AI<0.17 represents safe combustion, an AI>0.17<0.34 predicts probable fouling and an AI>0.34 predicts almost certain fouling [40]. For BAI, a value of BAI<0.15 predicts that bed agglomeration is likely to occur [298]. For the R_a^b a value of <0.5 indicates a low risk of slagging and an R_a^b>1.0 predicts a high to severe risk of slagging during biomass combustion. SI values below SI<0.6 predict a low slagging inclination, SI>0.6<2.0 predicts a medium slagging inclination and SI>2.0 predicts a high slagging inclination. For FI values below FI<0.6 indicate a low fouling inclination FI>0.6<40.0 medium fouling inclination and FI>40.0 indicate high fouling inclination. An SVI>72 indicates a low slagging indication where SVI>63<72 suggests a medium

indication and SIV<65 indicates a high slagging inclination. These indices have been calculated based on the inorganic and heteroatom analysis obtained in Section 3.6, albeit the values calculated in 3.6 were mg/kg on an element basis and these values will have to be corrected to oxides to be used in these equations.

Table 3.3: Predictive slagging and fouling indices

Slagging/fouling index	Expression	Limit
Alkali Index	$AI = \frac{Kg\ (K_2O + Na_2O)}{GJ}$	AI<0.17 safe combustion AI>0.17<0.34 probable fouling AI>0.34 almost certain fouling
Bed Agglomeration Index	$BAI = \frac{\%(Fe_2O_3)}{\%(K_2O + Na_2O)}$	BAI<0.15 bed agglomeration likely
Acid Base Ratio	$R\frac{b}{a} = \frac{\%(Fe_2O_3 + CaO + MgO + K_2O + Na_2O)}{\%(SiO_2 + TiO_2 + Al_2O_3)}$	$R\frac{b}{a}$ <0.5 low slagging risk
Slagging Index	$SI = (\frac{\%(Fe_2O_3+CaO+MgO+K_2O+Na_2O)}{\%(SiO_2+TiO_2+Al_2O_3)})$*%S(dry)	SI<0.6 low slagging inclination SI>0.6<2.0 medium slagging inclination SI>2.0 high slagging inclination
Fouling Index	$FI = (\frac{\%(Fe_2O_3+CaO+MgO+K_2O+Na_2O)}{\%(SiO_2+TiO_2+Al_2O_3)})* \%(K_2O + Na_2O)$	FI<0.6 low fouling FI>0.6<40.0 medium fouling FI>40.0 indicate high fouling
Slag Viscosity Index	$SVI = \frac{(\%\ SiO_2 * 100)}{\%(SiO_2 + MgO + CaO + Fe_2O_3)}$	SVI>72 low slagging indication SVI>63<72 medium slagging indication SIV<65 high slagging inclination

3.7.3. Determination of free ionic salts within fuel (fouling)

In addition to the ash fusion test, determination of water soluble salts can be a good indicators of the fouling propensity of the fuel as they are most easily volatilised and decomposed [39]. BS EN ISO 16995-2 provides a methodology for determining free ionic salts within a biofuel. The method works by accurately weighing out approximately 0.2 grams to 0.1 mg into 20 x 150 mm Pyrex Screw cap culture tubes with PTFE lined phenolic caps. 10 ml of deionised water was then added, tubes sealed and then heated to

120 °C in an autoclave (CertoClav, Austria) for one hour. The solid and liquid products were separated by filtration under vacuum using a Buchner funnel and 90 mm qualitative circles (Grade 3, Whatman, UK). The char was subsequently rinsed with deionised water to remove residual salts before the liquid product was transferred to a volumetric flask and made up to volume. Determination of salts was undertaken via ion exchange chromatography (Dionex, USA). Anions were analysed using a Dionex DX 100 with an IonPac AS14A 250 x 4 mm column and used an eluent solution composing of sodium carbonate (Na_2CO_3) (8 mM) and sodium bicarbonate $NaHCO_3$ (1mM). Cations were analysed using a Dionex LC20 fitted with an IonPac CS12A 250 x 4 mm column and used a sulphonic acid solution (1mM) as an eluent. Both systems used 5 ml sample volumes, with 25 µl sample injected onto the column using an automated sampler (Dionex, USA). For the recycling process water work presented in Chapter 6 and 7, this method demonstrated most of the alkali metal salts present were in the form of free ionic salts. While the data compared closely there was however slight discrepancy between the AAS and IC data. Rerunning the cation data on the AAS should overcome this but technical issues with AAS has meant undertaking this work has, at time of writing not been possible.

Chemical fractionating techniques similar to those descried in Miles et al., [205], Skrifvars et al. [267] and Koppejan and Van Loo (2012) whereby a standardised leaching process using progressive and more severe chemical reagents (water, then ammonium acetate and then hydrochloric acid) may also be more appropriate a technique. This is due to washing then leaching with ammonium acetate indicating the proportion of mono-valiant and di-valiant cations within the bio-coal, which it has been hypothesised that they may play a role in bio-coal formation.

3.8. Determination of combustion and pyrolysis behaviour by thermogravimetric analysis (TGA).

Temperature programmed oxidation (combustion) - thermogravimetric analysis (TPO-TGA) is one method originally developed by Babcock and Wilcox for comparing and evaluating the combustion behaviour of fuels [68]. This is done by gradually heating the fuel at a gradual rate of 10 °C $minute^{-1}$ in air to 900 °C and by calculating the first derivative thermogravimetric (DTG) curve. Form this four characteristic temperatures are typically interpreted [68]. The first initiation temperature occurs where the weight first begins to fall; the second initiation temperature occurs where the weight loss accelerates due to the onset of char combustion. The third is the peak temperature where the weight

loss is maximum; and the fourth is the burn-out temperature where the weight is constant, indicating the completion of combustion [68].

TPO was carried out using a programmed method consistent on both the Mettler Toledo TGA/DSC1 and TGA/DSC3, with both instruments using an identical programmed method and 70 µl alumina crucibles, annealed at 1100 °C (Mettler Toledo, Switzerland). Results shown in Figure 3.7 suggest sample size does limit the rate of oxidation during combustion, so samples were weighed to 10 mg ± 5%, to avoid mass transfer limitations. A sample size below <100 µm was used in order to reduce the effects of heat transfer through the particle and to ensure that combustion was controlled kinetically [299], in addition to ensuring homogeneity of fuel.

Determination of the pyrolysis behaviour was obtained by taking the derivative of the proximate data obtained under nitrogen at a heating rate of 25 °C minute^{-1} in air to 900 °C.

3.9. Determination of grindability

The importance of milling behaviour is discussed in Section 2.4.4.2. Resistance to milling was calculated using the Hardgrove Grindability Index (HGI), a scale used to assess a fuels resistance to grinding and thus the energy requirement to pulverise a fuel to the required 70 % below 75 µm needed for pulverised coal applications [300]. The HGI method is however not suitable for the lower density biomass which would be too voluminous to use in the Hardgrove grindability equipment. A modified HGI has been developed by Bridgeman et al. [196] that requires a fixed volume of sample rather than a fixed mass seen in the original HGI. A volumetric HGI test was undertaken for some of the feedstocks and fuels generated as part of this work, as recommended in Bridgeman et al. [196].

Unprocessed *Miscanthus* was milled in the Retsch SM300 Cutting Mill outlined in section 3.1.1. The milled sample was then sieved using 600 µm – 1.18 mm which is the size fraction required for the modified HGI test, while the HTC fuels were simply sieved for analysis to between 1.18 mm and 600 µm as the material had previously been processed. The HGI test was carried out in the 50 cm^3 Retsch Cryomill, discussed in section 3.1.3, which was operated as an impact mill without liquid nitrogen at room temperature. 10 cm^3 of sieved biomass was then accurately weighted to 0.1mg and ground in a ball mill for 30 seconds at 15 Hz before being passed through a 75 µm sieve. Separation was aided by a Retsch AS 200 vibratory sieve shaker. The mill was calibrated using four HGI reference coals (ACIRS, Australia) with HGI of 26, 49, 69 and 94, and a

line of best fit calculated using least squares. Calibration details are shown in Figure 3.14 and samples were analysed in triplicate.

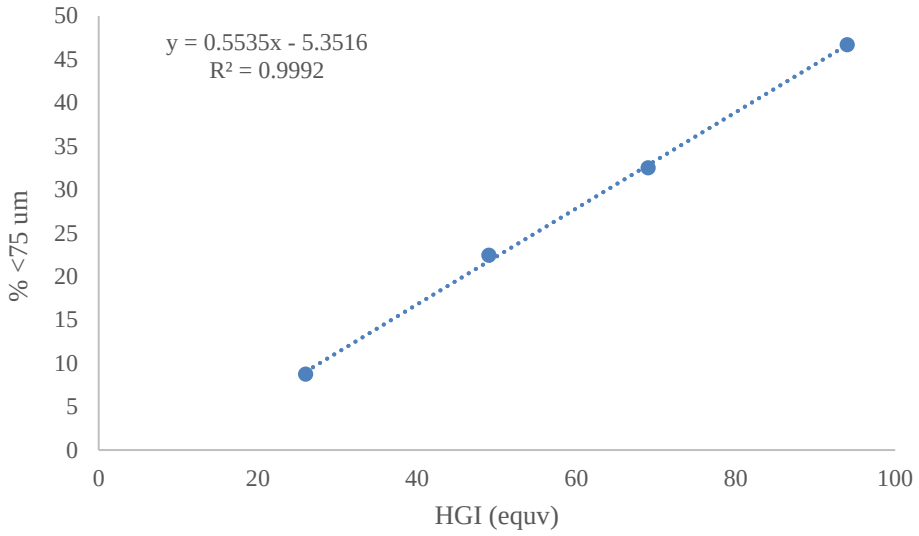

Figure 3.14, Percentage of HGI ranked coals (HGI of 26, 49, 69 and 94) passed through a 75 µm sieve in a 50 cm^3 Retch ball mill for 30 seconds at 15 Hz

3.10. Process water analysis

This study does not attempt to quantify the aqueous products within the process water, given it is extremely difficult to determine which chemical reactions take place [301], however gaining an insight into the process water chemistry is important to understand underlying mechanisms. This section discusses the various methods used to achieve this.

3.10.1. Total Organic Carbon analysis

Total Organic Carbon (TOC) is the amount of organic carbon present within the process waters. The carbon content of the process water was analysed using a Hach Lange IL550 (Germany) total carbon analyser. The method works by injecting a water sample into a high temperature furnace (1000 °C) within the analyser and any carbon within the sample is converted to carbon dioxide. The product gasses are passed through an inbuilt gas chromatography (GC) column onto a TCD. Based the retention time within the GC column, carbon dioxide is identified and a computer calculates the amount of carbon dioxide evolved, which is proportional to the amount of carbon in the sample.

To tell the difference between organic carbon and inorganic carbon, a sample of ‘untreated water’ is initially injected into the instrument giving total carbon (organic carbon plus inorganic carbon). Acid is then added to the next sample, reacting with the

inorganic carbon and removing the carbon as carbon dioxide. The sample is then injected into the furnace and the carbon dioxide detected is purely from the organic carbon. Inorganic carbon is calculated by subtracting organic carbon from total carbon. The instrument is accurate up to 2000 mg/l TC, so consequently process water is typically diluted x25 in a volumetric flask and in certain circumstances x50 (recycling process water work).

3.10.2. Free ionic salts by Ion Chromatography

Free ionic salts in the process waters were analysed by ion exchange chromatography (IC). IC works by injecting a sample (25 µl) into an ion exchange column where is transported in an eluent and the ions are separated by charge. At the end of the column there is a suppressor which acts to decrease any background eluent conductivity and noise as well as increasing the analyte conductivity before being passed to a conductivity detector. The suppressor greatly enhances the signal to noise ratio detected by the conductivity detector. The conductivity detector, analyses for changes in conductivity of the eluent as it passes though, giving the reading in µs. A schematic of the system is given in Figure 3.15.

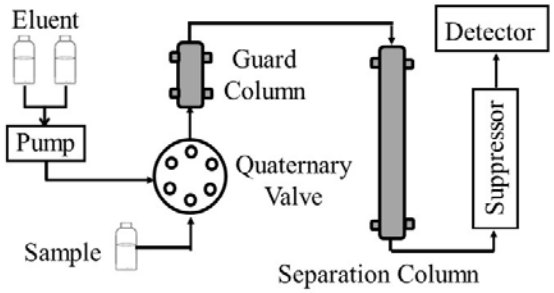

Figure 3.15 Schematic of an ion exchange chromatography system

Quantification is based on the retention time with the response proportional to the concentrations of ions present and the response is calculated using calibration standards. Given anions and cations require different configurations, analysis anions were analysed using a Dionex DX 100 with an IonPac AS14A 250 x 4 mm column and used an eluent solution composing of sodium carbonate (Na_2CO_3) (8 mM) and sodium bicarbonate $NaHCO_3$ (1mM). Cations were analysed using a Dionex LC20 fitted with an IonPac CS12A 250 x 4 mm column and used a sulphonic acid solution (1mM) as an eluent. Both systems used 5 ml sample volumes, with 25 µl sample injected onto the column using an automated sampler (Dionex, USA).

A limitation of this IC method is that it will only determine free ionic salts within the process waters, which is different to total ions within the process water as some metals and heteroatoms maybe ionically bound to the organic carbon. Analysis of nitric acid digested process waters using AAS identified a number of cations remain organically bound in the process waters. A process water total ion content methodology was developed as IC offers the advantage of being able to determine halogens, phosphorus, nitrogen and sulphur in addition to metals in the process water, as offered by the nitric acid / AAS method. The method developed involved adding a known volume of process water (typically 10 ml) to a 50 ml Erlenmeyer flask. The water was then taken to near dryness on a hotplate before being cooled. 20 ml hydrogen peroxide (30 % w/w) was then added before heating at 150 °C on a laboratory hotplate. A small refluxing funnel was placed in the mouth of the flask (see Figure 3.16) to avoid loss of liquid by spurting while enabling gas escape, while attempting to retain oxidant through reflux. After digestion samples needed to be taken to near dryness to volatilise any residual hydrogen peroxide, which could damage the IC column before being made up in deionised water. Residual carbon was analysed by TOC (Hach Lange, Germany), however residual carbon was detected. With increased digestion time, a white precipitate was achieved however this proved to be highly unstable and could spontaneously combust at near dryness. Consequently, a total metals by IC method was shelved.

Figure 3.16: Erlenmeyer flask with refluxing funnel

3.10.3. Organic compounds with process water via High Performance Liquid Chromatography

The organic compounds within the process waters were initially analysed by High Pressure Liquid Chromatography (HPLC). HPLC is an analytical technique used to separate and quantify components within a mixture by passing a pressurised liquid solvent containing the sample mixture through a column filled with a solid adsorbent material. Each component in the sample interacts slightly differently with the adsorbent material, causing different flow rates for the different components and leading to the separation of

the components as they flow out the column. The technique is particularly suitable for separation of HTC process waters as the chromatography is not limited to volatile and thermally stable samples, which limits GCMS [293]. HPLC is a common technique for quantifying organics in HTC process waters; for example Hoekman et al. [29], Reza et al. [126] and [302], and Kambo et al. [115].

HPLC was undertaken using a Dionex Ultimate 3000 (USA) setup, fitted with a column oven (Shimadzu CTO-10AC, Japan), ultraviolet detector and a refractive index detector (Shodex RI-101, Japan). Size exclusion chromatography (SEC) via gel filtration chromatography (GFC) was undertaken to show the size distribution of organic compounds present. This was undertaken using a Waters UltrahydroGel (USA) and ultra-high purity deionised water (Elga, UK) as the mobile phase. The column was heated in the column oven to 80 °C and detection was via the refractive index detector. Organic acids present were analysed by a Supelco (USA) organic acids column, SupelcoGel C610-H with 1% H_2PO_4 eluent. Detection was via the ultraviolet detector and while separation can be done at room temperature the column was heated to 30 °C, as temperature within the laboratory tends to fluctuate. Sugar analysis should be possible using SupelcoGel C610-H however poor resolution lead to the purchase of a SupelcoGel Pb column, more specific to sugars. This column was operated with distilled water eluent, heated to 80 °C and detection was via the refractive index detector. The process works in the same way as IC with the various columns designed to separate the compounds, with the sugar and organic acid column separating based on charge and the size exclusion column separating based on molecular size, with the smaller molecules being retained for longer because they interact with the gel within the column where larger molecules cannot.

The detector used is dependent on what is being analysed, with the sugars and SEC using a refractive index detector (differential refractometer), which detects compounds based on the different levels of refraction obtained when the analyte passes though the column relative to the solvent. The organic acids column uses a ultra-violet (UV) detector, which measured the compounds based on changes in absorbance of UV light as the solvent and analyses pass though the detector. Quantification of known compounds was possible using a range of calibration standards supplied in organics acids kit, carbohydrate kit and in addition 5-hydroxymethylfurfural (5-HMF) and levulinic acid standards (Sigma-Aldrich, USA).

Issues have however arisen when analysing sugars and organic acids within process waters due to interactions between the salts and the column packing which separate on charge. To overcome this process waters will be pre-processed though ion-exchange resins (Dowex® Marathon™ MR-3 hydrogen and hydroxide form) to extract the salts, and pH corrected to pH 5 before HPLC. This had partial success, although there were fears the ion exchange resin was extracting organics in addition to the inorganics. This was later replaced by an inline Bio-Rad deashing cartridge, which combines cation and anion exchange resins to remove inorganic salts from the sample, essentially purifying any carbohydrate which passes though, removing salt peaks and improving resolution [303].

Even with the inline deashing column, poor detection was still seen. It was unclear whether it was as a result of the deashing column changing the pH and thus the elution rate or whether the compounds we were searching for were even present. It is acknowledged that biomass degradation compounds which contain monomeric sugars (mainly glucose and fructose) along with various alditols, aliphatic acids, oligomeric sugars, and phenolic glycosides, are very reactive in hydrothermal media [304]. It could be possible that the simple sugars being produced via hydrolysis are almost immediately undergoing decarboxylation and dehydration to new compounds and consequently are not present. The Dionex Ultimate 3000 was not fitted with a mass spectrometer detector, so detection of a compound is dependent on the retention time of the analyte within the process water, maintaining the same retention time as the calibration standard.

While effort was taken to best matrix-match the standards, the process waters are a complex mixture of organic and inorganic compounds, which vary between samples. Analysis via HPLC-MS works by bombarding the eluted compound with electrons causing the molecule to fragment in a characteristic and reproducible way. The resulting fragmentation pattern can then be used to calculate the eluted compound. Consequently, for this work HPLC-MS would be a more appropriate method for organic compound determination within the process water, as this method will allow for peak shift brought about though interactions between the salts and the column packing and changes to pH though deashing.

More recently work by Hoekman and co-workers have begun to detect organic acids and sugars by Ion Chromatography using a method developed by Jaffrezo et al. [305] using a Dionex IonPac AS11 column [101, 173, 268, 306]. In addition to organic acids the Dionex IonPac AS11 column should resolve acetate and formate, something the

IonPac AS14A fitted within the Dionex DX 100 and used for anions, cannot (see Section 3.10.2). Given the apparent importance of acetate and formate within recycled process waters (see Chapter 6 and 7); a Dionex IonPac AS11 column has been fitted into a Dionex ICS-900 (Thermo Scientific, USA), however quantification has yet to be undertaken on process waters.

3.10.4. Organic compounds with process water via Gas Chromatography Mass Spectroscopy

While characterization of process waters is typically done using liquid chromatography, some groups Baccile, Titirici and co-workers, appear to use Gas Chromatography Mass Spectroscopy (GCMS) in their characterisation [301, 307, 308]. While GCMS has limitations as the chromatography is limited to volatile and thermally stable compounds which limits the compounds detection compared with HPLC; many of the key compounds in HTC responsible for char formation; 5-HMF, levulinic acid, dihydrohyacetone, acetic acid and formic acid [85, 86, 301, 309] are volatile and will need to be thermally stable to survive the hydrothermal reaction. The ability of the technique to positively identify the presence of a particular substance through analysis of the resulting fragmentation pattern determined by the mass spectrometer is also a major advantage over HPLC given the complex matrix of the process water appears to influence elution rate.

GCMS was undertaken using a Shimadzu GCMS QP2010SE (Japan). The system works by inputting a sample onto a sample column via an injector. The column is within a column oven which has a pre-determined heating regime. The column responsible for the separation of the components by interaction between the sample mixture and the stationary phase within the column. The pre-determined heating regime of the column oven aids the elution rate. The Shimadzu GCMS QP2010SE was setup to use capillary columns and for process waters, a Restek RTX-Wax (USA) was used. This column is in essence a 30 metre long thin capillary tube with an internal diameter of 0.25 mm and the inside coated with a thin coherent film of crossband carbowax polyethylene glycol. The RTX-Wax is a highly non-polar column and as such well suited to volatile fatty acid (VFA) analysis. Good separation was achieved using a start temperature of 100 °C and a heating rate of 15 °C minute^{-1} to 220 °C, followed by a 10 minute hold at 220 °C.

Once eluted from the column the carrier gas and eluted compounds enter a high vacuum environment in the mass spectrometer; the vacuum is required in order to convert molecules into gas phase ions with a lifetime long enough to be measured [293]. The

eluted molecules are then bombarded by ions from an ion source in order to ionize the sample before entering a quadrupole mass analyser. The quadrupole consists of four parallel metal rods set parallel to each other and are responsible for filtering the ions generated from the sample. Each opposing rod pair is connected together electrically, and a radio frequency (RF) voltage with a DC offset voltage is applied between one pair of rods and the other. Ions travel down the quadrupole between the rods and only ions of a certain mass-to-charge ratio will reach the detector for a given ratio of voltages: other ions have unstable trajectories and will collide with the rods. This permits selection of an ion with a particular m/z or allows the operator to scan for a range of m/z-values by continuously varying the applied voltage [293]. A schematic of a GCMS is given in Figure 3.17.

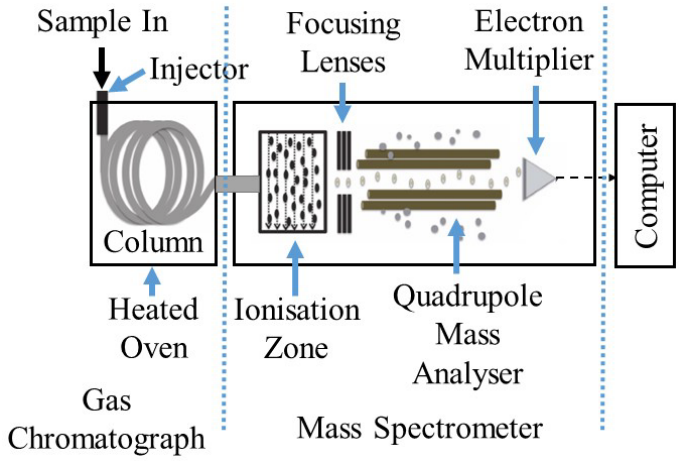

Figure 3.17. Schematic of a quadrupole gas chromatograph – mass spectrometer

For GCMS a chromatogram is given, which plots the Total Ion Current (TIC) detected by the mass spectrometer. This is sometimes known as Multi Ion Counting (MIC). As compounds are eluted into the mass spectrometer they are ionised and this changes the TIC. It should be noted that TIC is compound specific. An increase in TIC for a specific compound is directly proportional to an increase of that compound but double the TIC compared to another compound would not necessarily represent double the concentration of the second compound as TIC depends on the fragmentation behaviour of the compound. Consequently, to make this method quantitative calibration standards for the quantified chemicals are required.

The technique can positively identify the presence of a particular substance by plotting the mass spectrum for a specific point in time (i.e. a TIC peak). The mass spectrum consists of an intensity vs. mass-to-charge ratio (m/z) plot, which the Shimadzu instrument can then undertake a similarity search against the NIST-11 spectral database,

which is a database of compound specific mass spectrums. The ability to identify unknown peaks is a particular advantage given the hydrothermal reaction is a mixture of hydrolysis, degradation and hydrogenation reactions and a range of chemicals will be generated [84]. An example of this is the presence of valeric acid within the process water, which is a product of the hydrogenation of the levulinic acid [271], but is not typically reported in hydrothermal literature.

In an attempt to avoid the use of solvents and liquid-liquid extraction identification of the VFA within the process water was initially attempted using a purge and trap method. A CDS Analytical 5200 pyroprobe (USA) fitted to the GCMS was modified via a Swagelok septum fitted to the pyroprobe interphase. This allowed process water to be syringed into the heated interphase, evaporated and the VFA trapped on the instrument trap, which is then flashed onto the GCMS. This minimised the volume of water injected onto the column. A schematic of the setup is given in Figure 3.18.

After further reading direct water injection onto the column was developed as guidelines stated water could be injected as the column and injector temperatures are always above 100 °C to avoid condensation. An injection volume of 1µl is used to avoid back flash due to the solvent expanding. Consequently, process waters were directly injected via a Shimadzu AOC 20i auto sampler into a slit injector at 280 °C. An injection volume of 2 µl was used but with the slit ratio increased to 1:20 as this appeared to give better mixing within the injector. This method did not detect sugars such as fructose but was capable of detecting sugar derivatives such as furans and 5-HMF.

Detection of phenols was attempted using a mid-polarity 60 metre Restek RTX-50 capillary column (50 % phenyl – 50 % methyl polysiloxane). Direct water injection was undertaken with a starting column temperature of 100 °C and a heating rate of 8 °C $minute^{-1}$ to 290 °C, followed by a 1.25 minute hold at 290 °C. The analysis however gave poorer peak resolution to the RTX-Wax and did not enable identification of additional compounds. Consequently the RTX-50 data is not presented in this work. Phenols are believed to be present within the water based on protonated NMR analysis but these maybe in the form of larger polymers which would not be detected.

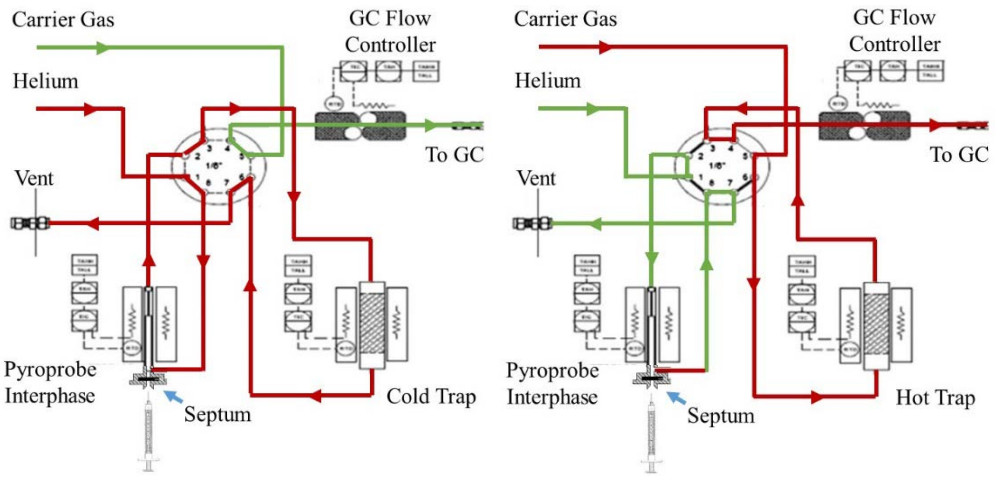

Figure 3.18 Schematic of CDS Analytical 5200 pyroprobe, with septum added. Left image represents pyroprobe in trap mode, with the right image purging the trap onto the GC.

3.10.5. Organic compounds with process water via protonated nuclear magnetic resonance

Due to the complex nature of the process waters a qualitative overview of the organic compounds present in the process waters was obtained using water corrected protonated nuclear magnetic resonance (NMR) using a Bruker AVANCE III HD-400 (USA). 2 ml of process water was added to 3 ml deuterium oxide sample shaken and then analysed. Deuterium oxide is added prior to analysis because labile protons, such as alcohols, amines, amides and hydroxyl groups have protons that exchange with other labile protons, including water, and bring about no characteristic chemical shift. By adding deuterium oxide the liable protons exchange with the deuterium and in the process are removed from the spectrum. Therefore, the NMR spectra only shows the narrow C-H protons. As water is present, labile peaks exchanging with water will appear at 4.7ppm and this is removed from the data by the water suppression program. Peaks were identified by developing a reference library using range of pure reference standards at known concentrations (Sigma-Aldrich, USA) and cross checked using data provided in Pretsch et al. [310] and AIST spectral database.

3.10.6. Biomethane potential from process water

AD of the organic compounds within the aqueous phase has been calculated alongside some of this work. While the ‘standard’ method for determination is now via chemical oxygen demand (COD), this was largely unused at the time of undertaking this work. Biological methane production (BMP) by using the Boyle equation was subsequently adopted as it had been used by authors including Danso-Boateng et al. [274].

This work also started to explore the potential for hydrogen production as the process water chemistry may lend itself better to that process, as discussed in Section 2.6.

3.10.6.1. Calculation of biomethane and bio-hydrogen production

The carbon, hydrogen, nitrogen, sulphur and oxygen content of the process water was calculated by drying a known volume of process water at 60 °C over a period of 48 hours to reduce loss of volatile organic compounds. The dried sample analysed using a Flash 2000 CHNS analyser (Thermo Scientific, USA) using the methodologies described in 3.4. Due to the high inorganic content of the process water calculation of ash by heating to 550 °C in a muffle furnace in air was not possible, due to the added weight of the incorporated oxygen when the slats are converted to oxides. Inorganics within the water were taken as the weight by difference using Equation 3.19. Calculations of potential gas yields by methanogenesis have been calculated based on the Boyle Equation (Equation 3.20) and hydrogen yields via hydrogenesis using Equation 3.21, with a,b,c,d and x,y,z being the molar fraction.

$$Inorganics_{db} = 100 - C_{db} - H_{db} - N_{db} - S_{db} - O_{db} \quad (3.19)$$

$$C_aH_bO_cN_d + ((4a-b-2c+3d)/4)\ H_2O \rightarrow ((4a+b-2c-3d)/8)\ CO_2 + ((4ab+2c+3d)/8)\ CH_4 + d\ NH_3 \quad (3.20)$$

$$C_xH_yO_z + (2x-z)\ H_2O = x\ CO_2 + ((y/2)+(2x-z))\ H_2 \quad (3.21)$$

3.11. Pyrolysis-gas chromatography-mass spectroscopy

Pyrolysis-gas chromatography-mass spectroscopy (Py-GCMS) is an analytical technique whereby a sample is thermally decomposed to produce smaller molecules that can be separated and detected by GCMS. The system enables the identification of volatile and non-volatile compounds and the way in which the polymer fragments can help identify the way that the sample polymer assembled itself. Py-GCMS was undertaken using a CDS Analytical 5200 pyroprobe (USA) fitted to a Shimadzu GCMS QP2010SE. Separation was done using a 60 meter 0.25 mm RTX-1701 capillary column (Restek, UK) which is a cross band 14% cyanopropylphenyl: 86% dimethyl polysiloxane. The column was initially heated to 40 °C for 2 minutes before being heated at 10 °C minute^{-1} to 280 °C, followed by a 25 minute hold at 280 °C.

The pyroprobe works by heading a sample within a quartz tube, which is placed within a platinum heating coil and heated to the a desired temperature up to 1200 °C at a desired heating rate. The CDS Analytical 5200 pyroprobe can directly pyrolyse the sample onto the column but is typically operated in trap mode, where by the sample is pyrolysed in a flow of helium with the helium flow passed through a Tanax porous

polymer absorbent trap which traps the evolved compounds. Once the sample is fully pyrolysed the gas flow is switched so helium passing though the polymer absorbent trap passes through a transfer line into the gas chromatograph injector port. On switching the gas flow the polymer absorbent trap is rapidly heated to 300 °C which releases the trapped volatiles into the gas flow and into the gas chromatograph injector. This is demonstrated in Figure 3.19. The injector is operated in split mode with a 1:10 bypass and the desorbed volatiles are injected onto the GC column and separated accordingly. The advantage of operating the pyroprobe in trap mode is it allows for analysis of all the volatile components of the analyte at slower heating rates: direct injection tends to favour the highly volatile compounds and high heating rates.

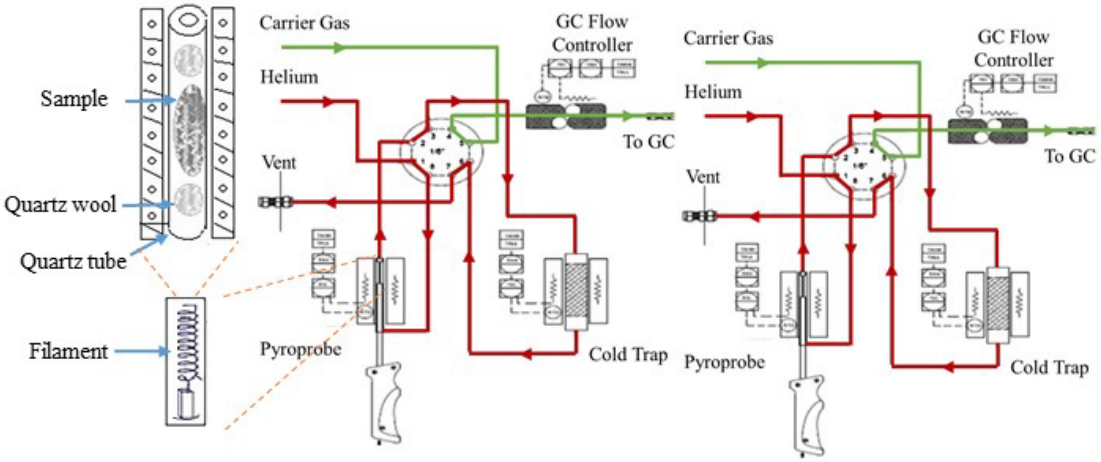

Figure 3.19. Pyroprobe schematic, left of image showing filament and sample positioning, middle showing gas flow during devolatilisation and right image showing gas flow when desorbing the trap.

When undertaking routine Py-GCMS, samples were analysed in duplicate with a pyrolysis temperature of 550 °C using 20 °Cms^{-1} heating rate. 550 °C was held for 1 minute at this temperature to fully devolatilise the sample before injection. To avoid condensation of volatiles the interphase, transfer line and valve gear on the pyroprobe was heated to 300 °C prior to the coil heating the sample. The trap was heated to 50 °C when absorbing and 300 °C when desorbing the volatiles. Samplers were prepared by taking quartz tubes 25 mm in length and 0.5 mm inner diameter supplied by CDS Analytical (USA) (Figure 3.19). The quartz tubes were cleaned in a flame using a Bunsen burner prior to the sample being added to remove any residual organic material which could contaminate the sample. Quartz wool (CDS Analytical, USA) was then inserted into the quartz tube to act as a sample holder and then further heated in the Bunsen burner to remove residues found on the fibres before 2-3 mg of sample was added. Another piece of heated quartz wool used to cap the top of the tube.

The pyrolysis behaviour of the samples were compared with the pyrolysis behaviour determined by TGA analysis as discussed in section 3.8. When particular changes were observed in the derivative data multistage desorptions were undertaken to understand the changes in chemistry. An example is the multistage desorptions at 250 °C, 400 °C and 600 °C undertaken on the recycled process water samples and the influence of retention time samples. In the event that the desorption temperature is below 300 °C the interphase temperature is lowered to the thermal desorption / pyrolysis temperature (e.g. 250 °C for the 250 °C desorptions).

3.12. Reactor gas analysis using gas chromatography-thermal conductivity detector.

Post hydrothermal carbonisation, reactor gas was subsequently depressurised into a 3 way ball vale (Swagelok, USA) with a gas sampling bag (Saint Gobain, France) fitted to the gas outlet port. Gas analysis was undertaken using a Shimadzu GC 2014 gas chromatograph (Japan) fitted with a 2 metre molecular sieve 5A 60-80 mesh and a 2 metre Hayesep N 100-120 mesh with argon carrier gas and TCD detector. Given the reactor had been cleared of air via a vacuum pump, flushed and then filled with argon prior to operation, it is generally assumed that gases detected by the GC are gases created during the reaction. Blank runs confirm this. Sample delivery was via 250 µl sample loops, which the instrument uses to automatically inject the sample onto the column. Sample is introduced by attaching the gas sampling bag via the spare outlet valve on the 3 way ball valve, attaching a 10 ml luer lock SGE syringe to the inlet port and pumping gas from the bag into the loop (see Figure 3.20). The instrument was setup with a 25 ml flow on both columns, with the injector set at 80 °C, the column heated at 40 °C and the TCD heated to 150 °C. Run time was 5 minutes on the Hayesep followed by 5 minutes on the molecular sieve. The instrument was calibrated for hydrogen oxygen, nitrogen, methane, carbon monoxide and carbon dioxide using 5 % and 10 % mixes of gas in an argon balance. Hydrogen, oxygen, nitrogen, methane and carbon monoxide were analysed using the Hayesep while carbon dioxide was analysed using the molecular sieve. It was discovered that the columns were susceptible to poisoning from carbon dioxide and moisture giving poor separation. Once this was realised regular flushes with an oven temperature at 120 °C overcame this issue.

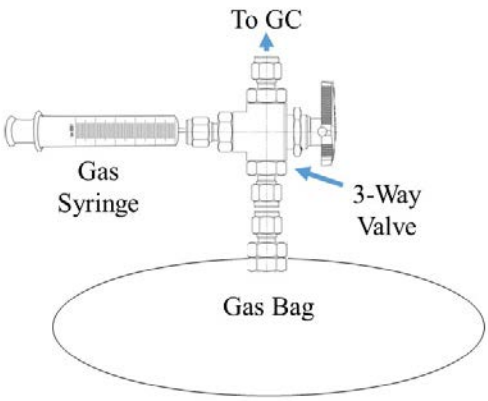

Figure 3.20, Gasbag configuration

3.13. Scanning electron microscopy – energy dispersive x-ray

Scanning electron microscopy (SEM) was used to provide an in depth image of a bio-coal particle surface, aiding the understanding of char formation process. In SEM imaging a beam of electrons are emitted from an electron gun (cathode) which is focused on the sample. The electrons beam is accelerated through a high voltage (in this case 5 or 15 kV) and pass through a system of electromagnetic lenses to produce a thin beam of electrons. The beam then reaches the surface of the sample and either secondary electrons (SE) or backscattered electrons (BSE) are released dependent on the analysis type selected. When SE is selected the beam hits the sample the electrons are absorbed and its own electrons are released which are then detected by a detector which uses the information to produce an image. In BSE mode the electrons focused onto the surface are reflected back from the sample surface and then detected allowing for the generation of the image.

SEM imaging of the raw fuels and chars were taken using a Carl Zeiss EVO MA15 SEM (Switzerland) with Oxford Instruments AZtecEnergy Energy Dispersive X-ray (EDX) system (UK). Ground samples were mounted onto 10 mm SEM stubs using carbon adhesive disks (Agar Scientific, UK) and the excess removed using a dry air duster. To prevent accumulation of electrons on the surface generating charge up, the samples were covered by a thin layer of carbon was added to prevent accumulation of electrons via a Quarumtech Q300 (UK) carbon coater. The samples were then placed onto the sample holder stand and installed in the SEM. Once installed the system was placed under vacuum and images taken at a range at 5 kV and over a range of magnifications. For the influence of size samples SEM-EDX was used to gauge silicon concentrations within the samples.

3.14. Experimental replication and statistical treatment

Analyses were routinely carried out using duplicate samples with errors given within this thesis calculated as standard errors, using Equation 3.22. In addition to analysing in duplicate, figures obtained by TOC and ICP analysis are based on multiple sample injections until a maximum standard deviation of ± 2% is achieved. For colorimetric analysis, duplicate samples were analysed and for each sample a minimum of three separate readings were taken to determine the abortion of the solution, with the absorption taken as the mean figure. An estimation of the error on the routine quantitative analyses is given in Table 3.4.

$$\text{Standard error} = \text{Standard deviation} / (\sqrt{\text{number of samples}}) \qquad (3.22)$$

Table 3.4: Repeatability and expected error within analyses

Analysis		Typical Data Range	Source(s) of error	Repeatability and Error
HTC Yield		80-20wt%	moisture correction	±0.2wt%
Moisture Content		60-40% and >5%	appropriate sampling	>0.2wt%
Volatile Carbon		80-20wt%	measurement error	±0.5wt%
Fixed Carbon		60-10wt%	measurement error	±0.5wt%
Ash Content		15-0wt%	incomplete incineration	±0.2wt%
CHNS	C	75-35wt%	measurement error/ capsule preparation	±0.3wt%
	H	4-7wt%		±0.3wt%
	N	5-0.5wt%		±0.1wt%
	S	1->0.1wt%		>0.1wt%
Oxygen		40-10wt%	measurement error/ capsule preparation	±0.3wt%
XRF	P	8000-400mg/kg	ashing and sample preparation	±5%
	Si	10,000-100mg/kg		±5%
	Fe	200-50mg/kg		±5%
	Mn	>50mg/kg		±5%
	Mg	600-200mg/kg		±5%
	Ca	10000-600mg/kg		±5%
AAS	Na	600-200mg/kg	rinsing error and complete digestion	±2%
	K	5000-400mg/kg		±2%
Colorimetry	Si	10,000-100mg/kg	sensitivity of analysis	±200mg/kg
	P	8000-400mg/kg	analyte preparation	±5%
Chlorine		5000-1000mg/kg	sample recovery from oxygen bomb	±2%

4. Fate of inorganic material during hydrothermal carbonisation of biomass: influence of feedstock on combustion

Work presented within this chapter is an abridged version of work presented in the Journal Fuel, for the unabridged version or to cite please use: Aidan M. Smith, Surjit Singh, and Andrew B. Ross. "Fate of inorganic material during hydrothermal carbonisation of biomass: influence of feedstock on combustion behaviour of hydrochar." *Fuel* 169 (2016): 135-145.

4.1. Abstract

A series of high moisture content biomass have been processed by hydrothermal carbonisation (HTC) in a batch reactor at two temperatures (200 °C and 250 °C). The feedstocks processed include food waste, secondary sewage sludge, AD press cake, microalgae, macroalgae and a fibre derived from municipal derived wastes. In addition, three lignocellulosic biomass including *Miscanthus*, willow and oak wood have been processed under identical conditions. The yields and properties of the resulting bio-coals including their HHV, CHNS, mineral content and ash fusibility properties have been determined and compared with their starting biomass. Typical char yields for lingocellulosic material range between 58-70 wt% at 200 °C and reduce to 40-46 wt% at 250 °C. The behaviour and mass balance is however very feedstock dependent and the higher lignin biomass produce higher yields of bio-coal. There is a significant upgrading of the energy density of the bio-coals with calculated HHV ranging from typically 24 $MJkg^{-1}$ at 200 °C to 28-31 $MJkg^{-1}$ at 250 °C for lignocellulosic material. The exception is for sewage sludge and AD press cake which result in a significant solubilisation of organic matter. A significant removal of alkali metals is observed and this in turn changes the ash chemistry. This change in ash chemistry has been shown to change the ash melting behaviour and the hemisphere temperatures (oxidizing conditions) were seen to increase substantially. A number of predictive slagging and fouling indices have been used to evaluate the influence of the ash chemistry on the fuel combustion behaviour and this combined with the ash fusion testing has shown that HTC reduces the potential fouling and slagging in some of the resulting bio-coal if combusted.

4.2. Introduction

As discussed in Chapter 2, when undertaking this project there had been limited research into the fate of inorganic material in the biomass during HTC. This is perhaps surprising given inorganics are a particular issue for biomass during combustion, pyrolysis and gasification as large amounts of alkali and alkaline metals, particularly

potassium and sodium, along with sulphur and chlorine influence ash chemistry and influence the behaviours of the fuel in terms of its tendency to corrode equipment and cause slagging and fouling [39]. Demineralization of the fuel through dissolution of these alkali salts into the process water during HTC could potentially remove a large fraction of the fuel mineral content thereby reducing the above mentioned ash problems.

Previous work by Saddawi et al. [43] and others have demonstrated that simple washing of biomass in distilled water (at room temperature and pressure) can remove simple ionic salts such as alkali earth chlorides which dissolve easily. During HTC the subcritical water used has a lower density and viscosity than that of water under normal conditions [255] and as such removal of simple ionic salts within the biomass matrix can be enhanced. The increased dielectric content [256], increased ionic dissociation constant [257] and lower pH [11] of the subcritical water could also aid the removal of ionic bonded inorganics though ion exchange and dissolve the inorganic salts, thus removing ionic bonded inorganics from the biomass structure. The modification of the biomass structure during HTC will also further aid the removal of the inorganic elements.

When undertaking this work, only Reza et al. [76] had investigated the fate of inorganics during HTC, investigating *Miscanthus*, corn stover, switch grass and rice hull. The results showed reductions in the amount of calcium, sulphur, phosphorus, magnesium and potassium in the original biomass when the biomass is processed under hydrothermal conditions at 200° C, 230° C and 260° C. Removal of silicon appears limited at 200° C and 230° C although there was some indication that silicon content starts to decrease when the lignin starts to degrade at 260° C. It should be noted that despite a decrease in the inorganic content relative to the starting biomass, the overall concentration of inorganics within the char can increase.

As an initial scoping exercise to determine the behaviour of inorganics during HTC, this chapter has investigated a range of different feedstock. These feedstock include wet biomass wastes such as food waste, anaerobic digestion (AD) press cake, sewage sludge, fibre derived from organically separated municipal wastes and greenhouse waste, a number of terrestrial biomass such as *Miscanthus*, oak and willow and the aquatic biomass: microalgae and macroalgae. The feedstock investigated have a diverse biochemical composition and wide ranging levels of inorganics. This work seeks to understand the fate of inorganic material, the production of high energy density bio-fuels, and the prediction of the slagging and fouling behaviour during combustion.

4.3.Methodology

4.3.1. Materials

Samples of willow, *Miscanthus*, oak, greenhouse waste, food waste, secondary sewage sludge, AD press cake, macroalgae (*Laminaria Hyperborea*), microalgae (*Chlorella* spp.) and fibre derived from municipal waste were used in this investigation. The sample sizes ranged from 1x1 cm to 2x1 cm cuttings for willow and oak, 1x1 cm cuttings for *Miscanthus*, macroalgae, food waste and greenhouse waste, 600-1200 µm for municipal solid waste derived fibre, sewage sludge and AD press cake and a freeze died powder for microalgae. Samples were air dried before treatment and used as received for HTC on the assumption that in an industrial process, HTC would be conducted on chipped fuels to avoid energy-intensive size reduction prior to processing, taking advantage of the improved grindability. For the quantification work a portion of each sample is ground to a size meeting the test requirement.

4.3.2. Hydrothermal carbonisation

HTC was performed in a 600 ml Parr bench top reactor (Parr, USA) at 200 °C and 250 °C at their isobaric pressures of 16 bar and 40 bar respectfully. The temperature of the reactor was controlled by a PID controller. For each run, 24 g of biomass and 220 ml of distilled water was loaded into the reactor giving 10 % solids loading. The reactor was then heated to the desired temperature at approximately 8 °C $minute^{-1}$ and the reaction temperature held for one hour. After one hour the reactor was allowed to air cool. When cooled, the gas product was released to the atmosphere and the solid and liquid products separated by filtration under gravity using 150 mm qualitative circles (Whatman, UK). The sample was not washed in water or organic solvent. The bio-coal was allowed to air dry in a ventilated fume cupboard for a minimum of 48 hours.

4.3.3. Analysis

4.3.3.1.Inorganic analysis

The bio-coal and raw biomass were air dried and homogenised as described in Section 3.1.2 on sampling and Section 3.1.3 on milling. To determine the inorganic elemental composition (excluding silicon) samples were microwave digested (Aston Parr, USA), as described in section 3.6.1, with 200 mg of sample in 10 ml concentrated nitric acid (HNO_3). Potassium, sodium, calcium, magnesium and iron were determined by AAS (Valiant, USA), as described in Section 3.6.3; phosphorus and silicon determined using

calorimetry based methods, as described in Section 3.6.4 and Section 3.6.5 respectively. Heavy metals determined by ICP-MS (Perkin Elmer, USA) as described in Section 3.6.2. The AAS colorimetric methods were calibrated using standard elemental stock solution (Spectrosol, UK) and two certified biomass reference materials (Elemental Microanalysis, UK) were used to check the calibration and extraction efficiency.

4.3.3.2. Organic analysis and ash measurement

Carbon, hydrogen, nitrogen and sulphur content of the raw biomass and bio-coal was analysed using a Flash 1112 CHNS analyser (CE Instruments, USA) using the methodology described in Section 3.4.1. The carbon, hydrogen and sulphur was corrected for moisture using Equation 3.5 and hydrogen corrected using Equation 3.6, in accordance with ASTM D3180-15. The instrument was calibrated and checked using calibration standards and certified biomass reference materials (Elemental Microanalysis, UK). Ash content within the raw biomass and bio-coal was calculated in accordance with BS EN ISO 18122:2015 using a muffle furnace as described in Section 3.3.2. Oxygen content of the biomass was calculated by difference using Equation 3.7 and higher heating value (HHV) subsequently calculated by Dulong's equation (see Equation 3.11). Moisture content was determined in accordance with BS EN ISO 13134-1: 2015 using a moisture oven (Carbolite, UK) as described in Section 3.3.1, with values corrected to a dry basis in accordance with ASTM D3180-15.

4.3.3.3. Prediction of slagging and fouling behaviour

Ash fusion testing (AFT) was performed using a Carbolite digital ash fusion furnace in accordance with the standard method for the determination of ash melting behaviour (DD CEN/TS 15370-1:2006) using the methodology described in Section 3.7.1. In addition, various slagging and fouling indices have been utilised with their equations 1-6 in Table 3.3. Their underlying theory and calculation methodologies given in Section 3.7.2.

4.4. Results and discussion

4.4.1. Hydrothermal carbonisation yields

The mass yields of the HTC bio-coals shown in Figure 4.1 are both feedstock and temperature dependant. The yields for the lignocellulosic biomass range between 58 % and 70 % at the lower process temperature (200 °C) and between 40 % and 46 % for the higher process temperature (250 °C). Greenhouse waste, which in this case is largely Paprika waste from Almaria, Spain produces similar yields to lignocellulosics with 59 %

and 46 % respectfully. The food waste has a different biochemical composition to that of lignocellulosic material, mainly comprising of protein, carbohydrate and lipid, and has lower yields for both high and low temperature HTC, with 40 % and 44 % respectfully. The smaller difference between the two treatments is linked to the different biochemical content of food waste. The results for the macroalgae and the microalgae, which have a similar biochemical content to the food waste, exhibit a greater reduction in yield compared with food waste with 56 % and 36 % for the macroalgae and 43 % and 28 % for the microalgae at 200 °C and 250 °C respectfully. These yields are significantly lower than for the lignocellulosic based biomasses for both the lower and higher temperature treatments, indicating biochemical composition is an important variable influencing the yield of bio-coal.

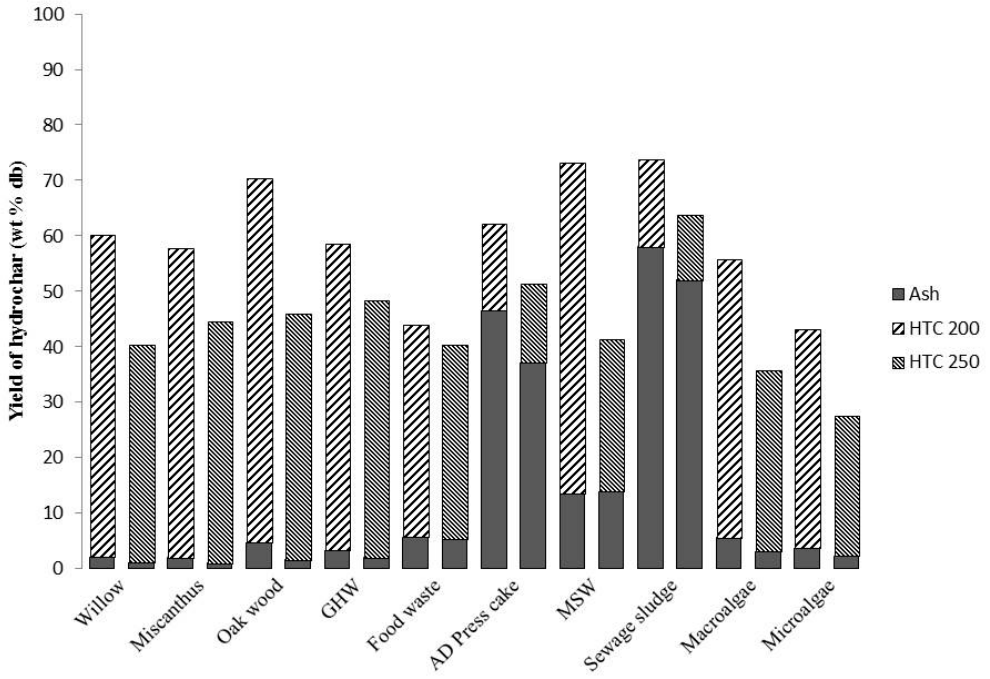

Figure 4.1: Bio-coal mass yields under hydrothermal conditions at 200° C and 250° C respectfully.

For the AD press cake, sewage sludge and to a lesser extent the municipal solid waste (MSW) the high yields are misleading due to the high ash content within the bio-coals. The reduction in yield between the lower and higher temperature treatments for the AD press cake appears to be mostly due to a decrease in the inorganic fraction (ash) within the bio-coal as opposed to greater degradation of the organic fraction. The HTC of AD press cake results in a significant solubilisation of the organic content into the process water. For sewage sludge, the resultant reduction in yield between 200 and 250° C is due to a combination of both degradation of the organic fraction and removal of the inorganic

fraction. For the MSW, the difference is largely due to degradation of the organic fraction of the bio-coal.

A decrease in ash relative to the starting biomass was observed in all samples, except the MSW which showed little change, however some caution is needed as the overall concentration of ash within the char can increase. The ash contents of the bio-coals are given in Table 4.1.

The decrease in yields between the lower and higher temperature treatments is believed to be primarily due to degradation of different biochemical components at the higher temperature. For lignocellulose based biomass, the significant degradation of cellulose occurring above 210° C [311] explains the higher mass yields at 200°C, with the yield decreasing between 200° C and 250° C due to degradation of the cellulose and to a lesser extent lignin, which begins to degrade between 220° C and 260° C [28, 75, 76]. Increasing the temperature from 200° C to 250° C also increases the pressure from 16 bar to 40 bar, which can exert an influence on the reaction equilibrium. Although this effect has been experimentally shown, it is thought to have a small impact during the HTC process [11].

4.4.2. Ultimate Analysis

The ultimate analysis of the feedstock and bio-coals produced at 200° C and 250° C are listed in Table 4.1. The ultimate analysis (CHNS) shows an increase in the carbon content (% db) for the bio-coals at 200° C and 250° C compared to the raw feedstock for all samples except sewage sludge (Table 4.1). Increased temperatures have been shown to favour higher carbon content, with carbon content increasing in all bio-coals when calculated on a dry ash free basis. Higher HHV is also observed with an increase in temperature. The exception to the rule is the processing of sewage sludge and AD press cake which result in lower HHV due to the large solubilisation of carbon proportional to the ash, although there are still significant increases in carbon density within the organic fraction for both feedstock when calculated on a dry ash free basis. The oxygen content determined by difference showed a significant reduction in all the bio-coals although the oxygen content of the sewage sludge and AD press cake samples maybe underestimated due to the high ash content.

The decreased oxygen content is due mainly to decarboxylation and dehydration reactions during HTC. Decarboxylation degrades the carboxyl (-COOH) and carbonyl groups (C=O), forming CO_2 and CO respectively. Dehydration removes hydroxyl groups

(-OH) from the feedstock leading to less hydrophilic functional groups. Both reactions can therefore reduce the oxygen content significantly in turn upgrading the energy density. Oxygen loss is of great importance, as its reduction increases the energy content (HHV) of the bio-coals. The reaction temperature also has a clear influence on the reducing oxygen content and increasing carbon content of the bio-coals. 250° C bio-coals contain higher carbon contents when compared to 200° C bio-coals (Table 4.1). This trend is further supported by the yields of bio-coal shown in Figure 4.1. Lower yields of bio-coal obtained at 250° C indicate that the decarboxylation and dehydration reactions are more favourable, with significant reductions in the level of oxygen at the higher temperature.

The increase in temperature also has a marked influence on the HHV of the respective bio-coals. The HHV is generally higher for bio-coals produced at 250°C. As discussed previously the extent of decarboxylation and dehydration is temperature dependent. High temperatures further concentrate the carbon, this coupled with a reduced oxygen content increase the HHV (Table 4.1). While higher temperatures are associated with lower yields, due to a greater amount of organic material undergoing decomposition, the enhanced removal of oxygen offsets this loss in energy terms of energy yield. However the energy yield at 200°C can be higher than bio-coals produced at 250°C due to the higher mass yields obtained at 200°C.

The O/C ratio and the H/C ratio of the bio-coals exhibit lower values when compared to the initial feedstock (Table 4.1). This will make the fuel more favourable as generally a fuel with low H/C and O/C ratios have reduced energy losses due to smoke and water vapour during the combustion process [265]. The reduction in the O/C and H/C ratios are a result of removal of CO_2 and H_2O indicating that the bio-coals possess a greater coal like behaviour than the feedstock. This agrees with the literature, which suggests that under hydrothermal conditions biomass undergoes removal of hydroxyl groups through dehydration, removal of carboxyl and carbonyl groups though decarboxylation, cleavage of ester and ether bonds through hydrolysis and for lignocellulose based biomass, increased aromatisation from the dehydration of lignin and aromatisation of carbohydrates [11].

Table 4.1: Ultimate analysis results for feedstock and bio-coals

Feedstock	% C (db)	% H (db)	% N (db)	%S (db)	% O (db)	HHV (MJ/kg db)	% Ash (db)	H/C (daf)	O/C (daf)	Energy Yield (%)
Willow	45.3±0.2	6.2±0.3	0.5±0.0	0.1±0.0	43.8	16.4	4.1	1.64	0.73	-
HTC 200	58.9±0.6	7.2±0.1	1.4±0.0	0.2±0.0	29.0	25.0	3.5	1.47	0.37	92.0
HTC 250	70.4±0.0	5.3±0.1	1.3±0.0	0.1±0.0	20.2	27.8	2.7	0.90	0.22	44.7
Miscanthus	46.0±0.0	5.7±0.1	0.5±0.0	0.1±0.0	42.8	16.1	4.9	1.49	0.70	-
HTC 200	61.1±0.6	6.2±0.1	0.8±0.0	0.1±0.0	28.3	24.5	3.5	1.22	0.35	88.0
HTC 250	71.0±0.6	7.9±0.0	1.1±0.0	0.2±0.0	17.5	32.1	2.3	1.34	0.18	58.5
Oak Wood	43.4±0.5	5.9±0.1	0.3±0.1	0.1±0.1	42.9	15.4	7.4	1.63	0.74	-
HTC 200	55.0±0.1	4.6±0.1	1.0±0.0	0.0±0.0	32.7	19.3	6.7	1.00	0.45	88.1
HTC 250	72.2±0.6	6.6±0.0	2.2±0.0	0.2±0.0	15.2	31.1	3.6	1.10	0.16	71.8
Greenhouse waste	45.7±2.6	6.7±0.3	1.1±0.5	0.2±0.0	36.4	18.5	9.9	1.76	0.60	-
HTC 200	59.6±0.1	6.3±0.1	1.9±0.0	0.0±0.0	26.5	24.4	5.7	1.27	0.33	77.8
HTC 250	68.5±0.1	6.1±0.1	3.6±0.0	0.2±0.0	17.4	28.8	4.2	1.07	0.19	54.3
Foodwaste	46.7±0.4	7.6±0.2	2.9±0.0	0.1±0.1	28.0	21.6	7.1	1.95	0.45	-
HTC 200	54.8±1.1	7.0±0.2	1.1±0.1	0.2±0.0	24.1	24.2	12.9	1.53	0.33	49.3
HTC 250	62.8±2.1	6.9±0.3	1.3±0.2	0.2±0.0	15.4	28.3	13.5	1.32	0.18	47.2

Table 4.1: Ultimate analysis results for feedstock and bio-coals continued…

Feedstock	% C (db)	% H (db)	% N (db)	%S (db)	% O (db)	HHV (MJ/kg db)	% Ash (db)	H/C (daf)	O/C (daf)	Energy Yield (%)
AD press cake	17.8±1.3	2.3±0.1	0.3±0.0	0.0±0.1	12.1	8.8	63.9	1.55	0.62	-
HTC 200	14.0±0.4	1.4±0.2	0.5±0.0	0.1±0.1	9.3	9.1	74.8	1.20	0.50	25.7
HTC 250	22.5±0.1	1.8±0.0	0.7±0.0	0.0±0.0	7.1	7.7	72.2	0.23	0.33	30.0
Municipal wastes	38.8±0.5	5.8±0.1	1.3±0.0	0.0±0.0	19.8	17.9	28.3	1.79	0.38	-
HTC 200	38.8±0.1	5.2±0.1	1.1±0.0	0.1±0.0	36.3	14.1	18.6	1.61	0.70	57.7
HTC 250	50.0±0.2	6.3±0.1	2.7±0.0	0.1±0.0	7.2	24.6	33.7	1.51	0.11	56.9
Sewage sludge	13.1±0.4	3.7±0.2	4.1±0.1	2.4±0.0	13.7	7.3	63.0	3.38	0.78	-
HTC 200	13.2±0.4	1.8±0.1	1.1±0.0	0.1±0.0	5.2	6.0	78.7	1.61	0.29	61.4
HTC 250	11.6±0.4	1.3±0.2	0.9±0.0	0.1±0.1	4.6	5.0	81.5	1.37	0.30	52.8
Macroalgae	31.6±0.1	5.2±0.0	2.8±0.0	4.5±0.0	35.3	11.8	20.6	1.97	0.84	-
HTC 200	48.2±0.2	4.7±0.2	2.3±0.0	0.1±0.1	34.5	16.8	10.2	1.17	0.54	79.6
HTC 250	59.5±1.7	5.4±0.3	5.9±0.1	0.1±0.0	20.5	24.6	8.6	1.09	0.26	52.9
Microalgae	48.4±0.3	7.2±0.1	7.8±0.1	0.3±0.0	27.1	21.8	9.2	1.79	0.42	-
HTC 200	58.0±0.3	7.0±0.0	5.3±0.0	0.0±0.0	20.8	25.8	8.8	1.44	0.27	51.1
HTC 250	62.1±0.1	6.8±0.1	4.8±0.0	0.0±0.0	17.9	27.5	8.4	1.32	0.22	29.2

4.4.3. Influence of HTC on bio-coal ash chemistry

Table 4.1 shows the ash content of the raw biomass and the resultant bio-coal on a dry basis. The results have shown that for the lignocellulosic materials and algae, increasing temperature results in a decrease in ash content, while for the organic wastes the reverse is true. Figure 4.1 shows the net removal of ash between the 200 °C and 250 °C bio-coals, implying that under hydrothermal conditions a proportion of ash is removed, with a greater proportion with increasing reaction severity. The reason ash decreases in some bio-coals but increases in others is due to the feedstock specific ash chemistry, with the lignocellulosics having a greater proportion of the inorganic material extracted than organic material. Organic wastes have a greater proportion of the organic material removed, thus even though inorganic material is removed, it can still become increasingly concentrated within the bio-coal.

The inorganic concentrations (wt%) within the biomass and the resultant bio-coals also appear to be both element and feedstock dependent. Samples with higher silicon and iron contents appear to result in an increasingly high concentration of ash within the bio-coal, while those without high silicon and iron have a decreasing concentration of ash within the bio-coal. The major ash forming elements within bio-coals and feedstock are given in Table 4.2 and the net percentage of metal remaining within the bio-coal for potassium, sodium, calcium, magnesium and phosphorus is given in Table 4.3. The net percentage of metal remaining within the bio-coal is calculated based on the ratio of the weight percentage inorganic content of the bio-coal with that of the raw feedstock multiplied by the mass yield at the given temperature. The percentage metal extracted is simply calculated by subtracting the percentage of original metal left within the bio-coal from 100.

Of the main inorganics investigated, potassium and sodium show the greatest percentage reduction, which is consistent with the leaching experiments undertaken in Saddawi et al. [43]. For potassium, excluding sewage sludge, between 84 % and 97 % of the potassium in the raw biomass was extracted at 250 °C. For HTC at 200 °C removal of potassium was less at between 60 % and 93 %. Sewage sludge had a reduction of approximately 50 % K for both the 200 and 250 °C hydrothermal treatments. This smaller reduction when compared to the other feedstock could be due to the chemical form in which the potassium exists. The potassium reduction is consistent with Reza et al. [76], which reported reductions in potassium ranging between 80 % and 90 % under hydrothermal conditions at 200, 230 and 260 °C, processing *Miscanthus*, albeit ground to

between 600 and 1180 µm. In Saddawi et al. [43], a washing procedure was used at ambient temperature involving water followed by ammonium acetate and hydrochloric acid, gave a potassium reduction of 46 % and 62 % for willow and *Miscanthus* from the starting biomass using similar sized fuel to this investigation.

Table 4.2 Major ash forming elements within bio-coals and feedstock

Feedstock	Na (wt%)	Mg (wt%)	P (wt%)	K (wt%)	Ca (wt%)	Fe (wt%)	Si (wt%)	S (wt%)
Willow	0.01	0.12	0.05	0.28	0.20	0.01	0.03	0.10
HTC 200	0.01	0.05	0.02	0.07	0.11	0.01	0.01	0.16
HTC 250	0.01	0.11	0.08	0.11	0.24	0.01	0.02	0.10
Miscanthus	0.02	0.06	0.02	0.17	0.20	0.01	2.10	0.10
HTC 200	0.01	0.04	0.02	0.08	0.09	0.01	2.81	0.10
HTC 250	0.01	0.04	0.01	0.05	0.05	0.01	2.91	0.21
Oak Wood	0.01	0.08	0.02	0.16	2.37	0.01	0.02	0.02
HTC 200	0.01	0.06	0.01	0.07	3.25	0.01	0.08	0.01
HTC 250	0.01	0.07	0.03	0.06	2.67	0.02		0.21
Greenhouse waste	0.04	0.81	0.08	4.03	1.58	0.01	0.20	0.24
HTC 200	0.03	0.57	0.06	2.58	2.44	0.02	0.15	0.02
HTC 250	0.02	0.61	0.16	0.51	1.34	0.08	0.10	0.19
Foodwaste	0.73	0.11	0.12	0.76	1.58	0.04	0.50	0.09
HTC 200	0.11	0.07	0.15	0.12	0.85	0.22	1.37	0.15
HTC 250	0.07	0.18	0.26	0.05	2.78	0.13	1.19	0.15
AD press cake	0.19	0.59	0.17	0.87	1.92	0.82	52.70	0.00
HTC 200	0.04	0.50	0.14	0.35	1.56	0.88		0.00
HTC 250	0.03	0.93	0.18	0.22	2.18	0.96	47.22	0.00
Municipal wastes	0.54	0.54	0.09	0.53	3.84	0.60	10.19	0.50
HTC 200	0.19	0.50	0.09	0.26	3.34	0.57	7.69	0.10
HTC 250	0.05	0.88	0.17	0.15	2.45	0.86	15.92	0.11
Sewage sludge	0.10	0.65	0.28	0.89	1.73	3.33	33.24	2.42
HTC 200	0.04	0.81	0.35	0.64	2.28	4.14	48.17	2.86
HTC 250	0.04	0.86	0.23	0.69	2.26	4.29	42.21	
Macroalgae	2.44	0.72	0.08	4.38	0.73	0.01	0.16	4.51
HTC 200	1.06	0.48	0.11	1.91	0.96	0.03	0.13	3.95
HTC 250	0.91	0.81	0.19	1.63	1.46	0.04	0.10	2.96
Microalgae	0.31	0.45	0.44	0.50	0.76	0.03	0.34	3.03
HTC 200	0.10	0.70	0.41	0.16	1.53	0.06	0.31	3.09
HTC 250	0.05	0.98	0.38	0.07	1.75	0.05	0.36	2.59

Table 4.3: The percentage of potassium, sodium, calcium, magnesium and phosphorus remaining within the bio-coal after hydrothermal processing

Feedstock	Na (%)	Mg (%)	P (%)	K (%)	Ca (%)
Willow	100	100	100	100	100
HTC 200	54	25	28	16	34
HTC 250	36	36	59	16	49
Miscanthus	100	100	100	100	100
HTC 200	26	41	50	29	28
HTC 250	21	31	30	12	11
Oak Wood	100	100	100	100	100
HTC 200	54	50	57	31	97
HTC 250	30	37	82	16	52
Greenhouse waste	100	100	100	100	100
HTC 200	48	44	41	40	91
HTC 250	22	26	67	4	30
Foodwaste	100	100	100	100	100
HTC 200	7	29	53	7	14
HTC 250	4	64	85	3	42
AD press cake	100	100	100	100	100
HTC 200	14	49	52	24	51
HTC 250	7	76	56	12	58
Municipal wastes	100	100	100	100	100
HTC 200	26	67	71	36	64
HTC 250	3	67	77	12	26
Sewage sludge	100	100	100	100	100
HTC 200	29	92	92	53	97
HTC 250	26	83	53	50	83
Macroalgae	100	100	100	100	100
HTC 200	24	37	76	24	73
HTC 250	13	41	88	13	71
Microalgae	100	100	100	100	100
HTC 200	14	67	40	14	86
HTC 250	5	60	24	4	63

Removal of sodium was observed for all samples, with the higher temperature associated with a greater reduction, although the percentage reduction appeared largely dependent on the sodium content of the starting biomass. For willow, *Miscanthus* and oak, reductions of between 46 % and 74 % were observed at 200 °C and reductions of between 64 % and 79 % were observed at 250 °C. The sodium content of the lignocellulosic material is however low in comparison to the other feedstock. Higher

sodium containing feedstock, such as AD press cake, food waste, municipal solid wastes, microalgae and macroalgae resulted in far greater sodium removal with between 74 % and 93 % removal at 200 °C and between 87 and 97 % removal at 250 °C. In comparison Saddawi et al. [43] reported a 30 % removal of sodium from willow and a 53 % reduction in sodium from *Miscanthus* after water washing. Reza et al. [76] reported reductions in sodium ranging between 31 and 40 % under hydrothermal conditions at 200, 230 and 260 °C, processing ground *Miscanthus*. The sodium content within the *Miscanthus* used in this investigation was similar to that in Saddawi et al. [43], 177 mg/kg and 192 mg/kg respectfully. The sodium content within Reza et al. [76] was 1451 mg/kg.

While all the bio-coals have a lower sodium and potassium content than the starting material, the alkaline metals magnesium and calcium along with phosphorus undergo more limited metal removal. For willow, all three metals are decreased at 200 °C but there is a smaller reduction at 250 °C. For willow, the magnesium, calcium and phosphorus concentration within the bio-coals is lower than that of the starting biomass but the magnesium, calcium and phosphorus reduction at 250 °C is almost proportional to the reduction in the organic fraction. The net removal of magnesium, calcium and phosphorus is also less at 250 °C. This phenomenon is common for the differing feedstock, with only *Miscanthus*, sewage sludge and microalgae having greater removal at 250 °C than 200 °C for magnesium, calcium and phosphorus. This reduced inorganics removal efficiency is also evident within the results for Reza et al. [76] which showed the inorganic element yields for *Miscanthus* were substantially lower at 260 °C compared with 200 °C for all elements investigated other than silicon.

The reason behind this decrease in metal extraction at higher temperatures could be due to increasing surface functionality of the bio-coals generated at higher temperatures reabsorbing metals from the process waters. It is known that the large number of carboxylic groups on the bio-coal surface can theoretically increase the cation exchange capacity (CEC) of the bio-coal [28]. The increased retention of cations could be due to increasing CEC of 250 °C bio-coals. The reduction may also be as a result of reduced extraction efficiency due to an increased build-up of hydrolysis derived products on the outer surface of the biomass macro-molecule at the higher temperature, as is hypothesised in Mosteiro-Romero et al. [98], reducing the extraction efficiency of the lower solubility salts. Finally there is also evidence that cations can play a role in polymerisation, with studies into the HTC of alginate (structural compound in seaweed) finding that divalent cations, such as calcium and magnesium promote cross linking of

alginates oligomers during char formation [147]. It could be that under the more severe conditions these metals are reincorporated into the bio-coal by this mechanism.

Calcium extraction appears most efficient in *Miscanthus* with 72 % removed at 200 °C and 89 % removed at 250 °C. Calcium extraction for *Miscanthus* in Reza et al. [76] was 88 % at 200 °C and 84 % removed at 260 °C. In contrast Saddawi et al. [43] extracted 19 % of the calcium using their water washing technique. In this investigation 66 % of the calcium from willow was removed at 200 °C and 51 % removed at 250 °C, while Saddawi et al. [43] extracted 3 % of the calcium though biomass washing. For the remaining feedstock investigated calcium varied as shown in Table 4.3 and this resulted in an increase in the calcium content in some of the bio-coals.

Magnesium extraction was most efficient for willow with 75 % extracted at 200 °C and 64 % removed at 250 °C; *Miscanthus* extraction was 60 % and 69 % respectfully. Reza et al. [76] extracted 88 % magnesium from *Miscanthus* at 200 and 250 °C. Saddawi et al. [43] extracted 14 % magnesium from willow and 56 % magnesium from *Miscanthus* using biomass washing. For the remaining feedstock in this study (excluding sewage sludge) between 33 % and 71 % magnesium was extracted at 200 °C and between 33 % and 67 % magnesium was extracted at 250 °C. For the lignocellulosic biomass and greenhouse wastes a net reduction in magnesium within the char was observed while for the remaining feedstock, magnesium became more concentrated within the char.

Phosphorus extraction followed similar trends to that of calcium and magnesium with the highest extractions associated with willow, *Miscanthus* and microalgae. Phosphorus extraction for willow was 72 % and 68 %; *Miscanthus* was 50 % and 70 %; and microalgae 60 % and 76 % for 200 °C and 250 °C respectively. Reza et al. [76] extracted 90 % phosphorus from *Miscanthus* at 200 °C and 58 % at 250 °C. Saddawi et al. [43] extracted 56 % phosphorus from willow and 49 % magnesium from phosphorus using biomass washing.

For most biomass materials, the major element speciation can be divided into three categories: (i) water soluble ionic salts, (ii) organically associated metals ionic or covalently bonded with tissue, and (iii) amorphous, crystalline or pure precipitated compounds [37, 38]. Most of the sodium and potassium within the biomass is in the form of ionic salts (>90%) such as sodium nitrate, sodium chloride, potassium nitrate and potassium chloride. For magnesium, between 60 and 90 % is in the form of ionic salts comprising of magnesium nitrate, chloride and phosphate, with a large proportion of the remainder being organically associated with chlorophyll and the biomass macromolecule.

For calcium, between 20 and 60 % is in the form of nitrate, chloride and phosphate ionic salts; a small proportion is incorporated into the biomass macromolecule, and the remainder is in the form of amorphous or crystalline compounds. Phosphorus occurs in both its ionic form and organically associated in protein, phospholipids and nucleic acids [37, 38]. The type of compound in which the metal is associated within the biomass is likely to strongly influence the extraction efficiency during HTC. A large proportion of potassium and sodium within the biomass is in the form of soluble ionic salts and this corresponds to a larger extraction of these metals. The magnesium, calcium and phosphorus is less easily extracted and corresponds to its association with organic matter in the biomass.

Limited leaching of silicon, titanium, iron and aluminium have been reported under hydrothermal conditions in Reza et al. [76] and several biomass washing experiments [205, 264, 312] using finely ground biomass. This is due to their very low solubility [205] and for the larger particle size used in these experiments it is assumed that there was only limited removal.

4.4.4. Influence of HTC on ash behaviour during combustion

The concentrations of the major ash forming elements within biofuels are listed in Table 4.2 and it is the behaviour of these elements within the ash, which brings about issues with slagging, fouling and corrosion, as discussed in Section 2.5.

The temperature at which the ash melts and fuses is strongly influenced by the alkali and alkaline metals which act as a flux for alumina-silicate ash [39]. Generally speaking calcium and magnesium increase the melting temperatures of ashes while potassium and sodium decrease it, although due to complex interactions between potassium, chlorine, sulphur, silicon and calcium each element cannot always be evaluated individually [39]. Table 4.4 contains the ‘deformation’ temperature, the point the ash starts to become sticky and potentially problematic, and the ‘flow’ temperature, the temperature in which it melts, for the ash fusion results for the raw feedstock and bio-coals as defined in DD CEN/TS 15370-1:2006 (see Section 3.7.1). Figure 4.2a-d give the transition temperatures between phases defined in Section 3.7.1 for willow, *Miscanthus*, macroalgae and microalgae feedstock. The results show that HTC has a strong influence on the ash fusion temperatures with the processed fuels becoming sticky (deformation) and melting (flow) at higher temperatures than the raw feedstock. This finding would support the theory that a large proportion of the potassium and sodium within the starting biomass is removed under HTC, reducing the flux effect they have on ash melting. The

more limited removal of magnesium and calcium under HTC, especially at 250 °C has been shown to result in increased concentrations of magnesium and calcium in the bio-coal. This could be advantageous, as the change in alkali to alkaline ratio within the char should increase the melting /fusion temperature.

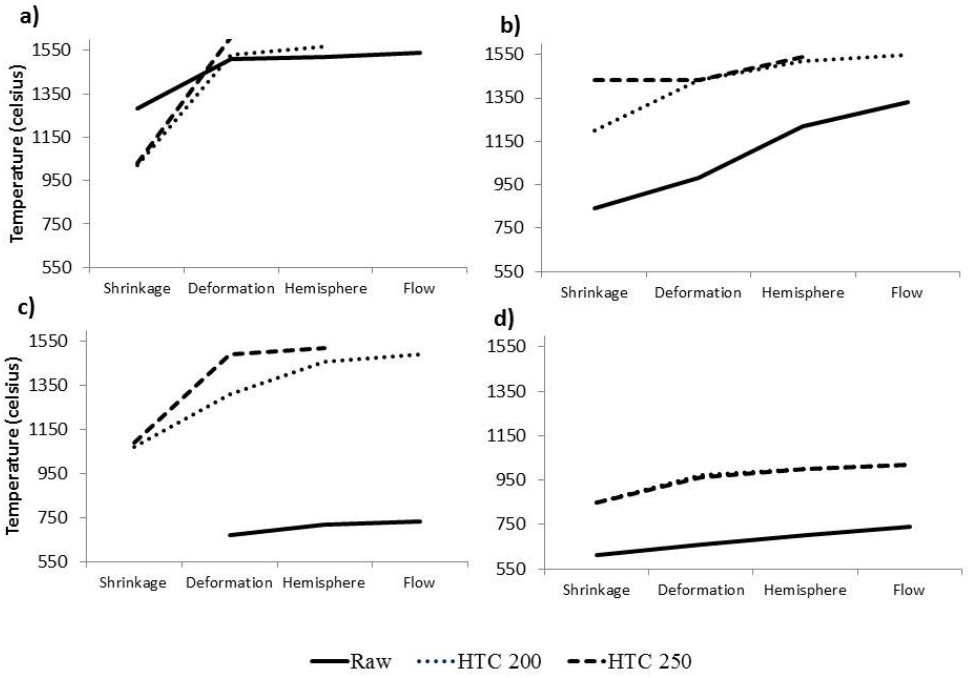

Figure 4.2: Ash fusion transition temperatures for a) willow, b) *Miscanthus*, c) macroalgae and d) microalgae.

Slagging potential is largely determined though fusion temperatures, with a decrease in fusion temperature indicating an increase in slagging potential [39]. The increase in fusion temperatures observed via the HTC consequently indicates slagging potential is reduced by HTC, with greater reductions brought about at higher temperatures. Table 4.4 also contains the results of a number of predictive slagging indices used to evaluate the influence of the ash chemistry, with their equations given in Table 3.3. The limited removal of iron under HTC, results in its accumulation within the char, which in turn results in improvements in bed agglomeration index (BAI), slag viscosity index (SVI) and base to acid ratio (R b/a). Some of the biomass is however predicted to have high slagging propensities, for example willow. Willow is predicted to have a high slagging propensity due to low silicon and titanium dioxide, when calculated using BAI, SVI and R b/a. This is despite high fusion temperatures outside of the furnace range (furnace limit 1570 °C).

Some caution is consequently needed when interpreting chemical composition based slagging indices as these indices are based originally on coal ash slagging and

assume the ashes will behave like alumino-silicate coal ashes. Biomass ash systems are chemically very different to alumino-silicate coal, with a lot of the ashes being low in both silicon and aluminium. Potassium tends to be the most predominant alkali metal in a form that is available to contribute to both fouling and slagging. Consequently, care is needed when comparing conventional slagging and fouling index values for biomass [39, 205]. This appears particularly applicable to the macroalgae results, as despite the 250 °C bio-coal having a flow temperature greater than that of the furnace limit, which suggests a low slagging potential (see Figure 4.2c), all slagging indices, indicate a high slagging inclination.

The actual slagging behaviour, compared to the indices predicted behaviour for samples such as microalgae, appears most likely due to the changes between ratios of ash components within the bio-coal ash and the resulting form the potassium takes in the fuel. It is likely that the retained calcium and phosphorus within the bio-coal is behaving in a similar way to calcium and phosphorus based additives used abate problems in biomass combustion [234]. Consequently, residual potassium chloride present could be either binding with calcium rich phosphates (see Equation 2.13), or become potassium phosphates (see Equation 2.14) which can then further react with calcium oxides (see Equation 2.15). These calcium potassium phosphate complexes are stable and removes the potassium available to form low temperature melting potassium silicates [200, 202]. Therefore, despite high levels of alkali metals, which would normally bring about a low ash melting temperature and slagging, the formation of thermally stabile complexes will remove the potassium available to form low temperature melting potassium silicates. While previous reports of high slagging seaweeds in Ross et al. [61] appear to be verified, it appears that hydrothermally processes seaweeds may perform significantly better. The low transition temperatures for microalgae could be due to the low silicon content within the feedstock. Strain selection could yield significantly higher transition temperatures.

In addition to slagging, fouling and corrosion is another major issue in commercial furnaces. HTC appears to result in a net improvement in the fouling indices with the Alkali Index (AI) improving for all feedstock, as HTC increases the calorific value of the fuel while reducing the potassium and sodium content. HTC should also reduce the chlorine within the fuel, chlorine being the main element in metal corrosion (see Section 2.5.2.3). Chlorine exists within biomass in the form of water soluble ionic salts (NaCl, KCl, $CaCl_2$, $MgCl_2$ and ionic chloride (Cl^-)) [37, 38] with the ionic salts making up a large proportion of the total inorganics extracted under HTC. The extraction of these

chloride based salts will result in the extracted chlorine appearing as chloride in the process waters. Biomass washing experiments have shown that between 85 % and 100 % of total chlorine within the biomass is extracted though washing [43, 205, 264]. The fouling inclination calculated by the Fouling Index (FI) is shown to improve after HTC however; a number of feedstock and bio-coal were calculated as having high fouling inclination due to low fuel silicon.

Table 4.4: Fouling indices and ash fusibility flow temperature

Feedstock	Fouling and Slagging Indices						Ash Behaviour (°C)	
	AI	BAI	R b/a	SI	FI	SVI	Deformation	Flow
Willow	0.16	0.03	2.1	0.2	39.4	6	1310±0	1540±0
HTC 200	0.04	0.11	0.6	0.1	9.9	4	1330±10	>1570
HTC 250	0.05	0.14	1	0.1	25.4	3	>1570	>1570
Miscanthus	0.11	0.06	0.3	0	1.7	84	980±10	1350±20
HTC 200	0.04	0.13	0.1	0	0.3	93	1430±0	1550±0
HTC 250	0.02	0.27	0.1	0	0.1	95	1430±0	>1570
Oak Wood	0.08	0.07	66.6	1.3	445.4	1	1390±0	1420±0
HTC 200	0.03	0.15	80.5	0.8	127	1	1360±10	1410±0
HTC 250	0.02	0.33	1.3	0.3	1.6	43	1480±0	1520±0
Greenhouse waste	2.45	0	2.1	0.5	93.9	6	1480±10	1550±0
HTC 200	1.28	0.01	37.8	0.8	1932.7	3	1410±0	1480±0
HTC 250	0.22	0.19	47	8.9	718	1	1500±0	1540±0
Foodwaste	0.71	0.03	7.2	0.7	179.5	18	1570±0	>1570
HTC 200	0.1	1.05	2.9	0.4	17.8	24	1450±10	>1570
HTC 250	0.04	1.2	5.1	0.8	10.4	13	1420±20	1530±0
AD press cake	1.14	0.9	0.1	0	0.2	92	1330±20	1430±10
HTC 200	0.95	2.62	3.2	0	2.1	0	1320±10	1530±10
HTC 250	0.3	4.65	0.1	0	0	89	1420±20	1550±20
Municipal wastes	0.66	0.63	0.6	0.3	2.9	59	1150±0	1200±0
HTC 200	0.4	1.43	0.6	0.1	1.8	55	1160±0	1190±0
HTC 250	0.1	5.01	0.3	0	0.2	73	1180±0	1240±0
Sewage sludge	1.71	3.95	0.3	0.6	0.5	80	1230±0	1430±0
HTC 200	1.67	7.2	0.2	0.6	0.2	82	1220±0	1440±0
HTC 250	0.88	6.93	0.2	0	0.3	80	1240±0	1470±0
Macroalgae	9.49	0	16.2	73.2	1525.8	5	670±0	730±0
HTC 200	2.03	0.01	11.1	44.1	411.9	5	1310±0	1490±0
HTC 250	1.28	0.02	14.1	41.8	522.6	4	1490±0	>1570
Microalgae	0.43	0.04	4.1	12.4	45.4	15	660±0	740±0
HTC 200	0.11	0.27	4.8	14.9	18.9	8	970±0	1020±0
HTC 250	0.07	0.5	4.9	12.8	6	8	1180±0	1020±0

4.5. Conclusions

It can be concluded that the bio-coal yields for lignocellulosics typically range from between 58 % and 70 % at the lower process temperature (200 °C) and between 40 % and 46 % for the higher process temperature (250 °C). The yields for the non-lignocellulosic materials such as sewage sludge, AD presscake and algae were significantly lower than for the lignocellulosic based biomasses for both the lower and higher temperature treatments indicating that biochemical composition has a significant impact on bio-coal yield. The lower yields of bio-coal obtained at 250° C indicate that the decarboxylation and dehydration reactions are more favourable, with significant reductions in the level of oxygen at the higher temperature. These decarboxylation and dehydration reactions subsequently increase the energy content (HHV) of the bio-coals.

This chapter has shown that a large proportion of the potassium and sodium within the feedstock is extracted during HTC, while magnesium and calcium along with phosphorus undergo more limited removal. The removal of these metals has a significant influence on the slagging and fouling propensity of the fuel, demonstrating the importance of metal removal in terms of combustion behaviour. The results show that treatment of biomass by HTC has a strong influence on the slagging propensity of the fuel, with ash fusion temperatures for the processed fuels melting at higher temperatures to that of the raw feedstock. This research demonstrates that HTC can produce a coal like bio-coal from a range of feedstock which is: (i) more energy dense, (ii) easily friable and (iii) more hydrophobic than the starting material, it also could overcome the issues of slagging and fouling associated with the starting material.

5. Valorisation of low quality biofuels by Hydrothermal Carbonisation

5.1. Overview

Chapter 4 showed that the treatment of biomass by HTC has a strong influence on the slagging propensity of the fuel, with ash fusion temperatures for the processed fuels melting at higher temperatures to that of the raw feedstock. The behaviour and mass balance is however very feedstock dependent and the higher lignin biomass produce higher yields of bio-coal. In this chapter, two low quality biomasses, *Miscanthus* and brown kelp, have been investigated further.

These two feedstocks are of particular interest as biofuels derived from aquatic biomass such as macroalgae offer an extensive and largely unutilised biomass resource which does not compete with agriculture or forestry for land and freshwater; overcoming drawbacks associated with using terrestrial biomass to produce biofuels. Brown kelp is however limited in fuel applications due its low heating value (HHV), high halogen content, high ash content and a high slagging and fouling propensity. *Miscanthus* is a perennial bio-energy crop which is currently being commercially utilised in both Europe and US. Conventional harvesting of *Miscanthus* is in late winter/ early spring after the crop has senesced and dropped its leaves. This late winter/ early spring harvest is in part to meet combustion quality requirements, as senescence and loss of leaves lower fuel nitrogen, chlorine, ash, alkaline metals and moisture content. Although this overwintering leads to a significant decline in ash content, it does not completely overcome combustion issues such as slagging, fouling and corrosion, and early harvesting of *Miscanthus* can increase dry mass yields by 40 % hectare^{-1}. Based on the findings in Chapter 4, HTC could be a promising pre-treatment in the valorisation of these low quality, problematic biofuels, offering the potential to exploit an extensive and largely unutilised biomass resource in the form of kelp and increase conventional yields of *Miscanthus* by up to 40 % per hectare.

The work within this chapter has been published in (i) Algal Research and (ii) the Journal Fuel, albeit the work presented in this chapter is abridged. For the unabridged version of the brown kelp work, please see: Aidan M. Smith and Andrew B. Ross "Production of bio-coal, bio-methane and fertilizer from seaweed via hydrothermal carbonisation." *Algal Research* 16 (2016): 1-11. For the unabridged version of the *Miscanthus* work, please see: Aidan M. Smith, Carly Whittaker, Ian Shield and Andrew B. Ross "Potential for production of high quality bio-coal from early harvested *Miscanthus* by hydrothermal carbonisation." *Fuel* 220 (2018): 546-557

5.2. Production of bio-coal from seaweed using hydrothermal carbonisation

5.2.1. Introduction

The macroalgae results, presented in Chapter 4, have indicated a significant energy densification of the starting feedstock by HTC. Perhaps more interestingly the bio-coals demonstrated very high ash melting temperatures in the ash fusion test, which suggested a low slagging potential (see Figure 4.2c); although numerical slagging indices still indicated a high slagging inclination. This result could be significant as macroalgae offers a potentially large and largely unutilised biomass resource [60]. A resource which due to its chemical composition being significantly different to terrestrial plants, has limited its energetic application [58].

Details on the chemical composition of macroalgae is given in Section 2.1.2, but generally macroalgae is high in chlorine, high in ash, has low calorific value and high moisture content, making 'conventional' biomass treatments less suitable [61]. Consequently, macroalgae is an unattractive option for combustion, pyrolysis and gasification without some form of pre-treatment. This is due to the energy requirements in thermal drying and unfavourable ash chemistry in terms of slagging, fouling and corrosion [61]. Research into the energetic application of macroalgae is therefore usually limited to biogas through anaerobic digestion (AD) [313-315] and fermentation for bio-ethanol [58, 316]. There have also been some investigations into acid washing, as a pre-treatment for thermal applications [317, 318]. At the time of undertaking this work, only Xu et al. [319] has published on the HTC of macroalgae with the aim to produce a fuel, albeit others have investigated the production of organic chemicals [320] and carbon microspheres [147] via hydrothermal processing of alginate.

The results presented in Chapter 4 appear to overcome the physiochemical problems associated with macroalgae, which prevent its utilisation in combustion, pyrolysis and gasification. The chemical compositions of microalgae however vary between species. This chapter sets out to investigate the feasibility of using HTC to produce a high quality solid fuel from brown kelp, which could be used in both domestic and commercial furnaces. This work looks at three species of UK indigenous brown kelp; (i) *Laminaria digitata* (ii) *Laminaria hyperborea* and (iii) *Laminaria esculenta* to assess whether the trends observed in Chapter 4 apply to other brown kelp species. Moreover the composition also varies within a single species, both seasonally and geographically [321]. Studies of the seasonal variation of seaweed composition have generally show that the carbohydrates such as laminarin and mannitol peak in the summer resulting in the

highest energy content. In contrast, the protein, ash and alginic acid content peak in the winter months resulting in lower calorific values [63, 322]. Harvesting toward the end of September results in a feedstock with the highest carbon content and the lowest nitrogen content [322]. The impact of this variation could influence the suitability of HTC as a pre-treatment. Therefore, the investigation also sets out to assess how the seasonal compositional variation of the seaweed affects the solid fuel quality.

5.2.2. Methodology

5.2.2.1. Hydrothermal carbonisation

HTC was performed in the 600 ml Parr reactor (Parr, USA) at 200 °C and 250 °C at their isobaric pressures. For each run, 24 g of freeze dried sample and 220 ml of distilled water was loaded into the reactor giving a solids loading of 10 %. The macroalgae used in HTC was processed unground and was simply rehydrated when mixed with the distilled water. The reactor heating rate was approximately 8 °C minute^{-1} and the reaction temperature held for one hour. After one hour, the reactor was air cooled to room temperature (approximately 2 ½ hours from 200 °C; three hours from 250 °C). When cooled, the reactor was depressurised and the reactor reweighed to calculate gas and moisture loss along with the remaining combined mass of process water and bio-coal. The solid and liquid products were separated by filtration under vacuum using 110 mm qualitative circles (Grade 15, Munktell, UK). The bio-coal was air dried in a fume cupboard for a minimum of 48 hours. Mass of process water was calculated by subtracting the dry mass of bio-coal from the combined mass of process water and bio-coal.

5.2.2.2. Materials

Samples of macroalgae were provided by the Scottish Association for Marine Science (SAMS) in Oban. *L. digitate, L. hyperborea and A. esculenta*, were harvested from wild kelp beds at Easdale on the west coast of Scotland in July 2009. In addition, samples of *L hyperborea* were collected in the spring (April), autumn (October) and winter (January) at the same location.

5.2.2.3. Analysis

5.2.2.4. Inorganic analysis

Samples were digested in a microwave (Aston Parr, USA), as described in section 3.6.1 and potassium, sodium, calcium, magnesium and iron determined by AAS (Valiant, USA), as described in Section 3.6.3. Phosphorus and silicon determined using calorimetry

based methods, as described in Section 3.6.4 and Section 3.6.5. Heavy metals determined by ICP-MS (Perkin Elmer, USA) as described in Section 3.6.2. Chlorine was analysed by combustion in an oxygen bomb (Parr, USA) followed by determination using ion exchange chromatography (Dionex, USA), as described in Section 3.6.7.

5.2.2.4.1. Organic analysis and ash measurement

Carbon, hydrogen, nitrogen, sulphur and oxygen content was determined using a Flash 2000 CHNS-O analyser (Thermo Scientific, USA), with the method described in Section 3.4.2. The volatile and fixed carbon component of the proximate analysis carried out using thermo-gravimetric analysis (Mettler Toledo, Switzerland) as described in Section 3.3.3. Ash content was determined using a muffle furnace, as described in Section 3.3.2. Moisture content was determined using a moisture oven (Carbolite, UK) as described in Section 3.3.1. The calorific value of the bio-coal and was calculated by both bomb calorimetry (Parr, USA) and Dulong's Equation (see Equation 3.11); as described in Section 3.5. Figures are given on a dry basis in accordance with ASTM D3180-15, with hydrogen and oxygen values corrected to account for moisture.

5.2.2.4.2. Prediction of slagging and fouling behaviour

Ash fusion testing (AFT) was performed using a Carbolite digital ash fusion furnace in accordance with the standard method for the determination of ash melting behaviour (DD CEN/TS 15370-1:2006) using the methodology described in Section 3.7.1. In addition, various slagging and fouling indices have been utilised with their equations 1-6 in Table 3.3. Their underlying theory and calculation methodologies given in Section 3.7.2.

5.2.2.4.3. Biological Methane Potential

The biological methane production (BMP) was calculated by drying a known volume of process water at 60 °C and calculating the carbon, hydrogen, nitrogen, sulphur and oxygen content analysed using a Flash 2000 CHNS analyser (Thermo Scientific, USA). Inorganic content within the process water was calculated by difference (see Equation 3.19) due to high minerals content of the water and high levels of oxygen being incorporated into the ash on drying. A full description of the process is given in Section 3.10.6.1. Calculations of potential gas yields by methanogenesis have been calculated based on the Boyle's equation (see Equation 3.20) and hydrogen yields via hydrogenesis using Equation 3.21.

5.2.3. Results and discussion

5.2.3.1. Influence of HTC on the bio-coal organic chemistry

The mass yields, calorific content and elemental composition of the bio-coals and starting feedstocks are given in Table 5.1. The results have shown a significant increase in energy density in the bio-coal, with the 'as received' CV of the fuel typically 22 MJ/kg for the 200 °C treatment and 25 MJ/kg for the 250 °C treatment. The CV of the initial feedstock typically ranges from 11.2 and 14.1 MJ/kg. It should be noted that the starting biomass has been dried, with a starting moisture content of between 80 and 90 %, which is consistent with Black [321], this energy penalty has not been considered in these figures; the bio-coal on the other hand have merely been air dried, with an air dried moisture content of between 2.1 and 3.5 %.

The energy densification of the bio-coal is as a result of changes to the ratio of carbon and oxygen (O/C) in the fuel, with the carbon content appearing to increase, while the oxygen and ash content appears to decrease. The Van Krevelen diagram given in Figure 5.1 shows how the O/C and hydrogen to carbon (H/C) ratios of the bio-coal compare with coals and lignin [20, 29]. The results show the bio-coal have a coal like morphology with an O/C ratio between that of bituminous coals and lignite as reported in Hatcher et al. [323]. The O/C ratios are similar to reported pine and fir 255 °C bio coals reported in Hoekman et al. [29].

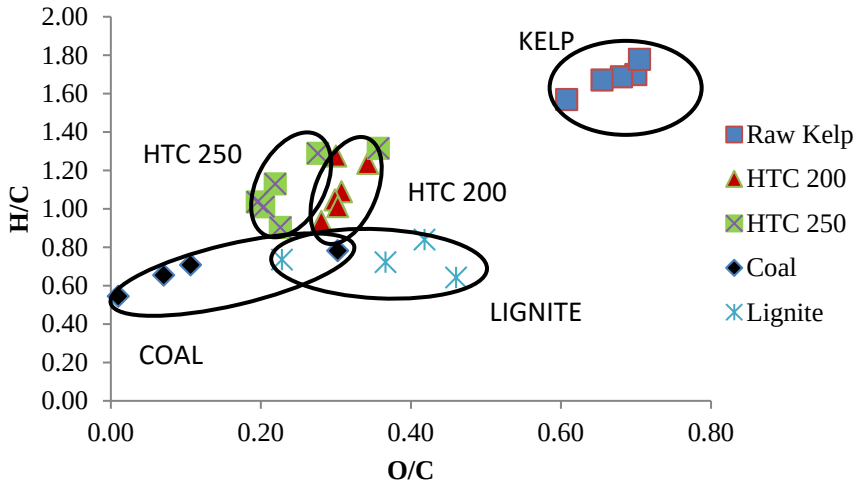

Figure 5.1: Van Krevelen diagram showing bio-coal, biomass, lignite and coals (lignite and coals adapted from Hatcher et al. [323])

Table 5.1: Proximate and ultimate analysis results for feedstock and bio-coal

Feedstock	Yield (% Mass db)	% C (db)	% H (db)	% N (db)	%S (db)	% O (db)	HHV (Dulong) (MJ/kg)	CV (Bomb) (MJ/kg) (ar)	% Ash (db)	H/C (daf)	O/C (daf)
Alaria	-	38.2±1.0	5.0±0.3	2.3±0.1	1.3±0.1	30.9±0.8	14.5	12.8	22.3±0.0	1.57	0.61
HTC 200	30.0	58.0±1.1	5.3±0.2	3.4±0.1	0.3±0.0	23.8±0.3	22.9	22.9	9.2±0.3	1.09	0.31
HTC 250	23.7	59.1±1.1	5.6±0.1	3.3±0.1	0.3±0.1	17.3±0.3	24.8	24.7	14.5±0.2	1.13	0.22
L.Digitata	-	33.3±2.4	4.7±0.2	1.7±0.1	0.9±0.3	31.1±2.1	12.4	11.4	28.3±0.0	1.70	0.70
HTC 200	21.8	50.2±0.4	5.3±0.1	2.4±0.0	0.7±0.1	20.1±0.7	21.0	22.5	21.2±0.3	1.27	0.30
HTC 250	18.4	55.9±0.6	6.1±0.0	2.9±0.0	0.1±0.0	26.6±1.2	22.9	22.6	8.3±0.1	1.31	0.36
L. Hyp' Spring	-	32.3±0.4	4.5±0.1	2.7±0.0	0.9±0.6	29.3±2.0	12.2	11.2	30.1±0.0	1.69	0.68
HTC 200	28.6	54.2±0.3	5.6±0.0	3.5±0.0	0.1±0.0	24.7±0.3	21.9	21.9	11.9±0.1	1.24	0.34
HTC 250	24.7	54.0±0.4	5.8±0.0	3.1±0.1	0.4±0.1	19.8±0.8	23.0	24.1	16.9±0.2	1.29	0.28
L. Hyp' Summer	-	38.2±0.1	5.3±0.0	1.9±0.0	0.6±0.0	33.3±0.7	14.5	12.9	20.6±0.0	1.67	0.65
HTC 200	31.2	62.3±0.9	5.4±0.2	3.1±0.0	0.1±0.0	24.8±0.2	24.4	23.0	4.3±0.1	1.05	0.30
HTC 250	24.3	67.1±0.9	5.7±0.1	3.2±0.1	0.1±0.0	18.2±0.4	27.5	26.5	5.7±0.1	1.01	0.20
L. Hyp' Autumn	-	42.0±0.5	6.2±0.1	2.0±0.0	0.0±0.0	39.5±0.0	16.1	14.1	10.2±0.0	1.78	0.70
HTC 200	33.0	64.6±0.6	5.0±0.0	2.6±0.0	0.0±0.0	24.1±0.4	24.7	22.6	3.6±0.1	0.93	0.28
HTC 250	31.7	66.9±0.3	5.0±0.1	2.8±0.1	0.0±0.0	20.1±0.2	26.2	25.9	5.1±0.1	0.90	0.23
L. Hyp' Winter	-	34.5±0.2	4.8±0.0	2.4±0.0	0.0±0.0	29.3±0.9	13.2	12.3	29.1±0.0	1.66	0.64
HTC 200	39.0	57.8±0.8	4.9±0.1	3.1±0.0	0.1±0.0	23.3±0.8	22.3	21.2	10.8±0.2	1.01	0.30
HTC 250	23.6	63.3±0.9	5.5±0.2	3.3±0.1	0.1±0.0	16.5±0.2	26.3	25.4	11.3±0.1	1.04	0.20

The H/C ratios are greater for the seaweed bio-coal than for coal, with all bio-coals typically between 0.9 and 1.3. This appears consistent with the H/C ratios presented in Chapter 4 (Smith et al. [213]) where lignocellulosic biomass was processed under identical conditions, while Hoekman et al. [29] reported H/C ratios between 0.8 and 1.0 for their 255 °C bio-coals. High H/C ratios can be associated with processing in alkaline conditions, and the alkaline metals extracted into the process waters maybe the cause [324]. The 250 °C seaweed bio-coals have a lower O/C ratio than the 200 °C seaweed bio-coal, as would be expected with lignocellulosic bio-coals and this would be due to increased dehydration. The H/C ratios for seaweed bio-coal are similar at each temperature, which differs from lignocellulosic biomass, where the lower temperature bio-coals had both higher O/C and H/C ratios [29].

5.2.3.1.1. Potential process chemistry routes

Although the bio-coals have undergone energy densification similar to that of lignocellulosic biomass, the yields appear to be lower for macroalgae than lignocellulosic biomass. The yields for the lignocellulosic biomass, presented in Chapter 4 and processed under similar conditions, range between 58 % and 70 % at the lower process temperature (200 °C) and between 40 % and 46 % for the higher process temperature (250 °C) for oak, willow and *Miscanthus* [213]. The low yields will largely be because of differences in biochemical composition. Brown kelps, as processed, comprise largely of carbohydrate in the form of parallel chains of polymeric alginic acid along with mannitol, laminarin, fucoidan and other polysaccharides [61], while lignocellulosic material is derived of cellulose, hemicellulose and lignin.

As discussed in Section 2.3.2, during HTC, lignin is hydrolysed into phenolic fragments, which are highly reactive and recombine quickly [28] and maintains a coke like macromolecule structure, which the hemicellulose and cellulose derived compounds condense onto [11]. For material with lower lignin content, crystalline cellulose scaffolds (present in grasses) act as the nucleus for the recondensation reactions [28, 77]. For biomass without a structural crystalline cellulose structure, carbonaceous nanoparticles / spheres are formed due to burst nucleation followed by LaMer particle formation [22, 77, 78]. It is unclear whether the alginic acid is crystalline in brown kelp, but given brown kelps comprise largely of carbohydrate [61], the latter (non-lignin) models of nucleation appear more likely.

There is very limited information on the HTC reactions during HTC of macroalgae. Jeon et al. [320] has looked into the hydrothermal degradation of sodium alginate, a water soluble alginate, at 200 °C and 250 °C using acid and base catalysts but did not report a char yield. The results showed that depolymerisation of alginic acid occurs from 150 °C; with hydrolysis converting the sodium alginate to monomers followed by subsequent reformation to organic acids, predominantly furfural, glycolic acid and formic acid. This would suggest that the decomposition chemistry of alginic acid is similar to that of cellulose. Consequently, polymerisation should follow a similar process chemistry to that described for cellulose in Section 2.3.2 and summarised in Figure 2.8.

The addition of calcium chloride to hydrothermally carbonised sodium alginate has been shown to promote the formation of carbon microspheres [147]. In Chen et al. [147], the authors hypothesise that calcium, being a divalent cation, binds poly-guluronic acid units, forming stable cross-linking chains enabling the formation of the sphere. It is unclear whether these metals are acting as seeding nuclei, bringing about initial polymerisation and in so triggering burst nucleation in a similar way to that reported by Antonietti and others in the early 2000's, with the HTC of sugars using noble metal catalysts [23, 25, 325]. Caution is however required when interpreting behaviour of alginate. Sodium alginate is widely exploited for its aggregative properties, particularly its ability to instantaneously and almost temperature-independently form a solid / gelatinous cross-linked structures in the presence of multivalent cations (e.g., Ca^{2+}), when dissolved in water [326]. Accordingly, its behaviour may be different to that of other carbohydrates.

It does however appear likely that calcium and magnesium play an important role in the formation of the bio-coals during HTC of macroalgae, with the divalent cations present in the process waters nucleating alginate hydrolysis fragments and forming nuclei from which the bio-coals can grow. This theory is supported by the metal analysis of the bio-coals (see Figure 5.2), which showed the calcium and magnesium increase in concentration within the bio-coals while the potassium and sodium are extracted. Moreover, there is evidence within the coal literature that may suggest multivalent cations can play a role in polymerisation of mineral coal, though interactions with oxygen functional groups [148, 149].

As part of this work electron microscopy images were not taken of these chars. Images would indicate whether the char is polymerised onto structural scaffolds or

derived though burst nucleation. In the case of the latter, increasing carbonisation time and organic concentration by increasing the water to solids ratio should increase yields [77, 78]. Likewise, if the cations are catalysing polymerisation, yields maybe improved though spiking with multivalent cations.

5.2.3.1.2. Influence of HTC on the bio-coal ash chemistry

While HTC appears to overcome the issues of moisture content and calorific value associated with seaweeds, the main issues which prevents its utilisation in combustion, pyrolysis or gasification is the high chlorine, high ash and high alkali metals content [61]. Figure 5.2, shows the main ash forming elements within the bio-coal and feedstock and Table 5.2 shows the percentage of metals extracted. Extraction efficiency is calculated by multiplying the concentration (mg/kg) of metal within the bio-coal with the product yield to give mg metal remaining per kg of feed. This is then divided by the initial feedstock concentration to give percentage removal.

Results show sodium is extracted in excess of 99 % for both treatments, with potassium extraction in the region of 97 % at 200 °C and 99 % at 250 °C. Chlorine is also removed in high quantities, typically around 99 % with slightly higher extraction associated with the increased reaction severity. The extraction efficiency of calcium and magnesium is less than the alkali metals, with the higher temperature treatments extracting less calcium and magnesium than the 200 °C treatment. This would suggest that these divalent cations are being retained by the bio-coal at higher temperatures. This retention could be because of interactions between the cations and the reactive oxygen functionalities on the char surface; the higher valiant cations being retained due to cation exchange [28]. The reduction in O/C would however suggest a reduced cation exchange capacity for the 250 °C bio-coals and may not explain increases in cation retention at the higher temperature. It appears more likely that the divalent cations are playing a role in char formation [147], forming a nuclei around which the bio-coal can form. The increased reaction temperature at 250 °C will result in greater degradation of the carbohydrates and therefore, the char formation is more dependent on repolymerisation. The repolymerisation is subsequently catalysed by the calcium and magnesium as hypothesised in Section 5.2.3.1.1. At 200 °C, it is likely that residual carbohydrate will remain within the char and therefore the char formation is less dependent on repolymerisation from organic fractions within the process water.

Development of a Pyrolysis-GCMS method to identify carbohydrate markers would be beneficial in this instance as qualification of residual carbohydrate, in much the

same way cellulose is quantified in Chapter 6, 7 and 8, would be beneficial in understanding char makeup.

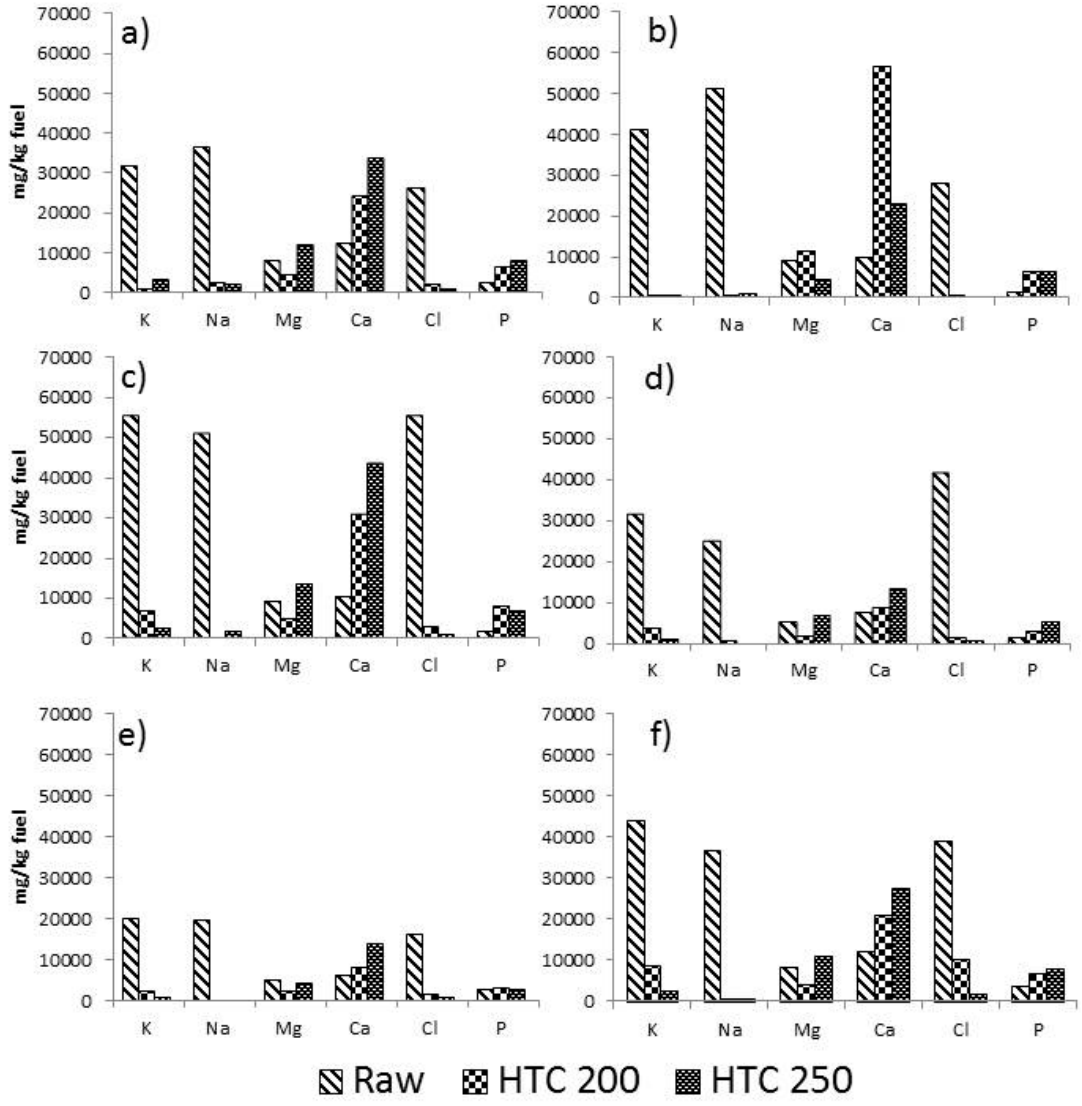

Figure 5.2. Concentrations of the main ash forming elements within the raw kelps and corresponding bio-coals. a) *A.* esculenta (summer), b) *L. Digitata* (summer), c) *L. Hyperborea* spring harvest, d) *L. Hyperborea* summer harvest, e) *L. Hyperborea* autumn harvest and f) *L. Hyperborea* winter harvest (concentrations and standard error of mean are given in Table 5.6)

Table 5.2: Percentage extraction of the main problematic ash forming elements within the raw kelps

	K (%)	Na (%)	Mg (%)	Ca (%)	Cl (%)	P (%)
A. Esculenta	100	100	100	100	100	100
HTC 200	99.2±0.1	98.4±0.0	87.4±1.2	56.1±2.2	98.2	44.6±6.8
HTC 250	98.1±0.3	99.0±0.0	73.3±0.4	51.2±1.1	99.3	44.3±2.2
L. Digitata	100	100	100	100	100	100
HTC 200	99.8±0.0	99.8±0.0	82.6±0.3	19.5±1.8	99.8	36.0±7.7
HTC 250	99.8±0.0	99.8±0.0	93.7±0.1	69.6±0.6	99.9	40.9±10.8
L. Hyp' Spring	100	100	100	100	100	100
HTC 200	97.7±0.4	99.9±0.0	89.4±0.5	44.5±2.9	99.0	16.5±2.2
HTC 250	99.3±0.0	99.5±0.0	76.8±0.2	35.1±2.1	99.7	39.9±2.8
L. Hyp' Summer	100	100	100	100	100	100
HTC 200	97.4±0.7	99.3±0.0	92.7±0.8	75.3±1.4	99.2	61.0±3.8
HTC 250	99.4±0.1	99.6±0.0	77.5±0.3	68.0±1.6	99.7	39.7±1.2
L. Hyp' Autumn	100	100	100	100	100	100
HTC 200	96.8±1.5	99.8±0.0	86.9±2.0	61.9±6.3	97.5	66.5±6.3
HTC 250	99.3±0.0	99.7±0.0	78.2±1.5	43.2±5.1	98.7	73.1±5.0
L. Hyp' Winter	100	100	100	100	100	100
HTC 200	94.5±0.0	99.6±0.0	86.8±0.6	52.0±0.3	92.8	48.2±0.3
HTC 250	98.8±0.2	99.6±0.0	72.3±1.4	52.8±0.5	99.1	53.3±1.4

While understanding extraction efficiency is important when understanding HTC mechanisms, the resulting concentration of metals and heteroatoms within the bio-coal is what is actually important when utilising the fuel, and these results are given in Figure 5.2. The results show significant reductions in the net concentrations of sodium, magnesium and chlorine, which will bring significant benefits in terms of the slagging and fouling properties of the char. The results show a net increase in the concentrations of the two divalent cations within the bio-coal, with magnesium concentration reducing in the 200 °C bio-coal but increasing in the 250 °C bio-coal. The increase in magnesium concentration is far greater than the decrease in mass yield at the higher temperature which shows that magnesium is being re-up taken at the higher temperatures, either due to increasing surface functionality or because at the higher temperatures it plays a role in the bio-coal formation. The calcium concentration increases in both treatments, but to a greater extent in the 250 °C treatment. As calcium's uptake is different to that of magnesium, it appears likely that calcium is playing a greater role in the bio-coal formation with its role increasingly important at higher temperatures. The presence of phosphates within the bio-coal (results given as elemental phosphorus) could indicate that

portions of the metals within the bio-coal are metal phosphates. This will be beneficial in terms of combustion due to their higher thermal stability when compared to metal oxides and thus improved ash behaviour [200].

The slagging and fouling indices for the seaweeds and corresponding bio-coal are given in Table 5.3. It is worth noting that the ash chemistry in the seaweeds is very different to that of a bituminous coal, which is predominantly comprised of silicon dioxide, iron oxide and aluminium oxide, while the ash of unprocessed raw kelp is largely alkali or alkaline earth metal salts. The large composition of alkali and alkaline earth metals results in an alkaline ash, which is why the acid base ratios are very high as the both the raw feedstock and the bio-coal have very low aluminium, silicon and titanium content resulting in base heavy ash. Likewise, the low silicon content results in low values for the slag viscosity index, which implies that there may be issues with slagging, based on the viscosity of the ash. The results for the slagging indices show large improvement in slagging propensity, with the slagging indices showing that the higher temperature bio-coal are safe for combustion, whereas the raw seaweeds are not. This is consistent with the results of the ash fusion testing which have shown large improvements (sometimes by up to 1000 °C increase in deformation temperature) in all the transition temperatures (see Figure 5.3).

Figure 5.3 shows the results of the ash fusion test. The raw *L. Hyperborea* ashes deform at 560 °C or below and go to flow (melt) at temperatures as low as 610 °C, demonstrating a very high slagging propensity. Contrary to this the *L. Hyperborea* 250 °C bio-coal not even deform before exceeding the furnace limit of 1570 °C. This shows how the fuel has been transformed from a high slagging fuel to a fuel with a low slagging potential [39]. The 250 °C bio-coal for *A. Esculenta* and *L. Digitata* started to deform at 1470 °C and 1260 °C and both went to flow but at temperatures 1550 °C and 1540 °C respectfully which are still high deformation and melting temperatures.

The 200 °C bio-coals melted at lower temperatures than the 250 °C bio-coals, with *A. Esculenta* and *L. Digitata* and *L. Hyperborea*; autumn and winter samples melting at 1490, 1490, 1530, 1510 °C respectfully, but had similar deformation temperatures to the 250 °C bio-coals, deforming at 1450, 1450, 1480 and 1470 °C respectfully. *L. Hyperborea* spring 200 °C bio-coal had gone to deformation at the furnace limit (1570 °C) but not gone to hemisphere or flow. *L. Hyperborea* summer 200 °C bio-coal had merely shrunk by the furnace limit (1570 °C). High flow temperatures were observed for the raw *A. Esculenta* and *L. Hyperborea* autumn samples, which would indicate a low slagging

propensity, but the low deformation temperatures of 620 °C and < 550 °C for the raw samples would indicate they would be highly problematic. For the raw *A. Esculenta* and *L. Hyperborea* autumn samples the ceramic tiles, on which the test pieces were placed were severely corroded and warped. This was not observed for any of the bio-coal test pieces.

The ash fusion test, being also inductive of fouling propensity, would suggest the bio-coals should have a low fouling propensity but the fouling index, given in Table 5.3, suggests a high fouling propensity for all bio-coals. Whether these fuels are fouling requires further investigation; however, these indices make assumptions on the ash mineralogy and don't take into account the role of phosphorus and calcium in abating sodium and potassium release, as discussed in Section 2.5.3.1. Moreover, it is shown in Figure 5.2 that a large portion of the chlorine has been extracted during the HTC process. Chlorine plays an important role in fouling and corrosion mechanisms, so at the least corrosion associated with any fouling deposits should be reduced [201]. Therefore, the bio-coals may, in practice, be low fouling but the presence of alkali and alkaline earth metals will always result in it being highlighted as having a high fouling risk when using fouling indices. This said, significant shrinkage of all the test pieces was observed. While it is believed that this is due to hydrothermally derived carbonates within the ash, it could still indicate volatilisation of potassium and sodium. Consequently, understanding of how the bio-coal ash chemistry changes as it is heated is a significant future step in determining the suitability of seaweed bio-coals in combustion. Ash fusion testing of the raw seaweed ashes resulted in significant fouling of the furnace optics which confirms the findings of Ross et al. [61] that fouling will be a significant problem when combusting seaweeds without pre-treatment.

Table 5.3: Fouling indices and ash fusibility flow temperature

Feedstock	Fouling and Slagging Indices						Ash Fusion		
	AI	BAI	R b/a	SI	FI	SVI	Deformation (°C)	Flow (°C)	Notes
A. Esculenta	6.86	0.81	68.25	84.1	2793.5	2	620	>1570	Tile deformed
HTC 200	0.12	0.28	6.17	0.0	19.1	10	1450	1490	
HTC 250	0.27	0.66	12.76	1.0	61.0	4	1470	1550	
L. Digitata	10.48	0.64	300.66	232.0	14139.8	0	550	1220	
HTC 200	0.07	0.61	35.20	0.3	26.8	1	1450	1490	
HTC 250	0.08	0.45	16.66	0.0	38.3	2	1260	1540	
L. Hyp' Spring	12.13	0.27	197.38	170.3	9297.6	1	570	610	
HTC 200	0.38	0.46	17.27	0.2	135.7	5	1540	>1570	
HTC 250	0.22	0.43	33.59	1.6	109.8	3	>1570	>1570	
L. Hyp' Summer	5.56	0.38	165.97	107.4	5763.1	1	550	680	
HTC 200	0.23	0.56	9.55	1.6	134.2	11	>1570	>1570	
HTC 250	0.07	0.61	15.83	0.9	56.6	5	>1570	>1570	
L. Hyp' Autumn	3.61	0.56	467.72	8.3	24757.7	0	<790	1520	Tile deformed
HTC 200	0.13	1.05	29.62	0.0	265.7	4	1480	1530	
HTC 250	0.04	0.94	49.87	0.4	103.4	2	>1570	>1570	
L. Hyp' Winter	8.36	0.51	354.96	12.4	12295.2	0	<800	1090	
HTC 200	0.50	0.45	27.32	1.0	297.7	3	1470	1510	
HTC 250	0.15	0.48	36.44	4.5	132.3	2	>1570	>1570	

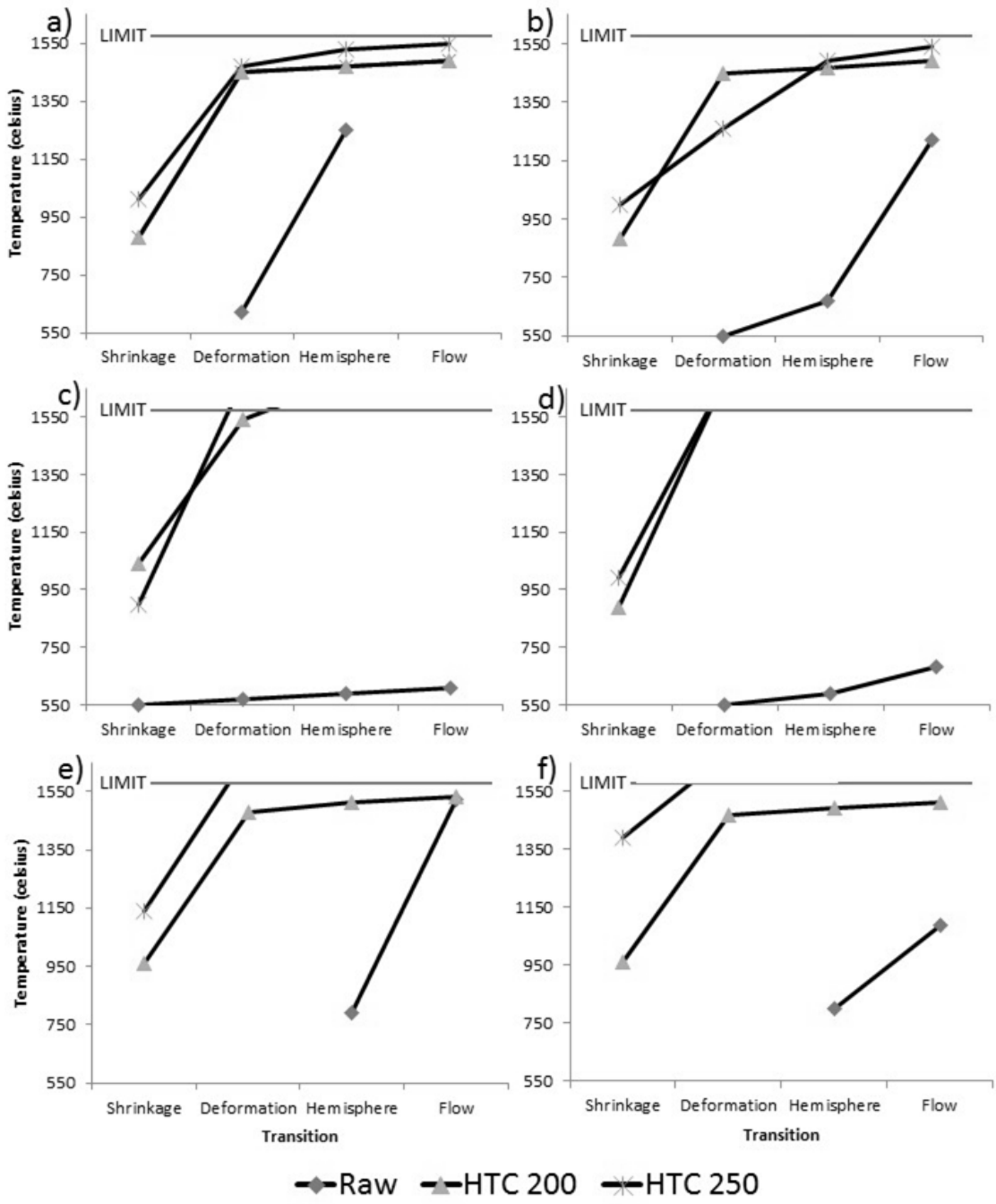

Figure 5.3: Ash fusion transition temperatures for the raw kelps and corresponding bio-coals. a) *A.* esculenta (summer), b) *L. digitata* (summer), c) *L. hyperborea* spring harvest, d) *L. hyperborea* summer harvest, e) *L. hyperborea* autumn harvest and f) *L. hyperborea* winter harvest

5.2.3.2. Process Water Chemistry

The anions and cations within the process waters were analysed by ion chromatography (IC) and the results are shown in the Table 5.4. The process water contains high concentrations of sodium and potassium along with high concentrations of the associated halogens; chlorine, fluorine and bromine. This correlates with the reductions seen in the bio-coal, which indicates that the fate of the alkali metals and their

associated anions is the process water. The divalent cations magnesium and calcium are also present within the process water although they are present in significantly lower concentrations, with approximately 5 grams of calcium per kg of feedstock, whereas potassium varies between 30 and 83 grams/ kg feedstock depending on the species and the season. In addition to the high cations present, there are also high concentrations of phosphate present within the process waters with concentrations varying from 12 g/kg feedstock to 76 g/kg feedstock. The presence of potassium and phosphate in high concentrations and to a lesser extent calcium and magnesium raises the prospect of recovering these salts for use in fertilizer. While this paper does not attempt to suggest potential extraction routes; for HTC of macroalgae to develop to a commercial scale it is essential to identify applications that offer technical or economic advantages over conventional biomass processes and the recovery of essential plant nutrients would be one such route.

In addition to the salts present within the process water there is also nitrogen in the form of nitrite, nitrate and ammonia. This will be largely derived from the organically bound nitrogen within the macroalgae. Table 5.1 shows the nitrogen content of the bio-coal and indicates that a significant portion of the nitrogen is transferred to the process water resulting in only a slight increase in nitrogen in the bio-coal. The relatively low concentrations of nitrogen detected by IC is indicative that the remaining nitrogen is in the form of organic compounds such as nitrogen heterocycles, pyrroles and indoles in the process waters due to the degradation of proteins [327] along with maillard reaction products due to interactions between the proteins and carbohydrates [89]. It is also likely that a number of organic compounds will also be associated with metals and heteroatoms, which will be undetectable by IC. Consequently the metals and heteroatoms detected by IC should be taken as free ionic salts in the process waters and not total extracted the metals and heteroatoms.

The process waters have been shown to be high in organic carbon (10-18 % of the carbon), due to the low bio-coal yields. As increasing the retention times and reducing the water to biomass ratio may well overcome this in the same way as has been done for low lignin, non-crystalline cellulose biomass [77, 78]. Recycling the process waters back into the HTC process may also have a similar impact [44, 48], although the extraction of salts could be problematic. Likewise, as hypothesised in this work addition of calcium may catalyse repolymerisation, while in addition acting as an additive in mitigating the

impacts of fouling and slagging. The second solution would be fermentation of the process waters by AD, a solution discussed in detail in the corresponding paper.

5.2.4. Influence of seasonal variation in bio-chemical composition on product yield

The energy yields from HTC of the three kelp species harvested in July and the energy yields of *L. hyperborea* harvested throughout the year are given in Figure 5.4. The results show that there is significant variation between the three species and the time of year of harvest. *L. hyperborea* appears to give the highest yields of bio-coal, with *A. esculenta* giving the second highest yields. Interestingly the higher temperatures appear to give lower energy yields, despite increased energy densification of the products. The reduced bio-coal energy yield is most likely due to increased decomposition of the carbohydrate present with the hydrolysed fractions then remaining within the process waters. Figure 5.4 also includes potential AD yields of methane and hydrogen, taken from Smith and Ross [259]. These results do however show that the lower energy yields of the higher temperature treatment can be offset by the increased potential energy yield from either hydrogen or methane production via AD. Moreover, with the improvements in slagging propensity of the solid fuel, the lower yields should not dissuade from this treatment.

The char yields appear highest in the autumn which correlates with the fuel having the highest carbon content [322]. The yields are lowest for material harvested in the spring, when ash is highest [63, 322]. This high ash content in the early spring also makes the fuel, even once hydrothermally treated at 250 °C, unsuitable for direct combustion due to fouling and slagging risk, although it still could be blended. The carbohydrate content of the algae, which peaks in the summer samples (July) [63, 322], appears less important than maximum carbon in terms of maximum bio-coal yield, although the higher carbohydrate content in the feedstock appears to increase the hydrogen and methane yields obtained by AD, which offsets the reduced energy yields in the bio-coal.

In summary, the results generally show that the highest energy yields are obtained in the summer and autumn harvested algae. This is different to direct seaweed AD which is reliant on carbohydrate content [63]. Consequently, it is not necessary to harvest in July to obtain maximum yield when processing by HTC. HTC will allow harvesting throughout the summer and autumn, which has the benefit of significantly extending the harvesting window, and will enable harvesting to be coordinated with maximum biomass yield as opposed to optimum composition. The results do imply harvesting in the spring is best avoided due to low yields and less favourable inorganic chemistry. If harvesting

in the autumn overruns, harvesting in the early winter should not be too detrimental to the fuels inorganic chemistry but will have a penalty on yields.

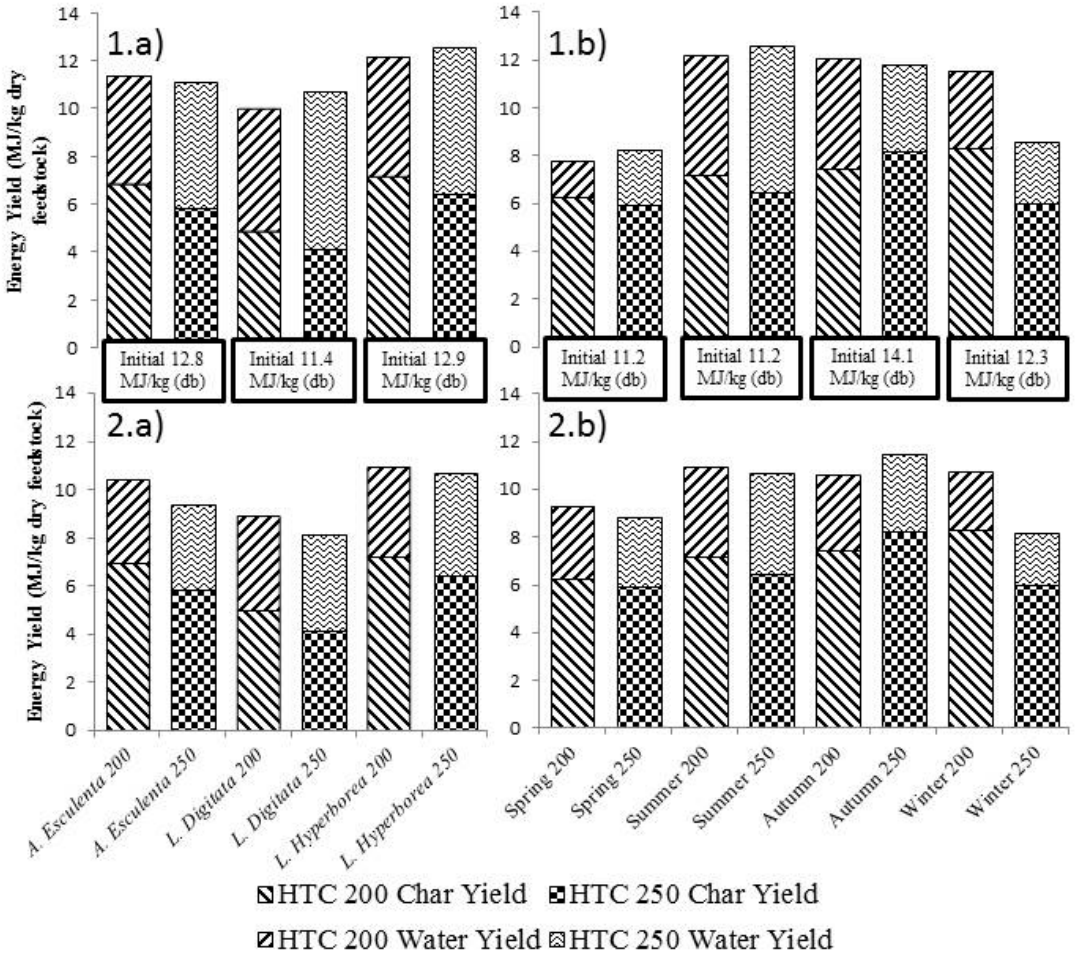

Figure 5.4: Bio-coal, hydrogen (1) and methane (2) yields (75 % of theoretical yield) from HTC followed by anaerobic digestion: 1a) variation between summer harvested species with hydrogeneses, 1b) variation between seasonal harvested *L. hyperborea* with hydrogeneses, 2a) variation between summer harvested species with methanogenesis, 2b) variation between seasonal harvested *L. hyperborea* with methanogenesis.

Table 5.4: Mass (g) of anions, cations and organic carbon in the process water after HTC of 1 kg feedstock using 10:1 water to solids ratio

Sample	Anions Process Water (g/kg feed)						Cations Process Water (g/kg feed)					Organic Carbon (g/kg)
	F^-	Cl^-	NO_2^-	Br^-	NO_3^-	PO_4^{3-}	Na^+	NH_4^+	K^+	Mg^{2+}	Ca^{2+}	
A. Esculenta 200	6.9	53.0	0.2	0.2	2.3	30.5	32.7	2.2	29.7	5.6	4.9	148.1
A. Esculenta 250	2.6	53.3	0.2	0.8	1.6	24.1	29.5	4.2	34.8	4.0	3.7	155.8
L. Digitata 200	8.6	65.7	0.5	1.9	2.3	35.7	37.1	0.0	40.8	6.5	5.9	177.1
L. Digitata 250	4.7	58.5	0.5	1.9	2.2	11.6	39.0	0.0	41.7	6.8	5.9	160.6
L. Hyp' Spring 200	5.9	81.0	0.5	10.7	0.9	44.6	36.9	2.0	43.0	5.8	2.5	100.1
L. Hyp' Spring 250	4.8	69.8	0.4	10.4	2.4	23.7	40.6	3.9	68.9	5.8	3.4	124.9
L. Hyp' Summer 200	2.7	24.7	0.5	1.0	1.3	29.0	19.3	1.6	33.8	3.3	3.7	154.1
L. Hyp' Summer 250	5.3	33.3	0.5	1.2	2.3	41.1	20.5	1.0	37.8	4.2	4.4	182.9
L. Hyp' Autumn 200	5.3	18.4	0.4	1.0	2.3	26.2	18.0	0.0	20.1	4.1	3.6	148.0
L. Hyp' Autumn 250	1.8	2.3	0.0	0.9	0.9	15.3	14.4	0.9	22.4	3.0	2.2	138.7
L. Hyp' Winter 200	7.3	64.6	0.5	4.7	2.5	64.1	26.4	3.8	75.3	5.5	3.5	87.2
L. Hyp' Winter 250	4.4	76.0	0.5	4.9	1.0	75.7	25.9	6.0	83.3	4.2	3.1	105.0

Table 5.5: Additional extractable anions and cations though bio-coal washing with distilled water (g/kg feedstock)

Sample	Anions Extracted (g/kg feed)						Cations Extracted (g/kg feed)					Organic Carbon (g/kg)
	F^-	Cl^-	NO_2^-	Br^-	NO_3^-	PO_4^{3-}	Na^+	NH_4^+	K^+	Mg^{2+}	Ca^{2+}	
A. Esculenta 200	0.8	4.1	0.0	0.2	0.2	0.9	4.6	0.0	4.1	0.8	0.9	24.4
A. Esculenta 250	0.3	3.2	0.0	0.2	0.2	0.6	3.0	0.4	3.6	0.4	0.4	18.7
L. Digitata 200	0.9	4.5	0.2	0.2	0.2	0.8	4.4	0.0	4.7	0.8	0.8	25.4
L. Digitata 250	0.4	3.7	0.2	0.2	0.2	0.5	4.4	0.0	4.7	0.8	0.7	18.2
L. Hyp' Spring 200	1.1	11.1	0.2	0.8	0.2	1.8	3.7	0.1	4.3	0.6	0.4	22.8
L. Hyp' Spring 250	0.8	8.8	0.2	0.7	0.3	1.0	6.3	0.6	10.8	0.9	0.5	25.0
L. Hyp' Summer 200	0.9	4.0	0.2	0.2	0.3	1.4	3.3	0.0	5.9	0.6	0.8	30.4
L. Hyp' Summer 250	0.2	2.3	0.2	0.2	0.0	0.9	2.1	0.0	3.5	0.3	0.4	20.7
L. Hyp' Autumn 200	0.8	2.7	0.2	0.2	0.2	1.2	3.3	0.0	3.9	0.8	0.7	34.7
L. Hyp' Autumn 250	0.4	2.3	0.0	0.2	0.2	1.1	2.2	0.0	3.4	0.4	0.4	25.6
L. Hyp' Winter 200	1.6	11.9	0.2	0.5	0.3	3.2	5.6	0.8	16.3	1.1	0.8	28.9
L. Hyp' Winter 250	0.6	7.0	0.2	0.3	0.2	2.0	3.1	0.7	10.0	0.5	0.5	15.1

5.2.5. Conclusions

This study has shown that processing macroalgae via HTC can produce a coal like product with improved combustion properties. Moreover, hydrothermal carbonisation can overcome the highly unfavourable inorganic and heteroatom chemistry of macroalgae, which will otherwise largely prevent its utilisation in combustion, pyrolysis or gasification due to slagging, fouling and corrosion.

The results indicate that HTC can produce a coal like product with an enhanced energy density. The resulting bio-coal has a typical CV of 22 MJ/kg(ar) for the 200 °C treatment and 25 MJ/kg(ar) for the 250 °C treatment. HTC results in almost complete removal alkali metals and chlorine. In addition, the bio-coals retain calcium and phosphorus, which inhibit the effects of the residual alkali metals in terms of slagging and fouling. Ash fusion testing has demonstrated that the slagging and fouling propensity of the resulting bio-coal is significantly reduced.

As brown kelp is largely derived of carbohydrate and absent of a lignin-derived structure, results suggest calcium may play an important role in the formation of the bio-coals during HTC of macroalgae. It is hypothesised that divalent cations present in the process waters nucleate the alginate hydrolysis fragments during HTC and form nuclei from which the bio-coals can grow.

Consequently, this study has shown that HTC is a promising pre-treatment for macroalgae producing a bio-coal with favourable combustion properties from a highly unfavourable feedstock. Further processing of the process water can generate bio-methane or, hydrogen and facilitate recovery of inorganics which will greatly improve the process economies. Moreover, the results would suggest that the cations have both an influence on the process chemistry in addition to influencing the ash chemistry.

Table 5.6: Concentrations of the main ash forming elements within the raw kelps and corresponding bio-coals with standard error of mean.

	K mg/kg	Na mg/kg	Mg mg/kg	Ca mg/kg	Cl mg/kg	P mg/kg
Alaria	31691±230	36658±172	8012±68	12489±109	26480	2652±73
HTC 200	1068±65	2641±9	4485±372	24286±1006	2093	6504±616
HTC 250	3312±463	2046±42	11906±73	33824±474	986	8205±103
L.Digitata	41300±201	51361±641	9209±10	9857±100	28224	1435±148
HTC 200	721±11	565±11	11431±176	56704±694	447	6563±109
HTC 250	560±20	842±17	4442±70	23044±251	294	6523±507
L. Hyp' Spring	55398±969	51136±14	9132±85	10428±282	55176	1824±24
HTC 200	6759±982	305±30	5151±218	30812±753	2922	8101±112
HTC 250	2555±132	1732±158	13583±1	43388±210	1218	7021±234
L. Hyp' Summer	31471±258	24940±145	5527±12	7752±363	41774	1635±29
HTC 200	3711±972	774±0	1837±187	8678±98	1484	2886±227
HTC 250	1051±108	496±20	6788±66	13540±50	714	5387±607
L. Hyp' Autumn	20050±94	19780±114	4845±69	6078±252	16155	2473±447
HTC 200	2287±1019	162±5	2232±305	8151±1010	1437	2920
HTC 250	554±32	230±23	4224±231	13799±656	846	2661
L. Hyp' Winter	44092±087	36659±1741	8228±370	12209±88	38908	3617±21
HTC 200	8602	514	3866	20909	10011	6698
HTC 250	2604±421	617±37	10871±71	27415±83	1637	8046±192

5.3. Production of high quality bio-coal from early harvested *Miscanthus* by hydrothermal carbonisation

5.3.1. Introduction

Miscanthus is a perennial bio-energy crop which is currently being commercially utilised in both Europe and the US. *Miscanthus* is viewed favourably as an energy crop, as being a C4 perennial rhizomatous grass, it offers enhanced carbon fixation, high water use efficiency and a rhizome which can store key nutrients to be utilised in early spring offering higher yields along with low fertilizer and pesticide requirements [328].

Current bio-energy applications for *Miscanthus* are largely focused on thermal conversion routes such as combustion, however such routes have feedstock quality requirements, with the fuel parameters set by the combustion system design. For *Miscanthus* to best fit the combustion quality requirements, it is conventionally harvested during the late winter or early spring in the UK, after which the crop has fully senesced and nutrients have been remobilised into the rhizome. Harvesting at that time tends to result in a fuel with a reduced above ground crop moisture content compared to that harvested at the peak of the growing season [329]. Also, the combined effect of leaf loss and nutrient translocation leads to a reduction in alkali metal content in the biomass in spring [330]: with Kahle et al., [331] reporting that the nitrogen, phosphorus and potassium content of the crop harvested late was 61 %, 64 % and 55 % respectively of that harvested in the autumn.

While the winter / late harvesting of *Miscanthus* may increase thermal feedstock quality, late harvesting has an impact on net biomass yield. Typically, the maximum biomass yield occurs in the early autumn months just prior to senescence [330]. After this, the crop dies back and the leaves and stems break as the crop dries over the winter resulting in an estimated decline in dry matter yield of 27 kg ha^{-1} day^{-1} [332] reaching an estimated total 30 % decline of peak dry matter yield by the conventional harvesting time, which would represent a 43% increase in yield working back [333-335]. Moreover while late harvested *Miscanthus* samples have improved fuel quality, with lower nitrogen, chlorine, ash and alkaline metal content, the results presented in Baxter et al. [336] indicate that slagging, fouling and corrosion is still most probable in most crops. Thus, the reduction in nutrients brought about by overwintering is still insufficient to lead to safe combustion and leads to a significant decrease in dry yield.

Delaying harvest until after senescence does have the advantage that the crop can remobilise key plant nutrients such as nitrogen into the rhizome for regrowth in the spring

and return some phosphorus and potassium to the soil through leaf fall [337, 338]. The longer term impact of continuous autumn harvesting is currently unknown, and there are concerns that earlier harvesting will prematurely exhaust the crop [335]. A number of studies have examined the impact of early harvesting on *Miscanthus* dry matter (DM) yields [330, 339, 340]. From these, there is some evidence that nitrogen management can play a role in ensuring sustainability of early cutting [330, 340]. In the scientific literature, two studies have demonstrated early harvesting of *Miscanthus* x *giganteus* can be performed for three to four consecutive years without seeing a noticeable drop in yield [330, 339]. One study identified a notable loss in yield in sites lacking nitrogen application [330]. A two-year study in Germany also found that *Miscanthus* x *giganteus* could tolerate early cutting [340], however without additional nitrogen, the yields were approximately half that of fertilised plots. In this case, the benefits of sustained yields must be offset though the moderate application of inorganic fertiliser [334]. Logistics of harvesting green crops should be similar to overwintered crops, with both crops harvested with forage harvesters. High moisture crops can pose storage difficulties due to microbial degradation and losses due to liquid effluent production and these factors would require further investigation [341].

Whether *Miscanthus* is harvested 'green' in the autumn or later after winter, a biomass pre-treatment which improves the fuels ash chemistry appears to be a pre-requisite for safe combustion and an autumn / green harvest will potentially achieve the highest possible yield per hectare. HTC appears an ideally suited pre-treatment for such an application as green harvested *Miscanthus* will have a high moisture content. Moreover, as demonstrated in Chapter 4 there is potential for a significant reduction in slagging, fouling and corrosion though the extraction of the alkali metals, along with chlorine. This section sets out to investigate the feasibility of using HTC to overcome the combustion limitations imposed by the inorganic chemistry of green/ early harvested *Miscanthus* while producing a high quality solid fuel for combustion, while increasing yields per hectare.

5.3.2. Methodology

5.3.2.1. Materials

Samples of *Miscanthus x giganteus* were obtained from Rothamsted Research (co-ordinates 51.801851, -0.366692 North). The crop used in this study is a naturally occurring triploid hybrid of diploid *M. sinensis* and a tetraploid *M. sacchariflorus* [342]. In autumn 2015, the crop was 22 years old. The site has a silty clay loam soil with flints

[343]. It was grassland for the majority of the previous 100 years and an adjacent *Miscanthus* crop had not responded (in terms of yield) to nitrogen fertiliser [344]. Therefore, no nitrogen or other fertilisers were applied.

For this experiment, the crop was harvested on the 24th November 2015 just after the initial onset of senescence, with the winter / spring harvest collected 8th March 2016. The site had previously been harvested in March 2015 and had a recorded yield of 14.4 t DM/ha. This was the first time the crop had been cut in autumn.

For this investigation, approximately 10 kg of crop was sampled at random as whole canes in both harvesting periods. Samples were shipped directly to the site of analysis. Upon receipt, the samples were split into a whole crop (leaves and stems), leaves only and stems only. Samples were then cut and homogenised in a garden shredder to a particle size of approximately 5 mm in diameter. The moisture content of the *Miscanthus* was calculated using a moisture oven following the procedure set out in BS ISO 11722:2013. The samples were further split using a riffle splitter, with one half processed as received and the other half oven dried at 60 ˚C for 72 hours. For analytical purposes, samples were further ground and homogenised to below 100 µm in a cryomill (Retsch, Germany).

5.3.2.2. Hydrothermal carbonisation

HTC was performed using the modified 2000 ml Parr reactor described in Section 3.2.2. For each run a 10 % solids loading (dry basis) was used with a combined mass of 1000 grams per run. HTC runs were performed on as received samples and oven dried samples, with the moisture content pre-determined and the biomass and deionised water corrected accordingly. The experiments were designed to ensure that each run contained an equivalent of 100 g of dry biomass. Other than sample loading, the runs were undertaken as described in Section 3.2.2.2. The bio-coal was allowed to air dry in a ventilated fume cupboard for a minimum of 48 hours, to gauge air dry moisture loss, and then oven dried at 60˚C overnight.

5.3.2.3.Analysis

5.3.2.3.1. Inorganic analysis

Inorganic elemental composition was determined by two methods; wavelength dispersive X-ray fluorescence (WD-XRF) and Atomic Absorption Spectroscopy (AAS). For XRF analysis, the samples were analysed using the fusion disk method described in Section 3.6.8.1. Due to the high temperatures required for glass fusion; potassium,

sodium, calcium, magnesium were determined by AAS as the alkali metals are known to volatilise below 900°C thus XRF may underestimate their concentration, as specified in PD ISO/TS 16996:2015. For AAS analysis, samples were digested using the hydrofluoric acid method described in Section 3.6.1 and determined by AAS (Valiant, USA) using the methods described in Section 3.6.3. Chlorine within the feedstock and bio-coal was analysed by combustion in an oxygen bomb (Parr, USA) followed by determination using ion exchange chromatography (Dionex, USA). The method is described in Section 3.6.7 and is consistent with BS EN ISO 16994-2016.

5.3.2.3.2. Organic analysis, combustion properties and ash measurement

Carbon, hydrogen, nitrogen, sulphur and oxygen content was determined using a Flash 2000 CHNS-O analyser (Thermo Scientific, USA), with the method described in Section 3.4.2. The volatile and fixed carbon component of the proximate analysis carried out using thermo-gravimetric analysis (Mettler Toledo, Switzerland) as described in Section 3.3.3. Ash content was determined using a muffle furnace, as described in Section 3.3.2. Moisture content was determined using a moisture oven (Carbolite, UK) as described in Section 3.3.1. The calorific value was determined using Dulong's Equation (see Equation 3.11). Figures are given to the appropriate base in accordance with ASTM D3180-15, with hydrogen and oxygen values corrected to account for moisture. Burning profiles, ignition, flame stability and burnout temperature were obtained by temperature programmed oxidation, as described in Section 3.8.

5.3.2.3.3. Prediction of slagging and fouling behaviour

Ash fusion testing (AFT) was performed using a Carbolite digital ash fusion furnace in accordance with the standard method for the determination of ash melting behaviour (DD CEN/TS 15370-1:2006) using the methodology described in Section 3.7.1. In addition, various slagging and fouling indices have been utilised with their equations 1-3 in Table 3.3. Their underlying theory and calculation methodologies given in Section 3.7.2.

5.3.2.3.4. Resistance to Milling

Resistance to milling was calculated using the Hardgrove Grindability Index (HGI), a scale. Experimental details are given on the HGI analysis in Section 3.9.

5.3.3. Results and discussion

5.3.3.1. Influence of HTC on the bio-coal organic composition

Table 5.7 shows the ultimate analysis results for both homogenised whole plants, key plant components and their corresponding bio-coals, Table 5.8 contains the mass yields, calorific values and proximate analysis for both homogenised whole plants, key plant components and their corresponding bio-coals. The results show a significant increase in carbon density for the 250°C treatments, with the 250°C bio-coals typically having around 70 wt% carbon. The hydrothermally treated leaves have slightly lower carbon densities due to the higher ash content. This increasing carbon density corresponds to an increase in the fuels energy density, with the HHV of the resulting bio-coal increasing from 18 MJ/kg (db) to 27 MJ/kg (db) for early and 18 MJ/kg (db) to 25 MJ/kg for conventionally harvested *Miscanthus* processed at 250°C. The HHV (gross calorific value) for the 'as received samples' were slightly higher at 28 MJ/kg for early and 26 MJ/kg conventionally harvested *Miscanthus*. This would suggest a higher energy density fuel for the early harvested *Miscanthus*.

Lower Heating Values (LHV) (net calorific value) have also been calculated for the fuels with the latter value taking into account the latent heat requirements for the water generated from the fuel bound hydrogen on a dry basis and, the water within the fuel and fuel bound hydrogen on an as received basis. Given in many combustion applications (e.g. coal power station) the latent heat is not recovered, LHV is often the more significant value, as it represents the overall energy available. The moisture contents given for the bio-coal in Table 5.8 are based on the moisture content after 48 hours of air drying. The moisture for the whole untreated *Miscanthus* is the moisture as received at the laboratory and the moisture for the unprocessed leaf and stems is post oven drying at 60˚C overnight. The LHV of the unprocessed green harvested autumn *Miscanthus* is 5 MJ/kg (a.r.); principally due to the 57.7 % moisture on harvesting. The same fuel, hydrothermally treated at 250 ˚C had a LHV of 26 MJ/kg (a.r.) after 48 hours air drying.

The energy densification of the 250°C bio-coals are as a result of changes to the ratio of carbon and oxygen (O/C) in the fuel, with the carbon content increasing, while the oxygen and ash content decreases. The Van Krevelen diagram shown in Figure 5.5 illustrates how the O/C and hydrogen to carbon (H/C) ratios of the bio-coals compare with coals and lignin [20]. The results show that the 250°C bio-coals have a more 'coal like' properties, with the O/C ratio predicting properties between lignite and bituminous coal, using coal data reported in Hatcher et al., [323]. The O/C ratios for the 250°C bio-

coals are reasonably consistent for both early harvested and conventionally harvested crops, with the H/C ratios varying more between the two harvests.

The early harvested *Miscanthus*, processed at 250°C, has a higher H/C ratio than the conventionally harvested *Miscanthus* processed at the same temperature. This variation could be due to changes in the composition of the feedstock, with the early harvested *Miscanthus* containing a higher proportion of leaf matter than when conventionally harvested. The results have shown that hydrothermally processing leaves at 250°C results in a higher H/C ratio, than processing stems of the whole sample. This change could be due to differences in biochemical composition, with the leaf matter containing a higher proportion of hemicellulose [345], thus increasing the amount of hemicellulose within the feedstock and altering the hydrothermal process chemistry. The leaf matter is also associated with a higher inorganic content, containing a greater concentration of alkali metals, alkaline earth metals and silicon (see Table 5.9). This higher H/C ratio was observed and discussed in Section 5.2.3.1 (see also Smith and Ross, [259]) and indicate these metals are having a catalytic influence bringing about higher H/C ratios. The potential mechanism for this would be the catalysis of liquid phase reactions accelerating the formation of low molecular weight compounds, for example formic acid, leading to decomposition and hydrogen donation [128, 142]. If alkali metals are bringing about this change, then it appears, temperature alone influences deoxygenation but temperature and metal content can influence fuel hydrogen.

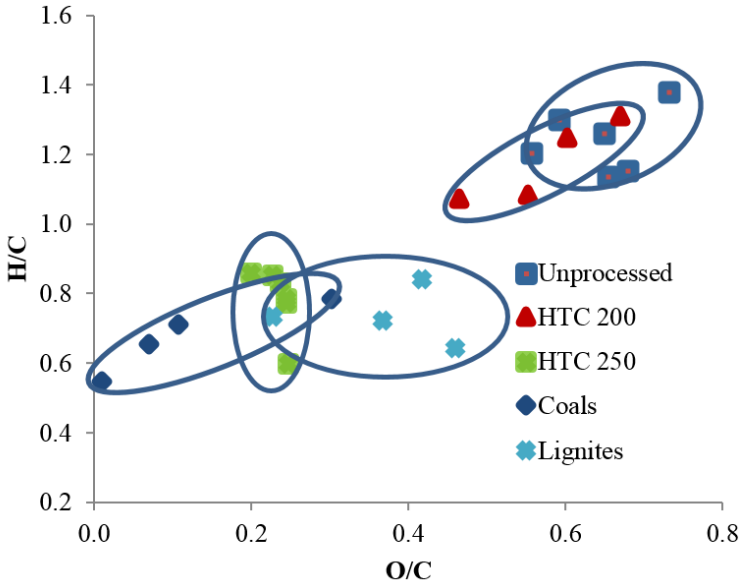

Figure 5.5. Van Krevelen diagram showing the bio-coals, unprocessed biomass, mineral lignite and mineral coals (lignite and coals adapted from Hatcher et al. [323])

The 200°C treatments result in more limited energy densification (with HHV of 18.2 MJ/kg to 19.5 MJ/kg and 15.2 MJ/kg to 17.9 MJ/kg), without noteworthy increases in carbon density and reductions in oxygen density. The reduction in mass of approximately 25-30 % suggests decomposition of some of the biochemical components at 200°C without significant repolymerisation. This limited energy densification, on its own should however not dissuade from this treatment, for the removal of some of the biochemical components makes the fuel more grindable, with a substantial improvement in the fuels HGI which could lead to energy savings when grinding and improvements in flame stability if used in pulverised coal applications. Moreover when the 'as received' moisture content of the unprocessed *Miscanthus* is considered, the 200°C treatments give significantly higher LHV and could avoid, or at least reduce the need for thermal drying. Treatment of the 'as received' feedstocks increased the LHV from 5 MJ/kg (a.r.) and 8 MJ/kg (a.r.) to 14 MJ/kg (a.r.) and 17 MJ/kg (a.r.) for the early and conventionally harvested *Miscanthus* respectively. This is principally due to the enhanced dewateribility of the bio-coal; due to its greater hydrophobicity [179].

Removal of the oxygen containing functional groups is advantageous as these can act as bonding sites for cations, such as sodium, potassium, magnesium, calcium, in biomass and lower-rank coals [68]. It has been suggested that HTC reduces the fouling risk though the combination of decreased oxygen and volatile matter content of the bio-coal [265]. Proximate analysis of the bio-coals in Table 5.8 shows that the volatile matter fraction is reduced from approximately 83 % for both early and conventionally harvested *Miscanthus* to approximately 60 % for the corresponding 250°C treated bio-coals.

5.3.3.2. Influence of HTC on the bio-coal combustion chemistry

Application of biomass in pulverised coal-fired power plants is discussed in Section 2.4.4, with the importance of combustion profiles and particle size discussed in Sections 2.4.4.1 and 2.4.4.2 respectively. One method for evaluating a fuels combustion behaviour is the Babcock and Wilcox TGA method, and this method is used in this chapter. A full description of this method is given in Section 3.8 but in essence, the method looks to identify differences in fuel burning characteristics (as shown by the burning profile). If the burning profiles are mismatched it could either result in a fuel burning in a way a furnace is not designed for or lead to poor burn interaction if co-fired (i.e. two fuels burning independently of each); either way resulting in an unstable flame.

Table 5.7: Elemental composition for both homogenised whole plants, key plant components and their corresponding bio-coals.

		% Dry Basis									
		N (wt %)		C (wt %)		H (wt %)		S (wt %)		O (wt %)		Ash (wt %)	
Whole Plant - Oven Dried Prior to Treatment	Autumn Whole Plant Raw	0.7	*±0.0*	52.2	*±0.5*	5.2	*±0.1*	0.1	*±0.0*	38.7	*±0.4*	3.1	*±0.0*
	Spring Whole Plant Raw	1.4	*±0.2*	46.2	*±0.2*	5.3	*±0.3*	0.1	*±0.0*	44.9	*±1.4*	2.1	*±0.1*
	Autumn Whole Plant HTC 200	1.0	*±0.0*	53.8	*±0.2*	5.6	*±0.2*	0.1	*±0.0*	43.1	*±1.3*	2.5	*±0.1*
	Spring Whole Plant HTC 200	0.9	*±0.0*	53.3	*±0.0*	4.8	*±0.2*	0.1	*±0.0*	39.3	*±0.2*	1.5	*±0.1*
	Autumn Whole Plant HTC 250	1.3	*±0.0*	69.7	*±0.3*	4.8	*±0.2*	0.1	*±0.0*	21.9	*±0.1*	2.2	*±0.0*
	Spring Whole Plant HTC 250	0.9	*±0.0*	70.7	*±0.4*	3.5	*±0.6*	0.1	*±0.0*	23.2	*±0.4*	1.4	*±0.0*
Plant Components - Oven Dried Prior to Treatment	Autumn *Miscanthus* Stems Raw	0.6	*±0.0*	48.9	*±0.0*	4.7	*± 0.1*	0.1	*±0.0*	42.7	*±0.9*	3.0	*±0.1*
	Spring *Miscanthus* Stems Raw	1.0	*±0.1*	48.3	*±0.4*	4.7	*±0.4*	0.1	*±0.0*	43.6	*±0.1*	2.3	*±0.2*
	Autumn *Miscanthus* Stems HTC 250	0.9	*±0.0*	70.9	*±0.4*	5.0	*±0.0*	0.1	*±0.0*	21.4	*±0.1*	1.7	*±0.1*
	Spring *Miscanthus* Stems HTC 250	0.9	*±0.0*	70.3	*±0.1*	4.5	*±0.7*	0.1	*±0.0*	23.0	*±0.0*	1.3	*±0.1*
	Autumn *Miscanthus* Leaves Raw	1.3	*±0.1*	48.6	*±0.6*	5.3	*±0.7*	0.1	*±0.0*	38.3	*±1.5*	6.4	*±0.4*
	Spring *Miscanthus* Leaves Raw	1.8	*±0.0*	47.7	*±0.3*	5.0	*±0.4*	0.1	*±0.0*	41.2	*±0.1*	4.1	*±0.2*
	Autumn *Miscanthus* Leaves HTC 250	1.5	*±0.0*	67.1	*±0.6*	6.5	*±0.7*	0.2	*±0.0*	18.0	*±0.3*	6.7	*±0.2*
	Spring *Miscanthus* Leaves HTC 250	1.7	*±0.0*	66.6	*±0.3*	5.5	*±0.2*	0.2	*±0.0*	21.1	*±0.0*	5.0	*±0.1*
Whole Plant - Treated as Received	Autumn Whole Plant HTC 200	0.6	*±0.0*	48.3	*±0.3*	5.3	*±0.5*	0.1	*±0.0*	43.1	*±0.2*	2.7	*±0.1*
	Spring Whole Plant HTC 200	0.8	*±0.0*	53.8	*±1.1*	4.8	*±0.3*	0.1	*±0.0*	33.4	*±0.8*	1.7	*±0.1*
	Autumn Whole Plant HTC 250	0.8	*±0.1*	72.3	*±0.7*	5.2	*±0.1*	0.1	*±0.0*	19.4	*±0.7*	2.2	*±0.4*
	Spring Whole Plant HTC 250	0.9	*±0.1*	70.3	*±0.3*	4.6	*±0.4*	0.1	*±0.0*	22.9	*±0.3*	1.4	*±0.0*

Table 5.8: Combustion and handling characteristics for both homogenised whole plants, key plant components and their corresponding bio-coals

		Yield (wt%) (dry)	Moisture (wt%) (a.r.)	HHV (MJ/kg) (dry)	HHV (MJ/kg) (a.r.)	LHV (MJ/kg) (dry)	LHV (MJ/kg) (a.r.)	Volatile Matter (wt%)	Fixed Carbon (wt%)	HGI	slagging and fouling indices		
											AI	**BAI**	**Rb/a**
Whole Plant - Oven Dried Prior to Treatment	Autumn Whole Plant Raw	n.a.	57.7[a]	18.2	7.7	17.1	5.1	84 ±0	12 ±0	0 ±0	0.31	0.02	0.90
	Spring Whole Plant Raw	n.a.	33.6[a]	15.2	10.1	14.0	8.1	83 ±0	15 ±0	0 ±0	0.23	0.01	0.65
	Autumn Whole Plant HTC 200	76	4.4[b]	19.5	18.6	18.3	17.3	75 ±0	20 ±0	36 ±3	0.09	0.02	0.43
	Spring Whole Plant HTC 200	71	8.0[b]	17.9	16.5	16.8	15.2	81 ±0	17 ±0	25 ±0	0.11	0.03	0.29
	Autumn Whole Plant HTC 250	49	3.7[b]	26.5	25.5	25.4	24.4	59 ±0	39 ±0	142 ±1	0.07	0.03	0.44
	Spring Whole Plant HTC 250	47	2.8[b]	24.8	24.1	24.0	23.3	42 ±0	150 *±2*	150 *±2*	0.05	0.04	0.44
Plant Components - Oven Dried Prior to Treatment	Autumn *Miscanthus* Stems Raw	n.a.	7.7[c]	15.6	14.4	14.6	13.2	75 ±0	22 ±0	0 ±0	0.34	0.01	0.87
	Spring *Miscanthus* Stems Raw	n.a.	7.1[c]	15.2	14.1	14.2	12.9	83 ±0	14 ±0	0 ±0	0.19	0.01	0.61
	Autumn *Miscanthus* Stems HTC 250	49	4.3[b]	27.4	26.2	26.3	25.0	58 ±0	41 ±0	144 ±1	0.06	0.13	0.51
	Spring *Miscanthus* Stems HTC 250	43	3.0[b]	26.1	25.3	25.1	24.2	56 ±0	43 ±0	145 ±2	0.05	0.03	0.73
	Autumn *Miscanthus* Leaves Raw	n.a.	7.5[c]	17.2	15.9	16.0	14.6	83 ±0	11 ±0	1 ±0	0.36	0.02	0.19
	Spring *Miscanthus* Leaves Raw	n.a.	7.1[c]	15.9	14.8	14.8	13.5	82 ±0	14 ±0	1 ±0	0.55	0.01	0.71
	Autumn *Miscanthus* Leaves HTC 250	45	4.1[b]	28.8	27.6	27.4	26.1	62 ±0	31 ±0	139 ±0	0.05	0.20	0.22
	Spring *Miscanthus* Leaves HTC 250	46	3.5[b]	26.6	25.7	25.4	24.4	58 ±0	37 ±0	144 ±2	0.09	0.05	0.27
Whole Plant - Treated as Received	Autumn Whole Plant HTC 200	76	7.1[b]	16.2	15.0	15.0	13.7	85 *±1*	11 *±1*	34 ±1	0.10	0.04	0.45
	Spring Whole Plant HTC 200	73	4.1[b]	19.1	18.3	18.0	17.2	85 *±1*	11 *±3*	25 ±0	0.10	0.02	0.39
	Autumn Whole Plant HTC 250	48	4.0[b]	28.4	27.3	27.3	26.0	60 *±1*	38 *±1*	151 ±1	0.05	0.04	0.41
	Spring Whole Plant HTC 250	49	3.0[b]	26.2	25.4	25.2	24.3	57 *±1*	42 *±1*	145 ±2	0.05	0.03	0.46

n.a. not applicable; a) as received; b) moisture 48 hours after treatment; c) oven dried at 60°C

Table 5.9. Fuel inorganic and heteroatom chemistry

		mg/kg $_{fuel}$ (db)										
		Na	K	Mg	Ca	Mn	Fe	Al	Si	P	S	Cl
Whole Plant - Oven Dried Prior to Treatment	Autumn Whole Plant Raw	660±30	3970 ±300	720±100	2150±200	80±<5	70±<5	80±<5	5370±50	410±5	860±30	4390±80
	Spring Whole Plant Raw	520±10	2360±80	830±120	2050±250	10±<5	30±<5	40±<5	5870±140	440±10	890±80	6300±270
	Autumn Whole Plant HTC 200	540±30	1440±20	590±40	1670±110	50±<5	30±<5	20±<5	6660±130	380±20	750±30	3440±10
	Spring Whole Plant HTC 200	280±40	1110±20	450±10	1000±10	70±<5	50±<5	50±<5	6940±230	470±10	590	2910
	Autumn Whole Plant HTC 250	360±30	1090±5	520±0	1760±100	70±<5	40±<5	30±<5	5750±70	720±20	850±30	1640±50
	Spring Whole Plant HTC 250	320±30	590±70	370±50	1040±40	70±<5	30±<5	10±<5	3670±70	550±10	960±40	1640±40
Plant Components - Oven Dried Prior to Treatment	Autumn *Miscanthus* Stems Raw	220±10	4120±40	810±40	2030±120	80±<5	30±<5	170±10	5210±80	490±10	600±20	4250±80
	Spring *Miscanthus* Stems Raw	300±10	2110±30	810±30	1430±80	80±<5	20±<5	n/d	5060±220	400±10	830±30	5560±100
	Autumn *Miscanthus* Stems HTC 250	350±80	940±80	380±20	1760±100	60±<5	140±10	190±10	4480±130	680±20	960±40	2530±60
	Spring *Miscanthus* Stems HTC 250	370±30	620±20	430±5	1360±40	50±<5	20±<5	n/d	2620±100	400±20	1030±30	5040±110
	Autumn *Miscanthus* Leaves Raw	1020±80	3970±30	720±20	2150±120	80±<5	70±<5	80±5	27330±800	410±20	900±30	5830±100
	Spring *Miscanthus* Leaves Raw	680±30	6470±80	1150±20	3390±240	130±<5	50±<5	50±5	10560±260	630±10	1250±50	7030±100
	Autumn *Miscanthus* Leaves HTC 250	290±10	850±70	550±20	6940±100	150±<5	200±10	240±10	27330±410	1800±20	1670±30	2120±40
	Spring *Miscanthus* Leaves HTC 250	280±10	1790±70	690±5	2360±100	160±<5	100±10	n/d	12760±130	2180±30	1970±80	1650±60
Whole Plant - Treated as Received	Autumn Whole Plant HTC 200	220±5	1050±10	360±10	1680±20	50±<5	50±<5	100±5	4870±130	440±20	760±20	2740±80
	Spring Whole Plant HTC 200	380±40	1170±20	470±10	920±10	50±<5	30±<5	n/d	5110±90	262±10	570±20	3140±200
	Autumn Whole Plant HTC 250	210±20	960±10	370±20	1830±30	60±<5	50±10	120±20	5420±150	674±60	860±20	2420±40
	Spring Whole Plant HTC 250	420±10	550±30	360±50	860±40	60±<5	30±<5	<10	3240±60	40±10	810±80	1330±100

Figure 5.6 shows the DTG curves for unprocessed *Miscanthus,* processed at 200°C, samples processed at 250°C and a reference bituminous coal (Elemental Microanalysis B2306, batch 203830). Figure 5.6a shows the burning profile of the unprocessed early and conventionally harvested *Miscanthus* and compares the profiles to a reference coal. The unprocessed biomass has a distinctive two peak profile at 300°C and 440°C respectfully. Here you have an initial volatile burn, with thermal decomposition starting at round 200°C for conventionally harvested *Miscanthus,* peaking at 300°C. The rate of loss then reduces before the char ignites and with a peak burn temperature at 440 ºC. Coal on the other hand has almost a single stage whereby the volatile burn starts at the first initiation temperature, around 325°C, with a 'shoulder' on the curve before the onset of char combustion at the second initiation temperature due to the onset of char combustion, around 460°C, with peak temperature around 550°C.

When firing this *Miscanthus* in a pulverised fuel application the first issue can arise within the pulverised fuel mill as thermal decomposition of the biomass needs to be avoided. Pulverised fuel mills generate heat through friction and energy requirements needed in milling and can operate in excess of 150°C. As shown in Figure 5.6a the *Miscanthus* starts undergoing thermal decomposition at approximately 200°C, where bituminous coal does not start until 325°C. The lower decomposition temperatures associated with many biomass fuels result in challenges in operation of the pulveriser mills and require lower temperatures compared to coal to avoid fuel decomposition.

The second issue comes once inside the furnace and when trying to achieve a stable flame. When burning fuel, it is important to achieve flame stability to sustain the flame and ensure safe boiler operation. Differences in the nature different fuels burn (as shown by the burning profile) when co-fired can lead to poor burn interaction, with essentially the two fuels burning independently of each other. When this happens maintaining flame velocity (rate of burning) is challenging as the flame can move higher or lower in the furnace due to the mismatch, which can result in either blow off or flash back [187]. The mismatched burning profiles of the coal and the unprocessed *Miscanthus* in Figure 5.6a may lead to a poor burn interaction as ignition temperatures do not overlap bringing about challenges in maintaining flame velocity and flame stability. Flame stability can be further exacerbated by differences in particle size as large particle sizes can act as heat sinks, increasing the resonance time of the particle before ignition and influencing the balance of heat loss and heat release.

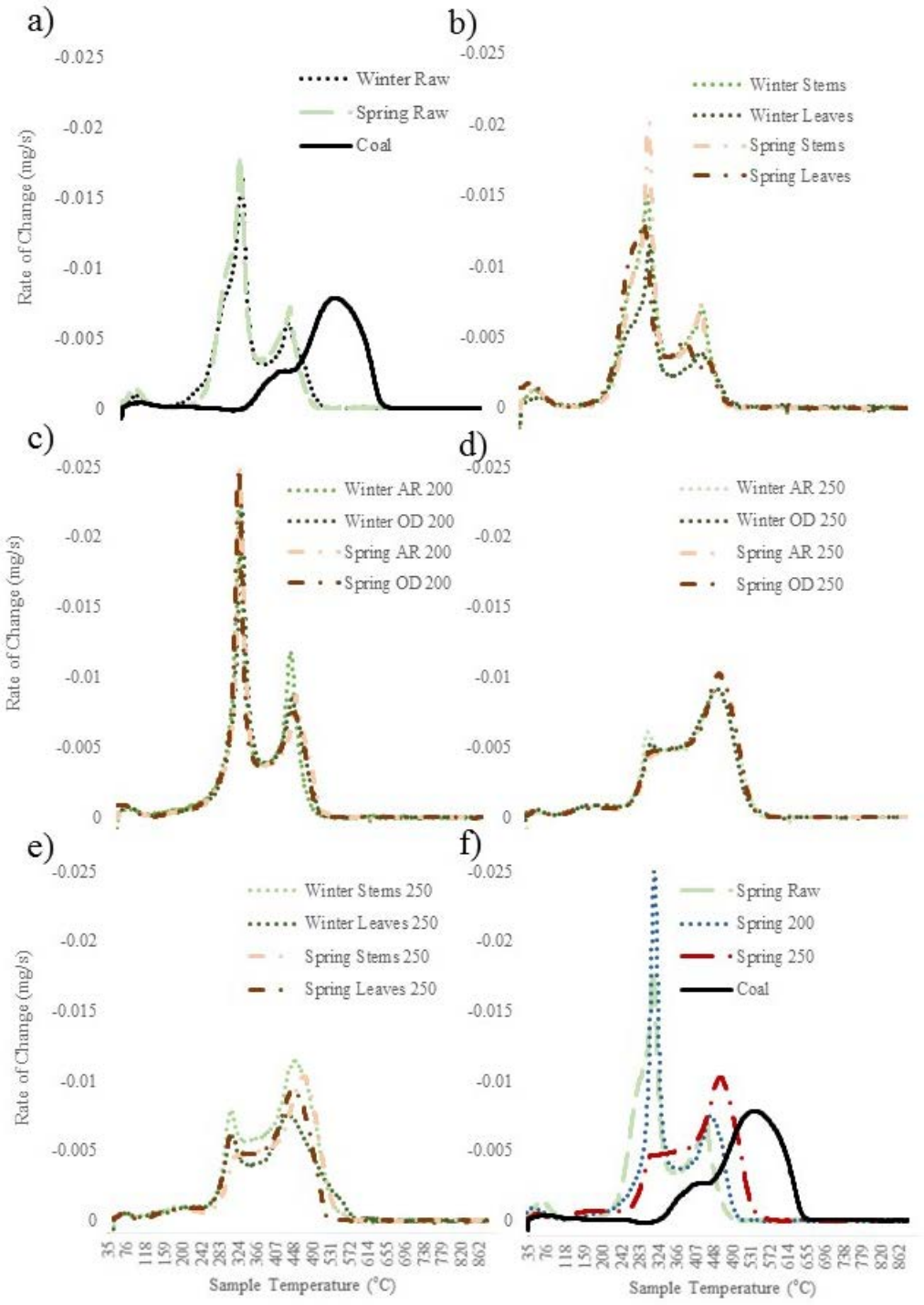

Figure 5.6: Derivative thermogravimetric (DTG) burning profiles for: a) early and conventionally harvested unprocessed *Miscanthus* and bituminous reference coal (Elemental Microanalysis B2306, batch 203830); b) early and conventionally harvested unprocessed *Miscanthus* leaf and stem; c) early and conventionally harvested *Miscanthus* hydrothermally treated at 200°C; d) early and conventionally harvested *Miscanthus* hydrothermally treated at 250°C; e) early and conventionally harvested leaf and stem hydrothermally treated at 250°C; and f) conventionally harvested *Miscanthus*, unprocessed, hydrothermally treated at 200°C, hydrothermally treated at 250°C and bituminous reference coal (Elemental Microanalysis B2306)

For a stable flame and good fuel burn out in a pulverised coal operation, pulverisation of fuel to 70% below 75µm is typically required and the ease in which this can be achieved is indicated by the HGI. The HGI for the unprocessed *Miscanthus* and processed bio-coals are given in Table 5.8. The unprocessed *Miscanthus* has an HGI of zero, which essentially implies under the test conditions, that no fuel would reach the desired 75µm, and thus, assuming co-milling, there would be either a greater energy requirement for milling to achieve 75µm or the pulverised fuel particles would be greater than 75µm in diameter. The lower first initiation temperature of the unprocessed *Miscanthus* would to a certain extent offset a larger particle diameter as heat loss due to the greater heat sink would be balanced by the earlier heat release. This would however only apply to a point after which the larger particles, on drying and de-volatilization, will became entrained in the gas stream and move higher in the furnace while still burning. This will promote flame instability [68].

Figure 5.6f shows the combustion profiles of the conventionally harvested unprocessed *Miscanthus*, processed at 200 °C and 250 °C and the reference coal. The profiles show the influence of HTC treatment on the fuels combustion profiles. The samples processed at 200°C retain the distinctive two peaks at 300°C and 460°C brought about by independent volatile and char burnout, similar to that of unprocessed *Miscanthus*. The 200°C treated samples do however differ from the unprocessed samples, and exhibit a slightly higher initiation temperature, approximately 240 °C, most likely due to the hydrolysis and removal of the hemicellulose from within the fuel [185]. There is also a greater rate of mass loss observed at 300°C, due to an increased level of cellulose within the fuel. This may be beneficial and allow pulverising mills to be run at a higher temperature consistent with coal operation. The HGI of 25 (see Table 5.8) for the samples processed at 200°C suggests that the fuel will pulverise, albeit like a high resistance coal. For reference, a change in HGI from 15 to 43 represents a 50% reduction in the energy requirement for milling, so going from an HGI of zero to 25 would represent a significant energy saving [197]. Bio-coal exhibiting a HGI of 25 would bring about a smaller particle size within the furnace, reducing issues with flame stability. Solid fuels exhibiting lower volatile ignition temperature, may not need the same amount of size reduction required for pulverised coal applications as heating of the particle to the volatile ignition temperature is lower. This allows for a larger particle diameter when compared to coal firing, so firing should be possible even if 70% of the 200°C hydrothermally treated fuel mass fails to meet the 75µm, as typically required in pulverised applications.

Figure 5.6f also shows that the samples processed at 250°C, adopts a 'coal like' single stage combustion profile, albeit with a lower first initiation temperature at 270°C compared with 325°C, and a lower peak temperature around 480°C as opposed to 550°C for the bituminous reference coal. The volatile burnout is also more pronounced for *Miscanthus* processed at 250°C than for the bituminous coal due to the higher volatile matter content of the bio-coal. The higher volatile matter content of the bio-coal can nevertheless be beneficial as this, along with the lower initiation temperature, will promote early ignition of the total fuel mass when co-fired; leading to better and more complete combustion. This early ignition in turn can also be beneficial for nitrogen oxide emissions as it will consume additional oxygen, increasing the fuel staging effects of low-NOx burners [68]. The HGI of 150 (see Table 5.8) for the samples processed at 250°C also imply that the fuel will easily pulverise and there should be limited issues with flame stability brought about though larger particle diameters encountered with untreated biomass.

Figure 5.6b shows the burning profiles of the unprocessed leaf and stem components. The burning profiles show differences between the stem and the leaf depending on the time of harvest, principally due to senescence and weathering degrading the plant biochemical components and removing inorganics, changing the ash content. These differences in composition also influence the burning profile of the bio-coal as shown in Figure 5.6e. The autumn stems, the autumn leaves and spring leaves both exhibit a distinct volatile peak, which may suggest the presence of residual cellulose or increased reactivity of the volatiles. This may account for the higher energy densities seen in the early harvested samples. For the conventionally harvested stems treated at 250 ºC, a coal like single stage combustion profile is observed whereby the transition between the volatile release and initiation of char burn (second initiation temperature) is marked more by a 'shoulder' as opposed to a distinct peak. This happens despite only a modest reduction in volatile matter (Table 5.8). The autumn components also appear more reactive than the conventionally harvested components with reduced peak temperature in the char burnout. This is most likely due to the higher potassium content (see Table 5.9) catalysing the volatile burn [208].

The two stage combustion profile described for the early harvested 250 °C plant component samples is also retained in the homogenised early harvest samples when compared with the conventionally harvested samples in Figure 5.6d. The 250 °C conventionally harvested samples displaying the single stage combustion profile similar

to the conventionally harvested stems treated at 250 °C. This change is brought about though a modest reduction in volatile matter content (Table 5.8), which brings about a slight change in the overall profile. Table 5.9 gives the inorganic content of the fuel, with the potassium content higher in the autumn samples. Higher potassium content is known to catalyse the volatile burn and could explain these differences [208] but the biochemical composition of the starting feedstock will be slightly different due to the higher proportion of leaf matter in the early harvested feedstock and needs to be also considered. Both these factors will influence the combustion profiles for the two unprocessed feedstock in Figure 5.6a. Figure 5.6c shows the early and conventionally harvested *Miscanthus* treated at 250°C and shows increased reactivity of the char burn in the autumn samples. The HGI appears reasonably constant for both the 200°C and 250°C treatments whether treating autumn or spring feedstock.

5.3.3.3.Influence of HTC on the *Miscanthus* inorganic chemistry

Inorganics can be a particular issue for *Miscanthus*, particularly early harvested *Miscanthus*, during combustion because of its tendency to corrode equipment and cause slagging, fouling and in certain furnaces bed agglomeration [336]. Figure 5.7 displays the deformation, hemisphere and flow temperatures for the autumn and spring whole plant unprocessed and treated at 200 °C and 250 °C. The safe combustion temperature is taken as the deformation temperature in Figure 5.7. Table 5.10 state the transition temperatures for all samples along with their standard errors.

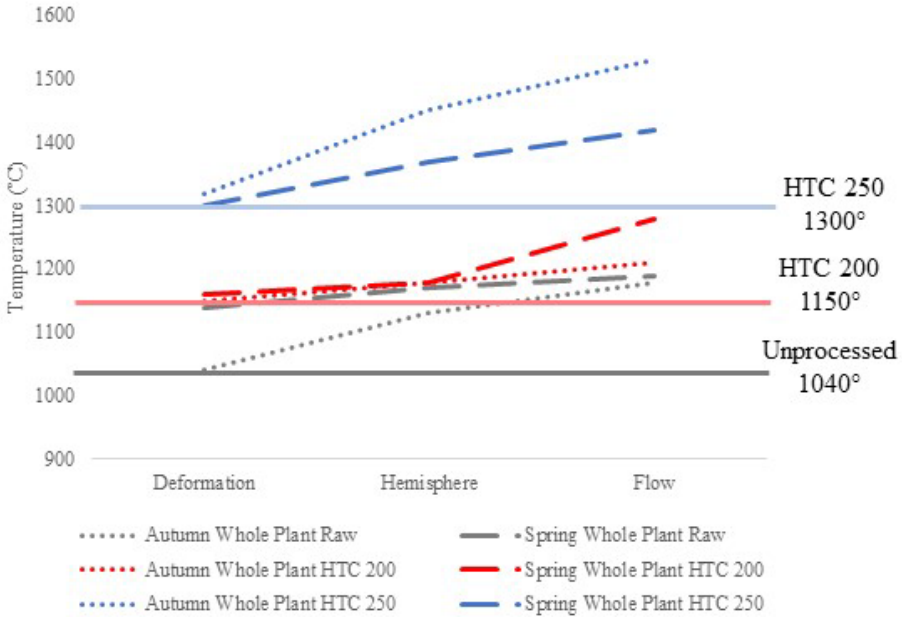

Figure 5.7. Ash Fusion Temperatures for the whole plant, oven dried prior treatment

Table 5.10. Ash fusion transition temperatures for both homogenised whole plants, key plant components and their corresponding bio-coals.

Sample		Onset Temperature (°C)							
		Shrinkage		Deformation		Hemisphere		Flow	
Whole Plant - Oven Dried Prior to Treatment	Autumn Whole Plant Raw	930	±0	1040	±15	1130	±0	1180	±0
	Spring Whole Plant Raw	960	±0	1140	±5	1170	±0	1190	±0
	Autumn Whole Plant HTC 200	1020	±0	1150	±0	1180	±0	1210	±0
	Spring Whole Plant HTC 200	900	±0	1160	±0	1180	±0	1280	±5
	Autumn Whole Plant HTC 250	850	±0	1320	±0	1450	±5	1530	±0
	Spring Whole Plant HTC 250	930	±25	1300	±15	1370	±5	1420	±30
Plant Components - Oven Dried Prior to Treatment	Autumn *Miscanthus* Stems Raw	1050	±0	1180	±0	1190	±0	1200	±0
	Spring *Miscanthus* Stems Raw	990	±0	1110	±0	1140	±0	1190	±0
	Autumn *Miscanthus* Stems HTC 250	990	±0	1300	±0	1350	±0	1370	±0
	Spring *Miscanthus* Stems HTC 250	830	±0	1250	±0	1320	±0	1360	±5
	Autumn *Miscanthus* Leaves Raw	1050	±0	1180	±0	1190	±0	1200	±0
	Spring *Miscanthus* Leaves Raw	700	±0	950	±0	1020	±5	1120	±0
	Autumn *Miscanthus* Leaves HTC 250	1060	±0	>1570					
	Spring *Miscanthus* Leaves HTC 250	880	±0	1390	±0	1530	±0	1570	±0
Whole Plant - Oven Dried Prior to Treatment	Autumn Whole Plant HTC 200	970	±5	1150	±5	1220	±5	1270	±5
	Spring Whole Plant HTC 200	990	±5	1140	±5	1200	±20	1230	±25
	Autumn Whole Plant HTC 250	850	±100	1320	±10	1450	±25	1530	±20
	Spring Whole Plant HTC 250	970	±70	1300	±0	1430	±0	1470	±60

The results show that the unprocessed early harvested *Miscanthus* behaves the most poorly in the AFT with the deformation temperature (i.e. safe combustion temperature) of only 1040°C. The conventionally harvested *Miscanthus* behaves better with a deformation temperature around 1140°C. The cause of this appears to be the higher potassium content within the fuel, relative to silicon content, in the unprocessed early harvested crop. Interpretation of this data requires some caution as despite the early harvested *Miscanthus* having the lower deformation temperature and the higher potassium content, the conventionally harvested crop has 2000 mg/kg more chlorine. Given the release of potassium depends more on the chlorine content than the potassium content alone [266], the corrosion and fouling potential may be higher for the conventionally harvested *Miscanthus,* with retention of potassium in the ash arguably more favourable.

Hydrothermally treating the early harvested *Miscanthus* at 200°C appears to reduce the potassium content from 4000 mg/kg to 1000 mg/kg (see Table 5.9) and this increases the deformation temperature to 1150°C, however there is only a minimal improvement with the conventionally harvested *Miscanthus* treated at 200°C. This change is due to the reduction of potassium in the 200°C treated samples being accompanied by reductions in fuel silicon and calcium. Calcium has been shown to increase the silicon fluxing temperature [261] and consequently its removal will reduce the melting temperature, while the reduction in potassium will lead to an increase in ash melting temperature. Consequently, for the 200°C treated samples, the change in the potassium to silicon ratio is less than the overall reduction in potassium due to corresponding reductions in silicon. The reduction of calcium will reduce the buffering offered by the calcium, which reduces the fluxing temperature of silicon due to potassium. Thus, despite the lower potassium content, the silicon melts at a similar temperature due to an overall reduction in silicon and calcium. It should however be noted that despite little change in deformation temperature, the overall ash content has reduced for both 200°C treated samples; this in turn changes the fuels from one with probable slagging and fouling to one which can be safely combusted according to the alkali index (See Table 5.8).

The 250°C treated samples exhibit a significant increase in transition temperature, with both the early and conventionally harvested *Miscanthus* increasing to 1320°C and 1300°C respectively, leading to a noteworthy increase in the safe combustion temperature. There is also a further increase in the hemisphere region with temperatures

up to 1450°C being observed (hemisphere temperature is reported as the upper limit for safe combustion by some authors). Of the early and conventionally harvested *Miscanthus* feedstocks, there appears to be a higher potassium content within the early harvested *Miscanthus* than conventional (approximately 1000 mg/kg and 600 mg/kg respectively) however the silicon content is also higher for the early harvested *Miscanthus* (approximately 5500 mg/kg and 3500 mg/kg respectively) and this appears to offset any fluxing brought about by the potassium. The early harvested *Miscanthus* also appears to contain a higher concentration of calcium and phosphorus, with the latter known to increase the thermal stability of potassium when present as potassium phosphate [200].

The highest ash thermal stability was observed for the hydrothermally related leaves, with the early harvested leaf deformation temperature exceeding the furnace limit at 1570°C. This high thermal stability is exhibited due to the high silicon content within the leaves. Silicon is largely retained within the bio-coal while the high potassium content of the leaves is largely extracted. This would suggest that harvesting the *Miscanthus* with an increased leaf content, as is done with early harvesting, does not adversely influence the ash chemistry, but potentially enhances it. The energy density of the hydrothermally treated leaves is not too dissimilar to the energy density of the stems (27.4 MJ/kg (db) to 28.3 MJ/kg (db)), and with similar HTC yields, the presence of leaves through early harvesting does not appear to have any adverse effect. In addition, the leaves will improve the acid base ratio due to increased silicon within the ash (see Table 5.8), while increasing the feedstock yield by up to 40 % by avoiding overwinter dry matter loss [333, 334].

The bio-coals have been shown to undergo significant reductions in alkaline metals, most notably potassium, on a mass basis and this is also associated with reductions in fuel chlorine (see Table 5.9). The feedstock is already low in sulphur, containing typically 0.1 wt % (db) with limited change in concentration through treatment (see Table 5.7 and Table 5.9). The inorganic analysis suggests that corrosion, associated with fouling should be reduced following treatment by HTC. The reductions in chlorine are however less than the reduction seen in comparable washing experiments, which have shown between 85 % and 100 % removal [43, 205, 264]. The assumption made in Chapter 4, published in Smith et al. [213] and assumed by subsequent authors, that, during HTC most chlorine within the biomass is extracted as demonstrated in washing experiments, may only in part be correct. The results suggesting there maybe other underlying chlorine retention mechanisms during HTC.

5.3.4. Conclusions

The results indicate that the inorganic chemistry of the raw *Miscanthus* would bring about probable slagging and fouling, whether harvested early or late. The low grindability would also make size reduction challenging when combusting in pulverised coal applications. Accordingly, whether *Miscanthus* is harvested early or conventionally, a biomass pre-treatment that improves the fuels ash chemistry and ideally grindability, appears to be a pre-requisite.

Hydrothermal carbonisation at 200°C showed only limited energy densification for both early and conventionally harvested *Miscanthus*. The HGI increases to 25, resulting in energy savings associated with grinding. HTC at 200°C reduces fuel alkali metal content, although additional reductions in fuel silicon and calcium result in only modest improvement in the ash deformation temperature, suggesting limited improvement in slagging propensity. Nonetheless, this should reduce the potential for deposit formation. This combined with a reduction in chlorine and low sulphur content of the fuel, should reduce fouling, active oxidation and corrosion. Slagging and fouling indices suggested safe combustion for both early and conventionally treated fuels.

HTC at 250°C results in a significant increase in carbon density and removal of oxygen functionality, with the resulting bio-coal reaching a HHV ranging from 27 to 28 MJ/kg for early and 25 to 26 MJ/kg for conventionally harvested *Miscanthus*. The 'coal like' single stage combustion profile, coupled with a HGI of 150, suggests the fuel will be easy to pulverise, overcoming issues associated with flame stability enabling a good burn interaction if co-fired with coal. HTC at 250°C can overcome slagging issues and increase the ash deformation temperature from 1040°C to 1320°C for early harvested *Miscanthus*. The chemistry also suggests a reduction in fouling and corrosion propensity for both 250°C treated fuels. Reductions in fuel chlorine were however less than that reported in the washing literature, suggesting chlorine is in part retained during HTC as opposed to washed out as previously assumed.

The results indicate that HTC at 250°C will valorise both conventional and early harvested *Miscanthus*. Harvesting and processing the crop early does not appear to have any adverse effect on the process yields and combustion properties of the resulting fuel. While the longer term agronomic impacts of early harvesting needs to be fully understood and optimum harvesting time determined, the combustion implications of early harvesting appear to be overcome by HTC and could provide a coal like bio-fuel with increased yields up to 40% per hectare due to avoidance of overwinter dry matter loss.

6. The influence of retention time on bio-coal combustion chemistry

6.1. Abstract

In this chapter, *M*iscanthus was hydrothermally carbonised at 200 °C and 250 °C, with varying retention times, from zero hours to 24 hours to understand what impact increasing retention time has on the resulting fuel's inorganic chemistry. The results are also used to establish a baseline to assess the additional impact of process water recycling on bio-coal yield and fuel properties, as discussed in the following chapter. Increasing retention times brought about dehydration of the fuel. However temperature appeared the more important variable, as after 24 hours at 200 °C the fuel had similar in properties to that of the 250 °C+0h bio-coal. After one hour, cellulose appears to be largely removed from the 250 °C bio-coal. This dehydration, repolymerisation and cellulose removal brings about a 'coal like' combustion profile, with decreasing reactivity with increasing retention time. This should aid combustion in existing pulverised coal power plants. Alkali metals are largely extracted at low retention times, but undergo further extraction with increasing retention times. Phosphorus and sulphur appear to undergo substantial extraction at 200 °C+0h but appear reincorporated with increasing retention time. Fuel chlorine is reduced with increasing retention time. Silicon content increases within the bio-coal with increasing severity, while calcium appears to reduce within the 250 °C bio-coal after one hour, thought to be due to organic acid leaching. Increasing reaction severity brings about a decrease in fuel fouling and slagging propensity, as demonstrated by the ash fusion test and various slagging and fouling indices.

6.2. Introduction

Retention time vary throughout the literature with some reports using residence times from less than five minutes to up to several days. However many studies which have looked into metal retention / removal have used 5 minute retention times, for example Reza et al. [76]. These short retention times may be favourable in terms of plant throughput but short retention times can impose kinetic limitations which prevent aromatization and repolymerisation [101]. It has been suggested by several authors that HTC is a two stage process with the initial hydrolysis reactions along with dehydration and decarboxylation reactions believed to have gone to completion by the time the hold temperature is reached [29, 98]. The advantage of retaining the reactor at temperature is it allows the ongoing repolymerisation of solved fragments in the liquid phase but this can also lead to the precipitation of insoluble salts [11]. Hoekman et al. [29] experimented with varying retention times with a spruce / fir mix and analysed the acids and sugars

present in the process water by IC and the mass yields and energy density of the chars. The results showed that sugars within the process water decreased as retention times increased, with organic acid increasing slightly but overall total organic carbon decreased which is indicative of repolymerisation. Furthermore, despite a small but noticeable decrease in mass recovery, energy content was shown to increase with residence time. Kruse et al. [99] demonstrated that increasing retention time at between 180 °C and 250 °C reduced nitrogen content of the bio-coal. It is generally assumed that longer residence times generally increase reaction severity [11], however with residence time there appears to be a trade-off between the costs associated with retaining a process at temperature (influence on throughput, increased energy costs etc.) and an enhanced product.

A number of authors in HTC have combined both the temperature and pressure parameters into a single factor known as the severity factor and is given in Equation 6.1 [84, 101-103]. The severity factor being the logarithm of the reaction ordinate; a reactivity a factor developed by Overend and Chornet [104] to characterize hydrolytic depolymerisation processes during wood pulping and similar operations. The principle dictates that similar products can be achieved through either increased retention times at a lower temperature or increased temperature with lower retention times. The equation is advantageous when predicting hydrolytic depolymerisation processes and will be suited to 'hydrothermal torrefaction' applications but becomes limited when you consider kinetic limitations imposed by aromatization and repolymerisation. Consequently shorter reaction times influence chemical composition of the products and simply operating hotter may not overcome this [101]. Influence of particle size, and solids loading are additional factors that will influence the required residence time, as both diffusion-controlled transport mechanisms during biomass decomposition and condensation polymerisation are likely to govern the overall rate of reaction.

$$\text{Severity Factor} = \text{Log}\,(\text{time (min)} * e^{[(\text{temp (°C)} - 100)/14.75]} \qquad (6.1)$$

In this research *Miscanthus* was hydrothermally carbonised at two temperatures 200^0C and 250^0C, with varying retention times, from zero hours to 24 hours to understand what impact increasing retention time has on both the fuels organic and inorganic combustion chemistry. This chapter is written to co-inside with Chapter 7, and the results presented in this chapter are used to establish a baseline in order to assess what additional impact of process water recycling has on the fuel's organic and inorganic combustion chemistry.

6.3.Methodology

6.3.1. Materials

Samples of *Miscanthus giganteus* were obtained from Rothamsed Research. Samples were initially cut garden shredder then further homogenised in a cutting mill (Retsch, Germany) using a 4 mm grate. Samples were then oven dried at 70 ˚C for 72 hours before processing.

6.3.2. Hydrothermal carbonisation

HTC was performed using the modified 2000 ml Parr reactor described in Section 3.2.2. For each run a 10 % solids loading was used with a combined mass of 1000 grams per run and undertaken as described in Section 3.2.2.2. The bio-coal was allowed to air dry in a ventilated fume cupboard for a minimum of 48 hours, to gauge air dry moisture loss, and then oven dried at 60˚C overnight.

6.3.3. Analysis

6.3.3.1.Inorganic analysis

Inorganic elemental composition was determined by two methods; wavelength dispersive X-ray fluorescence (WD-XRF) and Atomic Absorption Spectroscopy (AAS). For XRF analysis, the samples were analysed using the ash pressed pellet and lithowax binder method Section 3.6.8.2.1. The potentially volatile alkali and alkaline earth metals were determined by AAS analysis. Samples were digested using the hydrofluoric acid method described in Section 3.6.1 and determined by AAS (Valiant, USA) using the methods described in Section 3.6.3. Chlorine within the feedstock and bio-coal was analysed by combustion in an oxygen bomb (Parr, USA) followed by determination using ion exchange chromatography (Dionex, USA). The method is described in Section 3.6.7.

6.3.3.2.Organic analysis, combustion properties and ash measurement

Carbon, hydrogen, nitrogen, sulphur and oxygen content was determined using a Flash 2000 CHNS-O analyser (Thermo Scientific, USA), with the method described in Section 3.4.2. The volatile and fixed carbon component of the proximate analysis carried out using thermo-gravimetric analysis (Mettler Toledo, Switzerland) as described in Section 3.3.3. Ash content was determined using a muffle furnace, as described in Section 3.3.2. Moisture content was determined using a moisture oven as described in Section 3.3.1. The calorific value was determined using Dulong's Equation (see Equation 3.11). Figures are corrected in accordance with ASTM D3180-15, with hydrogen and oxygen

values corrected to account for moisture. Burning profiles, ignition, flame stability and burnout temperatures were obtained by TPO, as described in Section 3.8.

6.3.3.3.Prediction of slagging and fouling behaviour

Ash fusion testing (AFT) was performed using a Carbolite digital ash fusion furnace in accordance with the standard method for the determination of ash melting behaviour (DD CEN/TS 15370-1:2006) using the methodology described in Section 3.7.1. In addition, various slagging and fouling indices have been utilised with their equations 1-3 in Table 3.3. Their underlying theory and calculation methodologies given in Section 3.7.2.

6.3.3.4.Process water analysis

The carbon content of the process water was analysed using a total organic carbon analyser (TOC) (Hach, Germany) (see Section 3.10.1). Free ionic salts within the process waters were analysed by ion exchange chromatography (Dionex, USA) (see Section 3.10.2). Due to the complex nature of the process waters, a qualitative overview of the organic compounds present in the process waters was obtained using water corrected deuterium oxide spiked protonated nuclear magnetic resonance (NMR) (Bruker, USA), as described in Section 3.10.5. Peaks were identified by developing a reference library using range of pure reference standards at known concentrations (Sigma-Aldrich, USA) and cross checked using data provided in Pretsch et al., [310] and AIST spectral database. This method appears consistent with methods used by Berge and co-workers in [128, 141, 346]. Volatile compounds were further analysed by GCMS (Shimadzu, Japan) through direct injection onto 30 meter 0.25 mm RTX-Wax column (Restek, UK). This method appears consistent with methods of process water analysis used by Baccile, Titirici and co-workers [301, 307, 308]. Details on the GCMS method and its development given in Section 3.10.4. Reliable quantitative data via HPLC appeared unattainable in this instance. pH was determined using a digital probe meter (Hach, USA).

6.3.3.5.Gas phase analysis

Gas analysis was undertaken using a gas chromatograph (Shimadzu, Japan) fitted with a molecular sieve 5A 60-80 mesh and Hayesep N 100-120 mesh with argon carrier gas, 250 µl sample loops and TCD detectors, as described in Section 3.12.

6.3.3.6.Volatile component analysis

Volatile component analysis was carried out via pyrolysis-GCMS (CDS analytical, USA; Shimadzu, Japan) using a 60 meter 0.25 mm RTX-1701 column (Restek, UK). All

samples were routinely analysed in duplicate at 550 °C using 20 °Cms^{-1} heating rate and the pyroprobe operating in trap mode. In addition the samples processed at 250 °C with differing retention times, and run 1, 5 and 9 at 250 °C underwent multistage desorption's at 250 °C, 400 °C and 600 °C, with these temperatures corresponding to observed changes in DTG profiles obtained by the TGA proximate and oxidation programs.

6.4. Results

6.4.1. Influence of retention time on the bio-coal organic chemistry

The yields, energy density, proximate and ultimate analysis of bio-coals derived from differing retention times are given in Table 6.1. The results show for both temperatures, increasing retention time increases carbon density, reduces oxygen density and increases energy density. The results given in Table 6.1 would suggest that the bio-coal after 24 hours is similar to that of a bio-coal treated at 250 °C without a retention time. This said when the hydrogen and oxygen atomic ratios are plotted against carbon in a Van Krevelen diagram, given in Figure 6.1; it is shown that a more coal like material is obtained at 24h at 200 °C, than 0h at 250 °C. This result is constant with the calculated 'severity factor' given in Equation 6.1 and now adopted by a number of authors in HTC whom seek to combine both the temperature and pressure parameters into a single factor [84, 101-103].

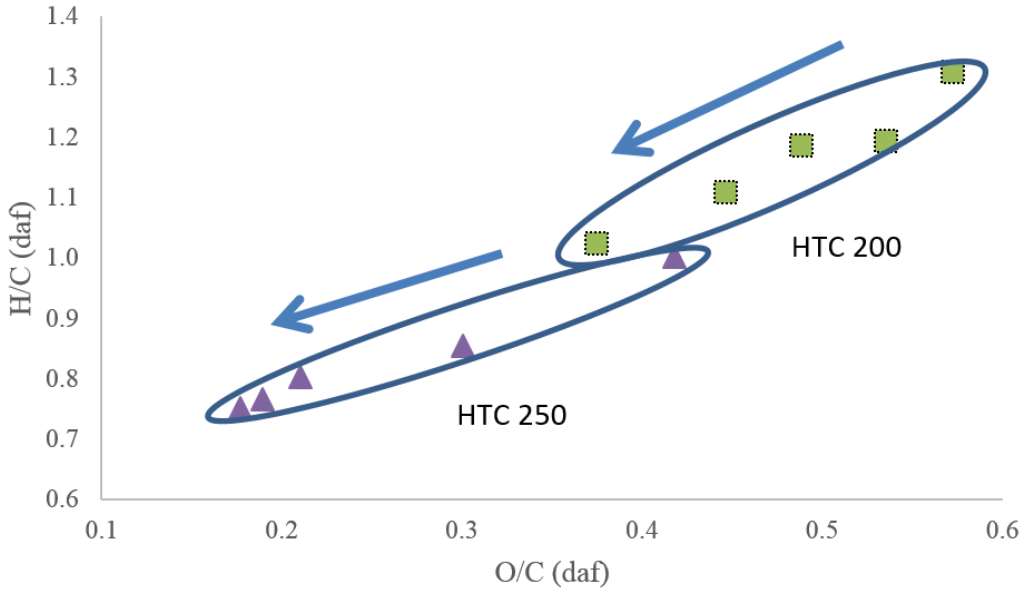

Figure 6.1: Atomic H/C-O/C rations of bio-coals derived from increasing retention times

Table 6.1: Yields, energy density, proximate and ultimate analysis of bio-coals derived from differing retention times

Temperature	Retention	% Dry Basis								HHV MJ/kg
		Yield	Nitrogen	Carbon	Hydrogen	Oxygen	Ash	Volatile Matter	Fixed Matter	
Unprocessed			0.7	52.2	5.2	38.7	3.1	84.5	12.3	18.2
	0h	67	0.7	51.8	5.6	39.5	2.4	80.4	16.0	18.5
	1h	65	0.7	53.6	5.3	38.2	2.2	77.4	18.9	18.9
HTC 200	4h	64	0.7	55.3	5.5	36.0	2.4	74.7	21.7	20.1
	8h	61	0.7	57.6	5.3	34.3	2.1	71.9	25.2	20.9
	24h	56	0.8	61.1	5.2	30.5	2.5	65.7	31.1	22.6
	0h	52	0.6	59.2	4.9	32.9	2.3	69.1	27.9	21.1
	1h	46	0.8	65.5	4.7	26.2	2.8	58.1	38.2	24.2
HTC 250	4h	44	0.8	71.6	4.8	20.1	2.7	53.5	42.3	27.5
	8h	43	0.8	73.4	4.7	18.6	2.5	51.7	44.1	28.2
	24h	43	0.8	74.1	4.6	17.5	2.9	49.3	45.8	28.5

It is important to recognise that while energy density increases, mass yields decrease, predominantly due to the removal of oxygen from within the fuel. The results presented in Figure 6.1 suggest dehydration is the predominant mechanism for oxygen and hydrogen removal increasing retention time. The decreasing mass yield has overall influence on the overall energy yield, with energy yield defined as the resulting fuels energy multiplied by the mass yield. The results show for the zero and one hour holds energy yields are around 68% and 61 % for the 200 °C and 250 °C treatments. Between one hour and four hours, the energy yield appears to increase, after which it appears reasonably consistent at around 70% at 200 °C and 67% at 250 °C, for the remaining treatments. For the 250 °C treatments there appears be an advantage in increasing retention time up to four hours due to the improvement in energy yield. Given increasing retention, times will decrease reactor/ plant throughput and invariably increase energy input due to heat losses, appropriate techno-economic assessment would be required. The increased production costs would have to be offset with energy savings brought about through haulage savings and handling improvements would be required to offset the likely higher cost of production. The severity factor given in Equation 6.1 also demonstrates that by increasing temperature retention time can be reduced, thus the improvement in energy yield seen after four hours in the 250 °C treatments, could be achieved by a shorter retention time at higher temperature. This said kinetic limitations resulting from shorter reaction times influence chemical composition of the products and simply operating hotter may not overcome this [101].

The increasing retention time also increases the fixed carbon content of the fuel. Results show the fixed carbon content increases at a rate greater than that of mass loss during the hydrothermal process for all but the zero and one hour 200 °C treated bio-coals, which from now will be referred to as HTC 200+0h and HTC 200+1h respectively. For the 200 °C treated bio-coals, the increasing fixed carbon yield indicates some of the fixed carbon is being derived from the condensation and repolymerisation of oligomers and monomers derived though the hydrolysis of hemicellulose and cellulose, which are readily degraded at temperatures of 180 °C and 200 °C respectively [71]. Lignin, of which content is closely correlated with fixed carbon content of raw biomass [347], is likely recalcitrant at 200 °C, being a cross linked phenolic polymer, degradation is more often associated with higher temperatures in the range of 230 °C to 260 °C dependent on retention time [28, 75, 76]. Consequently the lignin fraction is likely to remain within the 200 °C bio-coal, with possibly only limited removal of the hydroxy, methoxy and alkoxy

functional groups associated with its benzene units [25]. Accordingly, based on the literature the fixed carbon within the HTC 200+0h bio-coal, is likely derived predominantly of lignin. With increasing retention time water insoluble humic substances, often referred to as humins, are formed from the degradation and repolymerisation of cellulose and will make up a greater proportion of the fixed carbon [348]. These Humins are similar to that of the humic acids which are the thermal degradation products of lignin [25]. Pyrolysis GCMS has been undertaken analysis of the 200 °C derived bio-coals and the results are given in Figure 6.2. The results show with increasing retention time there are increasing concentrations of methyl furans (peaks 1 and 2), which are constant with humin formation via aldol addition or condensation of Hydroxymethylfurfural (5-HMF) and furfural like compounds [309]. Increasing retention times also brings about increasing conentrations of methyl and ethyl phenols (peaks 5, 21, 23, 25, 26 and 30), which indicate an increase in the humic substances within the bio-coal.

Interestingly all 200 °C bio-coals contain levoglucasan (peak 38), a pyrolysis product of starch and cellulose [349], indicating that the cellulose has not fully degraded after 24 hours at 200 °C. While this study does not attempt to quantify the aqueous products within the process water, given it is extremely difficult to determine which chemical reactions take place [301]. Total organic carbon (TOC) is given in Table 6.2 and shows a progressive decline in carbon concentration within the process water with increasing retention time and GCMS and H-NMR has been utilized to gain a qualitative overview of the changes within the process water. Figure 6.3 gives a GCMS trace of the predominant volatile fatty acids (VFA) within the process waters, and Figure 6.4a and Figure 6.4b gives an overview of the organic compounds present. Figure 6.4a shows that for HTC at 200 °C acetate salt is the overwhelming organic product within the process water, acetic acid (not to be confused with acetate) is at the greatest concentration of the VFA (Figure 6.3).

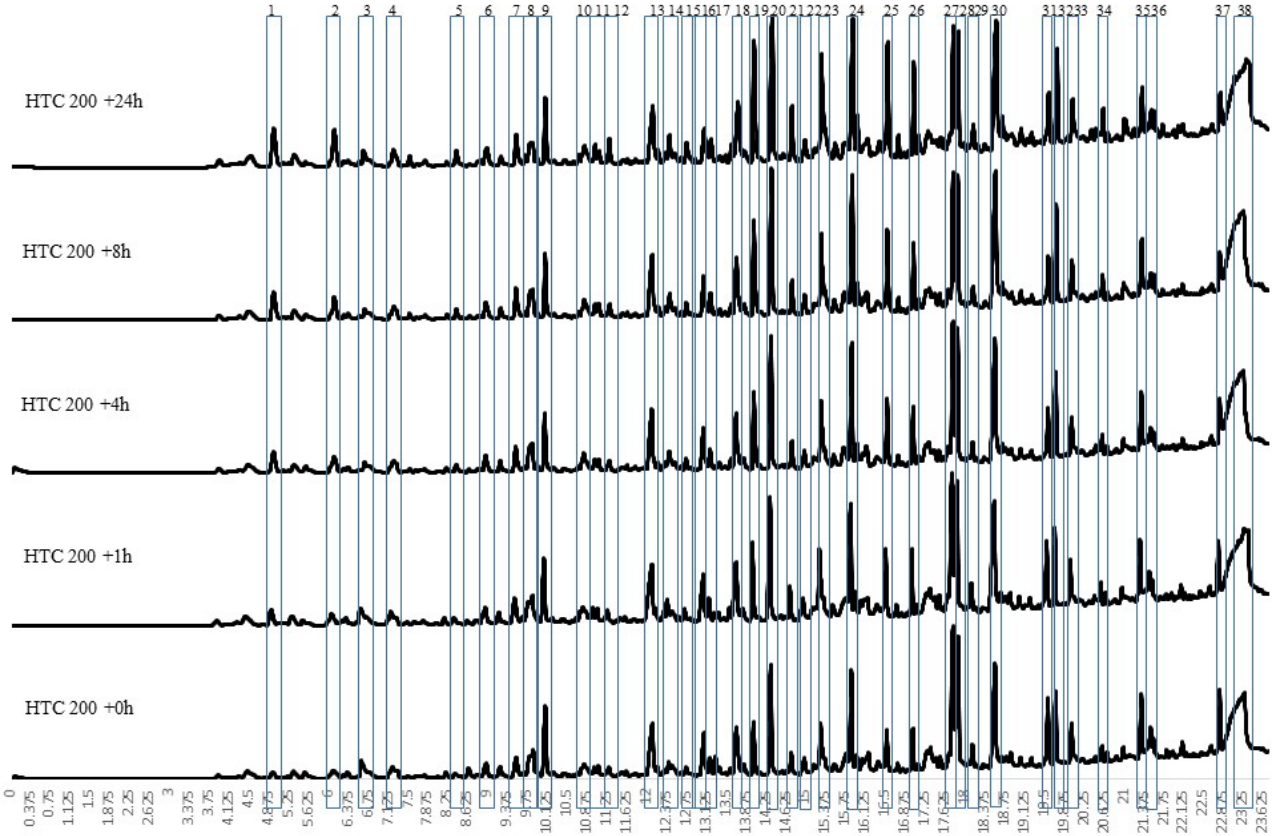

Figure 6.2: Pyrolysis GCMS spectra of volatile organics evolved at 550 °C from bio-coals treated at 200 °C with varying retention times. ((1) 2-methyl furan; (2) 2,5 dimethyl furan; (3) propanediol; (4) toluene; (5) 3-methyl phenol; (6) pentanoic acid; (7) cyclopentanone; (8) butanediol; (9) dimethylpyrazole; (10) 2-furanmethanol; (11) ethylhexaldehyde; (12) 1,3dimethylcyclopenten-3-one; (13) cyclopentadione; (14) 2-furan carboxadehyde; (15) 1methyl-1-cyclopenten-3-one; (16) furanone; (17) amino-3-pyridinol; (18) 3-methyl cyclopentanedione; (19) phenol; (20) 2-methoxyphenol; (21) 2-methyl phenol; (22) 2-cyclopenten-1-one: (23) 4-methyl phenol; (24) creasol; (25) 4-ethyl phenol; (26) 4-ethyl-2methoxy phenol; (27) dihydrobenzofuran; (28) 4-hydro-3-methyl acetophenone; (29) eugenol; (30) 2,6, dimethoxyphenol; (31) isoeugenol; (32) triethoxybenzene; (33) vanillin; (34) trimethoxytoluene; (35) dimethoxy acetophenone; (36) trimethylacealdehyde; (37) methoxy eugenol; (38) levoglucasan)

Initially the process water appears to be predominantly comprised of oligosaccharides, monosaccharides (glucose, fructose and maltose through isomerization, along with pentose) and aldehydes derived from the hydrolysis of cellulose and starch [79-81]. These compounds are readily decomposed giving rise to acetic acid [82, 83] bringing about the rapid drop in pH to 3.4 to 3.5 for the 200 °C treatments (see Table 6.2). As retention time is increased to HTC 200+1h TOC drops and acetate becomes overwhelmingly the main compound found in the NMR spectra. Due to the dominance of the acetate peak the acetate peaks at 2.0 ppm have been subsequently removed in Figure 6.4b to gain a better understanding of the changes in other components. At HTC 200+1h the 5-HMF becomes increasingly dominant, along with pyridinol, an organo-nitrogen compound, possibly derived from nitro-benzoamine (Figure 6.2 peak 19) in the raw biomass, furfural and formic acid in the VFA analysis. 5-HMF and furfural compounds being products which arise from the dehydration and fragmentation of the glucose, fructose and maltose derived from the starch and sugar [85, 86, 350].

Table 6.2: Total organic carbon, alkali and alkaline metals, chlorine, phosphate, sulphate and pH of process water with varying retention times.

Temperature	Retention	mg/l								pH
		Na	Mg	PO4	SO4	Cl	K	Ca	TOC	
HTC 200	0h	4	17	250	286	415	486	357	12637	3.54
	1h	6	50	193	229	1106	634	395	10935	3.41
	4h	6	18	209	277	498	526	442	8837	3.49
	8h	4	18	176	242	477	494	403	8210	3.44
	24h	5	37	169	209	477	487	183	7536	3.49
HTC 250	0h	5	56	292	274	354	482	227	12029	3.30
	1h	11	78	251	312	354	572	173	11946	3.30
	4h	6	65	274	281	390	474	282	10913	3.27
	8h	6	55	325	270	388	474	227	9707	3.28
	24h	5	41	370	262	351	521	324	8812	3.35

As retention time increases furfural appears not to be present in high concentrations within the process water, with pyridinol, acetic acid and 5-HMF appearing to be the main VFA products in the process water. Relatively low concentrations of furfural could be due to the furfural generated quickly decomposing to the VFA, aldehydes and phenols present [351], or quickly reacting with the monosaccharides present in the process water, forming the insoluble humins though polymeric condensation [350] making up the non-lignin derived char. The low yields could also be

due to the presence of the acetate and acetic acid within the process water, as acetyalization lowers the conversion yield of furfural from pentose [150].

Acetyalization is also known to reduce the reactivity of 5-HMF though protection of the formyl group, reducing polymeric condensation reactions with monosaccharides which would otherwise form humins (char) [150] increasing the resonance of 5-HMF in the process water. A reduction in the 5-HMF relative to pyridinol and reduction in TOC up to HTC 200+24h, combined with an increase in methyl furans in the corresponding Py-GCMS data (Figure 6.3), does however suggest that over increased retention times at 200 °C the 5-HMF is incorporated into the char by via aldol addition and/or condensation [309]. The low levels of levulinic acid and formic acid, common decomposition products of 5-HMF [270], indicate that under these conditions the 5-HMF does not decompose further to levulinic acid, unlike the 250 °C treatments (also shown in Figure 6.3), hence it appears to be reincorporated into the char.

Figure 6.4b does show the presence of formate which could suggest that formic acid formed during the hydrothermal process reacts with inorganics within the biomass to form metal formates. The NMR data also suggests the presence of formic acid but the GCMS analysis suggests that the formic acid is actually formic acid methylethyl ether / isopropyl fromate which gives proton shifts at both 1.28 and 8.01ppm and consequently would be double counted.

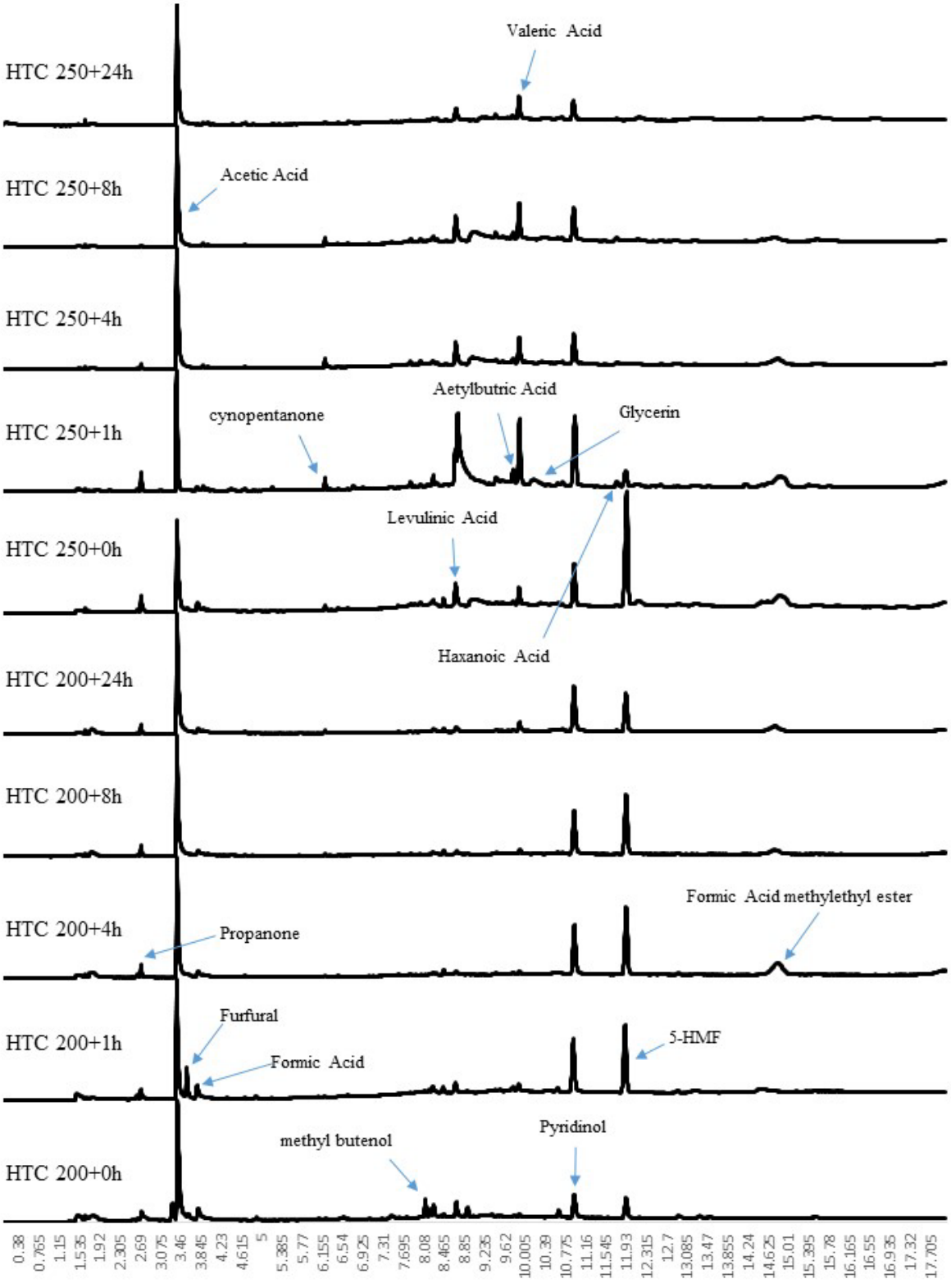

Figure 6.3: CGMS spectra of volatile fatty acids within of HTC process waters from 200 °C and 250 °C treatments at different retention times

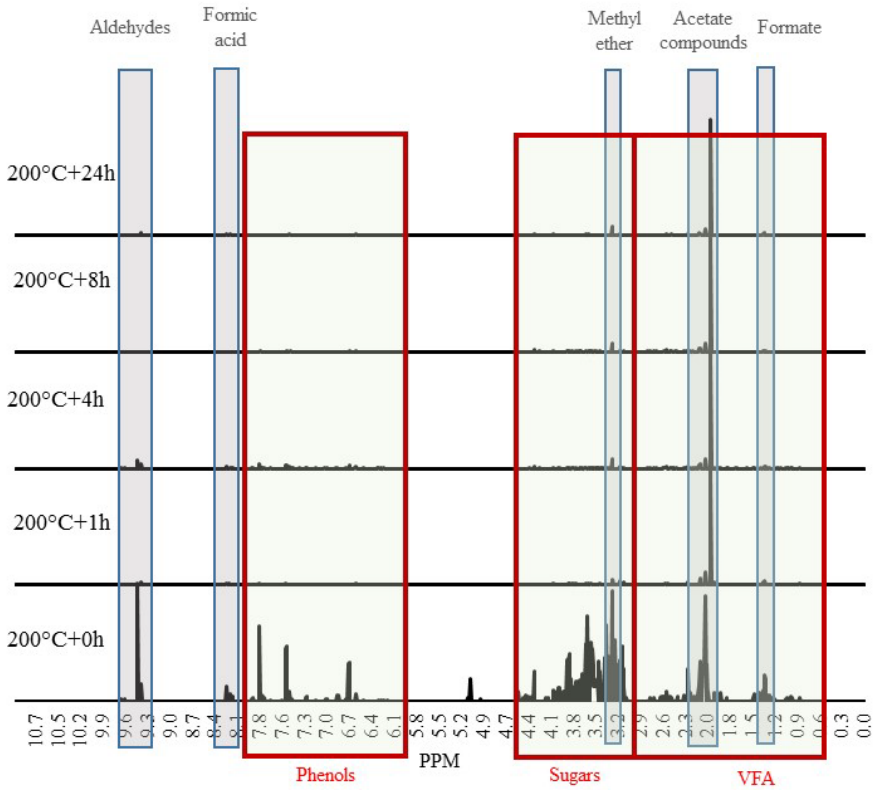

Figure 6.4a: H-NMR spectra of HTC process waters from 200 °C treatment at different retention times

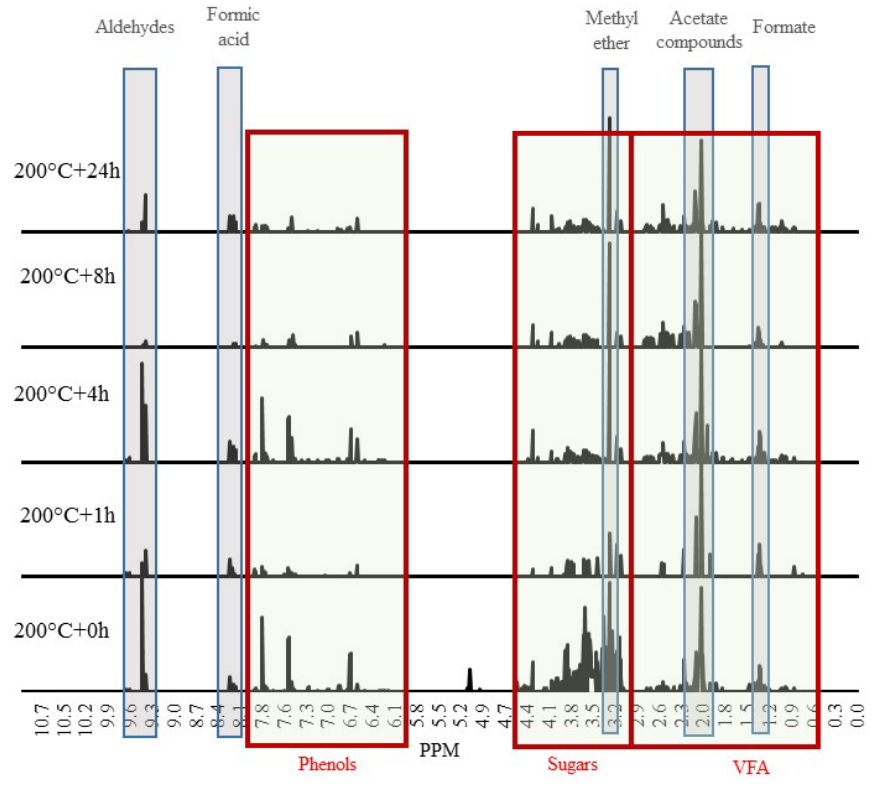

Figure 6.4b: H-NMR spectra of HTC process waters from 200 °C treatment at different retention times without acetate peak

For the 250 °C treatments TOC, given in Table 6.2 also shows a progressive decline in carbon concentration within the process water with increasing retention time. The py-GCMS results show a change in chemistry, with the loss of the large levoglucasan peak (peak 38), seen in all the HTC 200 °C treatments and the HTC 250+0h bio-coal (see Figure 6.5). While a small levoglucasan peak remains in the further four treatments with increasing retention time, the results imply that the cellulose is predominantly degraded after one hour at 250 °C (HTC 250+1h) and a recalcitrant fraction of cellulose remains despite increasing retention time. The presence of a large levoglucasan peak in HTC 250+0h implies that while cellulose degrades at and above 200 °C [71] there are still kinetic limitations, limited by reaction time, at 250 °C.

VFA analysis of the process water for HTC 250+0h, given in Figure 6.3, and indicates significant production of 5-HMF is high at this higher temperature and short retention time. At HTC 250+0h. The 5-HMF does however appear to be decomposing at 250 °C, with the appearance of the levulinic acid peak in the HTC 250+0h spectra. VFA analysis for HTC 250+0h process water indicates that there is reasonably low concentrations of formic acid but formic acid methylethyl ether / isopropyl fromate is present, suggesting that the formic acid quickly forms metal formates once produced.

By HTC 250+1h the VFA data shows the 5-HMF peak is largely gone, replaced with a levulinic acid peak and the appearance of the valeric acid peak. This shows that at 250 °C, 5-HMF is converted to levulinic acid and other compounds and is only an intermediate product at this temperature. The presence of 5-HMF in the HTC 250+0h process water would be due to the residual cellulose being present, producing 5-HMF at a rate greater than its conversion to levulinic acid or simply at the short retention time there is kinetic limitations, limiting its further conversion. This is significant as authors such as Kambo et al. [115] state that 5-HMF is a value added product in the process water of HTC 225 °C and HTC 260 °C. These results would suggest the 5-HMF detected by Kambo et al. [115] at 260 °C is more likely as a consequence of their fast heating rate and short retention time (>10 $C°min^{-1}$, <5 minutes) not fully converting the cellulose. Detection of levulinic acid at HTC 190 °C but no 5-HMF in Kambo et al. [115], could however indicate the compound reported as 5-HMF is actually a different compound and miss-identified by their HPLC method. In HTC 250+1h there is no visible formic acid peak, although formate is the third largest peak in Figure 6.6b, behind acetate and methyl ether, suggesting metal formates present in process water.

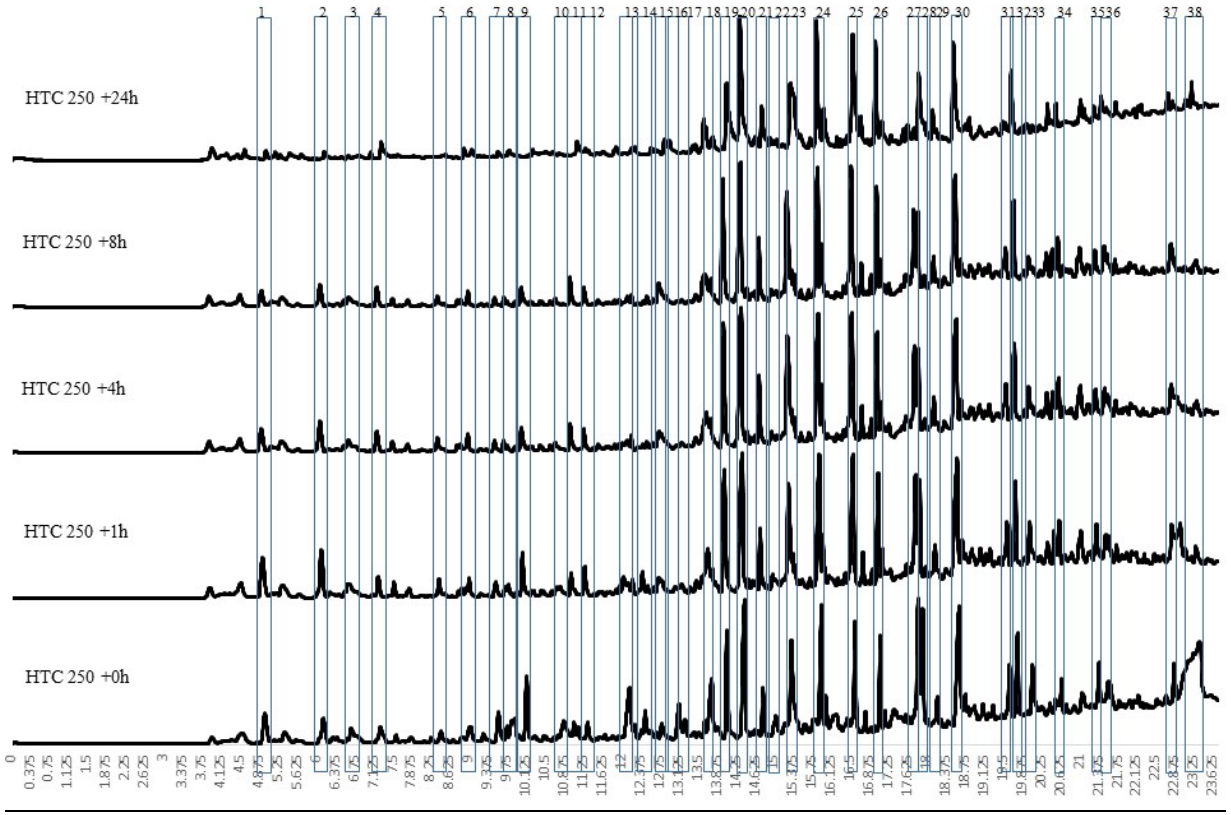

Figure 6.5: Pyrolysis GCMS spectra of volatile organics evolved at 550 °C from bio-coals treated at 250 °C with varying retention times. ((1) 2-methyl furan; (2) 2,5 dimethyl furan; (3) propanediol; (4) toluene; (5) 3-methyl phenol; (6) pentanoic acid; (7) cyclopentanone; (8) butanediol; (9) dimethylpyrazole; (10) 2-furanmethanol; (11) ethylhexaldehyde; (12) 1,3dimethylcyclopenten-3-one; (13) cyclopentadione; (14) 2-furan carboxadehyde; (15) 1methyl-1-cyclopenten-3-one; (16) furanone; (17) amino-3-pyridinol; (18) 3-methyl cyclopentanedione; (19) phenol; (20) 2-methoxyphenol; (21) 2-methyl phenol; (22) 2-cyclopenten-1-one: (23) 4-methyl phenol; (24) creasol; (25) 4-ethyl phenol; (26) 4-ethyl-2methoxy phenol; (27) dihydrobenzofuran; (28) 4-hydro-3-methyl acetophenone; (29) eugenol; (30) 2,6, dimethoxyphenol; (31) isoeugenol; (32) triethoxybenzene; (33) vanillin; (34) trimethoxytoluene; (35) dimethoxy acetophenone; (36) trimethylacealdehyde; (37) methoxy eugenol; (38) levoglucasan)

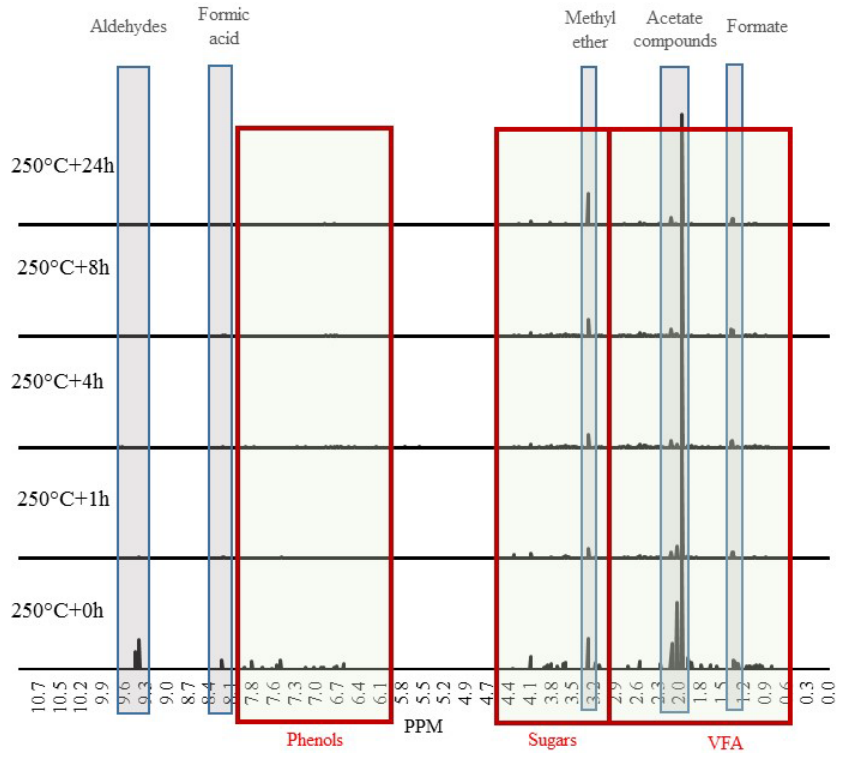

Figure 6.6a: H-NMR spectra of HTC process waters from 250 °C treatment at different retention times

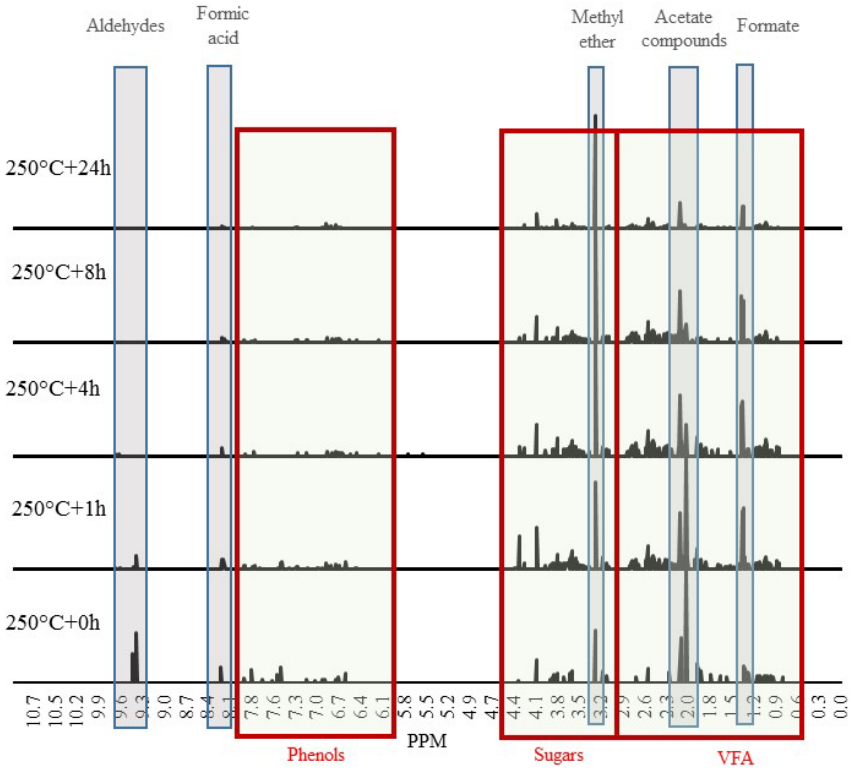

Figure 6.6b: H-NMR spectra of HTC process waters from 250 °C treatment at different retention times without acetate peak

For the 250 °C treatments methyl ether is the predominant proton after acetate in NMR analysis of process water, although based on this data it is unclear if it is in the form

of functional groups on larger compounds or as a metal methoxide. Valeric acid, which is present from HTC 250+1h onward in Figure 6.3 is a product of the hydrogenation of the levulinic acid, by either hydrogen or formic acid [271]. As retention time increases acetic and acetate become the increasingly dominant organic compounds in the process water based on GCMS and NMR data. With increasing retention time the levulinic acid peak appears to become less pronounced, with valeric acid becoming the most dominant VFA after acetic acid. With a progressive decline in carbon concentration within the process water with increasing retention time, this result could suggest that some of the levulinic acid is undergoing hydrogenation to valeric acid [271], while some is levulinic acid is undergoing oxidation to acetic acid [352], with the oxygen liberated from the biomass. Gas analysis was undertaken of the head gas for all runs but poor separation in early runs meant quantification of the data set was not possible (due to carbon dioxide poisoning of the Hayesep column giving poor peak resolution). The results did however show the appearance and distinct increase in gaseous oxygen and hydrogen in the head gas, with increasing retention time. This goes against the common assumption that the head gas is carbon dioxide but similar results have been stated in Lu et al. [128]. VFA such as formic acids are known to decompose to hydrogen under hydrothermal conditions [353] and possibly play a role in the hydrogenation of other VFA.

Figure 6.7 shows the pyrolysis/ devolatilisation behaviour of the 250 °C treated bio-coals generated under varying retention times and Figure 6.8a-c multistage py-GCMS desorption's at 250 °C, 400 °C and 600 °C respectively. Figure 6.7 show that at pyrolysis temperatures below 250 °C the bio-coals with extended retention time, (i.e. from HTC 250+1h) appear to have an early devolatalisation peak. Based on the Py-GCMS data this appears to be different in composition to the unprocessed *Miscanthus*, which at this temperature largely devolatilises methoxy-butadiene (peak 11) and benzylamine (peak 19), while the bio-coals appear to devolatilise methyl-cyclopenten-1-one (peak 6), dimethoxy-butedimine (peak 11), benzofuran (peak 12) and a series of phenols and methyl-phenols (peaks 13 to 18). These compounds are often associated with the thermal decomposition of lignin; however, such compounds are not seen to devolatilise in the unprocessed *Miscanthus* until between 400 and 600°C. This would suggest that these devolatilised phenols are either phenolic fragments of hydrolysed lignin liberated by the hydrothermal process or the humin products from aldol addition or condensation of 5-HMF and furfural like compounds [309].

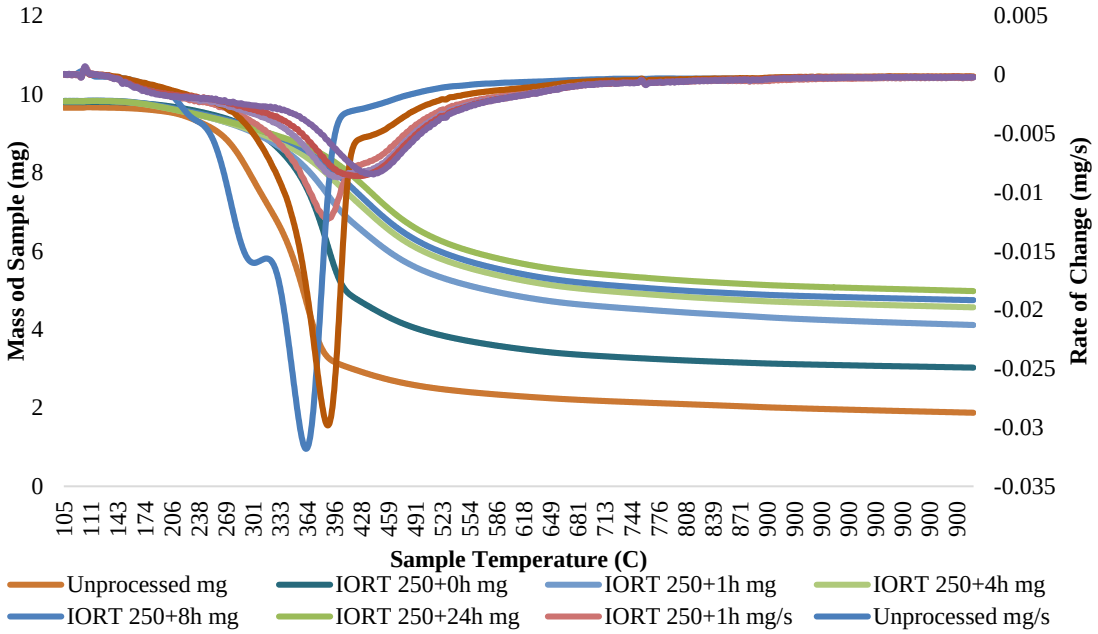

Figure 6.7: Weight loss and first derivative for the devolatilisation of bio-coals carbonised at 250 with varying retention times

At pyrolysis temperatures around 250 °C, the unprocessed *Miscanthus* and HTC 250+0h bio-coal start strongly devolatilizing. Figure 6.8b shows the compounds devolatilised between 250 °C and 400 °C. While there are some common compounds visible in all samples, for example phenol (peak 16), 2-methoxy phenol (peak 17), 2,3-dihydro benzofuran (peak 21), 4 hydroxy-3-acetophenone (peak 22) and 2,6 dimethyl phenol (peak 24); generally the unprocessed *Miscanthus* has a different volatile chemistry to the bio-coal. HTC 250+0h displays some peaks common with the unprocessed *Miscanthus* (acetic acid (peak a), isobutylacetic acid (peak d), 2-methoxybutenol (peak e), pyrolidethylamine (peak f), propanediol (peak g), furfural (peak h), furanmethanol (peak i), cyclopentanone (peak 11) and levolglucasan (peak o)), as well as the phenolic and furfural peaks associated with 250 °C bio-coals with longer retention times. This will indicate that at this sample, while partially carbonised, is less maturated than the 250 °C bio-coals with longer retention times. For HTC 250+1h some cyclopentanone (peak 11), is still present, which is not present in the bio-coals with longer retention times. Likewise the methyl furan and dimethyl furans present in HTC 250+0h and HTC 250+1h (the likely a product of humin formation via aldol addition or condensation of 5-HMF and furfural like compounds [309]), appear to reduce indicating these furans get further aromatized to the methyl and ethyl phenols (peaks 5, 21, 23, 25, 26 and 30) with longer retention times.

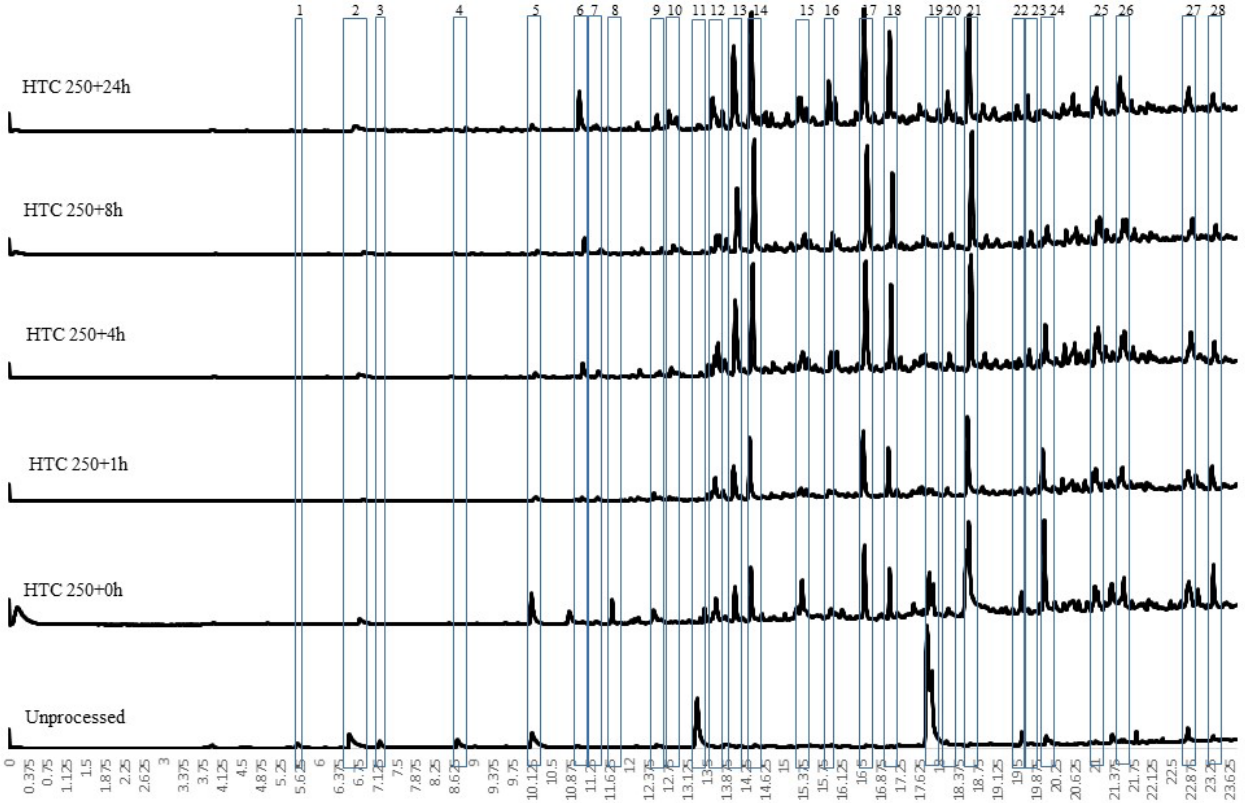

Figure 6.8a: Volatile organics evolved below 250 °C from bio-coals treated at 250 °C with varying retention times. ((1) pentenol; (2) acetic acid; (3) dihydro-dioxin; (4) propanoic acid methyl esther; (5) furfural; (6) 2-methyl-2-cyclopenten-1-one; (7) ethanone; (8) cymene; (9) furancarboxyldehyde; (10) 5 methyl-2-furancaboxaldehyde; (11) dimethoxybutedimine; (12) benzofuran; (13) phenol; (14) 2-methyl phenol; (15) 4-methyl phenol; (16) cresol; (17) 4-ethyl phenol; (18) 4-ethyl-2-methoxy phenol; (19) 2-methoxy-N-N-dymethyl benzoamine; (20) 2-methoxy-4-propyl phenol; (21) 2,6 dimethyl phenol; (22) eugenol; (23) trimethoxybenzene; (24) vanillin; (25) 2-furyl-5-methyl furan; (26) aethallymal; (27) 4-hydroxy-3,5-dimethyoxy benzaldehyde; (28) methoxyeugenol)

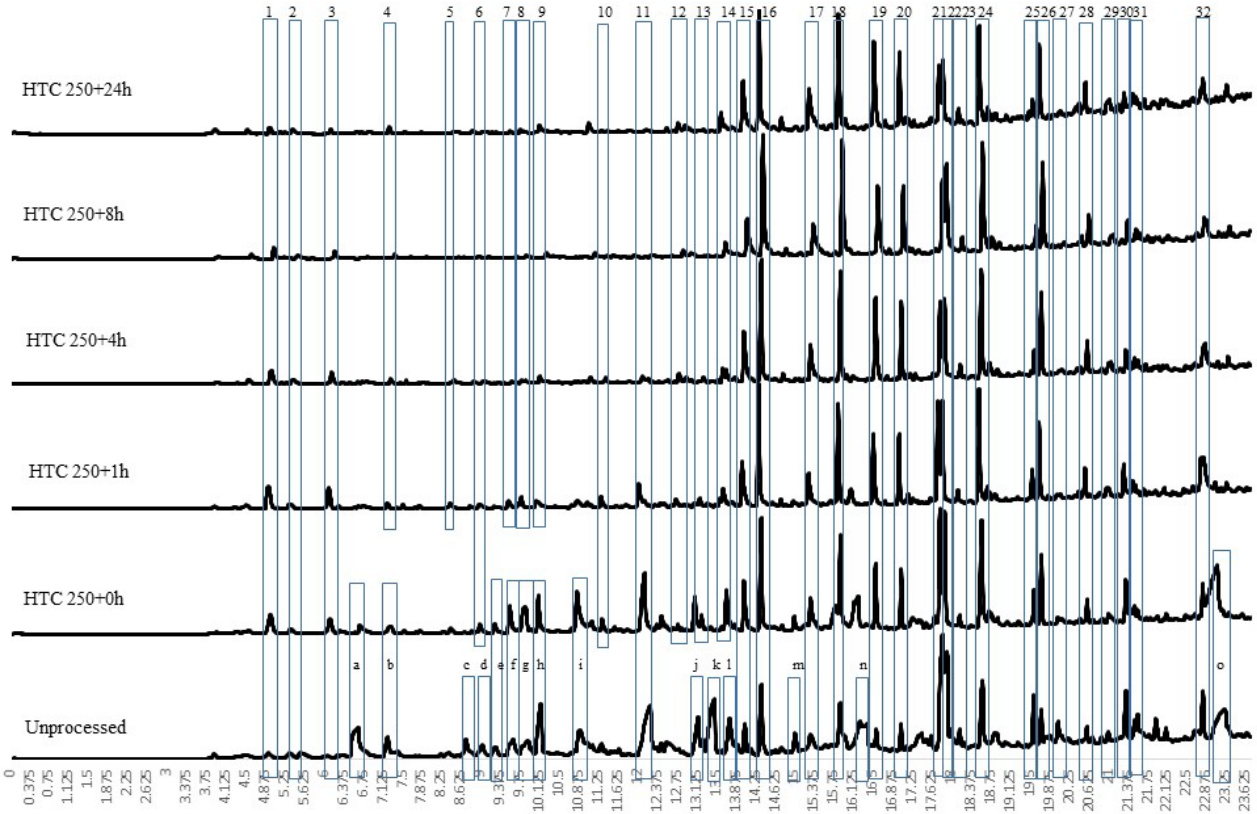

Figure 6.8b: Volatile organics evolved between 250 °C and 400 °C from bio-coals treated at 250 °C with varying retention times. ((1) 2, methyl furan; (2) 2-propenoic acid 2-hydroxy ethyl esther; (3) 2,5 dimethyl furan; (4) toluene; (5) 4 methyl phenol; (6) methyl-3-octyne; (7) dimethoxy butane; (8) cyclohexanol; (9) cyclopenten-1-one; (10) acetylfuran; (11) cyclopentanone; (12) methylcyclopenten-3-one; (13) benzenediol; (14) 3-methyl cyclopentanone; (15) phenol; (16) 2-methyl phenol; (17) 4-methyl phenol; (18) cresol; (19) 4-ethyl phenol; (20) 4-ethyl-2-methoxy phenol; (21) 2,3-dihydro benzofuran; (22) 4 hydroxy-3-acetophenone; (23) eugenol; (24) 2,6 dimethyl phenol; (25) eugenol; (26) 2 dihydro-2-methyl benofuran; (27) isoeugenol; (28) trimethoxybenzene; (29) trymethoxy-5-methyl benzene; (30) acetophenone; (31) dimethoxy phenone; (32) methoxyeugenol; a) acetic acid; (b) dihydrodioxin; (c) bioxirane; (d) isobutylacetic acid; (e) 2-methoxybutenol; (f) pyrolidethylamine; (g) propanediol; (h) furfural; (i) furanmethanol; (j) furanone; (k) dimethoxybutanamine; (l) cyclopent-1-one; (m) ethyl-2-hydroxy cyclopenten-1-one; (n) dimethyl heptane; (o) levoglucasan)

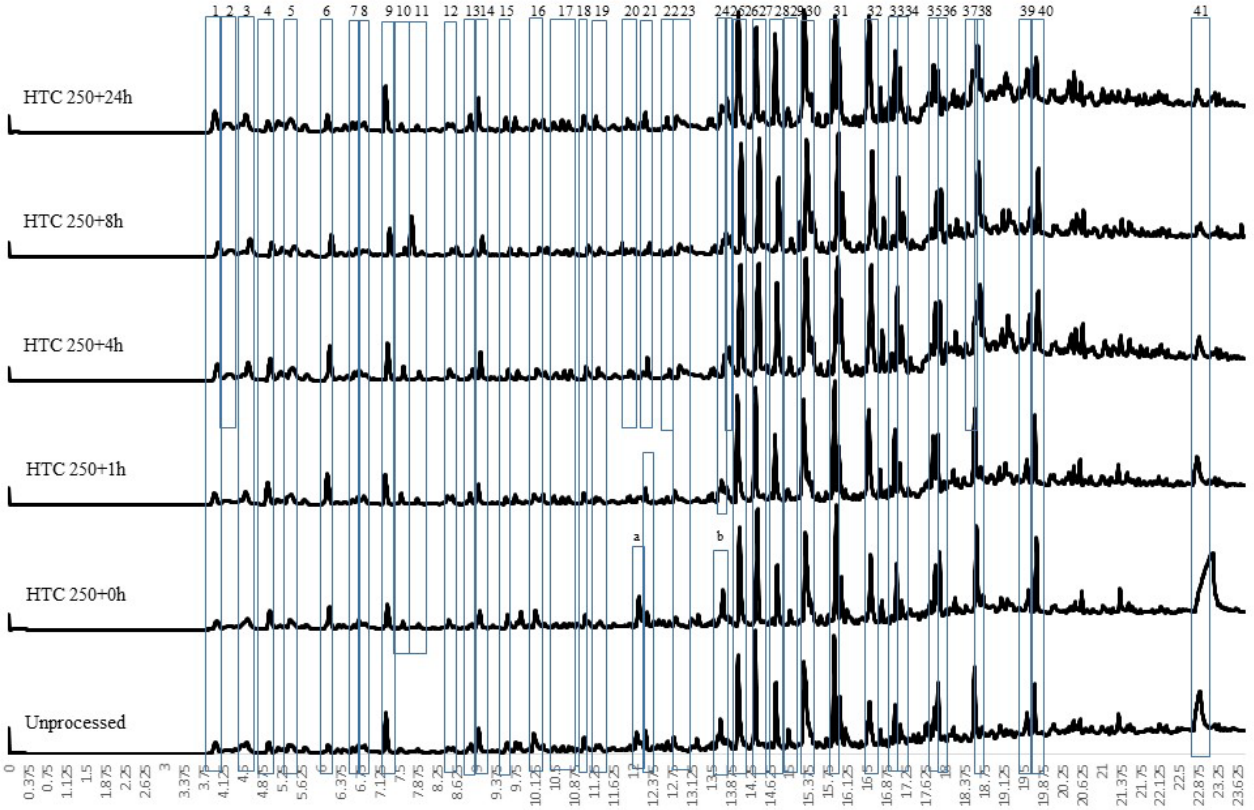

Figure 6.8c: Volatile organics evolved between 400 °C and 600 °C from bio-coals treated at 250 °C with varying retention times. ((1) Ethylcyclobutane; (2) Pentane; (3) Amino methyl propanol; (4) 2, methyl furan; (5) 2 ethyl butanal; (6) 2,5 dimethyl furan; (7) Valeric acid; (8) Octene; (9) Toluene; (10) Ethanone; (11) Trimethylimidazole; (12) Undecyonic acid methyl esther; (13) Ethylbenzene; (14) Xylene; (15) P-xylene; (16) 2-Cyclopenten-1-one; (17) Methyltoluene *spp.*; (18) Methyl cyclopentanone; (19) Triethylbenzene; (20) Fumeric acid ethyl esther; (21) Methoxy methyl benzene; (22) Indene; (23) 3-Methylcyclopenten-1-one; (24) 1-ethyl-4-methoxy benzene; (25) Acetonitrile benzene; (26) phenol; (27) 2-methyoxy phenol; (28) 2-methyl phenol; (29) Dimethyl phenol; (30) Cresol; (31) Creasol; (32) 2-ethyl phenol; (33) Ethylguaiacol; (34) 5-ethyl cresol; (35) 2,3 Dihydrobenzofuran; (36) 4-hydoxy-2-methylacetophenone; (37) Dioxybezene; (38) Dimethoxy phenol; (39) Eugenol; (40) Trimethoxybenzene; (41) Levolgucasan; (a) Cyclopentenone; (b) Hydroxy-3-methyl cyclopenten-1-one)

The presence of large levoglucasan peaks in the 400 °C and 600 °C Py-GCMS data (Figure 6.8b and Figure 6.8c) indicate the presence of cellulose within the unprocessed *Miscanthus* and HTC 250+0h. This would indicate that the bigger devolatilisation peaks, for the unprocessed *Miscanthus* and HTC 250+0h, which peak at 360 °C and 400 °C respectively on the DTG in Figure 6.7, will largely be cellulose. While the volatile chemistry of the two materials are not directly comparable, it is possible that the peak shift toward higher devolatilisation temperatures is, in part, due to reductions in alkali metal content within the fuel [160, 207-209, 212]. While fuel inorganics are discussed in detail in Section 6.4.2 and Section 6.4.3, data presented in Table 6.3 suggests alkali metals reduce after HTC and further reduce with increasing retention times. The 400 °C and 600 °C Py-GCMS data (Figure 6.8b and Figure 6.8c), indicate beyond HTC 250+4h the volatile chemistry of the 4, 8 and 24 hour 250°C bio-coals are all similar. Data presented in Figure 6.7, indicate devolatilisation temperature continues to increase with increasing retention time and this is in part brought about though reduced catalysis due to the reduction in alkali metals. It should be noted that the py-GCMS will not detect gaseous compounds in trap mode so carbon monoxide, carbon dioxide and other gaseous products devolatilised will not be detected but will account for at least part of the weight loss observed in Figure 6.7.

The devolatilisation of compounds released between 400 °C and 600 °C is given in Figure 6.8c. At this temperature the fragments from the lignin fraction within the unprocessed *Miscanthus* appears to devolatilise and the six profiles look distinctly similar, with largely phenolic compounds evolved. Slight differences arise with a large levoglucasan peak (peak 41) particularly prevent for HTC 250+0h, and the cyclopentenone (peak a) and hydroxy-3-methyl cyclopenten-1-one (peak b) present which are present in the untreated *Miscanthus* and HTC 250+0h. For the longer retention time samples there are increasing numbers of small peaks after 20 minutes on the GCMS spectra; with the mass spectrometer indicating increasing concentrations benzo-alcohols and phenolic acids with differing functional groups, brought about through increasing retention time.

6.4.2. Influence of retention time on the bio-coal inorganic chemistry

The results of a metal, phosphorus, chlorine and sulphur analysis are given in Table 6.3. The result for the 200 °C treatments suggest that there is an initial decrease in inorganics within the biomass with the ash content given in Table 6.1, dropping from 3.1 wt% (db) for the unprocessed *Miscanthus* to 2.4 wt% (db) for HTC 200+0h. While the

ash content, does not then significantly alter between treatments, varying between 2.1 and 2.5 wt% (db), the inorganic composition of the biomass and ash changes considerably, as shown in Table 6.3. The main change is the increase in concentration of silicon while the potassium continues to decrease with increasing retention time. Sodium appears to increase but is only present in the feedstock in low concentrations so extrapolating this to feedstocks with higher sodium concentrations should be done with caution.

Phosphorus appears to initially be extracted into the process water in HTC 200+0h but then steadily increases with increasing retention time. This suggests that it is incorporation of phosphorus into the bio-coal with increasing retention time. A similar trend is observed for the heteroatom sulphur, while the inverse is observed for the heteroatom chlorine, which is further reduced with increasing retention time. Chlorine exists within biomass in the form of water soluble ionic salts (NaCl, KCl, $CaCl_2$, $MgCl_2$ and ionic chloride (Cl^-)) [37, 38] with the ionic salts often making up a large proportion of the total inorganics within the starting biomass. The reduction in chlorine is however in steady decline with increasing retention time while the sodium, potassium, and magnesium, are predominantly removed in the initial heating for the biomass. Potassium undergoes continued decline over time, with the majority removed by the 200°C treatment with no retention time.

Calcium only undergoes limited removal and increases its relative concentration within the biomass. It is possible that the chloride is retaining an association with the calcium retained within the bio-coal. It is also likely that the sodium, potassium, and magnesium, are forming acetate and formate salts (as Figure 6.4a and Figure 6.6a suggest) and the residual chlorine is being retained through formation of week chlorine-hydrogen interactions with the hydrogens on the char [149]. This result does however support the findings in Section 5.3.3.3, which highlighted that the reductions in chlorine during HTC are less than the reduction seen in comparable washing experiments, which have shown between 85 % and 100 % removal [43, 205, 264]. The suggestion there may be other underlying roles retention mechanisms for chlorine during HTC appears correct and given the importance of chlorine in terms of combustion chemistry (see Section 2.5.2.3), further work is required on this. The assumption made in Chapter 4, published in Smith et al. [213] and assumed by subsequent authors, that, during HTC most chlorine within the biomass is extracted as demonstrated in washing experiments, is not strictly correct.

Table 6.3: Inorganic and heteroatom analysis of bio-coals derived from differing retention times and their influence of slagging and fouling indices

Temperature	Retention	mg/kg (Dry Basis)											AI	BAI	R b/a
		Na	Mg	Al	Si	P	S	Cl	K	Ca	Mn	Fe			
Unprocessed		520	920	30	6890	700	1130	3590	3030	3530	110	40	0.27	0.01	0.78
HTC 200	0h	100	540	80	6550	290	690	2710	1120	4060	50	90	0.08	0.08	0.58
	1h	150	400	70	6150	350	750	1760	1130	2800	50	120	0.08	0.09	0.49
	4h	120	480	110	6620	610	970	1650	900	4030	70	110	0.06	0.12	0.55
	8h	140	470	60	6960	670	880	1370	840	3780	80	50	0.06	0.05	0.50
	24h	190	470	100	7610	690	1170	1530	740	3630	60	100	0.06	0.10	0.44
HTC 250	0h	140	440	120	6320	710	1290	3500	920	3100	70	110	0.06	0.11	0.48
	1h	90	530	190	7840	1150	1130	1720	1040	5280	80	140	0.05	0.14	0.57
	4h	120	460	120	6770	1100	1230	2010	890	3570	80	120	0.05	0.12	0.49
	8h	110	350	110	6000	1290	1020	1510	650	2180	90	90	0.04	0.12	0.37
	24h	130	370	140	8080	1090	1070	1760	850	1450	70	130	0.04	0.14	0.24

The data in Table 6.3 shows that with increasing retention time the ash becomes predominantly calcium – silicon based, which should improve ash stability. Likewise, the reincorporation of phosphorus in the char should further increase ash stability. The increased silicon content along with decreased potassium chloride content within the bio-coal should also further reduce the fuels fouling propensity, as silicon oxide can also react with potassium chloride at high enough temperature forming potassium silicates (see Equation 2.5), abating the formation of gaseous potassium chloride [243-245]. This will be further aided by the phosphorus and calcium (see Equation 2.13, Equation 2.14 and Equation 2.15) [202, 242, 254]. Consequently the changes in inorganic and heteroatom chemistry with increasing retention time should reduce the fouling and the corrosion propensity of the fuel, increasing efficiency and reducing maintenance [201, 234].

Figure 6.9 shows the ash transition temperatures of the 200°C bio-coals with increasing retention time. The results show as retention times increase the deformation temperature increases, up to HTC 200+8h. For HTC 200+24h the ash deformation temperature (and hemisphere and flow temperature) decreases when compared to HTC 200+8h. The reduction in deformation temperature for HTC 200+24h appears to be due to an increase in silicon concentration within the fuel while the concentration of calcium reduces, altering the silicon to calcium ratio and the stasis brought about in the earlier samples. The removal of the calcium at longer retention times could be due to the presence of formic and acetic acids created with increasing retention time and discussed in Section 6.4.1 acid leaching the calcium. This result suggests that with increasing retention time at 200°C, there is an improvement in fuel slagging propensity, up to a point, after which organic acids generated within the process lead to increased removal of calcium and stasis brought about by the calcium. It is also possible that after 8 hours the continued dehydration of the bio-coal (see Figure 6.1) is reducing the oxygen functional groups on which calcium can bind, reducing the retention of calcium within the fuel. It is unclear at this point; whether it is these organic acids generated which are catalysing the dehydration of the fuel.

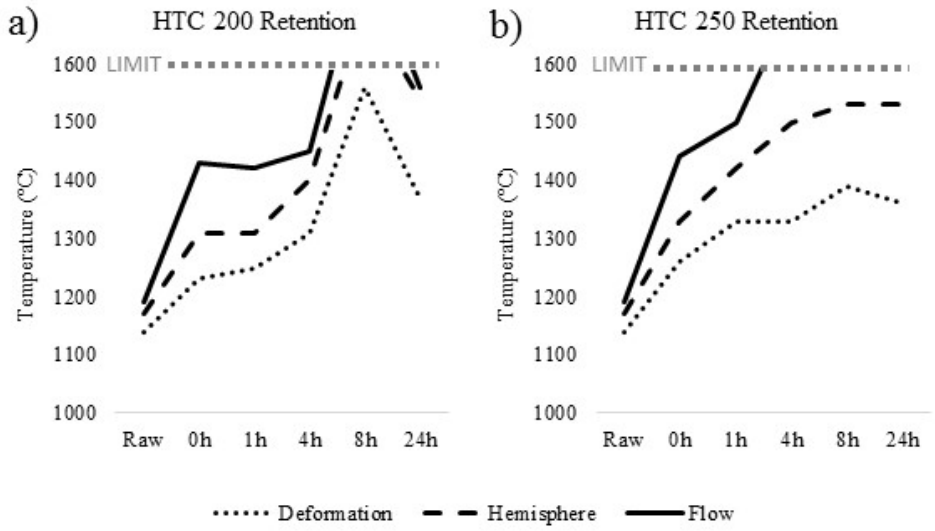

Figure 6.9: Ash transition temperatures for a) HTC at 200°C with varying retention times, b) HTC at 250°C with varying retention times

The result for the 250 °C treatments yield similar results to the 200 °C treatments, with the inorganic chemistry similar for HTC 200+0h and HTC 250+0h. Silicon is generally seen to increase with increasing retention time but whereas calcium content remained reasonably consistent in the 200 °C treatments, calcium content decreases with increasing retention time in the 250 °C treatments. Organic acid content within the process water increases with time so it appears likely that the increased calcium leaching with time is, in part, due to extraction by the organic acids created as part of the process. This said the pH appears to be buffered against the increasing organic acids with pH reaming reasonably consistent at pH 3.3 (see Table 6.2). Phosphorus appears to steadily increase with increasing retention time, although there is not the initial decrease seen in the 200 °C treatments, which would imply that phosphorus released on heating is reincorporated quickly into the bio-coal. Sulphur remains reasonably consistent in the 250 °C treatments, with a slight decrease with increasing retention time. The sulphur content is however higher in the 250 °C treatments than HTC 200+24h, which implies sulphur released on heating appears to have been also reincorporated by the time 250 °C has been reached. Like the 200 °C treatments, the chlorine content steady declines with increasing retention time, with the chlorine content slightly higher than the 200 °C treatments. Critically the fuels higher energy content will offset the higher chlorine content.

Figure 6.9 shows the ash transition temperatures for the 250 °C bio-coals and like the 200 °C bio-coals the ash fusion temperature increases with increasing retention time. A deformation temperature of 1330 °C was achieved within the one hour treatment, a

temperature reached between four and eight hours at 200 °C. The result should suggest that the severity factor given in Equation 6.1, ideally developed by Overend and Chornet [104] to characterize hydrolytic depolymerisation of wood may also apply to the fuels slagging propensity. While the 250 °C treatment produces a moderate improvement in deformation temperature, and thus the safe combustion temperature, it should be noted that there is a more substantial change in the hemisphere and flow temperature. This is evident with HTC 250+4h and longer not melting before reaching the furnace limit at 1570 °C. This would be beneficial for combustion as it would mean that if the ash is exposed to heat exceeding the deformation temperature, ash melting would still be unlikely, further reducing fuel slagging potential.

Table 3.3 gives slagging and fouling indices, which are based on the total alkali content of the fuel and as such are suited to biomass materials [205]. The results are given in Table 6.3 and show that the alkali index (AI) indicates that with the starting biomass is highly probable the fuel will slag and foul. The AI indicates all the hydrothermally treated fuels should be safe to combust in terms of slagging and fouling, with the results indicating for both the 200 ºC and 250 ºC treatments become progressively safer with increasing retention time. The acid base ratio (R b/a) indicates a similar trend. The bed agglomeration index (BAI) indicates a progressive improvement in the fuels agglomeration behaviour with increasing retention time but due to the low iron content within the initial biomass and within the bio-coals makes bed agglomeration appear likely. Iron does however appear to accumulate within the bio-coal so this could potentially be overcome with the blending and addition of a higher iron feedstock in the HTC process, which would increase the overall iron content within the fuel.

In the HTC method used there was no additional washing of the bio-coals, with the bio-coal filtered from the process water and allowed to dry prior to analysis. Analysis of the process waters given in Table 6.2, would suggest the potential for residual metal and chlorine containing process water to be left with the char. Additional leaching of these alkali metals and chlorine maybe possible with the incorporation of an additional washing procedure post carbonisation. This should further enhance removal of alkali metals and chlorine and further reducing fouling propensity, if required. The impact of an additional water treatment on the energy content and energy yields has not been assessed in this instance, nor have water treatment options such as anaerobic digestion been considered.

6.4.3. Influence of retention time on the bio-coal combustion behaviour

The concept of 'design' fuels and use of TGA and DTG analysis when comparing and evaluating fuels for blending to best match a boilers 'design' fuel has been introduced in Section 2.4.4 and fuel specific examples are given in section 5.3.3.2. Details on interpreting the data is given in Section 3.8. Figure 6.10 show the DTG curve for the 200 °C hydrothermally treated fuels, while Figure 6.10a shows the burning profile of the unprocessed *Miscanthus* and a reference coal for comparison. The first main change is the change in the onset of the first initiation temperature, which is delayed from 190 °C to 270 °C, due the removal of hemicellulose in all the treatments [185]. The removal of the alkali metals, discussed in Section 6.4.1 and known to catalyse the decomposition of biomass [208] also appear to delay in the volatile burn peak temperature and the fixed carbon peak temperature for HTC 200+0h.

As retention time increases the volatile burn peak temperature appears to advance, despite no notable increase in alkali metals within the fuel and likewise a reduction in calcium, which is also known to have significant catalytic influence on devolatilisation [211]. Consequently, it appears the increase in reactivity could be due to changes in the nature of the volatile material as opposed to shift in catalytic behaviour. Figure 6.2 shows that with increasing retention time there is a change in the composition of the volatile organics evolved and likewise Figure 6.8a has shown that hydrothermal treatment results in the formation and volatilization of 2-methyl phenol, 4-methyl phenol, 4-ethyl phenol, 2,6 dimethyl phenol and vanillin amongst others at a pyrolysis below 250 °C.

It should be noted that in the case of the 200 °C bio-coals and unprocessed *Miscanthus,* peak temperature is on the volatile burn as opposed to char combustion, seen in the coals and 250 °C bio-coals (excluding HTC 250+0h). With increasing retention time the second peak, which represents the onset and combustion of the char increases. This is fitting with the proximate analysis given in Table 6.1, which shows a decrease in volatile matter and an increase in fixed carbon with retention time. This trend continues with the 250 °C bio-coals shown in Figure 6.10c. In Figure 6.10c, the burning profile changes quickly from two distinct volatile and char burn peaks, as seen for HTC 250+0h, to a 'coal like' single stage combustion profile. With increasing retention time the volatile peak becomes increasingly less distinct and by HTC 250+24h the second initiation temperature being marked more by the acceleration in weight loss as opposed to a second peak.

For all the hydrothermally derived fuels the first initiation temperature appear similar around 270 °C, with the second initiation temperature appearing to increase slightly from 380 °C for HTC 250+0h to 390 °C for HTC 250+1h to HTC 250+24h. The inverse is observed for the 200°C bio-coals.

Peak temperature (char burn) also appears to increase from 390 °C for HTC 250+0h to 460 °C for HTC 250+4h to HTC 250+24h. Burnout temperature initially advances from 530 °C observed in the 200 °C bio-coals to 580 °C, which is consistent for HTC 250+1h to HTC 250+24h. The reference coal burns at a higher temperature than observed for the bio-coal, albeit with a similar burning curve to that of the longer retention time 250 °C bio-coal. The first initiation temperature being around 325°C, with the second initiation temperature around 460 °C, a peak temperature around 550°C and a burnout temperature at 650°C. The lower fuel characteristic temperatures of the 250 °C bio-coals can nevertheless be beneficial as this will promote early ignition of the total fuel mass, especially when co-fired; leading to better and more complete combustion. This early ignition in turn can also be beneficial for nitrogen oxide emissions as it will consume additional oxygen, increasing the fuel staging effects of low-NOx burners and lowering NOx emissions [68].

It should be noted that while increasing severity factor for HTC appears to offer greater flame stability, through a more coal like burning profile, particle size is as equally important parameter. In Chapter 5 (now published in Smith et al., [260]), an HGI of 25 was demonstrated for HTC 200+1h *Miscanthus*, while an HGI 150 was demonstrated for HTC 250+1h *Miscanthus*. This result would suggest that the 200 °C samples should pulverise if burnt in a PF plant. Likewise it appears likely HGI will increase with reaction severity, due to decomposition, removal and repolymerisation of the fibrous cellulose that provides strength to the biomass (as shown in Figure 2.1). An HGI of 25 would suggest the fuel would pulverise similar to that of a high resistance coal. The HGI of 150 would imply that the fuel will easily pulverise and there should be limited issues with flame stability. The lower the first initiation temperature of the bio-coals would, to a certain extent, allow for larger particle diameter, as heat loss due to the greater heat sink brought about though the larger particle, would be balanced by the earlier heat release when using an appropriate system [260].

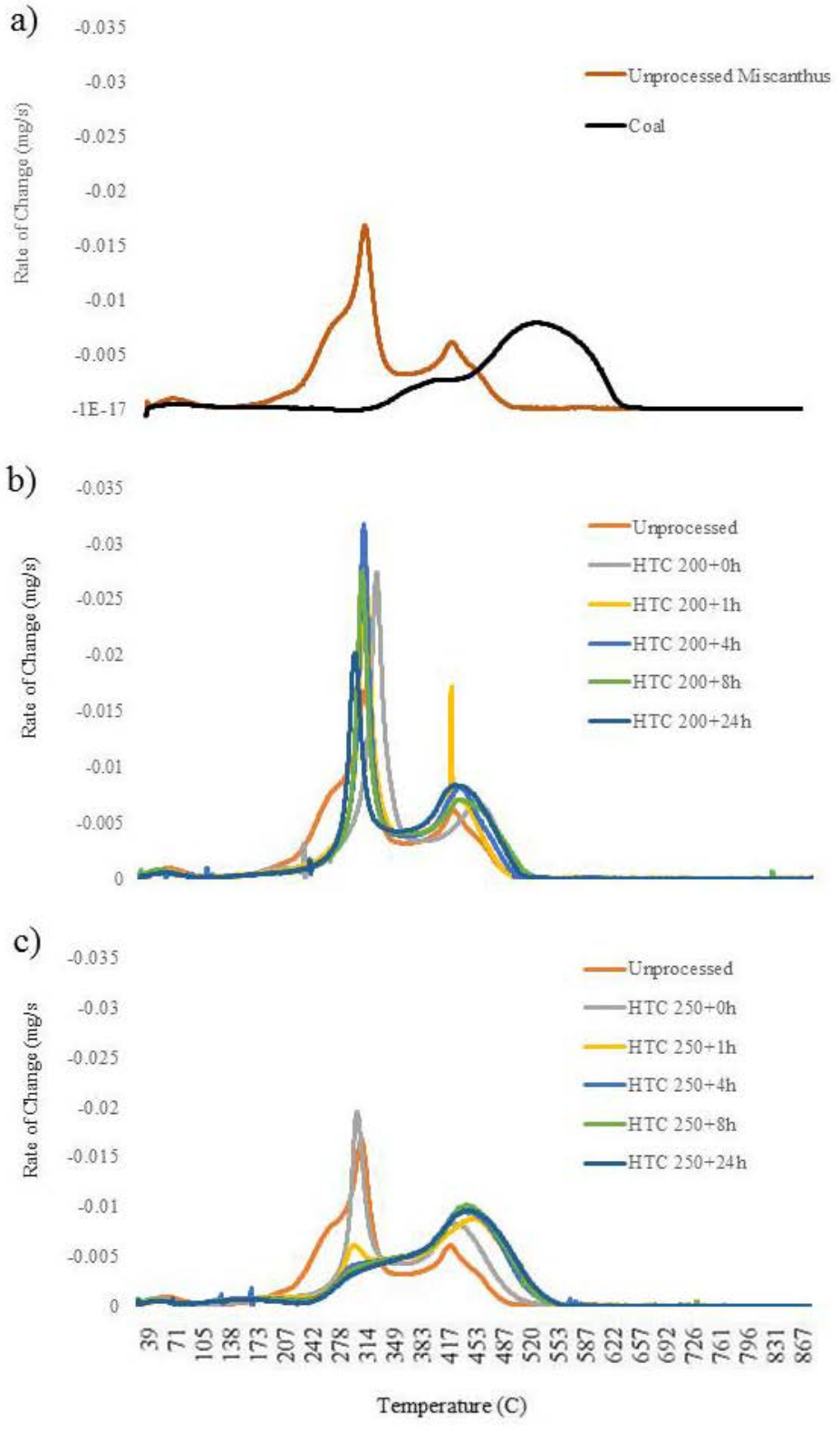

Figure 6.10: Derivative thermogravimetric (DTG) burning profiles for: a) unprocessed *Miscanthus* and bituminous reference coal (Elemental Microanalysis B2306, batch 203830); b) *Miscanthus* hydrothermally treated at 200°C with varying retention time and c) *Miscanthus* hydrothermally treated at 250°C with varying retention time

6.5. Conclusions

Miscanthus was hydrothermally carbonised at 200 ^{0}C and 250 ^{0}C, with varying retention times, from zero hours to 24 hours to better understand the influence of retention time on the bio-coal inorganic and combustion chemistry. Increasing retention severity brings about increased dehydration of the fuel, with temperature appearing the more important variable, with the HTC 200+24h having similar properties to that of the HTC 250+0h bio-coal. At 250 ^{0}C, 5-HMF, a commonly reported product of HTC, is quickly consumed, either being converted into char or decomposing to levulinic acid, which undergoes further conversion to valeric acid within the first hour. After one hour the 250 ^{0}C bio-coal continues to dehydrate, with evidence of repolymerisation of hydrothermally derived aromatics, with initially furanic then increasing aromatics observed with increasing retention time. By one hour most of the cellulose appears to have decomposed at 250 ^{0}C, albeit levolglucosan is observed in small quantities at 24 hours during analytical pyrolysis.

The dehydration, repolymerisation and cellulose removal at 250 ^{0}C brings about a more ‘coal like’ combustion profile, with decreasing reactivity with increasing retention time. This should aid combustion in existing pulverised coal power plants. Alkali metals are extracted at low retention times, but appear to further decrease with increasing retention times. Phosphorus and sulphur appear to undergo substantial extraction at HTC 200+0h but appear reincorporated with increasing retention time. Fuel chlorine is reduced with increasing retention time. Silicon content increases within the bio-coal with increasing severity, while calcium appears to reduce within the 250 ^{0}C bio-coals after one hour, thought to be due to organic acid leaching. Increasing reaction severity brings about a decrease in fuel fouling and slagging propensity, as demonstrated by the ash fusion test and various slagging and fouling indices.

7. The influence and implications of recycling hydrothermal process waters on bio-coal combustion chemistry

7.1. Abstract

It is understood that recycling HTC process waters can catalyse the HTC reaction and can improve the yields at little or no cost. These process waters do however contain alkali metals, chlorides, sulphates and nitrogen based compounds initially extracted by the HTC process. These inorganics and heteroatoms can bring about issues in combustion but could also offer advantages in terms of catalysis during the reaction. In this chapter, *M*iscanthus has been hydrothermally carbonised at two temperatures 200 ^{0}C and 250 ^{0}C with the process waters recycled nine times and a retention time of one hour for each treatment. Recycling process waters brings about an increase in product mass yield at both treatment temperatures; for 200 °C treatments yields increase from 65% and stabilise at between 71 % and 73 % after four cycles. The 250 °C treatments increased product mass yield from 46 % to 57 %, and by the final run it appeared not to have reached a stable value. A modest increase in energy density was seen for the for the 200 °C treatments from 18.9 MJ/kg to 19.7 MJ/kg, and thus the overall energy yield increases from 68% to 77 % after four cycles. For the 250 °C treatments energy density increased from 24.2 MJ/kg to 28.9 MJ/kg on the ninth cycle. This increases the overall energy yield from 61% to 91 %.

It is hypothesised that the recycled organic acids hydrolyse the hemicellulose and cellulose to furfural like compounds at a lower temperature and increase saccharide concentrations within the process water. This will favour aromatization and repolymerisation which better enables the decomposition products to undergo polymerization, which otherwise undergo further degradation to organic acids. It is proposed that the slow heating rate and hour long retention time overcome kinetic limitations imposed by faster heating rates and shorter retention times. After an initial improvement in fouling and slagging propensity brought about, through enhanced acid leaching of the fuel, recycling process water appears to have an adverse influence on the fouling and slagging propensity of the fuel. Mechanical water recovery and the incorporation of an additional washing procedure post carbonisation may however overcome this. The impact of an additional water treatment on the energy content, energy yields and inorganic chemistry has not been assessed.

7.2.Introduction

HTC is a biomass pre-treatment which uses hot compressed water to produce a high quality coal like solid fuel, often without the combustion limitations imposed by the starting feedstocks inorganic and heteroatom chemistry [76, 213]. In addition to the coal like product, HTC also produces an aqueous co-product, which contains about 10 to 15 % of the original organic matter in the form of sugars and organic acids from the HTC of herbaceous and woody biomass [268]. In order to maximise resource efficiency and avoid generation of wastewaters, which would require treatment, there has been growing interest in the potential utilisation for the process waters. Potential options include: the extraction and purification of organic acids and certain sugars; the anaerobic digestion of the process waters; and recycling the process waters back into the HTC process [113-115, 272]. The latter is of particular interest as it is understood that weekly acidic conditions improve the overall rate of reaction in HTC [26, 44, 118, 119, 121] and common organic acids generated, which include: acetic, formic, lactic and luvulinic acids have been identified as common reaction intermediates [11, 29], which, if added, act as reagents resulting in greater char yield [26, 44].

Recycling of these acids back into the HTC process has been shown to catalyse the reaction and can improve the yields at little or no cost [113-115] and may even be one of the most efficient means of heat recovery [116]. These process waters however also contain alkaline metals, chlorides, sulphates and nitrogen based compounds initially extracted by the HTC process [76, 173, 213]. While accumulation of these inorganic and heteroatoms within the recycled process waters may bring about a catalytic effect, for example chloride is associated with increased HHV [48], inorganic and heteroatoms within the solid fuel can also bring about significant issues in terms of slagging, fouling, corrosion and airborne emissions during combustion [39]. The effect and potential implications of recycling process waters on the fuel's inorganic chemistry has, until now, been overlooked.

In this research *Miscanthus*, was hydrothermally carbonised at two temperatures 200^{0}C and 250ºC, with the process waters were recycled nine times. The effect and potential implications of recycling process waters on the fuel's organic, and inorganic combustion chemistry has been investigated.

7.3.Methodology

The methodology used for the recycling process waters is the same methodology used in the influence of retention time work presented in Chapter 6. This work is intended

to be read alongside the work presented in that chapter, with the influence of retention time work intended to establish a baseline to assess what additional impact of process water recycling has on the process chemistry. Consequently, with the exception of the HTC methodology, please refer to the methodology in Section 6.3.3 for details of the analytical techniques used. This study used the same *Miscanthus giganteus* obtained from Rothamsed Research used in Chapter 6.

7.3.1. Hydrothermal carbonisation

HTC was performed using the modified 2000 ml Parr reactor described in Section 3.2.2. For each run a 10 % solids loading was used with a combined mass of 1000 grams per run and undertaken as described in Section 3.2.2.2. Following the first cycle, approximately 20 ml of process water was then sampled and stored at -18 °C for analysis. The Pyrex reactor liner was then cleaned, dried and then filled with a subsequent 100 grams of *Miscanthus*, the remaining process water from the previous run was then added and the combined mass made up to 1000 grams using deionised water, and the process repeated. The process water recycled nine times for each temperature. The bio-coal was allowed to air dry in a ventilated fume cupboard for a minimum of 48 hours, to gauge air dry moisture loss, and then oven dried at 60˚C overnight. Yields are defined as dry bio-coal mass compared with original dry mass of unprocessed *Miscanthus*.

Multistage desorption via pyrolysis-GCMS was undertaken at 250 °C, 400 °C and 600 °C, for the runs 1, 5 and 9 at HTC 250 °C.

7.4. Results

7.4.1. Influence of recycling process water on the bio-coal organic chemistry

The yields, energy density, proximate and ultimate analysis of bio-coal derived from recycling process waters are given in Table 7.1. The results show for both treatments increasing recycling process water increases the yield, with the mass yield for the 200 °C treatments increasing from 65% and stabilising at between 71 % and 73 % after four cycles. The mass yield for the 250 °C treatments increased from 46 % to 57 %, but on the 9th and final run it appeared not to have reached equilibrium. Energy yields were also seen to increase for both treatments, albeit from 18.9 MJ/kg to 19.7 MJ/kg, for the 200 °C treatments, with the latter remaining reasonably consistent for runs two to nine. The slight increase in energy content combined with the increase in mass yields had a positive impact on overall energy yield, increasing from 68% to 77 % after four cycles. For the 250 °C treatments, there was a more substantial increase in energy density, with the fuels

increasing from 24.2 MJ/kg to 28.9 MJ/kg on the ninth cycle. This energy densification appears predominantly due to the removal of oxygen, which is reduced from 26.2 % to 16.6 % combined with an increase in carbon density, which goes from 65.2 % to 72.7 %. This increases the overall energy yield from 61% to 91 %. The 250 °C treatment results differ from the results from the 260 °C treatments presented in Uddin et al., [114] and Kambo et al., [115] where the mass yields stabilise on the fourth cycle and energy density within the bio-coal decreases after the fifth sample in Kambo et al., [115]. In these two studies retention time was limited to five minutes and consequently differences in results are likely down to the one hour retention time used in this work. The longer retention time influences the chemical composition of the products by not imposing kinetic limitations brought about though the shorter retention times. In Kambo et al., [115], the hotter conditions used appear not to have overcome the shorter retention time. The 200 °C treatment results presented here appear to sit between the 200 °C and 230 °C treatments with 5 minute retention times as presented in Uddin et al. [114]

Figure 7.1 plots the change in hydrogen and oxygen atomic ratios against carbon in a Van Krevelen diagram and includes the influence of retention time data presented earlier. The results for the influence of retention time data suggest with increasing retention time dehydration is the predominant mechanism for oxygen and hydrogen removal. The 250 °C recycling treatment results however differ with H/C remaining consistent with increasing cycles but O/C reducing. This would suggest recycling process waters under these conditions is promoting decarboxylation. This differs from work presented in Stemann et al., [113] where it was demonstrated that recycling process waters at 220 °C for four hour retention times was catalysing dehydration. The 200 °C recycling treatment results in a reduction of O/C with increasing cycles but an increase in H/C. High H/C ratios appear to be associated with high alkali metal content within the process water as observed in the valorisation of algae and early harvested Miscanthus results in Chapter 5 [259, 354]. Given extracted alkali metals accumulate within the process waters; it appears likely that H/C ratio is increasing because of increasing alkali metals under these reaction conditions. Based on the results it is however unclear if this is hydrogen from the formation of metal hydroxides or organic hydrogen. This result is however consistent with work by Patwardhan et al. [142] which showed that mineral salt addition may accelerate the formation of low molecular weight compounds, including formic acid known to act as a hydrogen donor in hydrothermal reactions. The results presented in Lu et al. [128] showed significantly more hydrogen was measured in the gas-phase when carbonizing in the presence of $CaCl_2$ indicating conversion to hydrogen gas. Hydrogen

was detected in the reactor head gas, after repeated cycles, for both 200 °C and 250 °C recycling treatments, suggesting hydrogen donation from VFA such as formic acids accumulating in the process water [353].

Table 7.1: Yields, energy density, proximate and ultimate analysis of bio-coals derived from recycling process waters

Temperature	Cycle	% Dry Basis								MJ/kg (bomb)
		Yield	Nitrogen	Carbon	Hydrogen	Oxygen	Ash	Volatile Matter	Fixed Matter	(a.d.)
HTC 200	1	65	0.7	53.6	5.3	38.2	2.2	77.4	18.9	18.9
	2	69	0.7	54.7	5.4	35.9	3.3	75.2	20.0	19.8
	3	73	0.7	54.2	5.5	36.2	3.4	74.9	20.3	19.7
	4	71	0.8	54.1	5.5	36.0	3.6	73.2	22.3	19.7
	5	71	0.8	53.8	5.6	36.0	3.9	73.9	21.1	19.8
	6	73	0.9	54.3	5.1	35.8	3.9	74.0	21.0	19.3
	7	71	0.8	53.0	5.8	36.2	4.1	74.3	20.7	19.7
	8	73	0.9	55.7	6.2	33.5	3.6	71.6	24.1	21.7
	9	71	0.9	54.1	5.5	35.6	3.9	73.8	21.6	19.8
HTC 250	1	46	0.8	65.5	4.7	26.2	2.8	58.1	38.2	24.2
	2	51	0.7	66.8	4.8	23.4	4.2	57.1	38.0	25.3
	3	52	0.8	67.9	5.1	21.6	4.7	56.7	37.6	26.4
	4	52	0.8	69.4	4.8	20.3	4.7	57.8	37.0	26.7
	5	53	0.8	69.5	4.8	19.7	5.2	56.7	37.6	26.8
	6	53	0.8	71.1	4.9	19.0	4.2	57.1	38.5	27.6
	7	52	0.9	71.1	5.2	17.8	5.1	57.8	36.2	28.3
	8	55	0.8	71.2	5.0	17.8	5.2	57.5	36.8	28.0
	9	57	0.8	72.7	5.1	16.6	4.8	56.9	37.7	28.9

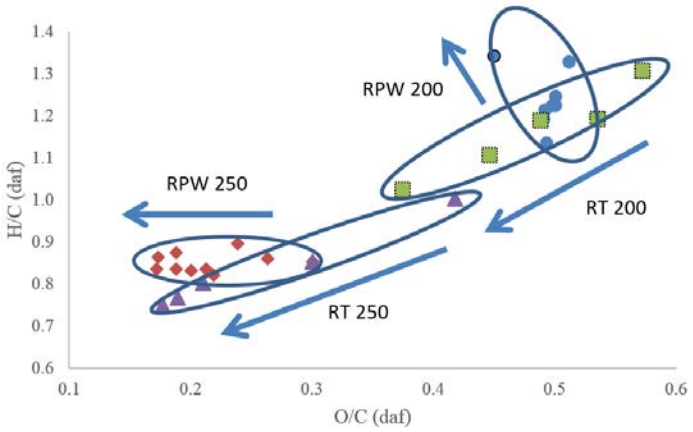

Figure 7.1: Atomic H/C-O/C rations of bio-coals derived from recirculation (RPW) and increasing retention times (RT)

The results for the 200 °C and 250 °C recycling treatments induced a slight reduction in volatile matter and an increase in fixed carbon for the 200 °C treatment. When corrected on a dry ash free basis there is however little change in the volatile matter and fixed carbon in the 250 °C recycling treatments, but a modest decrease in volatile matter and a modest increase in fixed carbon for 200 °C recycling treatments. The difference between the 'dry basis' results and the 'dry ash free basis' results coming about because the ash content is increasing with successive treatments.

7.4.1.1.200 °C Process chemistry

For the 200 °C treated bio-coals, the increasing fixed carbon yield and increasing mass yield would indicate the increased mass is a product of condensation and repolymerisation of oligomers and monomers derived though the hydrolysis of hemicellulose and cellulose. It had been demonstrated previously in work by Lynam et al. [44] that addition of acetic acid to HTC, inhibits further acetic acid generation during HTC. Based on this, the hypothesis that the reactions producing acetic acid could be reversible reactions was developed; i.e. added acetic acid pushes the equilibrium in the direction of reduced acetic acid production possibly resulting in hemicellulose, from which acetic acid is largely derived [82, 120, 121], remaining within the char and improving yields [44]. Figure 7.2 shows a CGMS VFA analysis of the process waters and acetic acid appears the predominant VFA present within the process water. The increase in fixed carbon would however suggest that the increase in mass yield is not due to hemicellulose remaining within the bio-coal. The DTG of temperature controlled combustion of the 200 °C recycled bio-coals (given in Figure 7.3) also indicates hemicellulose it is not present within the recycled bio-coal, given there appears no volatile material evolved between 190 °C and 270 °C.

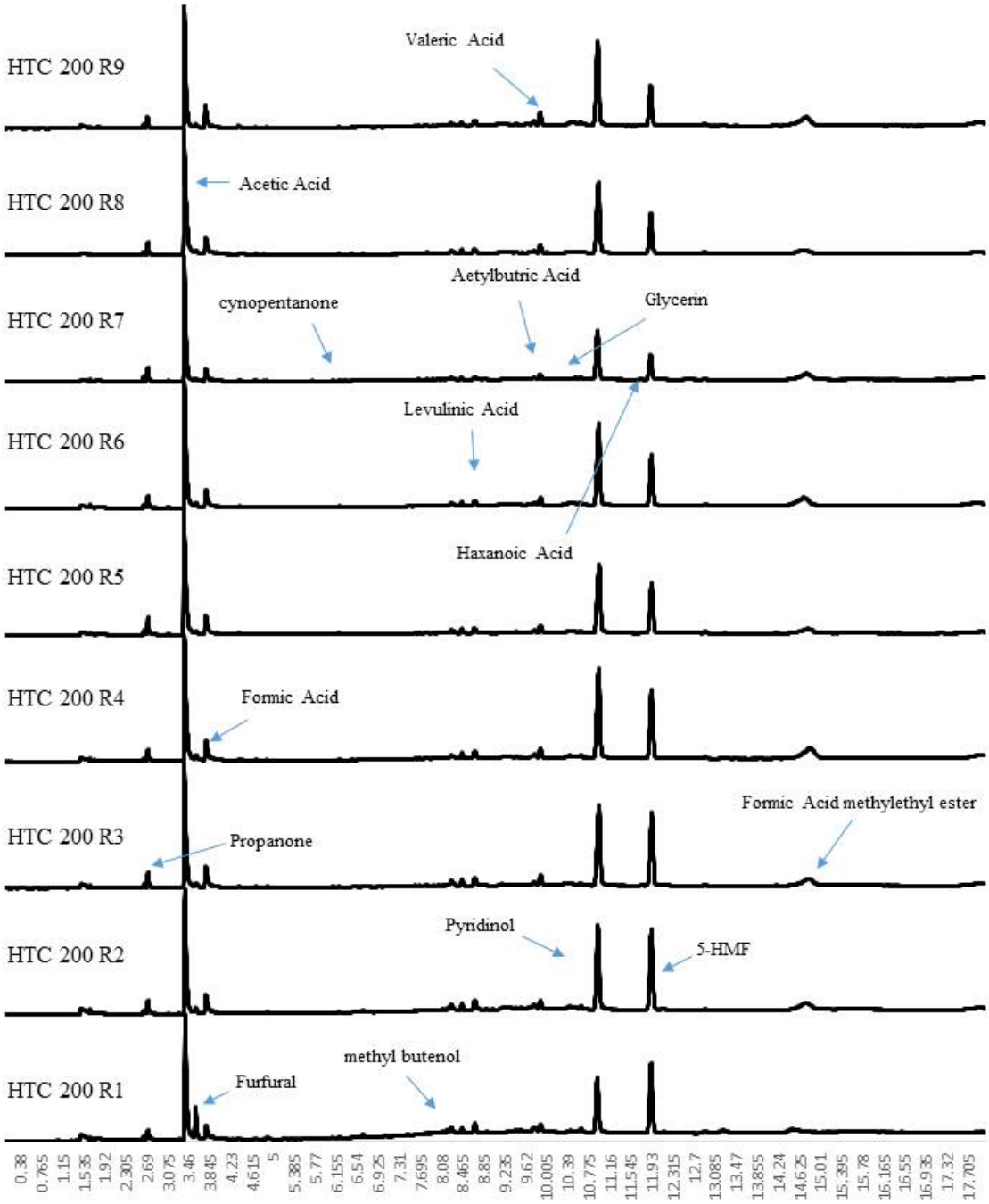

Figure 7.2: CG-MS spectra of volatile fatty acids within of process waters for the 200 °C recycling treatments

The presence of large amounts of acetate, as indicated within the protonated NMR analysis of the process water, would however suggest the presence of acetate salts within the process water (Figure 7.4a). It could appear that acetic acid, along with formic acid, formed during the hydrothermal process reacts with inorganics within the biomass to form metal acetates and formates. Metal acetates may not have the same influence acetic acid has on pushing reaction equilibriums in the direction of reduced acetic acid thus we don't see the retention of the hemicellulose as reported by Lynam et al. [44] in the case of recycling process water. This is due to the addition of inorganic material through the

addition of unprocessed biomass with every cycle. Accordingly, it is possible that the inorganics within the biomass are catalysing the removal of acetyl groups from the fuel.

TOC data given in Table 7.2 suggest that by cycle 3 in the 200 °C treatments TOC concentration within the process water remains reasonably constant at around 20,000 mg/l. The results given in Figure 7.2 suggest that pyridanol accumulates within the process water but the relative concentrations of 5-HMF appear to reduce. The low levels of levulinic acid indicate that under these conditions the 5-HMF does not decompose further to levulinic acid and thus the 5-HMF appears to be reincorporated into the char. Like in the retention time samples, furfural, a compound known to arise from the dehydration and fragmentation of the glucose, fructose and maltose derived from the starch and sugar [85, 86, 350], appears only present in low concentrations within the process water.

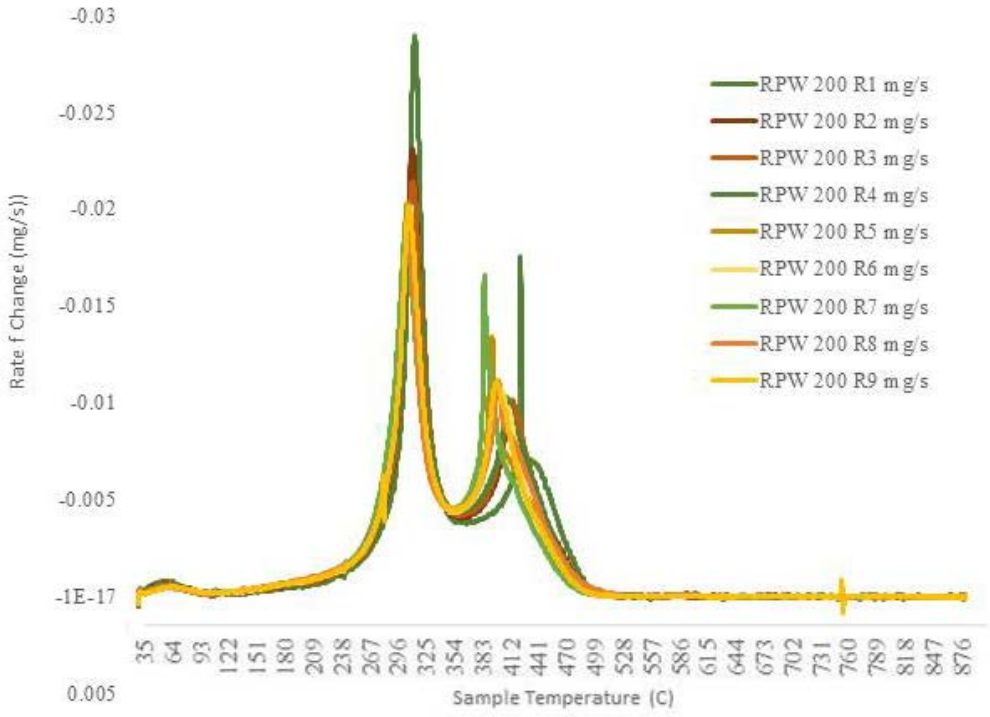

Figure 7.3: Derivative thermogravimetric (DTG) burning profiles for bio-coals derived from recycling process water at 200 °C

Table 7.2: Total organic carbon, alkali and alkaline metals, chlorine, phosphate, sulphate and pH of process water when recycling process waters.

Temperature	Cycle	Mg/l								pH
		Na	Mg	PO4	SO4	Cl	K	Ca	TOC	
HTC 200	1	11	78	251	312	354	572	173	10935	3.42
	2	17	199	477	581	553	1161	721	18197	3.41
	3	22	294	518	739	1070	1500	897	20680	3.45
	4	18	267	538	605	866	1532	737	18284	3.43
	5	21	322	986	814	1287	1898	989	22162	3.43
	6	17	268	481	571	969	1477	821	18660	3.42
	7	20	305	572	653	1077	1729	937	19973	3.43
	8	20	238	755	680	949	1656	834	19383	3.47
	9	19	283	676	618	1053	1592	880	20015	3.45
HTC 250	1	6	50	193	229	1106	634	395	11946	3.30
	2	14	138	393	494	1522	1207	877	20635	3.29
	3	18	216	404	587	2371	1605	1107	24837	3.29
	4	25	295	816	737	2718	2229	1540	30509	3.30
	5	29	408	841	827	3016	2760	1774	35853	3.30
	6	35	432	1193	907	3487	3015	1891	40246	3.28
	7	35	444	1140	789	3788	3164	1981	40664	3.29
	8	36	440	1353	850	4000	3156	1870	40262	3.28
	9	39	482				3373	1971	42311	3.28

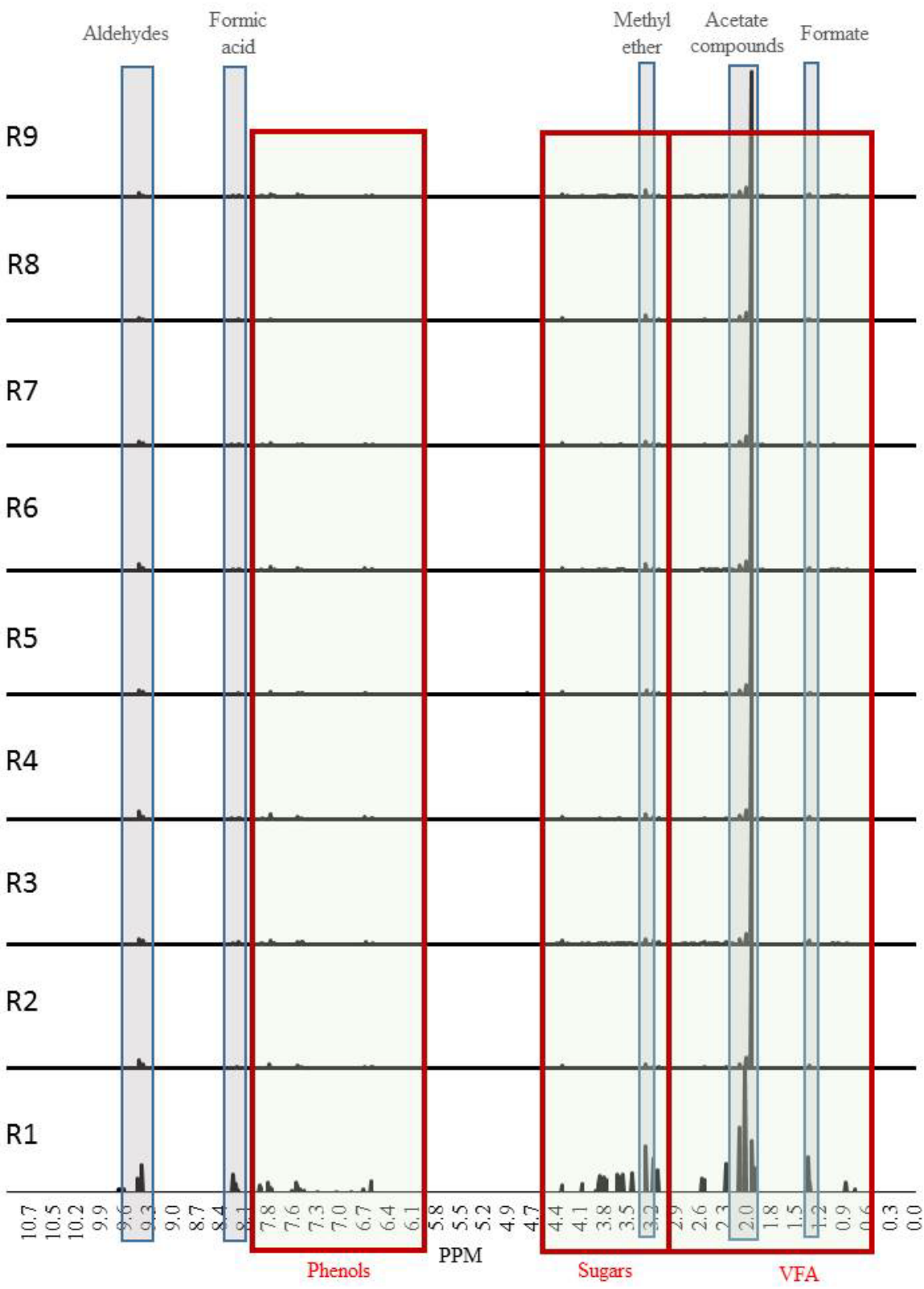

Figure 7.4: H-NMR spectra of HTC process waters 200 °C recycling treatments

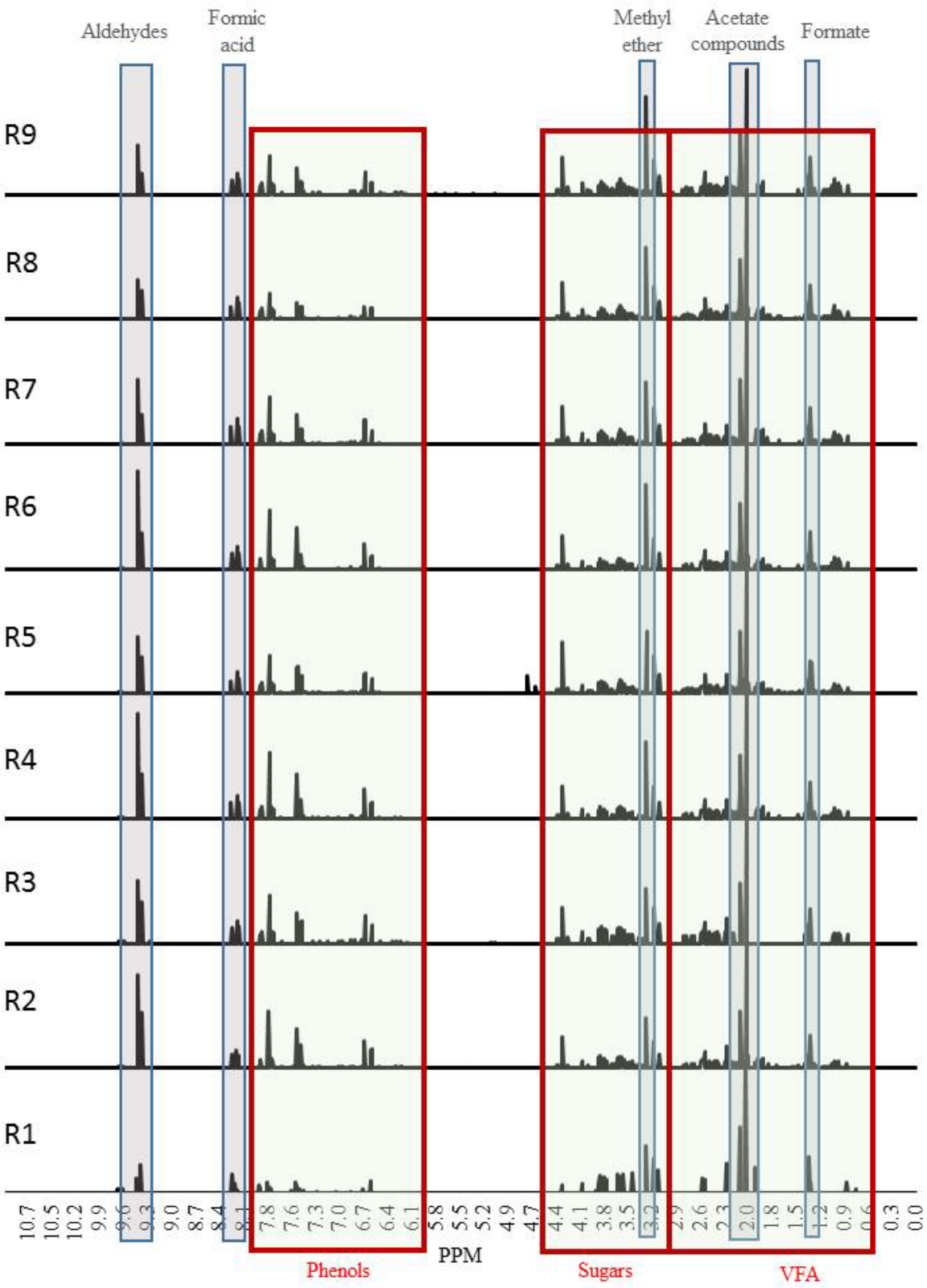

Figure 7.4b: H-NMR spectra of HTC process waters 200 °C recycling treatments without acetate peak

7.4.1.1.1. Proposed process chemistry for the 200 °C recycled bio-coals

It is proposed that when the process waters are recycled, organic acids already present within the process water, generated in the previous cycle, would generate

hydronium ions which along with the high dissociation of H^+ and OH^- brought about under hydrothermal conditions which would promote and catalyse hydrolysis of the hemicellulose and cellulose giving rise to their corresponding monosaccharides. Given 5-HMF and furfural (if it were present) would be already in the process water, there would be an enhanced chance that the 5-HMF and furfural would react with the newly created monosaccharides from the (hemi-) cellulose which would now be present in the process water. This reaction forms the insoluble humins though polymeric condensation which make up the char yield.

Py-GCMS has been undertaken for the 200 °C recycled bio-coals and the results are given in Figure 7.5b. The results show the volatile chemistry only changes subtly over the cycles with the following compounds becoming prevalent: 2-methyl furan (peak 1), 2,5 dimethyl furan (peak 2), 2-furanmethanol (peak 10), ethylhexaldehyde (peak 11), 1,3dimethylcyclopenten-3-one (peak 12), cyclopentadione (peak 13), furanone (peak 16), 3-methyl cyclopentanedione (peak 18), 2-methoxyphenol (peak 19), Dihydrobenzofuran (peak 27) and dimethoxyphenol (peak 30). This result is constant with humin formation via aldol addition or condensation of 5 furfural like compounds (5-HMF, furfural, 5-methylfurfural etc.) [309]. The results also suggest at a reduction in levoglucasan (peak 38) with increasing cycles, which would support the hypothesis that organic acids are catalysing the hydrolysis of the cellulose. This is further supported by the burning profile given in Figure 7.3, which, while showing a reduction in volatile burn, the peak shape remains ‘cellulose like’. Also, the pyrolysis data given in Figure 7.5b compares closely with the unprocessed *Miscanthus* (given in the same figure). This supports the assumption that the volatile material is predominantly from cellulose.

In Figure 6.2 of the previous chapter it was observed that there were increasing relative concentrations of methyl and ethyl phenols (peaks 5, 21, 23, 25, 26 and 30) as retention times increased. This phenomena is not as pronounced for the 200 °C recycled bio-coals. This would suggest that the kinetics required for aromatisation and formation of aromatic clusters at this temperature is still retention time dependent. This is despite increasing concentrations of cyclic and heterocyclic compounds, brought about through process water recycling.

Figure 7.4a and Figure 7.4b gives an overview of the organic compounds present using protonated NMR. Figure 7.4a shows that for 200 °C acetate salt is the main organic product within the process water and increases in overall concentration, in the subsequent run. TOC concentration within the process water remains reasonably constant after cycle

three and the acetate peak appears not to change relative to the other peaks after cycle three. In Figure 7.4b the acetate peaks at 2.0 ppm have been subsequently removed to gain a better understanding of the changes in other components. The results show that after the first cycle organic compounds with phenolic and aldehyde functional groups make a marked increase, within the process water. Monosaccharides and VFA within the process water also appear to diversify with the emergence of multiple peaks within their respective ranges. Acetyl and methyl ether functionalized compounds appear most abundant within the process water. The relative concentration of formic acids and formate appear reasonably unchanged throughout the cycles.

7.4.1.2.250 °C Process chemistry

For the 250 °C recycled process water bio-coal the dry ash free proximate analysis would suggest little change other than increasing ash content. Contrary to this though, the burning profile, given in Figure 7.6, shows a significant change in its combustion behaviour. The characteristic volatile peak, seen in Figure 6.10b profiles and Figure 6.10c combustion profiles for 250 °C treatment with zero and one hour retention times, becomes increasingly less distinct and by latter four cycles the second initiation temperature is marked more by the acceleration in weight loss as opposed to a second peak. Consequently, the bio-coal gains a more coal like burning profile with increasing cycles, with a similar burning profile to that seen for 250 °C treated bio-coal with 24 hour retention time. The 250 °C recycled bio-coals do not however have the increase in fixed carbon and the reduction in volatile matter observed for the 250 °C bio-coals with increasing retention given in Table 6.1. This appears due to the formation of a low temperature volatile peak starting around 100 °C and 270 °C whereby the first initiation temperature is reached.

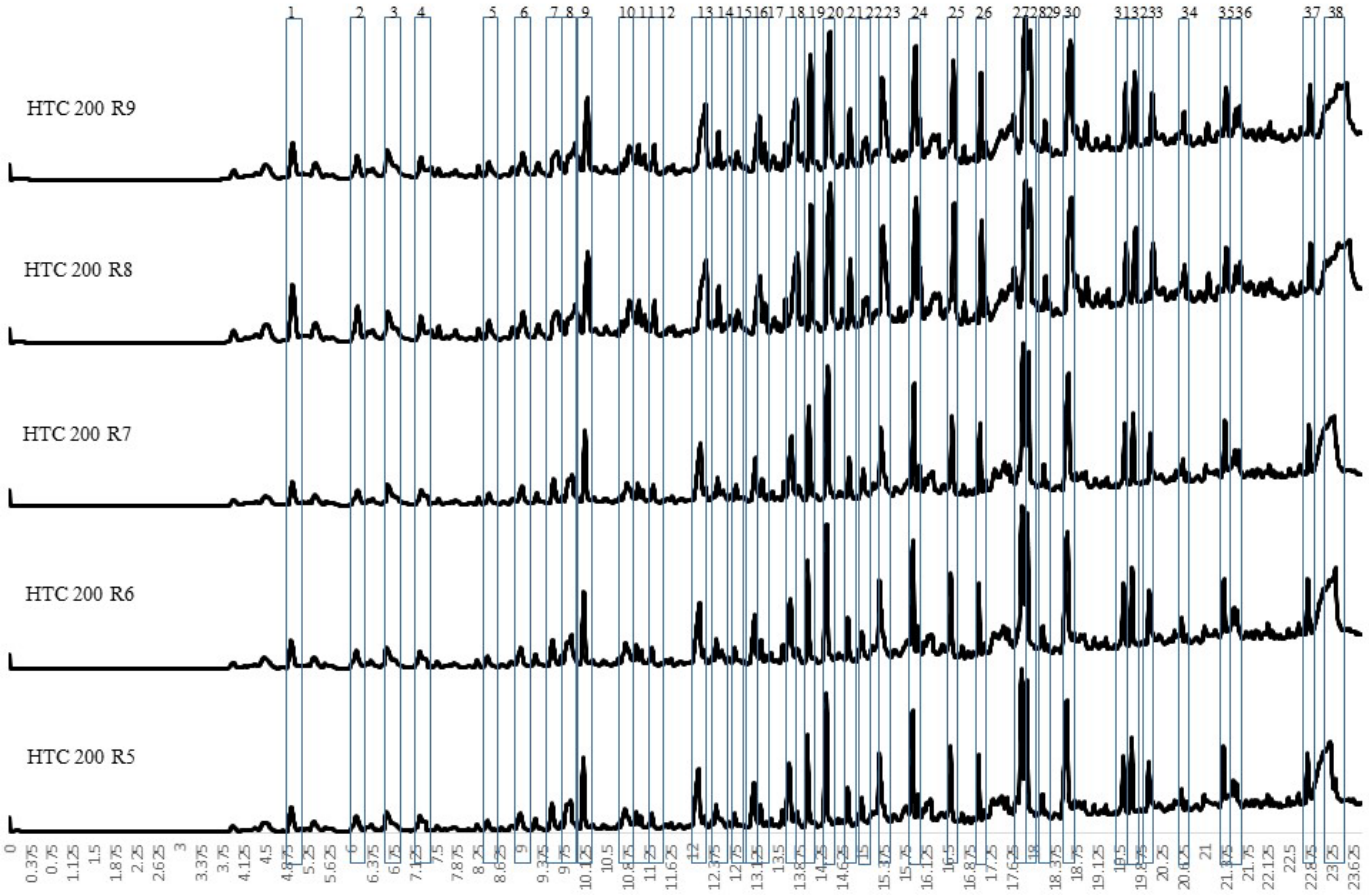

Figure 7.5a: Pyrolysis GCMS spectra of volatile organics evolved at 550 °C from recycled process water bio-coals treated at 200 °C

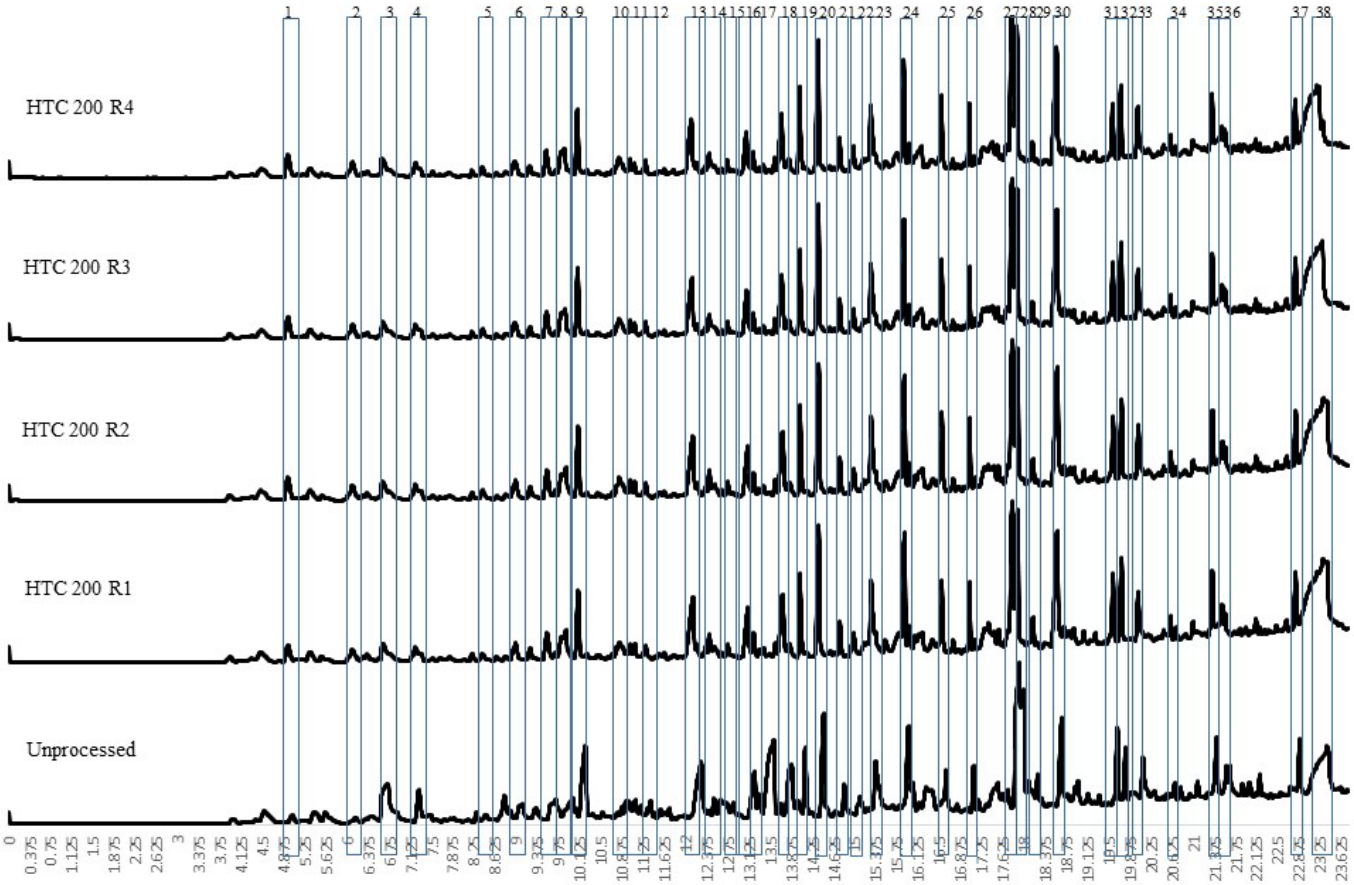

Figure 7.5b: Pyrolysis GCMS spectra of volatile organics evolved at 550 °C from recycled process water bio-coals treated at 200 °C ((1) 2-methyl furan; (2) 2,5 dimethyl furan; (3) propanediol; (4) toluene; (5) 3-methyl phenol; (6) pentanoic acid; (7) cyclopentanone; (8) butanediol; (9) dimethylpyrazole; (10) 2-furanmethanol; (11) ethylhexaldehyde; (12) 1,3dimethylcyclopenten-3-one; (13) cyclopentadione; (14) 2-furan carboxadehyde; (15) 1methyl-1-cyclopenten-3-one; (16) furanone; (17) amino-3-pyridinol; (18) 3-methyl cyclopentanedione; (19) phenol; (20) 2-methoxyphenol; (21) 2-methyl phenol; (22) 2-cyclopenten-1-one: (23) 4-methyl phenol; (24) creasol; (25) 4-ethyl phenol; (26) 4-ethyl-2methoxy phenol; (27) dihydrobenzofuran; (28) 4-hydro-3-methyl acetophenone; (29) eugenol; (30) 2,6, dimethoxyphenol; (31) isoeugenol; (32) triethoxybenzene; (33) vanillin; (34) trimethoxytoluene; (35) dimethoxy acetophenone; (36) trimethylacealdehyde; (37) methoxy eugenol; (38) evoglucasan).

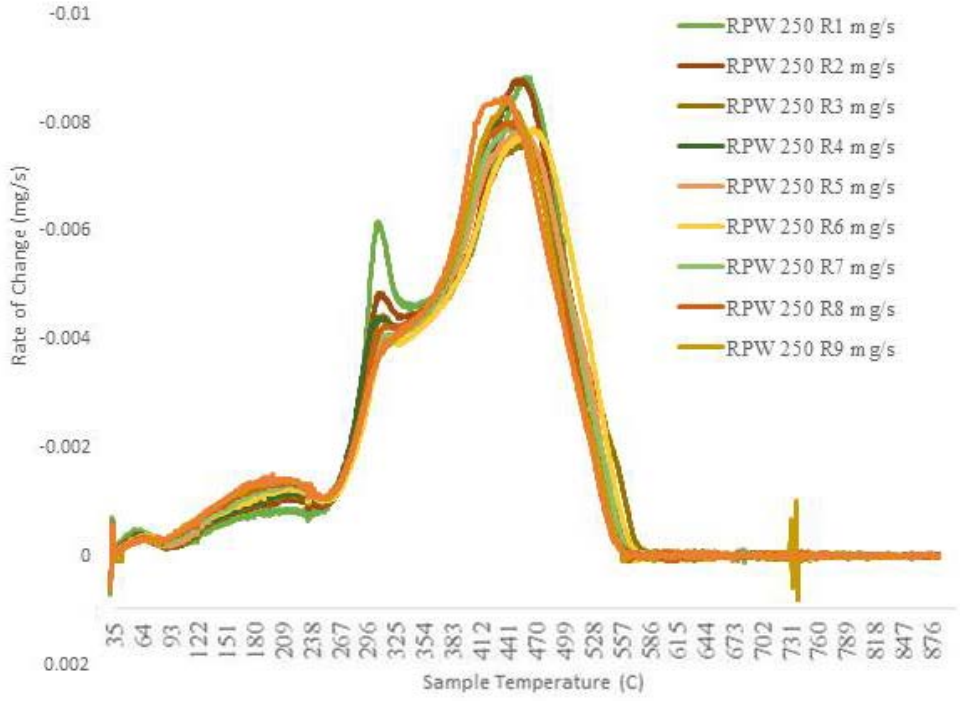

Figure 7.6: Derivative thermogravimetric (DTG) burning profiles for bio-coals derived from recycling process water at 250 °C

Py GCMS has been undertaken for the 250 °C recycled process water bio-coals at 550 °C, with these results given in Figure 7.7b. The results show the cyclic and heterocyclic compounds observed in the 200 °C recycled process water bio-coal and constant with humin formation via aldol addition or condensation of furfural like compounds (5-HMF, furfural, 5-methylfurfural etc.), are present in the 250 °C recycled bio-coals. This said the relative concertation of 2-methyl furan (peak 1), 2,5 dimethyl furan (peak 2), cyclopentanone (peak 8), 2-methyl-2-cyclopenten-3-one (peak 9), 3-methyl-1-cyclopentanedione (peak 11) and corylon (peak 12) reduce with increasing cycles indicating increased aromatisation. The pyrolysis products also become increasingly aromatic when compared with the 200 °C recycled bio-coal, as demonstrated by peaks 13 to 24, which are all phenolic. The phenolic peaks; phenol (peak 13), (14) 2-methoxyphenol (peak 14), creasol (peak 17) dihydrobenzofuran (peak 21) and a series of benzene derivatives (peak 25) appear to increase in relative concentration within the volatile material, while 2-methyl phenol (peak 15), 4-methyl phenol (peak 16), 2-ethyl phenol (peak 19), 4-hydro-3-methyl acetophenone (peak 22), and triethoxybenzene (peak 24) appear to reduce in relative concentration. This may suggest a change in group functionality with increasing cycles.

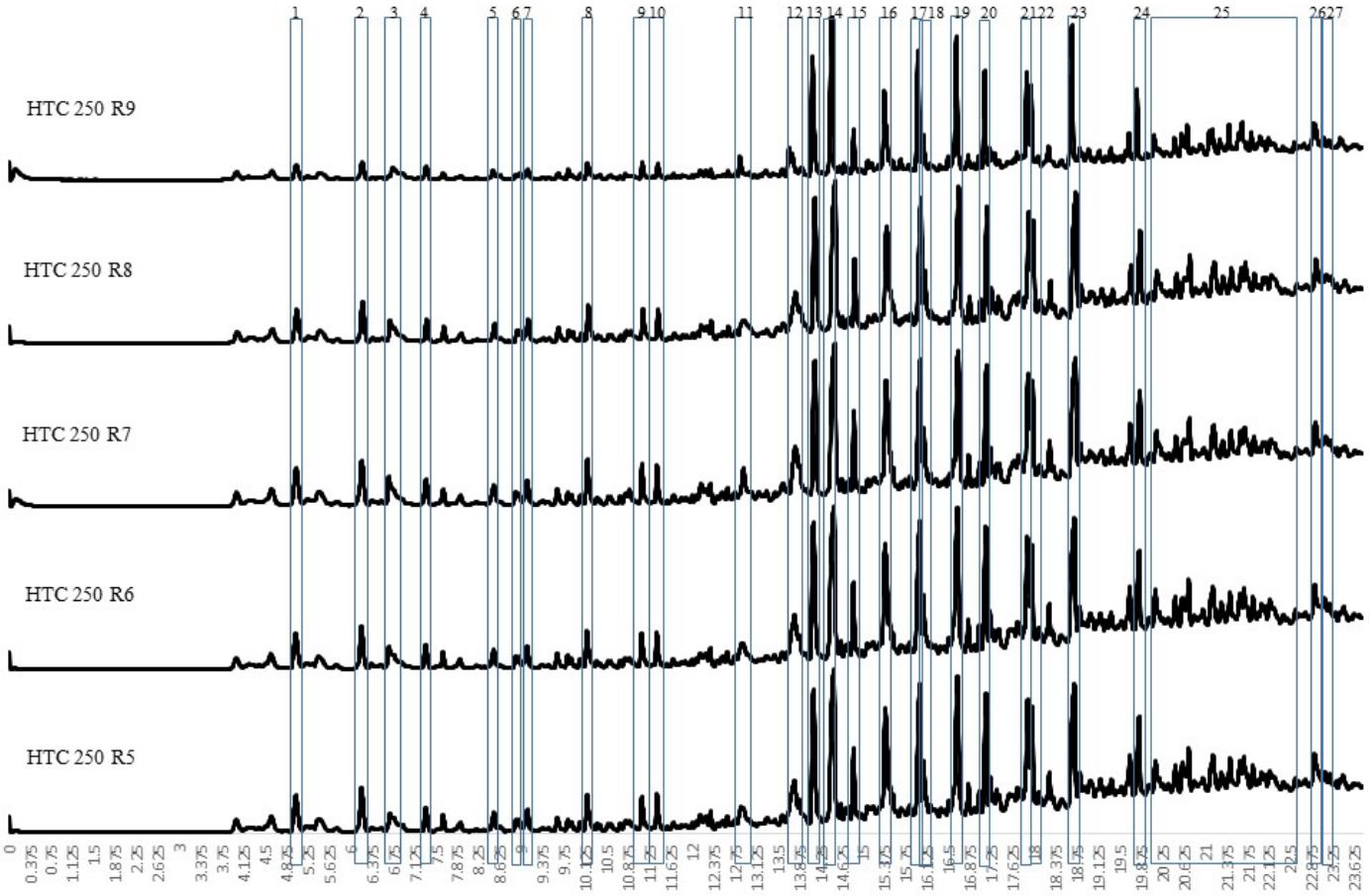

Figure 7.7a: Pyrolysis GCMS spectra of volatile organics evolved at 550 °C from recycled process water bio-coals treated at 250 °C

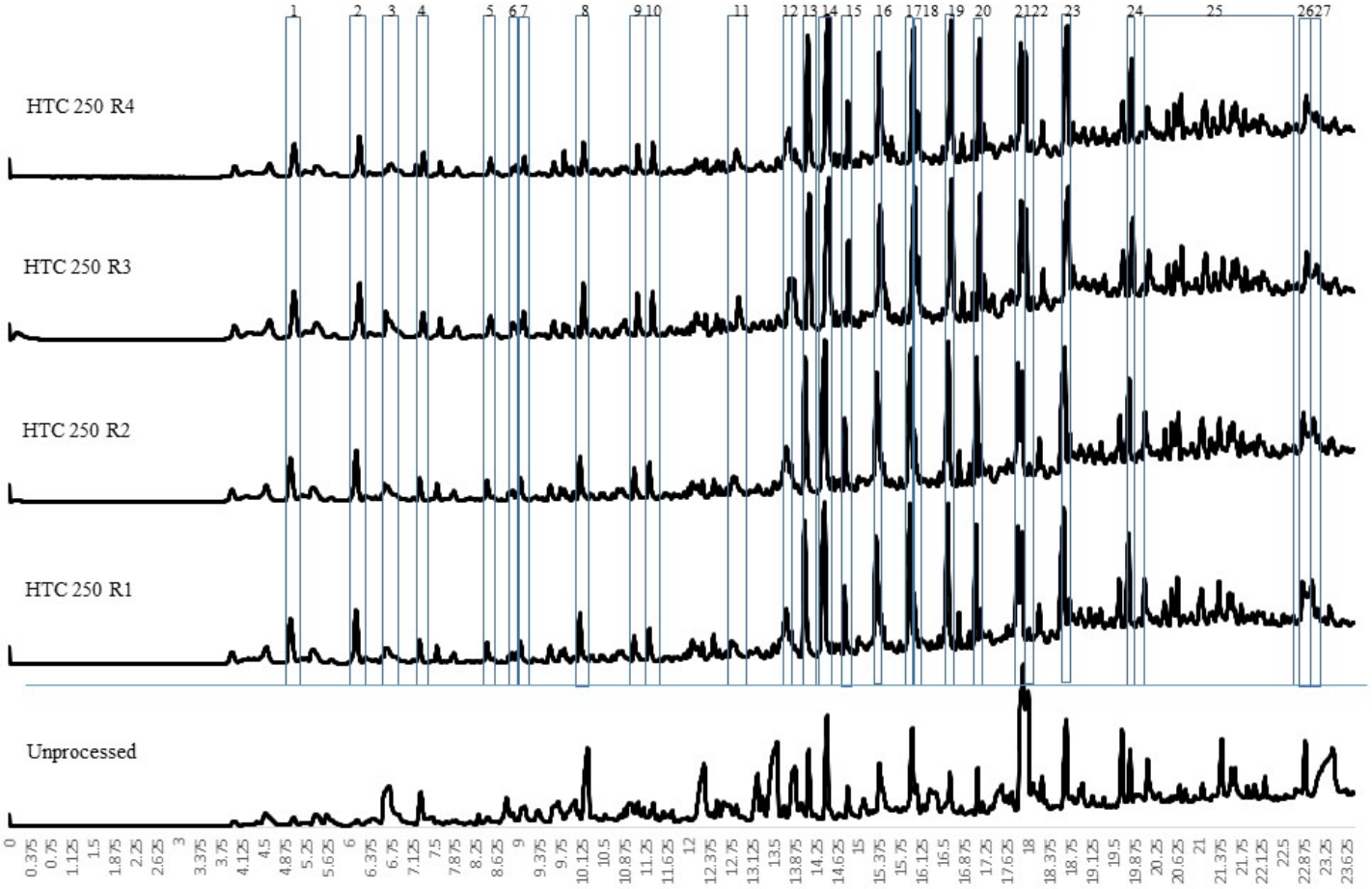

Figure 7.7b: Pyrolysis GCMS spectra of volatile organics evolved at 550 °C from recycled process water bio-coals treated at 250 °C ((1) 2-methyl furan; (2) 2,5 dimethyl furan; (3) propanediol; (4) toluene; (5) 3-methyl phenol; (6) ethylbenzene; (7) dimethylfulvene; (8) cyclopentanone; (9) 2-methyl-2-cyclopenten-3-one; (10) acetylfuran; (11) 3-methyl-1-cyclopentanedione; (12) corylon; (13) phenol; (14) 2-methoxyphenol; (15) 2-methyl phenol; (16) 4-methyl phenol; (17) creasol; (18) 4-ethyl phenol; (19) 2-ethyl phenol; (20) 4-ethyl-2methoxy phenol; (21) dihydrobenzofuran; (22) 4-hydro-3-methyl acetophenone; (23) 2,6 dimethoxyphenol; (24) triethoxybenzene; (25) benzene derivatives; (26) methoxy eugenol; (27) levoglucasan)

Levoglucasan, while present in first few cycles at gradually decreasing concentration, is not present in the latter cycles, indicating complete removal of cellulose. For the 250 °C treatments with increasing retention times (Chapter 6), levoglucasan was still present at 24 hours, albeit at decreasing concentrations with increasing retention time (see Figure 6.5), indicating residual cellulose at 24 hours. This would support the proposed mechanism that when the process waters are recycled, organic acids already present within the process water would promote and catalyse hydrolysis of the hemicellulose and cellulose giving rise to their corresponding monosaccharides.

VFA analysis via GC-MS of the process waters is given in Figure 7.8. The concentrations of 5-HMF and furfural appear low within the recycled process water, with the majority appearing to have decomposed to levulinic acid, a common decomposition product of 5-HMF [270], along with valeric acid a hydrogenation product of levulinic acid [271]. The relative concentrations of the levulinic acid, valeric acid and pyridinol do not significantly change between cycles, and the relative concentration with respect to acetic acid decrease. TOC data given in Table 7.2 does however suggest that TOC concentration continues to increase throughout the 250 °C treatments peaking at 42,000 mg/l in the ninth cycle, albeit the results suggest a decline in this increase after cycle five. Figure 7.9a shows that for the 250 °C cycles acetate salt is the overwhelming organic product within the process water. In Figure 7.9b the acetate peaks at 2.0 ppm have been subsequently removed to gain a better understanding of the changes in other components. The results, show reasonably limited change between the cycles with formate increasing in concertation with increasing cycles, supporting the hypothesis that formic acid and acetic acid leads to the formation of metal formate salts as inorganics are liberated from within the biomass. Whether the observed TOC increase after cycle five is due to, simply increasing acetate and formate would require further quantitative analysis of key compounds. The fact that the relative concentrations of the levulinic acid, valeric acid and pyridinol do not significantly change between cycles would suggest that decomposition products of cellulose and hemicellulose from the biomass do not decompose further to levulinic acid or hydrogenate further to valeric acid, but must be reincorporated into the bio-coal though humin formation.

Figure 7.9b indicates that the saccharide like compounds and VFA appear to initially increase in concentration on the first recycle but the composition appears to remain reasonably consistent thereafter, with saccharide like compounds and VFA the main constituents within the process water. The relative concentration of phenols and

aldehydes appear to decrease within the process water, although the NMR data is normalised so the increasing concentration of formate within the process water will also reduce the relative scaling of these components.

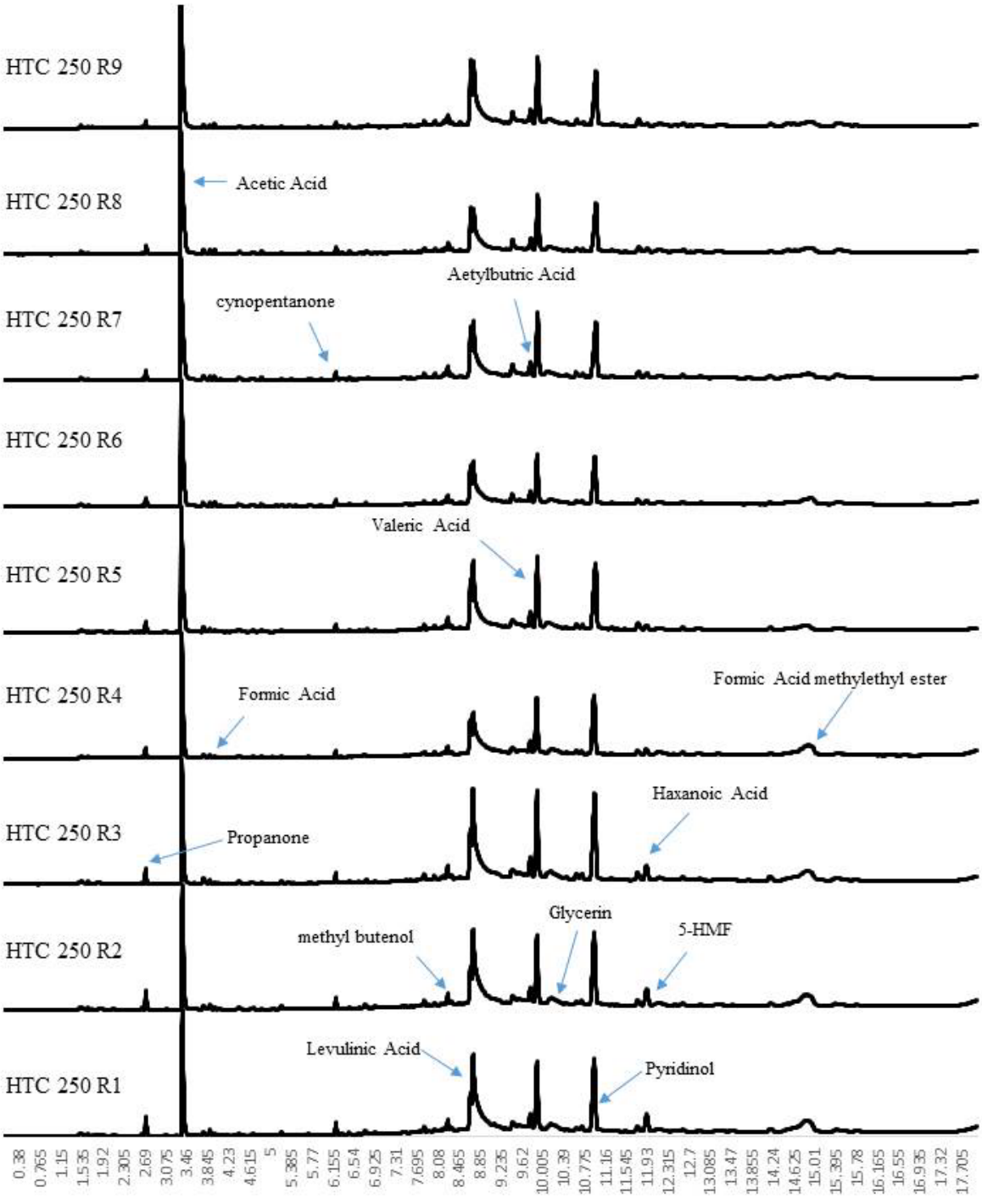

Figure 7.8: CG-MS spectra of volatile fatty acids within of process waters for the 250 °C recycling treatments

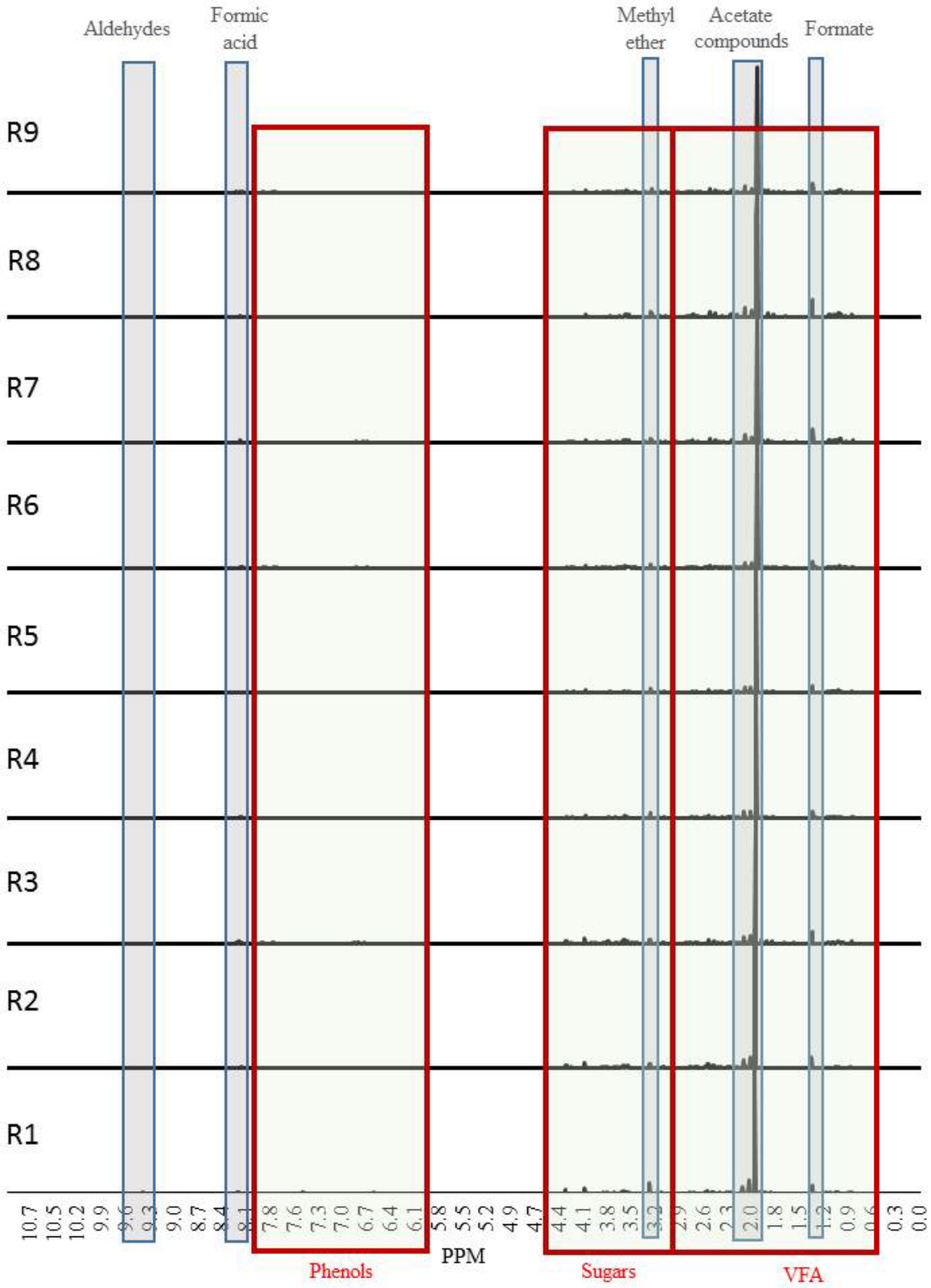

Figure 7.9: H-NMR spectra of HTC process waters 250 °C recycling treatments

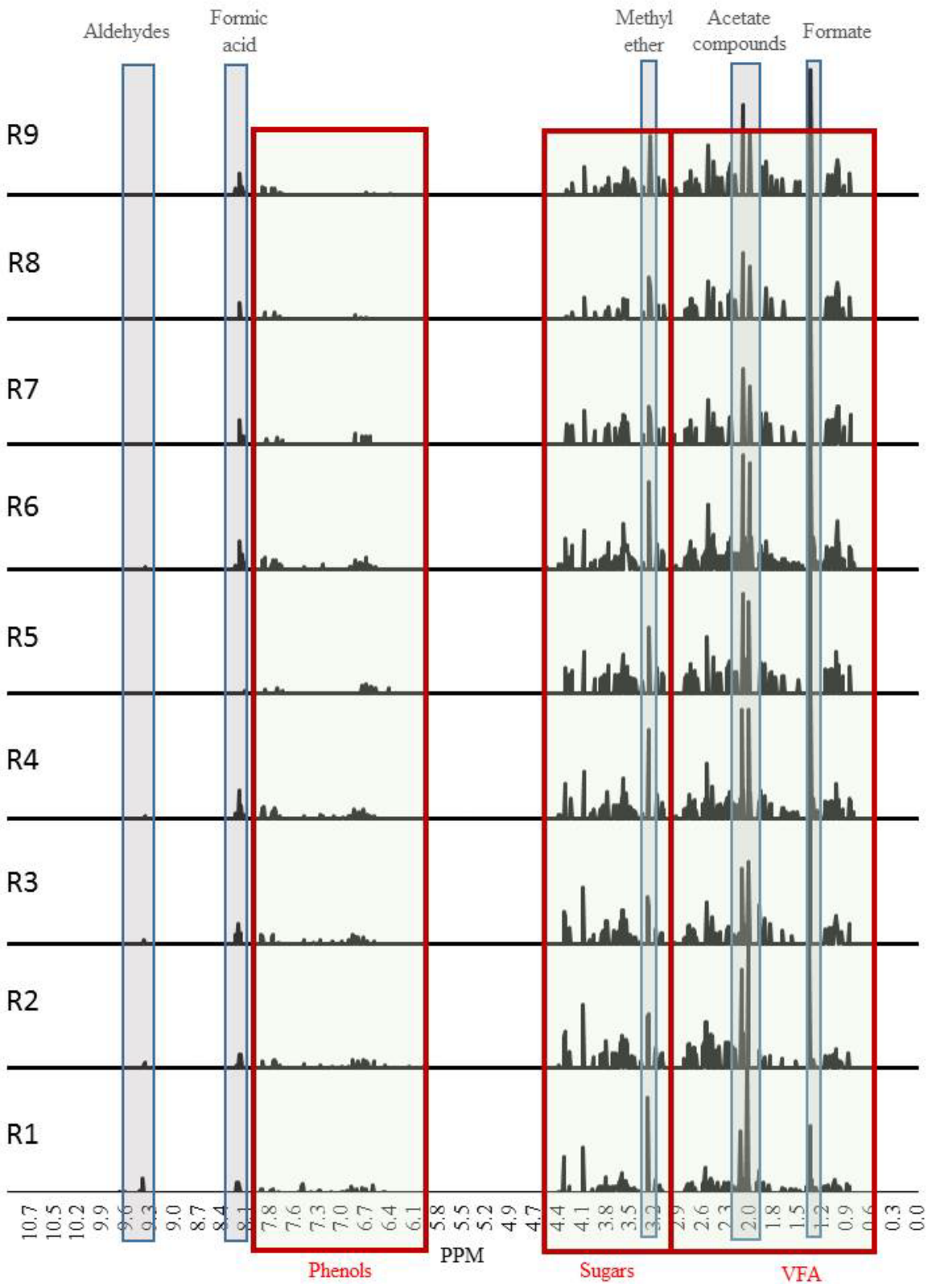

Figure 7.9b: H-NMR spectra of HTC process waters 250 °C recycling treatments without acetate peak

7.4.1.2.1. Proposed process chemistry for the 250 °C recycled bio-coals

The proposed mechanism is that the organic acids recycled from the previous cycle, combined with the change in ionic product of the subcritical water brings about

early hydrolysis of the hemicellulose and cellulose [79] as the reaction media is heating. The organic acids from the previous cycle go on to catalyse the degradation of the oligosaccharides generated from the hydrolysis of the hemicellulose and cellulose to monosaccharides which suffer dehydration and fragmentation (i.e. ring opening and C-C bond breaking) processes giving rise to different soluble products, such as furfural-like compounds and HMF related compounds, 1,2,4-benzenetrol, acids and aldehydes (acetaldehyde, acetonitrilacetone) [84, 85]. It is suggested that the recycled process waters catalyse this process thereby increasing the reaction rate at a lower temperature, which allows the monosaccharides and / or their decomposition products to undergo polymerization leading to the formation of soluble polymers. The polymerization or condensation reactions can be induced by intermolecular dehydration (two –OH groups react to leave a –O- bond thus removing water) or by aldol condensation. The formation of C=C can result from keto-enol tautomerism of dehydrated species or by intramolecular dehydration [85].

It is likely that the increased organic loading within the recycled process water, and increased saccharide concentrations within the process water (through enhanced hydrolysis of the hemicellulose and cellulose) would catalyse this, and that increased saccharide concentrations are known to favour aromatization and repolymerisation [85]. This process will be primarily catalysed by the levulinic acid and valeric acid derived from 5-HMF in the previous cycles. The increase in phenols seen in the py-GCMS, with increasing cycles will be due to the further decomposition of furfural like compounds [351] catalysed by the organic acids present in the recycled water and though fragmentation of the aromatic clusters formed as part of the char formation.

The formation of the bio-coal is believed to be produced by condensation by the intermolecular dehydration of the aromatized molecules described above [85]. The structure of which this takes is dependent on the biomass from which it is formed; biomass with ‘hard’ plant tissues, such as crystalline cellulose, maintain hierarchical shape (as is the case for *Miscanthus*), while soft plant tissues, without a scaffold do not keep their structure and form globular carboniferous particles [77]. Both structures are believed to follow the LaMer model of particle formation whereby when the concentration of aromatic structures reaches a certain point a burst nucleation takes place [22]. It appears likely that the higher organic loading encountered when recycling process waters, combined with the catalysis as a result of the organic acids, brings about the formation of aromatized molecules; this then would advance the point at which the burst nucleation

occurs. Initially the aromatic structures will be chemisorbed through reactive oxygen functionalities (hydroxyl, carboxyl, carboxylic etc.) which are present on the surface, which dehydrate to form stable oxygen groups, which are ether or pyrone, within the char formation. Reactive oxygen functionalities will remain on the surface and provide binding sites for more aromatic structures [85]. It should be noted that the reactor used in this study has a relatively slow average heating rate of 5 °C minute^{-1}. The slow heating rate is likely to have an influence on this reaction chemistry allowing more time for reactions to occur, for example polymerisation of monosaccharides and 5-HMF. Higher heating rates may impose kinetic limitations with compounds such as 5-HMF being converted to levulinic acid as opposed to polymerisation of monosaccharides to form humins (char).

The mechanism given for the char formation relies on dehydration whereas the van Krevelen results suggest decarboxylation is a dominant route. Polymerization and aromatization via decaboxylation while possible and appears less likely as carbon-carbon bonds are more stable. The 200 ºC recycled process water bio-coal results suggested increasing hydrogen via: (i) hydrogen donating, (ii) alkali metal catalysed reactions increasing organic hydrogen, or (iii) hydrogen is being added to the inorganics in the form metal hydroxides. It is possible that similar mechanisms are happening here, where by dehydration is the main char forming mechanism, but additional hydrogen is being incorporated via the above mechanisms, resulting in the van Krevelen plot given in Figure 7.1 suggesting decarboxylation. The HTC materials are reported to have a rich surface functionality and it is possible hydrogen donation is influencing this chemistry, for example through removal of removal of carboxyl groups, but more detailed surface analytical techniques, such as x-ray photon spectroscopy (XPS) would be required to draw any conclusions on such a change.

To better understand the changes in volatile release chemistry, multi stage pyrolysis GCMS was undertaken at three key temperatures, 250 °C, 400 °C and 600 °C, with these temperatures chosen based on changes observed in the DTG of the devolatilisation stage of the proximate analysis. The results are given in Figure 7.10. The results show that there is an increase in compounds evolved for the 250 °C desorption, which is consistent with the early volatile release between 100 °C and 270 °C in Figure 7.5. The results show the fuel from cycle one that there is some desorption of phenol (peak 16), 2-methyl phenol (peak 17), 4-ethyl phenol (peak 21), 4-ethyl-2-methoxy phenol (peak 22) and 2,6 dimethyl phenol (peak 26) in Figure 7.10a. These phenols are likely behaving like furfural compounds, i.e. they have undergone further decomposition

and become chemisorbed onto the char surface, as opposed to fragments of the aromatic clusters formed as part of the char formation. With increasing cycles there is the appearance of the VFA acetic acid (peak 4) and propanoic acid (peak 6), believed to be organics from residual process water as opposed to desorbed functional acetyl groups seen on the unprocessed biomass. Increasing cycles also bring about hydrolysed cellulose fragments, such as 2-cyclopenten-1-one (peak 8), 2-methyl-2-cyclopenten-1-one (peak 9) and ethanone (peak 10), in addition to the cyclic aldehydes, furancarboxyldehyde (peak 12) and 5 methyl-2-furancaboxaldehyde (peak 13). With increasing cycles the bulk of the compounds released are phenolic with benzofuran (peak 15), phenol (peak 16), 2-methyl phenol (peak 17), cresol (peak 18), 4-methyl phenol (peak 19), creosol (peak 20), 4-ethyl phenol (peak 21), 4-ethyl-2-methoxy phenol (peak 22), 2-methoxy-N-N-dymethyl benzoamine (peak 24), 2-methoxy-4-propyl phenol (peak 25), 2,6 dimethyl phenol (peak 26) and a host of methoxybenzoaldehydes which appear after peak 26. It appears likely that these are derivative aromatic structures which are chemisorbed through reaction reactive oxygen functionalities and are yet to form the stable ether or pyrone bonds formed within the char formation [85].

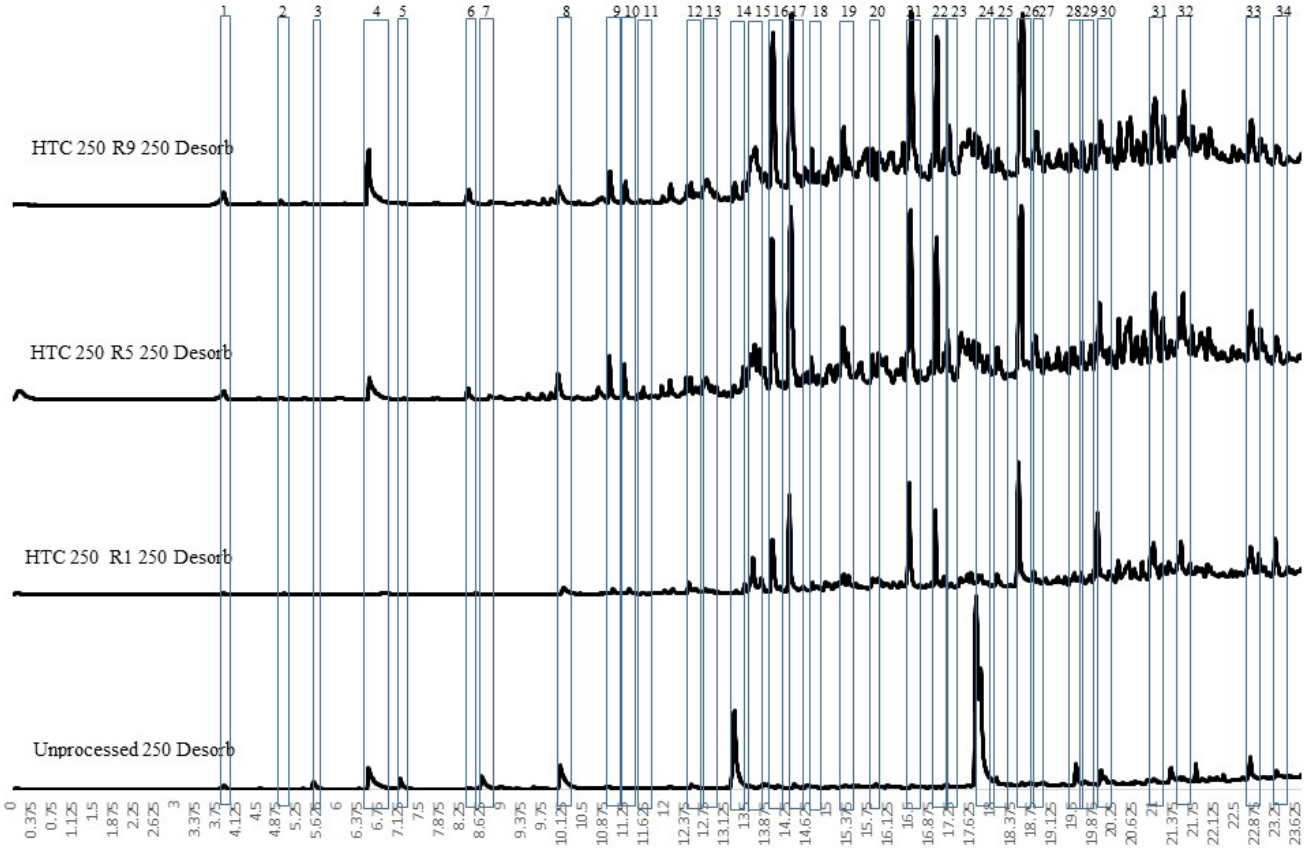

Figure 7.10a: Volatile organics evolved below 250 °C from bio-coals treated at 250 °C with recycled process waters ((1) ethylcyclobutane; (2) 2-methyl furan; (3) pentenol; (4) acetic acid; (5) dihydro-dioxin; (6) propanoic acid; (7) propanoic acid methyl esther; (8) 2-cyclopenten-i-one; (9) 2-methyl-2-cyclopenten-1-one; (10) ethanone; (11) cymene; (12) furancarboxyldehyde; (13) 5 methyl-2-furancaboxaldehyde; (14) dimethoxybutedimine; (15) benzofuran; (16) phenol; (17) 2-methyl phenol; (18) cresol; (19) 4-methyl phenol; (20) creosol; (21) 4-ethyl phenol; (22) 4-ethyl-2-methoxy phenol; (23) decanal; (24) 2-methoxy-N-N-dymethyl benzoamine; (25) 2-methoxy-4-propyl phenol; (26) 2,6 dimethyl phenol; (27) eugenol; (28) trimethoxybenzene; (29) vanillin; (30) isoeugenol; (31) 2-furyl-5-methyl furan; (32) aethallymal; (33) methoxyeugenol; (34) 4-hydroxy-3,5-dimethyoxy benzaldehyde)

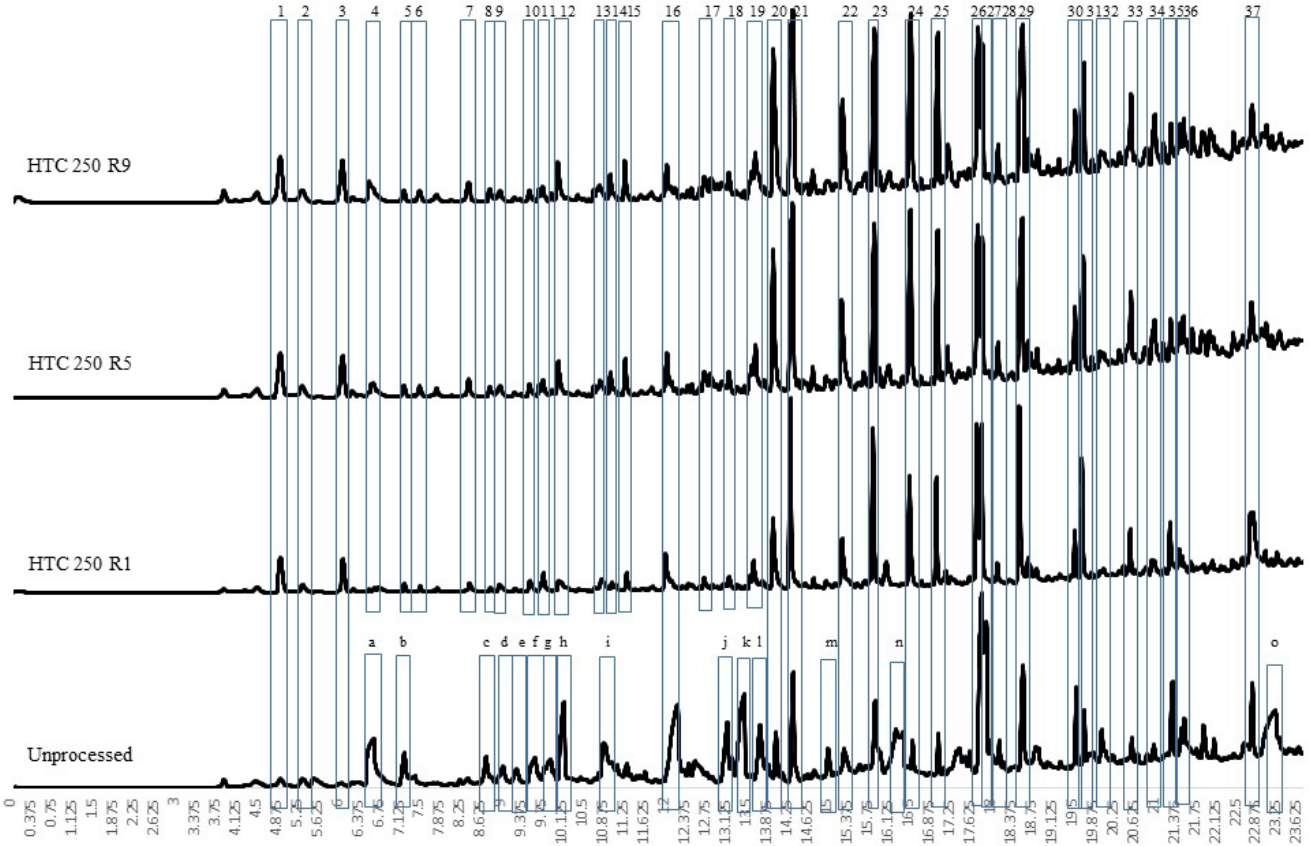

Figure 7.10b: Volatile organics evolved between 250 °C and 400 °C from bio-coals treated at 250 °C with recycled process waters. ((1) 2, methyl furan; (2) 2-propenoic acid 2-hydroxy ethyl esther; (3) 2,5 dimethyl furan; (4) valeric acid; (5) toluene; (6) ethanone; (7) 4 methyl phenol; (8) cyclopentanone; (9) methyl-3-octyne; (10) dimethoxy butane; (11) cyclohexanol; (12) cyclopenten-1-one; (13) furanmethanol; (14) methoxyclyclopentan-1-one; (15) acetylfuran; (16) cyclopentanone; (17) methylcyclopenten-3-one; (18) benzenediol; (19) 3-methyl cyclopentanone; (20) phenol; (21) 2-methyl phenol; (22) 4-methyl phenol; (23) cresol; (24) 4-ethyl phenol; (25) 4-ethyl-2-methoxy phenol; (26) 2,3-dihydro benzofuran; (27) 4 hydroxy-3-acetophenone; (28) eugenol; (29) 2,6 dimethyl phenol; (30) eugenol; (31) 2 dihydro-2-methyl benofuran; (32) isoeugenol; (33) trimethoxybenzene; (34) trymethoxy-5-methyl benzene; (35) acetophenone; (36) dimethoxy phenome; (37) methoxy eugenol; (a) acetic acid; (b) dihydrodioxin; (c) bioxirane; (d) isobutylacetic acid; (e) 2-methoxybutenol; (f) pyrolidethylamine; (g) propanediol; (h) furfural; (i) furanmethanol; (j) furanone; (k) dimethoxybutanamine; (l) cyclopent-1-one; (m) mthyl-2-hydroxy cyclopenten-1-one; (n) dimethyl heptane; (o) levoglucasan)

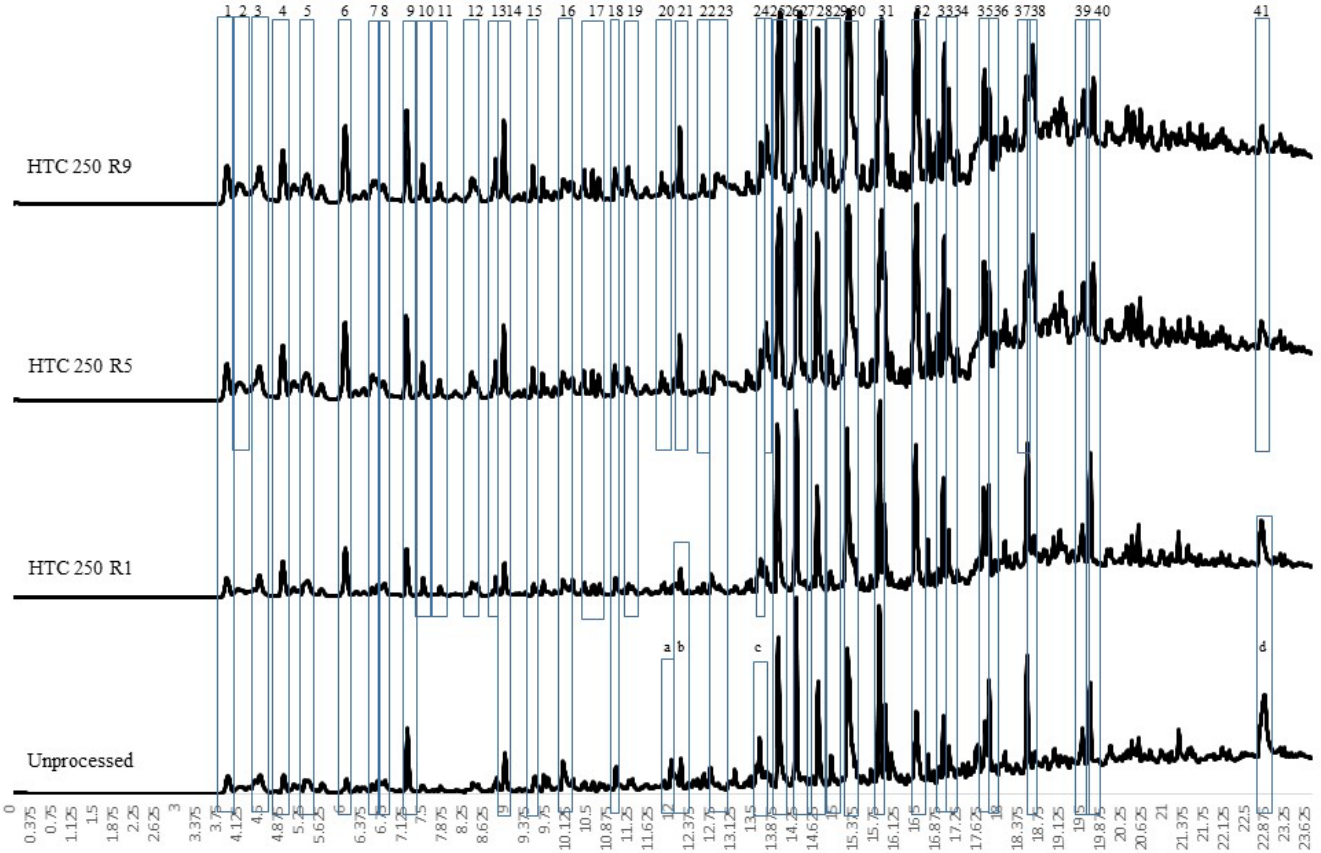

Figure 7.10c: Volatile organics evolved between 400 °C and 600 °C from bio-coals treated at 250 °C with recycling process waters ((1) ethylcycloputane; (2) pentane; (3) amino methyl propanol; (4) 2, methyl furan; (5) 2 ethyl butanal; (6) 2,5 dimethyl furan; (7) valeric acid; (8) octane; (9) toluene; (10) ethanone; (11) trimethylimidazole; (12) undecyonic acid methyl esther; (13) ethylbenzene; (14) xylene; (15) p-xylene; (16) 2-cyclopenten-1-one; (17) methyltoluene spp. (18) methyl cyclopentanone; (19) triethylbenzene; (20) fumeric acid ethyl esther; (21) methoxy methyl benzene; (22) indene; (23) 3-methylcyclopenten-1-one; (24) 1-ethyl-4-methoxy benzene; (25) acetonitrile benzene; (26) phenol; (27) 2-methyoxy phenol; (28) 2-methyl phenol; (29) dimethyl phenol; (30) cresol; (31) creasol; (32) 2-ethyl phenol; (33) ethylguaiacol; (34) 5-ethyl cresol; (35) 2,3 dihydrobenzofuran; (36) 4-hydoxy-2-methylacetophenone; (37) dioxybezene; (38) dimethoxy phenol; (39) eugenol; (40) trimethoxybenzene; (41) naphalene; (a) cyclopentenone; (b) methoxy toluene; (c) hydroxy-3-methyl cyclopenten-1-one; (d) levoglucasan)

For the 400 °C desorption (seen in Figure 7.10b), the chemistry between the recycled samples does not significantly differ, with the exception of the appearance of valeric acid (peak 4) from the process water in the latter runs. At 400 °C 2, methyl furan (peak 1) and 2,5 dimethyl furan (peak 3) appear with concentrations apparently increasing with repeated cycles; these are likely to be a product of humin formation via aldol addition or condensation of furfural like compounds. The phenolic compounds 4-methyl phenol (peak 22), cresol (peak 23), 4-ethyl phenol (peak 24) and 4-ethyl-2-methoxy phenol (peak 25) also increase in concentration, especially for the latter cycles. This possibly indicates the volatilisation of fragments of the aromatic clusters formed as part of the char formation in addition to the derived aromatic structures, which are chemisorbed to the char.

For the 600 °C pyrolysis run there was subtle differences between the cycles, with levoglucasan found within the first cycle bio-coal but not present in the fifth and ninth. While the data retains a peak in a similar area, this peak appears to be naphalene (peak 41) not levoglucasan (peak d), indicating the removal of cellulose. The compounds released at this temperature are predominantly phenolic, with toluene (peak 9), and many benzene based compounds including eithyl benzene (peak 13), xylene (peak 14), triethylbenzene (peak 19). Care is however required when interpreting this data as by this temperature the compounds detected are not necessarily the compounds desorbed off the char as secondary reaction chemistry during pyrolysis is likely taking place. The phenolic compounds seen in the previous runs appear strongly and are the predominant compounds evolved and are likely the fragments of the aromatic clusters formed as part of the char. After peak 40 (Trimethoxybenzene), the compounds afterward appear to be a multitude of different benzoalcohols and phenolic acids.

While the loss of the levoglucasan peak indicates the removal of cellulose, some caution is required when interpreting this data due potassium in the bio-coal. The presence of potassium is known to promote the decomposition of levoglucosan under pyrolysis [355]. While the fuels inorganic chemistry is discussed in detail the next section, Table 7.3 shows that the potassium within the bio-coal increases from 1000 mg/kg (db) in cycle 1, to 2300 mg/kg (db) and 3000 mg/kg (db) in cycles 5 and 9 respectively. It has been shown in Nowakowski et al. [356] and Nowakowski and Jones [357] that addition of 10,000 mg/kg potassium to willow and cellulose during pyrolysis leads the decomposition process of cellulose to different (low molecular weight) products such as acetic acid, propanoic acid and 1-hydroxy-2-butanone as opposed to levoglucosan. Consequently, the

removal of the levoglucasan peak would not definitively prove the removal of cellulose; albeit there is still evidence that cellulose is being removed in the thermogravimetric data presented in Figure 7.6. At the time of submission, reruns using demineralised samples were being undertaken but the impact of this potassium had yet to be assessed.

7.4.2. Influence of recycling process water on the bio-coal inorganic chemistry

Table 7.2 shows the changes in organic carbon, inorganic and heteroatom content and pH of the process water with increasing cycles. The notable main change is the accumulation of alkali metals and chlorine within the process water. For the 200 °C experiments, this appears to become stable by cycle six. This has an adverse effect on the slagging and fouling propensity of the bio-coal as it appears that the metals begin accumulating within the bio-coal. Metal analysis of the bio-coals are given in Table 7.3 along with the slagging and fouling indices. Note that the AI has increased from safe combustion before cycle 4 to probable slagging and fouling by cycle 9. The alkali index is still below that of the unprocessed *Miscanthus* given in Table 6.3, with an AI of 0.27, which would suggest a lower propensity. This is due to minimal re-accumulation of sodium and a higher energy density due to removal of oxygen. AI being based on kg of alkali per GJ as opposed to kg alkali per tonne of fuel.

For the 250 °C recycled bio-coals the same increase is observed, although the metal concentrations within the process water are approximately double in order of magnitude and still increasing by cycle nine. After cycle six there does appear a slowdown in accumulation of calcium, magnesium and sulphur within the process water, which also fits with the levelling of TOC within the process water but potassium, phosphate and chloride appear to be still increasing. The increasing concertation of metals within the process water is however not directly inversely proportional to the amount of metals within the bio-coal. The first recycle for example shows a decrease in magnesium, aluminium, phosphorus, calcium, magnesium and iron, with an increase in silicon. This is consistent with the results in Chapter 6 and supports the hypothesis that the organic acids created as part of the hydrothermal process are at least in part responsible for the extraction of the organically associated and precipitated inorganic materials within the starting biomass. By recycling the process waters back, the recycled acids aid the extraction of the organically associated and precipitated inorganic materials.

An ash fusion test was undertaken and the results are given in Figure 7.11. The results show that on the initial extraction there is a considerable improvement in deformation temperature, which increases from 1330 °C to 1570 °C for the 250 °C

treatment and remains similar for the third cycle. This change appears to be predominantly due to the increasing silicon fraction, which increases from 7,800 mg/kg to 15,100 mg/kg, and at the same time potassium increases from 1,040 mg/kg to 1,360 mg/kg. Thus, the relative ratio of potassium to silicon increases which reduces its fluxing potential. A similar increase in deformation temperature is seen for the 200 °C bio-coals, with an initial increase in deformation temperature from 1250 °C to 1350 °C. However this appears more due to an increase in calcium and magnesium as opposed to the significant reductions in potassium relative to silicon seen for the 250 °C bio-coals. The high silicon content of the recycled process water bio-coal may in fact be advantageous, from a fouling perspective as silicates are known to trap potassium within the ash, in the form of potassium silicates, preventing their potential volatilisation and subsequent fouling [358].

For the 250 °C cycles, the potassium within the bio-coal continues to increase with increased cycles, and its fluxing potential is offset initially by an increase in calcium on cycle three. After cycle three the increasing potassium starts to lower ash melting temperature, with a steady decline in deformation temperature, up to cycle 8 where the deformation temperature reaches 1140 °C, the same deformation temperature as the starting biomass (1140 °C), shown in Figure 6.9. A similar trend is shown for the 200 °C cycles, as despite increasing calcium content, the increasing potassium appears to bring about increased silicate fluxing, with 1150 °C reached by cycle four and deformation temperature dipping to 1110 °C by cycle 7. This result suggests that while recycling the process waters bring about an increase in both yield and energy density, recycling process waters during HTC does not overcome issues associated with slagging of the starting biomass, without an additional treatment stage.

Table 7.3: Inorganic and heteroatom analysis of bio-coals derived from recycling process waters and their influence of slagging and fouling indices

Temperature	Cycle	mg/kg Dry Basis											AI	BAI	R b/a
		Na	Mg	Al	Si	P	S	Cl	K	Ca	Mn	Fe			
HTC 200	1	148	400	74	6148	354	753	1764	1130	2802	50	115	0.08	0.09	0.49
	2	144	618	62	9535	423	640	2030	1848	3237	62	102	0.12	0.06	0.40
	3	183	714	75	9742	454	636	2673	2085	3582	86	94	0.14	0.04	0.44
	4	175	890	64	9753	538	709	2574	2633	4493	84	85	0.17	0.03	0.54
	5	156	991	77	10022	693	790	3186	2886	4684	116	106	0.18	0.04	0.56
	6	139	1147	61	9760	644	792	3217	3109	4988	125	105	0.19	0.04	0.62
	7	156	1247	106	10242	734	851	3560	3394	5160	119	112	0.21	0.04	0.63
	8	161	1050	80	9256	727	797	2762	2821	4697	110	88	0.17	0.03	0.61
	9	150	1143	77	9518	750	797	3196	3186	5877	111	108	0.20	0.04	0.70
HTC 250	1	82	525	191	7837	1145	1130	1721	1042	5279	82	143	0.05	0.14	0.57
	2	89	477	129	15106	596	1803	2142	1355	4172	56	92	0.07	0.07	0.26
	3	109	715	156	15018	954	1409	2581	1784	5227	76	104	0.09	0.06	0.34
	4	98	641	144	15459	746	1251	1969	1605	4559	58	95	0.08	0.06	0.29
	5	124	850	100	15463	943	1540	2586	2288	6383	117	124	0.11	0.06	0.41
	6	115	583	98	11376	1070	1146	2185	1395	3937	86	103	0.07	0.07	0.35
	7	114	800	118	13790	1146	1462	2687	2158	3914	114	134	0.10	0.07	0.33
	8	128	989	83	12799	1113	1345	3627	2713	4723	125	111	0.13	0.04	0.43
	9	115	1051	123	14532	796	1354	3354	2988	5645	114	99	0.14	0.04	0.43

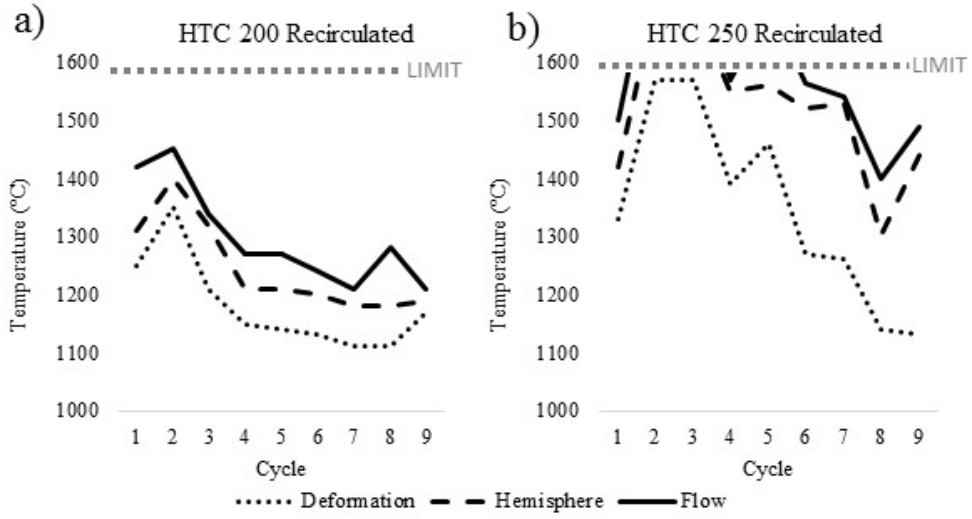

Figure 7.11: Ash transition temperatures for a) recirculation of process waters with HTC at 200°C, and b) recirculation of process waters with HTC at 250°C

In addition to slagging, the ash fusion test is often a good indicator of the fuels propensity to foul, the results would thus suggest an increase in fouling propensity with increasing treatments, and the increasing chlorine content would indicate increasing corrosion propensity. Slagging and fouling indices are given in Table 7.3 and show the AI, BAI and acid base ratio. Interestingly despite concentrations of alkali metals significantly increasing within fuel on repeated cycles the AI and acid base ratio suggest the fuel could still be managed in combustion systems in terms of slagging and fouling propensity. This appears due to the significantly higher energy density of the 250 °C recycled bio-coals; AI is based on kg of alkali per GJ as opposed to kg alkali per tonne of fuel. Consequently, despite similar levels of potassium and chlorine within the fuel as the starting feedstock, the energy density means less fuel would be required to meet the equivalent heat output and thus fouling should be lower per unit of energy. The low slagging risk indicated by the acid base ratio is predominantly due to significant increases in silicon concentrations within the fuel, which should reduce the fluxing brought about by the potassium.

In the HTC method used there was no additional washing of the bio-coals, the bio-coal was simply filtered from the process water and allowed to dry prior to analysis. Samples were not dewatered via centrifuge or mechanical process. Analysis of the process waters, given in Table 7.2, shows high levels of dissolved inorganics, particularly potassium which is found in concentrations of 3400 mg/l and chlorine which is in excess of 4000 mg/l by cycle nine. It is likely that residual process water is left within the char micro and macro pores on separation and will, on drying, deposit metal salts on the bio-

coal. The moisture content of the char appears to reduce with reaction severity, retention time, and increasing number of cycles, which would imply the sample is becoming increasingly hydrophobic and easier to dewater with increasing reaction severity and recirculation. This enhanced hydrophobicity and dewaterability is in agreement with the dehydration of the fuel [178, 179], observed in the results. The fuels were subsequently dried at 60 °C and while the wet mass of char is known it is difficult to proportion the free water (salt containing process water) to the bound water associated with the fuel. For the 250 °C recycled process waters, initial moisture content decreases from 76 % to 54 % over the nice cycles and as such it is likely a significant proportion of the process water will remain. It is likely that a proportion of the salts from the residual process water will be readily volatilised during combustion, contributing to fouling and corrosion. The chloride salts within the process water deposits, may however be retained within the char burn due to their higher thermal stability, and then be reincorporated and fixed into the ash [359].

Additional leaching of these alkali metals and chlorine would likely be possible, via mechanical water recovery post carbonisation and the incorporation of an additional washing procedure post carbonisation. This should remove metal salts deposited on the bio-coal and residual chloride which forms weak chlorine hydrogen interactions with the hydrogen atoms on the char surface and are easily removed by washing [149]. The impact of an additional water treatment on the energy content and energy yields has not been assessed in this instance. Dependent on the organic carbon removed as part of this washing procedure there could be scope for carbon recovery via treatment options such as anaerobic digestion with this ‘secondary’ wash water potentially less susceptible to inhibition of the methanogenic phase by volatile acids, long chain fatty acids, phenol, alkyl phenols alkali and alkaline earth metals, which foreseeably may cause issues in the direct anaerobic digestion of process waters [285, 286]. Lower organic carbon within the wash water may also make nutrient recovery more feasible.

7.4.3. Influence of recycling process water on the bio-coal combustion behaviour

The DTG burning profiles for bio-coal from the 200 °C recycling treatments and 250 °C recycling treatments are given in Figure 7.3 and Figure 7.6 respectively. The results for the 200 °C recycling treatments, shows there is no real shift in the first initiation temperature, nor the burn out temperature. The profile also maintains the characteristic two peak profile observed for the 200 °C bio-coals with varying retention time (Chapter 6). With increasing cycles the first volatile combustion peak decreases with increasing

cycles, while the second, char burning peak increases with increasing cycles. This gives the bio-coal a similar combustion profile to that produced at 200 °C 4-8 hour retention time. Proximate and ultimate analysis results support this. While the burn out temperature appears to remain the same, the char burn peak temperature decreases, which would imply the char burning is more reactive. This would fit with an increase in alkali metals observed in Table 7.3 and suggests a portion of the potassium remains within the char during combustion. Alkali metals, particularly potassium, increase char reactivity though metal catalysed oxidation of the carbon surface [207], through the intimate bonding with oxygen functionalities [160, 209].

For the 250 °C recycled process water bio-coal increasing cycles results in a fuel with a far more 'coal like' burning profile; the burning profile of the ninth cycle is similar to the burning profile to that seen for 250 °C treated bio-coal with 8 and 24 hour retention times. Unlike the treatments with increasing retention time, where burn out temperature increased with increasing duration of HTC, char burnout temperature reduces slightly along with a reduction in peak temperature (char burn). This would suggest, like the 200 °C recycled process water bio-coals, the char is more reactive. This also fits with an increase in alkali metals observed in Table 7.3 and suggests a portion of potassium remains within the char during combustion and intimate bonding between potassium and the char [160, 209].

The first initiation temperature / ignition temperature appears to remain similar for all cycles but the characteristic volatile peak seen in the 200 °C recycled process water bio-coals and the combustion profiles for the 250 °C treatment with zero and one hour retention times, becomes increasingly less distinct. By the latter four cycles, the second initiation temperature is marked more by the acceleration in weight loss as opposed to a second peak. Based on the pyrolysis GCMS spectra given in Figure 7.6b, this volatile reduction appears to be due to removal of cellulose from within the fuel, with the removal of the levoglucasan peak (peak 27), a characteristic compound derived from the thermal decomposition of cellulose, not present in the latter cycle. The 250 °C recycled process water bio-coals do however appear to undergo pre-ignition, low temperature thermal decomposition, with the formation of a low temperature volatile peak starting around 100 °C and 270 °C whereby the first initiation temperature is reached, and this increases with increasing cycles. Based on the pyrolysis GCMS spectra given in Figure 7.10a these compounds appear to be phenols and a host of methoxybenzoaldehydes and likely chemisorbed hydrothermally derived aromatic structures.

The low temperature evolution of these compounds could pose risk for handling and storage of the recycled bio-coal. In Chapter 5 (now presented in Smith et al. [260]) it was demonstrated that 250 °C treated *Miscanthus* was highly friable with a HTG of 150. This would suggest potential for generation of dust during handling and without appropriate housekeeping this dust can accumulate on hot surfaces of many electrical and mechanical devices, such as conveyers, dryers, hot bearings, and other machinery [360]. The low temperature volatilization of combustible gases could be a source of ignition. Bio-coal appears to have many properties more similar to coal than biomass; biomass is a reactive solid fuel capable of self-heating and self-igniting, especially during conveying and processing [181, 360] and consequently further analysis is needed to whether the same risks apply to bio-coal.

For biomass, spontaneous combustion is associated with storage, especially in the presence of moisture. Since coal is far less hydrophilic than biomass, open-air storage is possible for coal whereas biomass must usually be stored in silos. The stored biomass within the silos can then undergo biological and chemical processes, which consume oxygen, generate heat and release combustible gases, which when hot can ignite. Biomass also has a higher burning rate than coal, meaning that any ignition flame will propagate much more quickly for biomass and with the larger mixture ratio of biomass in co-firing plants [181].

A higher burn rate than coal appears likely for bio-coal based on the TGA burning profile but water immersion tests of bio-coal pellets, presented in Kambo and Dutta [179], would suggest that open air storage could be possible with bio-coal due to the enhanced hydrophobicity, which may overcome issues with silo storage. Ramírez et al. [361] developed a methodology for determination of ignition risk based on burning profiles in oxygen, with Jones et al. [207] and Chin et al. [360] developing the method to be based on burning profiles in air. The method uses the temperature of the maximum rate of weight loss temperature and the apparent first-order activation energy (E_a) at the point of maximum weight loss using the data from the conventional thermogravimetric analysis, to rank self-ignition propensity of fuels. Based on this, the bio-coal data would suggest a decreased risk of self-ignition when compared to biomass, especially for the 250 °C recycled process water bio-coal, but a higher risk to that of coal.

The low temperature thermal decomposition of the 250 °C recycled process water bio-coal could potentially be problematic for pulverizing mills, as pulverising mills are typically operated at elevated temperatures (approx. 150 °C) in pulverised fuel

applications and thermal decomposition of the fuel within the mill would be undesirable. The higher grindability of the 250 °C bio-coal, could however partially negate this as a HGI of 150 is higher than most coals (typically between 30 and 100) so the pulverisers should require lower energy input than would otherwise be required for coal and could therefore operate at lower temperature [260].

7.5. Conclusions

Recycling process waters brings about an increase in product mass yield at both treatment temperatures; for 200 °C treatments this increases from 65% and stabilises at between 71 % and 73 % after four cycles. For the 250 °C treatments, yields increased from 46 % to 57 %, and by the final cycle it appeared to still be increasing. A modest increase in energy density was seen for the for the 200 °C treatments from 18.9 MJ/kg to 19.7 MJ/kg, with the latter remaining reasonably consistent for runs two to nine, consequently the overall energy yield increases from 68% to 77 % after four cycles.

For the 250 °C treatments energy density increased from 24.2 MJ/kg to 28.9 MJ/kg on the ninth cycle, through reduction in fuel oxygen and an increase in carbon. This increases the overall energy yield from 61% to 91 %. The H/C ratio increases for the 200 °C bio-coals and remains constant for the 250 °C bio-coals, which appears to suggest hydrogen donation from organic acids or due to the influence of alkali metals. Process chemistry would suggest char formation though dehydration and addition of hydrogen as opposed to decarboxylation suggested by H/C O/C ratios. Recycling the process waters appears to catalyse the removal of cellulose from the bio-coal, with no cellulose apparent by cycle 5.

It is hypothesised that the recycled organic acids hydrolyse the hemicellulose and cellulose to furfural like compounds at a lower temperature and increase saccharide concentrations within the process water. Increased saccharide concentrations favour aromatization and repolymerisation which better enables the decomposition products to undergo polymerization, which otherwise undergo further degradation to organic acids. It is proposed that the slow heating rate and hour retention time overcome kinetic limitations imposed by faster heating rates and shorter retention times previously reported.

Recycling the process waters at 200 °C gives a combustion profile more similar to HTC 200°C+4h and HTC 200°C+8h, with a reduced volatile burn and increased char burn, the char burn is however more reactive. Recycling the process waters at 250 °C

gives an increasing ‘coal like’ burning profile, more similar to HTC 250°C+8h and HTC 200°C+24h but with a more reactive char burn. The 250 °C recycled bio-coals do however form a low temperature volatile peak evolving phenols and a host of methoxybenzoaldehydes. This could pose risks in terms of handling and further analysis is required.

After an initial improvement in fouling and slagging propensity brought about, though enhanced acid leaching of the fuel, recycling process water appears to have an adverse influence on the fouling and slagging propensity of the fuel. Mechanical water recovery and the incorporation of an additional washing procedure post carbonisation may however overcome this. The impact of an additional water treatment on the energy content, energy yields and inorganic chemistry has not been assessed.

8. Influence of particle size during hydrothermal carbonisation of lignocellulosic biomass

8.1. Abstract

HTC is known to improve grindability and thus it would be best to use the largest possible feedstock size to avoid energy intensive size reduction. Bio-coals are however known to develop an outer oily film and it has been suggested in the literature that the formation of this layer may limit the intimate contact between the biomass and process water. Given that the process chemistry relies on direct contact with water, this layer could change the process chemistry in larger particles, influencing the fuel properties. The formation of an oily layer may also prevent the extraction of inorganic materials from within the biomass, preventing the improvement in slagging and fouling propensity often reported. In this chapter, willow was processed using cylinders at between 1-2 mm and 4.0 cm in diameter. The results showed that at 4.0 cm there was still complete conversion of the cellulose, with limited change in hydrothermal chemistry. Increasing particle size also appears to initially improve energy density of the resulting fuel rising from 26 MJ/kg to 28 MJ/kg at 2.5-3.0 cm diameter. Beyond 3.0 cm there was a slight reduction in energy density to 27 MJ/kg, which is believed to be due to the start of heat transfer limitations when using retention times of one hour. This becomes more apparent when treating the biomass with bark as the bark retains the cylinder integrity. A reduction in volatile carbon with increasing size suggests that size reduces the diffusion of preliminary products into the bulk water which enhances hydrolysis and polymerisation within the particle. This significantly improves the grindability behaviour of the fuel with an HGI of 62 for the 1-2 mm samples, increasing to 177 at 3.0 cm. This would represent a huge reduction in the energy requirements for milling if the fuel is used in pulverised fuel applications. Metal analysis suggests that there is free movement of water though the particle at 4.0 cm in diameter and metal extraction is not limited though the formation of a low water permeable hydrolysis layer. Ash fusion testing has shown that processing willow with the bark has a positive influence on the slagging and fouling behaviour of the fuel due to the increased calcium and phosphorus in the ash.

8.2. Introduction

Studies into HTC have largely focused on ground lignocellulosic material, typically in the range of 600 to 1200 μm. As HTC of lignocellulosic material results in a bio-coal which is highly friable it is expected that an industrial process would take advantage of this and would use the largest possible chips to avoid energy intensive size

reduction [43]. There is however, uncertainty as to how the HTC mechanism works in larger particles with limited reports on the influence of particle size on HTC and even the more established HTL and HTG. In reviews such as Libra et al. [28] it is assumed the solid product of bio-coal is largely formed by re-condensation reactions, yet such findings were based on research using finely ground biomass, and high cellulose contents. In larger particles where the more recalcitrant crystalline cellulose and lignin is present the more recalcitrant nature of these materials mean they become 'hard templates' of which the 'secondary char' nucleates around [28, 77].

Mosteiro-Romero et al. [98] looked into the influence of size in HTL, but within temperature ranges still applicable to HTC, using 400–800 μm mesh particles along with spherical particles of diameters 0.4–0.5 cm and 0.9–1 cm. For HTL and HTG the feedstock is ideally completely liquefied, however, in practice, operational parameters prevent complete conversion leading to the production of char (bio-coal). This study indicated that at temperatures of 250 ºC typically, associated with HTC and heating rates of 20–35 ºC min^{-1}, there are two distinct zones; a hydrolysis zone on the outside of the particle which is in contact with the process water and a pyrolysis zone within the particle which forms due to limited contact with water, as shown in Figure 8.1. The extent of the pyrolysis zone appearing to be determined by the thickness of the hydrolysis zone [98]. To the best of the author's knowledge no similar study exists for HTC.

This result is significant as in HTC intimate contact with water is a pre-requisite for HTC as it is the water which catalyses the thermal decomposition of hemicellulose, cellulose and lignin at 180 °C, 200 °C and between 230 °C and 260 °C respectfully, along with providing the water required in hydrolysis [11, 28, 75, 76]. Additionally the water provides the medium for the hydrolysed fragments to react and recombine [11, 28, 86]. Without the presence of water the thermal decomposition of the biomass components will occur at higher temperatures and produce different products as the decomposition will typically not include the addition of water. For example under pyrolysis conditions hemicellulose will decompose between 200-260 ºC, decomposition of cellulose will start between 240 ºC and 350 ºC and lignin which decomposes between 280 ºC and 500 ºC [186]. Given HTC is typically undertaken between 180 ºC and 260 ºC, the formation of a 'pyrolysis zone' within the core of larger particles would result in a largely unreacted core, more similar to torrefied fuels, whereby the hemicellulose and some cellulose is degraded [10]. When hydrothermally treating at temperatures of 250 ºC, this will typically result in fuels with a higher oxygen content, higher volatile carbon content, lower fixed

carbon content and lower calorific value, as seen for the HTC 250+0h sample in Chapter 6, due to the presence of cellulose within the fuel, in the larger diameter particles. Moreover, the formation of a low water-permeable hydrolysis layer could be highly significant when trying to extract inorganics and heteroatoms from biomass, as development of the hydrolysis zone may reduce or prevent the extraction of these elements though water diffusion limitations preventing their extraction.

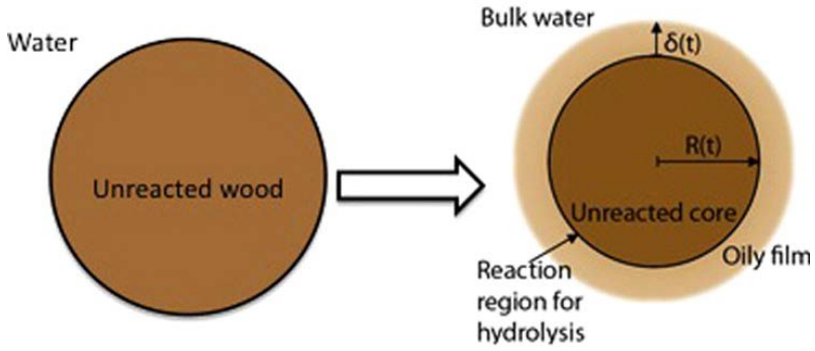

Figure 8.1: Formation of hydrolysis and pyrolysis zones within a wooden sphere undergoing hydrothermal treatment, adapted from Mosteiro-Romero et al. [98].

This chapter looks into larger feedstock sizes in an attempt to identify the optimum particle size and minimising energy intensive size reduction. The chapter will go on to demonstrate how particle size influences the organic and inorganic properties of the bio-coal and attempt to better understand the mechanisms of the HTC of larger particles of lignocellulosic biomass and how these properties will go on to influence the combustion properties of the resulting bio-coal.

8.3. Methodology

8.3.1. Materials

Samples of short rotation coppice willow (*Salix Spp.*) were obtained from Rothamsed Research. Samples were obtained as coppiced stems of varying diameters from the same plot and the same species to minimise sample variation. Samples were subsequently cut into cylinders according to sample diameter, to cylinders ranging between 1,0 and 4.0 cm, as shown in Figure 8.2. A 1-2 mm sample was obtained by putting samples though a cutting mill (Retsch, Germany) using a 4 mm grate. Cylinders were chosen as when perennial trees grow they grow from the cambium, a layer just below the bark, which produces the phloem and xylem cells. The phloem being the cells in the bark responsible for the transportation of soluble organic compounds made during photosynthesis, while the xylem, or wood as its more commonly referred, transports water

and nutrients from roots to shoots and leaves. As the tree grows new xylem cells are formed just below the bark while the more central cells undergo lignification, whereby lignin is deposited in a secondary cell wall, water is eliminated, forming a hydrophobic environment and the cells become both rigid and impermeable, before undergoing programmed cell death, forming the heartwood, with the living xylem the sapwood [362]. Consequently, plant tissue on the vertical plane should be of similar chemistry while chemistry will vary on the horizontal plane (see Figure 8.2). For each size, the samples were run with and without bark to see what influence the bark had on the process.

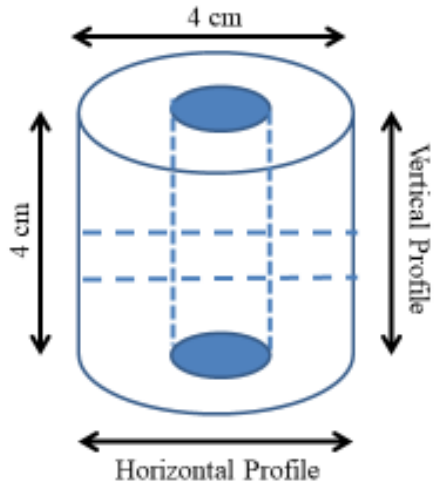

Figure 8.2: Schematic of a 4 cm willow cylinder, where the cross sections indicate sample location for analysis

8.3.2. Hydrothermal carbonisation

HTC was performed using the modified 2000 ml high pressure batch reactor (Parr, USA) at 250 °C as described in Section 3.2. For each run a 10 % solids loading was used, with a combined mass of approximately 1000 g a run. Obtaining exactly 100 g of sample using samples of a specific size was not possible so the reactor was loaded close to 100 g and the water adjusted accordingly. To ensure compete submersion 316 stainless steel mesh was used to submerge the particles and experiments were undertaken as described in Section 3.2.2.2.

8.3.3. Analysis

8.3.3.1. Sample preparation

For bulk property analysis samples were either homogenised for bulk property analysis by grinding below 100 µm using a cryomill (Retsch, Germany) or samples were taken on either the horizontal or vertical plane, as shown in Figure 8.2, using a 10 mm core borer in the HTC samples or a 10 mm drill bit in the unprocessed willow samples.

8.3.3.2.Inorganic analysis

Inorganic elemental composition was determined by AAS, as described in Section 3.6.3. 0.1 g of sample was digested in 10 ml nitric acid using 50 ml conical flasks and refluxing funnels, as described in Section 3.6.1. Phosphorus was determined using the colorimetric method described in Section 3.6.4 and shown in Figure 3.16.

8.3.3.3.Organic analysis, combustion properties and ash measurement

Carbon, hydrogen, nitrogen, sulphur and oxygen content was determined using a Flash 2000 CHNS-O analyser (Thermo Scientific, USA), with the method described in Section 3.4.2. The volatile and fixed carbon component of the proximate analysis carried out using thermo-gravimetric analysis (Mettler Toledo, Switzerland) as described in Section 3.3.3. Ash content was determined using a muffle furnace, as described in Section 3.3.2. Moisture content was determined using a moisture oven as described in Section 3.3.1. The calorific value was determined using Dulong's Equation (see Equation 3.11). Figures are corrected in accordance with ASTM D3180-15, with hydrogen and oxygen values corrected to account for moisture. Burning profiles, ignition, flame stability and burnout temperatures were obtained by TPO, as described in Section 3.8.

8.3.3.4.Ash fusion testing

Ash fusion testing (AFT) was performed using a Carbolite digital ash fusion furnace, as described in Section 3.7.1.

8.3.3.5.Volatile component analysis

Volatile component analysis was carried out via pyrolysis-GCMS (CDS analytical, USA; Shimadzu, Japan) using a 60 meter 0.25 mm RTX-1701 column (Restek, UK). All samples were routinely analysed in duplicate at 550 °C using 20 $°Cms^{-1}$ heating rate, with the pyroprobe operating in trap mode. Procedure described in Section 3.11.

8.3.3.6.Resistance to Milling

Resistance to milling was calculated using the Hardgrove Grindability Index (HGI). The HGI equivalent test procedure is described in Section 3.9.

8.3.3.7.Hydrophobicity testing

Moisture retention of samples was analysed by drying samples at 105 °C overnight in a laboratory oven (Memmert, Germany). Approximately 10 grams of sample

was then placed on a sample tray and loaded into a 48 litre sealed box with approximately 5 litres of water in the base, which acts as a humidity chamber. The humidity chamber was then placed in a large sample drying oven at 30 °C (Memmert, Germany), giving 100 % relative humidity and stored for 7 days in these conditions. Samples were removed from the humidity chamber and placed within a sample drying oven at 20 °C (Memmert, Germany); which is around 70 % relative humidity. Moisture content was determined by taking a representative sample and analysing in a moisture oven at 105˚C under nitrogen in accordance with BS EN ISO 18134-2:2015. Subsequent samples were taken every 24 hours.

8.3.3.8.Solid State C13 NMR analysis

For a limited number of samples Solid State C13 NMR was undertaken using a Bruker Avance III spectrometer and the EPSRC Solid Statye NMR service at Durham University. The instrument was operated at 75.4 MHz at room temperature, using both 13C direct-polarization Magic Angle Spinning (DPMAS) and cross-polarization MAS (CPMAS). Ground samples were packed into 4 mm o.d. zirconia rotors and a 4 mm HX MAS probe was used with a magic-angle spinning rate of 10 kHz and proton decoupling. For DPMAS, the 13C 90º pulse length was set at 2.5 Âµs with a recycle delay of 30s. 1500 scans were collected. For CPMAS a recycle delay of 1s was used, with between 10000-18000 scans.

8.4.Results

8.4.1. Influence of size on the bulk properties of the fuel

The bulk properties of the bio-coals derived from differing size willow cylinders are given in Table 8.1, with the carbon, oxygen and energy density (HHV) given in Figure 8.3. The results show that processing with increasing size results in an increase in carbon density up to 2.0 and 2.5 cm diameter stems for processing with and without bark. After which there is a slight reduction in carbon content up to 4.0 cm diameter stem. All samples above 1.0 cm in diameter have a higher carbon content than the starting biomass. When processing with bark, carbon content increases from 68.3 % to 70.8 % carbon at 2.0 cm particle diameter, reducing to 69.4 % at 4.0 cm. Processing without bark results in a higher carbon content in the bio-coal but this could be due to the feedstock without bark having an overall higher carbon content; bark having a slightly lower carbon content. When processing without bark a carbon content of 71.9 % is seen for 2.5 cm diameter, decreasing slightly to 71.0 % at 4.0 cm diameter. It is worth noting that despite the slightly

lower energy content with bark, bark accounted for between 12 and 16 % of dry matter depending on size. Consequently, removal of bark represents a reduction in feedstock and the lower energy density will be offset by the increase in product.

The inverse is seen for oxygen content decreasing from 23.9 % in the 1-2 mm sample, decreasing to 21.4 % oxygen at 2.0 cm particle diameter, before increasing to 22.7 % at 4.0 cm for the samples processed with bark. The oxygen content is slightly lower in the samples without bark, with the lowest oxygen content 20.7 % at 2.5 cm diameter. Oxygen content increases to 22.1 % for the 4.0 cm sample but the oxygen is still lower than the 1.0 cm diameter sample, which has 22.9 % oxygen. The influence of the increasing carbon content and decreasing oxygen content results in an increase in energy density with increasing size, and becoming reasonably constant at around 2 cm in diameter. The samples processed without bark have a higher overall energy density due to the higher carbon content and lower oxygen content and the influence this has on energy density, as shown in Dulong's Equation (see Equation 3.11). Energy density of the bio-coals begin to decline slightly above 2 cm in diameter, with the decline increasing after 3.5 cm in diameter albeit the energy density is still above that of the 1-2 mm and 1.0 cm samples. Ash content of the bio-coal appears to generally increase with increasing size for samples with and without bark.

The influence of bark appears to have the greatest impact on the volatile chemistry of the fuel. Figure 8.4 shows the volatile and fixed carbon of the samples treated at differing sizes with and without bark. While the samples without bark appear to remain reasonably consistent with between 51 and 52 % volatile carbon, the 1-2 mm sample has a volatile carbon content of 56 % reducing to 51 % in the 3.5 cm sample. The fixed carbon within the bio-coal increases as the volatile carbon decreases. The proximate analysis was undertaken using TGA and the 1st derivative (DTG) of the volatilisation stage is given in Figure 8.5. The DTG profile indicates significant difference between the profiles for the samples processed with bark and processed without. A double peak present on the samples treated with bark, which is not present in the sample processed without.

Appendix Figure 11.1 shows the same profiles but with the addition of unprocessed willow and unprocessed bark. The results show a large peak, with the greatest weight loss at approximately 350 ºC and most likely the thermal decomposition of cellulose, in the whole unprocessed willow and unprocessed bark, although this peak is smaller in the bark. A shoulder on the peak at around 300 ºC whole unprocessed willow is most likely the thermal decomposition of hemicellulose [185, 186]. Py-GCMS analysis

presented in Chapter 6 indicated that the cellulose is predominantly degraded during HTC with retention times of one hour or longer at 250 °C. The volatile material in bio-coals treated for one hour or longer at 250 °C appear to be methyl furans derived during humin formation via aldol addition or condensation of furfural like compounds [309], and methyl and ethyl phenols derived from humic substances derived within the hydrothermal process and from the decomposition of lignin [363]. The DTG results presented in Figure 8.5a, could suggest the presence of residual cellulose remaining within the bark, which is not degraded and not present within the debarked samples.

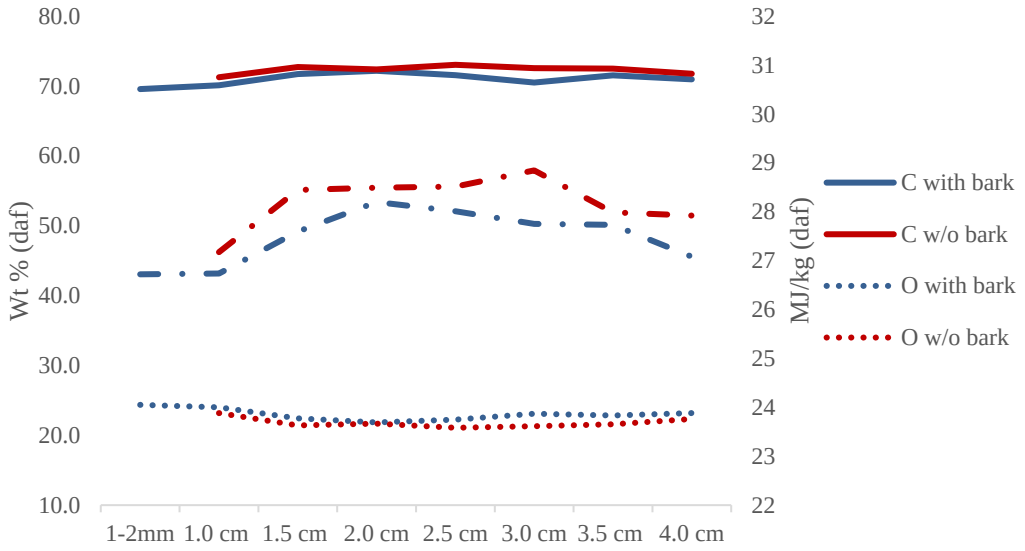

Figure 8.3: The carbon, oxygen and HHV of homogenised bio-coals derived from differing feedstock size, processed with and without bark and given on a dry ash free basis

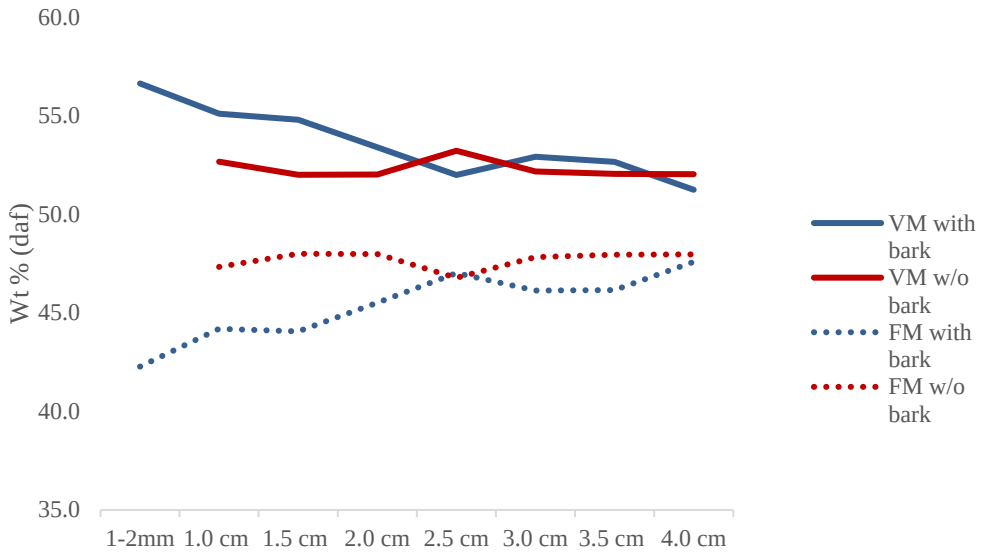

Figure 8.4: Proximate analysis of homogenised bio-coals derived from differing feedstock size and given on a dry ash free basis

Table 8.1: Bulk properties of homogenised bio-coals derived by varying feedstock size

Sample		% Dry Basis																
		C	H	N	S	O	Ash (%)	Volatile Matter (%)	Fixed Matter (%)	MJ/kg	HGI
Unprocessed with Bark		53.3 ± 2.0	6.5 ± 0.2	0.6 ± 0.0	0.0 ± 0.0	38.8 ± 0.0	0.9	88.9	10.3	20.4	0
Unprocessed Bark (only)		50.4 ± 0.7	5.5 ± 0.1	1.8 ± 0.0	0.0 ± 0.0	37.5 ± 0.4	5.0	74.4	20.6	18.3	-
HTC 250 With Bark	1-2 mm	68.3 ± 0.9	5.2 ± 0.1	0.7 ± 0.0	0.0 ± 0.0	23.9 ± 0.1	1.9	56.6	41.5	26.2	62
	1.0 cm	69.3 ± 1.1	5.1 ± 0.1	0.7 ± 0.0	0.0 ± 0.0	23.7 ± 0.2	1.3	55.1	43.6	26.4	153
	1.5 cm	70.3 ± 0.3	5.0 ± 0.0	0.7 ± 0.0	0.0 ± 0.0	22.0 ± 0.1	2.0	54.8	43.2	27.0	163
	2.0 cm	70.8 ± 0.5	5.3 ± 0.9	0.5 ± 0.0	0.0 ± 0.0	21.4 ± 0.2	2.0	53.4	44.6	27.7	172
	2.5 cm	70.3 ± 0.2	5.3 ± 0.1	0.7 ± 0.0	0.0 ± 0.0	21.8 ± 0.3	1.9	52.0	46.1	27.5	168
	3.0 cm	69.3 ± 0.9	5.5 ± 0.2	0.7 ± 0.0	0.0 ± 0.0	22.7 ± 0.0	1.8	52.9	45.3	27.3	173
	3.5 cm	70.0 ± 0.1	5.2 ± 0.3	0.4 ± 0.0	0.0 ± 0.0	22.4 ± 0.1	2.2	52.7	45.1	27.1	170
	4.0 cm	69.4 ± 0.9	4.9 ± 6.4	0.8 ± 0.0	0.0 ± 0.0	22.7 ± 0.3	2.2	51.2	46.5	26.5	167
Unprocessed without Bark		51.1 ± 0.8	6.4 ± 0.1	0.2 ± 0.0	0.0 ± 0.0	39.8 ± 0.1	0.5	85.4	10.1	20.0	0
HTC 250 Without Bark	1.0 cm	70.4 ± 0.4	5.0 ± 0.0	0.5 ± 0.0	0.0 ± 0.0	22.9 ± 0.5	1.2	52.0	46.7	26.8	135
	1.5 cm	71.8 ± 0.4	5.3 ± 0.6	0.4 ± 0.0	0.0 ± 0.0	21.1 ± 0.1	1.3	51.3	47.4	28.1	155
	2.0 cm	71.4 ± 1.3	5.4 ± 2.1	0.4 ± 0.0	0.0 ± 0.0	21.4 ± 0.2	1.4	51.3	47.3	28.1	168
	2.5 cm	71.9 ± 0.4	5.2 ± 0.1	0.5 ± 0.0	0.0 ± 0.0	20.7 ± 0.0	1.6	52.3	46.0	28.0	164
	3.0 cm	71.5 ± 0.1	5.6 ± 0.1	0.4 ± 0.0	0.0 ± 0.0	21.0 ± 0.1	1.6	51.3	47.1	28.4	177
	3.5 cm	71.0 ± 1.3	5.0 ± 0.9	0.6 ± 0.0	0.0 ± 0.0	21.1 ± 0.0	2.0	51.0	47.0	27.4	170
	4.0 cm	71.0 ± 0.3	5.3 ± 7.8	0.5 ± 0.0	0.0 ± 0.0	22.1 ± 0.1	1.1	51.5	47.5	27.6	163

The phloem fibres in bark are known to have think lignified cell walls [364], which may increase the recalcitrance of the cellulose as the lignin binds the cellulose microfibers within the secondary cell walls [362, 365]. Py-GCMS analysis of the bark at 550 °C, shown in Figure 8.6a, indicate however that there is only limited cellulose within the analysed bark sample as the levoglucasan peak (peak 35) is not present. This could be in part because the sample was taken from the periderm, which is the outer layer of the bark and may consist of dead lignified tissue similar to that of the heart wood of the xylem [362], the phloem fibres might have remained with the woody samples. This first peak in Figure 8.5a, which could suggest the presence of residual cellulose remaining within the bark, reduces with increasing size. This could be in part due to a reduction in the ratio of bark (phloem) to wood (xylem), however the results do suggest that by 3.5 cm there is complete removal of this first peak and a reduced bark to wood ratio would not explain this. Consequently, the results would indicate that with increasing size you get a more complete conversion of the cellulose within the larger particles, particularly in the phloem cells within the bark.

The finding that increasing size when processing with bark gives a more complete conversion would appear to contradict the findings of Mosteiro-Romero et al., [98], whereby at 250 ºC there is the formation of a hydrolysis zone on the outside of the particle which is in contact with the process water and a pyrolysis zone within the particle which forms due to limited contact with water, as shown in Figure 8.1. In Mosteiro-Romero et al., [98] increasing the particle size increased this pyrolysis zone. Given the thermal decomposition of cellulose will start between 240 ºC and 350 ºC [186], it would appear likely that cellulose would be present within centre of the particle. For the 2.5 cm to 4.0 cm samples, core samples have been taken on the vertical and horizontal planes as shown in Figure 8.2 and analysed by Py-GCMS to assess for any changes resulting from the presence of the hydrolysis and pyrolysis zones as described above. The results for the 4.0 cm samples are shown in Figure 8.6 and indicate complete removal of cellulose with the loss of the levoglucasan peak (peak 35) in all samples. Moreover, Figure 8.6c and Figure 8.6d give the vertical profiles of the samples hydrothermally reacted with and without bark. In these samples, the starting xylem should be of similar chemistry and show limited differences between both profiles. This would indicate there is not the presence of a hydrolysis and pyrolysis zone as hypothesised and complete hydrothermal carbonisation takes place in particles up to 4.0 cm in diameter when using retention times of one hour or more.

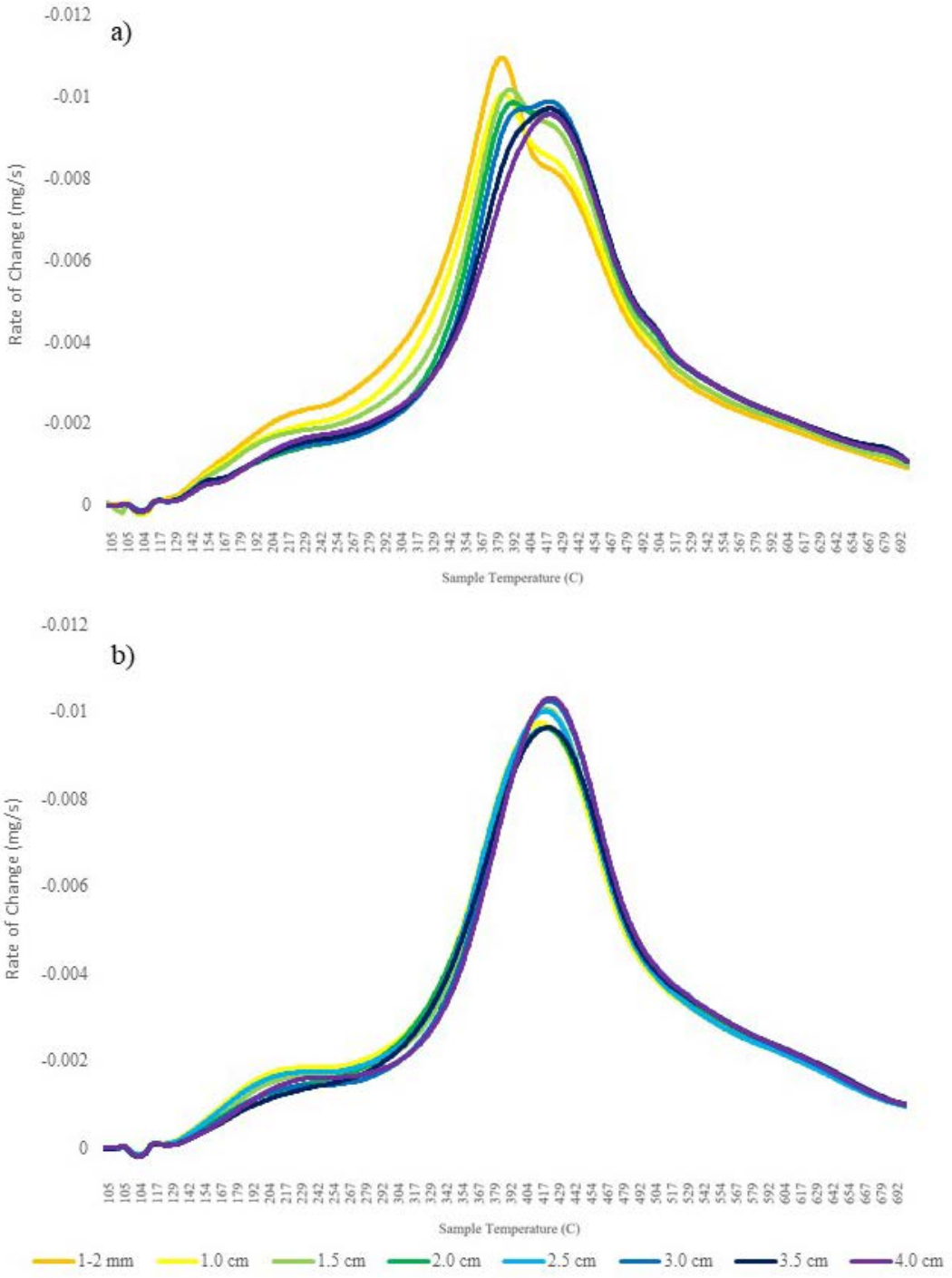

Figure 8.5: Derivative thermogravimetric (DTG) devolatilisation profiles for willow hydrothermally treated at 250 °C; a) with bark and b) without

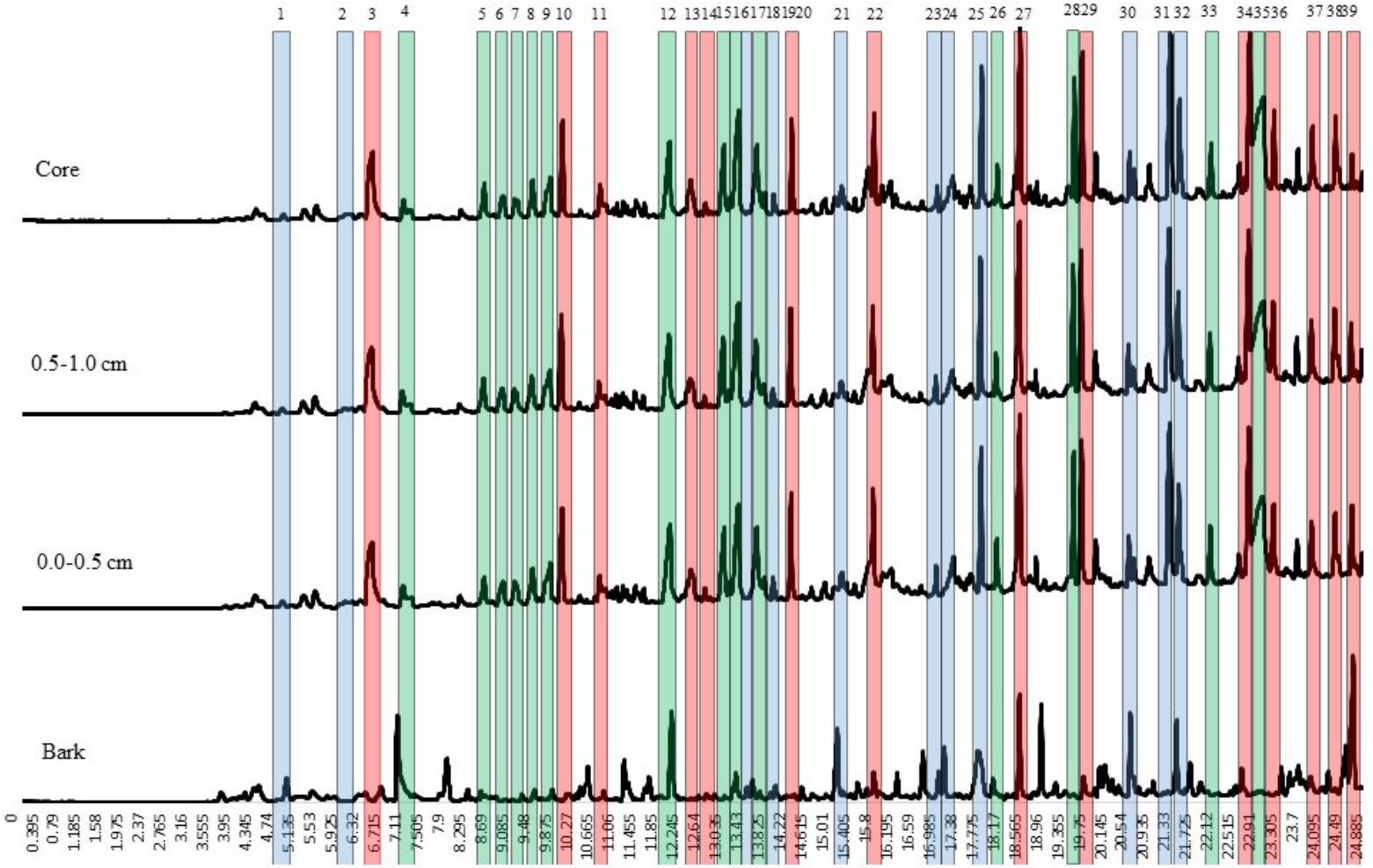

Figure 8.6a: Pyrolysis GCMS analysis at 550 °C of the changes volatile chemistry through the horizontal profile of the unprocessed willow in the 4.0 cm cylinders with bark.

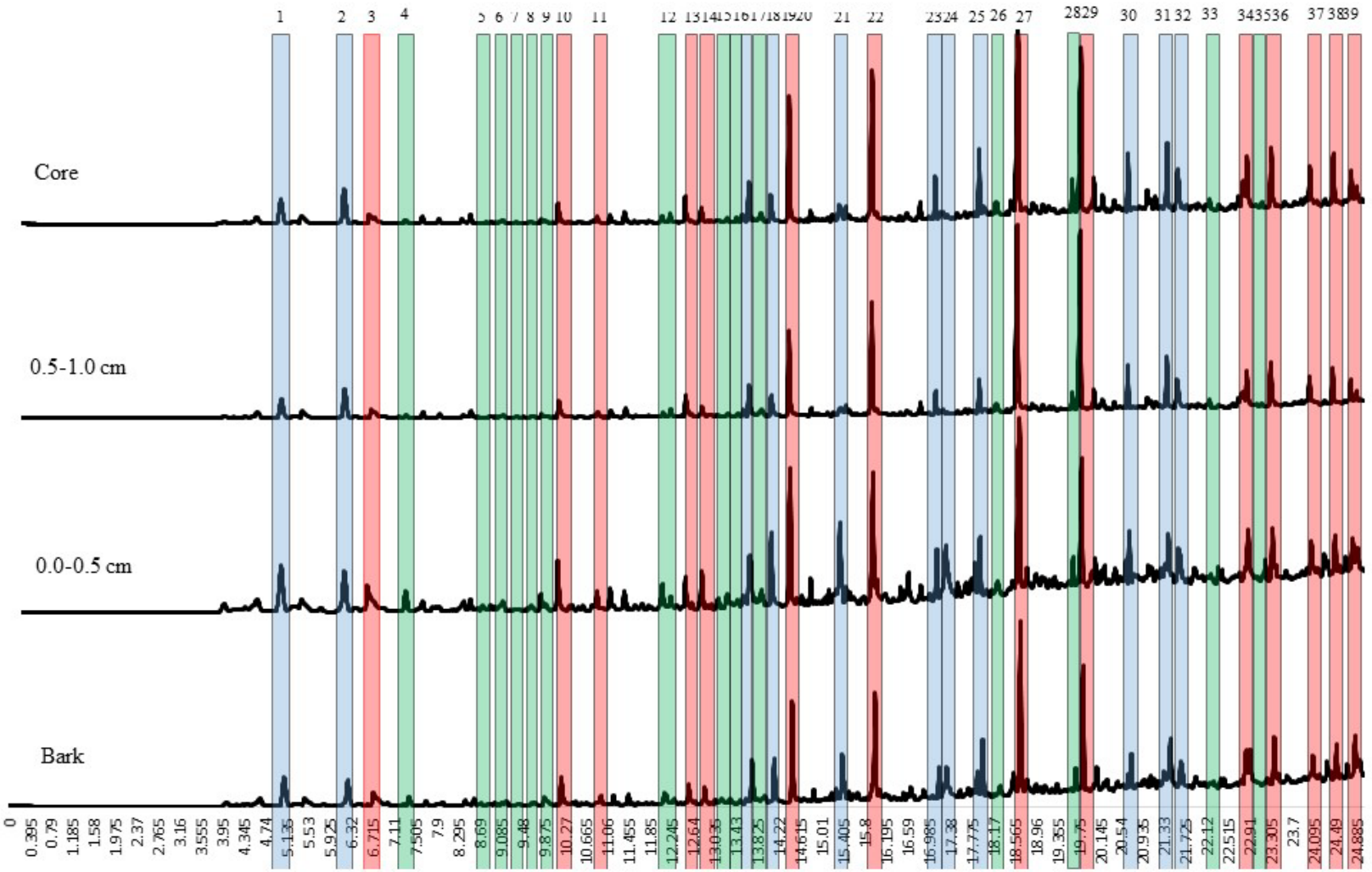

Figure 8.6b: Pyrolysis GCMS analysis at 550 °C of the changes volatile chemistry through the horizontal profile of the HTC 250 bio-coal in the 4.0 cm willow cylinders with bark

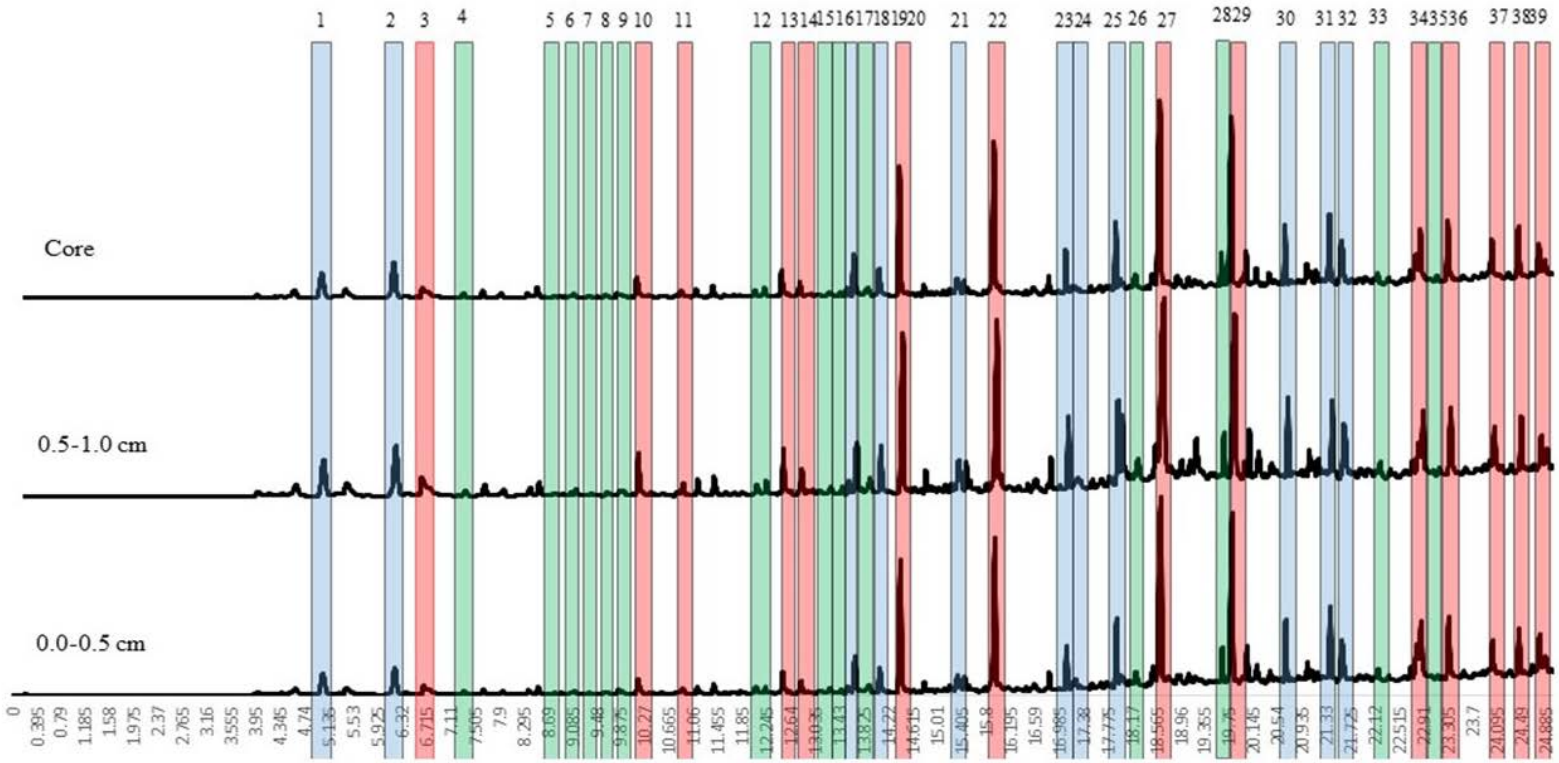

Figure 8.6c: Pyrolysis GCMS analysis at 550 °C of the changes volatile chemistry through the vertical profile of the HTC 250 bio-coal in the 4.0 cm willow cylinders with bark

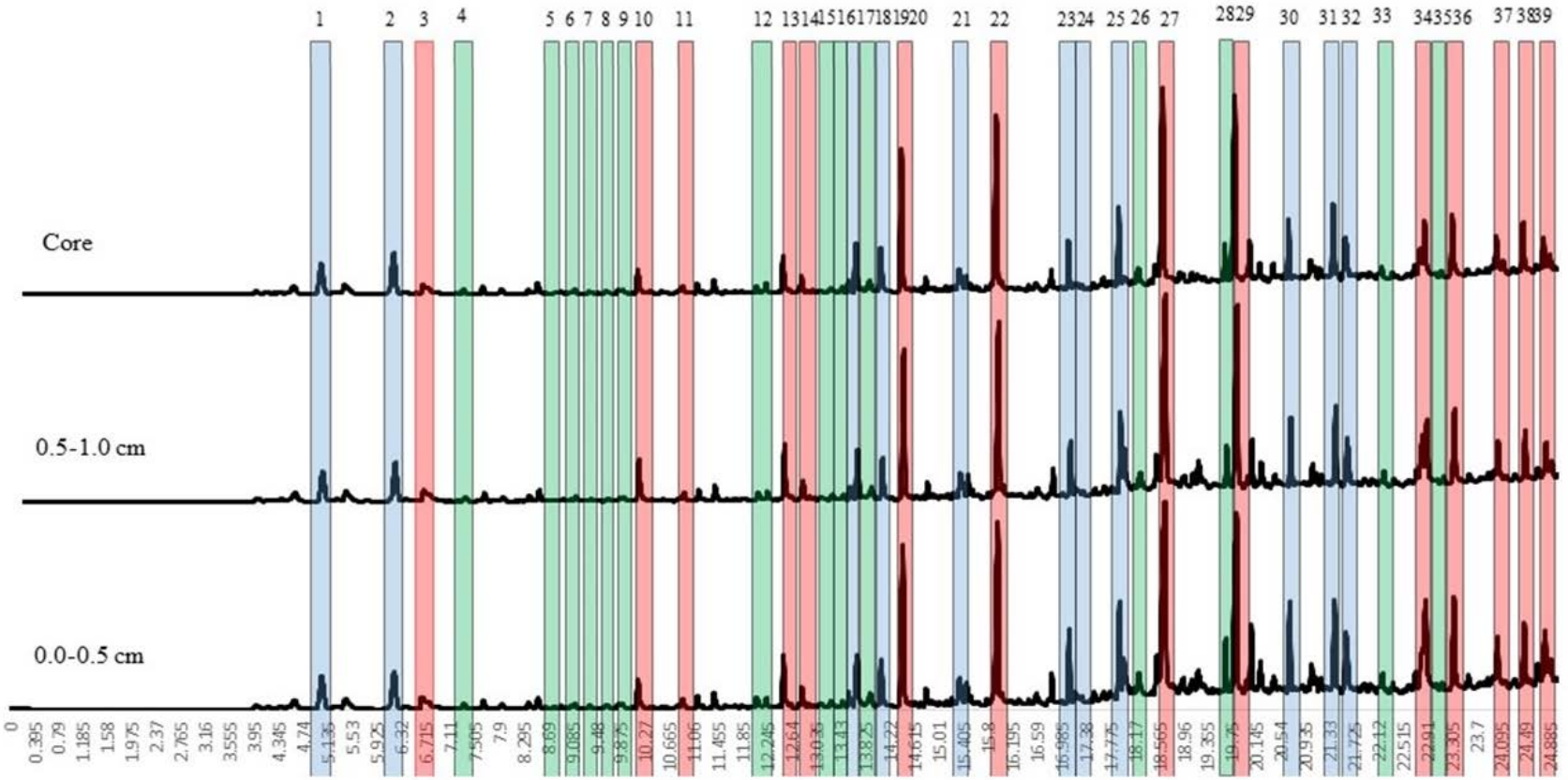

Figure 8.6d: Pyrolysis GCMS analysis at 550 °C of the changes volatile chemistry through the vertical profile of the HTC 250 bio-coal in the 4.0 cm willow cylinders without bark ((1) 2-methyl furan; (2) dimethyl furan; (3) acetic acid; (4) (dihydro)dioxin; (5) bioxirane; (6) propanoic acid; (7) methyl butenol; (8) pentylpenondione; (9) propanediol; (10) furfural; (11) cyclohexanone; (12) cyclopentandione; (13) acetylfuran; (14) corylone; (15) furanone; (16) dimethylbutane; (17) phenol; (18) eugenol; (19) methoxyphenol; (20) cresol; (21) creosol; (22) di-methyl toluene; (23) ethyl methoxyphenol; (24) hydroxyl-3methylacetophenone; (25) di-methoxy phenol; (26) corylone; (27) tri-methoxy phenol; (28) isoeugenol; (29) tri-methoxy toluene; (30) di-methoxyacetophenone; (31) paradol; (32) methoxyeugenol; (33) isoferulic acid; (34) methoxyeugenol; (35) levolgulcosan; (36) benzaldehyde; (37) acetosyringone; (38) ethyl barbutric acid; (39) hexadecanoic acid)

As shown in Figure 8.4, samples produced without bark appear to yield bio-coal which is reasonably consistent with between 51 % and 52 % volatile carbon. For the samples with bark, the 1-2 mm sample has a volatile carbon content of 56 % reducing to 51 % in the 3.5 cm sample. This reduction in volatile carbon appears to be due to the reduction and removal of cellulose originating from within the bark. Figure 8.5 shows a double peak present on the samples treated with bark, which are not present within the samples treated without bark. A reduced bark to wood ratio does not explain this reduction so these compounds must be undergoing increased conversion with increased size.

Figure 8.7 shows the samples with and without bark post carbonisation. One characteristic property of the bark samples is the bark helps retain the integrity of the cylinder (from 3.0 cm in diameter), while the equivalent samples without bark swell and disintegrate. It is generally assumed that char formation is formed though the hydrolysis of the hemicellulose and cellulose to monosaccharides which then undergo dehydration and fragmentation processes giving rise to different soluble products which undergo polymerization, condensation and aromatisation leading to the formation of the bio-coal [84, 85]. This chemistry is discussed in detail in Section 2.3.2. In the work presented in Mosteiro-Romero et al. [98] sperical particles were found to be abundant in the ‘pyrolysis zone’ within the 0.9–1 cm particles. These spherical particles are indicative of char formation by HTC and would suggest the core is undergoing hydrolysis, but the particle size is limiting diffusion of these preliminary products into the bulk water. If this is the case it will lead to an increase in organic acids, organic loading, and saccharide concentrations within the particle, catalysing the hydrothermal reaction and enhancing char formation within the core, which was assumed to be derived through pyrolysis reactions in Mosteiro-Romero et al. [98]. It is concequently hypothesised that in the smaller particles, with bark, the preliminary products diffuse into the bulk water, while they are retained within the larger particles due to diffision limitations. This enhances hydrolysis and polymerisation within the larger particles leading to the conversion of these volatile compunds which are seen in the smaller particles.

The carbon, oxygen, volatile carbon and fixed carbon contents of areas within the 2.5 cm to 4.0 cm samples have been calculated and are stated in Figure 8.8. Samples were taken on the vertical and horizontal plane, as shown in Figure 8.2, with the samples on the vertical plane believed to be of similar chemistry due to the growth characteristics of willow. In the unprocessed material it’s generally observed that the central core of the cylinder is highest in fixed carbon, highest in carbon and lowest in oxygen content. This

would be indicative of lignification [362]. There is variation in the carbon, oxygen and volatile carbon on the horizontal plane in the unprocessed samples as well as between samples of different sizes. The bark appears to have a higher ash and carbon content, lower oxygen content and lower volatile carbon content than the stem wood.

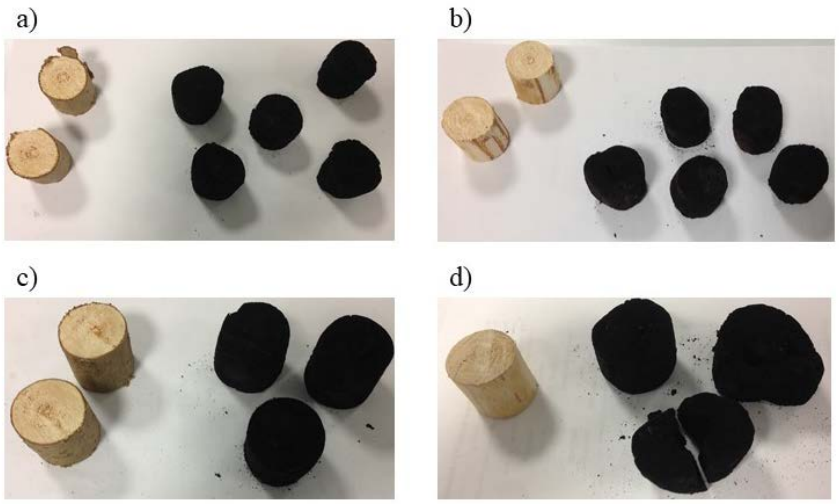

Figure 8.7: Unprocessed willow and the resulting bio-coals for a) 3.0 cm with bark, b) 3.0 cm without bark, c) 4.0 cm with bark, and d) 4.0 cm without bark

When comparing the HTC samples on the vertical profile there appears to be higher carbon contents on the outside of the cylinder than in the centre for all but the 2.5 cm samples. The cylinder profiles also appear to have slightly higher oxygen contents on the outside of the cylinder when compared to the centre. The exception to this being the 4.0 cm sample, which has a more oxygenated core. The volatile carbon content of the sample is also typically lower in the centre of the cylinder compared with the outside, with the exception once again being the 4.0 cm sample, which has a higher volatile content in the core.

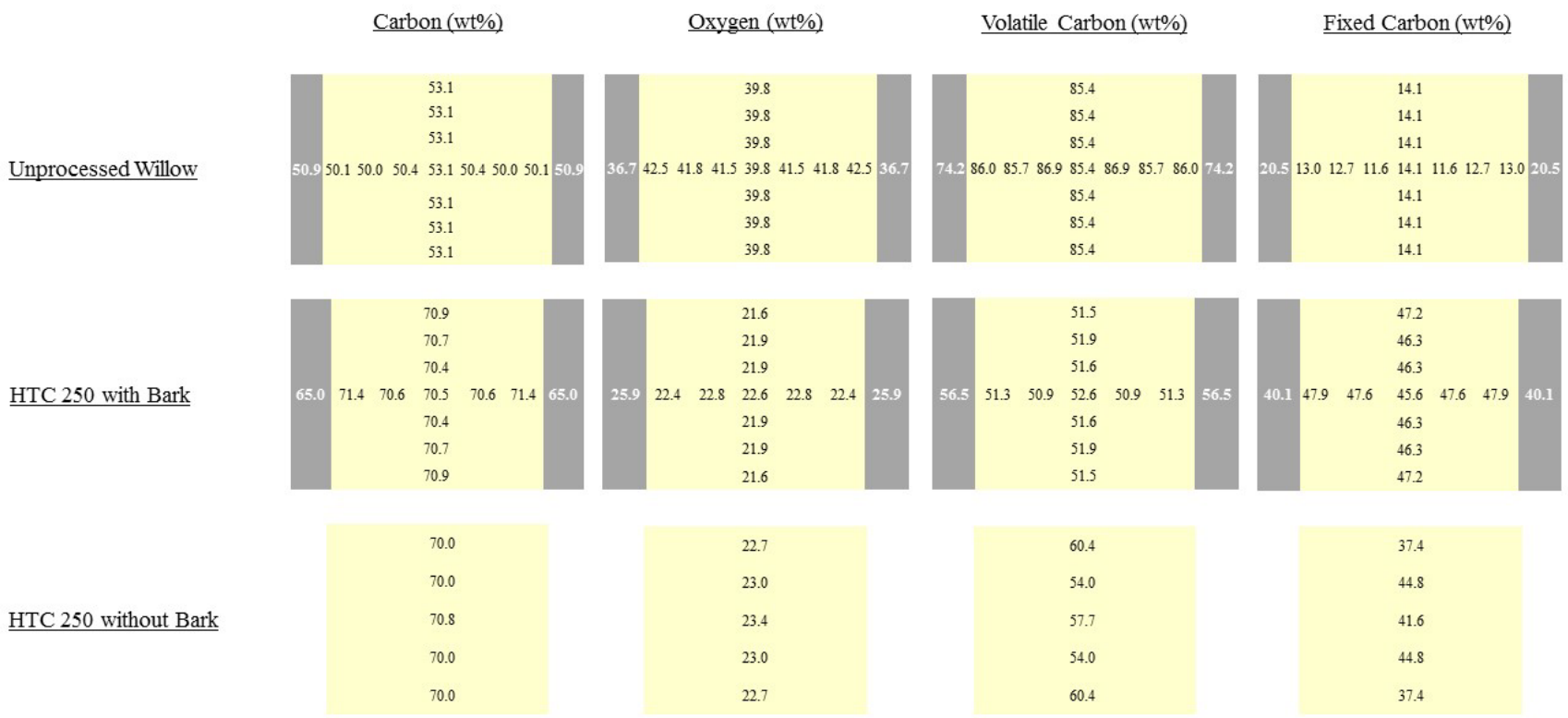

Figure 8.8a: variation in carbon, oxygen, volatile carbon and fixed carbon (d.b.) in the 4.0 cm willow cylinders.

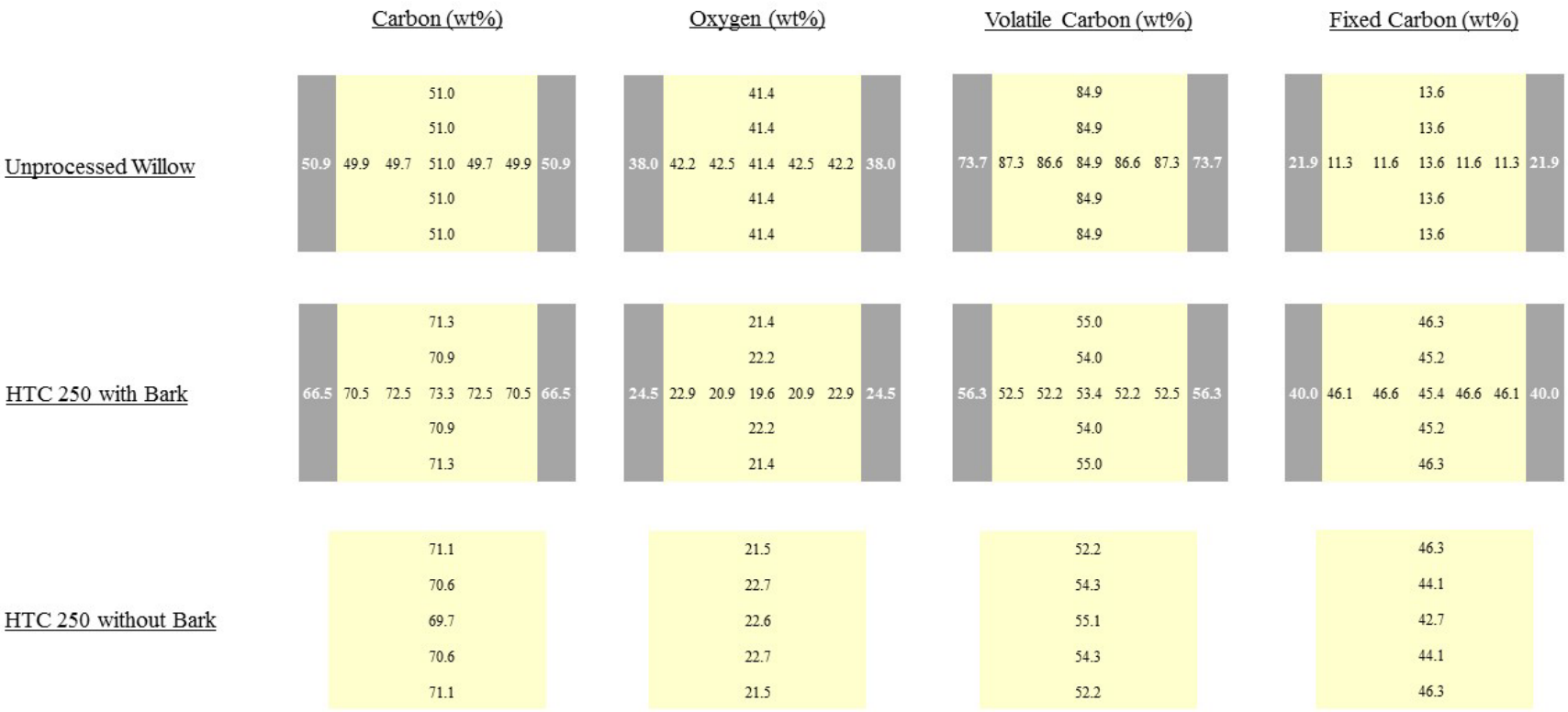

Figure 8.8b: variation in carbon, oxygen, volatile carbon and fixed carbon (d.b.) in the 3.5 cm willow cylinders.

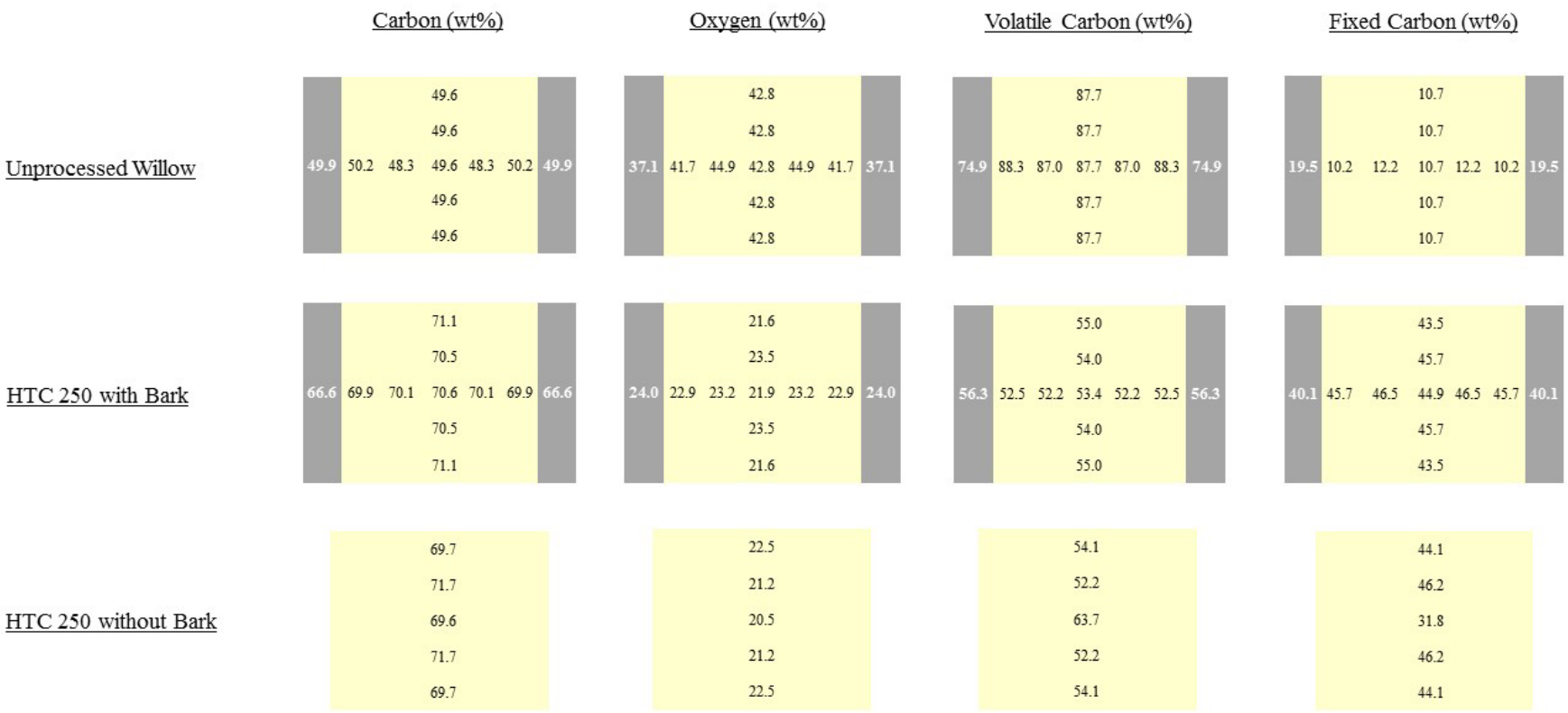

Figure 8.8c: variation in carbon, oxygen, volatile carbon and fixed carbon (d.b.) in the 3.0 cm willow cylinders.

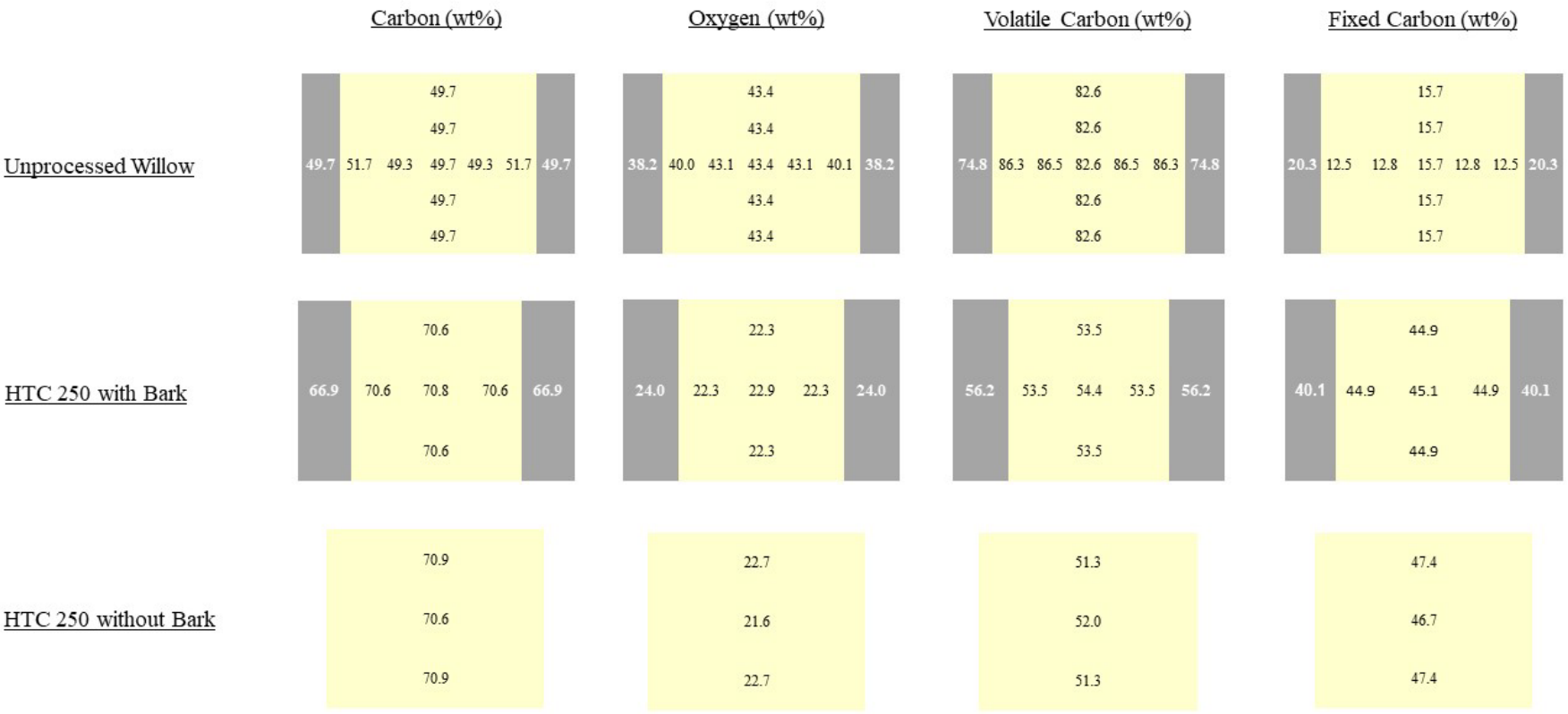

Figure 8.8d: variation in carbon, oxygen, volatile carbon and fixed carbon (d.b.) in the 2.5 cm willow cylinders.

The higher oxygen and volatile carbon content of the centre of the 4.0 cm diameter bio-coal samples may indicate the samples are less carbonised than the smaller cylinders, although Figure 8.6b still indicates that the cellulose has still been degraded within the sample, with the removal of the levoglucasan peak (peak 35). This increase in oxygen and volatile carbon within the 4.0 cm sample may well indicate that by 4.0 cm heat transfer may be becoming a limitation. In these experiments, all samples were retained for one hour at 250 ºC. As demonstrated in Chapter 6, increasing retention times increase fixed carbon and decrease volatile carbon of the sample. In larger particles / spheres, it will take longer for the centre of the particle to reach temperature than the outside of the particle, which would mean the centre of the particle has essentially had a lower retention time than the outside layers. While the central core has clearly carbonised based on the py-GCMS data any further increase in size beyond 4.0 cm or reduction in retention time could result in only a partially reacted core.

With the exception of the 4.0 cm diameter samples the higher volatile carbon, carbon and oxygen contents seen on the outside of the cylinders is indicative of the presence of an oily film on the outer surface of the particle, as shown in Figure 8.1. Solid State C13 NMR was undertaken on a limited number of samples and the spectra is given in Figure 8.9. The NMR spectra does indicate the presence of saturated short chain aliphatics, which would support this. Whether this layer is formed in-situ as hypothesised in Mosteiro-Romero et al., [98] or were water soluble, at temperature, due to the lower dielectric constant and have precipitated onto the surface of the char on cooling as hypothesised by others [88-90] is unclear. Either way the presence of this oily film does not appear to have hindered carbonisation.

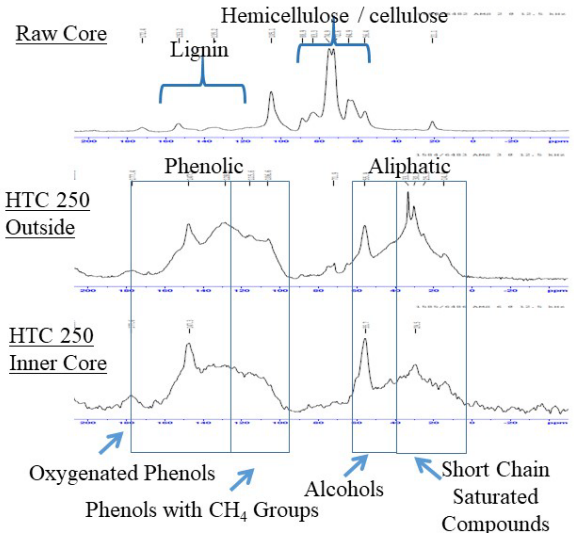

Figure 8.9. C13 NMR Spectra of the inside and outside of the 4 cm bio-coal with bark

8.4.2. Influence of size on the handling properties of the fuel

8.4.2.1. Moisture and hydrophobicity

Enhanced hydrophobicity of HTC bio-coal is a commonly stated handling improvement [178, 179]. The hydrophobicity is brought about though both the dehydration of the fuel [179] and the decreasing polarity of the bio-coal [366]. The polarity of the fuel can be calculated based on the polarity index which is mass ratio of oxygen and nitrogen to carbon [229]. Figure 8.10 shows the moisture content of the bio-coals after storage at 30 °C and 100 % RH. The results show that size has an influence on the hydrophobicity of the fuel, with the larger cylinders giving bio-coals with higher initial moisture contents for both with and without bark. Figure 8.10 also shows the equivalent sized unprocessed willow and in this instance all samples, irrespective of size obtain a similar equilibrium moisture content of around 22%. This result would imply that the increasing moisture content in the larger bio-coal samples is as a result of subtle changes in sample chemistry as opposed to simply size. Calculation of the polarity index of the samples shows that samples become less polar as they increase in size until around 2.0 cm in diameter, after which they begin to increase in polarity again. This trend follows the observed equilibrium moisture contents of the bio-coals closely. Treatment with and without bark appears a factor in the hydrophobicity of the bio-coal and appears more important than size, with samples with bark having higher equilibrium moisture contents than those without. This trend appears once again to be due to the polarity of the samples with the samples treated with bark being more polar than their no-bark equivalents.

Once the equilibrium moisture content at 30 °C and 100 % RH was determined, the samples were subsequently stored at 20 °C and 70 % RH and the moisture taken every subsequent 24 hours. Under these conditions, the bio-coals are shown to re-equilibrate to between 4 and 5 % moisture, with limited difference between sizes and whether they were treated with or without bark. For the unprocessed samples, only the 1.0 cm sized cylinders appear to reach equilibrium moisture content within 24 hours, with diffiusion limitations becoming increasingly apparent with regard to drying, as the samples get larger. The 4.0 cm samples appear not to have reached equilibrium by 72 hours. This result is significant as it shows that the diffision limitations brought about with larger particles are not so apparent with bio-coals. Figure 8.8 has demonstrated that the carbonisation is reasonably homogenous though the whole cylinder, with an increase in carbon and a decrease in oxygen. This suggests the hydrophobic properties of the bio-coal are reletively homogenous thoughout the cylinder up to a size of 4.0 cm. This could be significant as

some treatments such as torrefaction can lead to a hydrophobic surface, due to the removal of the hydroxyl functional groups, but the hydophobic properties are only superficial. When stored, coal will become increasingly hydrophillic as the surface oxidises though natural weathering during storage [367] and the same is applicable to bio-coals, charcoals and torrefied fuels. A homogenous hydrophobic fuel is beneficial as this will prolong the hydrophobic nature of the fuel as when the hydrophobic properties are limited to the surface these hydrophobic properties can be only temporary, as over time the surface will become hydrophillic again.

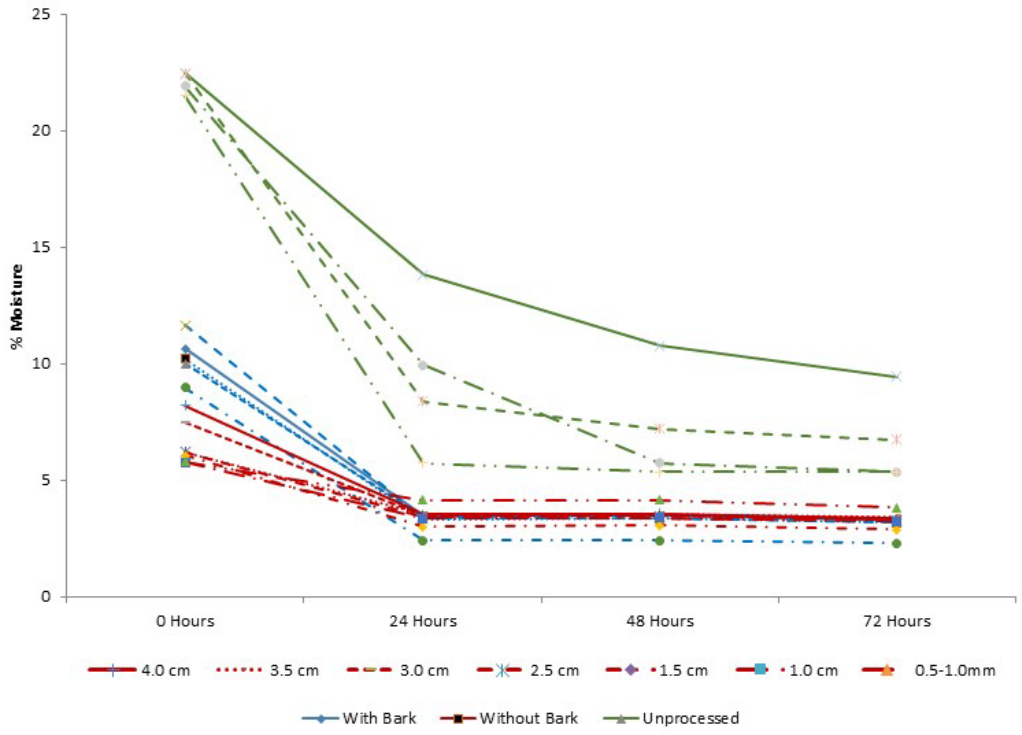

Figure 8.10: Moisture retention in hours at 20°C (70 % RH) after storage at 30°C (100 % RH) of unprocessed willow at differing sizes and bio-coals derived from feedstock size processed with and without bark

8.4.2.2.Size and grindability

Another property commonly reported for HTC is the enhanced friability or gridability of the bio-coal [33]. The enhanced grindability appears to be due to HTC degrading the hemicellulose and cellulose within the biomass, thus the fibrous material that provides strength to the biomass cell walls. The enhanced friability and grindability of the biomass is good for both dewatering the bio-coal post carbonisation as the removal of the fibrous material will allow for enhanced mechanical water recovery post carbonisation. Another benefit of the enhanced grindability comes in the form of enhanced flame stability and energy efficiency of pulverised fuel boilers [68]. In

Bridgeman et al. [196], unprocessed willow has an HGI of zero. This essentially implies under the test conditions, that no fuel would reach the desired 75µm and thus, assuming co-milling, there would be either a greater energy requirement for milling to achieve 75µm or the pulverised fuel particles would be greater than 75µm in diameter. Ndibe et al. [197] demonstrated that grade A1 wood pellets had an HGI of 15.

Investigations into the influence of torrefaction on enhanced grindability have been reported in Bridgeman et al. [196] and Ndibe et al. [197], with Bridgeman et al. [196] showing that the HGI went from zero to between 5 and 38 for willow with higher HGI associated with greater reaction severity. Ndibe et al. [197] investigated torrefied poplar between 250 °C and 300 °C, giving an HGI of between 30 and 43. For reference, a change in HGI from 15 to 43 represents a 50% reduction in the energy requirement for milling [197]. Results presented in Chapter 5 and Smith et al. [260], demonstrated that HTC of *Miscanthus* at 250 °C gives an HGI of 150, which suggests HTC fuel treated at 250 °C very easily pulverises.

To assess the impact size has on the grindability an HGI test was undertaken using a calibrated ball mill, with the results presented in Figure 8.11. For the unprocessed sample an HGI of 10 was achieved, although it should be noted that to undertake this test significant size reduction down to 0.6-1.18 mm was required using a cutting mill. The results for a 1-2 mm sample gave an HGI of 62, which is lower than the HGI of 150 reported for *Miscanthus* in Smith et al. [260]. The results however suggested as particle size increases grindability increases, with an HGI of 155 and 133 for the 1.0 cm samples with and without bark respectively. The grindability increases up to 3.0 cm with an HGI of 173 and 177 for the samples with and without bark respectively. After 3.0 cm the HGI starts to decrease with 167 and 163 for the samples with and without bark. This result would suggest that with the exception of the 3.0 cm sample the presence of bark during carbonisation makes the sample more grindable.

The result would suggest that the grindability of the bio-coal is not purely dictated by the removal of fibrous material that provides strength to the biomass cell walls. As previously discussed the higher volatile carbon, carbon and oxygen contents seen on the outside of the cylinders presented in Figure 8.8 and Figure 8.9 is indicative of the presence of an oily film on the outer surface of the particle, as shown in Figure 8.1. With increasing size the outer surface of the cylinders proportional to volume decreases and thus the film volume proportional to the remaining bio-coal. The presence of this oily film potentially reduces the efficiency of the size reduction. It is also shown in Figure 8.7 that one

characteristic property of the samples treated with bark is the bark retains the integrity of the cylinder while the equivalent samples without bark swell and disintegrate. This disintegration will increase the surface area on which the oily film can deposit and consequently could explain the lower grindability of the samples without bark. The reduction in HGI beyond 3.0 cm could be indicative of residual fibrous material, increasing the resistance to grinding. This fibrous material would be as a result of reduced heat transfer resulting in incomplete degradation of the biomass fibres and it is likely grindability will reduce as cylinder size exceeds 4.0 cm in diameter, as larger particles would only result in a partially unreacted core.

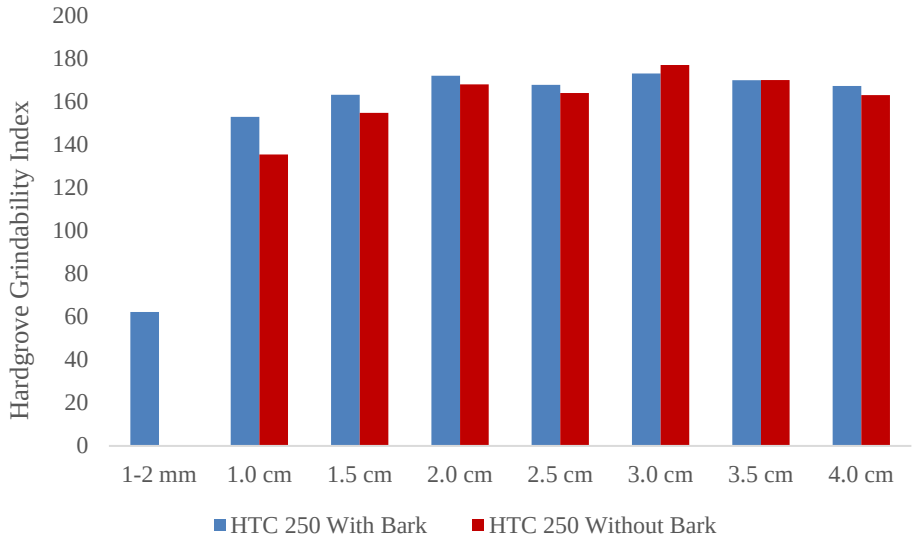

Figure 8.11: The Hardgrove Grindability Index of homogenised bio-coals derived from feedstock size processed with and without bark

8.4.2.3. Fuel burning properties

Figure 8.12 gives the burning profiles of homogenised samples from the samples treated at different sizes, with bark (Figure 8.12a) and without bark (Figure 8.12b). Interpretation and significance of fuel burning profiles have been discussed in Sections 2.4.4.1 and Smith et al. [260]. The burning profiles for all bio-coals give the ‘coal like’ burning profile. These ‘coal like’ profiles have almost a single stage profile whereby the volatile burn starts at around 310°C, with a ‘shoulder’ on the curve as opposed to characteristic independent peaks seen with unprocessed biomass. The second initiation temperature due to the onset of char combustion, around 400°C, with peak temperature is around 460°C. The results would suggest that the bio-coals produced with bark have a slightly higher volatile burn and slightly lower characteristic temperatures. This would indicate the samples processed with bark are more reactive, potentially due to the higher

alkali and alkaline earth metals present from the bark. These alkali metals are known to influence the devolatilisation and char reactivity during combustion [160, 207-209].

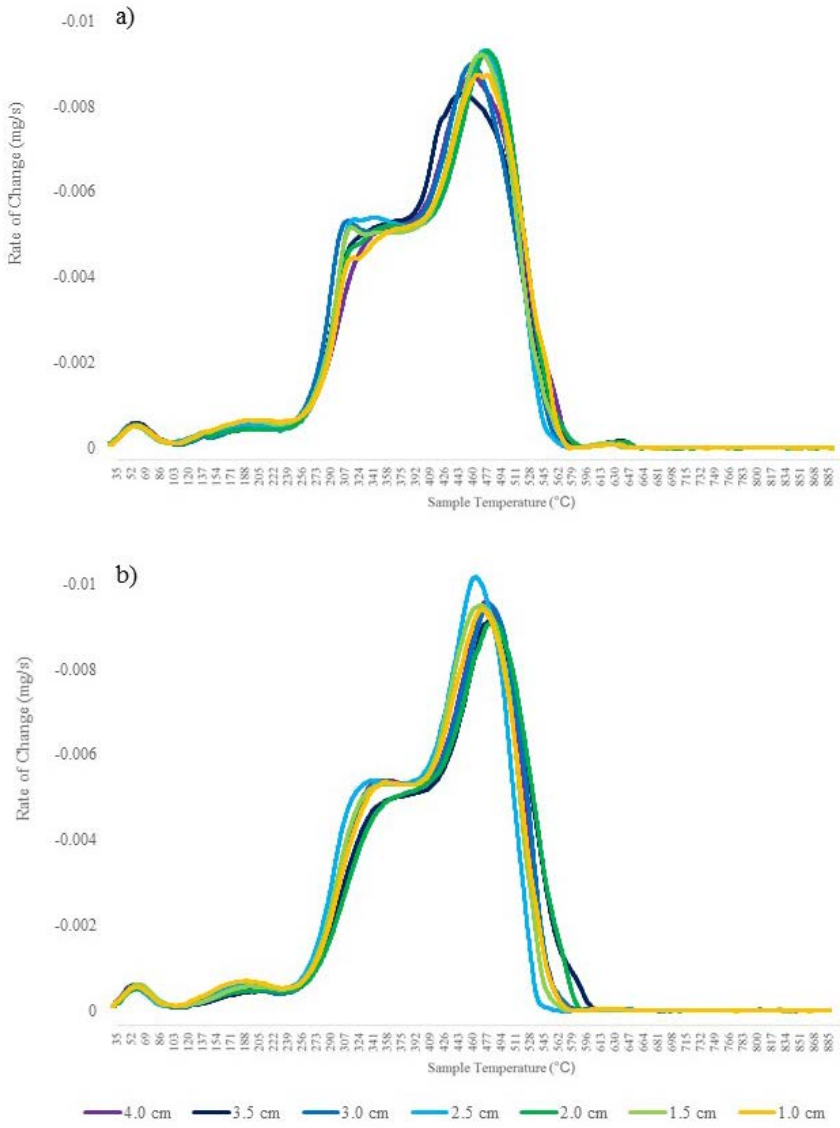

Figure 8.12: Derivative thermogravimetric (DTG) burning profiles for willow hydrothermally treated at 250 °C; a) with bark and b) without.

8.4.3. Influence of size on the inorganic content of the fuel

Table 8.2 gives the potassium, sodium, magnesium, calcium, iron, aluminium and phosphorus contents within the bio-coals; EDX analysis on the bio-coal ashes had demonstrated that these seven elements make up the bulk of metals present. The samples would suggest that for the samples with bark, the alkali metals concentration (sodium and potassium), decreases with increasing size to 3.0 cm in diameter, after which concentration increases. At 4.0 cm concentrations are still lower than the 1-2 mm sample but higher than the 1.0 cm samples. A similar trend has been observed for the samples without bark although these samples had lower potassium contents in the starting

feedstock as in the results the bark has a higher potassium content than the white wood. For all the samples the concentration of potassium is lower than the concentration of the starting feedstock. This would be beneficial in terms of slagging, fouling and corrosion as in biomass combustion, potassium is the main problematic element in these phenomena [39]. This said the concentrations of alkali metals in the starting feedstock should not be problematic in this instance.

The higher concentrations of potassium and sodium on the 1-2 mm sample could however suggest that surface area has an influence on the retention of metals, particularly these mono-valiant metals. Surface area (BET) testing has not been undertaken as part of this work but it is most likely that the 1-2 mm samples will have the highest surface area. Figure 8.13 shows how the metal concentrations vary throughout the cylinder for the 2.5 to 4.0 cm samples, with the results suggesting the outer surface of the cylinder has the highest concentrations of sodium and potassium once treated. As discussed earlier, there appears to be higher volatile carbon and oxygen on the outside of the cylinder, shown in Figure 8.8, which may be indicative of the presence of an oily film on the outer surface of the particle. This could suggest an interaction between the volatile carbon, in particular its oxygen containing functional groups, and alkali metals. It is known that surface oxygen containing functional groups can bind to cations such as sodium, potassium, magnesium, calcium, which can then be released upon thermal treatment [232]. Consequently, this could suggest the reuptake of metals from the process water onto the surface of the bio-coal. Given this material will be volatilised on combustion, this could lead to the volatilisation of these metals bringing about issues with fouling, as hypothesised in Section 2.5.3.2 and Smith et al. [354], where otherwise the potassium may be retained with the ash fraction due to interaction with calcium and silicates [234, 235]. If this the case increasing the particle size may well reduce the fuel's fouling potential.

The results also show a similar trend for calcium as seen with potassium, with a slight reduction for both the with bark and without bark samples up to 3.0 cm and then an increase in concentration thereafter. For calcium there is however a big difference in concentration between the with bark and without bark samples. The bark has a high calcium content compared to the white wood, with 12 mg/kg compared with 1.2 mg/kg for the white wood. This results in the samples treated with bark having a higher calcium content, than those without. The calcium appears to be largely retained within the bark and is not homogenously distributed through the fuel, as shown in Figure 8.13. The exception appears to be the 4.0 cm samples, which has reasonably high calcium

concentrations within the centre of the sample. It is however likely that this higher concentration of calcium in the core of the 4.0 cm diameter samples is due to retention of metal-containing process water as opposed to difference in chemistry. In these experiments separation of the solids and process water was undertaken using vacuum assisted filtration without the assistance of mechanical de-watering. It is likely that as the cylinders become larger more residual process water is left within the char micro and macro pores when filtered. This will, on drying, deposit metal salts on the bio-coal, as seen when recycling process waters in Section 7.4.2. This would explain the increase in metal concentrations from 3.0 cm with bark and 3.5 cm without.

Given the high HGI of these materials removal of this water retained within the micro and macro pores should be possible using mechanical dewatering presses, such as an extruder press. The presence of metal-rich process water in the central core does show that there is free movement of water though the particle, and consequently the formation of a low water permeable hydrolysis layer which may reduce or prevent the extraction of metals though water diffusion limitations does not appear to happen. While further work using mechanical dewatering appears that increasing size may, if anything, facilitate increased extraction due to the reuptake mechanisms discussed.

Of the elements analysed only phosphorus increases in concentration within the bio-coals compared to the starting feedstock. In HTC bio-coals, phosphorus appears to be associated with calcium [368] in much the same way as sulphur is associated with iron in coal [369]. The results given in Figure 8.13 could suggest that the calcium retained within the bio-coal is associated with the phosphorus. Low concentrations of iron, aluminium and magnesium in the samples mean there is only limited variation between the samples of varying size.

Table 8.2: The inorganic chemistry of homogenised bio-coals derived by varying feedstock size, processed with and without bark

Sample		metals and phosphorus (mg/kg)																				
		K			Na			Mg			Ca			Al			Fe			P		
Unprocessed With Bark		2.0	±	0.0	0.6	±	0.1	0.4	±	0.0	3.6	±	0.3	0.3	±	0.0	0.3	±	0.0	0.9	±	0.0
Unprocessed Bark (only)		4.6	±	0.1	0.7	±	0.0	1.0	±	0.0	12.0	±	0.5	0.2	±	0.0	0.2	±	0.0	1.6	±	0.0
HTC 250 With Bark	1-2 mm	0.9	±	0.1	0.9	±	0.2	0.3	±	0.0	3.1	±	0.0	0.2	±	0.0	0.5	±	0.0	1.0	±	0.0
	1.0 cm	0.5	±	0.0	0.8	±	0.1	0.2	±	0.0	2.6	±	0.3	0.2	±	0.0	0.6	±	0.0	1.0	±	0.0
	1.5 cm	0.6	±	0.1	0.8	±	0.1	0.2	±	0.0	1.9	±	0.5	0.2	±	0.0	0.4	±	0.0	0.8	±	0.0
	2.0 cm	0.3	±	0.0	0.5	±	0.2	0.1	±	0.0	2.8	±	0.1	0.1	±	0.0	0.3	±	0.1	0.8	±	0.1
	2.5 cm	0.4	±	0.1	0.6	±	0.0	0.2	±	0.0	1.9	±	0.2	0.1	±	0.0	0.3	±	0.0	0.8	±	0.0
	3.0 cm	0.3	±	0.0	0.9	±	0.0	0.2	±	0.0	2.5	±	0.3	0.2	±	0.0	0.5	±	0.0	0.8	±	0.1
	3.5 cm	0.5	±	0.1	0.7	±	0.1	0.2	±	0.0	3.5	±	0.2	0.1	±	0.0	0.3	±	0.0	0.9	±	0.0
	4.0 cm	0.6	±	0.1	0.7	±	0.0	0.3	±	0.0	2.8	±	0.5	0.1	±	0.0	0.4	±	0.1	0.9	±	0.0
Unprocessed Without Bark		0.9	±	0.0	0.7	±	0.1	0.2	±	0.0	1.2	±	0.2	0.3	±	0.1	0.4	±	0.1	0.4	±	0.0
HTC 250 Without Bark	1.0 cm	0.5	±	0.0	0.6	±	0.0	0.2	±	0.0	1.3	±	0.1	0.1	±	0.0	0.3	±	0.0	0.6	±	0.0
	1.5 cm	0.4	±	0.1	0.7	±	0.1	0.2	±	0.0	1.2	±	0.2	0.2	±	0.0	0.4	±	0.1	0.5	±	0.0
	2.0 cm	0.3	±	0.1	0.6	±	0.0	0.1	±	0.0	0.9	±	0.2	0.1	±	0.0	0.3	±	0.0	0.4	±	0.0
	2.5 cm	0.3	±	0.1	0.5	±	0.0	0.1	±	0.0	0.7	±	0.1	0.2	±	0.0	0.4	±	0.1	0.7	±	0.0
	3.0 cm	0.3	±	0.1	0.6	±	0.0	0.1	±	0.0	0.8	±	0.1	0.2	±	0.0	0.4	±	0.1	0.6	±	0.0
	3.5 cm	0.2	±	0.0	0.6	±	0.1	0.2	±	0.0	1.2	±	0.1	0.1	±	0.0	0.3	±	0.0	0.6	±	0.0
	4.0 cm	0.4	±	0.0	0.7	±	0.0	0.2	±	0.0	1.2	±	0.1	0.2	±	0.0	0.4	±	0.1	0.8	±	0.0

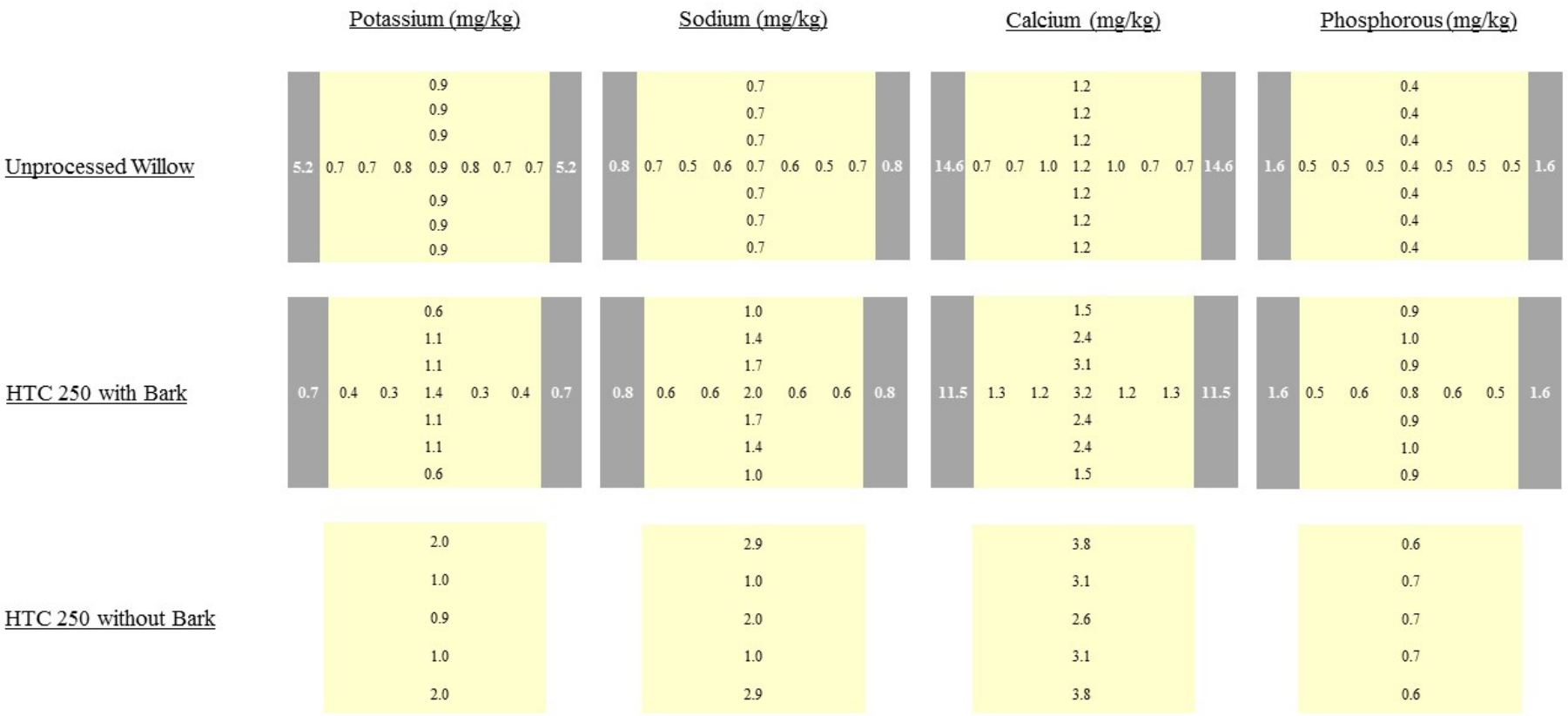

Figure 8.13a: variation in potassium, sodium, calcium and phosphorus in the 4.0 cm willow cylinders.

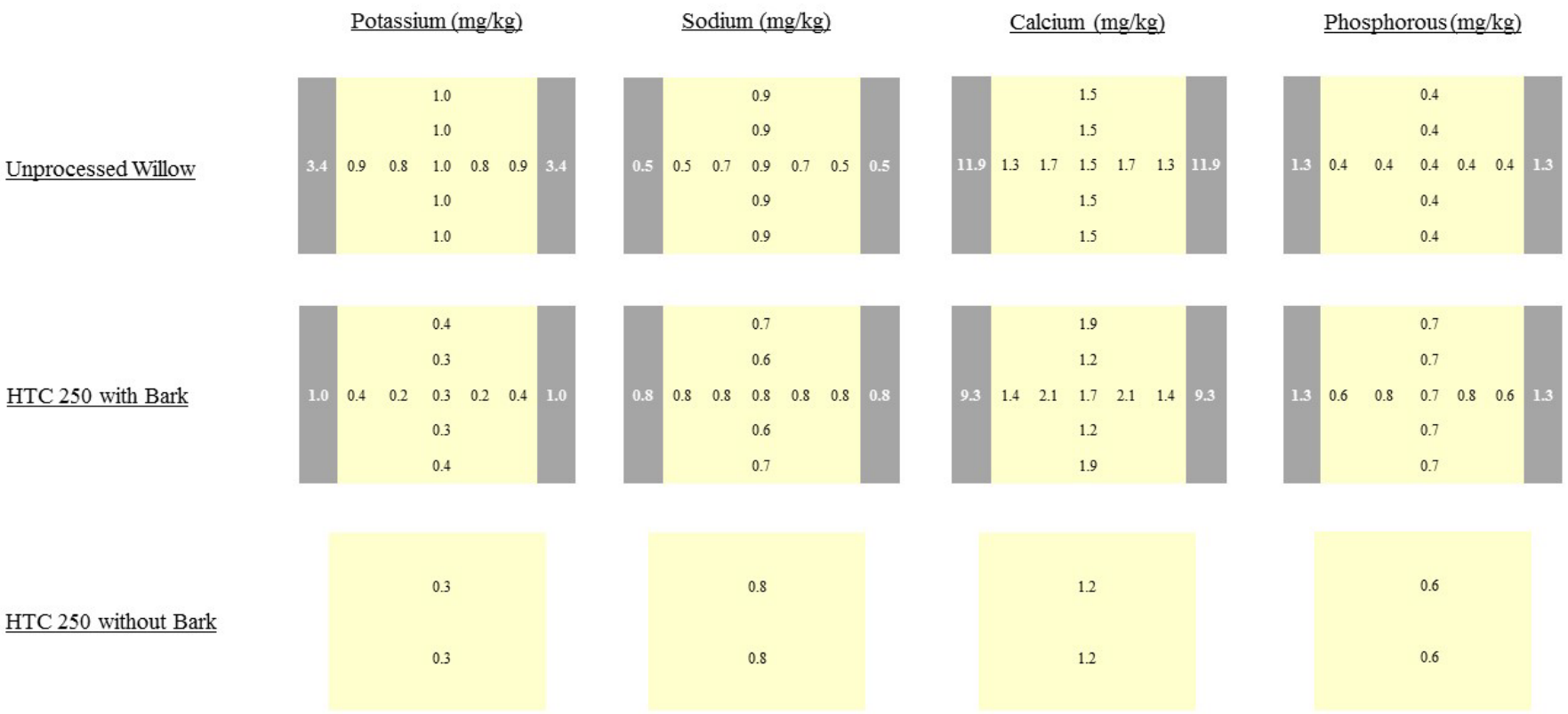

Figure 8.13b: variation in potassium, sodium, calcium and phosphorus in the 3.5 cm willow cylinders.

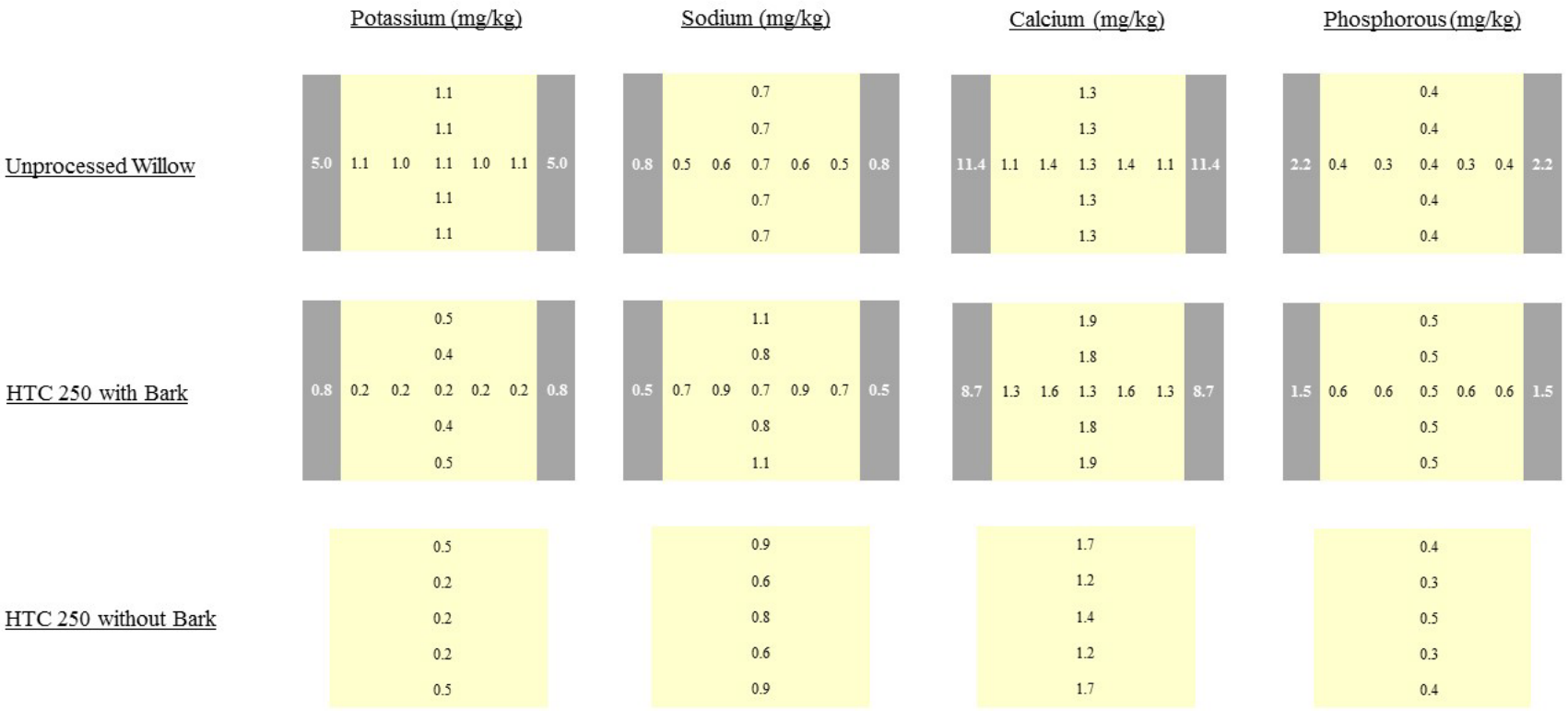

Figure 8.13c: variation in potassium, sodium, calcium and phosphorus in the 3.0 cm willow cylinders.

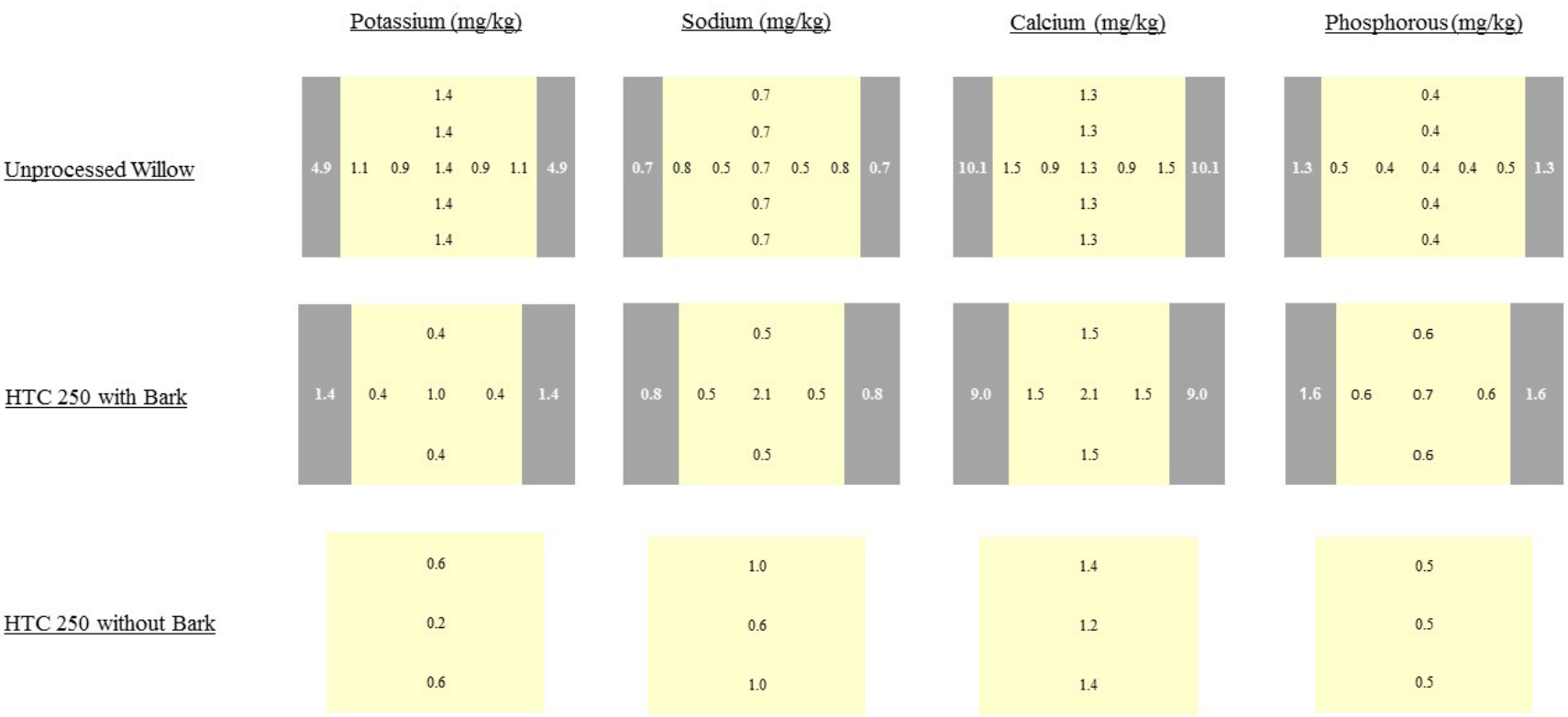

Figure 8.13d: variation in potassium, sodium, calcium and phosphorus in the 2.5 cm willow cylinders.

Ash fusion testing was undertaken to investigate how the extraction of metals with increasing size influences the slagging and fouling propensity of the fuel. The results are given in Table 8.3. The results show that the starting biomass has good fouling and slagging propensity with deformation temperature around 1530 ˚C. For the treatments with bark the ash transition temperatures remain relatively high, albeit slightly lower than the starting biomass. It should however be noted that despite a small increase in slagging propensity the temperatures are still very high so the fuels will be regarded as low slagging fuels. Fuels treated without bark appear to undergo a sharp decline in in both deformation and hemisphere temperatures. This would certainly indicate the fuels would have a greater propensity to slag during combustion and this propensity appears to increase with increasing size. The metal analysis of the fuels is given in Table 8.2 and it appears that the fuel's calcium content is the main driver behind this.

As discussed in the previous chapters, calcium is known to increase ash melting temperature and will restrain ash melting, ash sintering and slagging in bottom ash [39]. The high calcium content of the bark results in a higher calcium content in the fuel, which gives it a higher ash melting temperature. The higher level of phosphorus in the bark is also beneficial for the slagging and fouling propensity of the resulting bio-coal as calcium is more active in combustion of biomass fuels that are rich in phosphorus and potassium [202, 242, 254]. This is because potassium present within can either bind with calcium rich phosphates, or become potassium phosphates, which then further react with calcium oxides. These calcium potassium phosphate complexes are stable and removes the potassium available to form low temperature melting potassium silicates [200, 202]. The chemistry of this process is discussed in detail in Section 2.5.3.1. The calcium and phosphorus interaction is also more beneficial than that of just calcium as calcium on its own as when calcium present in the fuel dissolves into potassium silicate melts the reaction can result in the release of potassium into the gas phase, which can bring about the issues of fouling and corrosion. The presence of both calcium and phosphorus avoids this. Consequently, the results show that when undertaking HTC with willow, it is best to process with the bark as the presence of the calcium and phosphorus has a positive influence on the slagging and fouling propensity of the fuel. Processing without bark could result in a fuel with a higher slagging and fouling propensity than the starting biomass.

Table 8.3: Ash fusion behaviour of unprocessed and processed willow hydrothermally treated at 250 °C with and without bark, along with unprocessed bark.

Sample		Ash Transition Temperature (˚C)											
		Shrinkage			Deformation			Hemisphere			Flow		
Unprocessed With Bark		1010	±	0	1540	±	0	1560	±	0	1570	±	0
Unprocessed Bark (only)		1050	±	0	1510	±	0	1510	±	0	1510	±	0
HTC 250 With Bark	1.0 cm	1110	±	0	1480	±	10	1530	±	0	1530	±	0
	1.5 cm	1000	±	0	1540	±	0	1580	±	0	1580	±	0
	2.0 cm	1000	±	0	1480	±	0	1530	±	0	1530	±	0
	2.5 cm	1060	±	0	1510	±	0	1580	±	5	1580	±	0
	3.0 cm	1170	±	0	1490	±	0	1550	±	5	1550	±	5
	3.5 cm	1170	±	0	1520	±	0	1530	±	0	1530	±	0
	4.0 cm	1080	±	0									
Unprocessed Without Bark		850	±	0	1530	±	5	1550	±	5	1550	±	5
HTC 250 Without Bark	1.0 cm	970	±	0	1370	±	0	1400	±	0	1500	±	0
	1.5 cm	990	±	0	1430	±	0	1530	±	0	1580	±	0
	2.0 cm	990	±	0	1170	±	0	1330	±	0	1370	±	0
	2.5 cm	1020	±	0	1170	±	0	1250	±	0	1350	±	0
	3.0 cm	1010	±	0	1270	±	0	1290	±	0	1400	±	0
	3.5 cm	1020	±	0									
	4.0 cm	910	±	0	1370	±	10	1420	±	15	1490	±	0

8.5. Conclusions

The results have shown that the formation of an outer oily film on the bio-coal does not prevent the intimate contact between the biomass and process water. The results show that for 4.0 cm diameter cylinders there was still complete conversion of the cellulose, with limited change in hydrothermal chemistry. Larger particles do however impose some diffusion limitations, reducing the release of preliminary products into the bulk water which enhances hydrolysis and polymerisation within the particle. This appears to increase the energy density of the fuel, reduce the volatile carbon fraction and significantly improves the grindability behaviour of the fuel, which would represent a huge reduction in the energy requirements for milling, if the fuel is used in pulverised fuel applications. Size does appear to have some limitations on heat transfer with energy density reducing in samples beyond 2.5 cm in diameter when processed with bark and 3.0 cm when processed without bark. This difference appears to be due to the bark retaining the integrity of the cylinder and increasing retention time may overcome this.

Metal analysis suggests that there is free movement of water though the particle at 4.0 cm in diameter and metal extraction is not limited though the formation of a low

water permeable hydrolysis layer. Reduction in the ease at with residual process water can be extracted from the pores in the larger particles does however reduce metal extraction. The ease at which the bio-coal can be ground should enable further recovery using mechanical dewatering techniques. Ash fusion testing has shown processing willow with the bark has a positive influence on the slagging and fouling behaviour of the fuel due to the increased calcium and phosphorus in the ash. Consequently, with the incorporation of mechanical dewatering larger particle diameters, up to a particle size of 3.0 diameter, could result in an overall improvement in product quality under these test conditions.

9. Influence of pH on the combustion properties of bio-coal following hydrothermal treatment of Swine manure

9.1. Abstract

Swine manure has been hydrothermally treated between 120 and 250°C in water or solutions of 0.1M NaOH, 0.1M H_2SO_4 or 0.1M of the organic acid (CH_3COOH and HCOOH) and the influence pH has on the HTC process and combustion properties of the resulting fuels assessed. Results show pH most strongly influences ash chemistry, with decreasing pH increasing removal of ash. This reduction in ash has the biggest influence on the volatile carbon and energy content of the fuel, with lower ash contents bringing about higher energy densities when calculated on a dry basis for a given temperature. pH also influences dehydration, with a fuel's dehydration increased with decreasing pH, although with increasing temperature the influence pH has on dehydration becomes less. pH and temperature appear to influence yield, with lower pH increasing yields above 250 °C but decreasing yields below 200 °C. The lower yields below 200 °C appear to be due to the acids catalysing hydrolysis of 'cellulose like' fibres within the swine manure. The higher yields at 250 °C appear to be due to the low pH catalysing polymerisation due to its influence on the electrokinetic potential of the hydrothermal suspension. The untreated manure contains high levels of ionic sodium and potassium, which should bring about issues with deposition but ash fusion tests show the high calcium and phosphorus mitigates this. Treatment at 250 °C results in a more coal-like fuel with fuel properties similar to that of lignite coal and a HHV of between 21 and 23 MJ/kg depending on pH and can give very favourable ash chemistry in terms of slagging and fouling.

9.2. Introduction

As discussed in Section 2.3.10 the use of acid catalysts was initially widely investigated in HTC as it was reported early on that weekly acidic conditions improve the overall rate of reaction. While acid catalysts have largely fallen out of favour in HTC research the exception to this has been the application of acids in manures. The reason behind this has been due to environmental issues arising from the application of excessive amounts of manure to soil which brings about the accumulation of nutrients in soils with potential for surface and groundwater pollution [370]. Consequently there has been growing interest in using the technique for reclaiming key plant nutrients such as phosphorus while simultaneously making a fuel for energetic purposes [371].

Animal manures are usually a mixture of faeces, urine, discarded bedding, and waste feed with variable water content. Therefore HTC is well suited to the treatment of

manures as moisture will not be prohibitive in the processing [370]. The main advantage behind hydrothermal processing of manures is a number of key plant nutrients, including potassium and phosphorus form soluble phosphates and are extracted into the aqueous phase where they can be precipitated and recovered [87, 89]. The extent to which the phosphorus is converted is however feedstock dependent and it is largely associated with the inorganic content of the feedstock [372]. Previous studies looking into the HTC of manures have found that phosphorus within the manure feedstock is not easily extracted, leading to the immobilisation of the phosphorus in the bio-coal and this has prompted the application of acids in HTC to aid phosphorus extraction [131, 132, 371].

While the studies all suggest dilute acids could simultaneously facilitate nutrient recovery from manure while upgrading the manure to a bio-coal, these studies have not considered the implications that changes to the inorganic chemistry may have in terms of combustion. Work presented in the previous chapters has demonstrated that reduction in slagging and fouling propensity of HTC fuels is partially due to reduction in alkali metals, but also the retention of calcium and phosphorus within the bio-coal. As previously discussed phosphorus is often a controlling element in the ash transformation reactions during biomass combustion due to the high thermal stability of phosphate compounds [200] and its removal could be problematic.

In this work Swine manure has been hydrothermally treated between 120 and 250°C in water or solutions of 0.1M NaOH, 0.1M H_2SO_4 or 0.1M of the organic acid (CH_3COOH and HCOOH) and the influence pH has on the HTC process and combustion properties of the resulting fuels assessed.

9.3. Methods

9.3.1. Materials

Samples used in this study had been previously produced as part of a separate project looking into nutrient extraction under the ‘Biorefine’ project via the ERDF Interreg IVb NWE region programme and repurposed for this study. HTC was carried out by Dr Ugo Ekpo, with all additional analysis undertaken by Aidan Smith. Swine manure used in this study was collected from the University of Leeds farm. The manure was pre-dried in an oven at 60°C for several days after which it was ground into powder using an Agate Tema barrel before processing or characterisation.

9.3.2. Hydrothermal Processing

Hydrolysis and hydrothermal carbonisation of swine manure were performed in an unstirred 600mL high pressure batch reactor (Parr, USA). In each experiment, the reactor was charged with a slurry containing 24g of swine manure with either 220 mL of de-ionised water or solutions of 0.1M NaOH, 0.1M H_2SO_4 or 0.1M of the organic acid (CH_3COOH and HCOOH). Hydrothermal processing for each slurry was performed at 120°C, 170°C, 200°C and 250°C for 1hour. The residence time was taken from the point the reactor reached the desired temperature. The heating rate was approximately 10°C min^{-1} and the cooling rate was in a similar order. After processing, the reactor was allowed to cool to room temperature before separating the products. Yields are defined as dry bio-coal mass compared with original dry mass of unprocessed manure.

9.3.3. Analysis

9.3.3.1. Inorganic analysis

Inorganic elemental composition was determined using WD-XRF, using 550 °C derived ash, pressed without a binder. Full method can be found in Section 3.6.8.

9.3.3.2. Organic analysis, combustion properties and ash measurement

Carbon, hydrogen, nitrogen, sulphur and oxygen content was determined using a Flash 2000 CHNS-O analyser (Thermo Scientific, USA), with the method described in Section 3.4.2. The volatile and fixed carbon component of the proximate analysis carried out using thermo-gravimetric analysis (Mettler Toledo, Switzerland) as described in Section 3.3.3. Ash content was determined using a muffle furnace, as described in Section 3.3.2. Moisture content was determined using a moisture oven as described in Section 3.3.1. The calorific value was determined using Dulong's Equation (see Equation 3.11). Figures are corrected in accordance with ASTM D3180-15, with hydrogen and oxygen values corrected to account for moisture. Burning profiles, ignition, flame stability and burnout temperatures were obtained by TPO, as described in Section 3.8.

9.3.3.3. Prediction of slagging and fouling behaviour

Ash fusion testing (AFT) was performed using a Carbolite digital ash fusion furnace in accordance with the standard method for the determination of ash melting behaviour (DD CEN/TS 15370-1:2006) using the methodology described in Section 3.7.1. In addition, various slagging and fouling indices have been utilised with their equations 1-3 in Table 3.3. Their underlying theory and calculation methodologies given in Section 3.7.2.

9.4. Results

9.4.1. Influence of pH on fuel organic chemistry

The yields and ultimate analysis of the bio-coals derived from the swine manure are given in Table 9.1. The results show that with decreasing pH there increased removal of ash, with lower pH treatments having lower ash contents for their respective temperature. The exception being acetic acid (pH 2.88) which appears to have slightly lower ash content than formic acid (pH 2.38). Yields on a dry basis also appear influenced by pH, with higher yields associated with lower pH. The exception to this being sulphuric acid at lower temperatures, with lower yields observed at 120 °C than the higher pH treatments. This lower yield is in part because of the reduced ash content although lower yields can also be associated with enhanced oxygen removal. Due to the variation between ash contents with differing pH, Table 9.2 gives the ultimate analysis on a dry ash free (daf) basis, to enable direct comparisons between the organic chemistry of the different treatments. The results show that for the 120 °C treatment in sulphuric acid there is a higher carbon density and lower oxygen content for this treatment than the higher pH treatments at this temperature.

A Van Krevelen plot of the bio-coals from different pH and temperatures is given in Figure 9.1. The results show that with increasing temperature the bio-coals have more coal-like properties, with the plot indicating the fuel is undergoing increasing dehydration with increasing temperature and decreasing pH. pH appears to influence coalification with sulphuric acid (pH 1) giving the most dehydrated fuel at 120 °C and 170 °C; the 170 °C results show most clearly that the sulphuric acid is dehydrating the most, and the sodium hydroxide (pH 13) dehydrating the least at this temperature. This result fits with findings of Van Krevelen and co-workers in the 1950s and 1960's who, amongst other parameters, found the pH had an outcome of the carbonisation reaction [19, 20]. The results do however indicate that with increasing temperature the influence of the pH on dehydration becomes less, with the fuels from all conditions becoming similar in terms of atomic ratios at the higher temperatures.

The most dehydrated / coalified fuels for the 250 °C treatments are actually in the presence of formic acid followed by acetic acid (pH 2.38 and 2.88 respectively). The dry ash free ultimate analysis data presented in Table 9.2 indicates that these two acid-treated bio-coals have the highest carbon density with 71 % (daf). This higher carbon content could however be due to formic and acetic acid being organic acids, which would result in increased carbon within the hydrothermal reaction. This may well explain the higher

carbon content and lower O/C ratio. Use of a mineral acid at pH 2.38 and 2.88 respectively could well give an O/C ratio similar to that of water in Table 9.2 and Figure 9.1.

The results given in Table 9.2 suggest that the bio-coal from sulphuric acid at 250 °C has the lowest carbon content at 66 % (daf). The sulphuric-acid-samples have however acquired sulphur from the acid, which makes up 4 % (daf) of the fuel. Given the other samples are low in sulphur; the sulphur will reduce the relative carbon content of the fuel when compared to the other treatments, even when correcting to a dry ash free basis. The analysis of the 250 °C bio-coals in Table 9.2 would suggest the bio-coal is similar in property to Lignite A coal as described in Smith et al. [64] for all pH treatments.

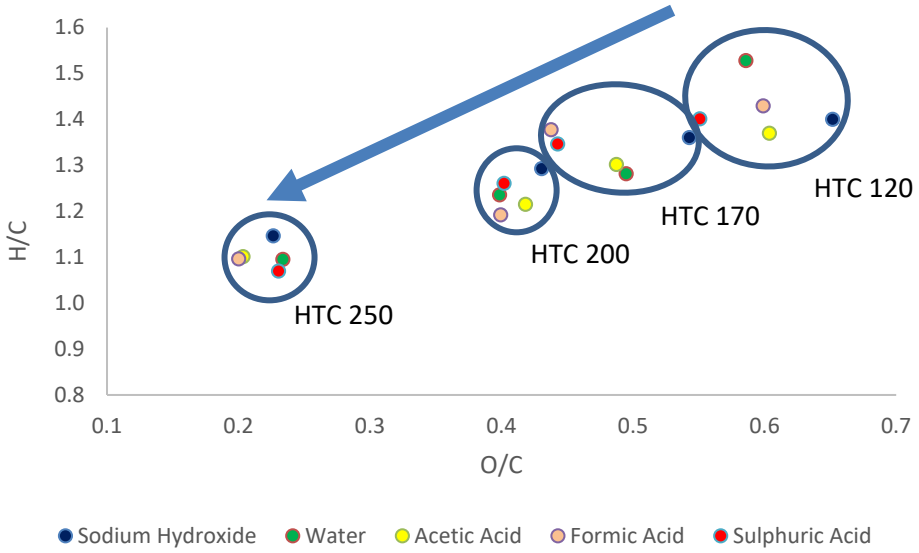

Figure 9.1: Van Krevelen plot of the bio-coals from different pH and temperature

Table 9.1: Ultimate analysis and yields of fuels on a dry basis

Sample Name	Dry Basis											
	Yield (%)	C (wt %)		H (wt %)		N (wt %)		S (wt %)		0 (wt%)		Ash (wt %)
Sodium Hydroxide 120°C	84	42.7	±0.3	5.0	±0.0	2.4	±0.0	0.1	±0.0	37.1	±0.5	12.6
Sodium Hydroxide 170°C	64	45.0	±0.2	5.1	±0.1	2.1	±0.0	0.1	±0.0	32.6	±0.9	15.2
Sodium Hydroxide 200°C	59	48.4	±0.2	5.2	±0.1	2.4	±0.0	0.2	±0.0	27.8	±0.0	16.0
Sodium Hydroxide 250°C	41	49.8	±0.0	4.8	±0.0	2.5	±0.0	0.3	±0.0	15.0	±0.1	27.6
Water 120°C	86	45.4	±0.5	5.8	±0.4	2.4	±0.1	0.1	±0.0	35.5	±1.0	10.7
Water 170°C	62	47.3	±0.3	5.0	±0.0	2.3	±0.1	0.2	±0.0	31.2	±0.4	14.0
Water 200°C	59	50.8	±0.3	5.2	±0.0	2.4	±0.0	0.2	±0.0	27.0	±0.1	14.3
Water 250°C	43	53.5	±3.4	4.9	±0.4	2.8	±0.2	0.3	±0.0	16.7	±0.3	21.9
Acetic Acid 120°C	83	45.0	±0.2	5.1	±0.0	2.6	±0.2	0.1	±0.0	36.2	±0.4	11.0
Acetic Acid 170°C	61	47.9	±0.7	5.2	±0.1	2.5	±0.1	0.1	±0.0	31.1	±0.6	13.0
Acetic Acid 200°C	59	50.1	±0.8	5.1	±0.1	2.3	±0.1	0.1	±0.0	27.9	±1.9	14.5
Acetic Acid 250°C	44	56.6	±0.6	5.2	±0.1	2.9	±0.0	0.2	±0.0	15.4	±0.1	19.7
Formic Acid 120°C	83	45.0	±1.1	5.4	±0.2	2.5	±0.1	0.2	±0.0	35.9	±1.4	11.0
Formic Acid 170°C	61	49.8	±0.1	5.7	±0.2	2.6	±0.0	0.2	±0.0	29.0	±0.9	12.7
Formic Acid 200°C	58	50.8	±0.2	5.0	±0.1	2.3	±0.1	0.2	±0.0	27.1	±0.3	14.6
Formic Acid 250°C	44	56.0	±1.4	5.1	±0.1	2.9	±0.1	0.3	±0.0	14.9	±0.3	20.8
Sulphuric Acid 120°C	75	47.9	±0.5	5.6	±0.0	2.2	±0.0	1.0	±0.0	35.2	±2.3	8.1
Sulphuric Acid 170°C	58	50.5	±0.6	5.7	±0.0	2.4	±0.1	1.7	±0.1	29.8	±0.7	10.0
Sulphuric Acid 200°C	57	52.4	±0.2	5.5	±0.0	2.2	±0.0	1.7	±0.0	28.1	±0.2	10.1
Sulphuric Acid 250°C	47	56.4	0±.7	5.0	±0.1	2.7	±0.0	3.4	±0.0	17.3	±0.3	15.1

Table 9.2: Ultimate analysis, proximate analysis and yields of fuels on a dry ash free basis

Sample Name	Dry Ash Free Basis									
	yield (%)	C (wt%)	H (wt%)	N (wt%)	S (wt%)	O (wt%)	H/C	O/C	Volatile Matter (%)	Fixed Matter (%)
Sodium Hydroxide 120°C	84	48.9	5.7	2.8	0.2	42.5	1.40	0.65	80	20
Sodium Hydroxide 170°C	62	53.0	6.0	2.4	0.1	38.4	1.36	0.54	80	20
Sodium Hydroxide 200°C	57	57.7	6.2	2.8	0.2	33.1	1.29	0.43	77	23
Sodium Hydroxide 250°C	34	68.8	6.6	3.4	0.4	20.8	1.15	0.23	68	32
Water 120°C	88	50.9	6.5	2.7	0.2	39.7	1.53	0.59	82	18
Water 170°C	61	54.9	5.9	2.7	0.3	36.2	1.28	0.49	78	22
Water 200°C	58	59.3	6.1	2.8	0.3	31.5	1.24	0.40	76	24
Water 250°C	38	68.5	6.2	3.6	0.4	21.3	1.09	0.23	67	33
Acetic Acid 120°C	85	50.5	5.8	2.9	0.2	40.7	1.37	0.60	80	20
Acetic Acid 170°C	61	55.1	6.0	2.9	0.2	35.8	1.30	0.49	79	21
Acetic Acid 200°C	58	58.6	5.9	2.7	0.2	32.7	1.21	0.42	75	25
Acetic Acid 250°C	40	70.5	6.5	3.7	0.3	19.1	1.10	0.20	67	33
Formic Acid 120°C	85	50.6	6.0	2.8	0.2	40.4	1.43	0.60	81	19
Formic Acid 170°C	61	57.0	6.5	3.0	0.2	33.2	1.38	0.44	79	21
Formic Acid 200°C	57	59.5	5.9	2.6	0.2	31.7	1.19	0.40	75	25
Formic Acid 250°C	40	70.7	6.5	3.6	0.3	18.9	1.10	0.20	68	32
Sulphuric Acid 120°C	79	52.1	6.1	2.4	1.1	38.3	1.40	0.55	83	17
Sulphuric Acid 170°C	60	56.1	6.3	2.6	1.9	33.1	1.35	0.44	83	17
Sulphuric Acid 200°C	59	58.3	6.1	2.4	1.9	31.3	1.26	0.40	76	24
Sulphuric Acid 250°C	46	66.4	5.9	3.2	4.0	20.4	1.07	0.23	66	34

Yields are corrected to give yield on a dry ash free basis in Table 9.2. It appears that decreasing pH increases yields for temperatures above 250 °C but decreases yields for temperatures below 200 °C. This would appear to be due to pH enhancing the rate of hydrolysis. The generation of hydronium ions due to the presence of acids are known to catalyse the hydrolysis of hemicellulose and cellulose into monosaccharides in lignocellulosic biomass [84]. Figure 9.2 shows the combustion profiles of the bio-coals following different treatment with different pH and temperature. While no fibre analysis has been undertaken as part of this work the 120 °C, 170 °C and 200 °C treatments have a distinct volatile burn peak at around 300 °C which is normally consistent with the presence of cellulose within a fuel [260]. For the 250 °C treatments the results displayed in Figure 9.2 show this peak is all-but-removed from the profiles of all fuel. This would suggest that cellulose or 'cellulose-like' components within the feedstock are removed by 250 °C. It appears likely that the lower yields associated with lower pH in the 120 °C, 170 °C and 200 °C treatments are due to the lower pH enhancing the hydrolysis of the cellulose or 'cellulose-like' components within the feedstock, resulting in its removal from the resulting bio-coal. For the 250 °C treatment the increased yield at lower pH would suggest that pH is also catalysing repolymerisation.

In HTC the hydrolysis of components such as hemicellulose and cellulose results in the formation of monosaccharides within the process water. These then undergo dehydration and fragmentation before repolymerisation and condensation leading to the formation of the char, as discussed in Section 2.3.2 [309, 348]. pH should play a key role in this polymerisation due to the influence pH has on zeta potential. Zeta potential, or as it is more correctly known, electrokinetic potential, is a key indicator of the stability of colloidal dispersions. The magnitude of the zeta potential indicates the degree of repulsion of likewise-charged particles in a dispersion. A high zeta potential will mean the solution or dispersion will resist agglomerating and flocculating. Bio-coals have a negative zeta potential as the HTC materials have negative acidic oxygenated groups on the surface, making them behave like weak acids [91]. When alkali is added to a hydrothermal suspension, the particles will tend to acquire a more negative charge and this will reduce the chance of them flocculating and forming the char. This is demonstrated in the bio-coal produced in sodium hydroxide solution at 250 °C, which has the lowest yield. If acid is added to the suspension a point is reached where the negative charge is neutralised [135]. The point zeta is at zero is the isoelectric point and would be the point the suspension is most likely to flocculate. For the water and acid treated experiments lower pH increases yields for the 250 °C treatments, which would suggest that lowering pH is

reducing the electrokinetic potential of the decomposition products within the aqueous phase enabling them to polymerise and increase char yield.

When looking at the bulk properties, excluding sulphur content, (carbon, hydrogen, nitrogen, oxygen, fixed carbon and volatile carbon) there appears limited difference between the bio-coals that have undergone HTC at 250 °C, other than yield. This would support the assertion that at this temperature pH is catalysing repolymerisation, with the char otherwise similar in composition. The exception being formic and acetic acid, albeit this difference appears to be due to these acids being organic acids, resulting in increased carbon within the hydrothermal reaction, as previously discussed.

The idea that lower pH is catalysing flocculation and polymerisation will also support the findings of Ghanim et al. [133]. Ghanim et al. [133] looked into the HTC of poultry litter at 250 °C for 2 h using various initial pH with sulphuric acid and found increasing sulphuric acid content appeared to both increase yield and decrease ash content. This however contradicts the findings in Chen et al. [134] who used sulphuric acid and bagasse, who found the inverse. Shorter retention times were however used in Chen et al. [134] (5 minutes, 15 minutes and 30 minutes). Given repolymerisation and aromatisation is considerably slower than hydrolysis, decarboxylation and dehydration reactions [11], it appears plausible that the longer retention time in Ghanim et al. [133] enabled greater repolymerisation than seen in Chen et al. [134].

9.4.2. Influence of pH on fuel inorganic chemistry

The metal analysis of the bio-coals and unprocessed pig manure is given in Table 9.3. The results show that despite apparent increases in ash content the overall inorganic chemistry changes depending on both the temperature of the treatment and the pH. For all treatments almost all potassium, sodium and strontium (typically in excess of 95 %) goes into the aqueous phase. The 120 °C treatment with water demonstrates that for all three metals around 11% of the original metal is retained within the char, with the remaining 11 % gradually reduced with increasing temperature. Almost complete removal is seen at 250 °C, regardless of pH. The exception being for the sodium hydroxide treatments. At 120 °C the sodium content actually increases due to residual sodium hydroxide being retained within the char. This said, by the 250 °C treatment, the bio-coal has the equivalent of only 12 % of the original sodium in the feedstock along with almost complete removal (98 %) of the potassium. This would suggest a reduced cation exchange capacity in the 250 °C bio-coals.

The results of the 120 °C treatment with water are significant as autoclaving fuel samples at 120 °C for one hour in water is a method for determining free ionic salts within a biofuel, as provided in BS EN ISO 16995-2. Consequently, metals removed in this treatment can, under BS EN ISO 16995-2, be regarded as in free ionic form. This result would suggest that around 90 % of the sodium, potassium and strontium are in free ionic forms, along with 40 % of the magnesium and 25 % of the phosphorus. The calcium, aluminium, silicon, manganese, iron, copper and zinc do not appear to be in a water soluble ionic form. In higher plants typically over 90 % of potassium and sodium is in ionic form, while 60-90 % and 30-85 % of magnesium and calcium is ionic [38]. The results for the 120 °C treatment with water would suggest that for pig manure there is a similar proportion of free ionic potassium and sodium in the fuel, but a greater proportion of the calcium, magnesium and phosphorus is either organically associated or present in mineral form than in lignocellulosic biomass [37, 39]. The relatively low extraction of phosphorus in water at 120 °C would suggest phosphorus is present as low solubility salts such as calcium and magnesium phosphate.

The behaviour of silicon is particularly notable in the results as for all pH treatments it appears to undergo increasing removal with increasing temperature, with between 45 and 60 % retained, depending on pH, at 250 °C. As stated in Chapter 4 and 5, silicon appears reasonably recalcitrant, largely being retained in the bio-coal. The removal is surprising, since while silicon can be water soluble, to become water soluble silicon has to be hydrated and become silicic acid (H_4O_4Si), which unless kept buffered within certain boundaries, readily degrades back to insoluble silicon dioxide (SiO_2) [213, 260]. Partial dissolution of silicon was reported in Fellinger et al. [150] so it appears under correct conditions part removal is possible.

Magnesium retention appears to be strongly influenced by pH with the highest retentions seen with the sodium hydroxide solutions (pH 13) and reduced retention with decreasing pH. Temperature also appears highly important with the highest removal typically at 170 °C and increasing retention at 200 °C and 250 °C at all pH.

Table 9.3: Main inorganics present within the unprocessed pig manure and derived bio-coals

Sample Name	mg/kg fuel (db)											
	Na	K	Mg	Ca	Al	Si	P	Mn	Fe	Cu	Zn	Sr
Unprocessed Pig Manure	1426	12100	9395	27035	434	3654	15197	314	1090	140	634	367
Sodium Hydroxide 120°C	2933	4126	9869	30212	413	3447	15431	445	1278	153	604	39
Sodium Hydroxide 170°C	2020	2927	10002	41385	620	4067	19254	633	1712	230	864	61
Sodium Hydroxide 200°C	1121	1371	7056	45915	715	3324	24748	531	1797	254	963	51
Sodium Hydroxide 250°C	404	577	17221	74240	1174	10311	41254	819	3177	394	1771	93
Water 120°C	193	1493	6232	31645	546	3710	13139	411	1464	195	701	45
Water 170°C	92	1043	5388	41790	674	3249	21806	599	1632	227	788	61
Water 200°C	156	411	6544	38053	660	3203	25178	452	1224	197	657	40
Water 250°C	n/d	392	10323	61727	1008	4533	36468	766	2287	380	1444	80
Acetic Acid 120°C	199	1920	4201	30840	572	4709	15020	433	1447	220	701	45
Acetic Acid 170°C	37	469	4201	38345	783	3699	20876	499	1527	262	758	45
Acetic Acid 200°C	105	425	4596	43490	721	3321	23494	573	1555	271	853	55
Acetic Acid 250°C	53	397	7123	57455	941	3504	34106	590	2252	324	1489	71
Formic Acid 120°C	114	1048	3685	30815	576	5344	15808	403	1523	208	653	42
Formic Acid 170°C	85	644	3624	37304	750	3995	20297	462	1336	234	642	48
Formic Acid 200°C	125	508	4542	43529	809	3646	24236	500	1411	286	803	55
Formic Acid 250°C	161	743	8307	60023	1023	4893	34543	901	2528	317	1516	89
Sulphuric Acid 120°C	171	1312	1490	19342	609	5182	2566	56	518	195	234	27
Sulphuric Acid 170°C	160	1252	1170	25280	670	4559	1728	n/d	593	222	226	28
Sulphuric Acid 200°C	125	1213	2152	24507	709	4287	3815	138	734	203	281	32
Sulphuric Acid 250°C	28	406	4083	34688	877	3472	6670	414	1295	336	923	55

For magnesium, there is an initial decrease in metal concentration in the bio-coal produced at up to 170 °C, followed by increased retention of metal in the bio-coal with increasing temperature between 200 °C and 250 °C. The metal retention behaviour is also observed for calcium, magnesium, iron and zinc, along with phosphorus. For these elements there appears almost complete retention within the bio-coal at 250 °C for the sodium hydroxide, water, acetic acid and formic acid treatments. The exception to this is sulphuric acid, which extracts 50 % of the calcium between 120 °C and 200 °C, with 60 %, retained at 250 °C. Most phosphorus is also extracted by the sulphuric acid with 87 % extracted at 120 °C and 200 °C respectively; over 90 % is extracted at 170°C. 80 % of the original phosphorus is extracted at 250 °C, leaving 20 % of the original phosphorus within the bio-coal. Similar extraction ratios observed for phosphorus are seen with magnesium using sulphuric acid. Aluminium and copper appear to remain within the bio-coal irrespective of temperature and pH.

The additional removal of the metals with the sulphuric acid is due to the high dissociation constant of sulphuric acid, which is a strong acid and forms hydronium ions in two stages, with the initial loss of a hydrogen (Equation 9.1) and the subsequent decomposition of the bi-sulphate (Equation 9.2). 0.1 molar sulphuric acid gives a pH of 1 but the same pH is possible using the same concentration of other strong mineral acids such as hydrochloric acid, or higher concentrations of weaker acids such as acetic acid which only partially dissociate, (hence pH 2.88 at the same molar concentration). The justification for using acid catalysts in HTC in Ekpo et al. [131], Dai et al. [132] and [371] is to principally mobilise the phosphorus into the aqueous phase for subsequent recovery.

The relatively low extraction of phosphorus in water at 120 °C would suggest phosphorus is present as low solubility salts such as calcium and magnesium phosphate. The high concentrations of hydronium ions generated by the sulphuric acid are required for the acid leaching of the phosphorus, with the mechanism for acid leaching of calcium given in Equation 9.3. With sulphuric acid the calcium is converted to calcium sulphate (see Equation 9.4) liberating the phosphorus as phosphoric acid [373]. Similar phosphorus extraction is possible using hydrochloric acid, albeit when leaching iron ores slightly higher efficiency is observed for sulphuric acid [373]. Greater calcium extraction maybe possible using hydrochloric acid as calcium chloride is more water soluble than calcium sulphate (745 g/l as opposed to 2.6 g/l at STP). This could explain the higher retention of calcium in the bio-coal when compared with magnesium, phosphorus,

manganese, iron and zinc, as the process water maybe saturated once cooled to room temperature.

$$H_2SO_4 + H_2O \rightarrow H_3O^+ + HSO_4^- \qquad K_1 = 2.4 \times 10^6 \text{ (Strong Acid)} \quad (9.1)$$

$$HSO_4^- + H_2O \rightarrow H_3O^+ + SO_4^- K_2 = 1.0 \times 10^{-2} \qquad (9.2)$$

$$Ca_{10}(PO_4)_6X(s) + 20H^+ = 6H_3PO_4\ 10Ca^{2+}\ H_2X \qquad (9.3)$$

$$Ca^{2+} + SO_4^{2-} = CaSO_4 \quad (9.4)$$

9.4.3. Influence of pH on fuel combustion chemistry

Table 9.4 gives the energy content, the volatile content and the results of slagging and fouling indices derived from the inorganic chemistry given in Table 9.3. The results show that the reaction temperature has the biggest impact on the energy content of the fuel, irrespective of the pH. The results show that HTC with sodium hydroxide gives the lowest energy density at all temperatures. This indicates that undertaking HTC in the presence of acids at decreasing pH increased the HHV of the bio-coal, as demonstrated in Ghanim et al. [133]. The highest HHV was observed for bio-coal formed in acetic and formic acid due to their higher carbon contents, i.e. increased carbon within the hydrothermal reaction, as previously discussed. Despite this, there still appears a trend of increasing HHV with decreasing pH.

The volatile carbon content of the bio-coal is given in Table 9.4. The volatile carbon content is important as it is derived by the thermal decomposition of the fuel in the pyrolysis stage of combustion. When devolatilising these volatiles prevent oxygen getting to the fuel particle, oxidising the carbon, hydrogen, and sulphur present. As thermal energy is able to penetrate the particle but the oxygen is not, a solid fuel particle undergoes pyrolysis until devolatilised [182]. Moreover the escaping volatiles burn much more quickly than the char (the fraction remaining after devolatilisation) and therefore understanding the devolatilisation behaviour of a fuel is important in terms of flame ignition, flame stability, flammability limits and the formation of pollutants such as nitrogen oxides [68]. The volatile content is also useful when determining the equivalent coal rank, with coals with higher ranks having lower volatile contents, as discussed in Section 2.2.

The volatile carbon appears to be most strongly influenced by reaction temperature, with lower volatile content present with increasing reaction temperature. This appears to be due to removal of fibrous material. Figure 9.2 shows the combustion profiles of the bio-coals following different treatments. In Figure 9.2 the 120 °C, 170 °C

and 200 °C treatments have a distinct volatile burn peak at around 300 °C which is normally consistent with the presence of cellulose within a fuel [260]. For the bio-coals produced at 250 °C and above this peak is much smaller in the profiles of all fuels. The repolymerised ‘humins’ derived from the hemicellulose and cellulose are similar to humic acids which are the thermal degradation products of lignin [25]. Consequently, the repolymerised material is likely to remain within the fixed carbon portion of the fuel along with the lignin. While pig manure is not strictly lignocellulosic in nature it is still likely from lignocellulosic origin and contain materials such as wheat straw so these assumptions should stand.

The results presented in Ghanim et al. [133] stated that low pH with sulphuric acid brought higher volatile carbon contents in the bio-coal, however this contradicts the findings in Chen et al. [134] who used sulphuric acid and bagasse and found the inverse. The volatile contents presented in Table 9.4 would initially support the findings of Ghanim et al. [133], however the reason the volatile carbon appears to increase is due to the decrease in ash content of the fuel, increasing the relative amount of volatile carbon present. Due to the variation between ash contents with differing pH the volatile contents have been calculated on a dry ash free basis in Table 9.4. This enables direct comparisons between the volatile chemistry of the different treatments. The results show little change between pH, perhaps even suggesting a small decrease in the volatile matter content of the 250 °C treatments with decreasing pH. In the work presented in Chen et al. [134] the fuel was considerably lower in ash than the samples used in Ghanim et al. [133], consequently there would not be the apparent increase in volatile carbon due to the decrease in ash content of the fuel. Thus, the results presented here support the findings of both studies.

Table 9.4 Energy content, volatile content and slagging and fouling indices for the bio-coals

Sample Name	Dry Basis					
	HHV (db)	Volatile Matter (%)	Fixed Matter (%)	AI	BAI	Rb/a
Sodium Hydroxide 120°C	14.9	70.9	18.1	0.86	0.14	9.05
Sodium Hydroxide 170°C	16.7	67.9	16.7	0.54	0.27	8.76
Sodium Hydroxide 200°C	18.9	62.8	18.8	0.25	0.55	9.91
Sodium Hydroxide 250°C	21.0	48.3	22.4	0.09	2.55	5.76
Water 120°C	17.3	76.9	16.9	0.13	0.90	6.63
Water 170°C	17.6	68.3	18.9	0.09	1.55	8.73
Water 200°C	19.8	65.7	20.3	0.05	1.92	8.31
Water 250°C	22.1	54.0	27.0	0.02	6.92	9.32
Acetic Acid 120°C	16.1	69.9	17.1	0.18	0.73	4.97
Acetic Acid 170°C	18.1	67.3	17.8	0.04	3.29	6.81
Acetic Acid 200°C	19.2	63.2	21.0	0.04	2.80	8.52
Acetic Acid 250°C	23.8	53.4	26.2	0.03	5.19	10.44
Formic Acid 120°C	16.5	73.5	16.9	0.10	1.39	4.27
Formic Acid 170°C	19.8	69.3	18.1	0.05	1.90	6.19
Formic Acid 200°C	19.6	63.4	21.1	0.05	2.12	7.72
Formic Acid 250°C	23.6	55.4	25.8	0.06	2.72	8.35
Sulphuric Acid 120°C	17.9	77.7	16.4	0.11	0.36	2.66
Sulphuric Acid 170°C	19.8	74.3	14.8	0.10	0.44	3.67
Sulphuric Acid 200°C	20.6	66.7	20.9	0.09	0.58	3.91
Sulphuric Acid 250°C	23.2	56.3	28.7	0.02	3.28	6.41

Figure 9.2 shows the DTG combustion profiles of the bio-coals following different treatments. For the 120 °C treatment in the presence of acids the first initiation temperature is lower, with weight loss starting at 160 °C for bio-coal from the three acid treatments but 200 °C for bio-coal from the water and alkali treatment. The water, acetic acid and formic acid treatments yield bio-coals which display an initial peak at 300 °C which can be consistent with the presence of the structural component hemicellulose, followed by a larger second peak at 325 °C which is typically associated with cellulose in lignocellulosic biomass [260]. This peak is the devolatilisation or volatile burn of the fuel and this temperature would be regarded as the second initiation temperature following the Babcock and Wilcox TGA method [374]. Given the Babcock and Wilcox TGA method is designed for coal and applied to biomass, normally for coal combustion

the fuel burn is predominantly associated with the char combustion (third initiation temperature), with coal giving a burning profile similar to the 250 °C bio-coals in Figure 9.2 [260].

For the sample produced in sulphuric acid at 120 °C there does not appear to be a distinct peak where the ‘hemicellulose like’ material decomposes but the presence of a shoulder at 300 °C. The higher mass loss between 160 °C and 300 °C when compared to the other samples may suggest that the ‘hemicellulose like’ component is still present but partially hydrolysed resulting in it thermally decomposing earlier. The sodium hydroxide treatment has only one distinct volatile peak, peaking about 300 °C. This result is most likely a consequence of the strong basic conditions degrading the ‘hemicellulose like’ material observed with the strong acid conditions but could also be the high sodium and potassium contents of the fuel (see Table 9.3) catalysing the volatile burn [208]. Both the sodium hydroxide and sulphuric acid treatments yield products which have higher char burn temperatures, with temperatures of 500 °C as opposed to 450 °C for the other treatments. The burnout temperature is similar at 580 °C for all treatments.

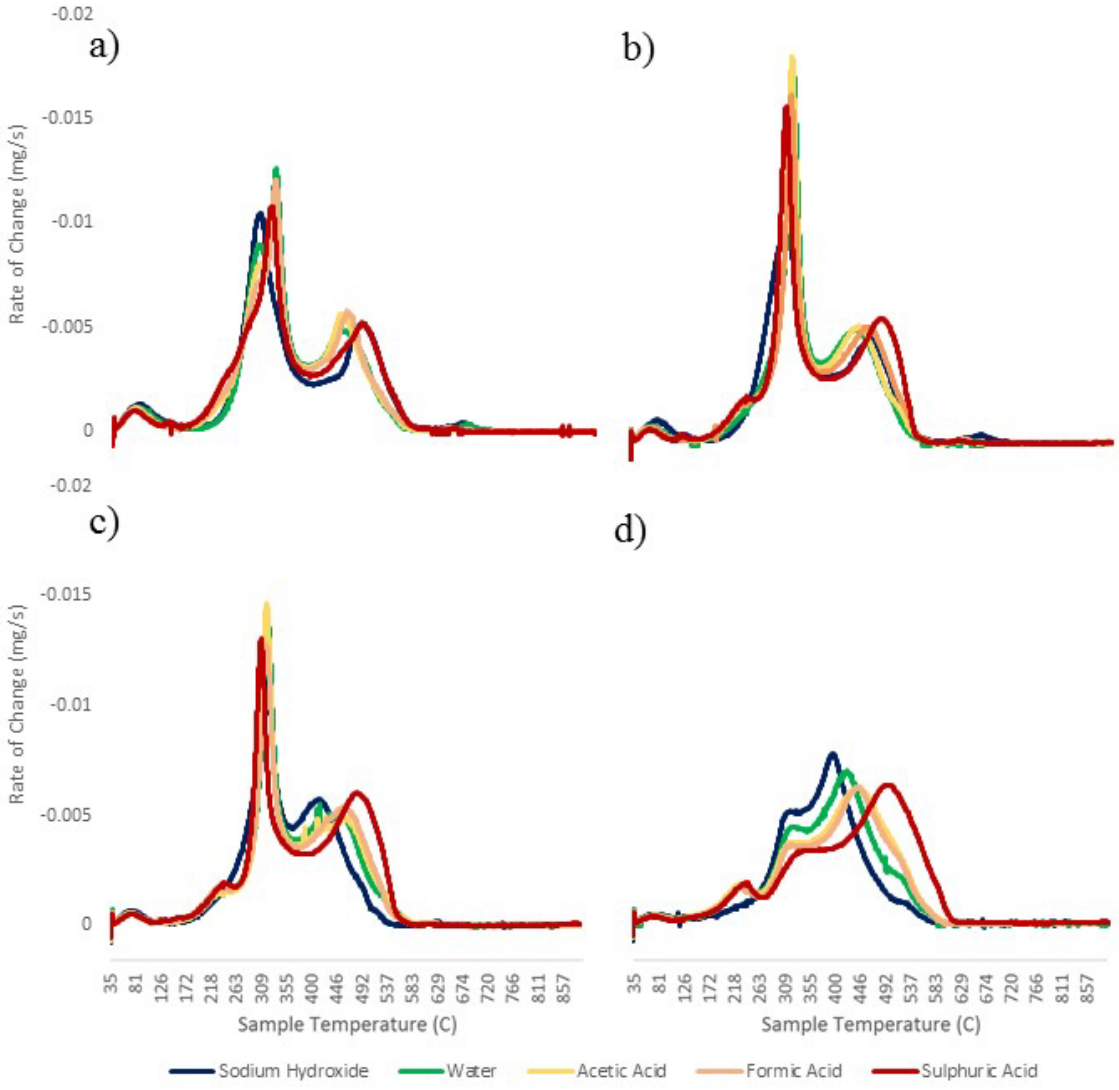

Figure 9.2: Derivative thermogravimetric (DTG) burning profiles for a) 120 °C, b) 170 °C, c) 200 °C and d) 250 °C treatments

As the process severity increases the profiles for the bio-coals generated at 170 °C, 200 °C and 250 °C retain the first initiation temperature of 160 °C and a new initial peak begins to arise at 235 °C for experiments in water and acids; this initially starts on the profile for the bio-coal generated at 170 °C but becomes increasingly pronounced into the 250 °C profile. This does not appear in the bio-coals produced in sodium hydroxide, which have a different combustion profile. This peak was also observed in bio-coals studied in Chapter 7 and Py-GCMS analysis identified the presence of a series of phenolic compounds with a host of methoxybenzoaldehydes. In Chapter 7 it was hypothesised that this peak was HTC-derived aromatic structures which are chemisorbed through reactive oxygen functionalities, yet to form the stable ether or pyrone bonds within the char

formation [85]. Their absence in alkaline conditions would suggest that this mechanism is acid catalysed or inhibited by alkaline conditions.

For all the bio-coals generated at 170 °C and 200 °C the combustion profiles contain a volatile peak which becomes increasingly dominant at 325 °C. This is most noticeable for 170 °C bio-coal as by treatment at 200 °C the volatile content within the fuel has decreased (see Table 9.4). By the 250 °C treatments the samples adopt a 'coal-like' overlapping combustion profile [260], whereby the transition between the volatile release and initiation of char burn (second initiation temperature) is marked more by a 'shoulder' as opposed to a distinct peak. This shoulder becomes less distinct with bio-coals formed at lower pH and correlates with a modest reduction in volatile matter. The benefits of this in terms of combustion are discussed in detail in 5.3.3.2.

For all the bio-coals with increasing reaction severity, lower pH increases char burnout temperature. This is particularly notable for those prepared at 250 °C as the peak temperature (char burn) increases from 400 °C for those produced in sodium hydroxide (pH 13) to 500 °C for those formed in sulphuric acid (pH 1). This result would suggest pH influences reactivity of the char. There is strong consensus in the literature that the alkali metals, potassium and sodium, catalyse char reactivity [160, 207-209], albeit the concentrations of alkali metals appears similar for the 250 °C bio-coals (see Table 9.3). The alkaline earth metals, calcium and magnesium, are understood to catalyse char reactivity but to a lesser extent than the alkali metals [209-211], with iron known to behave using similar mechanisms [212]. Given pH appears to more strongly influence alkaline earth metal content; with higher calcium and magnesium contents, along with iron, associated with higher pH (see Table 9.3), it is possible that the higher concentrations at higher pH is catalysing the thermal decomposition.

An ash fusion test was undertaken and Figure 9.3 displays the ash transition temperatures for the ashes of bio-coal from the four different temperatures and five different pH. Table 9.5 gives the transition temperatures for all samples along with the unprocessed sample and their standard errors. The results suggest that the unprocessed swine manure has a reasonably high deformation temperature, of 1320 °C, compared to between 980 °C and 1140 °C for the conventionally harvested *Miscanthus* [213, 260]. Despite this result, the slagging and fouling indices suggest almost certain slagging and fouling for these samples. The results of the ash fusion test certainly would suggest a low slagging fuel, possibly due to the high calcium and phosphorus content of the fuel. This would strongly suggest that calcium potassium phosphate complexes and calcium sodium

phosphate complexes are removing the potassium and sodium available to form low temperature melting potassium and sodium silicates [200, 202].

The results of the bio-coal formed in the 120 °C treatment with water would suggest that around 90 % of the sodium and potassium in the fuel is in the form of free ionic salts. Potassium and sodium when in the form of free ionic salts are more readily released into the vapour phase and likely to bring about issues with fouling [39, 205, 267]. The high calcium and phosphorus content of the fuel may however prevent this release, instead forming the stable calcium potassium phosphate complexes and calcium sodium phosphate complexes [234]. The slagging and fouling indices used in this paper would not consider such mechanisms when predicting the fuels propensity to slag and foul.

The deformation and hemisphere temperatures appear to change little, indicating limited change to slagging propensity. The exception to this being the sample produced at low temperature in sodium hydroxide and at 250 °C in sulphuric acid. The 120 °C, 170 °C and 200 °C sodium hydroxide samples showing increased deformation and hemisphere temperatures despite being the only hydrothermal samples where the alkali index (given in Table 9.5) suggests almost certain slagging and fouling. Given the sodium and potassium content is reduced compared to the starting feedstock, this reduction may explain the increase.

The bio-coal produced at 250 °C in sulphuric acid has the greatest improvement in ash behaviour with the sample not undergoing deformation within the test conditions (test limit 1570 °C). This is predominantly due to the ash becoming a highly stable magnesium calcium phosphate silicate complex. It should be noted that the samples generated in sulphuric acid have acquired sulphur from the acid, which makes up 3.4 % (db) of the fuel.

When combusting fuel in pulverised applications fuel sulphur can be desirable as while sulphur emissions are largely in the form of sulphur dioxide some sulphur trioxide is also formed. Sulphur trioxide plays an important role in the abatement of particulate emissions, by forming sulphuric acid in the flue gas which absorbs onto particulates in the flue gas [226]. This effects the surface electrical conductivity of the particulate, greatly increasing the efficiency of the electrostatic pacificators [224]. Biomass being typically low in sulphur can give a very low collection efficiency of electrostatic precipitators [225]. Consequently, when a fuel with high sulphur content is combusted, there is generally enough sulphur trioxide formed to bring the electrical resistivity of the fly ash into a range which results in good precipitator operation [225]. This could be particularly advantageous for the 250 °C treated sulphuric acid sample given Potential to

Emit (PTE) metals (strontium, copper and zinc) are present within the swine manure and the derived hydrothermal fuels. Precipitation of these in the fly ash would be required to avoid issues with emissions. The sulphur content of the 250 °C treated sulphuric acid sample is however high so blending with low sulphur biofuels or coal would bring within 'design fuel' specification. Moreover, the magnesium calcium phosphate silicate ash of the fuel would have an additive influence and could improve the slagging and fouling propensity of the blended biomass and coal. Consequently, with blending, the 250 °C treated sulphuric acid fuel could be safely combusted within the pulverised fuel plant, albeit care would be required due to the high ash, sulphur and nitrogen content.

Table 9.5: Ash transition temperatures from the ash fusion test

Sample Name	Ash Transition Temperature (°C)							
	Shrinkage		Deformation		Hemisphere		Flow	
Unprocessed	1260	±0	1320	±0	1380	±0	1500	±0
Sodium Hydroxide 120°C	1140	±0	1510	±0	1560	±10	>1570	
Sodium Hydroxide 170°C	1330	±0	1460	±20	1500	±10	>1570	
Sodium Hydroxide 200°C	1040	±0	1380	±10	1420	±0	1530	±0
Sodium Hydroxide 250°C	1100	±0	1290	±0	1300	±0	1360	±0
Water 120°C	1070	±0	1440	±0	1480	±0	1520	±0
Water 170°C	1120	±0	1340	±0	1360	±0	1490	±0
Water 200°C	1000	±0	1340	±0	1370	±0	1430	±0
Water 250°C	1040	±0	1300	±0	1350	±0	1410	±0
Acetic Acid 120°C	1100	±0	1290	±0	1330	±0	1370	±0
Acetic Acid 170°C	1100	±0	1340	±0	1370	±0	1410	±0
Acetic Acid 200°C	1160	±0	1310	±0	1370	±0	1410	±0
Acetic Acid 250°C	1000	±0	1310	±0	1370	±0	1420	±0
Formic Acid 120°C	970	±0	1320	±0	1360	±0	1400	±0
Formic Acid 170°C	1080	±0	1350	±0	1380	±0	1420	±0
Formic Acid 200°C	1040	±0	1370	±0	1400	±0	1440	±0
Formic Acid 250°C	1270	±0	1320	±0	1360	±0	1410	±0
Sulphuric Acid 120°C	960	±0	1400	±80	1460	±60	1520	±20
Sulphuric Acid 170°C	990	±0	1290	±0	1545	±5	1560	±0
Sulphuric Acid 200°C	880	±0	1340	±0	1350	±0	1390	±0
Sulphuric Acid 250°C	1010	±0	>1570					

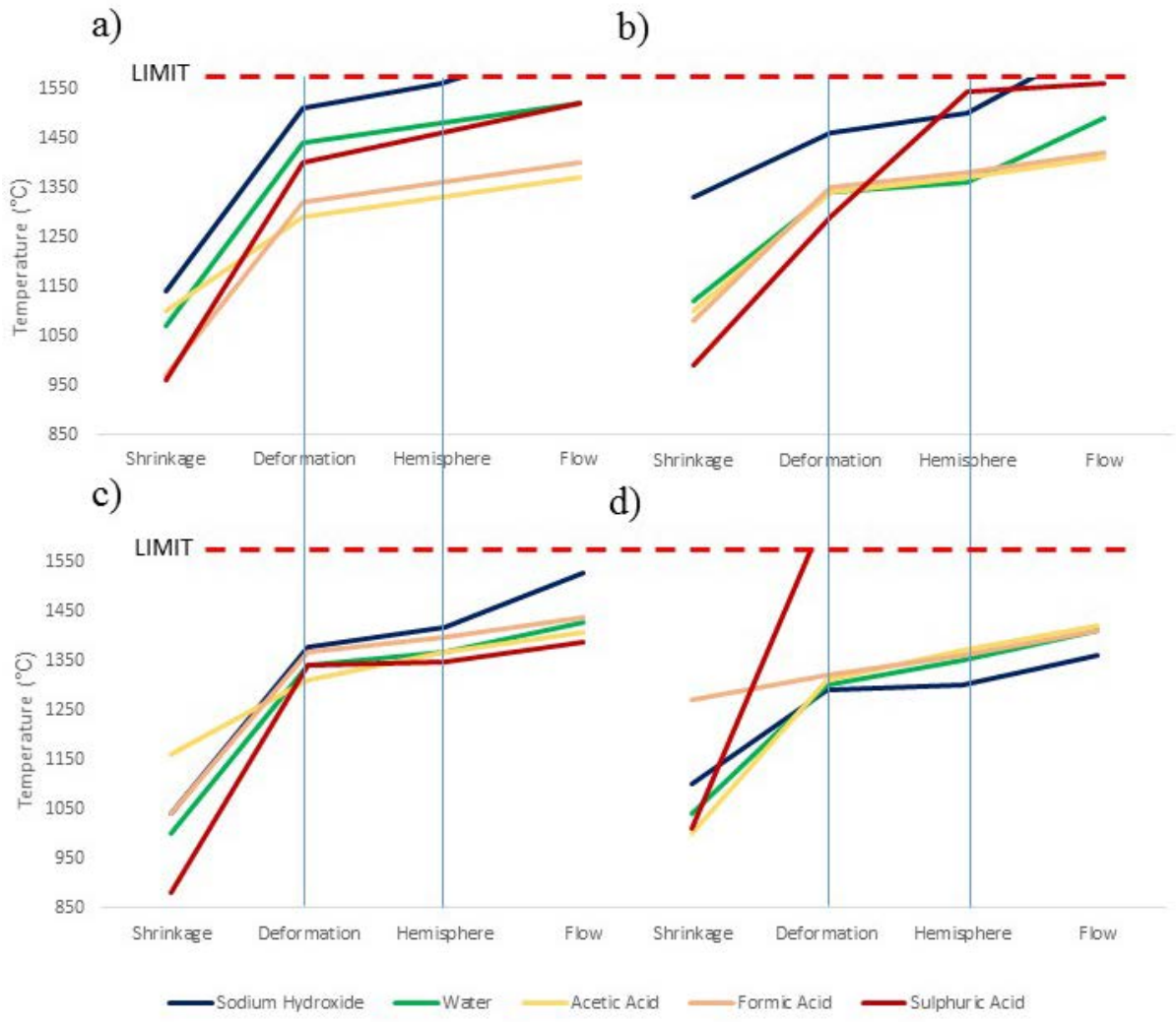

Figure 9.3: Ash transition temperatures from the ash fusion test

9.5. Conclusions

Control of pH during HTC most strongly influences ash chemistry of the resulting bio-coal, with decreasing pH increasing removal of ash. This reduction in ash has the biggest influence on the volatile carbon and energy content of the fuel; lower ash contents bring about higher energy densities when calculated on a dry basis. pH also influences dehydration, and the extent of dehydration increased with decreasing pH although when increasing the temperature the influence pH has on dehydration becomes less. pH and temperature appear to influence yield, with lower pH increasing yields for HTC above 250 °C but decreases yields below 200 °C. It is speculated that the lower yields below 200 °C are the result of the acids catalysing hydrolysis of 'cellulose like' fibres within the swine manure. The higher yields at 250 °C appear to be due to the low pH catalysing polymerisation due to its influence on the electrokinetic potential on the hydrothermal suspension.

HTC in water at 120 °C extracts free metal ions and results suggest that around 90 % of the sodium and potassium are in free ionic forms within the pig manure, along with 40 % of the magnesium and 25 % of the phosphorus. This free ionic sodium and potassium are more readily released into the vapour phase during combustion and likely to bring about issues with fouling; slagging and fouling indices suggest it cannot be safely combusted without treatment. The ash fusion test does however show reasonably high deformation temperature and would suggest low slagging and fouling. This seaming paradox is brought about through the high calcium and phosphorus content of the fuel which forms stable calcium potassium/sodium phosphate complexes. Hydrothermally treating the fuels achieves almost complete removal of sodium and potassium and should overcome their associated issues with fouling. Increasing reaction temperature appears to immobilise calcium, magnesium, iron, zinc and phosphorus within the bio-coal unless treated at low pH, which enables mobilisation of the phosphorus and alkaline earth metals.

Treatment at 250 °C results in a more coal-like fuel, with fuel properties similar to that of lignite coal and a HHV of between 21 and 23 MJ/kg depending on pH. The removal of the alkaline earth metal's and iron at pH 1 reduces the reactivity of the resultant bio-coal. Despite the mobilisation of calcium and phosphorus, using strong acid sufficient calcium and phosphorus is retained within the ash to give very favourable ash chemistry in terms of slagging and fouling.

10. Conclusions and further work

This research has set out to understand the role and fate of inorganics and heteroatoms during HTC of biomass. The objectives were: (i) to identify the behaviour of inorganics and heteroatoms in a range of biomass resources and their implications in combustion; (ii) understand how reaction parameters influence a fuel's inorganic and heteroatom chemistry; (iii) develop an understanding of the mechanisms behind the extraction of key metals and heteroatoms during the HTC of lignocellulosic biomass; and (iv) understand the potential catalytic mechanisms and roles inorganics and heteroatoms have during HTC. The specific chemistry for the main inorganics and heteroatoms found in biomass are summarised in the following sections but the findings have also led to a greater understanding of the fuel's handling and combustion chemistry, along with the underlying chemistry of the process itself. These findings are summarised below.

HTC, under the correct conditions, can lead to a significant improvement in fuel quality, with energy density improving from 10-18 MJ/kg to typically 25-30 MJ/kg on a dry basis, depending on feedstock. For uncatalysed HTC, the properties of this bio-coal is comparable to that of a low rank coal for *Miscanthus*, brown kelp and willow. In most of this work, two operating temperatures were typically used; 200 °C and 250 °C, with an hour retention time at the respective temperature. HTC at 200 °C improves the grindability of the biomass but results in limited energy densification in *Miscanthus*. HTC at 250 °C results in increased energy densification, producing a bio-coal with a HHV ranging from 25 to 30 MJ/kg depending on the feedstock. HTC can also increase the HGI of the fuel from 0 to in excess of 150 at 250 °C for *Miscanthus* and willow. This would represent a huge reduction in the energy requirements for milling if the fuel is used in pulverised fuel applications. At higher HTC temperatures, the combustion profile of the bio-coal exhibits a 'coal-like' overlapping volatile and char combustion profile and this, combined with the fact that the bio-coal grinds like coal, will overcome some of the limitations of burning biomass in pulverised coal plant.

Increasing retention times brings about dehydration of the fuel; however, temperature appeared the more important variable, as after 24 hours at 200 °C the fuel had similar properties to that of the 250 °C bio-coal with no retention time when processing *Miscanthus*. After one hour, cellulose appears to be largely removed from the 250 °C *Miscanthus* bio-coals. This dehydration, repolymerisation and cellulose removal brings about a 'coal-like' combustion profile, bio-coals with decreasing reactivity are formed with increasing retention time. Recycling process waters brings about an increase

in product mass yield at both treatment temperatures when processing *Miscanthus*. For 200 °C treatments the yields increase from 65% and stabilise at between 71 % and 73 % after four cycles. For the 250 °C treatments, increased product mass yield is seen from 46 % to over 57 %. A modest increase in energy density was seen for the for the 200 °C treatments from 19 MJ/kg to 20 MJ/kg, with corresponding energy yields increases from 68% to 77 % after four cycles. For the 250 °C treatments energy density increased from 24 MJ/kg to 29 MJ/kg on the ninth cycle. This increases the overall energy yield from 61% to 91 %. Under these conditions, the bio-coal falls under the classification of a high volatile sub-bituminous coal.

By recycling the process waters, the recycled organic acids hydrolyse the hemicellulose and cellulose to saccharides and furfural-like compounds at a lower temperature. This further increases saccharide and furfural-like concentrations within the process water, as the low temperatures do not further degrade them to organic acids. This will favour aromatization and repolymerisation, and better enables the decomposition products to undergo polymerization, before they undergo further degradation to organic acids. It is proposed that the slow heating rate and hour long retention time can overcome kinetic limitations imposed by faster heating rates and shorter retention times. pH also influences dehydration in the swine manure samples and these findings are likely applicable to lignocellulosics, with a fuel's dehydration increased with decreasing pH although with increasing temperature, the influence of pH on dehydration becomes less. pH and temperature appear to influence yield, with lower pH increasing yields for treatment above 250 °C but decreases yields for treatment below 200 °C. The lower yields below 200 °C is due to the acids catalysing hydrolysis of cellulose; the higher yields at 250 °C are due to the low pH catalysing polymerisation due to its influence on the electrokinetic potential of the hydrothermal suspension.

Given HTC improves grindability it would be best to use the largest possible feedstock size to avoid energy intensive size reduction. Bio-coals are however known to develop an outer oily film and it has been suggested in the literature that the formation of this layer may limit the intimate contact between the biomass and process water. This would prevent larger particles being used. Results presented in this work showed that for 4.0 cm diameter willow cylinders there was still complete conversion of the cellulose, with limited change in hydrothermal chemistry. Increasing particle size also appears to improve energy density of the resulting fuel for willow cylinders up to 2.5-3.0 cm diameter. A reduction in volatile carbon with increasing size suggests that size reduces

the diffusion of preliminary products into the bulk water which enhances hydrolysis and polymerisation within the particle. This significantly improves the grindability behaviour of the fuel. Metal analysis suggests that there is free movement of water though the particle at 4.0 cm in diameter and metal extraction is not limited though the formation of a low water permeable hydrolysis layer.

Based on the results, HTC has been shown to valorise low value fuels such as green harvested *Miscanthus* and seaweeds. This demonstrates the technology's potential to produce a direct substitute bio-coal from an expanded range of terrestrial and aquatic biomass.

10.1. Fate and influence of oxygen during HTC

Oxygen has an adverse impact on energy content, reducing HHV, as demonstrated by Dulongs Equation (see Equation 2.1), and it is also associated with many of the handling issues associated with biomass, as discussed in Section 2.5.2.4. Oxygen none the less plays a critical role in the reactions involved in HTC. The energy densification of the bio-coal is because of changes to the ratio of carbon and oxygen (O/C) in the fuel, with the carbon content increasing, while the oxygen content decreases. In many respects, HTC can be thought of as simply a deoxygenation process.

The main mechanisms involve removal of hydroxyl groups through dehydration, removal of carboxyl and carbonyl groups though decarboxylation, and cleavage of many ester and ether bonds through hydrolysis under the modified aqueous conditions. This process reduces the oxygen and hydrogen content (described by the molecular O/C and H/C ratio), destroys the colloidal structures and reduces the hydrophilic functional groups, giving the bio-coal its enhanced properties such as its change in polarity making the fuel less hydrophilic. Hydrolysed fragments are highly reactive and recombine quickly and dehydration and decarboxylation reactions, which have removed carboxyl and hydroxyl groups, leave unsaturated compounds, which can polymerise easily. The polymerization, condensation and aromatisation reactions are brought about by intermolecular dehydration (two –OH groups react to leave a –O- bond removing water) or by aldol condensation.

Oxygen plays a critical role in repolymerisation, with aromatic structures initially chemisorbed though reactive oxygen functionalities (hydroxyl, carboxyl, carboxylic etc.) which are present on the bio-coal surface. Once chemisorbed these functionalities dehydrate to form stable oxygen groups, which are ether or pyrone, within the char formation. Reactive oxygen functionalities will remain on the surface and provide binding

sites for more aromatic structures. The similar structures seen for high volatile bituminous coal, where oxygen often forms the stable bridges between cyclic aromatic carbon rings (Figure 2.3), are also seen for bio-coal (Figure 2.8). This would imply similar chemisorption and dehydration mechanisms underlie coal formation.

Increasing both temperature and retention time during HTC reduces fuel oxygen with the results suggesting that increasing reaction severity (or severity factor) results in dehydration of the fuel (see Equation 2.2). The results presented for *Miscanthus* in Chapter 6 suggest that with increasing temperature and retention time in HTC, dehydration is the predominant mechanism for oxygen and hydrogen removal. It has been shown throughout this work that alkali metals may influence H/C ratios in a range of feedstock, but alkali metals do not appear to influence deoxygenation (dehydration) and deoxygenation is predominantly determined by reaction severity. The exception may be with regard to their Lewis acidity, as pH appears to influence dehydration at lower temperatures, as shown in Chapter 9. With increasing temperature in HTC, bio-coals become similar in terms of atomic ratios, irrespective of pH.

With regard to the treatment of swine manures in Chapter 9, yields were seen to increase with lower pH despite no further deoxygenation at this temperature. This could be due to the influence of oxygenated functional groups on the particles electro kinetic potential. Bio-coals have a negative electro kinetic potential; as the oxygenated groups on the char surface are acidic, they behave like weak acids. Addition of acids to the process waters neutralises this negative charge and increases flocculation. While pH appears to have reduced influence on dehydration at higher temperatures, the exception is the application of organic acids, which enhances dehydration. Similarly, when recycling process waters (see Chapter 7), there is a further increase in fuel dehydration despite unchanging reaction severity. In this instance, it is believed that the organic acids within the process waters, increase dehydration by catalysing the hydrolysis of hemicellulose and cellulose at a lower temperature. The increase in organic carbon due to the presence of the organic acid must influence the subsequent polymerisation and repolymerisation reactions, hence the enhanced dehydration when processing with organic acids. Results presented in Chapter 8 on HTC of willow cylinders suggest that increasing particle size also increases deoxygenation, most likely due to diffusion limitations which prevent organic acids generated within the particle defusing into the process water. This results in localised increases in organic acid concentrations, which catalyse the reaction in a similar manner to that seen for recycling process waters.

From a combustion perspective, oxygen is primarily associated negatively with fuel energy density but the binding of cations to surface oxygen functional groups could also have a significant influence on a fuel's propensity to slag and foul. While the significance of individual metals is discussed in detail in the subsequent sections, the surface oxygen functional groups can bind to cations such as sodium, potassium, magnesium, calcium which is certainly an underlying mechanism for the retention and removal of metals that go on to influence the ash slagging propensity. It is these same oxygen functional groups, which, on combustion, devolatilise, transport their associated cations, and assist the volatilisation of both volatile and non-volatile metals. It has been proposed that HTC reduces the fouling risk due to a combination of decreased oxygen and volatile matter content of the bio-coal. While the reduction in oxygen and volatile carbon is true, the assumption that this then reduces the fouling propensity of the bio-coal may not be correct. This is because this mechanism does not take into account the re-uptake of metals from the process water onto the surface of the bio-coal. Given the bio-coals are essentially stewed in the metal rich process water, metal saturation of these functional groups may be greater than would otherwise be expected from biomass. Consequently, the bio-coal could lead to a greater fouling propensity than would otherwise be expected, due to an increase in the proportion of cations associated with oxygen functional groups. The significance of this requires further investigation.

10.2. Fate and influence of nitrogen during HTC

Issues associated with nitrogen within a fuel revolve around issues with nitrogen oxide emissions during combustion. Given in most combustion applications the fuel is burnt in air, these nitrogen emissions can also be generated from nitrogen within the air, with the latter referred to as thermal nitrogen oxides. Thermal nitrogen is usually controlled though fuel staging effects using low-nitrogen oxide burners. In this process, initial combustion occurs in a zone where the air to fuel ratio is above stoichiometry (fuel rich), consuming additional oxygen and reducing nitrogen oxides back to gaseous nitrogen. In addition, nitrogen can also influence the polarity of the fuel and thus its hydrophilic behaviour,

In HTC, nitrogen appears to be largely formed from the protein fraction of the feedstock. Malliard chemistry plays an important role in the behaviour of these proteins within HTC and is likely the main route for nitrogen incorporation within the bio-coal. Analysis of process waters of brown kelps presented in Chapter 5 has revealed a significant portion of the nitrogen is transferred to the process water, albeit nitrogen

within the bio-coal was slightly higher than the starting feedstock. It does appear that a lot of the nitrogen extracted remains as organic compounds such as nitrogen heterocycles, pyrroles and indoles, with ionic nitrogen (nitrate, nitrite, ammonia) being only a relatively small portion of the nitrogen extracted.

Authors have suggested that increasing retention time under HTC conditions at between 180 °C and 250 °C reduced nitrogen content of the bio-coal, albeit this trend was not observed for *Miscanthus* in chapter 6. Data presented in Chapter 9 for swine manure showed that extraction of nitrogen is not strongly influenced by pH but higher treatment temperatures did result an increase in fuel nitrogen (2.7 wt % at 120 °C to 3.6 wt % at 250 °C when treated in water). Recycling process waters brought about a slight increase in fuel nitrogen as the higher concentrations of glucose and amines within the process water should promote Malliard reactions. In the case of the bio-coals derived from *Miscanthus* while recycling process waters fuel nitrogen is still below 1 % so is still relatively low. Extrapolation of the swine manure results to lignocellulosic material is challenging, as swine manure is likely to contain a higher protein fraction. While overall fuel nitrogen appears largely unchanged during HTC of lignocellulosics, the early ignition of the bio-coals could be beneficial for nitrogen oxide emissions, as it will consume additional oxygen, increasing the fuel staging effects of low-NOx burners.

10.3. Fate and influence of sulphur during HTC

Sulphur dioxide within the flue gas plays an important role in corrosion and active oxidation of fouling deposits on heat exchangers, hence is often a heteroatom of interest. Fuel sulphur content does also play an important role in reducing suspended particle matter from thermal power stations, as it improves the efficiency of electrostatic precipitators (ESP) in large power station, reducing particulate emissions. Consequently, sulphur is typically required when operating a furnace with ESP and many modern power plants use flue gas desulphurisation (FDG), a set of technologies used to remove sulphur oxides from exhaust flue gases, post ESP to abate air quality issues.

Like oxygen, sulphur is present within coal linking some of the cyclic aromatic carbon rings, in the form of sulphide, disulphide or mercaptan in both aliphatic and aromatic structures in coal. Sulphur is known to be incorporated into bio-coals during HTC via Malliard reactions, albeit not through the classical Malliard reaction cascade.

All results have shown reductions in the amount of sulphur compared to the original biomass when processed by HTC. For seaweeds the reduction is greatest, going from 1 wt % (db) fuel sulphur to 0.1 wt % (db) fuel sulphur. All remaining samples were

already low in sulphur containing typically 0.1 wt % (db) with limited change in concentration through treatment. For *Miscanthus*, sulphur is initially extracted into the process water at low temperatures (200 °C), with greater reincorporation into the bio-coal as retention time is increased, albeit using a feedstock with a low sulphur content (see Table 6.3). These reactions may however be temperature dependent, as the highest sulphur reincorporation occurs at HTC 250 with no retention time, followed by a reduction in sulphur with increasing retention time (see Table 6.3). Sulphur content does increase slightly within the bio-coal when recycling process waters but it is unclear whether this is increased sulphur incorporation into the bio-coal or simply an increase in concentration of sulphur in the process water, remaining within the voids of the bio-coal (pore water).

Sulphuric acid is a common acid used when investigating acid catalysed HTC, with sulphuric acid appearing to promote more decarboxylation when compared to normalised concentrations of hydrochloric acid. Due to the importance of sulphur in ESP operation, utilisation of sulphuric acid catalysed HTC could be appropriate for use in combustion systems, if the bio-coal is blended/co-fired with low sulphur fuel.

10.4. Fate and influence of chlorine during HTC

Chlorine is very corrosive to stainless steel and present as an essential micronutrient in biomass, so removal would be highly desirable. Most issues are associated with fouling and the interaction between alkali chloride deposits and sulphur in the flue gas. Chlorine is no less desirable in the ash as chlorine can also react with silicates and the alkali metals to form an undesirably stable and corrosive slag. Chlorine is a particular problem when combusting *Miscanthus*, grass and straw which contain higher amounts of chlorine than wood.

Chlorine exists within biomass in the form of water soluble ionic salts (NaCl, KCl, $CaCl_2$, $MgCl_2$ and ionic chloride (Cl^-)) Biomass washing experiments have shown that between 85 % and 100 % of total chlorine within the biomass is extracted though washing, primarily though the removal of these salts. Chlorine is seldom analysed in HTC, with the assumption commonly made that given chlorine exists within biomass in the form of water soluble ionic salts, chlorine within the biomass is extracted. The brown kelp results, presented in chapter 5 support this hypothesis, with typically around 99 % extracted and slightly higher extraction associated with the increased reaction severity. Work on *Miscanthus*, also presented in chapter 5, showed chlorine reduces but the reductions in

chlorine are less than the reduction seen in comparable washing experiments. The results suggest there maybe other underlying chlorine retention mechanisms during HTC.

Work on the influence of retention time showed the reduction in chlorine is in steady decline with increasing retention time (50 % removal for both HTC 200+0h and HTC 250+0h, increasing to 80 % removal for HTC 250+24h). Meanwhile sodium, potassium, and magnesium, are predominantly removed in the initial heating for the biomass, with the majority removed (87, 75 and 60% respectively) by the 200 °C treatment with no retention time. Given calcium only undergoes limited removal (23 % removal for HTC 200+0h) and increases its relative concentration within the biomass (see Table 6.3), it is possible that the chloride is retaining an association with the calcium retained within the bio-coal. It is also possible that chlorine is being retained through formation of weak chloride-hydrogen interactions with the hydrogens on the char. When recycling the process waters there is significant accumulation of alkali metals and chloride within the process water and this does result in fuel chlorine increasing from approximately 1750 mg/kg to 3200 mg/kg by cycle nine for both 200 °C and 250 °C treatments. This is still below the 3600 mg/kg in the starting biomass and energy density has increased from 18 MJ/kg to 29 MJ/kg so still represents a substantial reduction in fuel chlorine on a MJ basis.

In the HTC method used there was no additional washing of the bio-coals; the bio-coal was filtered from the process water and allowed to dry prior analysis. It is likely that residual metal and chloride containing process water is left with the char. Incorporation of an additional washing procedure post carbonisation could further enhance removal of chlorine. Further work is required on this.

While chlorine extraction maybe less than reported in washing experiments, changes to the inorganic chemistry (as discussed in the following sections), could give an ash chemistry which works using similar chemical absorption chemistry used by commercial additives to mitigate the impacts of chlorine. This would suggest that mitigation of the fouling and corrosion issues associated with chlorine may be achieved by HTC by several different mechanisms, over and above simple extraction.

10.5. Fate and influence of phosphorus during HTC

Unlike the heteroatoms nitrogen and sulphur, phosphorous does not appear to be incorporated via Malliard cascades. Its retention and incorporation into the bio-coal appears to be more associated with the inorganic chemistry. While the alkali metals are largely extracted during HTC, magnesium, calcium and phosphorus undergo more limited

metal removal. This has a significant influence on the slagging and fouling propensity of the fuel as this forms calcium potassium phosphate complexes that are thermally stable and prevents the formation of low melting temperature potassium silicates or the volatilisation of potassium chloride. Consequently, in addition to alkali metal extraction, the retention of the calcium and phosphorus means that this calcium and phosphorous behave in a similar way to calcium and phosphorus additives in further abating and ash related issues associated with residual alkali metal.

When undertaking experiments at different retention times using *Miscanthus* feedstock, phosphorus undergoes substantial extraction in samples treated at 200 °C with no retention time (72 % removal for HTC 200+0h). The phosphorous then appears to be reincorporated as retention time is increased (only 45 % removal for HTC 200+24h). Under the same regime, calcium only undergoes limited removal (23 % removal for HTC 200+0h) and increases its relative concentration within the biomass (see Table 6.3), with this calcium potentially associated with chlorine, before exchanging with the phosphorus present in the process water. At 250 °C, phosphorus extraction decreases with increasing retention time (47 % removal for HTC 250+0h, decreasing to 33 % removal for HTC 250+24h). There is not the initial decrease, as seen in the 200 °C treatments, which would imply that phosphorus released on heating is reincorporated quickly into the bio-coal. The results seen throughout this study suggest that in HTC bio-coals, phosphorus appears to be associated with calcium, in much the same way, as sulphur is associated with iron in coal.

While phosphorus retention within the fuel offers advantages in terms of slagging and fouling during combustion, there is a lot of interest in using HTC as a technique for reclaiming phosphorus from manures while simultaneously making a fuel for energetic purposes. Investigations into swine manures suggested phosphorus is present as low solubility salts such as calcium and magnesium phosphates. When processing at different temperatures there is an initial reduction in phosphorus concentration in the bio-coal produced at up to 170 °C, followed by increased retention of phosphorus with increasing temperature between 200 °C and 250 °C. The exception being when sulphuric acid is added as this appears to dissolve low solubility calcium and magnesium phosphate.

In conclusion, calcium and magnesium phosphate present within the feedstock appears to remain within the bio-coal during HTC, with additional calcium phosphate likely generated under the hydrothermal conditions. Processing biomass with higher phosphorus concentrations also appears to be beneficial in terms of slagging and fouling.

Willow samples processed with bark or *Miscanthus* processed with leaves (early harvested) have better ash fusion test performance than samples processed without.

10.6. Fate and influence of potassium during HTC

The temperature at which the ash melts and fuses is strongly influenced by the potassium, which act as a flux, lowering the melting temperature of alumina-silicate ash. It is this low ash melting temperature, which brings on the phenomena of slagging. Potassium is also the main element responsible for fouling during biomass combustion as the potassium is generally in a form that is available for release by devolatilisation and consequently potassium is readily volatilised as potassium chloride in a flame.

Of the main inorganics investigated, potassium has shown the greatest overall reduction and in all runs bio-coals have a lower potassium content than the starting material. When processing at 200 °C using *Miscanthus*, 75 % of the potassium is removed without retention at this temperature, but further removal is possible with increasing retention times, with 86 % removed when processed over 24 hours. This trend continues at 250 °C, but at this temperature increasing retention time does not significantly increase potassium extraction. This extraction can bring about significant improvements in the fuel's slagging propensity as demonstrated by the ash fusion test. This is particularly prevalent when processing at 250 °C as retention of calcium and reincorporation of phosphorus results in the formation of calcium potassium phosphate complexes that are thermally stable and prevent the formation of low melting temperature potassium silicates or the volatilisation of potassium chloride. To the best of the author's knowledge, this has not been previously reported.

Work on HTC of willow cylinders, presented in Chapter 8, indicates that surface functionality does appear to have some influence on potassium retention. The outer surface of the chars are seen to have the highest concentrations of potassium once treated. This could have a significant influence on a fuel's propensity to foul as on combustion these functional groups devolatilise, volatilising the associated potassium. Consequently, the bio-coal could lead to a greater fouling propensity than would otherwise be expected and the significance of this requires further investigation.

It is believed that a lot of the residual potassium seen in the bio-coals is likely residual process water left over in the pore space. The improvements seen with increasing retention time at 200 °C, is likely because the dewatering properties of the bio-coal are improved with increasing reaction severity, along with reduced surface functionality. In this HTC method, there was no additional washing of the bio-coals, with the bio-coal

filtered from the process water and allowed to dry prior analysis. Mechanical dewatering using a screw press and even incorporation of a second water washing step (potentially important if recycling process waters), is likely to further remove this residual process water left with the char micro and macro pores, which on separation currently dries and deposit metal salts in the bio-coal. A better understanding of the partitioning of potassium would however be of benefit as it is also possible that residual potassium has formed carbonates or has reacted with other inorganic elements present in the fuel to form minerals such as K_2CaSiO_4 and $KAlSi_3O_8$ during the HTC reaction.

Potassium does not appear to play a role in bio-coal formation and coal experiments validate this. Solubilisation and metal precipitation experiments of low rank coals have suggested potassium plays no role in the cleating of aromatic structures. However, there is no experimental evidence either way for HTC. There is however evidence that potassium may increase the bio-coal's H/C ratio. This is potentially due to the potassium catalysing hydrogen donation from organics within the process water.

10.7. Fate and influence of sodium during HTC

The behaviour of sodium is very similar to that of potassium in terms of its influence on slagging and fouling and its behaviour in HTC. Consequently, throughout the text sodium and potassium are collectively referred to as the alkali metals. Within the literature sodium chloride addition has been investigated. It has been found that sodium chloride addition increases the dissolution of cellulose. There is also some evidence that sodium chloride addition can reduce the oxygen content of the fuel. In the results of this work alkali metals do not appear to influence deoxygenation (dehydration) with deoxygenation predominantly determined by reaction severity. Sodium chloride, along with potassium chloride, for that matter, are Lewis acids and their presence may catalyse the hydrolysis of cellulose accelerating the formation of organic acids, which have been shown to deoxygenate the fuel.

10.8. Fate and influence of calcium during HTC

During HTC, calcium appears to have a strong influence on the resulting fuels properties. While the alkali metals are known to decrease ash melting temperatures, calcium has been shown to increase the silicon fluxing temperature and it is this property which brings about its use in ash additives to abate slagging and fouling. The behaviour of calcium in HTC is feedstock specific but generally, calcium only undergoes limited removal and increases its relative concentration within the biomass. This combined with its close association with phosphorus, results in increased ash deformation and melting

temperatures of the bio-coal ash. Residual potassium appears also to form calcium potassium phosphate complexes, which are thermally stable, and prevent the formation of low melting temperature potassium silicates or the volatilisation of potassium chloride.

It has been observed that calcium at 200 ^{0}C undergoes limited removal (23 % removal for HTC 250+0h when processing *Miscanthus*) and increases its relative concentration within the biomass. At 250 ^{0}C, calcium appears to reduce within the bio-coal after one hour (54 % removal for HTC 250+0h, increasing to 82 % removal for HTC 250+24h when processing *Miscanthus*). Calcium extraction is also brought about when recycling process waters or though the addition of acid so calcium extraction is believed to be due to organic acid leaching. Based on the results and literature it is unclear whether the residual calcium within the bio-coal is in the form of a low solubility compound (such as calcium phosphate) or whether it is organically associated with oxygen. Organic acids are known to both dissolve compounds such as calcium phosphate and deoxygenate the fuel, so organic acids will work on both retention mechanisms. It is more than likely that calcium is present as both organically bound calcium and low solubility minerals, with the ratio of the two determined by the feedstock. When processing samples with bark, calcium remains within the bark, which indicates calcium is relatively immobile during HTC. Processing high calcium feedstock appears particularly advantageous during HTC with early harvested *Miscanthus* and samples with bark outperforming samples processed without.

In addition to the influence calcium has on the slagging and fouling propensity of a bio-coal, results in this work and in the literature would also suggest calcium plays a role in the repolymerisation process. Solubilisation and metal precipitation experiments of low rank coals have suggested removal of calcium can result in their solubilisation and subsequent addition of divalent cations (calcium and magnesium) has been shown to re-precipitate the coal. Moreover work modelling brown coal formation has shown that di-valiant cations could aid bio-coal formation with metal ions appearing to become surrounded by oxygen fictional groups, and carboxyl groups potentially acting as bi-dentrate ligands to calcium ions (e.g. R-COO^{-}(Ca^{2+})$^{-}$OOC-R). This has also been observed in the HTC of alginate with divalent cations binding poly-guluronic acid units during the reaction and providing nuclei for the formation of carbon microspheres.

Addition of calcium chloride and calcium carbonate has been investigated within the literature, with calcium carbonate known to act as a template around which nucleation can occur. Calcium chloride being a Lewis acid is somewhat different, but has been

shown to influence cellulose dissolution in a completely different way to that of sodium chloride. Being a stronger Lewis acid cellulose dissolution initially increases when compared to sodium chloride but calcium chloride does not appear to deoxygenate the feedstock, as seen with sodium chloride. Instead calcium appears to prevent further decomposition of the cellulose, while it catalyses the process water chemistry (e.g. decomposition of HMF to levulinic acid and decomposition of organic acids to hydrogen). It is believed the calcium binds to the surface oxygen functional groups but after this it prevents the further decomposition of the feedstock (surface passivation). This area appears to need further investigation as the results indicate calcium could make for a good hydrothermal catalyst, catalysing both the hydrolysis and repolymerisation reactions while improving the ash chemistry. The literature results do however suggest obtaining the right calcium concentration within the process water is of critical importance as excessive calcium could have the inverse effect.

10.9. Fate and influence of magnesium during HTC

Being a divalent cation the behaviour of magnesium is very similar to that of calcium in terms of its influence on slagging and fouling and its behaviour in HTC. Magnesium appears more soluble under HTC conditions, with 200 °C treatments leading to a greater removal of magnesium than seen for calcium (61 % removal for HTC 200+0h when processing *Miscanthus*) albeit percentage extraction is similar at longer retention times (approximately 80 % for HTC 250+24h). Like calcium, it appears that phosphorus may have an association with magnesium in the bio-coals obtained at 250 °C. Modelling of magnesium in brown coal formation along with solubilisation and metal precipitation experiments of coal suggest that magnesium will behave in much the same way as calcium, potentially catalysing both the hydrolysis and repolymerisation reactions while improving the ash chemistry. Magnesium is however present in biomass in lower concentrations than calcium and experiments using magnesium salts are less common. Whether magnesium chloride salts have the same surface passivation properties of calcium remain unknown.

10.10. Fate and influence of other metals during HTC

Iron, aluminium and the metalloid silicon are the final macro elements within biomass. Of these, silicon is probably the most important as it is the silicate in combination with calcium, potassium, sodium and phosphorus, which in part determines the volatilisation of metals, and the ash melting behaviour. Within the presented results and results presented in the literature it appears silicon is not in a water soluble form in

biomass and appears to remain within the bio-coal, increasing in concertation with increasing reaction severity. This higher silicon content of the bio-coal may be advantageous from a fouling perspective, as, silicates are known to trap potassium within the ash, in the form of potassium silicates, preventing their potential volatilisation and subsequent fouling. The influence on slagging depends on the other elements within the ash, as reviewed in the previous sections.

While silicon appears to remain insoluble, the swine manure results have indicated some removal of silicon into the aqueous phase with increasing temperature. This result is surprising as while silicon can be water soluble, to become water soluble silicon has to be hydrated and become silicic acid (H_4O_4Si), which unless kept buffered within certain boundaries, readily degrades back to insoluble silicon dioxide (SiO_2). None the less, other authors have reported similar findings under certain conditions so it does appear under certain conditions silicon can be removed from the bio-coal. Silicon does however provide a role in HTC, with silicon dioxide proving a template around which the bio-coal can polymerise.

Like silicon, iron and aluminium also undergo limited removal during HTC and accumulate within the bio-coal. Recycling process water does however remove some iron and aluminium from the bio-coal, which shows that organic acids created as part of the hydrothermal process, can extract these metals. Iron and aluminium are both interesting metals as when in salt form they will act as strong Lewis acids, with iron shown to catalyse complete carbonisation of cellulose at 200 °C, where incomplete carbonisation was observed in the absence of the salt. Solubilisation and metal precipitation experiments of low rank coals have suggested addition of iron and aluminium, being trivalent cations can re-precipitate the coal. This said, modelling work on brown coal formation has shown that trivaliant cations form less energetically favoured, distorted structures, associating with carboxyl and phenoxy groups, so appear less effective than calcium or magnesium.

The results have shown the low iron content within the initial biomass and subsequently within the bio-coals makes bed agglomeration appear likely so application of iron as a HTC catalysts could be of benefit in terms of ash chemistry, improving: bed agglomeration index (BAI), slag viscosity index (SVI) and base to acid ratio (R b/a).

10.11. Further work

10.11.1. Recycling process waters followed by mechanical dewatering and post-process washing

Recycling process waters brings about an increase in product mass yield, energy density and energy yield at both treatment temperatures. At 250 °C the treatments yield a bio-coal with an energy density of 29 MJ/kg on the ninth cycle and an energy yield of 91 %, moreover, this bio-coal falls under the classification of a high volatile sub-bituminous coal. Recycling process water does however have an adverse influence on the fouling, slagging propensity of the fuel, most likely due to residual process water is left with the char micro and macro pores on separation. This will, on drying, deposit metal salts on the bio-coal. It is hypothesised mechanical water recovery using a screw press would recover more process water and reduce this metal deposition, overcoming the slagging and fouling issues while truly producing a direct substitute coal. The incorporation of an additional washing procedure post carbonisation may further improve the combustion characteristics of the fuel. When washing additional carbon would be leached and treatment of this water via anaerobic digestion should also be investigated.

10.11.2. The influence of oxygen functionality on the fouling propensity of bio-coals

Binding of cations onto surface oxygen functional groups on a bio-coal could have a significant influence on a fuel's propensity to foul. Surface oxygen functional groups can bind to cations such as sodium, potassium, magnesium, calcium. These same oxygen functional groups, which, on combustion, devolatilise, could transport their associated cations, assisting the volatilisation of both volatile and non-volatile metals. While it has been proposed that HTC reduces the fouling risk due to a combination of decreased oxygen and volatile matter content of the bio-coal. This mechanism does not take into account the re-uptake of metals from the process water onto the surface of the bio-coal. Given the bio-coals are essentially stewed in the metal rich process water metal saturation of these functional groups maybe greater than would otherwise be expected from biomass. Consequently, the bio-coal could lead to a greater fouling propensity than would otherwise be expected, due to an increase in the proportion of cations associated with oxygen functional groups.

This volatilization of metals could be highly significant for bio-coal and the significance of this requires further investigation. Initially combustion of small bio-coal

pellets could be measured by use of flame emission spectroscopy as described in Mason et al. [375], could be sufficient to assess the significance of the devolatilisation mechanism.

10.11.3. The influence of cation valency on HTC

It is known that reactive oxygen functionalities (hydroxyl, carboxyl, carboxylic etc) act as both binding sites for aromatic structures and cations present within the process water during bio-coal formation. It is also understood that in bio-coal formation these oxygen fictional groups, initially chemisorb and then dehydrate to form stable oxygen groups, which are ether or pyrone, within the char formation. The influence the metals have on this mechanism is not yet clear. In fossil coal, metals are known to exist within the coal matrix as salts of carboxylic acids, alcohols and phenols. Removal of metals from within the coal matrix of low rank coals is known to lead to the solubilisation of low rank coals. Likewise the addition of divalent cations (Ca^{2+}, Mg^{2+} and Fe^{2+}) and trivalent cations (Fe^{3+} and Al^{3+}) has been shown to re-precipitate the coal (taking into account potential for acid precipitation), while monovalent cations (Na^{+}) had no effect on re-precipitation.

Moreover work modelling brown coal formation has shown that divalent cations aid the formation of energetically favoured, undistorted structures. In the models, metal ions appear to become surrounded by oxygen fictional groups, with carboxyl groups potentially acting as bi-dentrate ligands to calcium ions (e.g. R-COO-(Ca^{2+})-OOC-R). The trivalent cations form less energetically favoured, distorted structures, associating with carboxyl and phenoxy groups but still appear to play a role in coal formation. This binding would suggest that a that multivalent cations play a role in the bio-coal formation though the cleating of aromatic structures though carboxyl groups and interactions with the surrounding functional groups which then dehydrate to form stable oxygen groups. The reduction in calcium with retention time in the 250 °C treatments with increasing retention time and lower calcium in the 250 °C recycles could be in part be due to the removal of hydroxyl bonding sites during repolymerisation (e.g. R-OH(Ca^{2+})HO-R → R-O-R+H_2O+Ca^{2+}) in addition to acid leaching. The greater stability of carboxyl and carboxylic functional groups would mean that these sites and associated metals would likely remain within the bio-coal.

The results of this study have shown that many of the multivalent cations undergo only limited removal and it has been suggested throughout this work that calcium may play a role in polymerisation. Experimental validation of this using a range of different cations, salts and concentrations of salts would be required to demonstrate if this is the

case. As highlighted in Section 10.8 obtaining the right cation concentration appears of high importance in order to avoid surface passivation.

10.12. HTC in a broader context

This thesis predominantly focuses on the application of bio-coal in pulverised fuel applications and the results have shown that in particular the 250 °C bio-coals derived from lignocellulosic material have good coal-like properties and have real potential as substitute fuels pulverised coal applications. This is particularly true when recycling process waters and assuming the metal accumulation issues, discussed in the further work, can be overcome, then the product, a high grade, high volatile sub-bituminous equivalent bio-coal with high yields, may well have commercial promise as a direct substitute fuel.

Coal still provides almost 30% of the world's primary energy and will continue to be a dominant energy source in energy intensive industrial applications for the foreseeable future. In some applications, replacement with alternative renewable technologies may not be possible. Particular examples include the use of coal and carbon in metallurgy but could extend to newer ultra-supercritical power plants and reserve generating capacity. In such examples, production of a commercially viable, low carbon, direct substitute fuel will have a critical application in abating carbon emissions. Bioenergy CCS is also forecast to play a critical role in removal of atmospheric CO_2, required if we are not to exceed 430 ppm CO_2 by 2100. Consequently, the application of bio-coal and CCS in coal dependent industrial applications may well be an ideal combination, bringing about the required carbon negative industrial emissions to meet climate change targets.

With regard to the current status of HTC, a number of companies are offering 'commercial' HTC plant, with Ingelia perhaps the most established. Specific details on plant design and operating conditions are however sparse, with the Ingelia process operating at temperatures between 180-200 °C. To the best of the author's knowledge, no commercial plants are operating at 250 °C and recycling process water. From a practical perspective, recycling process water overcomes the issue with process water, which still appears largely unresolved. Recycling the process water and slow heating rates should lead to high heat recoveries if operating in a counter-current continuous system, albeit this increases resonance time and decreases throughput, increasing cost and plant size. Techno-economic assessments and lifecycle assessments are available for HTC, however, they are only applicable to the specific process assessed (temperature, resonance time, system configuration, feedstock etc.) and these system boundaries vary throughout the literature making extrapolation of the results to other HTC configurations difficult.

11. Appendix

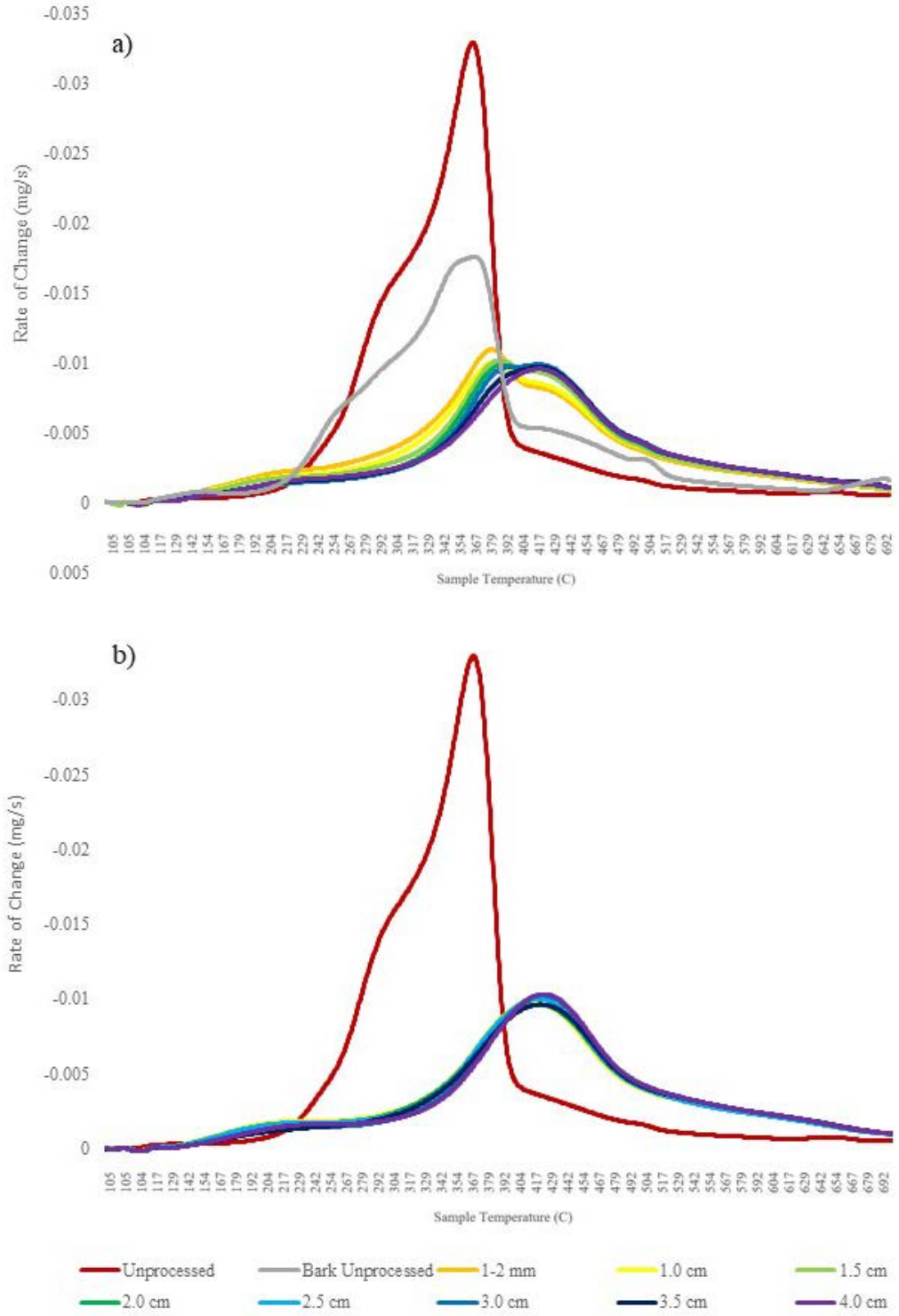

Figure 11.1: Derivative thermogravimetric (DTG) devolatilisation profiles for unprocessed willow and hydrothermally treated willow at 250 °C; a) with bark and b) without

12. References

[1] van Wyk JPH. Biotechnology and the utilization of biowaste as a resource for bioproduct development. Trends in Biotechnology 2001;19(5):172-7.

[2] Lichtenthaler FW, Peters S. Carbohydrates as green raw materials for the chemical industry. Comptes Rendus Chimie 2004;7(2):65-90.

[3] Schellnhuber HJ. Global sustainability: a nobel cause. Cambridge University Press; 2010.

[4] WMO. WMO. Globally Averaged CO2 Levels Reach 400 parts per million in 2015 [online]. [Accessed 12/02/2018]. Available from:https://public.wmo.int/en/media/press-release/globally-averaged-co2-levels-reach-400-parts-million-2015 2016.

[5] Flato G, Marotzke J, Abiodun B, Braconnot P, Chou SC, Collins WJ, et al. Evaluation of climate models. In: climate change 2013: the physical science basis. Contribution of working group I to the fifth assessment report of the intergovernmental panel on climate change. Climate Change 2013 2013;5:741-866.

[6] Rhodes CJ. The 2015 Paris climate change conference: COP21. Science progress 2016;99(1):97-104.

[7] IPCC. Climate Change 2014–Impacts, Adaptation and Vulnerability: Regional Aspects. Cambridge University Press; 2014.

[8] IPCC. Mitigation of Climate Change. Contribution of Working Group III to the Fifth Assessment Report of the Intergovernmental Panel on Climate Change. Cambridge University Press, Cambridge, UK and New York, NY 2014.

[9] Rackley SA. Carbon capture and storage. Butterworth-Heinemann; 2017.

[10] Ibrahim RHH, Darvell LI, Jones JM, Williams A. Physicochemical characterisation of torrefied biomass. Journal of Analytical and Applied Pyrolysis 2013;103(0):21-30.

[11] Funke A, Ziegler F. Hydrothermal carbonization of biomass: A summary and discussion of chemical mechanisms for process engineering. Biofuels, Bioproducts and Biorefining 2010;4(2):160-77.

[12] Bergius F. . Zeitschrift fur Komprimierte und Flussige Gase 1915;17.

[13] Bergius F. Beiträge zur Theorie der Kohleentstehung. Naturwissenschaften 1928;16(1):1-10.

[14] Bergius F. Production of hydrogen from water and coal from cellulose at high temperatures and pressures. Journal of Chemical Technology and Biotechnology 1913;32(9):462-7.

[15] Bergius F. Zeitschrift Des Vereines Deutscher Ingenieure 1925;69:1359-62.

[16] Titirici M-M. Sustainable carbon materials from hydrothermal processes. John Wiley & Sons; 2013.

[17] Berl E, Schmidt A. Über das Verhalten der Cellulose bei der Druckerhitzung mit Wasser. European Journal of Organic Chemistry 1928;461(1):192-220.

[18] Berl E, Schmidt A, Koch H. Über die Entstehung der Kohlen. Angewandte Chemie 1932;45(32):517-9.

[19] Schuhmacher J, Vanvucht H, Groenewege M, Blom L, Vankrevelen D. Chemical Structure and Properties of Coal XV-Constitution of Low Temperature Hydrogenation Products. Fuel 1956;35(3):281-90.

[20] Schuhmacher JP, Huntjens FJ, Van Krevelen DW. Chemical structure and properties of coal XXVI studies on artificial coalification. . Fuel 1960;39:223-34.

[21] Wang Q, Li H, Chen L, Huang X. Monodispersed hard carbon spherules with uniform nanopores. Carbon 2001;39(14):2211-4.

[22] Sun X, Li Y. Colloidal carbon spheres and their core/shell structures with noble-metal nanoparticles. Angewandte Chemie International Edition 2004;43(5):597-601.

[23] Yu SH, Cui XJ, Li LL, Li K, Yu B, Antonietti M, et al. From Starch to Metal/Carbon Hybrid Nanostructures: Hydrothermal Metal-Catalyzed Carbonization. Advanced Materials 2004;16(18):1636-40.

[24] Qian H-S, Yu S-H, Luo L-B, Gong J-Y, Fei L-F, Liu X-M. Synthesis of uniform Te@ carbon-rich composite nanocables with photoluminescence properties and carbonaceous nanofibers by the hydrothermal carbonization of glucose. Chemistry of Materials 2006;18(8):2102-8.

[25] Haenel MW. Recent progress in coal structure research. Fuel 1992;71(11):1211-23.

[26] Titirici M-M, Thomas A, Antonietti M. Back in the black: hydrothermal carbonization of plant material as an efficient chemical process to treat the CO 2 problem? New Journal of Chemistry 2007;31(6):787-9.

[27] Sevilla M, Maciá-Agulló JA, Fuertes AB. Hydrothermal carbonization of biomass as a route for the sequestration of CO2: Chemical and structural properties of the carbonized products. Biomass and Bioenergy 2011;35(7):3152-9.

[28] Libra JA, Ro KS, Kammann C, Funke A, Berge ND, Neubauer Y, et al. Hydrothermal carbonization of biomass residuals: A comparative review of the chemistry, processes and applications of wet and dry pyrolysis. Biofuels 2011;2(1):71-106.

[29] Hoekman SK, Broch A, Robbins C. Hydrothermal carbonization (HTC) of lignocellulosic biomass. Energy and Fuels 2011;25(4):1802-10.

[30] Briesemeister L, Kremling M, Fendt S, Spliethoff H. Air-Blown Entrained Flow Gasification of Biocoal: Gasification Kinetics and Char Behavior. Energy and Fuels 2017;31(9):9568-75.

[31] Briesemeister L, Kremling M, Fendt S, Spliethoff H. Air-Blown Entrained-Flow Gasification of Biocoal from Hydrothermal Carbonization. Chemical Engineering and Technology 2017;40(2):270-7.

[32] Trautmann M, Lang S, Traa Y. Direct liquefaction of lower-rank coals and biocoals with magnetically separable catalysts as a sustainable route to fuels. Fuel 2015;151:102-9.

[33] Tremel A, Stemann J, Herrmann M, Erlach B, Spliethoff H. Entrained flow gasification of biocoal from hydrothermal carbonization. Fuel 2012;102(Supplement C):396-403.

[34] Eberhardt G, Odening M, Lotze-Campen H, Erlach B, Rolinski S, Rothe P, et al. The impact of transportation costs on the profitability of industrial hydrothermal carbonisation. Berichte uber Landwirtschaft 2011;89(3):400-24.

[35] Hoekman SK, Broch A, Robbins C, Purcell R, Zielinska B, Felix L, et al. Process Development Unit (PDU) for Hydrothermal Carbonization (HTC) of Lignocellulosic Biomass. Waste and Biomass Valorization 2014;5(4):669-78.

[36] Kambo HS, Dutta A. A comparative review of biochar and hydrochar in terms of production, physico-chemical properties and applications. Renewable and Sustainable Energy Reviews 2015;45:359-78.

[37] Korbee R, Kiel J, Zevenhoven M, Skrifvars B, Jensen P, Frandsen F. Investigation of biomass inorganic matter by advanced fuel analysis and conversion experiments. Proc Power Production in the 21st Century: Impacts of Fuel Quality and Operations United Engineering Foundation Advanced Combustion Engineering Research Center Snowbird UT, Oct 2001.

[38] Marschner H, Marschner P. Marschner's mineral nutrition of higher plants. Academic press; 2012.

[39] Koppejan J, Van Loo S. The handbook of biomass combustion and co-firing. Routledge; 2012.

[40] Jenkins B, Baxter L, Miles T. Combustion properties of biomass. Fuel processing technology 1998;54(1):17-46.

[41] Fahmi R, Bridgwater AV, Darvell LI, Jones JM, Yates N, Thain S, et al. The effect of alkali metals on combustion and pyrolysis of Lolium and Festuca grasses, switchgrass and willow. Fuel 2007;86(10–11):1560-9.

[42] Gudka B, Jones JM, Lea-Langton AR, Williams A, Saddawi A. A review of the mitigation of deposition and emission problems during biomass combustion through washing pre-treatment. Journal of the Energy Institute 2015.

[43] Saddawi A, Jones JM, Williams A, Le Coeur C. Commodity fuels from biomass through pretreatment and torrefaction: Effects of mineral content on torrefied fuel characteristics and quality. Energy and Fuels 2012;26(11):6466-74.

[44] Lynam JG, Coronella CJ, Yan W, Reza MT, Vasquez VR. Acetic acid and lithium chloride effects on hydrothermal carbonization of lignocellulosic biomass. Bioresource Technology 2011;102(10):6192-9.

[45] Benavente V, Calabuig E, Fullana A. Upgrading of moist agro-industrial wastes by hydrothermal carbonization. Journal of Analytical and Applied Pyrolysis 2014.

[46] Liu Z, Balasubramanian R. Upgrading of waste biomass by hydrothermal carbonization (HTC) and low temperature pyrolysis (LTP): A comparative evaluation. Applied Energy 2014;114:857-64.

[47] Zhao P, Shen Y, Ge S, Chen Z, Yoshikawa K. Clean solid biofuel production from high moisture content waste biomass employing hydrothermal treatment. Applied Energy 2014;131:345-67.

[48] Lynam JG, Toufiq Reza M, Vasquez VR, Coronella CJ. Effect of salt addition on hydrothermal carbonization of lignocellulosic biomass. Fuel 2012;99(0):271-3.

[49] Kruse A, Gawlik A. Biomass Conversion in Water at 330−410 °C and 30−50 MPa. Identification of Key Compounds for Indicating Different Chemical Reaction Pathways. Industrial & Engineering Chemistry Research 2003;42(2):267-79.

[50] Sarkanen KV, Tillman DA. Progress in biomass conversion. Elsevier; 2013.

[51] Amaducci S, Facciotto G, Bergante S, Perego A, Serra P, Ferrarini A, et al. Biomass production and energy balance of herbaceous and woody crops on marginal soils in the Po valley. Gcb Bioenergy 2017;9(1):31-45.

[52] Shankar Tumuluru J, Sokhansanj S, Hess JR, Wright CT, Boardman RD. A review on biomass torrefaction process and product properties for energy applications. Industrial Biotechnology 2011;7(5):384-401.

[53] O'Sullivan AC. Cellulose: the structure slowly unravels. Cellulose 1997;4(3):173-207.

[54] Scheller HV, Ulvskov P. Hemicelluloses. Annual Review of Plant Biology 2010;61(1):263-89.

[55] Alonso DM, Wettstein SG, Dumesic JA. Bimetallic catalysts for upgrading of biomass to fuels and chemicals. Chemical Society Reviews 2012;41(24):8075-98.

[56] Zakzeski J, Bruijnincx PCA, Jongerius AL, Weckhuysen BM. The Catalytic Valorization of Lignin for the Production of Renewable Chemicals. Chemical Reviews 2010;110(6):3552-99.

[57] Obernberger I, Biedermann F, Widmann W, Riedl R. Concentrations of inorganic elements in biomass fuels and recovery in the different ash fractions. Biomass and bioenergy 1997;12(3):211-24.

[58] Jung KA, Lim S-R, Kim Y, Park JM. Potentials of macroalgae as feedstocks for biorefinery. Bioresource technology 2013;135:182-90.

[59] Gao K, McKinley K. Use of macroalgae for marine biomass production and CO2 remediation: a review. J Appl Phycol 1994;6(1):45-60.

[60] Rowbotham JS, Dyer PW, Greenwell HC, Theodorou MK. Thermochemical processing of macroalgae: A late bloomer in the development of third-generation biofuels? Biofuels 2012;3(4):441-61.

[61] Ross AB, Jones JM, Kubacki ML, Bridgeman T. Classification of macroalgae as fuel and its thermochemical behaviour. Bioresource Technology 2008;99(14):6494-504.

[62] Horn SJ. Bioenergy from brown seaweeds. 2000.

[63] Adams JMM, Ross AB, Anastasakis K, Hodgson EM, Gallagher JA, Jones JM, et al. Seasonal variation in the chemical composition of the bioenergy feedstock Laminaria digitata for thermochemical conversion. Bioresource Technology 2011;102(1):226-34.

[64] Smith KL, Smoot LD, Fletcher TH, Pugmire RJ. The structure and reaction processes of coal. Springer Science & Business Media; 2013.

[65] IEA. Medium-Term Coal Market Report 2016 - Market Analysis and Forecasts to 2021. 2016.

[66] Speight JG. The Chemistry and Technology of coal. CRC press; 2013.

[67] Miller BG. Coal energy systems. Academic Press; 2004.

[68] Tillman DA, Duong DNB, Harding NS. Chapter 4 - Blending Coal with Biomass: Cofiring Biomass with Coal. In: Tillman DA, Duong DNB, Harding NS, editors. Solid Fuel Blending. Boston: Butterworth-Heinemann; 2012, p. 125-200.

[69] Van Krevelen DW. Coal: typology, physics, chemistry, constitution. Elsevier Amsterdam; 1993.

[70] Shinn JH. From coal to single-stage and two-stage products: a reactive model of coal structure. Fuel 1984;63(9):1187-96.

[71] Peterson AA, Vogel F, Lachance RP, Fröling M, Antal Jr MJ, Tester JW. Thermochemical biofuel production in hydrothermal media: a review of sub-and supercritical water technologies. Energy & Environmental Science 2008;1(1):32-65.

[72] Toor SS, Rosendahl L, Rudolf A. Hydrothermal liquefaction of biomass: A review of subcritical water technologies. Energy 2011;36(5):2328-42.

[73] López Barreiro D, Prins W, Ronsse F, Brilman W. Hydrothermal liquefaction (HTL) of microalgae for biofuel production: State of the art review and future prospects. Biomass and Bioenergy 2013;53(0):113-27.

[74] Kritzer P, Dinjus E. An assessment of supercritical water oxidation (SCWO): Existing problems, possible solutions and new reactor concepts. Chemical Engineering Journal 2001;83(3):207-14.

[75] Pastor-Villegas J, Pastor-Valle JF, Rodríguez JMM, García MG. Study of commercial wood charcoals for the preparation of carbon adsorbents. Journal of Analytical and Applied Pyrolysis 2006;76(1–2):103-8.

[76] Reza MT, Lynam JG, Uddin MH, Coronella CJ. Hydrothermal carbonization: Fate of inorganics. Biomass and Bioenergy 2013;49(0):86-94.

[77] Titirici MM, Thomas A, Yu S-H, Müller J-O, Antonietti M. A direct synthesis of mesoporous carbons with bicontinuous pore morphology from crude plant material by hydrothermal carbonization. Chemistry of Materials 2007;19(17):4205-12.

[78] Baccile N, Laurent G, Babonneau F, Fayon F, Titirici M-M, Antonietti M. Structural characterization of hydrothermal carbon spheres by advanced solid-state MAS 13C NMR investigations. The Journal of Physical Chemistry C 2009;113(22):9644-54.

[79] Oomori T, Khajavi SH, Kimura Y, Adachi S, Matsuno R. Hydrolysis of disaccharides containing glucose residue in subcritical water. Biochemical Engineering Journal 2004;18(2):143-7.

[80] Nagamori M, Funazukuri T. Glucose production by hydrolysis of starch under hydrothermal conditions. Journal of chemical technology and biotechnology 2004;79(3):229-33.

[81] Bobleter O. Hydrothermal degradation of polymers derived from plants. Progress in Polymer Science 1994;19(5):797-841.

[82] Antal MJ, Mok WSL, Richards GN. Mechanism of formation of 5-(hydroxymethyl)-2-furaldehyde from d-fructose and sucrose. Carbohydrate Research 1990;199(1):91-109.

[83] Jin F, Zhou Z, Moriya T, Kishida H, Higashijima H, Enomoto H. Controlling Hydrothermal Reaction Pathways To Improve Acetic Acid Production from Carbohydrate Biomass. Environmental Science & Technology 2005;39(6):1893-902.

[84] Garrote G, Domínguez H, Parajó JC. Hydrothermal processing of lignocellulosic materials. Holz als Roh- und Werkstoff 1999;57(3):191-202.

[85] Sevilla M, Fuertes AB. Chemical and Structural Properties of Carbonaceous Products Obtained by Hydrothermal Carbonization of Saccharides. Chemistry – A European Journal 2009;15(16):4195-203.

[86] Sevilla M, Fuertes AB. The production of carbon materials by hydrothermal carbonization of cellulose. Carbon 2009;47(9):2281-9.

[87] Heilmann SM, Davis HT, Jader LR, Lefebvre PA, Sadowsky MJ, Schendel FJ, et al. Hydrothermal carbonization of microalgae. Biomass and Bioenergy 2010;34(6):875-82.

[88] Heilmann SM, Jader LR, Harned LA, Sadowsky MJ, Schendel FJ, Lefebvre PA, et al. Hydrothermal carbonization of microalgae II. Fatty acid, char, and algal nutrient products. Applied Energy 2011;88(10):3286-90.

[89] Heilmann SM, Jader LR, Sadowsky MJ, Schendel FJ, von Keitz MG, Valentas KJ. Hydrothermal carbonization of distiller's grains. Biomass and Bioenergy 2011;35(7):2526-33.

[90] Levine RB, Pinnarat T, Savage PE. Biodiesel production from wet algal biomass through in situ lipid hydrolysis and supercritical transesterification. Energy & Fuels 2010;24(9):5235-43.

[91] Baccile N, Antonietti M, Titirici M-M. One-Step Hydrothermal Synthesis of Nitrogen-Doped Nanocarbons: Albumine Directing the Carbonization of Glucose. ChemSusChem 2010;3(2):246-53.

[92] Baccile N, Laurent G, Coelho C, Babonneau F, Zhao L, Titirici M-M. Structural Insights on Nitrogen-Containing Hydrothermal Carbon Using Solid-State Magic Angle Spinning 13C and 15N Nuclear Magnetic Resonance. The Journal of Physical Chemistry C 2011;115(18):8976-82.

[93] White RJ, Yoshizawa N, Antonietti M, Titirici M-M. A sustainable synthesis of nitrogen-doped carbon aerogels. Green chemistry 2011;13(9):2428-34.

[94] Steinhart H. The Maillard Reaction. Chemistry, Biochemistry and Implications. By Harry Nursten. Angewandte Chemie International Edition 2005;44(46):7503-4.

[95] Ledl F, Schleicher E. New Aspects of the Maillard Reaction in Foods and in the Human Body. Angewandte Chemie International Edition in English 1990;29(6):565-94.

[96] Wohlgemuth S-A, Vilela F, Titirici M-M, Antonietti M. A one-pot hydrothermal synthesis of tunable dual heteroatom-doped carbon microspheres. Green Chemistry 2012;14(3):741-9.

[97] Hashaikeh R, Fang Z, Butler IS, Hawari J, Kozinski JA. Hydrothermal dissolution of willow in hot compressed water as a model for biomass conversion. Fuel 2007;86(10–11):1614-22.

[98] Mosteiro-Romero M, Vogel F, Wokaun A. Liquefaction of wood in hot compressed water: Part 1—Experimental results. Chemical Engineering Science 2014;109:111-22.

[99] Kruse A, Koch F, Stelzl K, Wüst D, Zeller M. Fate of Nitrogen during Hydrothermal Carbonization. Energy & Fuels 2016;30(10):8037-42.

[100] Bach Q-V, Tran K-Q, Khalil RA, Skreiberg Ø, Seisenbaeva G. Comparative Assessment of Wet Torrefaction. Energy & Fuels 2013;27(11):6743-53.

[101] Hoekman SK, Broch A, Felix L, Farthing W. Hydrothermal carbonization (HTC) of loblolly pine using a continuous, reactive twin-screw extruder. Energy Conversion and Management 2017;134:247-59.

[102] Roos AA, Persson T, Krawczyk H, Zacchi G, Stålbrand H. Extraction of water-soluble hemicelluloses from barley husks. Bioresource Technology 2009;100(2):763-9.

[103] Kim DS, Myint AA, Lee HW, Yoon J, Lee Y-W. Evaluation of hot compressed water pretreatment and enzymatic saccharification of tulip tree sawdust using severity factors. Bioresource Technology 2013;144(Supplement C):460-6.

[104] Overend RP, Chornet E. Fractionation of lignocellulosics by steam-aqueous pretreatments. Philosophical Transactions of the Royal Society of London Series A, Mathematical and Physical Sciences 1987;321(1561):523-36.

[105] Anastasakis K, Ross AB. Hydrothermal liquefaction of the brown macro-alga Laminaria Saccharina: Effect of reaction conditions on product distribution and composition. Bioresource Technology 2011;102(7):4876-83.

[106] Venderbosch RH, Sander C. Hydroconversion of wet biomass a review Report GAVE-9919 2000.

[107] Volpe M, Fiori L. From olive waste to solid biofuel through hydrothermal carbonisation: The role of temperature and solid load on secondary char formation and hydrochar energy properties. Journal of Analytical and Applied Pyrolysis 2017;124:63-72.

[108] Volpe M, Goldfarb JL, Fiori L. Hydrothermal carbonization of Opuntia ficus-indica cladodes: Role of process parameters on hydrochar properties. Bioresource Technology 2018;247:310-8.

[109] Sermyagina E, Saari J, Kaikko J, Vakkilainen E. Hydrothermal carbonization of coniferous biomass: Effect of process parameters on mass and energy yields. Journal of Analytical and Applied Pyrolysis 2015;113:551-6.

[110] Álvarez-Murillo A, Román S, Ledesma B, Sabio E. Study of variables in energy densification of olive stone by hydrothermal carbonization. Journal of Analytical and Applied Pyrolysis 2015;113:307-14.

[111] Sabio E, Álvarez-Murillo A, Román S, Ledesma B. Conversion of tomato-peel waste into solid fuel by hydrothermal carbonization: Influence of the processing variables. Waste Management 2016;47:122-32.

[112] Mäkelä M, Benavente V, Fullana A. Hydrothermal carbonization of lignocellulosic biomass: Effect of process conditions on hydrochar properties. Applied Energy 2015;155:576-84.

[113] Stemann J, Putschew A, Ziegler F. Hydrothermal carbonization: Process water characterization and effects of water recirculation. Bioresource Technology 2013;143:139-46.

[114] Uddin MH, Reza MT, Lynam JG, Coronella CJ. Effects of water recycling in hydrothermal carbonization of loblolly pine. Environmental Progress & Sustainable Energy 2014;33(4):1309-15.

[115] Kambo HS, Minaret J, Dutta A. Process Water from the Hydrothermal Carbonization of Biomass: A Waste or a Valuable Product? Waste and Biomass Valorization 2017:1-9.

[116] Stemann J, Ziegler F. Assessment of the energetic efficiency of a continuously operating plant for hydrothermal carbonisation of biomass. *World Renewable Energy Congress-Sweden; 8-13 May; 2011; Linköping; Sweden.* Linköping University Electronic Press; 2011:125-32.

[117] Geissler C, Belau L. Zum Verhalten der stabilen Kohlenstoffisotope bei der Inkohlung. Zeitschrift für Angewandte Geologie 1971;17(1/2):13-6.

[118] Hu B, Yu S-H, Wang K, Liu L, Xu X-W. Functional carbonaceous materials from hydrothermal carbonization of biomass: an effective chemical process. Dalton Transactions 2008(40):5414-23.

[119] Demir-Cakan R, Baccile N, Antonietti M, Titirici M-M. Carboxylate-rich carbonaceous materials via one-step hydrothermal carbonization of glucose in the presence of acrylic acid. Chemistry of Materials 2009;21(3):484-90.

[120] Lu X, Yamauchi K, Phaiboonsilpa N, Saka S. Two-step hydrolysis of Japanese beech as treated by semi-flow hot-compressed water. J Wood Sci 2009;55(5):367-75.

[121] Lu X, Zhang Y, Angelidaki I. Optimization of H 2 SO 4-catalyzed hydrothermal pretreatment of rapeseed straw for bioconversion to ethanol: focusing on pretreatment at high solids content. Bioresource technology 2009;100(12):3048-53.

[122] Ando H, Sakaki T, Kokusho T, Shibata M, Uemura Y, Hatate Y. Decomposition behavior of plant biomass in hot-compressed water. Industrial and Engineering Chemistry Research 2000;39(10):3688-93.

[123] Pedersen TH, and Rosendahl, L.A. Synergetic Wood-glycerol Co-liquefaction in Supercritical Water for High Yield of High Quality Bio-crude. Proceedings from 23rd European Biomass Conference and Exhibition 2015.

[124] Yang W, Shimanouchi T, Kimura Y. Characterization of the Residue and Liquid Products Produced from Husks of Nuts from Carya cathayensis Sarg by Hydrothermal Carbonization. ACS Sustainable Chemistry & Engineering 2015;3(4):591-8.

[125] Ye T, Wei Z, Spinney R, Tang C-J, Luo S, Xiao R, et al. Chemical structure-based predictive model for the oxidation of trace organic contaminants by sulfate radical. Water Research 2017;116:106-15.

[126] Reza MT, Rottler E, Herklotz L, Wirth B. Hydrothermal carbonization (HTC) of wheat straw: Influence of feedwater pH prepared by acetic acid and potassium hydroxide. Bioresource Technology 2015;182:336-44.

[127] Goering H, Van Soest P. Forage fiber analysis. Agricultural handbook no. 379. US Department of Agriculture, Washington, DC 1970:1-20.

[128] Lu X, Flora JRV, Berge ND. Influence of process water quality on hydrothermal carbonization of cellulose. Bioresource Technology 2014;154:229-39.

[129] Krässig HA. Cellulose: structure, accessibility and reactivity. Gordon and Breach Science Publ.; 1993.

[130] Wikberg H, Ohra-aho T, Pileidis F, Titirici M-M. Structural and Morphological Changes in Kraft Lignin during Hydrothermal Carbonization. ACS Sustainable Chemistry & Engineering 2015;3(11):2737-45.

[131] Ekpo U, Ross AB, Camargo-Valero MA, Fletcher LA. Influence of pH on hydrothermal treatment of swine manure: Impact on extraction of nitrogen and phosphorus in process water. Bioresource Technology 2016;214:637-44.

[132] Dai L, Tan F, Wu B, He M, Wang W, Tang X, et al. Immobilization of phosphorus in cow manure during hydrothermal carbonization. Journal of Environmental Management 2015;157:49-53.

[133] Ghanim BM, Kwapinski W, Leahy JJ. Hydrothermal carbonisation of poultry litter: Effects of initial pH on yields and chemical properties of hydrochars. Bioresource Technology 2017;238:78-85.

[134] Chen W-H, Ye S-C, Sheen H-K. Hydrothermal carbonization of sugarcane bagasse via wet torrefaction in association with microwave heating. Bioresource Technology 2012;118:195-203.

[135] Yu L, Falco C, Weber J, White RJ, Howe JY, Titirici M-M. Carbohydrate-Derived Hydrothermal Carbons: A Thorough Characterization Study. Langmuir 2012;28(33):12373-83.

[136] Baccile N, Weber J, Falco C, Titirici M-M. Characterization of Hydrothermal Carbonization Materials. Sustainable Carbon Materials from Hydrothermal Processes. John Wiley & Sons, Ltd; 2013, p. 151-211.

[137] Zhao L, Baccile N, Gross S, Zhang Y, Wei W, Sun Y, et al. Sustainable nitrogen-doped carbonaceous materials from biomass derivatives. Carbon 2010;48(13):3778-87.

[138] Marson GA, El Seoud OA. A novel, efficient procedure for acylation of cellulose under homogeneous solution conditions. Journal of Applied Polymer Science 1999;74(6):1355-60.

[139] Remsing RC, Swatloski RP, Rogers RD, Moyna G. Mechanism of cellulose dissolution in the ionic liquid 1-n-butyl-3-methylimidazolium chloride: a 13C and 35/37Cl NMR relaxation study on model systems. Chemical Communications 2006(12):1271-3.

[140] Yu Y, Lou X, Wu H. Some recent advances in hydrolysis of biomass in hot-compressed water and its comparisons with other hydrolysis methods†. Energy & Fuels 2007;22(1):46-60.

[141] Lu X, Pellechia PJ, Flora JRV, Berge ND. Influence of reaction time and temperature on product formation and characteristics associated with the hydrothermal carbonization of cellulose. Bioresource Technology 2013;138:180-90.

[142] Patwardhan PR, Satrio JA, Brown RC, Shanks BH. Influence of inorganic salts on the primary pyrolysis products of cellulose. Bioresource Technology 2010;101(12):4646-55.

[143] Hamid SBA, Teh SJ, Lim YS. Catalytic Hydrothermal Upgrading of α-Cellulose using Iron Salts as a Lewis Acid. BioResources 2015;10(3):5974-86.

[144] Fechler N, Wohlgemuth S-A, Jaker P, Antonietti M. Salt and sugar: direct synthesis of high surface area carbon materials at low temperatures via hydrothermal carbonization of glucose under hypersaline conditions. Journal of Materials Chemistry A 2013;1(33):9418-21.

[145] Cui X, Antonietti M, Yu S-H. Structural Effects of Iron Oxide Nanoparticles and Iron Ions on the Hydrothermal Carbonization of Starch and Rice Carbohydrates. Small 2006;2(6):756-9.

[146] Ryu J, Suh Y-W, Suh DJ, Ahn DJ. Hydrothermal preparation of carbon microspheres from mono-saccharides and phenolic compounds. Carbon 2010;48(7):1990-8.

[147] Chen J, Chen Z, Wang C, Li X. Calcium-assisted hydrothermal carbonization of an alginate for the production of carbon microspheres with unique surface nanopores. Materials Letters 2012;67(1):365-8.

[148] Quigley DR, Breckenridge CR, Dugan PR, Ward B. Effects of Multivalent Cations on Low-Rank Coal Solubilities in Alkaline Solutions and Microbial Cultures. Energy and Fuels 1989;3(5):571-4.

[149] Domazetis G, James BD. Molecular models of brown coal containing inorganic species. Organic Geochemistry 2006;37(2):244-59.

[150] Fellinger T-P, White RJ, Titirici M-M, Antonietti M. Borax-Mediated Formation of Carbon Aerogels from Glucose. Advanced Functional Materials 2012;22(15):3254-60.

[151] Paraknowitsch JP, Zhang J, Su D, Thomas A, Antonietti M. Ionic Liquids as Precursors for Nitrogen-Doped Graphitic Carbon. Advanced Materials 2010;22(1):87-92.

[152] Schüth F. Endo- and Exotemplating to Create High-Surface-Area Inorganic Materials. Angewandte Chemie International Edition 2003;42(31):3604-22.

[153] Ryoo R, Joo SH, Kruk M, Jaroniec M. Ordered mesoporous carbons. 2001.

[154] White RJ, Antonietti M, Titirici M-M. Naturally inspired nitrogen doped porous carbon. Journal of Materials Chemistry 2009;19(45):8645-50.

[155] Soorholtz M, White RJ, Zimmermann T, Titirici M-M, Antonietti M, Palkovits R, et al. Direct methane oxidation over Pt-modified nitrogen-doped carbons. Chemical Communications 2013;49(3):240-2.

[156] Ryoo R, Joo SH, Jun S. Synthesis of Highly Ordered Carbon Molecular Sieves via Template-Mediated Structural Transformation. The Journal of Physical Chemistry B 1999;103(37):7743-6.

[157] Liang C, Hong K, Guiochon GA, Mays JW, Dai S. Synthesis of a Large-Scale Highly Ordered Porous Carbon Film by Self-Assembly of Block Copolymers. Angewandte Chemie International Edition 2004;43(43):5785-9.

[158] Liang C, Dai S. Synthesis of mesoporous carbon materials via enhanced hydrogen-bonding interaction. Journal of the American Chemical Society 2006;128(16):5316-7.

[159] Meng Y, Gu D, Zhang F, Shi Y, Yang H, Li Z, et al. Ordered mesoporous polymers and homologous carbon frameworks: amphiphilic surfactant templating and direct transformation. Angewandte Chemie 2005;117(43):7215-21.

[160] Huang HY, Yang RT. Catalyzed Carbon–NO Reaction Studied by Scanning Tunneling Microscopy and ab Initio Molecular Orbital Calculations. Journal of Catalysis 1999;185(2):286-96.

[161] Huang Y, Cai H, Yu T, Zhang F, Zhang F, Meng Y, et al. Formation of Mesoporous Carbon With a Face-Centered-Cubic Fd $\bar 3$ m Structure and Bimodal Architectural Pores From the Reverse Amphiphilic Triblock Copolymer PPO-PEO-PPO. Angewandte Chemie 2007;119(7):1107-11.

[162] Attard TM, McElroy CR, Gammons RJ, Slattery JM, Supanchaiyamat N, Kamei CLA, et al. Supercritical CO2 Extraction as an Effective Pretreatment Step for Wax Extraction in a Miscanthus Biorefinery. ACS Sustainable Chemistry & Engineering 2016;4(11):5979-88.

[163] Meng Y, Gu D, Zhang F, Shi Y, Cheng L, Feng D, et al. A family of highly ordered mesoporous polymer resin and carbon structures from organic− organic self-assembly. Chemistry of materials 2006;18(18):4447-64.

[164] White RJ, Tauer K, Antonietti M, Titirici M-M. Functional hollow carbon nanospheres by latex templating. Journal of the American Chemical Society 2010;132(49):17360-3.

[165] Zhai Y, Liu X, Zhu Y, Peng C, Wang T, Zhu L, et al. Hydrothermal carbonization of sewage sludge: The effect of feed-water pH on fate and risk of heavy metals in hydrochars. Bioresource Technology 2016;218:183-8.

[166] Yun J, Jin F, Kishita A, Tohji K, Enomoto H. Formic acid production from carbohydrates biomass by hydrothermal reaction. *Journal of Physics: Conference Series.* 215. IOP Publishing; 2010:012126.

[167] Hunter SE, Savage PE. Acid-Catalyzed Reactions in Carbon Dioxide-Enriched High-Temperature Liquid Water. Industrial & Engineering Chemistry Research 2003;42(2):290-4.

[168] Hunter SE, Savage PE. Quantifying rate enhancements for acid catalysis in CO2-enriched high-temperature water. AIChE Journal 2008;54(2):516-28.

[169] Bach Q-V, Tran K-Q, Skreiberg Ø. Accelerating wet torrefaction rate and ash removal by carbon dioxide addition. Fuel Processing Technology 2015;140:297-303.

[170] Miyazawa T, Funazukuri T. Polysaccharide Hydrolysis Accelerated by Adding Carbon Dioxide under Hydrothermal Conditions. Biotechnology Progress 2005;21(6):1782-5.

[171] Peter Van Walsum G, Garcia-Gil M, Chen S-F, Chambliss K. Effect of dissolved carbon dioxide on accumulation of organic acids in liquid hot water pretreated biomass hydrolyzates. Applied Biochemistry and Biotechnology 2007;137(1):301.

[172] Ross AB, Biller P, Kubacki ML, Li H, Lea-Langton A, Jones JM. Hydrothermal processing of microalgae using alkali and organic acids. Fuel 2010;89(9):2234-43.

[173] Broch A, Jena U, Hoekman S, Langford J. Analysis of Solid and Aqueous Phase Products from Hydrothermal Carbonization of Whole and Lipid-Extracted Algae. Energies 2013;7(1):62.

[174] Zhang G, Ma D, Peng C, Liu X, Xu G. Process characteristics of hydrothermal treatment of antibiotic residue for solid biofuel. Chemical Engineering Journal 2014;252:230-8.

[175] Akimoto M, Ninomiya K, Takami S, Ishikawa M, Sato M, Washio K. Hydrothermal Dechlorination and Denitrogenation of Municipal-Waste-Plastics-Derived Fuel Oil under Sub- and Supercritical Conditions. Industrial & Engineering Chemistry Research 2002;41(22):5393-400.

[176] Wu Z. Fundamentals of pulverised coal combustion. IEA Clean Coal Centre Reports 2005.

[177] Acharjee TC, Coronella CJ, Vasquez VR. Effect of thermal pretreatment on equilibrium moisture content of lignocellulosic biomass. Bioresource Technology 2011;102(7):4849-54.

[178] Escala M, Zumbühl T, Koller C, Junge R, Krebs R. Hydrothermal Carbonization as an Energy-Efficient Alternative to Established Drying Technologies for Sewage Sludge: A Feasibility Study on a Laboratory Scale. Energy & Fuels 2013;27(1):454-60.

[179] Kambo HS, Dutta A. Strength, storage, and combustion characteristics of densified lignocellulosic biomass produced via torrefaction and hydrothermal carbonization. Applied Energy 2014;135(Supplement C):182-91.

[180] Wilk M, Magdziarz A. Hydrothermal carbonization, torrefaction and slow pyrolysis of Miscanthus giganteus. Energy 2017;140:1292-304.

[181] Jones JM, Saddawi A, Dooley B, Mitchell EJS, Werner J, Waldron DJ, et al. Low temperature ignition of biomass. Fuel Processing Technology 2015;134(Supplement C):372-7.

[182] Miller BG, Tillman DA. Combustion Engineering Issues for Solid Fuel Systems. Elsevier; 2008.

[183] Williams A, Jones J, Ma L, Pourkashanian M. Pollutants from the combustion of solid biomass fuels. Progress in Energy and Combustion Science 2012;38(2):113-37.

[184] Glassman I, Yetter RA, Glumac NG. Combustion. Academic press; 2014.

[185] Yang H, Yan R, Chen H, Lee DH, Zheng C. Characteristics of hemicellulose, cellulose and lignin pyrolysis. Fuel 2007;86(12):1781-8.

[186] Dahlquist E. Technologies for Converting Biomass to Useful Energy. 1 ed.: CRC Press; 2013.

[187] Su S, Pohl JH, Holcombe D, Hart JA. Techniques to determine ignition, flame stability and burnout of blended coals in p.f. power station boilers. Progress in Energy and Combustion Science 2001;27(1):75-98.

[188] Yarin LP, Hetsroni G, Mosyak A. Combustion of two-phase reactive media. Springer Science & Business Media; 2013.

[189] Liu Z, Quek A, Hoekman SK, Srinivasan M, Balasubramanian R. Thermogravimetric investigation of hydrochar-lignite co-combustion. Bioresource technology 2012;123:646-52.

[190] Parshetti GK, Kent Hoekman S, Balasubramanian R. Chemical, structural and combustion characteristics of carbonaceous products obtained by hydrothermal carbonization of palm empty fruit bunches. Bioresource Technology 2013;135:683-9.

[191] Tillman DA, Duong DNB, Harding NS. Chapter 1 - Introduction to Fuel Blending. In: Tillman DA, Duong DNB, Harding NS, editors. Solid Fuel Blending. Boston: Butterworth-Heinemann; 2012, p. 1-29.

[192] Zhang J, Yuan J-W, Sheng C-D, Xu Y-Q. Characterization of coals utilized in power stations of China. Fuel 2000;79(1):95-102.

[193] Bryers RW. Investigation of the reactivity of macerals using thermal analysis. Fuel processing technology 1995;44(1-3):25-54.

[194] Su S, Pohl JH, Holcombe D, Hart JA. A proposed maceral index to predict combustion behavior of coal. Fuel 2001;80(5):699-706.

[195] Tillman DA, Duong DNB, Harding NS. Chapter 3 - Blending Coal on Coal. In: Tillman DA, Duong DNB, Harding NS, editors. Solid Fuel Blending. Boston: Butterworth-Heinemann; 2012, p. 71-123.

[196] Bridgeman TG, Jones JM, Williams A, Waldron DJ. An investigation of the grindability of two torrefied energy crops. Fuel 2010;89(12):3911-8.

[197] Ndibe C, Vonk G, Yuan S, Maier J, Scheffknecht G. Characterizing the Grinding Behavior of Pre-Treated Biomass Fuels for Coal Pulverizer Application. Proceedings of 24th European Biomass Conference and Exhibition 2016:457 - 65.

[198] McNamee P, Adams PWR, McManus MC, Dooley B, Darvell LI, Williams A, et al. An assessment of the torrefaction of North American pine and life cycle greenhouse gas emissions. Energy Conversion and Management 2016;113:177-88.

[199] Masiá AT, Buhre B, Gupta R, Wall T. Characterising ash of biomass and waste. Fuel Processing Technology 2007;88(11):1071-81.

[200] Grimm A, Skoglund N, Boström D, Ohman M. Bed agglomeration characteristics in fluidized quartz bed combustion of phosphorus-rich biomass fuels. Energy & Fuels 2011;25(3):937-47.

[201] Riedl R, Dahl J, Obernberger I, Narodoslawsky M. Corrosion in fire tube boilers of biomass combustion plants. *Proceedings of the China International Corrosion Control Conference 1999.* 1999.

[202] Lindström E, Sandström M, Boström D, Öhman M. Slagging Characteristics during Combustion of Cereal Grains Rich in Phosphorus. Energy & Fuels 2007;21(2):710-7.

[203] Thy P, Jenkins BM, Grundvig S, Shiraki R, Lesher CE. High temperature elemental losses and mineralogical changes in common biomass ashes. Fuel 2006;85(5):783-95.

[204] Thy P, Lesher CE, Jenkins BM. Experimental determination of high-temperature elemental losses from biomass slag. Fuel 2000;79(6):693-700.

[205] Miles TR, Miles Jr T, Baxter L, Bryers R, Jenkins B, Oden L. Alkali deposits found in biomass power plants: A preliminary investigation of their extent and nature. Volume 1. National Renewable Energy Lab., Golden, CO (United States); Miles (Thomas R.), Portland, OR (United States); Sandia National Labs., Livermore, CA (United States); Foster Wheeler Development Corp., Livingston, NJ (United States); California Univ., Davis, CA (United States); Bureau of Mines, Albany, OR (United States). Albany Research Center; 1995.

[206] Williams PT, Horne PA. The role of metal salts in the pyrolysis of biomass. Renewable Energy 1994;4(1):1-13.

[207] Jones JM, Darvell LI, Pourkashanian M, Williams A. The role of metals in biomass char combustion. 2005.

[208] Saddawi A, Jones JM, Williams A. Influence of alkali metals on the kinetics of the thermal decomposition of biomass. Fuel Processing Technology 2012;104:189-97.

[209] Backreedy RI, Jones JM, Pourkashanian M, Williams A. Burn-out of pulverised coal and biomass chars☆. Fuel 2003;82(15):2097-105.

[210] Kannan MP, Richards GN. Gasification of biomass chars in carbon dioxide: dependence of gasification rate on the indigenous metal content. Fuel 1990;69(6):747-53.

[211] Stojanowska G, Jones J. Influence of added calcium on thermal decomposition of biomass, lignite and their blends. Archivum Combustionis 2006;26(3/4):91.

[212] Backreedy RI, Jones JM, Pourkashanian M, Williams A. Modeling the reaction of oxygen with coal and biomass chars. Proceedings of the Combustion Institute 2002;29(1):415-21.

[213] Smith AM, Singh S, Ross AB. Fate of inorganic material during hydrothermal carbonisation of biomass: Influence of feedstock on combustion behaviour of hydrochar. Fuel 2016;169:135-45.

[214] Lane DJ, Truong E, Larizza F, Chiew P, de Nys R, van Eyk PJ. Effect of Hydrothermal Carbonization on the Combustion and Gasification Behavior of Agricultural Residues and Macroalgae: Devolatilization Characteristics and Char Reactivity. Energy & Fuels 2017.

[215] Bach Q-V, Chen W-H, Lin S-C, Sheen H-K, Chang J-S. Wet torrefaction of microalga Chlorella vulgaris ESP-31 with microwave-assisted heating. Energy Conversion and Management 2017;141:163-70.

[216] Bach Q-V, Tran K-Q, Skreiberg Ø. Comparative study on the thermal degradation of dry- and wet-torrefied woods. Applied Energy 2017;185:1051-8.

[217] Bach Q-V, Tran K-Q, Skreiberg Ø, Khalil RA, Phan AN. Effects of wet torrefaction on reactivity and kinetics of wood under air combustion conditions. Fuel 2014;137:375-83.

[218] Bach Q-V, Tran K-Q, Skreiberg Ø. Combustion kinetics of wet-torrefied forest residues using the distributed activation energy model (DAEM). Applied Energy 2017;185:1059-66.

[219] Miller JA, Bowman CT. Mechanism and modeling of nitrogen chemistry in combustion. Progress in energy and combustion science 1989;15(4):287-338.

[220] Gardiner WC. Gas-phase combustion chemistry. Springer Science & Business Media; 2000.

[221] Bowman CT. Control of combustion-generated nitrogen oxide emissions: technology driven by regulation. *Symposium (International) on Combustion*. 24. Elsevier; 1992:859-78.

[222] Heschel W, Rweyemamu L, Scheibner T, Meyer B. Abatement of emissions in small-scale combustors through utilisation of blended pellet fuels. Fuel processing technology 1999;61(3):223-42.

[223] Kim K-H, Kabir E, Kabir S. A review on the human health impact of airborne particulate matter. Environment International 2015;74:136-43.

[224] Parker KR. Applied electrostatic precipitation. Springer Science & Business Media; 2012.

[225] Shanthakumar S, Singh DN, Phadke RC. Flue gas conditioning for reducing suspended particulate matter from thermal power stations. Progress in Energy and Combustion Science 2008;34(6):685-95.

[226] Dahlin RS, Vann Bush P, Snyder TR. Fundamental mechanisms in flue-gas conditioning. Topical report No. 1, Literature review and assembly of theories on the interactions of ash and FGD sorbents. Southern Research Inst., Birmingham, AL (United States); 1992.

[227] Córdoba P. Status of Flue Gas Desulphurisation (FGD) systems from coal-fired power plants: Overview of the physic-chemical control processes of wet limestone FGDs. Fuel 2015;144:274-86.

[228] White PJ, Broadley MR. Chloride in soils and its uptake and movement within the plant: a review. Annals of Botany 2001;88(6):967-88.

[229] Rutherford DW, Chiou CT, Kile DE. Influence of soil organic matter composition on the partition of organic compounds. Environmental Science & Technology 1992;26(2):336-40.

[230] Huéscar Medina C, Phylaktou HN, Andrews GE, Gibbs BM. Explosion characteristics of pulverised torrefied and raw Norway spruce (Picea abies) and Southern pine (Pinus palustris) in comparison to bituminous coal. Biomass and Bioenergy 2015;79:116-27.

[231] Saeed MA, Slatter DJF, Andrews GE, Phylaktou HN, Gibbs BM. Combustion of Pulverized Biomass Crop Residues and Their Explosion Characteristics. Combustion Science and Technology 2016;188(11-12):2200-16.

[232] Miles TR, Miles Jr TR, Baxter LL, Bryers RW, Jenkins BM, Oden LL. Boiler deposits from firing biomass fuels. Biomass and Bioenergy 1996;10(2–3):125-38.

[233] Vuthaluru HB, Brooke RJ, Zhang DK, Yan HM. Effects of moisture and coal blending on Hardgrove Grindability Index of Western Australian coal. Fuel Processing Technology 2003;81(1):67-76.

[234] Wang L, Hustad JE, Skreiberg Ø, Skjevrak G, Grønli M. A Critical Review on Additives to Reduce Ash Related Operation Problems in Biomass Combustion Applications. Energy Procedia 2012;20(Supplement C):20-9.

[235] Clery DS, Mason PE, Rayner CM, Jones JM. The effects of an additive on the release of potassium in biomass combustion. Fuel 2018;214:647-55.

[236] Aho M. Reduction of chlorine deposition in FB boilers with aluminium-containing additives. Fuel 2001;80(13):1943-51.

[237] Pettersson A, Åmand L-E, Steenari B-M. Chemical fractionation for the characterisation of fly ashes from co-combustion of biofuels using different methods for alkali reduction. Fuel 2009;88(9):1758-72.

[238] Tran K-Q, Iisa K, Steenari B-M, Lindqvist O. A kinetic study of gaseous alkali capture by kaolin in the fixed bed reactor equipped with an alkali detector. Fuel 2005;84(2):169-75.

[239] Tobiasen L, Skytte R, Pedersen LS, Pedersen ST, Lindberg MA. Deposit characteristic after injection of additives to a Danish straw-fired suspension boiler. Fuel Processing Technology 2007;88(11):1108-17.

[240] Åmand L-E, Leckner B, Eskilsson D, Tullin C. Deposits on heat transfer tubes during co-combustion of biofuels and sewage sludge. Fuel 2006;85(10):1313-22.

[241] Steenari BM, Lindqvist O. High-temperature reactions of straw ash and the anti-sintering additives kaolin and dolomite. Biomass and Bioenergy 1998;14(1):67-76.

[242] Steenari B-M, Lundberg A, Pettersson H, Wilewska-Bien M, Andersson D. Investigation of Ash Sintering during Combustion of Agricultural Residues and the Effect of Additives. Energy & Fuels 2009;23(11):5655-62.

[243] Uberoi M, Punjak WA, Shadman F. The kinetics and mechanism of alkali removal from flue gases by solid sorbents. Progress in Energy and Combustion Science 1990;16(4):205-11.

[244] Kyi S, Chadwick BL. Screening of potential mineral additives for use as fouling preventatives in Victorian brown coal combustion. Fuel 1999;78(7):845-55.

[245] Llorente MJF, Arocas PD, Nebot LG, García JEC. The effect of the addition of chemical materials on the sintering of biomass ash. Fuel 2008;87(12):2651-8.

[246] Wang L, Skjevrak G, Hustad JE, Grønli MG. Effects of Sewage Sludge and Marble Sludge Addition on Slag Characteristics during Wood Waste Pellets Combustion. Energy & Fuels 2011;25(12):5775-85.

[247] Elled AL, Davidsson KO, Åmand LE. Sewage sludge as a deposit inhibitor when co-fired with high potassium fuels. Biomass and Bioenergy 2010;34(11):1546-54.

[248] Aho M, Yrjas P, Taipale R, Hupa M, Silvennoinen J. Reduction of superheater corrosion by co-firing risky biomass with sewage sludge. Fuel 2010;89(9):2376-86.

[249] Wang L, Skjevrak G, Hustad JE, Grønli MG. Sintering characteristics of sewage sludge ashes at elevated temperatures. Fuel Processing Technology 2012;96:88-97.

[250] Broström M, Kassman H, Helgesson A, Berg M, Andersson C, Backman R, et al. Sulfation of corrosive alkali chlorides by ammonium sulfate in a biomass fired CFB boiler. Fuel Processing Technology 2007;88(11):1171-7.

[251] Jiménez S, Ballester J. Influence of operating conditions and the role of sulfur in the formation of aerosols from biomass combustion. Combustion and Flame 2005;140(4):346-58.

[252] Jiménez S, Ballester J. Formation of alkali sulphate aerosols in biomass combustion. Fuel 2007;86(4):486-93.

[253] Aho M, Vainikka P, Taipale R, Yrjas P. Effective new chemicals to prevent corrosion due to chlorine in power plant superheaters. Fuel 2008;87(6):647-54.

[254] Gilbe C, Öhman M, Lindström E, Boström D, Backman R, Samuelsson R, et al. Slagging Characteristics during Residential Combustion of Biomass Pellets. Energy & Fuels 2008;22(5):3536-43.

[255] Wagner W, Pruß A. The IAPWS formulation 1995 for the thermodynamic properties of ordinary water substance for general and scientific use. Journal of Physical and Chemical Reference Data 2002;31(2):387-535.

[256] Archer DG, Wang P. The Dielectric Constant of Water and Debye-Hückel Limiting Law Slopes. Journal of physical and chemical reference data 1990;19(2):371-411.

[257] Bandura AV, Lvov SN. The ionization constant of water over wide ranges of temperature and density. Journal of Physical and Chemical Reference Data 2006;35(1):15-30.

[258] Mäkelä M, Fullana A, Yoshikawa K. Ash behavior during hydrothermal treatment for solid fuel applications. Part 1: Overview of different feedstock. Energy Conversion and Management 2016;121:402-8.

[259] Smith AM, Ross AB. Production of bio-coal, bio-methane and fertilizer from seaweed via hydrothermal carbonisation. Algal Research 2016;16:1-11.

[260] Smith AM, Whittaker C, Shield I, Ross AB. Production of high quality bio-coal from early harvested Miscanthus by hydrothermal carbonisation. awaiting.

[261] Mäkelä M, Yoshikawa K. Ash behavior during hydrothermal treatment for solid fuel applications. Part 2: Effects of treatment conditions on industrial waste biomass. Energy Conversion and Management 2016;121:409-14.

[262] Mäkelä M, Kwong CW, Broström M, Yoshikawa K. Hydrothermal treatment of grape marc for solid fuel applications. Energy Conversion and Management 2017;145:371-7.

[263] PetroviĿ J, PerišiĿ N, MaksimoviĿ JD, MaksimoviĿ V, KragoviĿ M, StojanoviĿ M, et al. Hydrothermal conversion of grape pomace: Detailed characterization of obtained hydrochar and liquid phase. Journal of Analytical and Applied Pyrolysis 2016;118:267-77.

[264] Deng L, Zhang T, Che D. Effect of water washing on fuel properties, pyrolysis and combustion characteristics, and ash fusibility of biomass. Fuel Processing Technology 2013;106:712-20.

[265] Liu Z, Quek A, Kent Hoekman S, Balasubramanian R. Production of solid biochar fuel from waste biomass by hydrothermal carbonization. Fuel 2013;103(0):943-9.

[266] Müller M, Wolf K-J, Smeda A, Hilpert K. Release of K, Cl, and S Species during Co-combustion of Coal and Straw. Energy & Fuels 2006;20(4):1444-9.

[267] Skrifvars B-J, Laurén T, Hupa M, Korbee R, Ljung P. Ash behaviour in a pulverized wood fired boiler—a case study. Fuel 2004;83(10):1371-9.

[268] Hoekman SK, Broch A, Robbins C, Zielinska B, Felix L. Hydrothermal carbonization (HTC) of selected woody and herbaceous biomass feedstocks. Biomass Conv Bioref 2013;3(2):113-26.

[269] Weiner B, Poerschmann J, Wedwitschka H, Koehler R, Kopinke F-D. Influence of Process Water Reuse on the Hydrothermal Carbonization of Paper. ACS Sustainable Chemistry & Engineering 2014;2(9):2165-71.

[270] Assary RS, Redfern PC, Hammond JR, Greeley J, Curtiss LA. Computational Studies of the Thermochemistry for Conversion of Glucose to Levulinic Acid. The Journal of Physical Chemistry B 2010;114(27):9002-9.

[271] Lange J-P, Price R, Ayoub PM, Louis J, Petrus L, Clarke L, et al. Valeric Biofuels: A Platform of Cellulosic Transportation Fuels. Angewandte Chemie International Edition 2010;49(26):4479-83.

[272] Wirth B, Mumme J. Anaerobic Digestion of Waste Water from Hydrothermal Carbonization of Corn Silage. *Applied Bioenergy*. 1. 2014.

[273] Wood BM, Jader LR, Schendel FJ, Hahn NJ, Valentas KJ, McNamara PJ, et al. Industrial symbiosis: Corn ethanol fermentation, hydrothermal carbonization, and anaerobic digestion. Biotechnology and bioengineering 2013;110(10):2624-32.

[274] Danso-Boateng E, Shama G, Wheatley A, Martin S, Holdich R. Hydrothermal carbonisation of sewage sludge: Effect of process conditions on product characteristics and methane production. Bioresource technology 2015;177:318-27.

[275] Wirth B, Reza T, Mumme J. Influence of digestion temperature and organic loading rate on the continuous anaerobic treatment of process liquor from hydrothermal carbonization of sewage sludge. Bioresource Technology 2015;198(Supplement C):215-22.

[276] Nyktari E, Danso-Boateng E, Wheatley A, Holdich R. Anaerobic digestion of liquid products following hydrothermal carbonisation of faecal sludge at different reaction conditions. Desalination and Water Treatment 2017;91:245-51.

[277] Guellout Z, Clion V, Benguerba Y, Dumas C, Ernst B. Study of the dark fermentative hydrogen production using modified ADM1 models. Biochemical Engineering Journal 2018;132:9-19.

[278] Hu B-B, Li M-Y, Wang Y-T, Zhu M-J. High-yield biohydrogen production from non-detoxified sugarcane bagasse: Fermentation strategy and mechanism. Chemical Engineering Journal 2018;335:979-87.

[279] Guo L, Zhang Z, Gao M, She Z, Zhao Y, Guo Y, et al. Comparison of thermophilic bacteria and alkyl polyglucose pretreatment on two-stage anaerobic digestion with waste sludge: Biogas production potential and substrate metabolism process. Bioresource Technology 2018;249:694-703.

[280] Amorim NCS, Amorim ELC, Kato MT, Florencio L, Gavazza S. The effect of methanogenesis inhibition, inoculum and substrate concentration on hydrogen and carboxylic acids production from cassava wastewater. Biodegradation 2018;29(1):41-58.

[281] Aragón-Briceño C, Ross AB, Camargo-Valero MA. Evaluation and comparison of product yields and bio-methane potential in sewage digestate following hydrothermal treatment. Applied Energy 2017;208(Supplement C):1357-69.

[282] Nuchdang S, Frigon JC, Roy C, Pilon G, Phalakornkule C, Guiot SR. Hydrothermal post-treatment of digestate to maximize the methane yield from the anaerobic digestion of microalgae. Waste Management 2018;71:683-8.

[283] Villamil JA, Mohedano AF, Rodriguez JJ, de la Rubia MA. Valorisation of the liquid fraction from hydrothermal carbonisation of sewage sludge by anaerobic digestion. Journal of Chemical Technology & Biotechnology 2018;93(2):450-6.

[284] Rajagopal R, Massé DI, Singh G. A critical review on inhibition of anaerobic digestion process by excess ammonia. Bioresource Technology 2013;143(0):632-41.

[285] Stronach SM, Rudd T, Lester JN. Toxic Substances in Anaerobic Digestion. Anaerobic Digestion Processes in Industrial Wastewater Treatment. Berlin, Heidelberg: Springer Berlin Heidelberg; 1986, p. 71-92.

[286] Camarillo R, Rincón J. Effect of inhibitory compounds on the two-phase anaerobic digestion performance of diluted wastewaters from the alimentary industry. Chemical Engineering Journal 2012;193-194(Supplement C):68-76.

[287] Reza MT, Wirth B, Lüder U, Werner M. Behavior of selected hydrolyzed and dehydrated products during hydrothermal carbonization of biomass. Bioresource Technology 2014;169:352-61.

[288] Agler MT, Wrenn BA, Zinder SH, Angenent LT. Waste to bioproduct conversion with undefined mixed cultures: the carboxylate platform. Trends in biotechnology 2011;29(2):70-8.

[289] Gerlach RW, Dobb DE, Raab GA, Nocerino JM. Gy sampling theory in environmental studies. 1. Assessing soil splitting protocols. Journal of Chemometrics 2002;16(7):321-8.

[290] Keenan JH, Keyes FG. Thermodynamic properties of steam. 1936.

[291] Krevelen DW. Coal--typology, chemistry, physics, constitution. Elsevier Science & Technology; 1961.

[292] Corbitt RA. Standard handbook of environmental engineering. 1990.

[293] Mendham J, Denney R, Barnes J, Thomas M, Denney R, Thomas M. Vogel's Quantitative Chemical Analysis. Prentice Hall, New York 2000;71:65-70.

[294] Klinkenberg H, van der Wal S, de Koster C, Bart J. On the use of inductively coupled plasma mass spectrometry as an element specific detector for liquid chromatography:

optimization of an industrial tellurium removal process. Journal of Chromatography A 1998;794(1):219-32.

[295] Vogel AI. Quantitative Inorganic Analysis. Longmans, Green and Co, London 1939.

[296] Parr. 207M - Analytical Methods for Oxygen Bombs. 2013.

[297] Xing P, Mason PE, Chilton S, Lloyd S, Jones JM, Williams A, et al. A comparative assessment of biomass ash preparation methods using X-ray fluorescence and wet chemical analysis. Fuel 2016;182(Supplement C):161-5.

[298] Bapat D, Kulkarni S, Bhandarkar V. Design and operating experience on fluidized bed boiler burning biomass fuels with high alkali ash. American Society of Mechanical Engineers, New York, NY (United States); 1997.

[299] Hayhurst AN. The kinetics of the pyrolysis or devolatilisation of sewage sludge and other solid fuels. Combustion and Flame 2013;160(1):138-44.

[300] Hardgrove R. Grindability of coal. Trans ASME, Fuels and Steam Power 1932;54:37-46.

[301] Chuntanapum A, Matsumura Y. Formation of Tarry Material from 5-HMF in Subcritical and Supercritical Water. Industrial & Engineering Chemistry Research 2009;48(22):9837-46.

[302] Reza MT, Freitas A, Yang X, Coronella CJ. Wet Air Oxidation of Hydrothermal Carbonization (HTC) Process Liquid. ACS Sustainable Chemistry & Engineering 2016;4(6):3250-4.

[303] Fitt L. Convenient, in-line purification of saccharide mixture in automated high-performance liquid chromatography. Journal of Chromatography A 1978;152(1):243-6.

[304] Chen S-F, Mowery RA, Scarlata CJ, Chambliss CK. Compositional Analysis of Water-Soluble Materials in Corn Stover. Journal of Agricultural and Food Chemistry 2007;55(15):5912-8.

[305] Jaffrezo JL, Calas N, Bouchet M. Carboxylic acids measurements with ionic chromatography. Atmospheric Environment 1998;32(14):2705-8.

[306] Reza MT, Uddin MH, Lynam JG, Hoekman SK, Coronella CJ. Hydrothermal carbonization of loblolly pine: reaction chemistry and water balance. Biomass Conv Bioref 2014;4(4):311-21.

[307] Titirici M-M, Antonietti M, Baccile N. Hydrothermal carbon from biomass: a comparison of the local structure from poly- to monosaccharides and pentoses/hexoses. Green Chemistry 2008;10(11):1204-12.

[308] Baccile N, Falco C, Titirici M-M. Characterization of biomass and its derived char using 13C-solid state nuclear magnetic resonance. Green Chemistry 2014;16(12):4839-69.

[309] Patil SKR, Lund CRF. Formation and Growth of Humins via Aldol Addition and Condensation during Acid-Catalyzed Conversion of 5-Hydroxymethylfurfural. Energy & Fuels 2011;25(10):4745-55.

[310] Pretsch E, Bühlmann P, Affolter C, Pretsch E, Bhuhlmann P, Affolter C. Structure determination of organic compounds. Springer; 2009.

[311] Kumar S, Gupta R, Lee YY, Gupta RB. Cellulose pretreatment in subcritical water: Effect of temperature on molecular structure and enzymatic reactivity. Bioresource Technology 2010;101(4):1337-47.

[312] Werkelin J, Skrifvars B-J, Zevenhoven M, Holmbom B, Hupa M. Chemical forms of ash-forming elements in woody biomass fuels. Fuel 2010;89(2):481-93.

[313] Adams J, Gallagher J, Donnison I. Fermentation study on Saccharina latissima for bioethanol production considering variable pre-treatments. J Appl Phycol 2009;21(5):569-74.

[314] Gurung A, Van Ginkel SW, Kang W-C, Qambrani NA, Oh S-E. Evaluation of marine biomass as a source of methane in batch tests: A lab-scale study. Energy 2012;43(1):396-401.

[315] Hughes AD, Kelly MS, Black KD, Stanley MS. Biogas from Macroalgae: Is it time to revisit the idea? Biotechnology for Biofuels 2012;5.

[316] Horn SJ, Aasen IM, Østgaard K. Ethanol production from seaweed extract. J Ind Microbiol Biotech 2000;25(5):249-54.

[317] Ross A, Anastasakis K, Kubacki M, Jones J. Investigation of the pyrolysis behaviour of brown algae before and after pre-treatment using PY-GC/MS and TGA. Journal of analytical and applied pyrolysis 2009;85(1):3-10.

[318] Bae YJ, Ryu C, Jeon J-K, Park J, Suh DJ, Suh Y-W, et al. The characteristics of bio-oil produced from the pyrolysis of three marine macroalgae. Bioresource technology 2011;102(3):3512-20.

[319] Xu Q, Qian Q, Quek A, Ai N, Zeng G, Wang J. Hydrothermal carbonization of macroalgae and the effects of experimental parameters on the properties of hydrochars. ACS Sustainable Chemistry and Engineering 2013;1(9):1092-101.

[320] Jeon W, Ban C, Park G, Yu TK, Suh JY, Woo HC, et al. Catalytic hydrothermal conversion of macroalgae-derived alginate: Effect of pH on production of furfural and valuable organic acids under subcritical water conditions. Journal of Molecular Catalysis A: Chemical 2015;399:106-13.

[321] Black W. The seasonal variation in weight and chemical composition of the common British Laminariaceae. Journal of the Marine Biological Association of the United Kingdom 1950;29(01):45-72.

[322] Schiener P, Black K, Stanley M, Green D. The seasonal variation in the chemical composition of the kelp species Laminaria digitata, Laminaria hyperborea, Saccharina latissima and Alaria esculenta. J Appl Phycol 2015;27(1):363-73.

[323] Hatcher PG, Breger IA, Szeverenyi N, Maciel GE. Nuclear magnetic resonance studies of ancient buried wood—II. Observations on the origin of coal from lignite to bituminous coal. Organic Geochemistry 1982;4(1):9-18.

[324] López Barreiro D, Beck M, Hornung U, Ronsse F, Kruse A, Prins W. Suitability of hydrothermal liquefaction as a conversion route to produce biofuels from macroalgae. Algal Research 2015;11(0):234-41.

[325] Sun X, Li Y. Colloidal Carbon Spheres and Their Core/Shell Structures with Noble-Metal Nanoparticles. Angewandte Chemie International Edition 2004;43(5):597-601.

[326] Hecht H, Srebnik S. Structural Characterization of Sodium Alginate and Calcium Alginate. Biomacromolecules 2016;17(6):2160-7.

[327] Biller P, Ross AB. Potential yields and properties of oil from the hydrothermal liquefaction of microalgae with different biochemical content. Bioresource Technology 2011;102(1):215-25.

[328] Lewandowski I, Clifton-Brown JC, Scurlock JMO, Huisman W. Miscanthus: European experience with a novel energy crop. Biomass and Bioenergy 2000;19(4):209-27.

[329] Lewandowski I, Heinz A. Delayed harvest of miscanthus—influences on biomass quantity and quality and environmental impacts of energy production. European Journal of Agronomy 2003;19(1):45-63.

[330] Yates NE, Riche AB, Shield I, Zapater M, Ferchaud F, Ragaglini G, et al. Investigating the Long-term Biomass Yield of Miscanthus giganteus and Switchgrass when

Harvested as a Green Energy Feedstock. . *23rd European Biomass Conference and Exhibition.* Vienna, Austria; 2015:61 – 7.

[331] Kahle P, Beuch S, Boelcke B, Leinweber P, Schulten H-R. Cropping of Miscanthus in Central Europe: biomass production and influence on nutrients and soil organic matter. European Journal of Agronomy 2001;15(3):171-84.

[332] Gezan SA, Riche AB. Over-winter decline in switchgrass and miscanthus. Aspects of Applied Biology 90 2008:219.

[333] Godin B, Lamaudière S, Agneessens R, Schmit T, Goffart J-P, Stilmant D, et al. Chemical characteristics and biofuel potential of several vegetal biomasses grown under a wide range of environmental conditions. Industrial Crops and Products 2013;48:1-12.

[334] Yates N, Riche AB, Shield I. long term biomass yield. 2015.

[335] Clifton-Brown JC, Breuer J, Jones MB. Carbon mitigation by the energy crop, Miscanthus. Global Change Biology 2007;13(11):2296-307.

[336] Baxter XC, Darvell LI, Jones JM, Barraclough T, Yates NE, Shield I. Miscanthus combustion properties and variations with Miscanthus agronomy. Fuel 2014;117, Part A:851-69.

[337] Roncucci N, Di Nasso NO, Tozzini C, Bonari E, Ragaglini G. Miscanthus× giganteus nutrient concentrations and uptakes in autumn and winter harvests as influenced by soil texture, irrigation and nitrogen fertilization in the Mediterranean. GCB Bioenergy 2015;7(5):1009-18.

[338] Cadoux S, Riche AB, Yates NE, Machet J-M. Nutrient requirements of Miscanthus x giganteus: conclusions from a review of published studies. Biomass and Bioenergy 2012;38:14-22.

[339] Mayer F, Gerin PA, Noo A, Lemaigre S, Stilmant D, Schmit T, et al. Assessment of energy crops alternative to maize for biogas production in the Greater Region. Bioresource Technology 2014;166(0):358-67.

[340] Kiesel A, Lewandowski I. Miscanthus as biogas substrate – cutting tolerance and potential for anaerobic digestion. GCB Bioenergy 2017;9(1):153-67.

[341] Emery IR, Mosier NS. The impact of dry matter loss during herbaceous biomass storage on net greenhouse gas emissions from biofuels production. Biomass and Bioenergy 2012;39(Supplement C):237-46.

[342] Purdy SJ, Cunniff J, Maddison AL, Jones LE, Barraclough T, Castle M, et al. Seasonal Carbohydrate Dynamics and Climatic Regulation of Senescence in the Perennial Grass, Miscanthus. BioEnergy Research 2015;8(1):28-41.

[343] Avery B, Catt J. The soil at Rothamsted, Lawes Agricultural Trust. IACR-Rothamsted, Harpenden, Hertfordshire, United Kingdom 1995.

[344] Shield I, Barraclough TJP, Riche AB, Yates NE. Growing the energy crop miscanthus for 22 years. Asp Appl Biol 2015;128:173–9.

[345] van der Weijde T, Kiesel A, Iqbal Y, Muylle H, Dolstra O, Visser RGF, et al. Evaluation of Miscanthus sinensis biomass quality as feedstock for conversion into different bioenergy products. GCB Bioenergy 2017;9(1):176-90.

[346] Lu X, Berge ND. Influence of feedstock chemical composition on product formation and characteristics derived from the hydrothermal carbonization of mixed feedstocks. Bioresource Technology 2014;166(0):120-31.

[347] Demirbaş A. Relationships between lignin contents and fixed carbon contents of biomass samples. Energy Conversion and Management 2003;44(9):1481-6.

[348] Kei-ichi S, Yoshihisa I, Hitoshi I. Catalytic Activity of Lanthanide(III) Ions for the Dehydration of Hexose to 5-Hydroxymethyl-2-furaldehyde in Water. Bulletin of the Chemical Society of Japan 2001;74(6):1145-50.

[349] Lakshmanan CM, Hoelscher HE. Production of Levoglucosan by Pyrolysis of Carbohydrates. Pyrolysis in Hot Inert Gas Stream. Product R&D 1970;9(1):57-9.

[350] van Putten R-J, van der Waal JC, de Jong E, Rasrendra CB, Heeres HJ, de Vries JG. Hydroxymethylfurfural, A Versatile Platform Chemical Made from Renewable Resources. Chemical Reviews 2013;113(3):1499-597.

[351] Kabyemela BM, Adschiri T, Malaluan RM, Arai K. Glucose and Fructose Decomposition in Subcritical and Supercritical Water: Detailed Reaction Pathway, Mechanisms, and Kinetics. Industrial & Engineering Chemistry Research 1999;38(8):2888-95.

[352] Fang Y, Zeng X, Yan P, Jing Z, Jin F. An Acidic Two-Step Hydrothermal Process To Enhance Acetic Acid Production from Carbohydrate Biomass. Industrial & Engineering Chemistry Research 2012;51(12):4759-63.

[353] Holmelid B, Barth T, Brusletto R, Kleinert M. Production of monomeric phenols by formic acid assisted hydrous liquefaction of lignin. Biomass and Bioenergy 2017;105(Supplement C):298-309.

[354] Smith AM, Whittaker C, Shield I, Ross AB. The potential for production of high quality bio-coal from early harvested Miscanthus by hydrothermal carbonisation. Fuel 2018;220:546-57.

[355] Julien S, Chornet E, Tiwari PK, Overend RP. Vacuum pyrolysis of cellulose: Fourier transform infrared characterization of solid residues, product distribution and correlations. Journal of Analytical and Applied Pyrolysis 1991;19:81-104.

[356] Nowakowski DJ, Jones JM, Brydson RMD, Ross AB. Potassium catalysis in the pyrolysis behaviour of short rotation willow coppice. Fuel 2007;86(15):2389-402.

[357] Nowakowski DJ, Jones JM. Uncatalysed and potassium-catalysed pyrolysis of the cell-wall constituents of biomass and their model compounds. Journal of Analytical and Applied Pyrolysis 2008;83(1):12-25.

[358] Jensen PA, Frandsen FJ, Dam-Johansen K, Sander B. Experimental Investigation of the Transformation and Release to Gas Phase of Potassium and Chlorine during Straw Pyrolysis. Energy & Fuels 2000;14(6):1280-5.

[359] van Lith SC, Jensen PA, Frandsen FJ, Glarborg P. Release to the gas phase of inorganic elements during wood combustion. Part 2: Influence of fuel composition. Energy & Fuels 2008;22(3):1598-609.

[360] Chin YS, Darvell LI, Lea-Langton AR, Jones JM, Williams A. Ignition Risks of Biomass Dust on Hot Surfaces. Energy & Fuels 2016;30(6):4398-404.

[361] Ramírez Á, García-Torrent J, Tascón A. Experimental determination of self-heating and self-ignition risks associated with the dusts of agricultural materials commonly stored in silos. Journal of Hazardous Materials 2010;175(1):920-7.

[362] Déjardin A, Laurans F, Arnaud D, Breton C, Pilate G, Leplé J-C. Wood formation in Angiosperms. Comptes Rendus Biologies 2010;333(4):325-34.

[363] Smith AM, Ross AB. The influence and implications of recycling hydrothermal process waters on hydrochar combustion chemistry. Fuel Awaiting Publication.

[364] Nakagawa K, Yoshinaga A, Takabe K. Anatomy and lignin distribution in reaction phloem fibres of several Japanese hardwoods. Annals of Botany 2012;110(4):897-904.

[365] Laurans F, Dejardin A, Leple J, Pilate G. Physiologie de la formation des parois de fibres de bois. REVUE DES COMPOSITES ET DES MATERIAUX AVANCES 2006;16(1):25.

[366] Wu B, Taylor CM, Knappe DRU, Nanny MA, Barlaz MA. Factors Controlling Alkylbenzene Sorption to Municipal Solid Waste. Environmental Science & Technology 2001;35(22):4569-76.

[367] Kruszewska KJ, Labuschagne BCJ, du Cann VM. Relating coal oxidation and hydrophobicity: a petrographic approach. Fuel 1996;75(14):1611-6.

[368] Smith AM, Ekpo U, Ross AB. Influence of pH on the properties of hydrochar following hydrothermal treatment of Swine manure. awaiting.

[369] Baruah MK, Gogoi PC. A new form of sulphur in coal: the discovery of an iron-sulphur coordination compound. Fuel 1998;77(9):979-85.

[370] Szogi AA, Vanotti MB, Ro KS. Methods for Treatment of Animal Manures to Reduce Nutrient Pollution Prior to Soil Application. Current Pollution Reports 2015;1(1):47-56.

[371] Heilmann SM, Molde JS, Timler JG, Wood BM, Mikula AL, Vozhdayev GV, et al. Phosphorus Reclamation through Hydrothermal Carbonization of Animal Manures. Environmental Science & Technology 2014;48(17):10323-9.

[372] Ekpo U, Ross AB, Camargo-Valero MA, Williams PT. A comparison of product yields and inorganic content in process streams following thermal hydrolysis and hydrothermal processing of microalgae, manure and digestate. Bioresource Technology 2016;200:951-60.

[373] Jin Y-s, Jiang T, Yang Y-b, Li Q, Li G-h, Guo Y-f. Removal of phosphorus from iron ores by chemical leaching. Journal of Central South University of Technology 2006;13(6):673-7.

[374] Tillman DA, Duong DNB, Harding NS. Chapter 2 - Principles of Solid Fuel Blending. In: Tillman DA, Duong DNB, Harding NS, editors. Solid Fuel Blending. Boston: Butterworth-Heinemann; 2012, p. 31-70.

[375] Mason PE, Darvell LI, Jones JM, Williams A. Observations on the release of gas-phase potassium during the combustion of single particles of biomass. Fuel 2016;182:110-7.